



HAL
open science

Conception de complexes de cobalt (III) pour la commutation entre les mécanismes de polymérisation radicalaire et d'ouverture de cycle

Maxime Michelas

► **To cite this version:**

Maxime Michelas. Conception de complexes de cobalt (III) pour la commutation entre les mécanismes de polymérisation radicalaire et d'ouverture de cycle. Chimie de coordination. Université Paul Sabatier - Toulouse III, 2023. Français. NNT : 2023TOU30033 . tel-04204269

HAL Id: tel-04204269

<https://theses.hal.science/tel-04204269>

Submitted on 12 Sep 2023

HAL is a multi-disciplinary open access archive for the deposit and dissemination of scientific research documents, whether they are published or not. The documents may come from teaching and research institutions in France or abroad, or from public or private research centers.

L'archive ouverte pluridisciplinaire **HAL**, est destinée au dépôt et à la diffusion de documents scientifiques de niveau recherche, publiés ou non, émanant des établissements d'enseignement et de recherche français ou étrangers, des laboratoires publics ou privés.



THÈSE

En vue de l'obtention du
DOCTORAT DE L'UNIVERSITÉ DE TOULOUSE
Délivré par l'Université Toulouse 3 - Paul Sabatier

Présentée et soutenue par
Maxime MICHELAS

Le 11 janvier 2023

**Design of cobalt(III) carboxylate complexes for switching
between radical and ring opening polymerization mechanisms**

Ecole doctorale : **SDM - SCIENCES DE LA MATIERE - Toulouse**

Spécialité : **Chimie Organométallique et de Coordination**

Unité de recherche :

LCC - Laboratoire de Chimie de Coordination

Thèse dirigée par

Christophe FLIEDEL et Rinaldo POLI

Jury

M. Vincent MONTEIL, Rapporteur

M. Andreas DANOPOULOS, Rapporteur

M. Dider GIGMES, Examineur

Mme Blanca MARTIN-VACA, Examinatrice

M. Christophe FLIEDEL, Directeur de thèse

M. Rinaldo POLI, Co-encadrant de thèse

Remerciements

Tout d'abord, je souhaite vivement remercier le Dr. Vincent Monteil et le Prof. Andreas Danopoulos, ainsi que le Dr. Blanca Martin-Vaca et le Dr. Didier Gignes pour avoir accepté d'évaluer mes travaux de thèse en tant que rapporteurs et examinateur(-trice). Ce fut un honneur d'avoir pu rassembler vos expertises respectives pour mon jury de thèse, les questions et discussions qui en ont découlées ont été des plus intéressantes pour la suite de ce projet de recherche et nous ont permis d'avoir un nouveau regard sur celui-ci.

Évidemment, je remercie mes directeurs de thèses, le Prof. Rinaldo Poli dont je suis heureux d'avoir pu faire partie de la longue lignée de doctorants ayant pu profiter de son savoir et de ses idées. Et bien sûr, le Dr. Christophe Fliedel avec qui je suis très heureux d'avoir pu partager la vie de laboratoire et nos idées au cours de ces 3 ans. Un homme bourré de talent, à l'esprit vif, qui m'a apporté un enrichissement scientifique et personnel inestimable et m'emplit de gratitude. Au démarrage de ce projet je ne pensais pas participer à autant d'événements, tel que ton mariage ou la naissance de tes filles, qui furent des événements remplis de joies. Je pense qu'aucun doctorant ne peut rêver meilleur encadrement surtout en période de COVID (en toute objectivité bien sûr). Outre l'encadrement, j'aimerais remercier Jean-Claude Daran pour la diffraction des rayons X, Pascal Guillo pour sa bonne humeur et toujours ses petites blagues bien placées, mes stagiaires qui m'ont aidé à faire progresser mon sujet de thèse (Jadhe Salin, Gabrielle Dufaut et Thomas Caparros) ainsi que tout le staff du LCC pour leur accueil.

Trois ans de thèse c'est aussi toute une équipe et dans un premier temps j'aimerais remercier tous les gens qui sont passés dans le bureau C226 que j'ai partagé pendant ces 3 ans avec Illia, mais aussi Chantal. D'autre part, je dois aussi remercier les autres doctorants, qui ont partagé les galères de la thèse avec moi, et notamment Quentin Le De (mon bras droit) avec qui j'ai passé tous ces samedis de dur labeur avec moi, mais aussi toutes les soirées beuveries, matchs de rugby et sessions de ski. Sa compagnie a rendu la thèse en période COVID des plus agréables à vivre et je lui souhaite tout le meilleur pour la suite de sa carrière professionnelle et aussi au niveau personnel. Ainsi que tous les autres doctorants tels que Paul, Juliette, Caroline, Aurèle, Romane, Chloé, Dylan, Arno, Clément avec qui j'ai pu passer et passerai encore j'espère de folles soirées.

En dehors du laboratoire, je remercie les colocs Thomas Gerardon et Léo Vergnes les aventuriers, l'un plus sur fortnite quand même. Ce qui est sûr c'est qu'avec vous je n'ai pas passé un jour sans rire ou déconner ce qui m'a beaucoup aidé à décompresser les jours de longues manip ou les semaines sans résultats concluants. D'autre part, un petit mot à tous les copains de Valence que l'on peut citer par leurs surnoms : Benji, Tobe, Totoje, Mimitos, Romy, Sylvestre, Cyp, Mathou, Totor avec qui j'ai tout partagé depuis le collège ou même avant pour certain (je pense à toi Juju), pour leur soutien indéfectible, qui aura été pour moi une énorme source de motivation.

J'aimerais ajouter une mention spéciale pour Marie-Aurore ou « Chaton » à qui je dois énormément, car tu m'as permis de me concentrer à 100% sur la rédaction de la thèse en t'occupant d'absolument de tout le reste. Et surtout tu as su supporter mon humeur parfois terrible (Il paraît que je suis un gros râleur...) lorsque tout ne passé pas comme je le voulais.

J'aimerais finir ces remerciements avec Jean Luc Boit, qui m'a beaucoup inspiré dans ma jeunesse, bien que décédé, je suis certain qu'il aurait été très fier d'assister à l'aboutissement de cette aventure. Et bien évidemment mes parents sans qui rien de tout cela n'aurait été possible, car ils m'ont toujours poussé à donner le meilleur de moi-même. Je dédie donc ma réussite personnelle à eux mais aussi à toutes les personnes qui ont contribué à faire de moi ce que je suis aujourd'hui.

*“C’est le désir qui transforme les rêves en réalité.
Plus vous demanderez à la vie, plus vous recevrez d'elle.”*

Napoleon Hill

*“On ne juge pas un Homme sur le nombre de fois qu’il tombe
Mais sur le nombre de fois qu’il se relève.”*

Jigoro Kano

“Un jour je suis né, depuis je profite.”

Benjamin M’zoughi

“Il faut savoir travailler avec sa tête.”

Jean Luc Boit

Résumé

Dans le monde entier, les matériaux polymères prennent une grande place et remplacent bons nombres de matériaux traditionnels tels que le bois, l'acier ou le verre. En effet, ces polymères ont apporté une large gamme de propriétés intéressantes utiles à la vie de l'Homme comme celle de barrière aux gaz pour les emballages alimentaires, ou encore, permettent la constitution de matériaux légers pour l'automobile, réduisant ainsi les émissions de CO₂. De plus, les besoins en polymères bien définis avec un contrôle sur l'architecture (*c-à-d.* masse molaire, dispersité contrôlée, ou des bouts de chaînes fonctionnalisés) ne cessent d'augmenter avec le temps pour de nouveaux matériaux de hautes performances. Néanmoins, en raison de l'émergence des problèmes environnementaux et des pressions sociétales, l'amélioration de nos matériaux usuels s'inscrit dans une stratégie de développement durable visant à remplacer ceux issus de la pétrochimie par des matériaux biosourcés et/ou biodégradables. C'est dans cette optique que s'inscrit notre recherche, qui consiste à utiliser des métaux abondants, peu coûteux et moins toxiques que les complexes métalliques déjà utilisés pour la production industrielle de polymères. Les objectifs de ce projet visent ainsi à développer un composé de coordination à base de cobalt, qui servira d'amorceur et de modérateur pour deux types de polymérisations différentes : la polymérisation par ouverture de cycle (ROP) et la polymérisation radicalaire à médiation organométallique (OMRP). De plus, ce nouvel outil fonctionnerait sans aucun co-agent pour l'amorçage et le contrôle de ces polymérisations et permettrait la commutation entre ces 2 mécanismes sans aucune modifications chimiques. Ces travaux de thèse s'articuleront avec différentes architectures autour du centre métallique : des ligands à base de (N₂O₂) ou entièrement oxygénés et le fragment amorceur avec la structure carboxylate (Co-O(O)R). Ce mémoire se divisera notamment en trois parties : la première sur l'OMRP où des complexes à base de cobalt(III) ont été développés et peuvent effectuer une dissociation homolytique de la liaison Co-O(O)R par activation thermique et ainsi générer un radical primaire oxygéné pour l'amorçage directe des monomères vinyliques (VAc, MA, S, ...). Cette dissociation libère également un complexe de cobalt(II), qui joue le rôle de modérateur en piégeant de manière réversible la chaîne polymère en croissance. Par la suite la deuxième partie amènera la discussion sur les polymères biosourcés et biodégradables produit par ROP d'esters cycliques, notamment pour les monomères L-lactide (LA) ou ε-caprolactone (CL). Nous proposons que la même espèce cobalt-carboxylate puisse permettre la formation d'un nucléophile, en raison de la plus grande polarité de la liaison Co-O(O)R par rapport à la liaison Co-carbone, permettant ainsi la ROP. Par conséquent, un composé unique sera mis en évidence, qui peut fournir un radical et un nucléophile en fonction des conditions expérimentales et du type de monomères sans aucune modification chimique. L'idée sous-jacente décrite dans une troisième partie est de synthétiser des copolymères à bloc en couplant des monomères non-biodégradables et biodégradables, avec un mécanisme de commutation de polymérisation de l'OMRP à la ROP, sans aucune modification chimique entre chaque bloc. De façon plus large et appliquée, ces travaux visent à découvrir et maîtriser de nouvelles voies de synthèse de matériaux aux propriétés biodégradables.

Mots clés : Radicalaire, ouverture de cycle, polymère, complexe métallique.

Abstract

Throughout the world, polymer materials take a large place and substitute large quantities of traditional materials such as wood, steel or glass. In fact, these polymers possess a large window of interesting properties for the human daily life like gas barrier for food packaging, light weight to contribute reducing automotive carbon dioxide emission, or many other useful features of interest in the pharmaceutical field. Moreover, well-defined polymers with predictable M_n , controlled dispersity (D) or end-chain functionalization become more and more needed for the conception of new materials with original features to answer specific issues. Nevertheless, due to the emergence of environmental issues and driven by the societal pressure, an improvement of the usual materials by employing a sustainable development strategy, through replacing petrochemical-based materials by bio-based and biodegradable materials, is strongly desirable. This is the context in which our research takes place, which consists of using abundant, non-expensive and less toxic metal catalysts than those currently used for industrial polymer production. That is why this project aims to develop coordination compounds based on cobalt able to act as initiator and moderator for two different types of polymerizations: the Ring Opening Polymerization (ROP) of cyclic esters and the Organometallic Mediated Radical Polymerization (OMRP) of vinyl monomers. Moreover, this new tool should operate without any co-agent for the initiation and the control of these polymerizations. This thesis work deals with the various architectures around the cobalt center and will be presented in two parts: (N_2, O_2)- or fully O-based ligands. The initiating fragment is mainly the carboxylate (Co-O(O)R) architecture. For the OMRP polymerization method, which is based on the radical mechanism, we developed a cobalt(III) catalyst capable of homolytically cleaving the Co-O(O)R bond under thermal activation to generate the oxygenated primary radical for the direct initiation of vinyl monomers (*i.e.*, VAc, MA, S). This cleavage allows the release of a cobalt(II) complex in the medium, which can act as a moderator by reversibly trapping the growing polymer chain. Thus, the cobalt-carboxylate abilities for homolytic cleavage and control polymerization of more or less activated monomers, respectively with (N_2, O_2)- and fully O-based ligands, will be discussed. Concerning, the bio-based and biodegradable polymers produced by the ROP of cyclic ester, notably L-lactide (LA) or ϵ -caprolactone (CL), we propose that the same cobalt-carboxylate species can also allow the nucleophilic initiation of the ring opening process. Indeed, the higher polarizability of the Co-O(O)R bond compared to the Co-carbon bond should allow the nucleophilic attack of the monomer carbonyl function. Therefore, we wish to highlight a unique cobalt-carboxylate compound that is able to form a radical and act as a nucleophile depending on the experimental conditions, the monomer and the type of external stimulus, with the aim of initiating and controlling the polymerization of vinyl monomers and cyclic esters without any chemical modification. The final objective is to synthesize block copolymers with coupling of common non-biodegradable and biodegradable monomers with a polymerization mechanism switch from OMRP to ROP, without any chemical modification between the growth of each block. The ambition of this work is to open the way to the development of new materials with biodegradable properties.

Key words: Radical, organometallic complex, ring opening, polymer.

List of Symbols and abbreviations

Symbols

Mt	Metal
R [•]	Radical
R ₀	Primary radical
P _n	Polymer chain
M	Monomer
K	Equilibrium constant
k	Rate constant
M_n	Average molecular weight in number
<i>D</i>	Dispersity

Abbreviations

RDRP	Reversible Deactivation Radical Polymerization
DT	Degenerative Transfer
RT	Reversible Termination
OMRP	Organometallic Mediated Radical Polymerization
ROP	Ring Opening Polymerization
ROCoP	Ring Opening Copolymerization
RAFT	Reversible Addition-Fragmentation (chain) Transfer
NMP	Nitroxide Mediated (radical) Polymerization
ITP	Iodine Transfer Polymerization
LAM	Less Activated Monomer
MAM	More Activated Monomer
DFT	Density Functional Theory
BDE	Bond Dissociation Energy
NMR	Nuclear Magnetic Resonance
MALDI-TOF	Matrix Assisted Laser Desorption Ionisation- Time of Flight
GPC	Gel Permeation Chromatography
SEC	Size Exclusion Chromatography
DSC	Differential Scanning Calorimetry
ESI	Electrospray Ionization
DOSY	Diffusion Ordered Spectroscopy
EPR	Electron Paramagnetic Resonance
CV	Cyclic Voltammetry

SQW	Square-Wave Voltammetry
GC-MS	Gas chromatography-mass spectrometry
CCT	Catalytic Chain Transfer
<i>H</i>	Enthalpy
G	Gibbs free energy

Chemical compounds

DCM	Dichloromethane
DMC	Dimethylcarbonate
CL	ε-Caprolactone
PCL	Polycaprolactone
LA	Lactide (independently of the stereochemistry)
PLA	Poly(lactide)
St	Styrene
PS	Polystyrene
MA	Methyl acrylate
PMA	Polymethyl acrylate
VAc	Vinyl acetate
PVAc	Poly(vinyl acetate)
MMA	Methyl methacrylate
PMMA	Poly(methyl methacrylate)
BA	Butyl acrylate
PBA	Poly(butyl acrylate)
BPO	Benzoyl peroxide
LPO	Di-lauroyl peroxide
TBPO	Di-tertbutyl peroxide
APO	Di-acetyl peroxide
acac	Acetylacetonate
TTMSS	Tris(trimethylsilyl)silane
TBT	Tributyl tin
AIBN	Azobis(isobutyronitrile)
TPO	2,4,6-trimethylbenzoyl diphenylphosphine oxide
Co	Cobalt
^t Bu	<i>Tert</i> -butyl

Outline

General introduction.....	I
Chapter I. Bibliographic review	1
I. Introduction	5
II. General aspects of Organometallic-Mediated Radical Polymerization (OMRP) and overview of the contribution of each metal in this field	6
1. Titanium	9
2. Vanadium	12
3. Chromium	13
4. Molybdenum.....	16
5. Manganese and Rhenium	17
6. Iron, Ruthenium and Osmium.....	18
7. Rhodium.....	20
8. Copper.....	20
9. Cobalt.....	20
10. Conclusion.....	26
III. Ring Opening Polymerization of cyclic esters using d-block metal complexes	27
1. General aspects of Ring Opening Polymerization (ROP)	27
2. Rare-earth metals	29
3. Group 4 (Titanium, Zirconium and Hafnium).....	30
4. Vanadium	35
5. Chromium	37
6. Manganese.....	38
7. Iron.....	39
8. Cobalt.....	42
9. Nickel.....	44
10. Copper.....	45
11. Conclusion.....	49
IV. Original copolymers synthesis	50
1. Sequential polymerization based on difunctional initiators.....	51
2. Difunctional initiators for one-pot copolymerizations	52
3. Multistep copolymer synthesis based on a monofunctional initiator.....	54

4. Conclusion.....	58
V. References	59

Chapter II. Cobalt(III) carboxylate complexes 77

I. Introduction and strategy targeting	80
II. Cobalt complexes with (N ₂ ,O ₂)-type ligands	82
1. Introduction	82
2. (N ₂ ,O ₂) ligand architectures.....	82
3. Cobalt(II) complexes with Schiff-base ligands	84
4. Cobalt(III) carboxylate complexes with (N ₂ ,O ₂)-type ligands	85
5. Conclusion.....	95
III. Cobalt complexes with an (O ₂ ,O ₂)-type ligand	96
1. Introduction	96
2. (Acetylacetonato)-cobalt(III) carboxylate complexes.....	96
IV. Conclusion and outlook	110
V. Experimental section	111
1. Materials	111
2. Characterizations	111
3. Methods.....	113
VI. References	118

Chapter III: Polymerization processes 125

I. Introduction and strategy	129
II. Radical polymerization (OMRP)	131
1. (N ₂ ,O ₂)-Cobalt(III) complexes for the polymerization of MAMs.....	131
2. Conclusion on the use of (N ₂ ,O ₂)-based complexes as initiating systems	140
3. (O ₂ ,O ₂)-Cobalt(III) carboxylate complexes.....	141
4. Conclusion	160
III. Ring opening polymerization (ROP)	161
1. Introduction	161

2.	(N ₂ ,O ₂)-Cobalt complex (3.1)	162
3.	(O ₂ ,O ₂)-Cobalt carboxylate complexes	169
4.	Conclusion	171
IV.	Polymerization switch	173
1.	Sequential polymerization processes (Block copolymers)	174
2.	One pot procedure (Mixture of PVAc & PCL)	180
3.	Selective degradation of copolymer (OMRP-b-ROP)	183
V.	Conclusion and outlook	185
VI.	Experimental section	186
1.	Materials	186
2.	Characterizations	186
3.	Methods	187
	General conclusion and perspectives	190
	References	192
	Annexes Chapter I	198
	Annexes Chapter II	217
	Annexes Chapter III	243
	Résumé en Français	255

General introduction

While polymers are too often abusively associated to simple “plastics” used for packaging, they represent in fact a material of choice used in many fields such as automotive engineering, aeronautics, fuel cells, paints or in the biomedical area (*e.g.* for drug delivery). In many of these areas, polymeric materials replaced traditional ones such as wood, steel or glass. Although several techniques are available for the synthesis of polymeric materials (anionic, cationic...), a large part of the worldwide production of polymers is achieved by conventional radical polymerization, especially due to its easy implementation and high tolerance to many functional groups. Nevertheless, the increasing demand of well-defined polymers (predictable M_n , narrow dispersity (\mathcal{D}), chain-end fidelity/functionalization, block copolymers...) for high-tech applications led to the development of new polymerization methods or to the improvement of the existing ones, in particular *via* the reversible-deactivation radical polymerization (RDRP) techniques.¹

In the framework of the present thesis, we were especially interested in polymerization methods that make use of coordination compounds. Industrial polymerization processes using metal complexes have been applied over more than sixty years. The most famous example is the Ziegler-Natta process developed by Karl Ziegler and Giulio Natta in 1950 for the polymerization of olefins with a titanium-based complex as shown in *Figure 1* (left).²

Another important breakthrough in the field was the discovery, in the mid 90's, of Atom Transfer Radical Polymerization (ATRP),^{3, 4} and especially all further developments of the copper-based ARTP that can be essentially attributed to Matyjaszewski and coll. (*Figure 1*, middle).⁵⁻⁷ This technique uses a metal-halide complex as moderator of the polymerization, the role of which is to establish a reversible equilibrium between the active radical species (growing polymer chain) and a dormant species that results from the radical trapping by an halogen atom present in the complex (*Figure 1*, right). Among the important improvements of this technique are the development of more active catalysts (allowing their use in only *ppm* amounts)^{8, 9} and the development of methods allowing 1) the regeneration of the activator, 2) to perform the polymerization under aerobic conditions, 3) the temporal control of the polymerization.¹⁰ Altogether, these properties account for the growing use of ATRP at an industrial level and/or for the fabrication of high-performance consumer products.¹¹

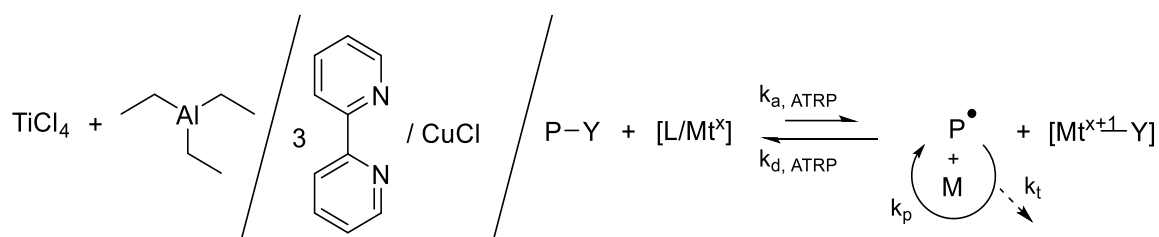


Figure 1: First Ziegler-Natta (left) and ATRP (middle) complexes used for polymer production and ATRP equilibrium.^{2, 12, 13}

While ATRP has pushed the limits of radical polymerization, new challenges have appeared. Indeed, the control of the polymerization of certain monomers like vinyl acetate (VAc) and vinylidene fluoride (VDF) was low.^{14, 15} These monomers belong to the “less activated monomers” (LAMs) class. In the radical polymerization area, they are known as the most difficult monomers to control because they are associated to highly reactive/non-stabilized radicals, and therefore they make very strong bonds with the moderator in the dormant species, which are difficult to reactivate.¹⁶ Another RDRP technique that was developed much more recently and that uses coordination compounds as moderators, namely Organometallic-Mediated Radical Polymerization (OMRP) was found very promising for the controlled polymerization of LAMs.^{17, 18} The development of new initiators/moderators and OMRP initiation mechanistic studies are topics that were investigated during the present thesis work.

Besides the important developments discussed above, societal and environmental issues have led, over the last decades, to the development of sustainable strategies to replace petrochemical-based materials with bio-based and biodegradable materials. The most famous approach is the Ring Opening Polymerization (ROP) of cyclic esters, such as lactide (LA), originating from renewable resources.¹⁹ The corresponding biodegradable and biocompatible polylactide material is highly studied and has many applications in the biomedical area for implants or drug delivery, but also for packaging to replace common polystyrene or polyethylene. The pioneering work in this field dates back to the 50's with the reports by Klein *et al.*²⁰⁻²² using Sn- and Al-based complexes as ROP initiators (*Figure 2*).

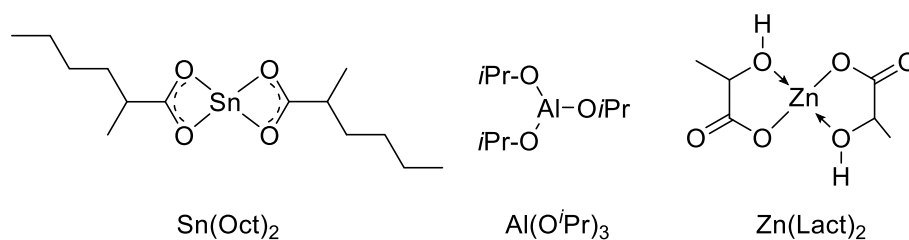


Figure 2: First metal complexes reported for industrial ROP.²⁰⁻²²

Figure 3 shows the number of publications per year in function of a series of topics; a) concerns three RDRP techniques, *i.e.* ATRP, reversible addition–fragmentation chain-transfer (RAFT) and nitroxide mediated radical polymerization (NMP), and b) compares ROP and RDRP methods. These graphs underline that the techniques making use of a coordination compound as initiator/moderator/catalyst for polymer production are still intensively studied.

The enthusiasm around these kinds of polymerization methods motivated the scientific community to think about how to couple different techniques to produce new classes of polymers. Several approaches were proposed to produce original block copolymers, such as by click chemistry, by using multifunctional initiators or by post-modification of the chain end of a first block for chain extension.²³ However, to the best of our knowledge, no single compound that allows to switch from a RDRP method to ROP and *vice-versa* has yet been reported, and this will be the aim of the present project.

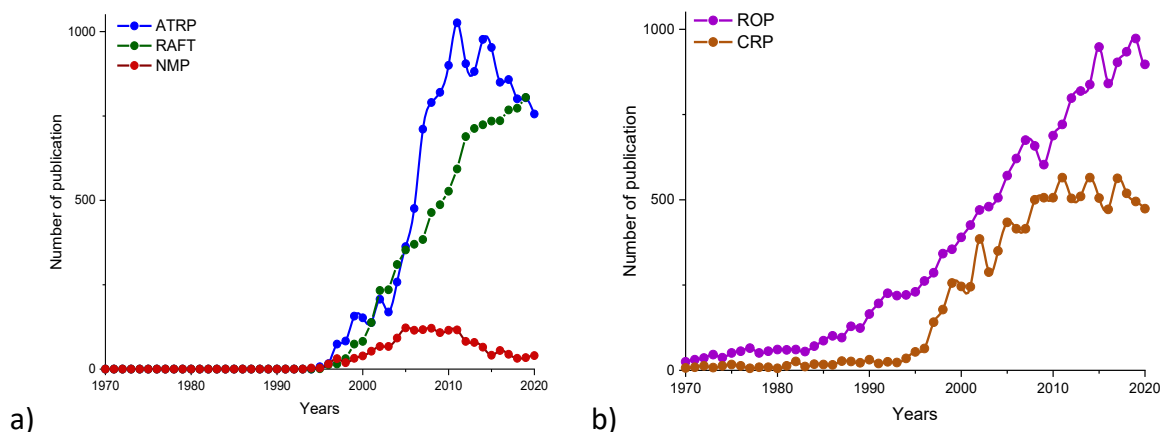


Figure 3: Publications per years mentioning the terms a) “Atom Transfer Radical Polymerization” (ATRP), “reversible addition-fragmentation (chain) transfer” (RAFT), “nitroxide mediated (radical) polymerization” (NMP), b) “controlled radical polymerization” (CRP), “ring opening polymerization” (ROP).

Searches were carried out in June 2022 using SciFinder-*n*TM

The present project aims at the development of metal complexes able to efficiently initiate and moderate both OMRP and ROP types of polymerizations. Moreover, if these processes are well-controlled, the metal complex should be linked to one chain-end of the macromolecule ($[L/Mt-P_m]$). We expect to reactivate this chain end for the formation of block copolymers, but not by using the same technique used for the previous block (*i.e.* OMRP/OMRP or ROP/ROP), but rather by switching from one to the other mechanism, *i.e.* OMRP to ROP and ROP to OMRP. If successful, these switches would allow accessing unprecedented copolymers with unknown properties.

The thesis manuscript will be divided into the following three chapters:

Chapter 1 is a bibliographic review that presents, in a first part, the OMRP and (metal-mediated) ROP methods, from general principles and mechanisms to the more recent and striking results. A second part will present the state of the art in the access of original copolymers produced by coupling, click, a switch, and chain-end post-functionalization.

Chapter 2 is dedicated to the synthesis and characterization of cobalt(III) complexes that can be potential initiators and moderators of a polymerization reaction, following either a radical (OMRP) or a coordination insertion (ROP) path.

Chapter 3 describes, in a first part, the results of obtained by OMRP or ROP with several complexes. A second part, will be dedicated to the tests of “switch” from OMRP to ROP and from ROP to OMRP, without any chemical modification between the first and second block synthesis.

References

1. Jenkins, A. D.; Jones, R. G.; Moad, G., Terminology for reversible-deactivation radical polymerization previously called "controlled" radical or "living" radical polymerization (IUPAC Recommendations 2010). *Pure and Applied Chemistry* **2009**, *82* (2), 483-491.
2. Kazuo, S., Takesi, S., Ziegler-Natta catalysts for olefin polymerizations. *Pmg. Polym. Sci.* **1997**, *23*, 1503-1546.
3. Wang, J.-S.; Matyjaszewski, K., Controlled/"living" radical polymerization. atom transfer radical polymerization in the presence of transition-metal complexes. *J. Am. Chem. Soc.* **1995**, *117* (20), 5614-5615.
4. Kato, M.; Kamigaito, M.; Sawamoto, M.; Higashimura, T., Polymerization of Methyl Methacrylate with the Carbon Tetrachloride/Dichlorotris-(triphenylphosphine)ruthenium(II)/Methylaluminum Bis(2,6-di-tert-butylphenoxide) Initiating System: Possibility of Living Radical Polymerization. *Macromolecules* **1995**, *28* (5), 1721-1723.
5. Matyjaszewski, K., Atom Transfer Radical Polymerization (ATRP): Current Status and Future Perspectives. *Macromolecules* **2012**, *45* (10), 4015-4039.
6. Matyjaszewski, K., Ranking living systems. *Macromolecules* **2002**, *26* (7), 1787-1788.
7. Xia, K. M. a. J., Atom Transfer Radical Polymerization. *Chem. Rev.* **2001**, *101*, 2921-2990.
8. Matyjaszewski, K.; Enciso, A. E.; Lorandi, F.; Mehmood, A.; Fantin, M.; Szczepaniak, G.; Janesko, B. G., p-Substituted tris(2-pyridylmethyl)amines as ligands for highly active ATRP catalysts: Facile synthesis and characterization. *Angew. Chem. Int. Ed.* **2020**, *in press*, 10.1002/anie.202004724.
9. Ribelli, T. G.; Fantin, M.; Daran, J. C.; Augustine, K. F.; Poli, R.; Matyjaszewski, K., Synthesis and Characterization of the Most Active Copper ATRP Catalyst Based on Tris[(4-dimethylaminopyridyl)methyl]amine. *J. Am. Chem. Soc.* **2018**, *140* (4), 1525-1534.
10. Ribelli, T. G.; Lorandi, F.; Fantin, M.; Matyjaszewski, K., Atom Transfer Radical Polymerization: Billion Times More Active Catalysts and New Initiation Systems. *Macromol. Rapid Commun.* **2019**, *40* (1), e1800616.
11. Matyjaszewski, K., Advanced Materials by Atom Transfer Radical Polymerization. *Adv Mater* **2018**, *30* (23), e1706441.
12. Matyjaszewski, K., Introduction to living polymerization. Living and/or controlled polymerization. *Journal of physical organic chemistry* **1995**, *8*, 197-207.
13. Wang, J.-S.; Matyjaszewski, K., Controlled/"living" radical polymerization. atom transfer radical polymerization in the presence of transition-metal complexes. *Journal of the American Chemical Society* **2002**, *117* (20), 5614-5615.
14. Moad, G., Living and controlled RAP (reversible activation polymerization) on the way to RDRP (reversible deactivation radical polymerization). No chance for immortality. A mini-review on the terminological development of RDRP. *Polymer International* **2022**.
15. Fliedel, C.; Poli, R., Homolytically weak metal-carbon bonds make robust controlled radical polymerizations systems for "less-activated monomers". *Journal of Organometallic Chemistry* **2019**, *880*, 241-252.
16. Debuigne, A.; Jérôme, C.; Detrembleur, C., Organometallic-mediated radical polymerization of 'less activated monomers': Fundamentals, challenges and opportunities. *Polymer* **2017**, *115*, 285-307.
17. Auras, R.; Harte, B.; Selke, S., An overview of polylactides as packaging materials. *Macromol Biosci* **2004**, *4* (9), 835-64.
18. Philippe Degée, P. D., Robert Jerome, Sven Jacobsen and HansGerhard Fritz, New catalysis for fast bulk ring-opening polymerization of lactide monomers. *Macromol. Symp.* **1999**, *144*, 289-302
19. Löfgren, A.; Albertsson, A.-C.; Dubois, P.; Jérôme, R., Recent Advances in Ring-Opening Polymerization of Lactones and Related Compounds. *Journal of Macromolecular Science, Part C: Polymer Reviews* **1995**, *35* (3), 379-418.
20. Odile Dechy-Cabaret, B. M.-V., and Didier Bourissou, Controlled Ring-Opening Polymerization of Lactide and Glycolide. *Chem. Rev.* **2004**, *104*, 6147-6176.
21. Jakubowski, W.; Matyjaszewski, K., New Segmented Copolymers by Combination of Atom Transfer Radical Polymerization and Ring Opening Polymerization. *Macromolecular Symposia* **2006**, *240* (1), 213-223.

1. Jenkins, A. D.; Jones, R. G.; Moad, G., Terminology for reversible-deactivation radical polymerization previously called "controlled" radical or "living" radical polymerization (IUPAC Recommendations 2010). *Pure and Applied Chemistry* **2009**, *82* (2), 483-491.
2. Kazuo, S., Takesi, S., Ziegler-Natta catalysts for olefin polymerizations. *Pmg. Polym, Sci.* **1997**, *23*, 1503-1546.
3. Wang, J.-S.; Matyjaszewski, K., Controlled/"living" radical polymerization. atom transfer radical polymerization in the presence of transition-metal complexes. *J. Am. Chem. Soc.* **1995**, *117* (20), 5614-5615.
4. Kato, M.; Kamigaito, M.; Sawamoto, M.; Higashimura, T., Polymerization of Methyl Methacrylate with the Carbon Tetrachloride/Dichlorotris-(triphenylphosphine)ruthenium(II)/Methylaluminum Bis(2,6-di-tert-butylphenoxide) Initiating System: Possibility of Living Radical Polymerization. *Macromolecules* **1995**, *28* (5), 1721-1723.
5. Matyjaszewski, K., Atom Transfer Radical Polymerization (ATRP): Current Status and Future Perspectives. *Macromolecules* **2012**, *45* (10), 4015-4039.
6. Matyjaszewski, K., Ranking living systems. *Macromolecules* **2002**, *26* (7), 1787-1788.
7. Xia, K. M. a. J., Atom Transfer Radical Polymerization. *Chem. Rev.* **2001**, *101*, 2921-2990.
8. Matyjaszewski, K.; Enciso, A. E.; Lorandi, F.; Mehmood, A.; Fantin, M.; Szczepaniak, G.; Janesko, B. G., p-Substituted tris(2-pyridylmethyl)amines as ligands for highly active ATRP catalysts: Facile synthesis and characterization. *Angew. Chem. Int. Ed.* **2020**, *in press*, 10.1002/anie.202004724.
9. Ribelli, T. G.; Fantin, M.; Daran, J. C.; Augustine, K. F.; Poli, R.; Matyjaszewski, K., Synthesis and Characterization of the Most Active Copper ATRP Catalyst Based on Tris[(4-dimethylaminopyridyl)methyl]amine. *J. Am. Chem. Soc.* **2018**, *140* (4), 1525-1534.
10. Ribelli, T. G.; Lorandi, F.; Fantin, M.; Matyjaszewski, K., Atom Transfer Radical Polymerization: Billion Times More Active Catalysts and New Initiation Systems. *Macromol. Rapid Commun.* **2019**, *40* (1), e1800616.
11. Matyjaszewski, K., Advanced Materials by Atom Transfer Radical Polymerization. *Adv Mater* **2018**, *30* (23), e1706441.
12. Matyjaszewski, K., Introduction to living polymerization. Living and/or controlled polymerization. *Journal of physical organic chemistry* **1995**, *8*, 197-207.
13. Wang, J.-S.; Matyjaszewski, K., Controlled/"living" radical polymerization. atom transfer radical polymerization in the presence of transition-metal complexes. *Journal of the American Chemical Society* **2002**, *117* (20), 5614-5615.
14. Kermagoret, A.; Jérôme, C.; Detrembleur, C.; Debuigne, A., In situ bidentate to tetradentate ligand exchange reaction in cobalt-mediated radical polymerization. *European Polymer Journal* **2015**, *62*, 312-321.
15. Faliereas, P. G.; Ladmiral, V.; Debuigne, A.; Detrembleur, C.; Poli, R.; Ameduri, B., Straightforward Synthesis of Well-Defined Poly(vinylidene fluoride) and Its Block Copolymers by Cobalt-Mediated Radical Polymerization. *Macromolecules* **2019**, *52* (3), 1266-1276.
16. Moad, G., Living and controlled RAP (reversible activation polymerization) on the way to RDRP (reversible deactivation radical polymerization). No chance for immortality. A mini-review on the terminological development of RDRP. *Polymer International* **2022**.
17. Fliedel, C.; Poli, R., Homolytically weak metal-carbon bonds make robust controlled radical polymerizations systems for "less-activated monomers". *Journal of Organometallic Chemistry* **2019**, *880*, 241-252.
18. Debuigne, A.; Jérôme, C.; Detrembleur, C., Organometallic-mediated radical polymerization of 'less activated monomers': Fundamentals, challenges and opportunities. *Polymer* **2017**, *115*, 285-307.
19. Auras, R.; Harte, B.; Selke, S., An overview of polylactides as packaging materials. *Macromol Biosci* **2004**, *4* (9), 835-64.

20. Philippe Degée, P. D., Robert Jerome, Sven Jacobsen and HansGerhard Fritz, New catalysis for fast bulk ring-opening polymerization of lactide monomers. *Macromol. Symp.* **1999**, *144*, 289-302
21. Löfgren, A.; Albertsson, A.-C.; Dubois, P.; Jérôme, R., Recent Advances in Ring-Opening Polymerization of Lactones and Related Compounds. *Journal of Macromolecular Science, Part C: Polymer Reviews* **1995**, *35* (3), 379-418.
22. Odile Dechy-Cabaret, B. M.-V., and Didier Bourissou, Controlled Ring-Opening Polymerization of Lactide and Glycolide. *Chem. Rev.* **2004**, *104*, 6147–6176.
23. Jakubowski, W.; Matyjaszewski, K., New Segmented Copolymers by Combination of Atom Transfer Radical Polymerization and Ring Opening Polymerization. *Macromolecular Symposia* **2006**, *240* (1), 213-223.

Chapter I. Bibliographic review

Chapter I is a bibliographic review that presents, in a first part, the OMRP and (metal-mediated) ROP methods, from general principles and mechanisms to the more recent and striking results. A second part will present the state of the art in the access of original copolymers produced by coupling, click, a switch, and chain-end post-functionalization.

Table of contents

Chapter I. Bibliographic review	1
I. Introduction	5
II. General aspects of Organometallic-Mediated Radical Polymerization (OMRP) and overview of the contribution of each metal in this field	6
1. Titanium	9
2. Vanadium	12
3. Chromium	13
4. Molybdenum	16
5. Manganese and Rhenium	17
6. Iron, Ruthenium and Osmium	18
7. Rhodium	20
8. Copper	20
9. Cobalt	20
a. Porphyrin system	21
b. β -Diketonate system.....	22
c. Other planar macrocyclic systems	24
d. Other ligand systems	25
10. Conclusion	26
III. Ring Opening Polymerization of cyclic esters using d-block metal complexes	27
1. General aspects of Ring Opening Polymerization (ROP)	27
2. Rare-earth metals	29
3. Group 4 (Titanium, Zirconium and Hafnium)	30
4. Vanadium	35
5. Chromium	37
6. Manganese	38
7. Iron	39
a. Iron chloride precursors	39
b. Iron trimethylsilylamide	40
c. Iron alkoxide complexes	41
8. Cobalt	42

9.	Nickel	44
10.	Copper	45
11.	Conclusion	49
IV.	Original copolymers synthesis	50
1.	Sequential polymerization based on difunctional initiators	51
2.	Difunctional initiators for one-pot copolymerizations	52
3.	Multistep copolymer synthesis based on a monofunctional initiator	54
4.	Conclusion	58
V.	References	59

I. Introduction

The synthesis of hybrid copolymers based on vinyl monomers and cyclic esters has already been reported. Nevertheless, these approaches include either a chemical modification between the blocks to modify the chain-end, which could then be reactivated for the growing of the second block with the second method,¹ or the use of a di- or tri-functional initiator, in which each function can initiate a specific type of polymerization.^{2,3} The limitation of the latter remains that it can only provide a diblock copolymer (for a di-functional initiator), one block growing on each specific site.

Our approach consists in the design of a new tool, a single coordination compound, that could behave, as a function of the experimental conditions (monomers, stimulus used for activation, *etc.*), as an initiator for an OMRP process, by furnishing radicals *via* the homolytic cleavage of either an Mt-C_{OMRP}-polymer or an Mt-O_{ROP}-polymer bond, or as a ROP initiator, furnish a nucleophile from either an Mt-C_{OMRP}-polymer or an Mt-O_{ROP}-polymer bond. The concept is schematically presented in *Figure I-1*.

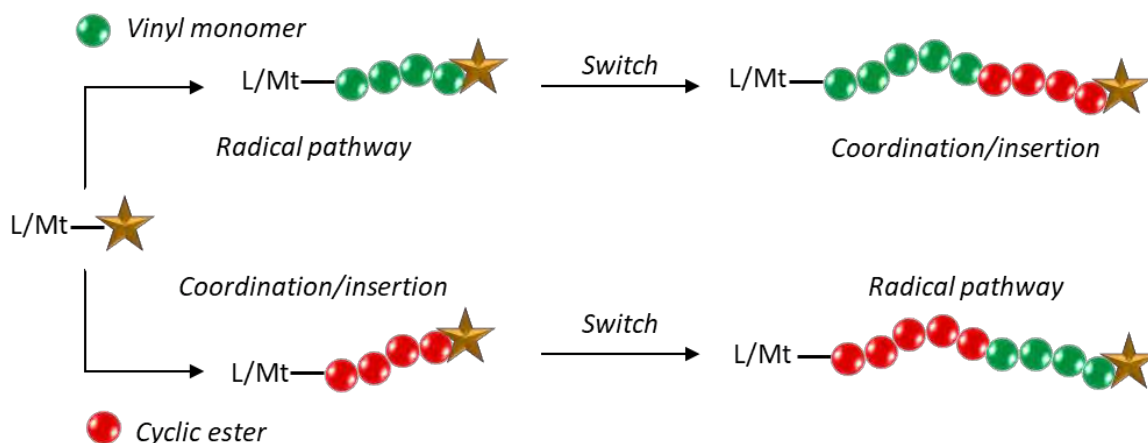


Figure I-1: General strategy for polymerization switching by a single metal complex.

This bibliographic review will be divided into three parts. The first will be dedicated to the controlled polymerization of vinyl monomer by organometallic-mediated radical polymerization (OMRP). The second part will summarize the recent developments in the field of ring opening polymerization (ROP) of cyclic esters, with a special emphasis on initiators based on group 5 to group 11 metals. The last section will present the original diblock copolymers already reported in the literature that combine a poly(vinyl monomer) block produced *via* a radical mechanism and a polyester block produced *via* a coordination mechanism.

II. General aspects of Organometallic-Mediated Radical Polymerization (OMRP) and overview of the contribution of each metal in this field

The industrial production of polymeric materials based on radical polymerization follows a conventional radical polymerization path (*Figure II-1*), which involves fast propagation and high tolerance of many functional groups. This technique is based on four fundamental steps: 1) primary radical generation by an external stimulus (*e.g.* temperature, UV, visible light, pH), 2) propagation, where the propagating radical species (P_n^\bullet) reacts with other vinyl monomers in order to extend the polymer chain, 3) termination reactions (disproportionation or coupling), and 4) chain transfer to an external molecule (transfer agent) that stops the growth of the original chain and starts a new chain. The terminations and chain transfer are responsible for the poor control of the process.

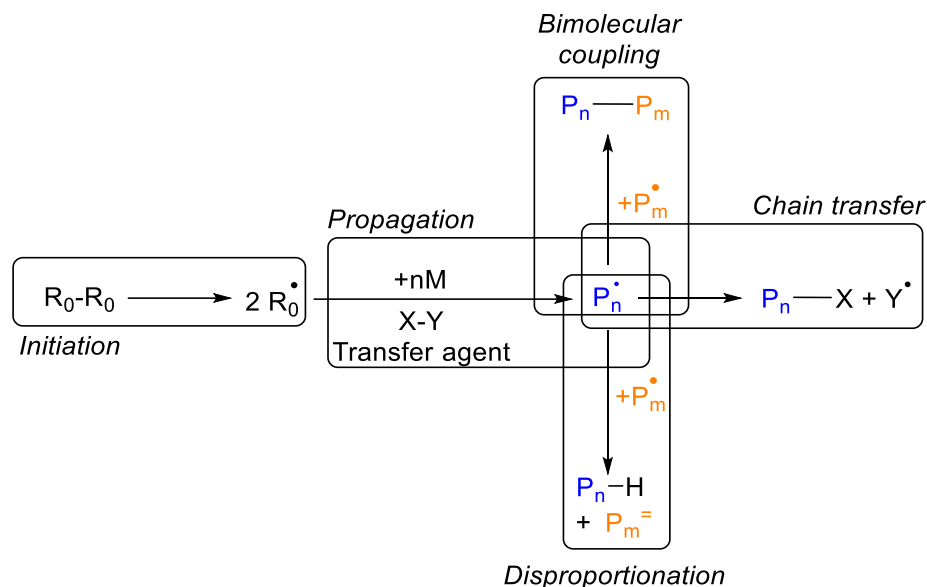


Figure II-1. Conventional radical polymerization.

The aforementioned limitations led to the development of new methods that aimed at improving the control of the polymerization (chain length and dispersity) and the chain-end fidelity/functionality, allowing the design of complex architectures. The terminology “Controlled Radical Polymerization” appeared in 1994, and the improvements relative to conventional radical polymerization, in terms of the impact of the termination reactions, were such that these new methodologies were (abusively) compared to living polymerization techniques. The terminology used nowadays, and recommended by IUPAC, is “Reversible-Deactivation Radical Polymerization” (RDRP).^{4,5} All the RDRP methods are based on the same principle (*Figure II-2*); after the initiation step, which can be *direct* or *reverse*, the propagation is controlled by a dynamic equilibrium between the active radical species ($P_{n/m}^\bullet$) and a

dormant species ($T-P_{n/m}$), resulting from the trapping of the radical by a controlling agent (T). The objective is to reduce the radical concentration to favour the controlled chain growth and limit the bimolecular terminations. The propagation can follow a Reversible Termination (RT) equilibrium, such as in ATRP or NMP^{6,7} or a Degenerative Transfer (DT) equilibrium, such as in RAFT or ITP.⁸⁻¹²

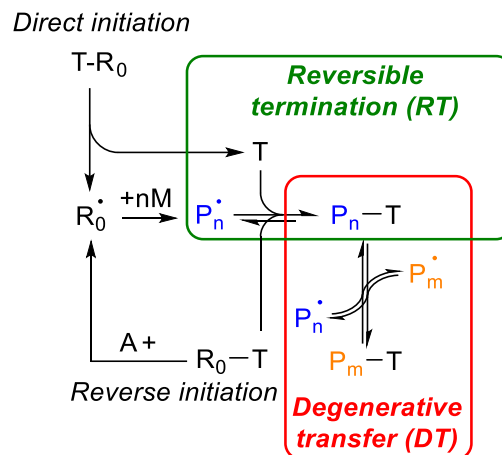


Figure II-2: General mechanism of Reversible-Deactivation Radical Polymerization (RDRP).

The control of the polymerization is also dependent on the experimental conditions and on the type of monomer used. In this regard, the controlled polymerization of the so-called “Less Activated Monomer” (LAMs, Figure II-3), such as vinyl acetate (VAc), remains challenging for the RDRP methods. These monomers generate a highly reactive/non-stabilized radicals, and therefore form very strong bonds with the moderators, and therefore the corresponding dormant species are difficult to reactivate. Organometallic-Mediated Radical Polymerization (OMRP), which uses a coordination compound (L/Mt^x) as moderator, has proven to be a method of choice for the controlled polymerization of such monomers.¹³ The detailed mechanisms/equilibria involved in OMRP are depicted in Figure II-4.

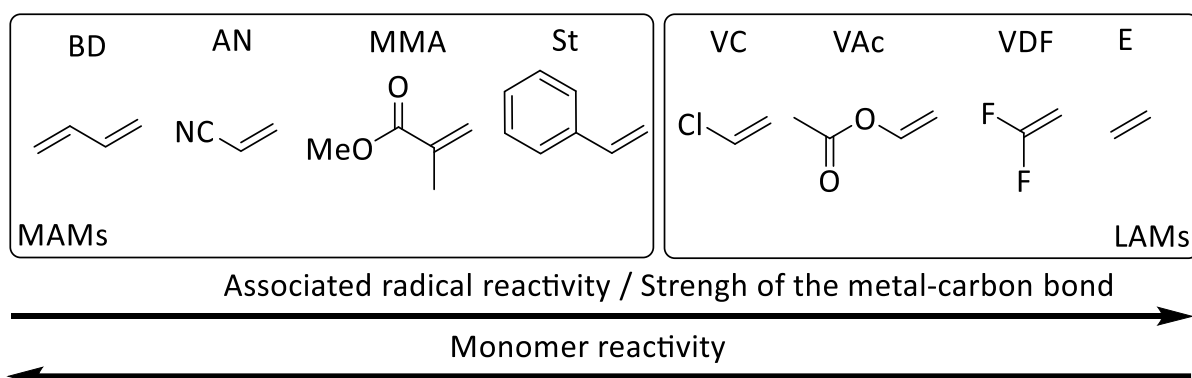


Figure II-3. Reactivity scale of MAMs and LAMs.

BD = 1,3-butadiene; AN = acrylonitrile; MMA = methyl methacrylate; St = styrene; VC = vinyl chloride; VAc = vinyl acetate; VDF = vinylidene fluoride; E = ethylene.

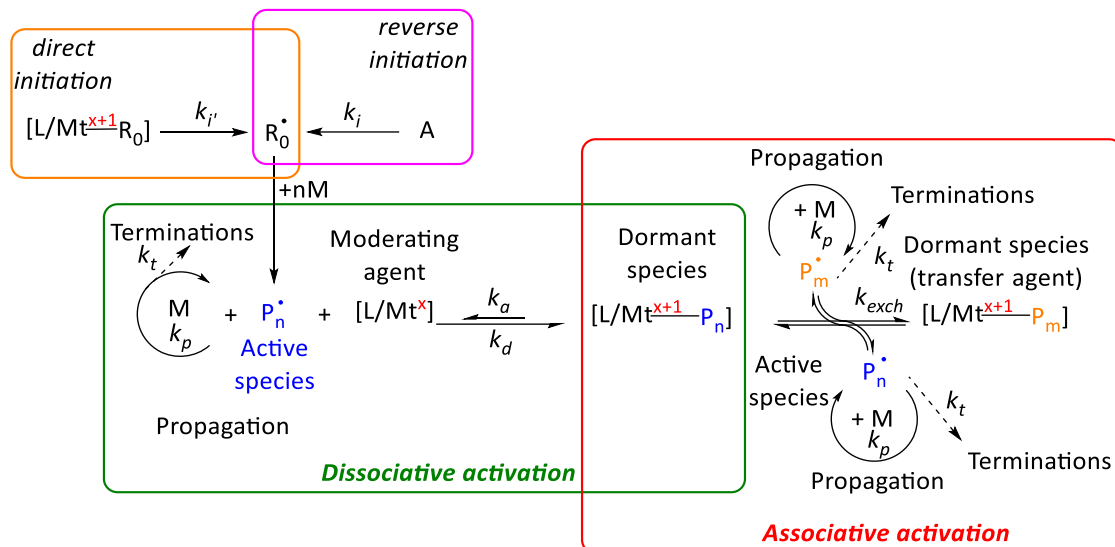


Figure II-4. Mechanisms/equilibria involved in OMRP.

As shown above, an OMRP process can be initiated either by “reverse initiation”, by using an external source of radicals (AIBN or V-70) and the moderator (L/Mt^x), or by “direct initiation”, by using a unimolecular coordination compound ($Mt^{x+1}-R_0$). The latter complex should contain a $Mt-R_0$ bond that can be cleaved homolytically to afford a primary radical (R_0^\bullet) and release the moderator (L/Mt^x) in the medium. After that, the control of the polymerization is established by reversible trapping of growing radical chain by the moderator, to form $Mt^{x+1}-P_n$ (dormant species). A controlled growth in OMRP may be ensured by either a reversible termination or a degenerative transfer mechanism.

The prerequisites of this method are to use a metal centre that; *i*) easily switches between oxidation states x and $x+1$, *ii*) can arrange a vacant coordination site for the trapping, and *iii*) forms relatively weak $Mt^{x+1}-C(\text{polymer})$ bonds to allow homolytic cleavage. Indeed, the Mt -polymer bond dissociation energy (BDE) is the only parameter that controls the OMRP equilibrium. As illustrated in Figure II-5, if the BDE is too small, the Mt -polymer bond will be too fragile (no efficient trapping) and the polymerization will not be controlled. Inversely, if the BDE is too high, irreversible trapping will occur and this will stop of the polymerization.

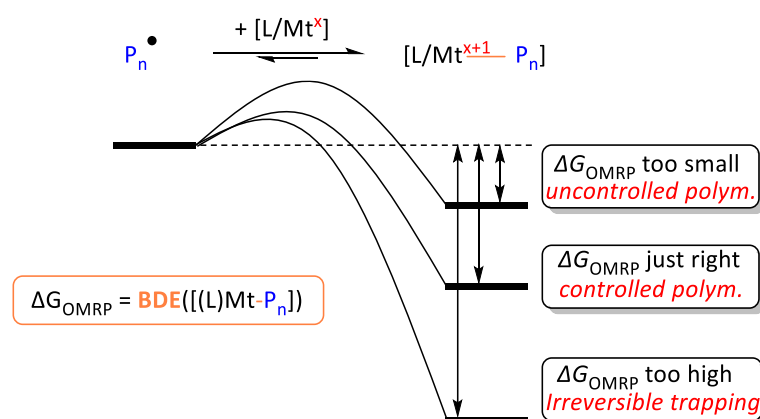


Figure II-5. Relationship between OMRP equilibrium and $Mt-P_n$ Bond Dissociation Energy.

On the basis of the relationship between the OMRP equilibrium constant and the Mt-P_n BDE, coordination chemistry plays a determining role because it is in principle possible to modulate “on demand” the Mt-P_n bond strength *via* the choice of the metal centre and/or by ligand engineering (steric and electronic properties), and therefore, in theory, OMRP may be adaptable to all vinyl monomers.

Several systems were already reported for the controlled polymerization of MAMs or LAMs by OMRP, and the following section will provide an overview of these systems by metal, with a special emphasis on cobalt, which is the most successful metal and also the one studied in the present thesis project. All of the experimental data from the literature are summarized in the annexes Table S1-S2. This section is the part I wrote of a book chapter in *Comprehensive Organometallic Chemistry IV* during the first COVID-19 lockdown.¹⁴

1. Titanium

Compounds with a Ti^{IV}-R bond are extensively used to polymerize alkenes by the coordination/insertion mechanism. Nevertheless, this bond has sufficiently low homolytic strength for reversible homolysis in certain systems, compatible with mediation of radical polymerizations. Since 2004,¹⁵ Asandei and coworkers have applied this chemistry for the controlled polymerization of styrene,¹⁵⁻²⁹ butadiene³⁰⁻³⁴ and isoprene.^{35, 36} The mediating agent is a Ti^{III} complex, generated *in situ* by reduction of a stable Ti^{IV} precursor. Zinc was shown to be the best reducing agent²⁰ and [Cp₂TiCl₂] (**1.1**, *Figure II-6*, Y = Cl) the best precursor amongst several investigated Ti^{IV} complexes,^{18-20, 37, 38} yielding [Cp₂Ti^{III}Cl]. This complex operates, at the same time, as polymerization moderator and as part of the initiating system in combination with various other molecules, see *Figure II-7*. The [Cp₂Ti^{III}Cl] reducing power, combined with the oxophilicity/halidophilicity of titanium(IV), produces primary radicals by electron transfer in combination with many stable molecules such as aldehydes,^{17, 39} active halides R-Y (α,α' -dihalo-*p*-xylene^{27, 31, 33, 34}, 1,10-dibromodecane,²⁹ 4-methoxybenzenesulfonyl chloride,²⁴ (1-bromoethyl)benzene²⁵), peroxides^{16, 21, 22, 40} and also epoxides by radical ring opening (RRO).^{15, 20, 23, 28, 32, 36} Subsequently, a second [Cp₂Ti^{III}Cl] molecule reversibly traps the growing radical chain to generate the organometallic Ti^{IV} dormant species, rather than by Cl atom transfer to generate a Cl-capped chain. The NMR and IR analyses of the recovered polymer products obtained by aldehyde or epoxide RRO initiations have confirmed the presence of the Cp₂TiCl-O fragment at the α chain-end and the absence of Cl atoms at the ω chain-end (hence, no ARTP mechanism).^{15, 31, 33, 36}

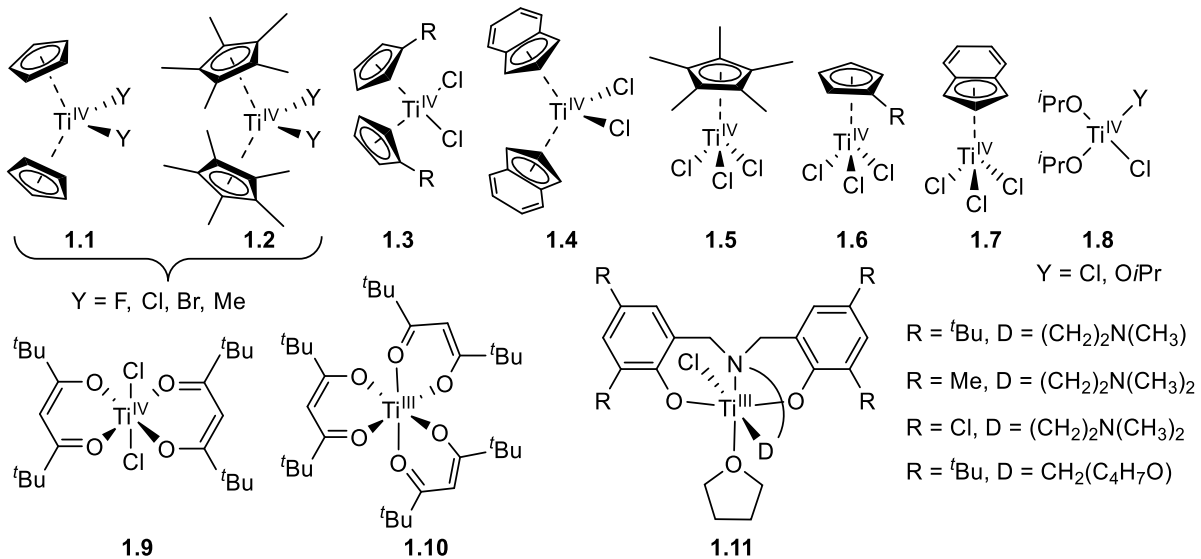


Figure II-6: Titanium(IV) complexes evaluated in radical polymerization.

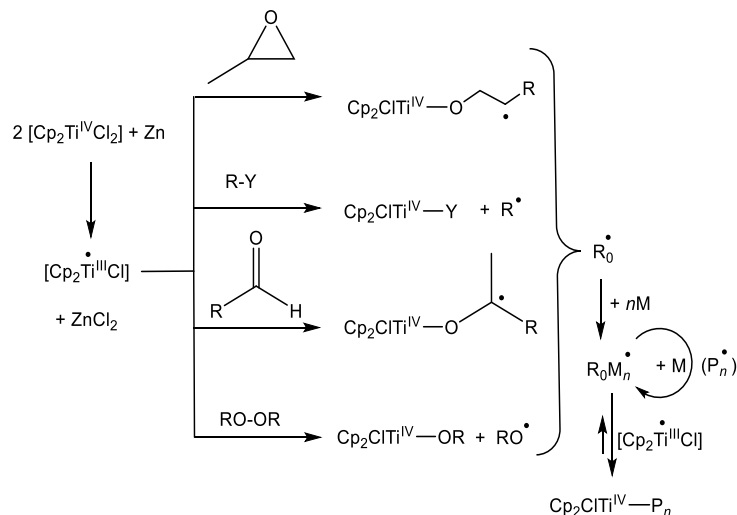


Figure II-7: Initiation systems for the $[\text{Cp}_2\text{Ti}^{\text{III}}\text{Cl}]$ -mediated OMRP.

The Figure II-6 summarizes all Ti complexes evaluated as moderators or initiators/moderators in OMRP. Among the sandwich complexes (**1.1-1.4**) with different η^5 and monodentate wedge ligands,^{18-20, 37, 38} the most efficient one in terms of controllability is the simplest and least expensive $[\text{Cp}_2\text{TiCl}_2]$.¹⁵ The half-sandwich complexes (**1.5-1.7**) required higher temperatures for $\text{Ti}^{\text{IV}}\text{-C}$ bond homolysis and also led to broader dispersities.¹⁹ Improved control resulted from a decrease of the five-membered ring electron donating power ($^t\text{BuCp}$, $^i\text{PrCp}$, EtCp and Cp).¹⁹ The alkoxide (**1.8**) and diketonato (**1.9-1.10**) complexes were tested in styrene polymerization.^{37, 41} Only **1.8** ($\text{Y} = \text{Cl}, \text{O}^i\text{Pr}$) provided some control, although with low initiation efficiencies, whereas **1.9** only led to free radical polymerization and the Ti^{III} complex **1.10** gave no initiation.

The readily accessible amine bis(phenolate) complexes of Ti^{III} , **1.11**, provided excellent control ($\mathcal{D} = 1.14$) for the MMA polymerization in toluene at 80°C in combination with azo-initiators (V-70 or AIBN).⁴² This polymerization, however, does not involve reversible $\text{Ti}^{\text{IV}}\text{-C}$

homolysis. Rather, the radically initiated polymer chains are trapped as enolates (Ti^{IV}-O bond) and continue to grow by a bimetallic Group Transfer Polymerization (GTP) mechanism. In this respect, other reports of MMA polymerizations with radical initiations in the presence of highly oxophilic metallic complexes, including [Cp₂TiCl₂],⁴³⁻⁴⁵ and described as controlled radical polymerizations, may need reconsideration. The OMRP mechanism with this highly oxophilic metal is unambiguously demonstrated only for styrene and diene monomers. An attempt to polymerize VDF with this system led to no polymer production.⁴⁶

The effect of various parameters (solvent and additives,³⁸ metal/initiator/monomer stoichiometry, temperature,⁴⁷ and initiation method^{26, 28}) has been studied in detail for the best-performing [Cp₂Ti^{III}Cl] system. Initiation by aldehyde reduction, yielding Cp₂Ti^{IV}-OCHR*, is more efficient than the RRO method (lower proportion of side reactions). Peroxides may function either by the classical thermal decomposition or by a redox process and the resulting ether chain-end groups are less easily post-modified. The alkyl halide initiation method is the most sensitive and difficult one to optimize.²⁸ A summary of the most significant result is provided in Table 1. Low-dispersity (1.10 - 1.18) polystyrenes were obtained with each initiation modes, the optimum temperature being 70-90°C for the [Cp₂Ti^{IV}Cl₂]/Zn system.^{26-28, 48} For polyisoprene, a lower but still satisfactory level of control (*Đ* of 1.2–1.3) and optimum initiator efficiency were achieved for [DBPX]/[Cp₂TiCl₂]/[Zn] = 1/6/20 at 70°C.³⁵ *Random* and *block* styrene-isoprene copolymers with *Đ* of 1.39–1.50 were also obtained using [Cp₂TiCl₂] at 110°C.⁴⁹ Polybutadiene, on the other hand, could only be obtained with *Đ* ≥ 1.5.³²

Table 1. Best results for the OMRP of styrene, isoprene and butadiene with the [Cp₂Ti^{IV}Cl₂]/Zn initiating-controlling system.

Initiating method	Compound (I) ^a	[M]/[I]/[Ti]/[Zn]	<i>Đ</i> at 50% conv.	T/°C	Ref.
Styrene					
Aldehyde	BA	100/1/4/8	1.11	90	26, 28, 39, 48
	TCA	100/1/4/8	1.10	90	48
RRO	BDGE	50/1/6/12	1.11	90	18, 26, 28, 47
	BEB	100/1/2/6	1.18	75	25, 28
	DCPX	?	1.10	90	27
Halide	DBPX	?	1.14	90	27
	DIPX	?	1.12	90	27
	DBD	100/1/2/4	1.38	90	29
	MBSC	100/1/1/1	1.20	60	24
Peroxide	BPO	100/1/3/6	1.13	90	21, 22, 26, 28, 40
Butadiene					
Aldehyde	BBA	200/1/3/3	1.8	130	30
RRO	MPEG	100/1/2.5/2	1.5	130	32
Halide	DBPX	200/1/6/20	1.6	130	31
Isoprene					
Aldehyde	BA	200/1/3/10	1.37	100	35
RRO	MPEG	200/1/4/12	1.40	110	35
Halide	DBPX	100/1/6/20	1.25	70	35

^a BA = benzaldehyde; TCA = thiophen-2-carboxaldehyde; BDGE = 1,4-butanediol diglycidyl ether; BEB = (1-bromoethyl)benzene; DCPX = α, α' -dichloro-p-xylene; DBPX = α, α' -dibromo-p-xylene; DIPX = α, α' -diiodo-p-xylene; MBSC = 4-Methoxybenzenesulfonyl Chloride; DBD = 1,10-dibromodecane; BPO = Benzoyl peroxide; BBA = benzyloxybenzaldehyde; MPEG = glycidyl 4- methoxyphenyl ether.

2. Vanadium

Shaver *et al.* reported that bis(iminopyridine)vanadium(III) complexes **2.1**, also active coordination/insertion polymerization catalysts for olefins and dienes,⁵⁰⁻⁵³ are able to control the radical VAc polymerization (\bar{D} ca. 1.3) at 120°C using AIBN as thermal initiator (*Figure II-8*). Control, however, was satisfactory only for relatively small monomer conversions (ca. 30%) because of slow moderating complex decomposition, possibly by irreversible radical additions to the non-innocent diiminopyridine ligand.^{54, 55}

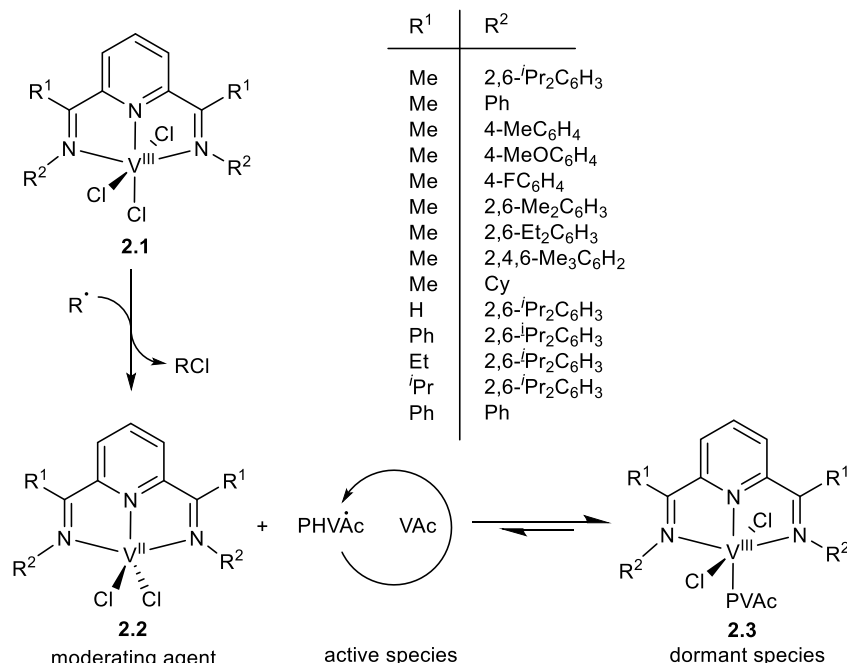


Figure II-8: Bis(iminopyridine) vanadium complexes used in OMRP and their mechanism of action.

The main point of interest is the controlling mechanism, because the presence of Cl ligands raises the question of a possible reverse ATRP *via* the reversibility of the reduction step to **2.2**. Additionally, OMRP may be promoted by either a V^{III}/V^{IV}-R pair (**2.1** with a putative V^{IV} radical trapping product) or by the V^{II}/V^{III} **2.2/2.3** pair generated after *in situ* Cl atom transfer. The presence of metallic chain-ends was indicated by the isolated polymer color, ¹H NMR and derivatization studies. A distinction between V^{III} and V^{IV} at the chain end was possible from the polymer molecular weights, because direct trapping by V^{III} would produce one chain per initiating radical, whereas reduction to V^{II} consumes two radicals per chain – one to initiate the propagation and one for metal reduction – hence double average molar masses. Further characterization by EPR and XPS of the recovered polymer, the identification of Me₂C(CN)Cl in solution and validation by DFT calculations confirmed the mechanism shown in *Figure II-8*.^{54, 55}

Extension of this system to other vinyl esters (propionate, pivalate) gave equally good control, whereas vinyl benzoate and styrene are less well-controlled ($\bar{D} > 1.5$)^{54, 55} and other more activated monomers (methyl methacrylate, acrylonitrile) showed no control.⁵⁵

Therefore, the V^{III} -C BDE for this system is only suitable for more reactive radicals. Reducing the aryl 2,6 substituents steric bulk or removing them altogether (*i.e.* $R^2 = C_6H_3-2,6-Et_2$, $C_6H_3-2,6-Me_2$, Ph) led to poorer control, whereas electronic variations at the *para* position are relatively unimportant.⁵⁶ Steric bulk was proposed to offer protection against the unwanted ligand attack by the radical, while not negatively affecting the productive reversible addition to the metal center. Use of a bulky aliphatic R^2 group (Cy) also led to poor control, with fast uncontrolled polymerization suggesting a weakening of the V^{III} -C bond. Variations of the R^1 substituents while keeping the same R^2 ($C_6H_3-2,6-^iPr_2$) confirm the steric protection hypothesis: for H, rapid complex degradation only led to short oligomers, but good control was maintained for $R^1 = Et$ and iPr .

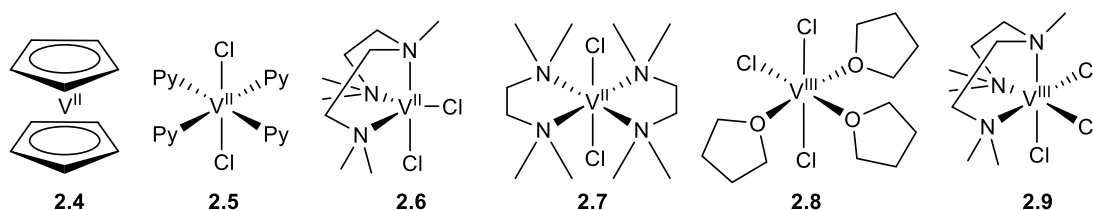


Figure II-9: Other vanadium complexes tested in OMRP.

Other vanadium complexes (Figure II-9) are less efficient.⁵⁵ Polystyrene radical chains are apparently incapable of reducing V^{III} -Cl to V^{II} and/or the used (or *in situ* produced) V^{II} complex does not efficiently trap the chains. The more strongly binding PVAc $^{\bullet}$ chains, on the other hand, produce polymers with a certain degree of control, especially when used in combination with the V^{III} precursors (2.8 and 2.9), but lower than with the above-described bis(imino)pyridine systems 2.1.

3. Chromium

Starting in 1978, Minoura *et al.* described the polymerization of various vinyl monomers by redox initiation with the combination of chromous acetate and a peroxide and pointed out their “living” character.⁵⁷⁻⁶⁰ Controlled polymerizations were also obtained when using an “aged” system, namely by introducing the monomer after all Cr^{2+} was converted to Cr^{3+} , although longer ageing gave lower initiation efficiencies. The polymerizations were kinetically well-defined, with slower monomer consumption than in the free radical process and a linear molar mass increase with monomer conversion. They were controlled, however, only at low temperatures (< 30°C). Although the formation of a direct metal-carbon bond was not invoked by the authors, an interaction between the growing radical chain and the metal ion was explicitly suggested. These are therefore the first reports, for any metal, of what we now know as dissociative OMRP.

The moderating effect of various vinylarene tricarbonylchromium(0) complexes 3.1 (Figure II-10) was highlighted for the AIBN-initiated polymerization of acrylic monomers.⁶¹⁻⁶⁴ The MMA polymerization, for instance, was moderately controlled in the 50-70°C range ($\mathcal{D} = 1.5-$

1.8), whereas broader molar mass distributions were obtained at higher temperatures. The proposed mechanism involves radical addition to the vinyl function to produce a benzylic radical **3.2** with spin delocalization on the metal center, which would then be capable of reversibly trapping the growing radical chain. This trapping may involve the formation of weak Cr^{II}-C bonds in a putative (cyclohexadienyl)alkyl tricarbonylchromium(II) dormant species, though this was not explicitly suggested by the authors.

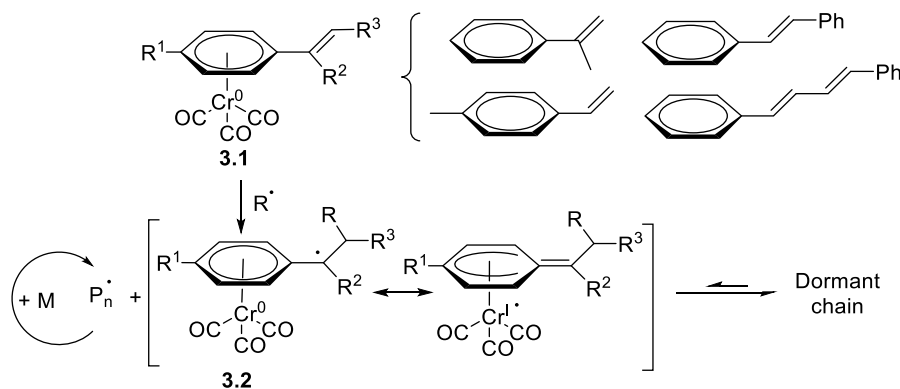


Figure II-10: Vinylarenes used in (arene)tricarbonylchromium(0)-mediated polymerization and proposed mechanism of action.⁶¹⁻⁶⁴

A controlled VAc polymerization takes place when V-70-initiated and moderated by half-sandwich β -diketiminato systems, Figure II-11, presumably yielding Cp(nacnac^{Ar,Ar'})Cr^{III}-PVAc dormant species.⁶⁵⁻⁶⁷ The polymerization rates were highly dependent on the aryl group steric encumbrance, being faster for complexes with bulkier ligands (e.g. **3.3a**), though the dispersities were relatively broad. All other systems (**3.3b-h**) gave low conversions. No control, on the other hand, was observed for polystyrene in the presence of **3.3a**, suggesting trapping inefficiency.

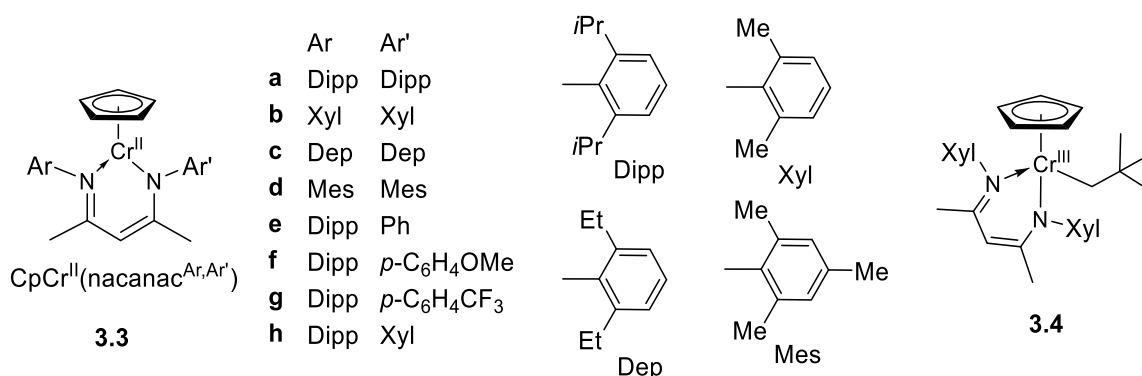


Figure II-11: Structures of half-sandwich Cr complexes used in the OMRP of vinyl acetate.

A model compound, CpCr^{III}(nacnac^{Xyl,Xyl})(Np) (**3.4**; Np = neopentyl), was structurally characterized and shown to be a suitable thermal initiator, yielding better results in terms of targeted molar masses and dispersity ($\mathcal{D} < 1.5$), upon working at room temperature.⁶⁶ However, the polymerization was very slow and progressively became even slower as a result

of inverted monomer additions. Thermolysis of **3.4** in vinyl acetate (50°C) induced a color change and conversion to the inactive acetate complex $[\text{CpCr}^{\text{III}}(\text{nacnac}^{\text{Xyl,Xyl}})(\text{OAc})]$, **3.5** (Figure II-12). The proposed deactivation mechanism involves β -acetate abstraction from the minor tail radical by the oxophilic chromium. These results suggest that controlled polymerizations can only occur at low temperatures for homolytically labile complexes, whereas thermally more robust bonds give rise to either very slow polymerizations at low temperature or to deactivation upon warming.

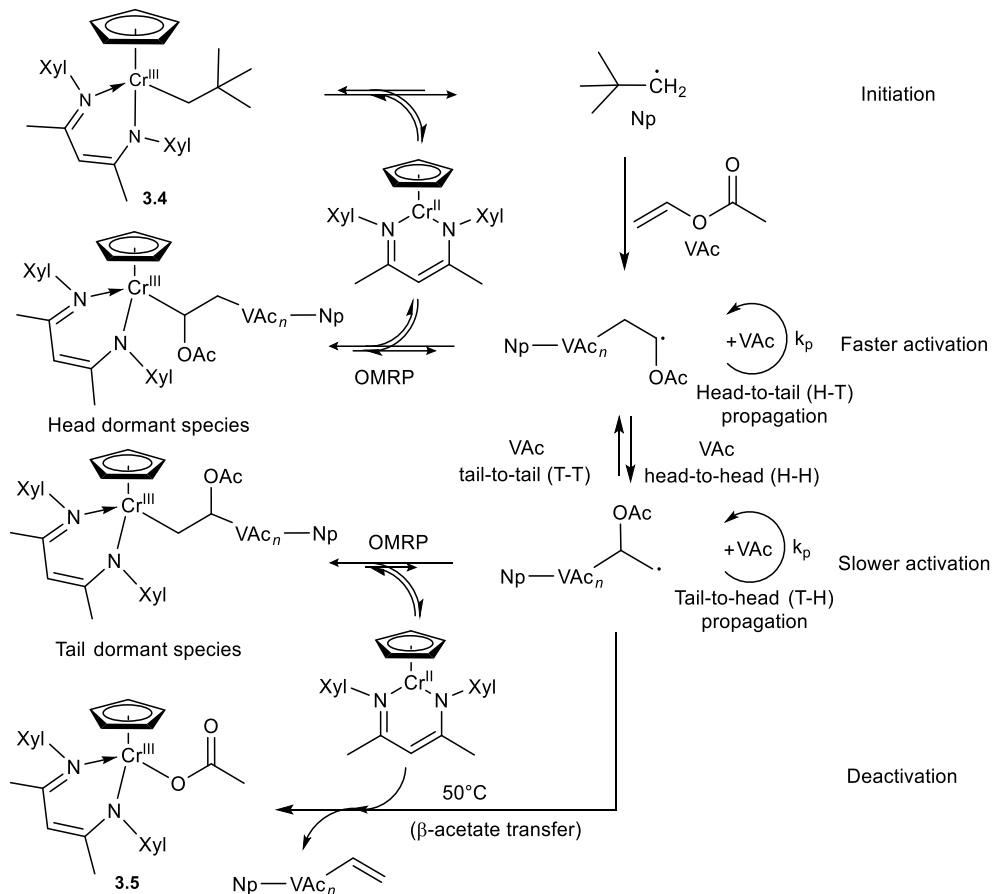


Figure II-12: Mechanism, slowdown and moderator deactivation for the VAc polymerization initiated by $[\text{CpCr}^{\text{III}}(\text{nacnac}^{\text{Xyl,Xyl}})\text{Np}]$ (**3.4**).

All these results were rationalized by DFT calculations of the $\text{Cr}^{\text{III}}\text{-C}$ bond strength as a function of radical nature and ligand steric bulk, Table 2.^{65, 66} The BDE value decreases, and the $\text{Cr}^{\text{III}}\text{-C}$ distance correspondingly increases, going from the stronger vinyl acetate model radical, $\cdot\text{CH}(\text{CH}_3)\text{OOCCH}_3$, to the weaker styrene model radical, $\cdot\text{CH}(\text{CH}_3)\text{Ph}$ (method A), from the primary $\cdot\text{CH}_2\text{Ph}$ to the secondary $\cdot\text{CH}(\text{CH}_3)\text{Ph}$ (method A), and from smaller to larger aryl groups ($\text{Ph} > \text{Xyl} > \text{Dipp}$; methods A and B).

Table 2: BDEs and bond lengths in $[Cp(nacnac^{Ar,Ar})Cr^{III}-R]$ complexes from DFT calculations.

Ar	R	Method ^a	BDE/kcal mol ⁻¹	Distance/Å	Ref.
Ph	CH(CH ₃)Ph	A	11.8	2.173	65
Ph	CH ₂ Ph	A	20.8	2.136	65
Ph	CH(CH ₃)OOCCH ₃	A	28.4	2.109	65
Ph	CH(CH ₃)OOCCH ₃	B	25.9	2.091	66
Xyl	CH(CH ₃)Ph	A	2.0	2.197	65
Xyl	CH ₂ Ph	A	13.3	2.146	65
Xyl	CH(CH ₃)OOCCH ₃	A	19.7	2.214	65
Xyl	CH(CH ₃)OOCCH ₃	B	20.6	2.115	66
Dipp	CH(CH ₃)OOCCH ₃	B	18.6	2.139	66

^a Full QM calculations with the B3LYP functional and the 6-31G** basis set. ^bQM/MM calculations with B3LYP/UFF (cutoff at the N-Ar bonds) with SDD (Cr), 6-31G* (O,N,C) and 6-31G** (H) basis sets.

4. Molybdenum

The 17-electron Mo^{III} complexes **4.1-4.3** control the AIBN-initiated styrene polymerization and are ineffective for the MMA polymerization (Figure II-13).⁶⁸ The absence of halogenated chain ends excludes an ATRP mechanism and suggests the formation of organomolybdenum(IV) dormant species. The same complexes, however, are also ATRP catalysts with bromoalkane initiators through reversible Br-atom transfer with production of a L/Mo^{IV}-Br moderator.

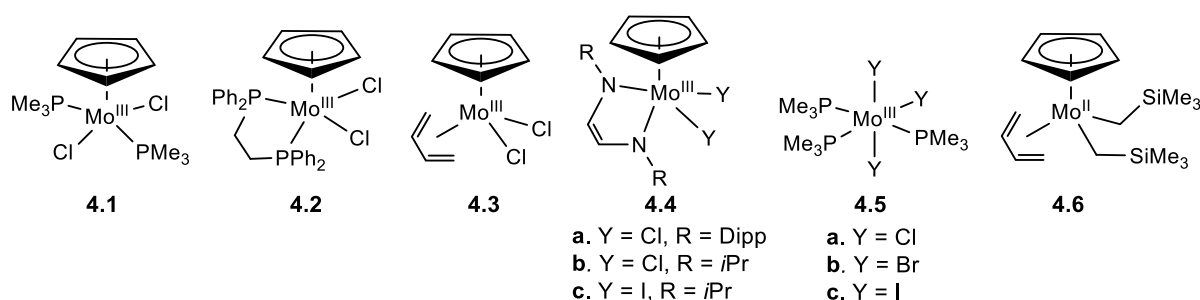


Figure II-13: Molybdenum-based complexes used in ATRP/OMRP.

The RN=CH-CH=NR (R₂-dad) ligands gave access to steric modulation for complexes **4.4**, the structure of which suggests a Mo^V ene-diamido rather than a Mo^{III}(diazadiene) formulation. The sterically more encumbered **4.4a** led to reversible dissociative activation of polystyrene chains,⁶⁹ whereas the less congested **4.4b** gave irreversible trapping of both polystyrene and poly(methyl acrylate) chains. Moving from to the diiodo complex **4.4c**, however, restored reversible homolysis.⁷⁰ Octahedral [Mo^{III}Y₃(PMe₃)₃] complexes (**4.5**) efficiently control styrene polymerization by ATRP,^{71, 72} but poorly perform by OMRP. With **4.5a**, slower polymerization than without metal complex and a polymer molar mass increase with conversion suggest the presence of a moderating equilibrium, though insufficient for good control. Conversely, identical results as in free radical polymerization were obtained with **4.5c**.⁷² Complex **4.6** was also tested as a unimolecular initiator, probing a possible Mo^{III}-CH₂SiMe₃ bond homolysis, but no polymerization occurred at 80°C. Polystyrene did form at 110°C, but at similar rate and with

the same characteristics as for the self-initiated metal-free process. This suggests a significant Mo-C BDE decrease upon increasing the metal oxidation state from III to IV, as also indicated by DFT calculations. It also suggests that the self-initiated polystyrene radical chains are not efficiently trapped to yield a putative $\text{CpMo}^{\text{IV}}(\text{P}_n)(\text{CH}_2\text{SiMe}_3)_2$, underlining the importance of the one-electron ligand (Cl in **4.3** vs. CH_2SiMe_3 in **4.6**).⁶⁸

5. Manganese and Rhenium

The $[\text{Mt}^{\text{I}}(\text{CO})_5^{\bullet}]$ radicals (Mt = Mn, Re), generated from the photolytic splitting of their dimers, are able to initiate the polymerization of a few monomers. The resulting polymers feature $[(\text{CO})_5\text{Mt-P}_n]$ chain ends, indicating the initiation ability of the metalloradicals, but no moderating action was demonstrated for these polymerizations.⁷³ The same radicals were subsequently used in the CRP of VDF by the iodine transfer (ITP) controlling method (*Figure II-14*).^{74, 75} However, the role of these radicals appeared limited to the reactivation by iodine atom abstraction of the less reactive iodine-capped dormant species, which forms by non-degenerative transfer after an inverted (head-to-head) monomer addition. The formation and possible reactivation of the organometallic dormant species, $[(\text{CO})_5\text{Mt-PVDF}_{\text{H/T}}]$, which may also be produced by the direct trapping of the growing chain by the continuously generated $[\text{Mt}(\text{CO})_5^{\bullet}]$ radicals, was not considered.

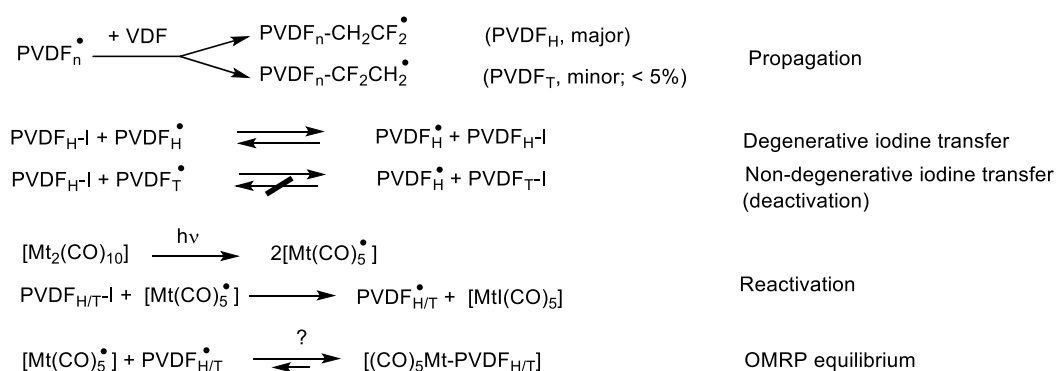


Figure II-14: Scheme 41. Action of the $[\text{Mt}(\text{CO})_5^{\bullet}]$ (Mt = Mn, Re) radicals in the reactivation of PVDF-T-I dormant species in the ITP of VDF and possible role of metal-carbon bond homolysis.

For this reason, subsequent work has analyzed the homolysis of model complexes of these putative dormant species for manganese, namely $[(\text{CO})_5\text{Mn-R}_F]$ ($\text{R}_F = \text{CF}_3, \text{CHF}_2, \text{CH}_2\text{CF}_3$, **5.1** in *Figure II-15*), as well as $[(\text{CO})_5\text{Mn-COCF}_2\text{CH}_3]$ (**5.2**),⁷⁶ finding that these bonds are too strong (46-54 kcal mol⁻¹) for significant generation of R_F under the VDF ITP conditions. However, they photoinitiate the VDF polymerization under both visible and UV light irradiation, though without ensuring controlled growth.⁷⁷ Therefore, if any such $[(\text{CO})_5\text{Mt-PVDF}_{\text{H/T}}]$ dormant species form during the ITP process, they can be reactivated under irradiation but the controlled polymer growth is entirely ensured by ITP. The significantly weaker Mn^I-C bond (35.3±2.8 kcal mol⁻¹) in $[(\text{CO})_5\text{Mn-CH}(\text{Me})\text{COOMe}]$ (**5.3**) allows thermal initiation of methyl

acrylate polymerization at relatively low temperatures, but the polymerization was uncontrolled, as expected from the rapid $[\text{Mn}(\text{CO})_5^*]$ radical disappearance by dimerization.⁷⁸

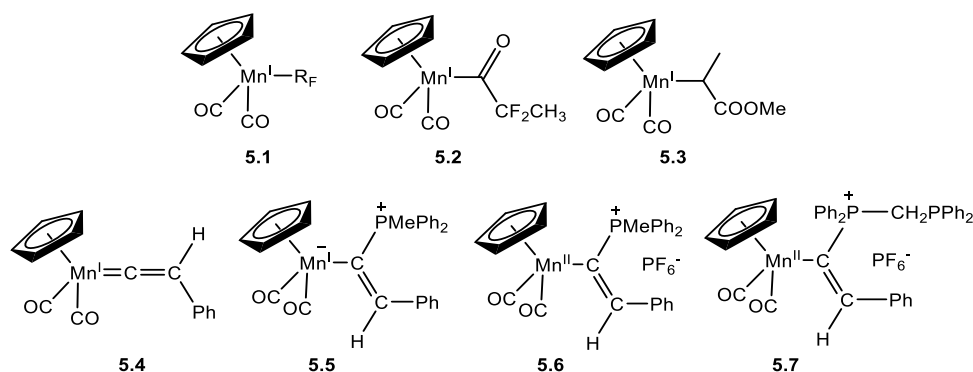


Figure II-15: Half-sandwich manganese complexes used in radical polymerization.

A few additional half-sandwich Mn^{I} (18-electron) and Mn^{II} (17-electron) complexes (compounds **5.4-5.7** in Figure II-15) were tested as moderating agents for the polymerization of MMA initiated by AIBN,⁷⁹ but polymerization rates and polymer properties similar to the metal-free control were observed in all cases, indicating no significant moderating effect. When heated in the presence of AIBN and in the absence of monomer, the 18-electron **5.4** and **5.5** decomposed, whereas **5.6** and **5.7** were stable. The latter could in principle bind an organic radical but the product would be an unlikely organomanganese(III) complex. Indeed, DFT calculations indicated that only of a weak van der Waals adduct is formed between the model PhCH^*Me radical and **5.6**, with an insignificant stabilization energy of -1.4 kJ mol^{-1} (ca. $-0.3 \text{ kcal mol}^{-1}$).

6. Iron, Ruthenium and Osmium

The area of iron-mediated CRP (both ATRP and OMRP) has been reviewed in 2014.⁸⁰ Although there is intensive activity on Fe-based ATRP catalysts, only few contributions address the reversible Fe-C bond homolysis. The main investigated systems are shown in Figure II-16. Under thermal AIBN initiation, the porphyrin (**6.1**), phthalocyanine (**6.2**) and Schiff base (**6.3**, **6.4**) systems control the styrene polymerization, although with higher than target molar masses and rather broad dispersities.⁸¹ While VAc polymerization was inhibited by **6.2**, controlled growth could be provided by complex **6.5**, demonstrating an Fe^{III} -C BDE tuning by the coordination environment (weaker for O_4 relative to O_2N_2 and N_4).⁸² For VAc, however, **6.5** performed more poorly than its cobalt analogue because of a lower trapping efficiency and the formation of $[\text{Fe}^{\text{II}}(\text{acac})_2]$ oligomers, reducing the moderator efficiency. Control improved when operating under more dilute conditions or in the presence of Lewis bases, especially PMe_2Ph . Complex **9.7** also controlled the VAc polymerization by degenerative transfer, indicating its ability to undergo associative radical exchange. The isolated $[\text{Fe}^{\text{III}}(\text{acac})_2\text{-PVAc}]$ was shown to function as a single-component macroinitiator for the OMRP of VAc. Similar results were also reported when using $[\text{Fe}^{\text{III}}(\text{acac})_3]$ in the presence of a reducing agent with the best results given by ascorbic acid.⁸³

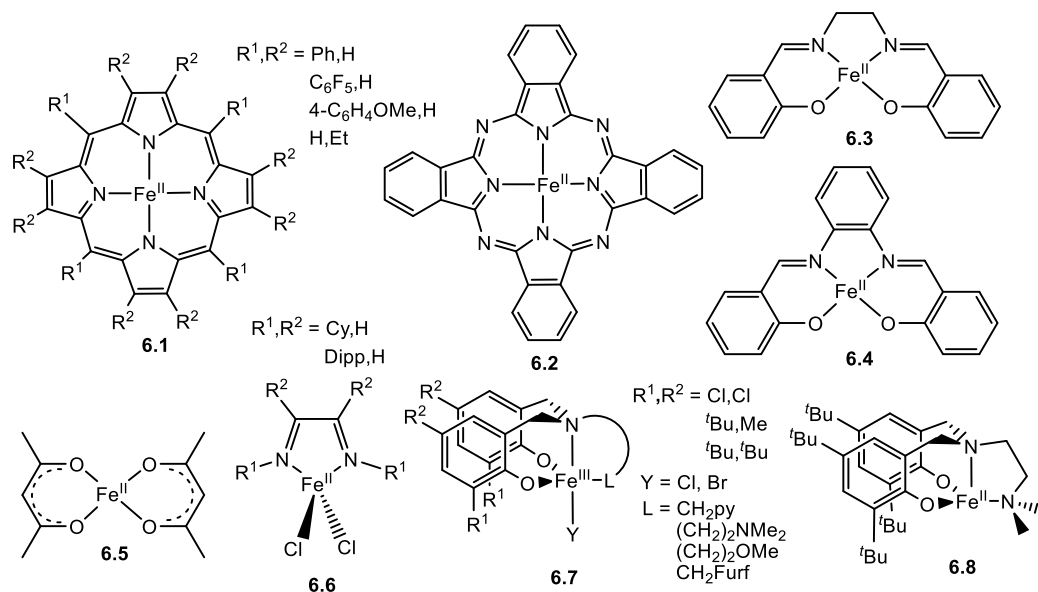


Figure II-16: Main iron complexes used in OMRP.

The α -diimine system **6.6** in combination with alkyl halide initiators controls styrene polymerization by ATRP. Although the involvement of direct radical trapping (OMRP/ATRP interplay) was invoked as a path leading to catalytic chain transfer via β -H elimination,⁸⁴ a later study suggested that this occurs by HAT instead, without $\text{Fe}^{\text{III}}\text{-C}$ bond formation.⁸⁵ The bis(phenolate) systems **6.7**, on the other hand, lead to ATRP/OMRP interplay for the polymerization of substituted styrenes and MMA after *in situ* reduction (reverse ATRP conditions).⁸⁶⁻⁸⁸ The reduced Fe^{II} complex **6.8** (presumably dimeric in the solid state) was isolated and independently shown to exert control in the V-70-initiated polymerization of styrene and MMA. For VAc, on the other hand, irreversible radical trapping occurs.⁸⁹ DFT calculations suggested that the diaminebis(phenolate) ligand geometry does not allow the Fe^{II} system to attain the preferred tetrahedral geometry whereas the trigonal bipyramidal dormant species is not strained, thus leading to a stronger $\text{Fe}^{\text{III}}\text{-C}$ bond relative to system **6.6**.⁹⁰

Ruthenium yields very successful ATRP catalysts of type $[\text{Ru}^{\text{II}}\text{Cl}_2\text{L}_3]$ ⁹¹ and $[\text{Cp}^*\text{Ru}^{\text{II}}\text{YL}_2]$,⁹² working through the $\text{Ru}^{\text{II}}/\text{Ru}^{\text{III}}\text{-Y}$ couple, but radical trapping to yield Ru^{III} -capped dormant chains has not been demonstrated. The osmium complex $[\text{Os}^{\text{II}}\text{Cl}_2(\text{PPh}_3)_3]$, on the other hand, contributes with reversible chain trapping to the alkyl halide-initiated ATRP of styrene and (meth)acrylates. This is shown by its independent ability to provide moderate control in the AIBN-initiated polymerization.⁹³ The vertical trend in Mt-R BDE ($\text{Ru} < \text{Os}$) is responsible for this phenomenon, as confirmed by DFT calculations.⁹⁴

7. Rhodium

Whereas the (octaethylporphyrinato)rhodium(II) dimer, $[(\text{OEP})\text{Rh}^{\text{II}}]_2$, adds irreversibly to both head and tail ends of acrylates to yield $[(\text{OEP})\text{Rh}^{\text{III}}-\text{CH}_2\text{CH}(\text{CO}_2\text{R})-\text{Rh}^{\text{III}}(\text{OEP})]$, the steric demand of $[(\text{TMP})\text{Rh}^{\text{II}}]$ precludes both its dimerization and strong binding to the acrylate head end, but allows tight binding to the tail end, yielding $[(\text{OEP})\text{Rh}^{\text{III}}-\text{CH}_2\text{CH}(\text{CO}_2\text{R})\text{CH}(\text{CO}_2\text{R})\text{CH}_2-\text{Rh}^{\text{III}}(\text{OEP})]$ after dimerization by head-head coupling. The $\text{Rh}^{\text{III}}-\text{CH}_2$ bond is too strong for reversible dissociation, but the photoinitiated MA polymerization is controlled, demonstrating moderation through reversible binding to the head end.⁹⁵ The high cost of rhodium certainly discourages further development of OMRP applications.

8. Copper

Copper is undoubtedly the most successful metal for ATRP through $[\text{L}/\text{Cu}^{\text{I}}]$ and $[\text{L}/\text{Cu}^{\text{II}}-\text{Y}]$ complexes as catalyst and moderator, respectively, but there are no reports of successful $[\text{L}/\text{Cu}^{\text{I}}]$ -based OMRP. The ATRP activity is very ligand dependent, spanning several orders or magnitude.^{96, 97} Interplay with OMRP for these systems would lead to $[\text{L}/\text{Cu}^{\text{II}}-\text{P}_n]$ dormant chains.

Organocopper(II) compounds are rare and characterized by low BDEs,⁹⁸ hence suggesting that $[\text{L}/\text{Cu}^{\text{I}}]$ complexes might be suitable as OMRP moderators for LAMs. Indeed, reversible radical trapping by $[\text{L}/\text{Cu}^{\text{I}}]$ has been evidenced by a slowdown of the polymerization rates.⁹⁹⁻¹⁰¹ However, the resulting $[\text{L}/\text{Cu}^{\text{II}}-\text{P}_n]$ bond is apparently too weak (too high dissociation constant) to yield controlled chain growth. Another problem negatively affecting OMRP with $[\text{L}/\text{Cu}^{\text{I}}]$ complexes is catalysed radical termination (CRT), which has been highlighted for acrylate polymerizations.¹⁰⁰⁻¹⁰⁶ This occurs via a $[\text{L}/\text{Cu}^{\text{II}}-\text{P}_n]$ intermediate, which then reacts with a second radical to yield terminated chains and regenerate $[\text{L}/\text{Cu}^{\text{I}}]$. The most active ATRP catalysts, which also lead to the strongest $[\text{L}/\text{Cu}^{\text{II}}-\text{P}_n]$ bonds,^{101, 107} are also the most efficient radical termination catalysts. The negative impact of CRT in an ATRP process can be minimized by working at very low catalyst concentrations, because CRT depends on $[\text{L}/\text{Cu}^{\text{I}}]$, whereas the ATRP activity depends only on the $[\text{L}/\text{Cu}^{\text{I}}]/[\text{L}/\text{Cu}^{\text{II}}-\text{Y}]$ ratio.^{108, 109}

9. Cobalt

Cobalt is undoubtedly the most investigated and successful transition metal for OMRP and is the metal on which this thesis work is focused.^{110, 111} It always operates via a diamagnetic 5- or 6-coordinate $[\text{L}/\text{Co}^{\text{III}}-\text{P}_n]$ dormant species and the $[\text{L}/\text{Co}^{\text{II}}]$ moderator may be a 4- (square planar or tetrahedral) or 5-coordinate complex, either spin doublet or quartet. In the presence of donor solvents or additives (D), 6-coordinate (18-electron) $[\text{L}(\text{D})/\text{Co}^{\text{III}}-\text{P}_n]$ dormant species and 5- or 6-coordinate $[\text{L}(\text{D})/\text{Co}^{\text{II}}]$ and $[\text{L}(\text{D})_2/\text{Co}^{\text{II}}]$ moderating complexes may also be involved. The alkylcobalt(III) compounds **9.1** ($\text{R} = \text{CH}_2\text{tBu}$)¹¹² and **9.2**^{113, 114} (Figure II-17) were first used

as initiators in a dissociative activation mode, yielding controlled polymerizations of acrylates under thermal or photochemical activation, respectively. The polymerizations can also be initiated by a classical radical source with a cobalt(II) complex. In this case, injection of a substoichiometric amount of primary radicals (R_0^\bullet) can only sustain the dissociative activation mode, whereas an excess ($R_0^\bullet/Co^{II} > 1$) may ensure control by DT provided a vacant site is available in $[L/Co^{III}-R]$ for an associative exchange.

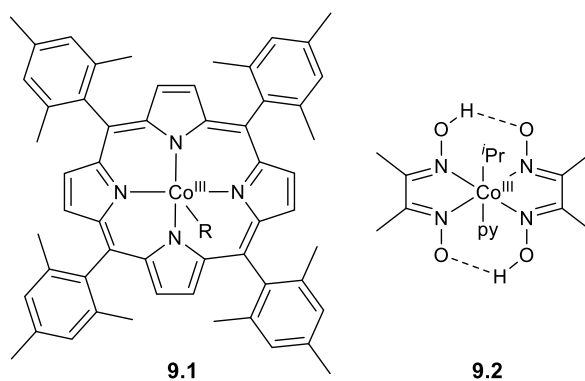


Figure II-17: First cobalt complexes used in OMRP.

a. Porphyrin system

After the seminal report of OMRP with **9.1**, further studies have focused on more readily accessible Co^{II} species (Figure II-17) and a classical radical source. The lipophilic **9.3a-c** control the polymerization of acrylates esters,¹¹⁵⁻¹¹⁹ while water-soluble **9.3d,e** control the polymerization of acrylic acid in water.¹²⁰ The intermediate polarity of **9.4** is compatible with a wider array of lipo/hydrophilic acrylates and acrylamides in both polar and non-polar media and also allows to control *t*BA, whereas **9.3a** is inefficient.¹²¹ This results from the Co^{III} -*t*BA bond strengthening by the release of steric strain linked to the removal of two *o,o'*-Me groups from one aryl substituent, as confirmed by DFT calculations.¹²² The dissociative OMRP of VAc with **9.3a** is completely inhibited, but becomes possible by DT, though control is good only up to moderate conversion.¹²³⁻¹²⁵ Dissociative activation of $[(TMP)Co^{III}-PVAc]$ becomes possible by addition of excess pyridine,¹²⁵ by the same principle that was elucidated first for $[Co^{II}(acac)_2]$ (see next section).¹²⁶

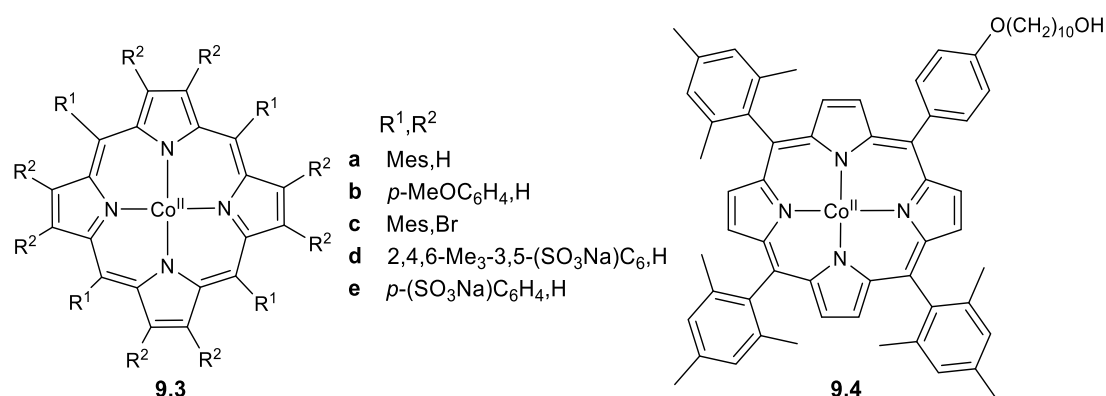
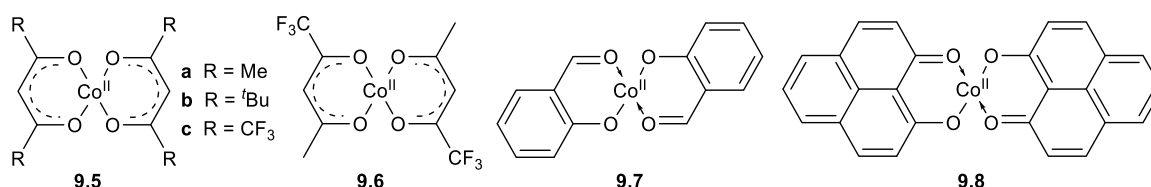


Figure II-18: Cobalt porphyrin complexes used in OMRP.

After thermal AIBN-initiated MA or DMA polymerization with **9.3a** and **9.4**, the resulting [L/Co^{III}-PMA] and [L/Co^{III}-PDMA] ($M_n = 1-1.8 \cdot 10^4 \text{ g mol}^{-1}$) were used as macroinitiators for the room temperature OMRP of acrylamides under visible-light irradiation, demonstrating a positive effect of photocleavage in dissociative OMRP. Well-controlled diblock copolymers were obtained only with moderate light intensity.^{127, 128} Complex [(TMP)Co^{III}-CO₂Me] also photoinitiated the OMRP of acrylates and acrylamides at room temperature, with good control even for tBA.¹²⁸

b. β -Diketonate system

The application of β -diketonate and related systems (Figure II-19) has marked a turning point in OMRP with cobalt. The O₄ donor set weakens the Co^{III}-C bond with respect to the N₄ donor set of porphyrins, making these systems better suited for the OMRP of LAMs. The simplest and commercially available **9.5a** affords excellent control for VAc in bulk and aqueous suspension, with either thermal (V-70 at 30-40°C)^{129, 130} or redox (benzoyl or lauroyl peroxide)¹³¹ initiation. **9.5b**¹³² and **9.6**¹³³ yield similar results, whereas **9.5c** is inefficient. Benzene ring fusion in the salicylate (**9.7**)¹³⁴ and 9-oxyphenalenone (**9.8**)¹³⁵ systems results in poorer control, while **9.8** also leads to CCT, which is rarely observed for LAMs. **9.5a** controls well also other LAMs such as other vinyl esters,¹³⁶ vinyl amides,¹³⁶⁻¹⁴⁰ vinyl chloride,¹⁴¹ VDF,^{142, 143} and the copolymerizations of VAc with ethylene,¹⁴⁴ 1-octene^{145, 146} and perfluorohexyl ethylene.¹⁴⁷ More reactive monomers are not well controlled by **9.5a**, but acceptable results were obtained for acrylonitrile^{148, 149} and nBA¹⁵⁰ under optimized conditions. Allyl radicals, being quite stabilized, cannot be efficiently trapped by **9.5a**. Thus, addition of dienes to dormant [L/Co^{III}-P_n] chains results in the formation of P_n-diene• which, because of the slow diene radical homopropagation and termination by coupling, selectively generates mid-chain-functionalized P_n-diene-diene-P_n products, including symmetric A_nB_{2m}A_n triblock copolymers from [(acac)₂Co^{III}-B_mA_n] diblock dormant chains.¹⁵¹⁻¹⁵³ Use of the unimolecular [(acac)₂Co^{III}-(VAc)_nR₀] initiator ($n \sim 4$, R₀ = Me₂C(OMe)CH₂CMeCN) in the dissociative mode generally leads to better control. This compound is prepared by V-70/**9.5a**-initiated VAc polymerization at small VAc/**9.5a** ratio and is sufficiently stable to be purified by chromatography.¹⁵⁴

Figure II-19: β -Diketonate and cobalt complexes used in OMRP.

Donor solvents or additives (D) strongly affect the polymerization rate and control mode with **9.5a**.¹²⁶ In their absence, the 5-coordinate dormant species can be stabilized by carbonyl

group chelation from the chain ultimate monomer,¹⁵⁴ if this is a vinyl ester or amide (*Figure II-20*). The chelation equilibrium still allows access to the vacant site for a DT polymerization. Coordination of D, on the other hand, negates a DT polymerization and stabilizes the moderating species, increasing the propensity to dissociative activation. The latter effect is modulated by the D concentration and binding constant, water being a particularly efficient donor.¹⁵⁵ Since water is a common contaminant of commercial **9.5a** and solvents, it is possible to witness dissociative activation or shorter than expected induction times for OMRP-DT under supposedly “anhydrous” conditions.¹⁵⁶

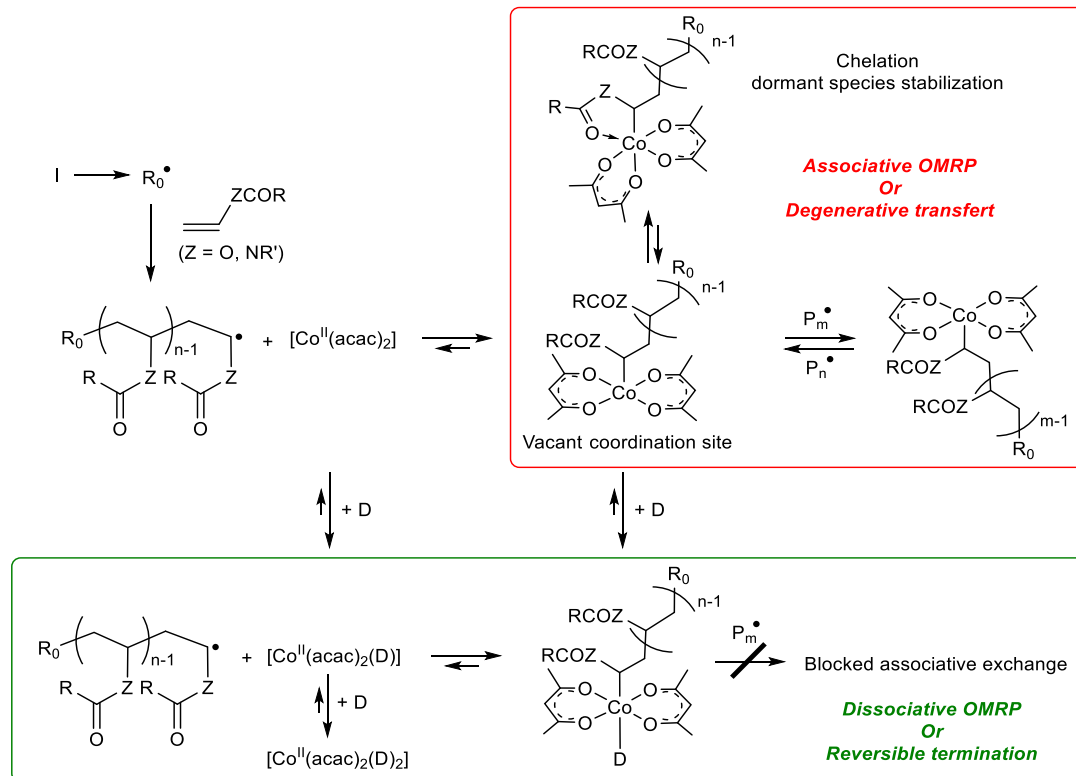


Figure II-20: Effect of donor additives in the [Co(acac)₂]-mediated polymerization of vinyl esters and amides.

Chelation by the ultimate monomer rationalizes a few observations such as the reactivity trend for different ring size N-vinyl lactams,¹³⁹ the lack of control for γ -methylene- γ -butyrolactone (though its copolymerization with VAc is controlled)¹⁵⁷ and the absence of slowdown or of a worsening of control at high conversions for the VAc polymerization, contrary to other $[L/Mt^{x+1}-PVAc]$ species where this chelation is impossible.¹⁵⁸ The latter phenomenon results from compensation of the stronger $Co^{III}-CH_2CH(OAc)$ bond by a weaker 6-membered chelate in the tail dormant species formed after an inverted monomer addition, relative to the weaker $Co^{III}-CH(OAc)CH_2$ bond and stronger 5-member chelate in the head dormant species. VDF, like VAc, is better controlled by OMRP with **9.5a** than by other techniques. This is not due to a chelation phenomenon but rather to the polar effect of the α - and β -F substituents on the BDE, as shown by DFT calculations. Thus, the $[(acac)_2Co^{III}-CF_2CH_2-PVDF]$ (head) and $[(acac)_2Co^{III}-CH_2CF_2-PVDF]$ (tail) dormant species have bonds of equal

strengths, whereas the other techniques, after an inverted monomer addition, yield less labile tail dormant species.¹⁵⁹ Steric effects also modulate the $[L/Co^{III}-P_n]$ BDE: the VAc OMRP-DT is equally fast with **9.5a** and **9.5b**, but much slower with the former in the dissociative mode without D. Conversely and for the same steric reason, the D effect is stronger for **9.5a**.¹³²

c. Other planar macrocyclic systems

The success of cobalt porphyrins has naturally led to interest in other related systems with well-developed $[L/Co^{III}-R]$ chemistry. After the seminal report of the acrylate polymerization with **9.2**,^{113, 114} the water-soluble cobaloxime has not led to other OMRP applications, whereas it has extensively been investigated as a CCT catalyst, mostly for methacrylates and styrenics.¹⁶⁰⁻¹⁶³ The equally water-soluble cobalamin has yielded the controlled polymerization of 2-hydroxyethyl acrylate at pH 7, whereas polyethylene glycol methacrylate gave catalytic chain transfer oligomerization.¹⁶⁴

Greater attention has been devoted to salicylidene diamine (Salen-type) systems (*Figure II-21*). A moderately controlled MA polymerization occurs when initiated by V-70/**9.9** at 50°C,¹⁶⁵ slowly for $R_0^*/Co^{II} < 1$ by dissociative activation and rapidly by OMRP-DT with excess radicals. When using $[(Salen)Co^{III}-Et]$ as initiator, the strong $Co^{III}-Et$ bond relative to $Co^{III}-PMA$ results in poor initiation efficiency. The substituted *trans*-cyclohexane-1,2-diyl-bridged (Salen*) system **9.10a** controls both MA and VAc with AIBN initiation at 60°C. While both dissociative and associative activation modes cooperate for MA, VAc polymerizes only by OMRP-DT. The dissociation equilibrium constants for $[(Salen^{tBu,tBu})Co^{III}-PMA]$ and $[(Salen^{tBu,tBu})Co^{III}-PVAc]$ were estimated as $\sim 4.2 \cdot 10^{-8}$ and $< 10^{-12}$, respectively.¹⁶⁶ A peculiar phenomenon for this $Co(Salen^*)$ -terminated PVAc is its selective conversion to $[(Salen^*)Co^{III}-OPVAc]$ (i.e. with insertion of only one O atom) upon treatment with O_2 (3 bar) at 60°C, allowing a switch from an OMRP to a coordination/insertion mechanism for a chain extension by CO_2 /epoxide copolymerization.¹⁶⁷ Interestingly, like with **9.5a** but unlike with **9.3a**, the VAc polymerization remains well-controlled at high conversions.

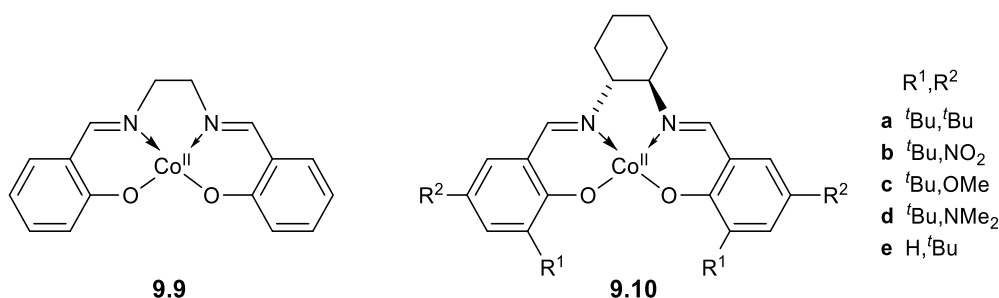


Figure II-21: Schiff-base cobalt complexes used in OMRP.

The **9.10a**-moderated dissociative OMRP of several monomers can also be operated at room temperature, though slowly and only for acrylates and acrylamides, when photoinitiated by $[(Salen^{tBu,tBu})Co^{III}-CO_2Me]$,¹⁶⁸ but becomes faster and can be extended to VAc when

transferred to the DT regime by addition of the ArCOP(O)Ph₂ photoinitiator (Ar = 2,4,6-C₆H₂Me₃), either to [(Salen^{tBu,tBu})Co^{III}-CO₂Me]¹⁶⁸ or to **9.10a**.¹⁶⁹ By this method, controlled random copolymers of acrylates or acrylamides and 1-octene, a less activated monomer, have also been obtained.¹⁷⁰ A [(Salen^{tBu,tBu})Co^{III}-CO₂PPE] (PPE = poly(propylene phthalate)) macroinitiator also photoinitiates the room temperature OMRP of MA, yielding uniform PPE-*b*-PMA macromolecules. This macroinitiator was made from [(Salen^{tBu,tBu})Co^{III}-OPPE], obtained by living coordination/insertion copolymerization of propylene oxide and phthalic anhydride, by CO insertion. Hence, this procedure allows a switch from a coordination/insertion to an OMRP mechanism.¹⁷¹

The substituents effect in the **9.10a-e** series was assessed for the polymerizations of VAc, styrene and MMA with AIBN initiation (AIBN/**9.10** = 0.6), aiming at dissociative activation conditions.¹⁷² DFT calculations on the [(Salen*)Co^{III}-CHMePh] models suggest that stronger donation from R² stabilizes preferentially the [L/Co^{II}] system, thereby weakening the Co^{III}-C bond: NO₂ (15.4) > *t*Bu (14.1) > OMe (13.7) > NMe₂ (13.3) (values are BDEs in kcal mol⁻¹). For VAc at 120°C, **9.10b** gave only low conversions without any control, while higher conversions and M_n close to target were given by the other systems. On the basis of the above-mentioned studies,^{166, 169} the intervention of OMRP-DT with excess radicals seems possible, at least for **9.10a**. However, the generation of a good quality PVAc when AIBN/**9.10** was lowered to 0.4 for **9.10c** suggests that genuine dissociative activation may also occur. The styrene polymerizations were only poorly controlled and those of MMA only gave CCT oligomers.¹⁷²

d. Other ligand systems

The additional coordination geometries shown in *Figure II-22* have also been considered as OMRP moderating agent. The 1,3-bis(2-pyridylimino)isoindolates (bpi) complexes **9.11** provide control for MA and *n*BA under thermal initiation (V-70/Co^{II} = 1:1) at 60°C. DFT calculations show a negligible effect of the bpi substituents on the [(bpi)(acac)Co^{III}-CH(CO₂Me)Et] BDE, in agreement with the polymerization results.¹⁷³ Systems **9.12** control styrene and MMA only rather poorly under ATRP conditions (ethyl-2-bromo-isobutyrate initiator). OMRP trapping may be involved in these polymerizations, but the polymer tacticity suggests that non-radical mechanisms may also contribute for **9.12a,b**.¹⁷⁴ The β-ketoiminates **9.13** are isolobal with the β-ketonates by substitution of one O atom with NR and thus may sterically tune the Co^{III}-P_n bond strength. Similarly to **9.5a**, these systems are able to promote the VAc dissociative and associative OMRP, but slower radical trapping (in the order **c** > **a** > **b**) leads to poorer control and D additives have little impact on the polymerization results.¹⁷⁵ The bis(phenoxy-imine) complexes **9.14** also show poor trapping ability in the thermally initiated VAc polymerization. In addition, **9.14b,d,e,f** revealed CCT activity. Excellent control could be achieved with **9.14a** when photoinitiated by ArCOP(O)Ph₂ (Ar = 2,4,6-C₆H₂Me₃) at 24°C, whereas MA polymerization could not be controlled under any conditions.¹⁷⁶

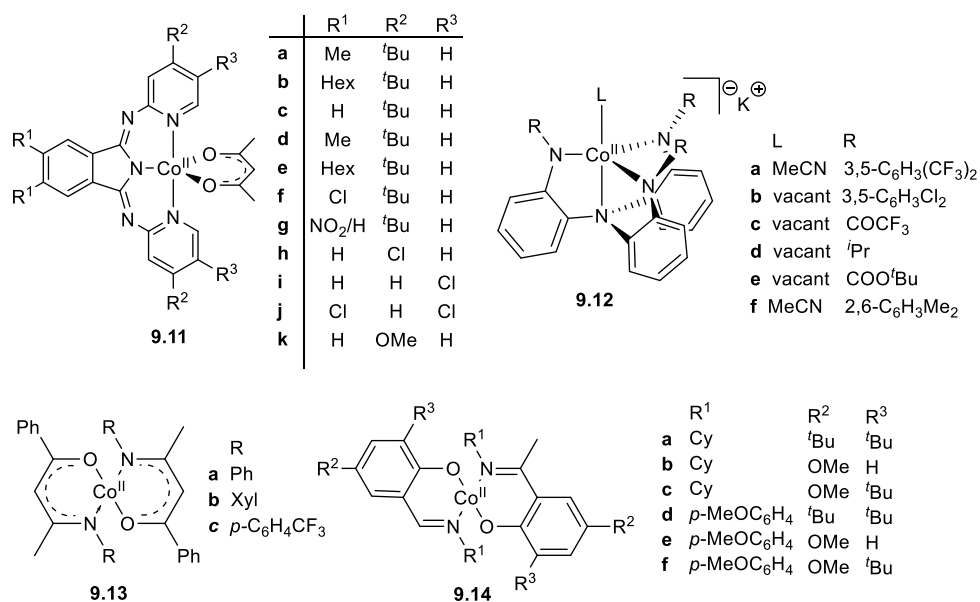


Figure II-22: Other coordination spheres for cobalt complexes used in OMRP.

10. Conclusion

As a conclusion, several systems, based on a large variety of transition metals, were developed and their success in OMRP is variable. Some studies clearly highlighted that small modifications on the ligand scaffold strongly affected the reactivity of the corresponding complexes in OMRP (see *e.g.* the CrCp(nacnac^{Ar,Ar'}) systems). This fact clearly illustrated that fine tuning of the Mt-P_n bond strength (BDE), *via* ligand/complex engineering, is the key for an efficient OMRP process and that it should be adaptable to a large variety of monomers.

In relation to the objectives of the present thesis work, which is the development of unimolecular systems of cobalt(III) that would allow OMRP direct initiation (green box in Figure II-23) and ROP initiation (red box in Figure II-23), the present section addressed the OMRP part and the following section will be dedicated to ROP.

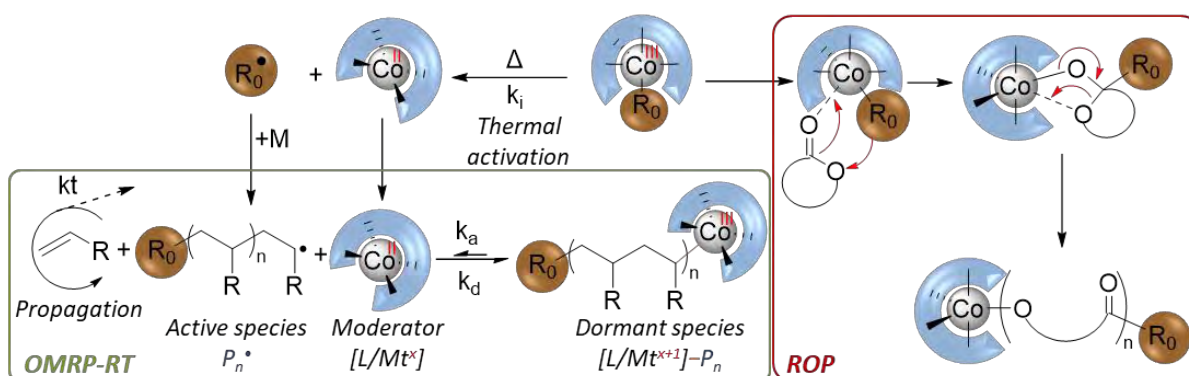


Figure II-23: Strategy for the application of the same Co^{III} initiator to two polymerization mechanisms (OMRP on the left, ROP on the right)

III. Ring Opening Polymerization of cyclic esters using d-block metal complexes

This section will discuss general aspects and mechanisms of Ring-Opening Polymerization (ROP) and provide an overview of the contribution of the different d-metals in this field, based on the experimental data highlighted in the annexes (Table S3). Certain monomers used in ROP are of great interest, because they are made from renewable resources (biobased), such as lactide, and their corresponding polymers are biodegradable.¹⁷⁷

1. General aspects of Ring Opening Polymerization (ROP)

Environmental and societal pressures led to increasing interests on the production of sustainable polymers. The research on renewable alternatives to fossil raw materials is largely investigated to reduce the environmental impact of human industries.¹⁷⁸ In 2014, among the 300 megatons of polymers produced globally, only 1.7 megatons were bioderived, and they concern three main products: polyethylene terephthalate (PET), polyethylene (PE) and polylactide (PLA).^{178, 179} In this context, polyesters made from biobased cyclic esters have been identified as materials of choice, because they are biodegradable and could be used in many areas, such as food packaging, pharmaceutical applications etc.^{177, 180, 181}

Therefore, Ring Opening Polymerization (ROP), the method of choice to access polyesters, has attracted much attention over the last two decades. The two mechanisms that a ROP can follow are depicted in *Figure III-1*. Both are based on the ester C=O bond polarization by the Lewis acidic metal centre, followed by nucleophilic attack that induces the ring opening. The “coordination/insertion” mechanism take place when the metal-coordinated monomer is attacked by the metal-bonded (via an Mt-O bond) macromolecular growing chain, while the “activated monomer mechanism” take place when the complex only acts as a Lewis acid and the monomer is attacked by the OH-terminated free macromolecule.

The first generation of complexes used for the ROP of lactide were simple homoleptic metal complexes, such as tin(II) bis(2-ethylhexanoate) [Sn(Oct)₂], zinc(II) lactate [Zn(Lact)₂] and aluminium(III) tris(isopropoxide) [Al(OⁱPr)₃] (*cf. Figure 2 - General Introduction*).¹⁸² However, these catalysts required high temperatures and therefore led to many side reactions, such as intra- or inter-chain transesterification or chain transfer. Several studies followed these initial findings with two main objectives: 1) improve the reaction conditions and the control of the polymerization, for which aluminum-based complexes proved quite successful,¹⁸³⁻¹⁸⁵ and 2) use non-toxic metal for biomedical applications.¹⁸⁶

The objective of the present thesis work, in terms of ROP, was to synthesize and use complexes based on cobalt, which is a non-toxic, inexpensive and abundant metal, as initiators, because it should provide stable and easy-to-handle complexes in the oxidation state +III. Moreover, (L)Co-R₀/P_n species should also be suitable for an OMRP initiation.

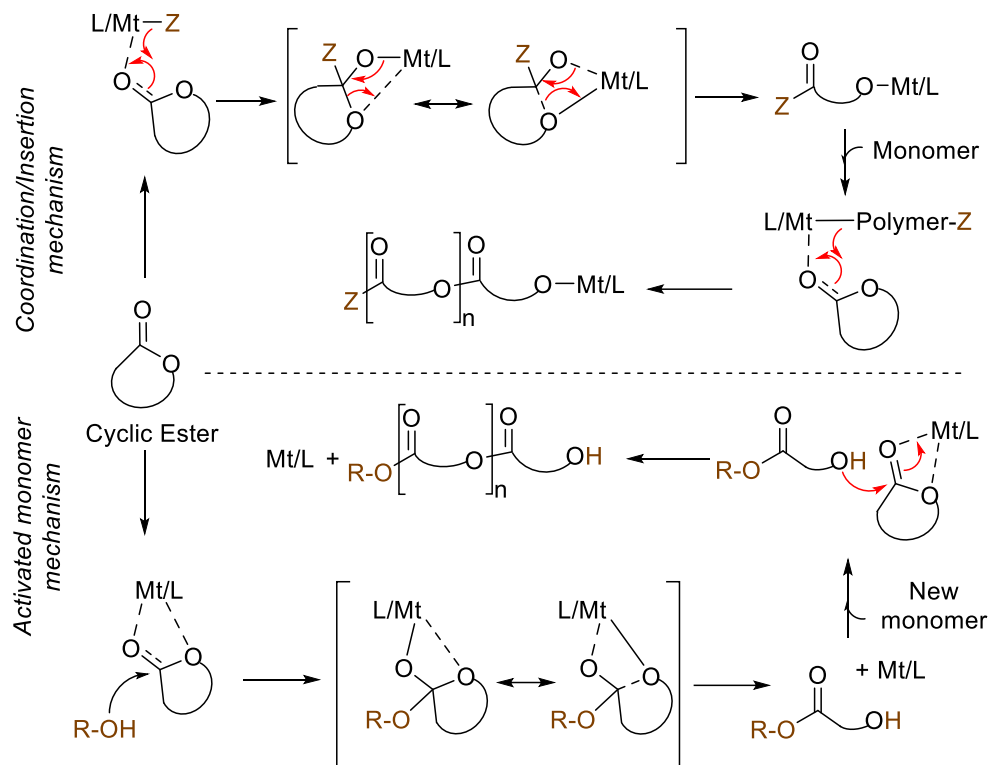


Figure III-1: Coordination/insertion (top) and activated monomer (bottom) ROP mechanisms.¹⁸⁷

As for OMRP, a few side reactions that can interplay with the coordination insertion mechanism may occur, as shown in Figure III-2. Inter- and intra-chain transesterification reactions can occur and lead generally to increased dispersities and lower M_n values than expected.¹⁸⁸

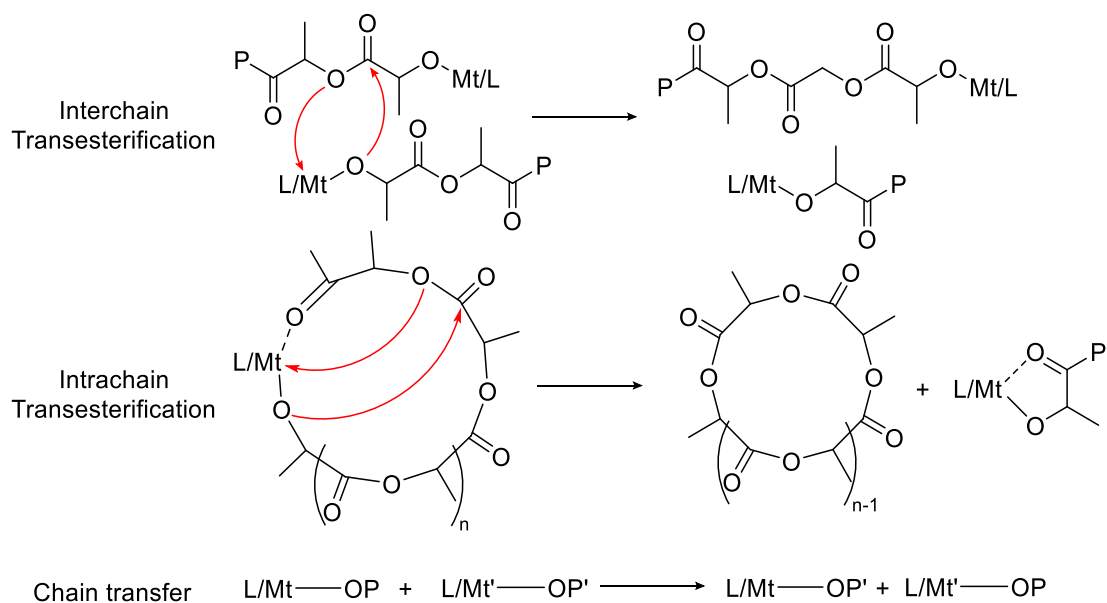


Figure III-2: Metal catalysed side reactions involved in ROP.

The mechanical and biodegradability properties of polylactide (PLA) greatly depends on its microstructure (tacticity). The ROP of *rac*-lactide (*rac*-LA) can lead to several outcomes, as depicted in *Figure III-3*. A non-selective process will lead to random sequence of D- or L-lactide, *i.e.* an atactic amorphous polymer. In contrast, a stereoselective polymerization of *rac*-LA can lead to heterotactic or isotactic (diblock, multiblock or separate blocks) PLA. The polymerization of *meso*-LA can lead to heterotactic or syndiotactic PLA. While chiral complexes rarely lead to high degrees of stereoregularity, the incorporation of bulky substituents on the ligand scaffold has proven to increase the stereoselectivity of the process. In other words, heterotactic or isotactic PLAs may be produced *via* the ROP of *rac*-LA initiated by an achiral complex, provided the polymerization proceeds *via* a chain-end stereocontrolled mechanism, *i.e.* the last inserted LA unit stereo-controls the insertion of the incoming monomer. Isotactic PLA reaches $T_m \geq 180^\circ\text{C}$ vs. T_m around 150°C for syndiotactic PLA obtained from *meso*-LA. Many studies aiming at a stereoselective ROP of *rac*-LA were reported, and summarized in recent comprehensive reviews.^{177, 187, 189}

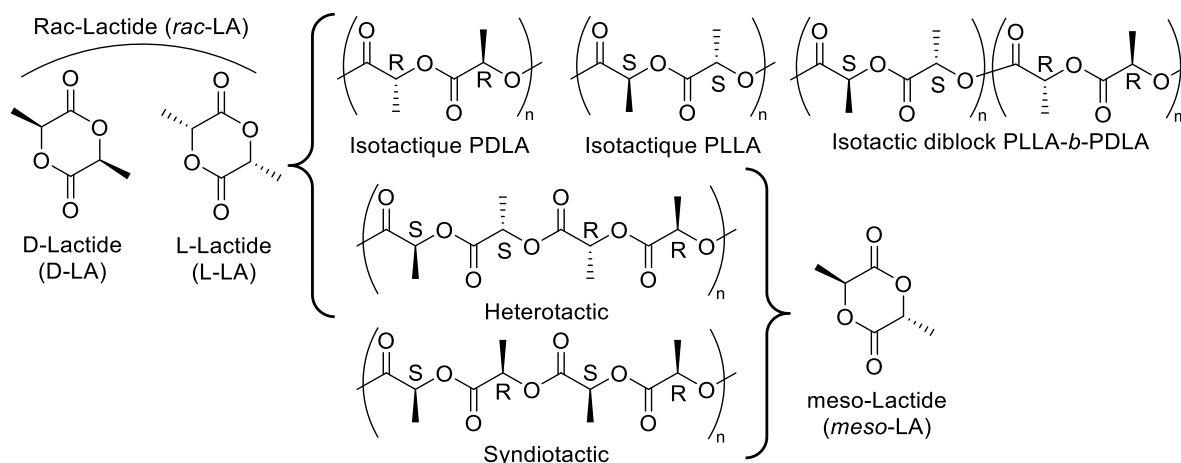


Figure III-3: Common cyclic ester monomers and possibility of tacticity with chiral monomer.

In the subsequent sections of the present chapter, I will provide an overview of the recent d-metal- and lanthanide-based systems applied to the ROP of cyclic esters with a special emphasis on cobalt, the metal investigated in the present project. I have excluded Zn from this overview because, many reviews are already available, as well as the metals of Groups 1, 2 and 13.^{185, 190-193}

2. Rare-earth metals

In 2000, Hillmyer, Tolman *et al.*¹⁹⁴ described a series of di- and tri-nuclear yttrium complexes for the ROP of *rac*-LA and ϵ -caprolactone (ϵ -CL). These complexes were well characterized by NMR and X-rays diffraction (XRD) studies. The polymerization tests performed in dichloromethane (DCM) at 25°C revealed a linear evolution of the molar masses (M_n) as a function of conversion, attesting the polymerization control, even though the dispersity values were quite high (\bar{D} 1.20-1.77).

Afterwards, the group of Carpentier described monomeric complexes of Group 3 (Figure III-4), which were able to control the stereoselective ROP of *rac*-LA to form heterotactic-enriched PLA.^{195, 196} The experiments performed in THF at 20°C with reaction times between 5 and 20 min demonstrated that all of these complexes are active initiators for the controlled ROP of *rac*-LA and afforded heterotactic PLA. Altogether, narrow dispersities (1.07-1.34) and the experimental molar masses close to the theoretical values accounted for a living process (cf. Section III-2). Block copolymers of the PLA-*b*-PCL type could also be developed by sequential monomer addition.¹⁹⁵ In these different contributions, the authors carefully analysed the structure-tacticity relationship, highlighting the non-innocent role of the size of the R¹ substituent in *ortho* position of the phenolate groups.¹⁹⁵⁻¹⁹⁷ The reported Y-based systems also successfully controlled the polymerization of other monomers such as four-membered lactones, *rac*- β -butyrolactone (*rac*-BL), *rac*- β -malolactonate (*rac*-MLA^Rs) and *rac*-4-alkoxymethylene- β -propiolactone (*rac*-BPL^{OR}s).¹⁹⁸

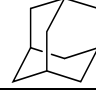
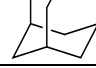
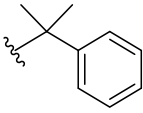
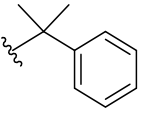
Complex	M	R ¹	R ²	R ³	X
2.1	Y	Me	Me		N(SiMe ₃) ₂
2.2	Y				N(SiHMe ₂) ₂
2.3	Y	^t Bu	^t Bu		CH ₂ SiMe ₃
2.4	La				N(SiHMe ₂) ₂
2.5	Nd				N(SiMe ₃) ₂
2.6	Y	Adamantane	Me	OMe	N(SiHMe ₂) ₂
2.7	La	C ₁₀ H ₁₆	Me		N(SiHMe ₂) ₂
2.8	Nd		Me		N(SiMe ₃) ₂
2.9	Y		^t Bu		N(SiHMe ₂) ₂
2.10	Y				N(SiHMe ₂) ₂
2.11	Y	^t Bu	^t Bu	N(Me) ₂	N(SiHMe ₂) ₂
2.12	Y	CMe ₂ Ph	CMe ₂ Ph		
2.13	Y	CMe ₂ ^t Bu	Me		
2.14	Y	CMe ₂ (4CF ₃ C ₆ H ₄)	Me	OMe	N(SiHMe ₂) ₂
2.15	Y	CPh ₃	Me		
2.16	Y	Cl	Cl		

Figure III-4: Rare-earth metals-based initiators for the stereoselective ROP of *rac*-LA.¹⁹⁵⁻¹⁹⁷

3. Group 4 (Titanium, Zirconium and Hafnium)

Group 4 metals-based ROP initiators were widely investigated and very well described in many reviews until 2015.¹⁹⁹ A large library of supporting ligands was reported, which includes bidentate bis(aryloxo),²⁰⁰ thioetherphenolate,²⁰¹ tri- and tetra-dentate amino and iminophenolate (salan, salen, salalen), half Schiff-base, (OSSO)-type, (OSNO)-type, and NHC-bis(phenolate) ligands.^{199, 202, 203} The present section will provide an updated overview (since

2015) of the Group 4 metals-based initiators and will be divided in four parts, the first three dealing with Ti complexes and the last one focusing on Zr and Hf.

a. Mononuclear Ti complexes of tridentate ligands

In 2015, Muneeswaran, Velmathi *et al.*²⁰⁴ reported the ROP of ϵ -CL with the novel tridentate Ti complex **3.1** (Figure III-5). The reaction was carried out in bulk at 150 °C and reached 96% conversion after 24 h to yield a polymer with moderate dispersity (1.33). The PCLs synthesized with **3.1** were used for the preparation of a novel two-phase polymer nanocomposite with nanocrystalline multiferroic BiFeO₃.

In 2018, Durr and Williams reported the preparation of Ti(IV) complexes of half Schiff-base ligands that exhibited good activities for the controlled ROP of ϵ -CL and ω -pentadecalactone.²⁰⁵ As presented in Figure III-5, the steric bulk of the ligand led to different coordination modes, which influenced the polymerization rate, with the catalytic activities decreasing in the order: type IV (**3.7**, **3.8** and **3.9**) > type III (**3.5** and **3.6**) > type I and II (with **3.2**, **3.3** and **3.4**), for both monomers.

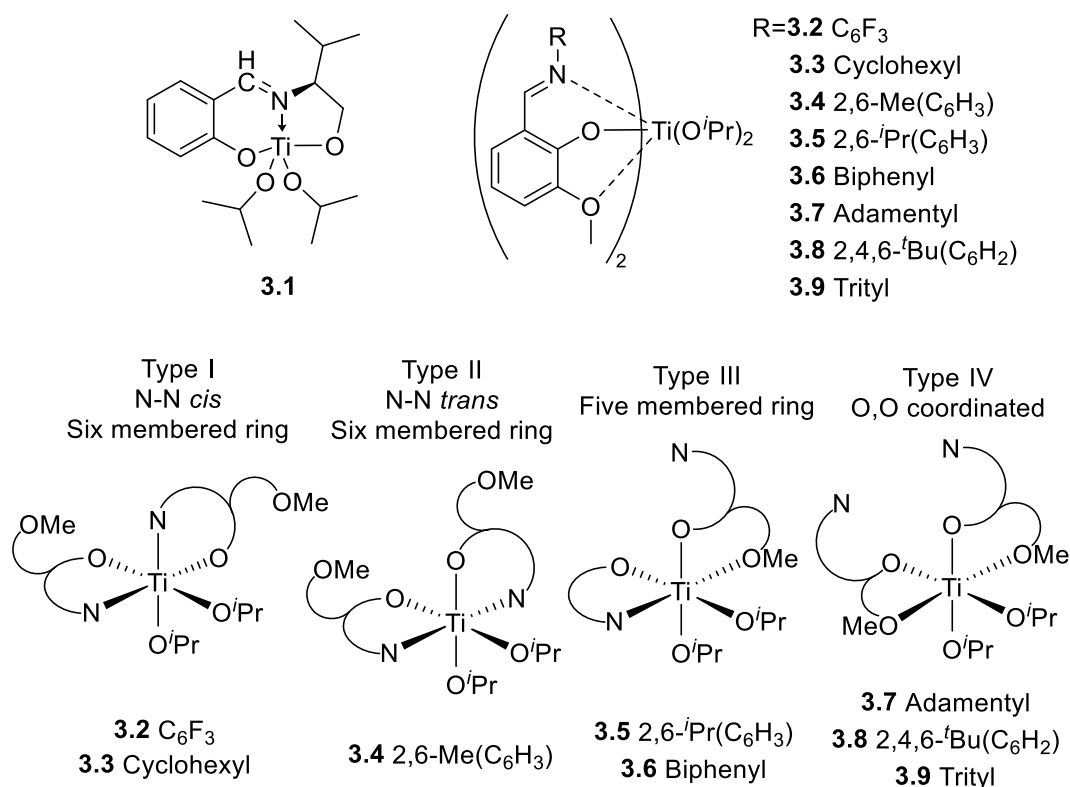


Figure III-5: Geometries of the titanium(IV) complexes of half Schiff base ligands. ^{204, 205}

b. Dinuclear Ti complexes of tridentate ligands

Chand, Chakraborty *et al.*²⁰⁶ reported a new library of dinuclear Ti alkoxide complexes containing (NNO)-type ligands (**3.10**, **3.11** and **3.12**). All of these complexes were well

characterized by ^1H , ^{13}C NMR, mass spectrometry (MS) and also by XRD. All of them were found in a distorted octahedral geometry. The ligand is disposed in a *meridional* fashion, the alkoxide bridge are located *cis* to each other and the terminal alkoxide in *anti*-fashion with respect to each other. All compounds exhibited a high activity ($\geq 90\%$ conv. in ≤ 21 min) and good control ($\bar{D} \leq 1.21$) for the bulk ROP of ϵ -CL and *rac*-LA, at 100°C and 140°C , respectively. The high polymerization rate was tentatively attributed to the presence of CN substituents on the ligand backbone, with strong electron-withdrawing power, therefore increasing the Lewis acidity of the Ti center. On the other hand, the increase of the steric bulk in the phenolate group *ortho*-position also increased the activities, indeed the reaction times for complexes **3.10**, **3.11** and **3.12** were 21, 15 and 8 min, respectively.²⁰⁶

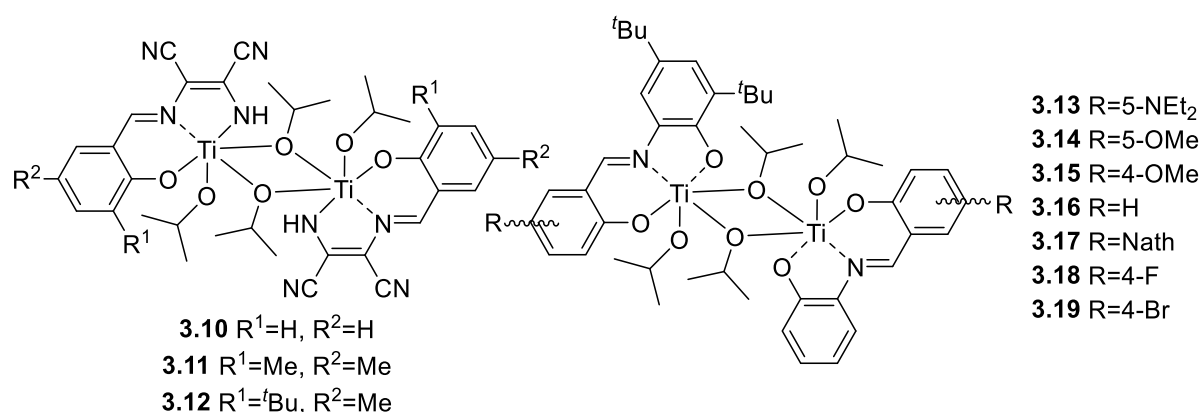


Figure III-6: Dinuclear titanium complexes with tridentate ligand.

Lin, Chen *et al.*²⁰⁷ reported a series of titanium complexes with ONO-tridentate Schiff base ligands that are active for the controlled ROP of *rac*-LA and ϵ -CL at 70°C and 30°C , respectively. In all cases, the experimental M_n values agreed well with the theoretical ones and the dispersities were low. The ROP tests assessed the influence of the R group on the catalytic activity and tendency for the ROP of CL is as follows: **3.17** > **3.18** \approx **3.19** \approx **3.13** > **3.14** \approx **3.15** > **3.16**; while that for the ROP of LA is: **3.13** > **3.14** \approx **3.15** \approx **3.16** \approx **3.17** > **3.14** > **3.19**.

c. Ti complexes of tetradentate ligands

In 2018, Wu *et al.* reported a series of Ti^{IV} complexes of tetradentate unsymmetrical N_2O_2 ligands that exhibited good activities in the bulk (130°C) ROP of *rac*- and L-LA. However, the chloride complexes (**3.20** and **3.21**) required the addition of alcohol in the medium (*cf. annex table*) Figure III-7.²⁰⁸

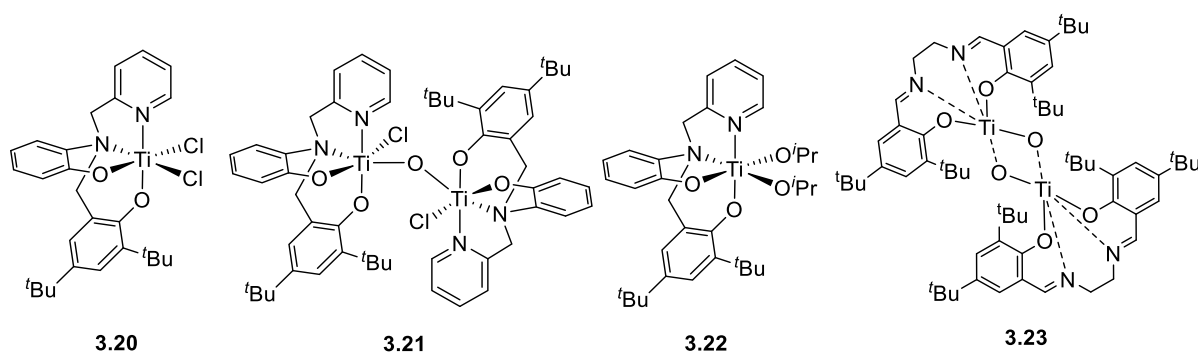


Figure III-7: Mono- and Dinuclear titanium complexes with tetradentate ligand.

The dinuclear Ti^{IV} complex **3.23**, supported by a salen-type ligand performed well in the ROP of *rac*-LA at 160°C for 16 h to afford a polymeric material with $\bar{D} \leq 1.4$.

d. Zr and Hf complexes

Jones *et al.* reported a series of unsymmetrical Schiff base complexes of Zr and Hf (**3.24-3.28**, Figure III-8) that were active for the ROP of *rac*-LA in melt at 130°C for Zr complexes or 80°C for Hf complexes.²⁰³ The authors also reported the half-Schiff base Zr complexes **3.29-3.34**, which exhibited good activities in the ROP of *rac*-LA in toluene at both 20°C and 80°C. The polymerization worked also well in bulk, achieving higher molecular weight, but the dispersity raised above 1.20.²⁰²

The tetranuclear zirconium complex **3.35**, supported by an unsymmetrical amino-bisphenolate ligand, reported in 2015, is active for the ROP of *rac*-LA and allowed the formation of PLA within 26 h at 70°C in toluene with an acceptable dispersity (\bar{D} 1.27).²⁰⁹

The Zr (**3.36a-c**) and Hf (**3.37a-c**) analogues of the Ti-based initiators (**3.10-3.12**) were also reported and behaved similarly to the latter.²⁰⁶

In 2019, within a series of nine Zr and Hf complexes with Schiff based ligands, only three of them, with Mt-OR groups, revealed good activities for the controlled ROP of *rac*-LA and ϵ -CL, at 140°C and 80°C respectively, while the homoleptic complexes were inactive.²¹⁰ As often observed, the hafnium derivative **3.40** was less reactive than the zirconium complexes **3.38** and **3.39**. The Zr^{IV} bis(dbzm) complex (**3.41**) and its ROP of ϵ -CL was reported, including a computational investigation of the mechanism, however only using semi empirical method (PM3).²¹¹

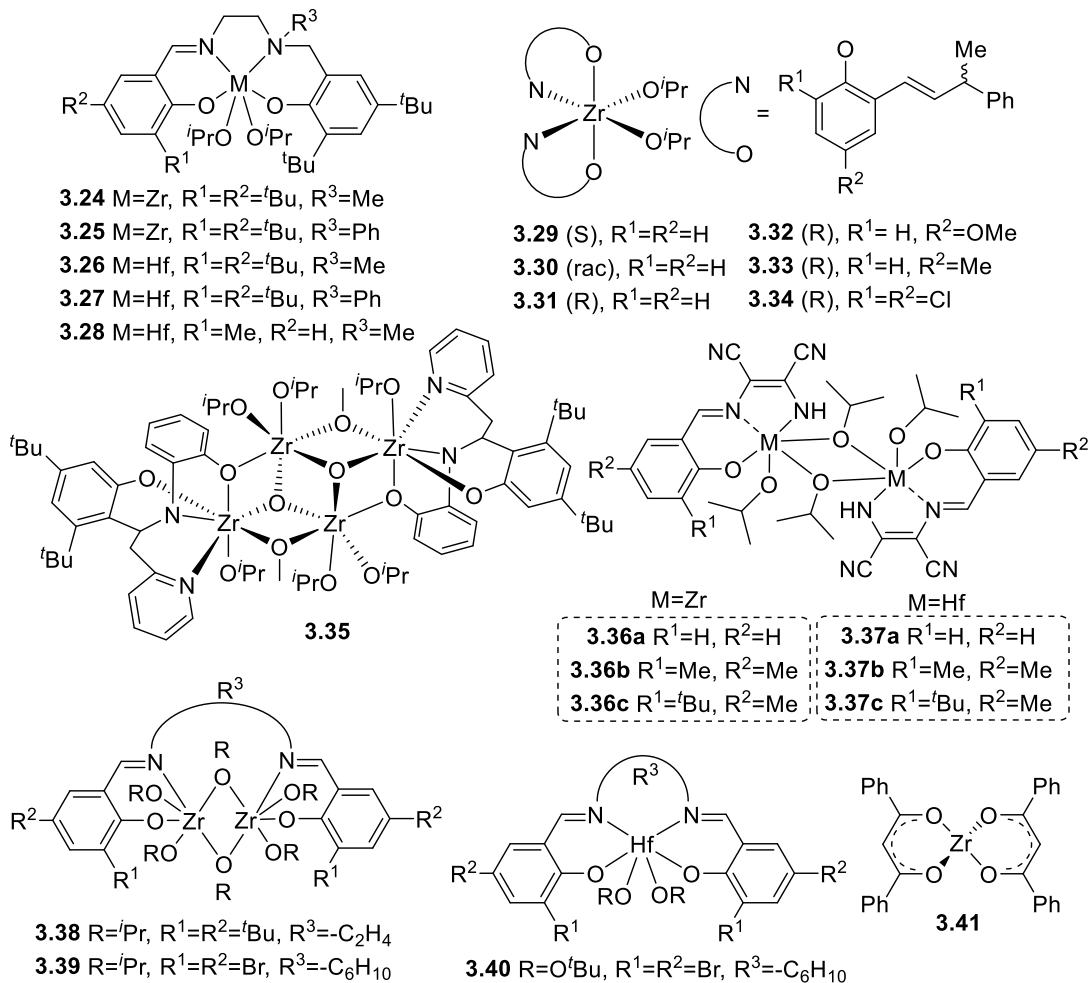


Figure III-8: Zirconium and Hafnium complexes library for ring opening polymerization.

Diaconescu *et al.* described in 2019 a redox switchable ROP system, namely (salfen)Zr(O^{*i*}Pr)₂ (salfen = *N,N'*-bis(2,4-di-*tert*-butylphenoxy)-1,1'-ferrocenediimine), which promoted the homopolymerization of cyclic esters or epoxides as a function of the ferrocene oxidation state.²¹² This properties was exploited for the formation of multiblock copolymers. The reduced form of the complex, **3.42**, readily mediated the ROP of L-LA at 100°C in C₆D₆, achieving the formation of the first PLA block. After addition of a chemical oxidant, the Zr^{Ox} species (**3.43**) was formed, and further addition of cyclohexene oxide (CHO) led to the formation of a diblock copolymer PLA-*b*-PCHO. The latter could further be extended, after reduction and addition of L-LA to a PLA-*b*-PCHO-*b*-PLA terpolymer. Similar systems, based on (salfan)Zr(O^{*t*}Bu)₂, (thiolfan)*Ti(O^{*i*}Pr)₂ and (phosfen)Y(O^{*t*}Bu), were reported earlier.^{213, 214}

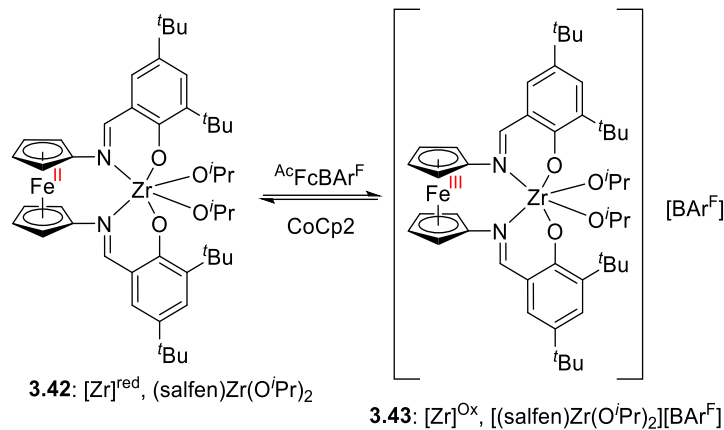


Figure III-9: Red/Ox switchable system based on a zirconium complex.²¹²

4. Vanadium

Vanadium was thoroughly studied and applied to the polymerization of ethylene.²¹⁵⁻²²³ The use of vanadium complexes in the ROP of cyclic esters will be detailed in the present section.

In 2005, Nomura and coll.²²⁴ synthesised the ketimide aryloxy complex $(\text{ArN})\text{V}(\text{Me})(\text{OAr})(\text{N}=\text{C}^t\text{Bu}_2)$ (**4.1**, Figure III-10) which initiated the ROP of ϵ -CL at 100 °C and afforded PCL with rather low dispersities (\bar{D} 1.2-1.5). Subsequently, Redshaw *et al.* described a series of vanadium complexes with chelating bis-aryloxy ligands that were characterized by NMR and XRD (Figure III-10).²²⁵ These mono- and dinuclear compounds were shown to be active initiators for the ROP of ϵ -CL. While the mononuclear complexes **4.2a**, **4.2b** and **4.2c** produced PCL at 40°C within 24 h ($\leq 25\%$) in the presence of 1 eq BnOH, they remained less efficient than the dinuclear complexes **4.3a-4.3h** (41%-78%). Between 2011 and 2016, the group of Redshaw reported the synthesis of a series of dimeric oxo- and imido-vanadium alkoxide complexes with 1,3-calix[4]arene ligands (**4.4**, **4.5a** and **4.5b**), which converted ϵ -CL to PCL with low to high conversions (**4.4** = 94%, **4.5a** = 46% and **4.5b** = 20%) at 80 °C within 72 h.^{226, 227} These differences were rationalized by the easier accessibility of the metal centre in **4.4**, and the bulkiness of the alkoxide, *i.e.* the more bulky, the less active.

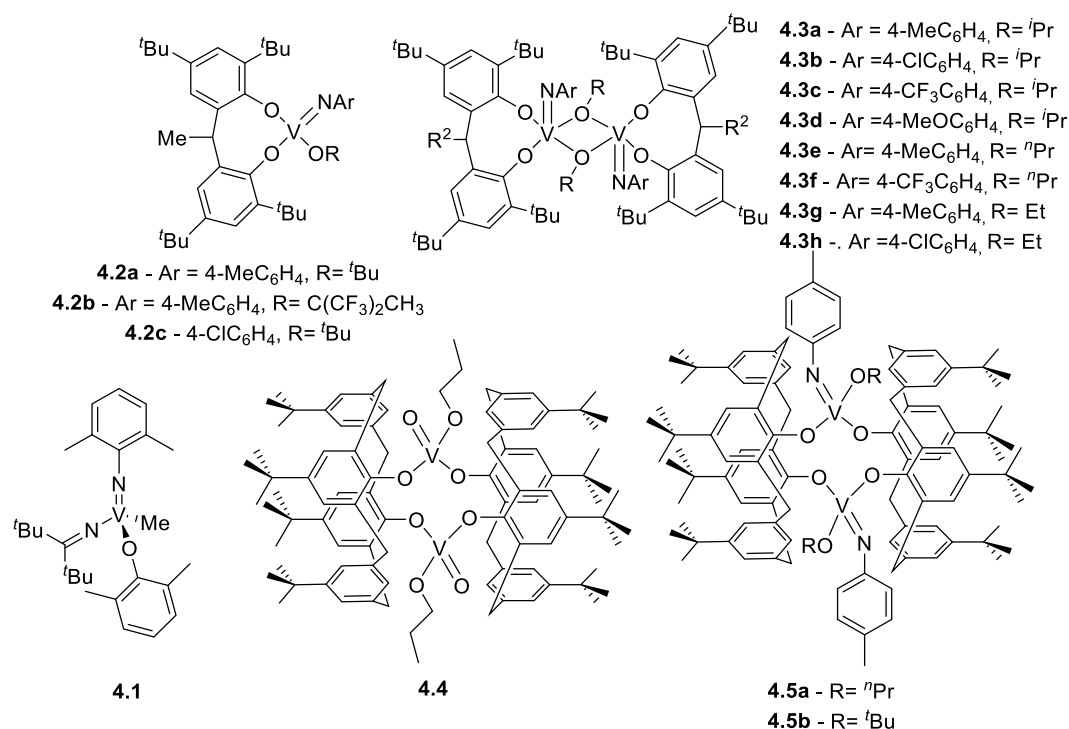


Figure III-10: Mono- and di-nuclear vanadium complexes for ROP of caprolactone.

In 2013, Redshaw *et al.* developed another series of mono- and dinuclear vanadium complexes with (half) Schiff base ligands for the polymerizations of ethylene and ϵ -CL (Figure III-11).²²⁸ For reactions performed in toluene at 110 °C over 72 h with a ratio of [M]/[V]/[BnOH] = 400/1/1, complexes **4.8b-4.9c** and **4.11**, **4.12** reached 70% conversion or higher, while complexes **4.6a**, **4.6b** and **4.8a** only reached 50% conversion, and **4.13**, **4.7a**, **4.7b** and **4.9d** less than 50%. In all cases, the experimental M_n values were lower than expected. However, the dispersities remained narrow (\mathcal{D} 1.2-1.4), except for **4.8b** (\mathcal{D} 2.3).

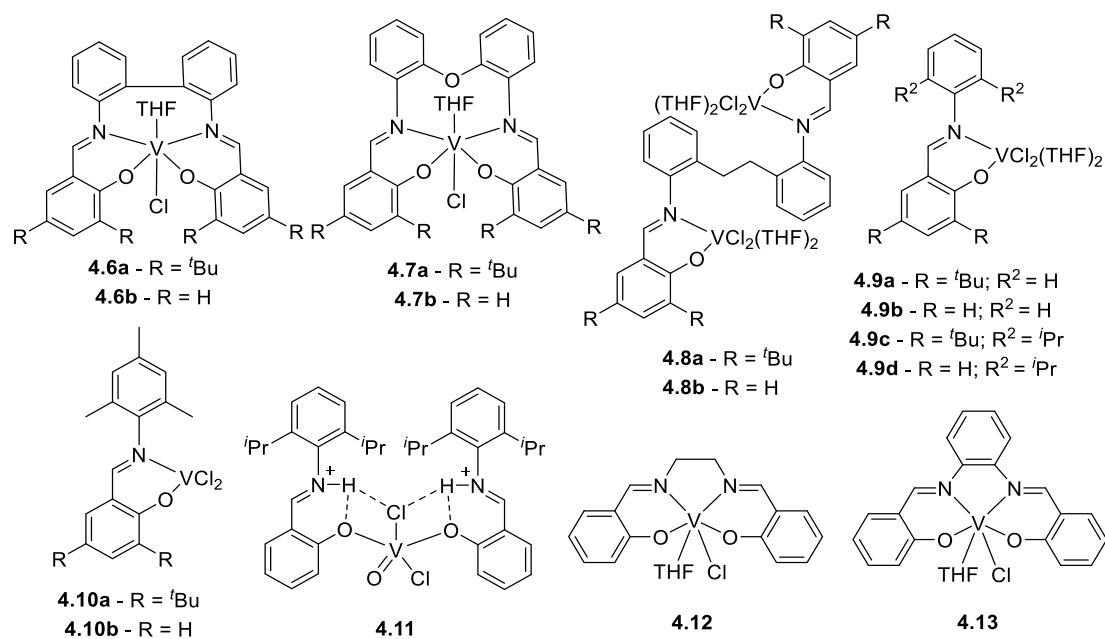


Figure III-11: Vanadium complexes of (half) Schiff base ligands.

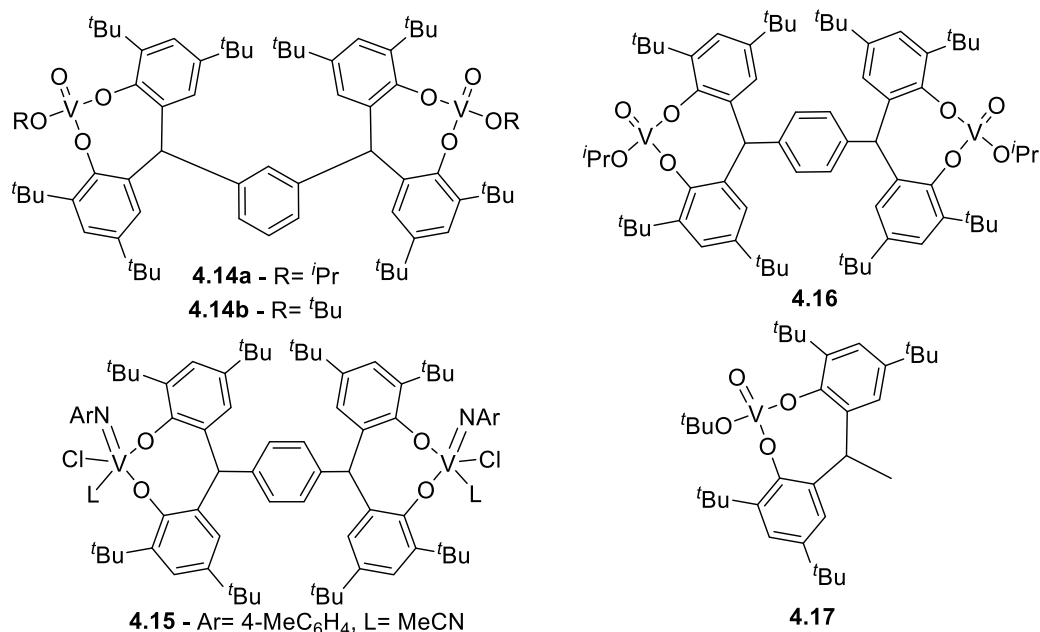


Figure III-12: Oxo- and amido-vanadium complexes of chelating bis- or tetra(aryloxoide) ligands.

In 2016, the group of Redshaw described oxo- and amido-vanadium complexes with bis- (**4.17**) and tetra(aryloxoide) (**4.14-4.16**) ligands for applications in the ROP of ϵ -CL (bulk, 80°C, 30 min) and *L*-LA (toluene, 80°C, 24 h) (Figure III-12).²²⁹ A nearly complete conversion of ϵ -CL was observed in each case, while the conversions for LA reached 15-20% for **4.14a** and **b**, and ca. 50% for the other complexes. In all cases, the M_n values were much lower than expected and the molar mass distributions were quite broad for CL (\bar{D} 1.20-1.5) and slightly better for LA (\bar{D} 1.10-1.34).

5. Chromium

Rieger *et al.* described mono- and dinuclear chromium(III) chloride complexes supported by salen-type ligands (**5.1-5.4**, Figure III-13) that were only moderately active for the ROP of β -butyrolactone (β -BL).^{230, 231}

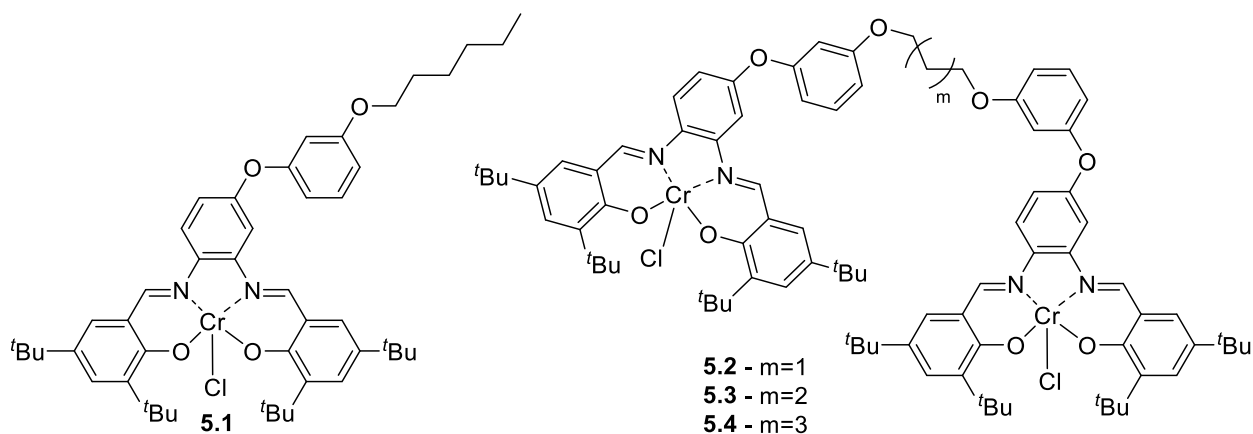


Figure III-13: Chromium complexes applied to the ROP of β -BL.^{230, 231}

6. Manganese

Various manganese salts, *i.e.* $[\text{MnCl}_2]$, $[\text{Mn}(\text{OAc})_2]$ and $[\text{Mn}(\text{SO}_4)_2]$ were shown to polymerize L-LA. However, they required several days at 150 °C to achieve complete conversions.^{232, 233} In 2015, Daneshmand and Shaper reported a series of manganese(III) complexes of tetradentate diamino-bis(phenolate) ligands (**6.1-6.3**) that were evaluated in the ROP of *rac*-LA (Figure III-14).²³⁴ While complexes **6.1**, **6.2** and **6.3** were inactive in DCM at room temperature and in toluene at 70°C, they exhibited a moderate activity in bulk conditions at 130°C, reaching 50-90% conversion after 2-4 h. Complex **6.3** reached a higher conversion, probably due to its greater thermal stability (*vs.* **6.1** and **6.2**). The recovered polymeric materials exhibited dispersities between 1.1 and 1.5.²³⁴

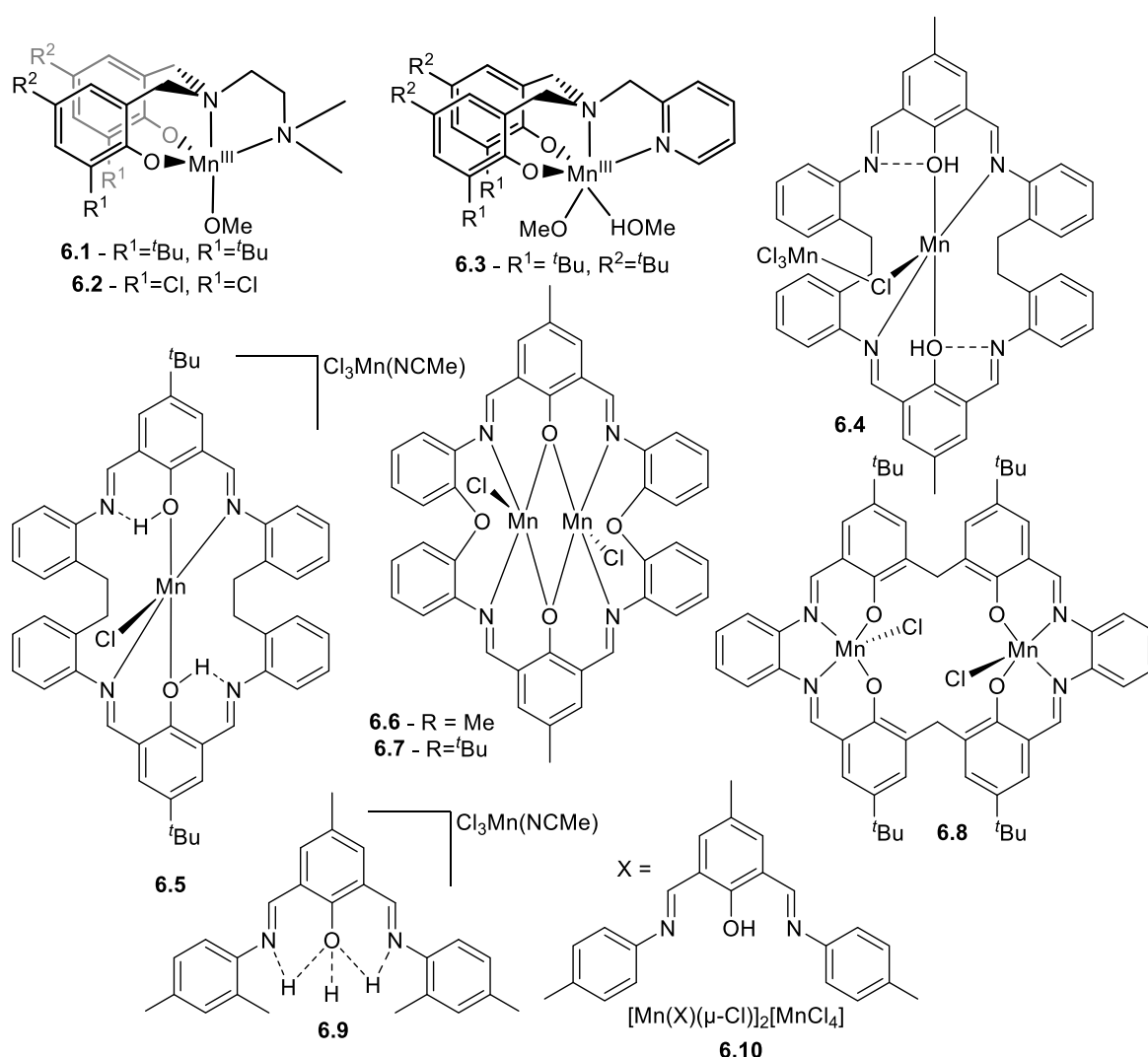


Figure III-14: Manganese complexes applied to the ROP of cyclic esters.

Within a library of manganese complexes of bis(imino)phenoxide macrocyclic ligands developed by Redshaw, Elsegood *et al.*,²³⁵ only complexes **6.4** and **6.5** mediated the ROP of ϵ -CL, however reaching only low conversion ($\leq 15\%$) at temperatures above 60°C (Figure III-14).

7. Iron

a. Iron chloride precursors

Iron chloride complexes were found to be suitable initiators for ROP processes. However, they required an initiation step consisting of a reaction with propylene oxide (PO) to generate, *in situ*, an iron alkoxide species *via* epoxide ring-opening, which then initiates the ROP following the classical coordination/insertion mechanism, as shown in *Figure III-15*.

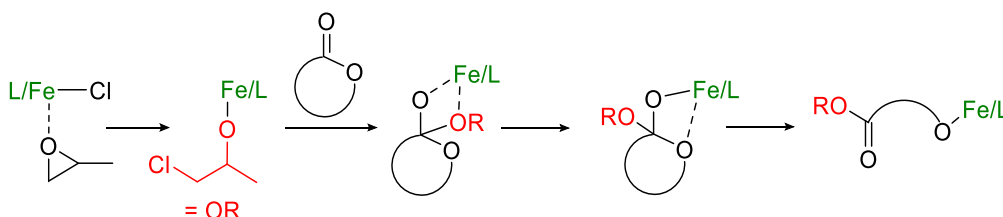


*Figure III-15: ROP Initiation mechanism for Iron chloride complexes.*²³⁶

In 2017, Pang *et al.* reported a series of iron(III) chloride of salen-type ligands (**7.1-7.8**, *Figure III-16*), which were activated by PO for the ROP of LA.²³⁷ Complexes **7.1**, **7.2** and **7.3** allowed studying the influence of the backbone flexibility and chirality on the polymerization, while complexes **7.4**, **7.5**, **7.6**, **7.7** and **7.8** allowed identifying a potential impact of the phenol substituents. All ROP were carried out in 2 mL of PO, with a [M]/[Fe] = 100/1 ratio. Within the first series of complexes, **7.1** and **7.2** required one day at 60°C to reach a 90% conversion (\bar{M}_n 1.46–1.58), while the more flexible complex **7.3** only needed 4 h to reach a 90% conversion (\bar{M}_n 1.54). Concerning the second series, while complex **7.4** (*o*-H substituents) was completely inactive, **7.5** showed a modest activity (40% conversion, 10 h, 2 h induction period) and the complex **7.7** exhibited a high activity (2 h, 94% conversion, no induction period). Clearly, the presence of electron-withdrawing chloride groups (EWGs) increases the Lewis acidity of the iron centre and boosts the reactivity. However, the introduction of a Me group on the ethylene backbone did not affect much the reactivity (**7.5** vs. **7.6** and **7.7** vs. **7.8**).

In 2018, Lamberti *et al.* showed that moving from salen-type ligands to their diamino-bis(phenolate) (**7.9**) or mixed imino/amino-bis(phenolate) (**7.10**, *Figure III-16*) analogues is detrimental to the ROP of L-LA, while it is beneficial to the ROP of ϵ -CL.²³⁸ The surprising result obtained for LA was explained by an increased Lewis acidity of the metal centre in **7.9** and **7.10**, which could lead to a stable lactate intermediate.

Jones *et al.* published a study that aimed at identifying a structure/activity relationship within a series of salalen iron chloride complexes (**7.10-7.16**, *Figure III-16*).²³⁹ Within the **7.10-7.13** series, it can be noticed that the presence of electron-donating groups (EDGs) on the phenol moieties slows down the polymerization rate (3 days for **7.10** (*t*Bu), 2 days for **7.13** (Me) at 60 °C for *ca.* 75% conv), while the presence of EWGs boosted the activity (6 h for **7.12** (Cl) at 60 °C for 80% conv). Complex **7.11** exhibited a similar activity to **7.12**. Concerning the influence of the backbone, no trend clearly appeared. Indeed, **7.14** (C₆H₄) and **7.16** (C₆H₁₀)

were slightly more and slightly less active, respectively, than their CH₂CH₂ analogues, **7.10** and **7.11**, respectively. Nevertheless, all of these complexes exhibited a good control of the polymerization, with experimental molar masses of the polymers increasing linearly as a function of the conversion and relatively close to the theoretical values. The dispersities ranged between 1.11 and 1.30.

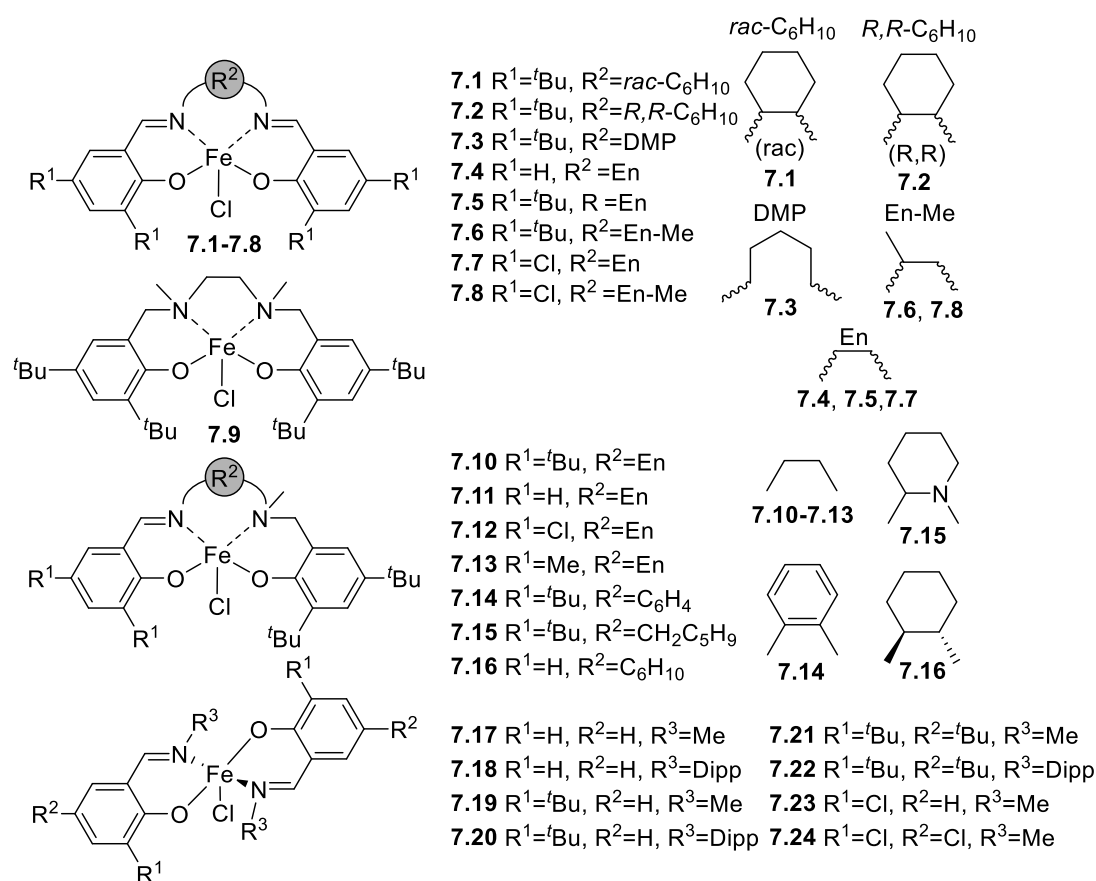


Figure III-16: Iron chloride complexes applied to the ROP of cyclic esters.

In 2018, Garden, Shaver *et al.* evaluated a series of iron chloride precursors supported by two half Schiff-base ligands (**7.17-7.24**, Figure III-16) in the ROP of *rac*-LA.^{240, 241} Performing the polymerization in toluene at 120 °C with a LA/Fe/PO ratio of 100/1/50, nearly complete conversion was obtained, but the *M_n* values were lower than expected and the dispersities were quite large (*D* 1.4-1.7).

b. Iron trimethylsilylamide

In 2019, Thomas *et al.* described one of the more impressive results for the stereoselective ROP of *rac*-LA in solution.²⁴² Complexes **7.32-7.36** (in the presence of *i*PrOH, Figure III-17) converted up to 800 eq. of *rac*-LA in toluene at room temperature within minutes to afford high molecular weight stereo-complexes of PLA.

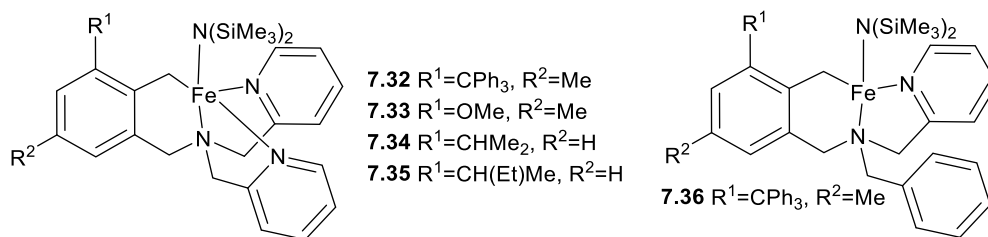


Figure III-17 : Iron trimethylsilylamide complexes.

c. Iron alkoxide complexes

At the beginning of the 2000's, a few groups started to work on the ROP of LA mediated by iron alkoxide complexes. The group of Tolman used simple homoleptic ferric alkoxides, such as ferric ethoxide (**7.37**), *n*-propoxide (**7.38**), isopropoxide (**7.39**) and *n*-butoxide (**7.40**, Figure III-18), which led to over 90% conversion within 36 h at 130°C (bulk conditions).^{243, 244} Nearly at the same time, Hillmyer, Tolman *et al.* reported that complexes **7.41a-c** (Figure III-18) were efficient initiators for the ROP of ϵ -CL and LA.²⁴⁵ All of these polymerizations were carried out in toluene, with [M] = 1 M at 25 °C for CL and 70 °C for LA. The produced PCL with **7.41c** exhibited narrow dispersity ($\mathcal{D} < 1.20$, at 100% conv. within 20 min). In contrast, the molar mass distributions of the produced PLA were quite broad (\mathcal{D} 1.40-2.00, at 100% of conversion).²⁴⁵ During the same period, several other systems were reported, such as the well-defined iron(II) complex **7.42** (Figure III-18), which is highly active for the ROP of both LA and CL in toluene at room temperature, though less controlled for CL.²⁴⁶ The heterobimetallic iron(II) alkoxide or aryloxo complexes, [(THF)NaFe(O^{*t*}Bu)₃]₂ (**7.43**) and [(THF)₄Na₂Fe(2,6-diisopropylphenolate)₄] (**7.44**, Figure III-18), respectively, efficiently initiated the ROP of LA at room temperature in dichloromethane, affording high molecular weight PLA with quite high dispersities (\mathcal{D} = 1.57 (**7.43**), 1.89 (**7.44**)).^{247, 248}

The bis(imino)pyridine iron bis(alkoxide) complex **7.45** (Figure III-18), reported by Byers *et al.*, initiated the ROP of LA. However, the rate of polymerization was very low (14% conversion in 24 h at room temperature) and gave an ill-defined polymeric material.²⁴⁹ Nevertheless, complex **7.45** could be converted *in situ* to its bis(alkoxide) counterparts **7.46a**, **7.46b**, **7.46c**, by reaction with the appropriate alcohol, and these complexes were much more active and led to well-defined PLA samples. Complex **7.46a** could be used as a switchable “on/off” ROP initiator. Indeed, chemical oxidation of the Fe^{II} complex **7.46a** by addition of ferrocenium hexafluorophosphate (FcPF₆) led to its Fe^{III} counterpart (**7.48**, Figure III-18), which is completely inactive.²⁴⁹ The reversibility of the switch was shown by the addition of cobaltocene (CoCP₂), which reduced the Fe^{III} to Fe^{II}, affording again an active ROP initiator and comparable ROP rates were observed ($k_{\text{obs}} = 1.5 \times 10^{-4} \text{ s}^{-1}$ before oxidation to Fe^{III} and $k_{\text{obs}} = 2.2 \times 10^{-4} \text{ s}^{-1}$ after reduction back to Fe^{II}). The monoalkoxide complexes analogous to **7.46a** and **7.46c**, namely **7.47a** and **7.47c** (Figure III-18), respectively, were applied to the ROP of LA in toluene or chlorobenzene solutions.^{250, 251} Both the monoalkoxide initiators **7.47a** and **7.47c** were shown to be more active than their bis(alkoxide) analogues. While complex **7.47a** also

initiated the ROP of ϵ -CL at room temperature (80% in 24 h), **7.46a** was totally inactive (active at 70°C, 99% conv. in 18 h).^{250, 251} Lee, Park *et al.* highlighted that the dinuclear iron complexes **7.49** and **7.50** (Figure III-18), readily initiated the bulk ROP of LA 130°C (100 eq. LA, conv. 97% (**7.50**), 47% (**7.49**)), affording relatively well-defined PLA samples (M_n values close to theoretical ones, $\bar{D} = 1.23$ -1.4).²⁵² Silvino *et al.* reported the use of the phenoxy-imine iron(III) complex **7.51** (Figure III-18) in the ROP of L-LA. However, under bulk conditions (500 eq LA, 120°C) its efficiency remained modest (48% conv.) and the obtained polymeric material had lower molecular weight than expected and exhibited a broad dispersity (\bar{D} 1.5).²⁵³

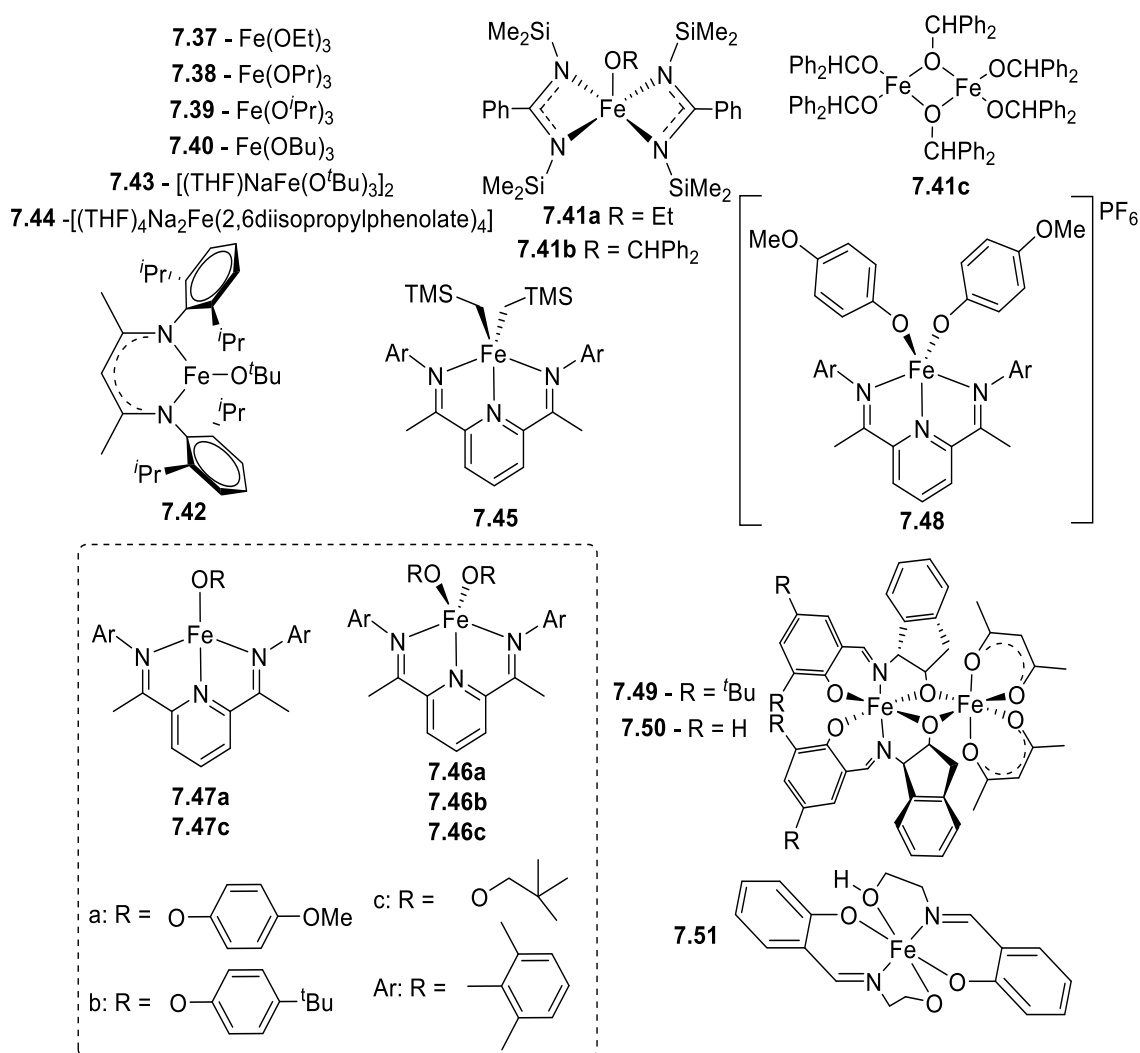


Figure III-18: Iron alkoxide complexes applied to the ROP of cyclic esters.

8. Cobalt

Cobalt-based systems were much more applied to the ring-opening copolymerization of CO₂ and epoxides than to the ROP of cyclic ester.^{254, 255} In 2012, Xiaoping and Shunjun reported that the anionic homoleptic tris(aryloxide) cobalt complex (**8.1**, Figure III-19) achieved complete conversion of 100 equiv. of LA after 4 h at 70°C in toluene.²⁵⁶ The reaction could be

carried out at room temperature, however it required three days to achieved the same level of conversion.

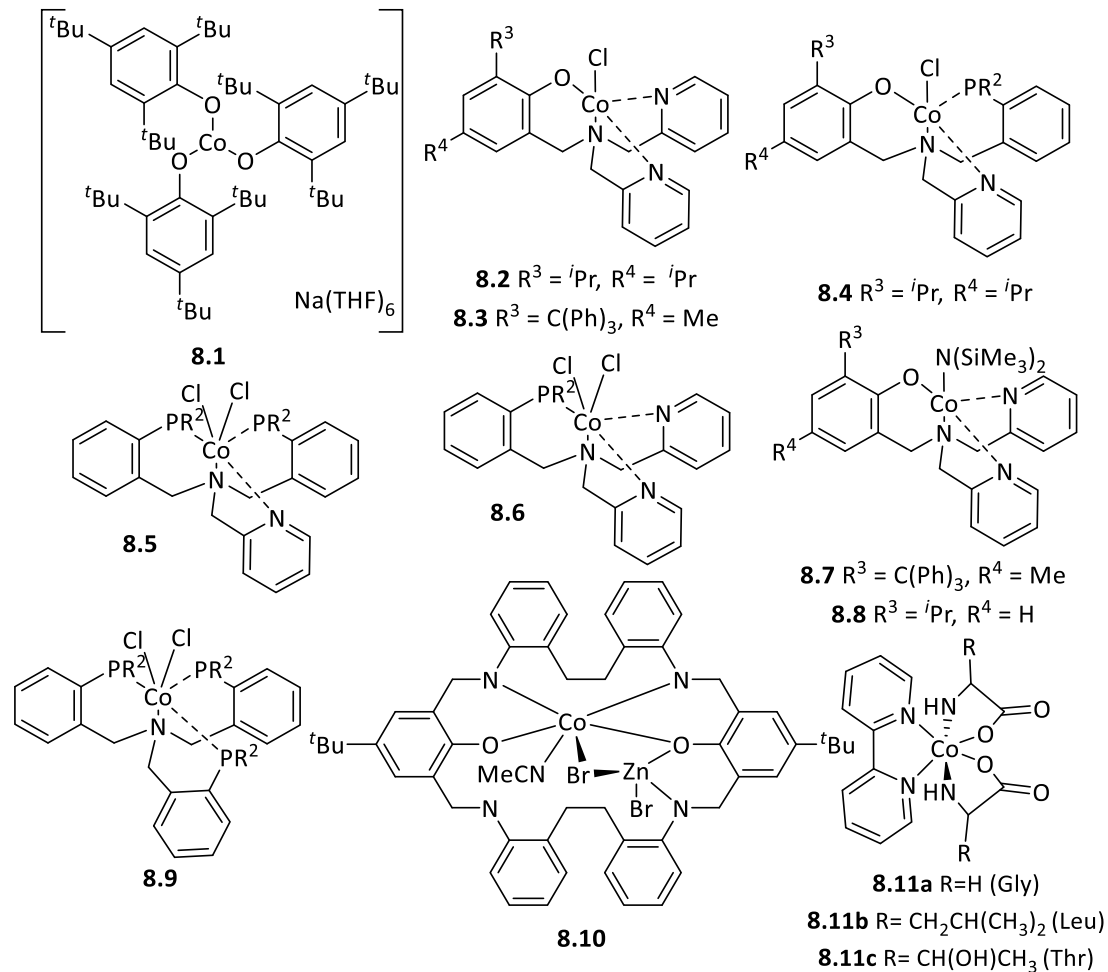


Figure III-19: Unimolecular cobalt complexes applied to the ROP of LA.

Thomas *et al.* reported a series of (zinc(II) and) cobalt(II) complexes of tetradentate tripodal ligands applied to the ROP of LA (Figure III-19).^{257, 258} This family of compounds comprises mono- and dichloride complexes as well as an amido $[\text{N}(\text{SiMe}_3)_2]$ derivative. Within the chloride complexes only compounds **8.3** and **8.6** exhibited good activity, affording well-defined PLAs (narrow \mathcal{D} and good agreement between experimental and theoretical M_n values), obtained in bulk at 130°C with addition of BnOH.²⁵⁸ The results of the ROP tests initiated by complexes **8.2**, **8.4**, **8.5** and **8.9** were unsatisfactory. The use of the $\text{N}(\text{SiMe}_3)_2$ derivative improved the activity. For the ROP of LA in toluene at room temperature (with one equivalent of $i\text{PrOH}$), the measured TOF values were 496 h^{-1} for **8.7** (bulkier CPh_3 *ortho*-substituent) vs. 2430 h^{-1} for **8.8** ($i\text{Pr}$ *o*-substituent) and the dispersities of the high molecular weights PLA samples were low (\mathcal{D} 1.06-1.09).²⁵⁷

More recently, Redshaw *et al.* reported the use of a bimetallic Zn/Co complex (**8.10**), supported by a macrocyclic [2+2] Schiff base ligand, to mediate the ROP of δ -VL, L-LA and ϵ -

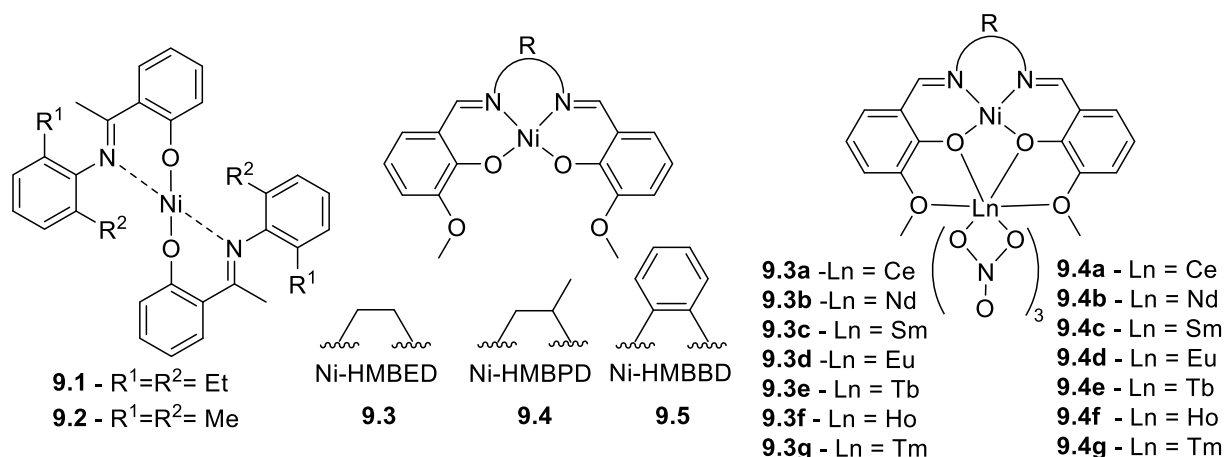
CL, and very good results were obtained (*Figure III-19*).²⁵⁹ The reaction were carried out in the presence of 1 equivalent of BnOH at 130°C and achieved high conversions ($\geq 80\%$) and low \bar{D} values in the 1.15-1.30 range. The group of Suman reported a synthetic route to access aminoacid cobalt complexes (with glycine **8.11a**, leucine **8.11b** and threonine **8.11c**, *Figure III-24*), which initiated the ROP of LA and led to high conversions ($>70\%$) in 60 min.²⁶⁰ While complex **8.11a** produced PLAs with M_n values in good agreement with the theoretical ones, the MW of the PLAs produced with **8.11b** and **8.11c** were higher than expected, probably due to a slower initiation rate, which was attributed to a larger steric hindrance around the Co centre.²⁶⁰

9. Nickel

Nickel complexes benefit from high electron transfer ability and stability, which make them attractive for many applications, including catalysis and polymerization.

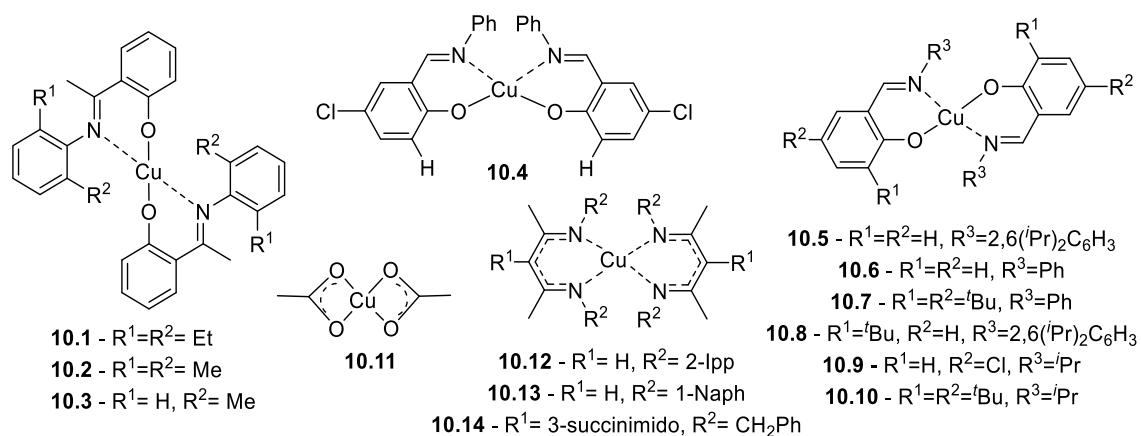
In 2007, Ghosh *et al.* applied to nickel the same ligand scaffold that gave rise to active Cu-based initiators for the ROP of LA.²⁶¹ However, complexes **9.1** and **9.2** (*Figure III-20*) were found inactive for the ROP of LA. In 2016, Maharana *et al.* applied the same strategy (from Cu to Ni) using salen-type ligands. After optimization, complexes **9.3-9.5** were found to initiate the controlled (moderate in view of the M_n values) ROP of LA in DCM at room temperature in the presence of BnOH (*Figure III-20*).²⁶² The absence of BnOH was detrimental to the activity. The several ROP runs allowed the followed ranking in terms of the observed polymerization rate: **9.3** > **9.4** > **9.5**.

Coordination of a $\text{Ln}(\text{NO}_3)_3$ moieties to salen-type nickel(II) complexes led to the bimetallic Ni-Ln complexes **9.3a-g** and **9.4a-g** (HMBED and HMBPD backbones, respectively), inducing a distortion of the square planar geometry and an increased Lewis acidity of the Ni centre (*Figure III-20*).^{263, 264} The increase in steric hindrance around the Ni could have a negative impact in the ROP activity, but in fact these compounds were found to be active in the bulk ROP of LA, affording high molecular weight and well-defined PLA samples (\bar{D} 1.05-1.19). The difference in terms of activity follows the trend: **9.4a** > **9.4b** > **9.4c** > **9.4d** > **9.4e** > **9.4f** > **9.4g**, which suggests that increasing the Ni-Ln bond length induces a decrease in activity. Complex **9.3c** shows activity and well controlled LA polymerization, but it is less efficient than the corresponding complex Ni(II) (**9.3**, **9.4** and **9.5**). The groups of Bao *et al.*²⁶⁵ and Lü, Fan *et al.*²⁶⁴ extended the library of bimetallic Ni/Ln complexes derived from **9.3**, namely **9.3a** (Ce), **9.3b** (Nd), **9.3d** (Eu), **9.3e** (Tb), **9.3f** (Ho) and **9.3g** (Tm, *Figure III-20*). Generally, the activity of the bimetallic complexes was lower than their monometallic Ni counterparts, and they required to work in bulk at high temperatures (130-160 °C, vs. DCM at room temperature). However, they allowed to reach high molar weight polymeric materials.

Figure III-20: Nickel complexes applied to the ROP of LA.²⁶¹⁻²⁶⁵

10. Copper

Copper is the most studied metal, within Groups 5-11, in ROP catalysis. In 2007, Ghosh *et al.* reported a series of phenoxy-ketimine copper(II) complexes (**10.1-10.3**, Figure III-21), which were found efficient for the ROP of LA in bulk (160 °C, 4 h, 55-70% conversion, \bar{D} 1.43-1.58).²⁶¹ In 2010, Luximon *et al.* reported a series of salicylaldimine copper complexes (**10.4-10.10**, Figure III-21) and studied the effect of the substituents on the ROP performances.¹⁹³ Compounds **10.5**, **10.6** and **10.9** do not initiate the polymerization, whereas all others initiated and controlled the ROP of LA. However, their activity was variable: **10.7** did not exhibit any activity below 100°C (and obtained 10% of conversion in 68 h at 100 °C), **10.4** led to 18% conv. in 24 h at 70 °C and **10.8** and **10.10** were the most effective (55% and 80%, respectively, in 35 h at 70°C). Chakraborty *et al.* highlighted that the commercially available copper bis(acetate) complex (**10.11**, Figure III-20) was an effective initiator for the controlled ROP of *rac*-LA and L-LA, either in bulk or in solution (H₂O or *i*PrOH).²⁶⁶ Schaper *et al.* reported a series of diketimate copper complexes (**10.12-10.14**, Figure III-20) that were very efficient for the controlled ROP of LA in DCM at room temperature in the presence of BnOH **10.14** (\bar{D} 1.07-1.53).²⁶⁷

Figure III-21: Mononuclear copper complexes applied to the ROP of LA.^{193, 261, 266-268}

Jin *et al.* reported a comparative study between the copper(II) complex **10.15** and its bimetallic copper-neodymium derivative (**10.16**, *Figure III-21-22*).²⁶⁸ The addition of the $\text{Nd}(\text{NO}_3)_3$ moiety increased the Lewis acidity of the copper centre, which influenced its ROP activity. Both complexes exhibited a good activity in bulk at 130°C and provided PLAs with narrow molar mass distributions (\mathcal{D} 1.11-1.38). For **10.15**, the higher molar weights were achieved at 24 h, after which the M_n values decreased, suggesting the occurrence of transesterification reactions. In contrast, complex **10.16** reached higher MW polymers, which could be attributed to the higher steric protection of the active copper centre. Moreover, the coordination of a water molecule in complex **10.15** has a detrimental effect on the polymerization, *i.e.* a deactivating effect, as shown by the low activity: 18.13 g/mol/h for complex **10.15** versus 259 g/mol/h for complex **10.16** after 12 h.

Schaper *et al.* reported the *N,N'*-dibenzyl diketimate copper isopropanolate ($\text{nacnac}^{\text{Bn}}\text{-CuOiPr}_2$) complexes **10.17** and **10.18**, which exhibited a very high activity for the ROP of *rac*-LA in DCM at room temperature, and the process followed first-order kinetics (*Figure III-21*).^{267, 269} It was assumed that the *N*-benzyl substituent on the ligand provides enough flexibility to allow monomer coordination, but has sufficient steric bulk to destabilize the LA-coordinated square planar intermediate and favour the insertion. In 2013, Huang *et al.* reported copper complexes based on benzotriazole phenoxide-type ligands (BTP) (**10.19**, **10.20**, **10.21**, *Figure III-22*).²⁷⁰ While complex **10.19** only gave 10% conversion after 6 h (toluene, 110°C in the presence of 9-AnOH (9-anthracenemethanol)), complexes **10.20** and **10.21** led to 92% and 93% conversion, respectively. The authors showed that the use of specific initiators, *i.e.* 2,2'-hexadecylimino)diethanol ($\text{NC}_{16}\text{H}_{33}/2\text{ROH}$), *tert*-butyl bis(2-hydroxyethyl)carbamate (BOC/2ROH) or triethanolamine (TEA/3ROH), allowed producing 2- or 3-arm polymeric materials. Shaver *et al.* reported the copper(II) complexes of tridentate N-based ligands (**10.22** and **10.23**, *Figure III-22*), which however acted as bidentate ligands because the five-member ring constrain disfavoured the pincer mode.²⁷¹ These complexes were shown to be very effective initiators for the ROP of LA in C_6D_6 at room temperature and with an excellent control (predictable M_n and narrow \mathcal{D}). In contrast to **10.22**, complex **10.23** presented an induction time of 60 min, which was attributed to the stronger coordination of the pyridine donor (vs. dimethyl amine) in the bridging alkoxide ligand.

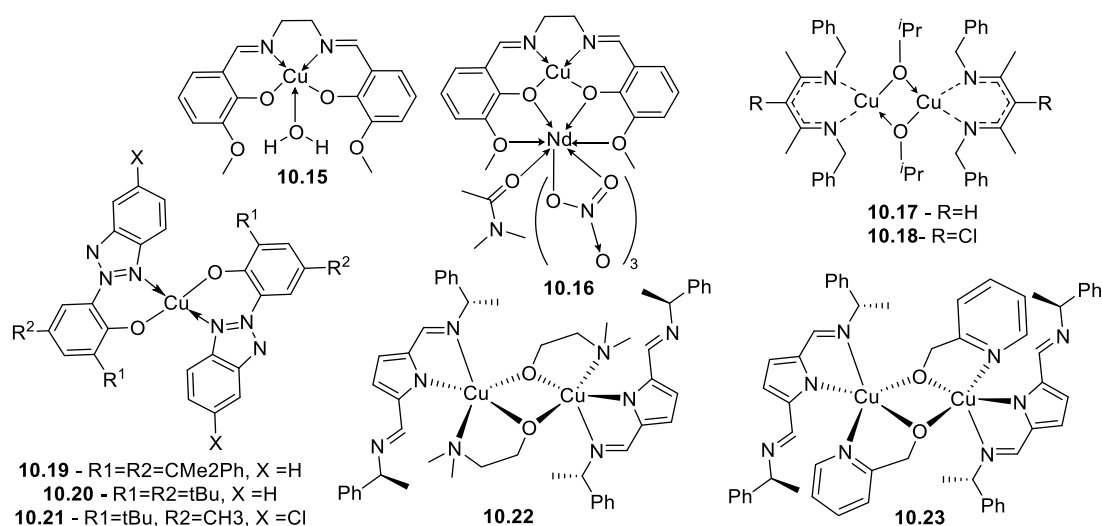


Figure III-22: Copper complexes applied to the ROP of LA. ^{193, 267, 269, 271}

In 2018, Schaper *et al.* investigated a large scope of copper complexes that can be divided in the following categories as a function of their supporting ligands: dinuclear β -diketimine (**10.24**), mononuclear β -aminoketone (**10.25**) and dinuclear iminophenol (**10.28A**, **10.29A**, **10.30A**, **10.31A**, **10.32A**, **10.33A**, **10.33B**, Figure III-23).^{272, 273} Complexes of types **A** and **B** integrate a dimethylaminomethoxy and pyridinemethoxy initiating group, respectively. While complex **10.24** initiates the ROP of LA at room temperature, leading to complete conversion in 5 h, the produced PLA samples exhibited lower M_n values than expected and quite broad dispersities (\mathcal{D} 1.7-2.6). Complex **10.25**, in contrast, is inactive at room temperature, but afforded a 24% conversion at 50 °C. The ROP mediated by **10.29A** follows clean first order kinetics without any notable induction period or catalyst decomposition, and the resulting well-defined PLA (exp. M_n vs. theo. M_n values, narrow \mathcal{D}) was atactic.²⁷³ Complexes **10.31B** and **10.34B** exhibited similar activity and improved again the control, with a better fit of the MWs. Complexes **10.33A** and **10.33B** revealed low efficiency and led to only 36% and 26% conversion, respectively, after 3 days of reaction. Complexes **10.26**, **10.27** and **10.35B** are inactive at room temperature.²⁷²

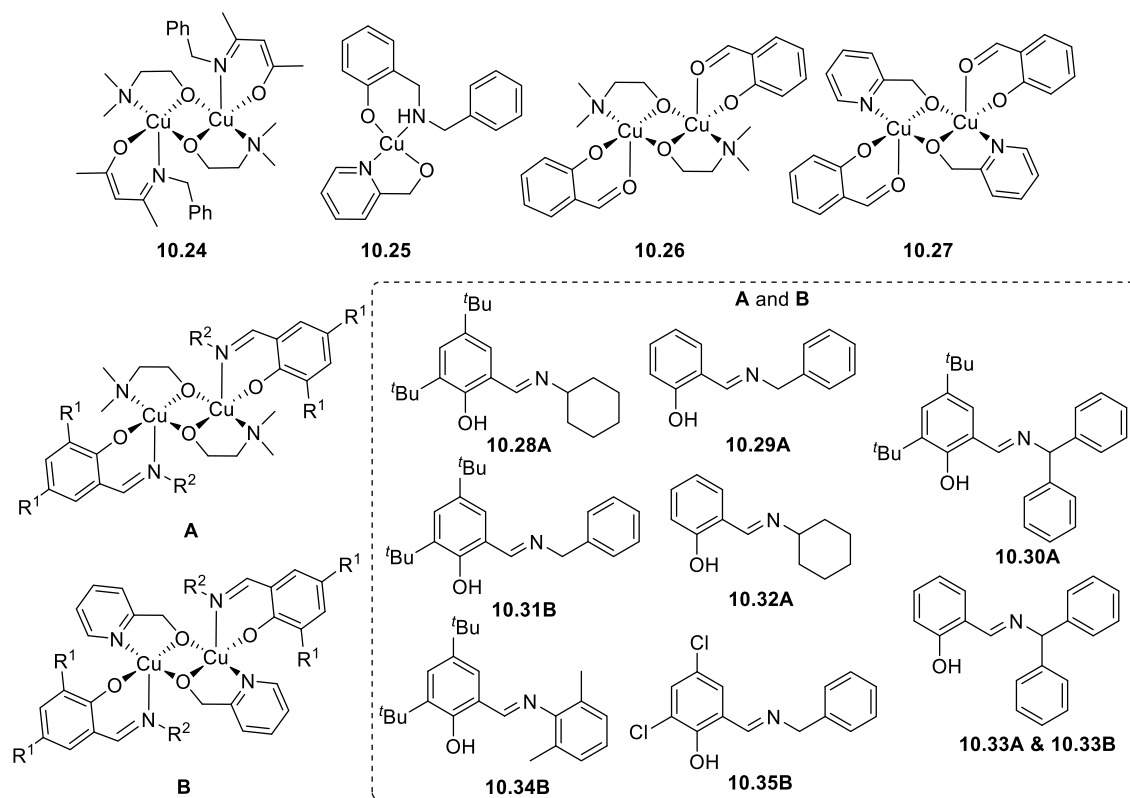


Figure III-23: Copper(II) complexes developed by Schaper and coll.^{272, 273}

The series of Cu^{II} complexes based on iminomethylpyridine (**9.36-9.41**, Figure III-24), reported by Lee, Neyab *et al.*²⁷⁴ and Roy *et al.*,²⁷⁵ were evaluated as initiators for the ROP of *rac*-LA and converted 100 equivalents of monomer in DCM at -25 °C within 2 h, after activation with MeLi (conversion of CuCl₂ to CuMe₂). The only data that changed within the series are the M_n et \bar{D} values of the recovered PLA samples. The increase of the N,N'- or N,O-linker length from two carbon atoms (**9.36**, **9.41**, respectively) to three carbon atoms (**9.37**, **9.40**, respectively), did not affect these properties, both complexes led to too high MWs and \bar{D} around 1.5. The best improvement for this system was the introduction of the morpholine (**9.39**) or piperidine (**9.38**) groups, which allowed to bring the M_n values closer to the theoretical ones and to lower the dispersities (\bar{D} 1.25-1.50).

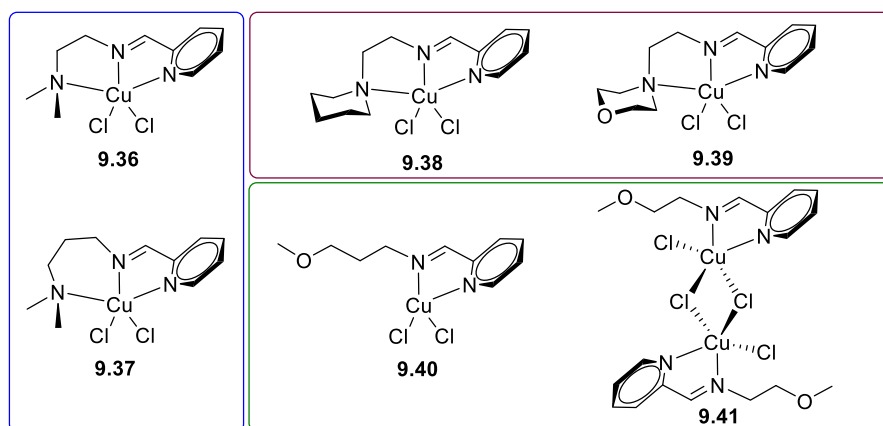


Figure III-24: Series of iminomethylpyridine copper (II) complexes.^{274, 275}

11. Conclusion

This section highlighted that a wide variety of transition metal complexes were applied to the ROP of cyclic esters. Their performances were highly dependent of the nature of the metal and the ligand scaffold. As mentioned at the beginning of this part, the mechanism of this technique is based on the polarity of the Mt-Z bond, which is the nucleophile responsible of the ring opening. Therefore, the most efficient systems are based on complexes containing an Mt-O bond, the latter being already present in the precursor or generated *in situ* by addition of an alcohol.

The present thesis work will focus on cobalt-based systems, although the complexes of this metal have not been the most studied nor the most efficient (for now). On the other hand, they appear as the most versatile to combine the ROP and OMRP mechanisms (see above). According to *Figure III-25*, we propose to use our know-how in cobalt coordination chemistry to design complexes able to produce an alkoxide radical (R_0^\bullet) to initiate an OMRP process (green square) and have a sufficiently nucleophilic $R_0\text{-Co}^{\text{III}}$ bond to initiate a ROP process (red square).

Addition of a system having such properties to the polymer chemist toolbox would allow the production of original materials, the properties of which remain to study. The incorporation of a biobased and/or biodegradable segment within a polyvinyl material could allow better recycling properties. Methods to access polyester-polyvinyl copolymers will be detailed in the following section.

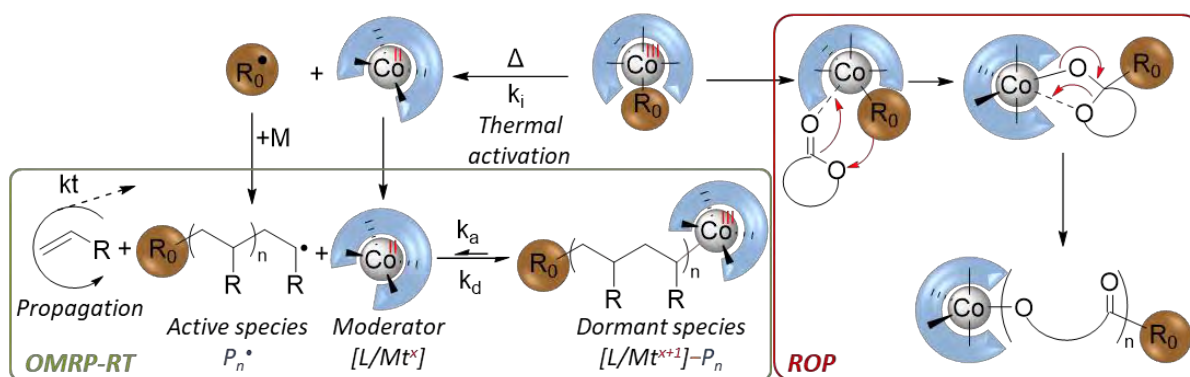


Figure III-25: ROP of cyclic ester using a metal-alkoxide catalyst (Red box).¹⁸⁷

IV. Original copolymers synthesis

The development of the synthesis methods affording block copolymers remains a contemporary challenge, due to the different reactivity of the monomers. However, the access to copolymers with a block or sequenced architecture is of great importance, because it allows to tune/improve the thermal and mechanical properties of materials. The first achievements in this field were the formation of copolymers made of monomers within the same category, *i.e.* LAM/LAM²⁷⁶ or MAM/MAM^{5, 277} in radical polymerization or lactone/lactone in ROP. Subsequently, the copolymerization of slightly different monomers was targeted, such LAM/MAM²⁷⁸ or cyclic ester/cyclic carbonate copolymers. Nowadays, researchers in the field are trying to combine different polymerization techniques to access new classes of polymers with new original properties. The major interest of this new challenges is to produce sustainable polymers, due to societal and environmental issues. In fact, the polymers of tomorrow should be derived from sustainable resources, should be highly efficient (for the targeted use), and should offer sustainable solutions after use.²⁷⁹

The present section will provide an overview of studies allowing the “coupling” of two polymerization techniques, following the strategies highlighted in *Figure IV-1*. One path consists in using a difunctional initiator designed with two different functions for the initiation of two different polymerizations either sequentially (**1**) or simultaneously (**2**). A second one features the use of a monofunctional initiator that can be chemically modified after the first block synthesis for chain extension (**3**).

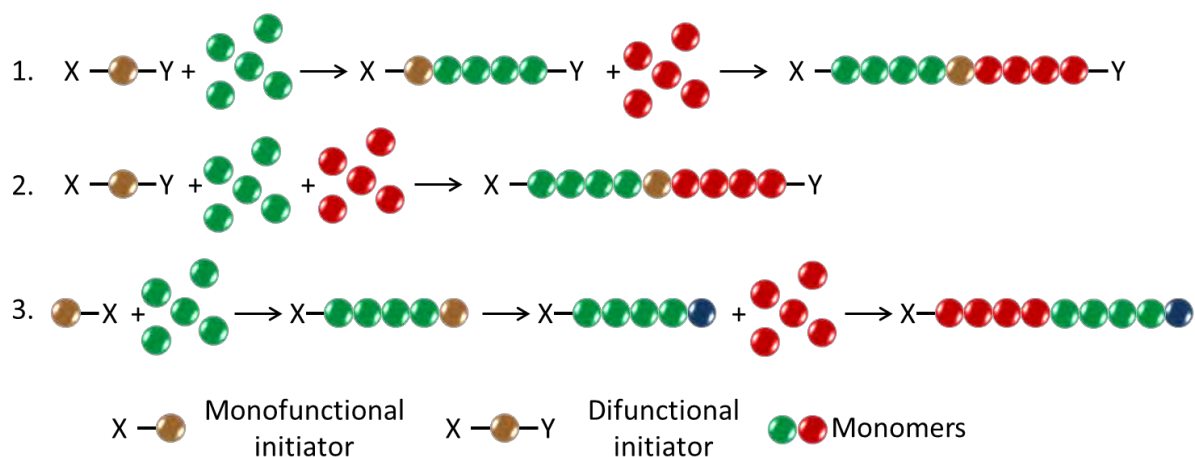


Figure IV-1: General strategies for the combination of CRP and ROP: (a) Two-step method using a difunctional initiator; (b) One-step method using a difunctional initiator (c) Multi-step method using a monofunctional initiator and transformation of the chain-end functionality.¹

1. Sequential polymerization based on difunctional initiators

As shown in *Figure IV-2*, difunctional initiators designed for a ROP/ATRP copolymerization were composed of an alcohol function at one end and a bromine atom at the other end. In the case of system I, reported by Sinturel *et al.* in 2011, the 2,2,2-tribromoethanol was used for the ATRP of styrene, catalysed by CuBr/HMTETA at 100°C, to afford a well-defined polymer (M_n 24 300 g mol⁻¹, D 1.30).²⁸⁰ The preservation of the alcohol function allowed, in a second time, to promote the ROP of LA in toluene at 80°C, leading to a PS-*b*-PLA block copolymer, as confirmed by a shift of the GPC signal to M_n 30 400 g mol⁻¹, and by the appearance of the characteristic PLA signals in the NMR spectrum of the polymer. A similar approach was reported based on a chloro-substituted initiator.²⁸¹

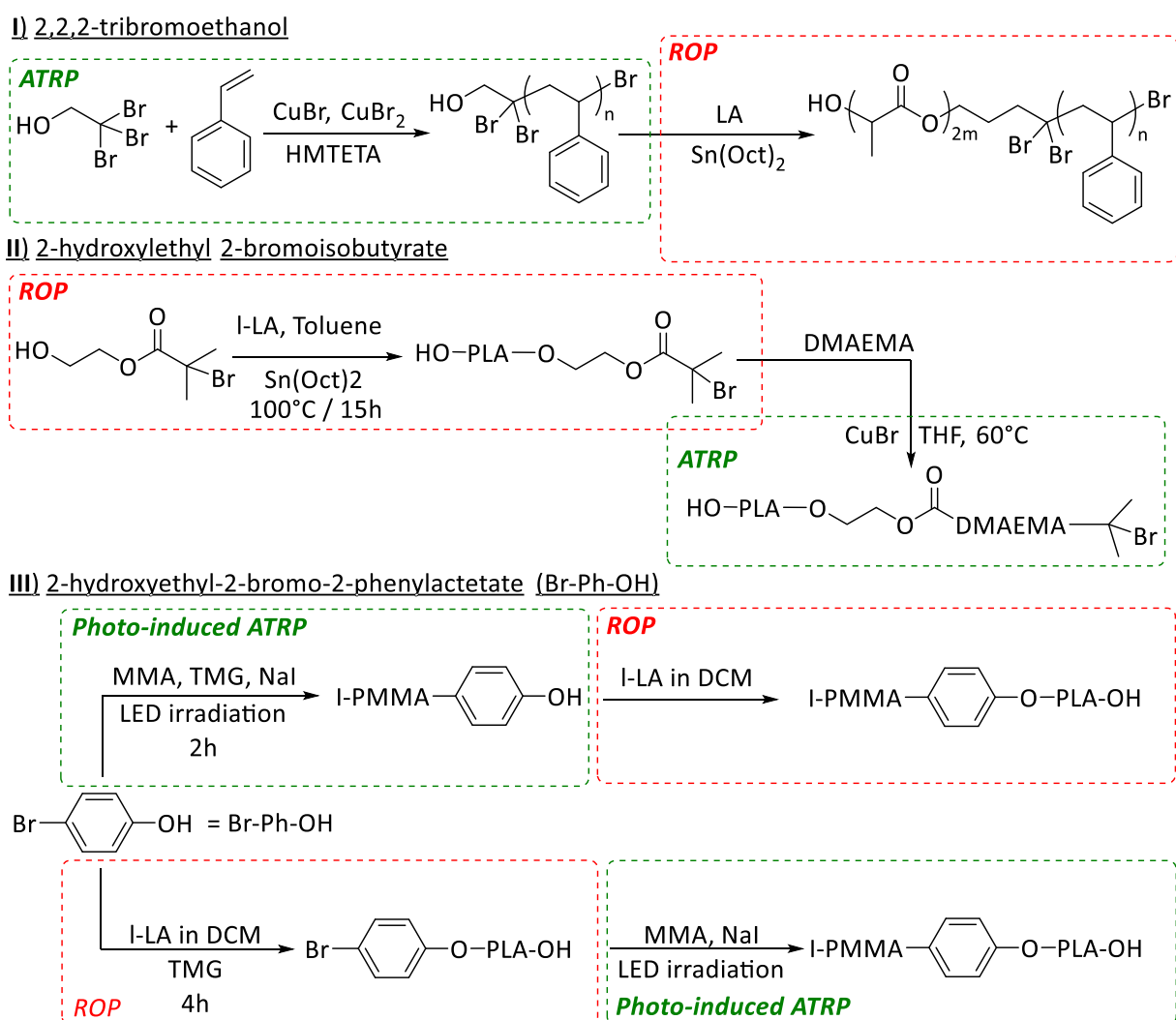


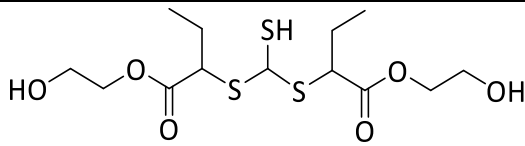
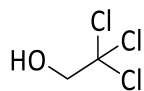
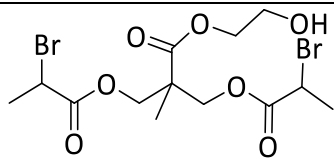
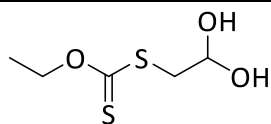
Figure IV-2: Sequential polymerization methods based on bifunctional initiators.^{280, 282-284}

A polymerization sequence in the opposite direction, from ROP to ATRP (II), was reported by Frey *et al.*²⁸⁵ and Bo, Ji *et al.*²⁸³, allowing to produce an amphiphilic PLA-*b*-PDMAEMA block copolymer with pH- and temperature responsive behaviour. In fact, at low pH, the PMAEMA

block becomes hydrophilic, resulting in the formation of micelles. Dispersities below 1.11 account for a good control of both polymerizations. For the third example (system III), reported in 2020 by Lie *et al.*,²⁸² the ATRP was photoinitiated with white LED irradiation and led to an iodine-mediated photo-ATRP, while the alcohol function allowed to initiate the ROP of LA. Thus, both the ROP to ATRP and ATRP to ROP transitions were shown to be possible.

Based on the same principle, initiators with an increased number of functionalities were developed to access more complex polymeric architectures, as shown in *Table IV-1*.

Table IV-1: Other initiators with several functionalities for a sequential ROP-CRP process.

Entry	Multifunctional initiators	Functionalities	ref
1		1 RAFT 2 ROP	286 287
2		1 ROP 3 ATRP	281
3		2 ATRP 1 ROP	3
4		1 RAFT 2 ROP	288

2. Difunctional initiators for one-pot copolymerizations

One-pot syntheses with difunctional initiators present the advantage of producing copolymers in one step, instead of requiring preliminary purification of the first polymer block before chain extension. The initiators presented below simultaneously mediate ROP and a controlled radical polymerization such as NMP, RAFT or ATRP (*Figure IV-3*).

The first example of original diblock copolymer produced via the simultaneous occurrence of two polymerization mechanisms was reported by Jerome, Hawker, Hedrick *et al.*² in 1998. They applied a difunctional alcohol/nitroxide initiator for simultaneous polymerization by ROP and NMP (*Figure IV-3a*). Later, a difunctional alcohol/alkyl halide initiator was applied to concurrent ROP and ATRP (*Figure IV-3b*).^{2, 289} Another example of ROP/ATRP simultaneous polymerization, was reported by Yilmaz, Yagci *et al.*²⁹⁰ The authors used 2-hydroxyethyl 2-bromo-2-methylpropanoate (HBM) as dual initiator, perylene as ATRP photocatalyst and phosphazene base (P₁-*t*-Bu) as ROP catalyst (*Figure IV-3c*). Technically, all these reactants were mixed together in THF and the polymerizations proceeded. Several combinations were tested:

St/CL, NIPAM/CL, BuA/CL, MMA/LA, and monomodal GPC traces were observed with dispersities ranging from 1.21 (for PS-*b*-PCL) to 1.67 (for PBuA-*b*-PCL).

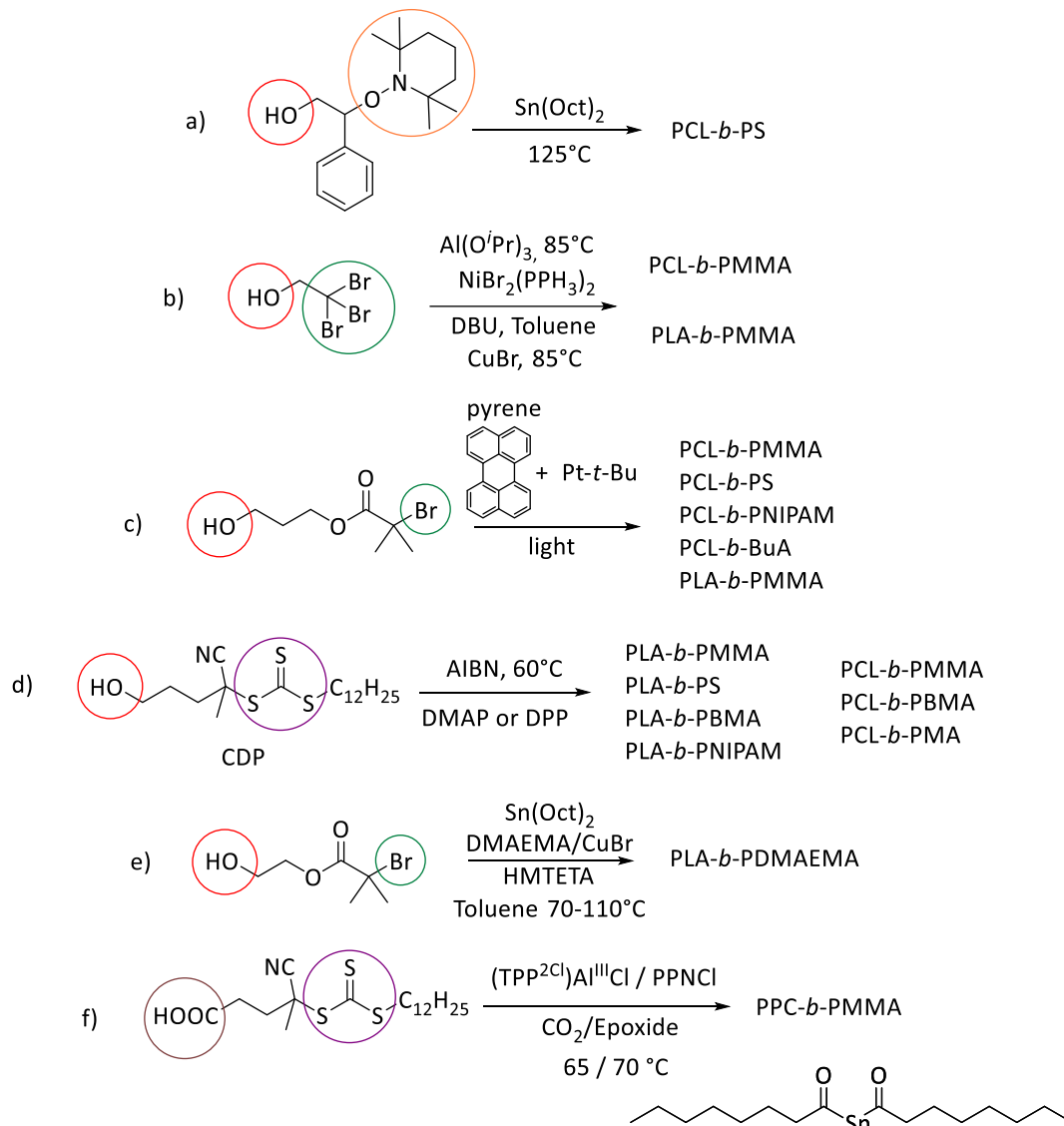


Figure IV-3: One step diblock syntheses using difunctional initiators.

Colour coding for initiating group/polymerization technique: ROP, ATRP, NMP, RAFT and RoCOP - CO₂/epoxides.

In 2012, Youk *et al.*²⁹¹ used the 4-cyano-4-(dodecylsulfanylthio carbonyl)sulfanylpentano (CDP) initiator to produce several well-defined block copolymers by ROP/RAFT (Figure IV-3d). CDP presents a trithiocarbonate function for RAFT polymerization of vinyl monomers, such as St, MA, BMA or NIPAM, and an alcohol function for the ROP of cyclic monomers, such as VL, CL, TMC or LA, with 4-dimethylamino pyridine (DMAP) as catalyst for LA and diphenyl phosphate (DPP) for the other. The difunctional initiator presented by Detrembleur, Baziun *et al.*²⁹² (Figure IV-3e) for the one pot and simultaneous copolymerization was an evolution of the system presented on Figure IV-2. More recently, Wang, Xie *et al.*²⁹³ applied this strategy for combining RAFT and ROCOP (CO₂/epoxides) polymerizations, with various vinyl and

epoxides monomers such as MMA, styrene, benzyl methacrylate, propylene oxide (PO) and cyclohexene oxide (CHO), respectively (Figure IV-3f). The authors highlighted the relatively good results, because after 8 h reaction at 65°C, the experimental M_n values were in good agreement with the theoretical ones and narrow molar mass distributions were observed (\mathcal{D} 1.09-1.14).

In 2016, Boyer *et al.*²⁹⁴ described a one-pot copolymer synthesis by coupling ROP and RAFT polymerizations. However, this system worked by photoswitches, which were triggered by specific wavelengths irradiations (Figure IV-4). The photo-ROP polymerization is mediated by a photochromic molecule, here merocyanine-based photoacid (PAH). The blue light ($\lambda = 428$ nm) induced intramolecular cyclisation and produce a strong acid (PA⁻), which is able to catalyse the ROP of the cyclic ester (Figure IV-4a). The second compound, zinc tetraphenylporphyrin (ZnTPP), plays the role of catalyst for photo-induced electron/energy transfer RAFT (PET-RAFT) and works under red light at 635 nm (Figure IV-4b). As shown in the conversion vs. time plot (Figure IV-4c) each polymerization is switched on at a different wavelength, allowing the synthesis of a block copolymer. With this technique, a PVL-*b*-PMA block copolymer with $M_n = 4610$ g mol⁻¹ and $\mathcal{D} = 1.15$ was obtained (Figure IV-4d).

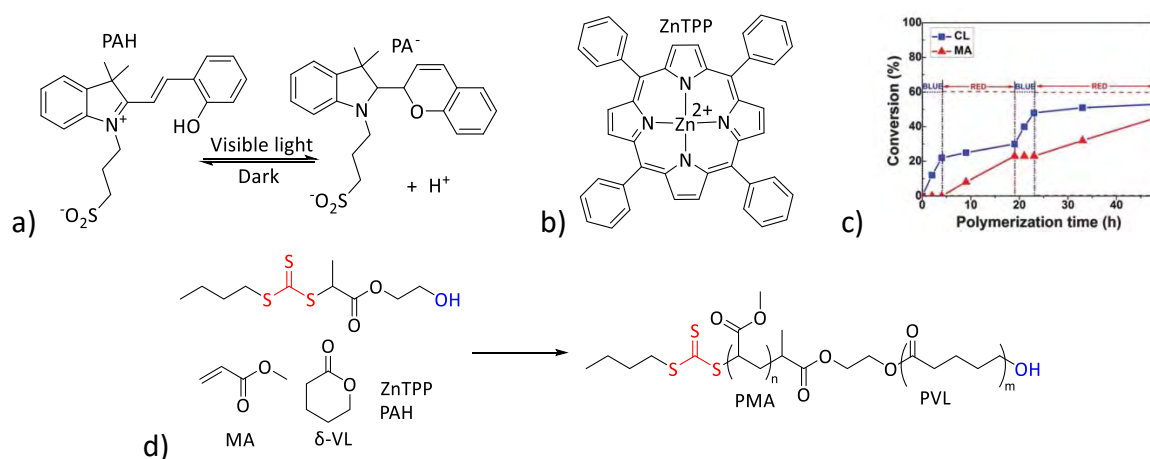


Figure IV-4: a) PAH, b) ZnTPP, c) Kinetics and d) copolymerization reaction mediated by the system of Boyer *et coll.*²⁹⁴

3. Multistep copolymer synthesis based on a monofunctional initiator

The last strategy to produce original diblock copolymers *via* ROP and CRP is based on the use of a monofunctional initiator, which is further chemically modified to be able to initiate another polymerization type and produce the second block of the polymerization. This strategy corresponds to pathway 3 presented in Figure IV-1.

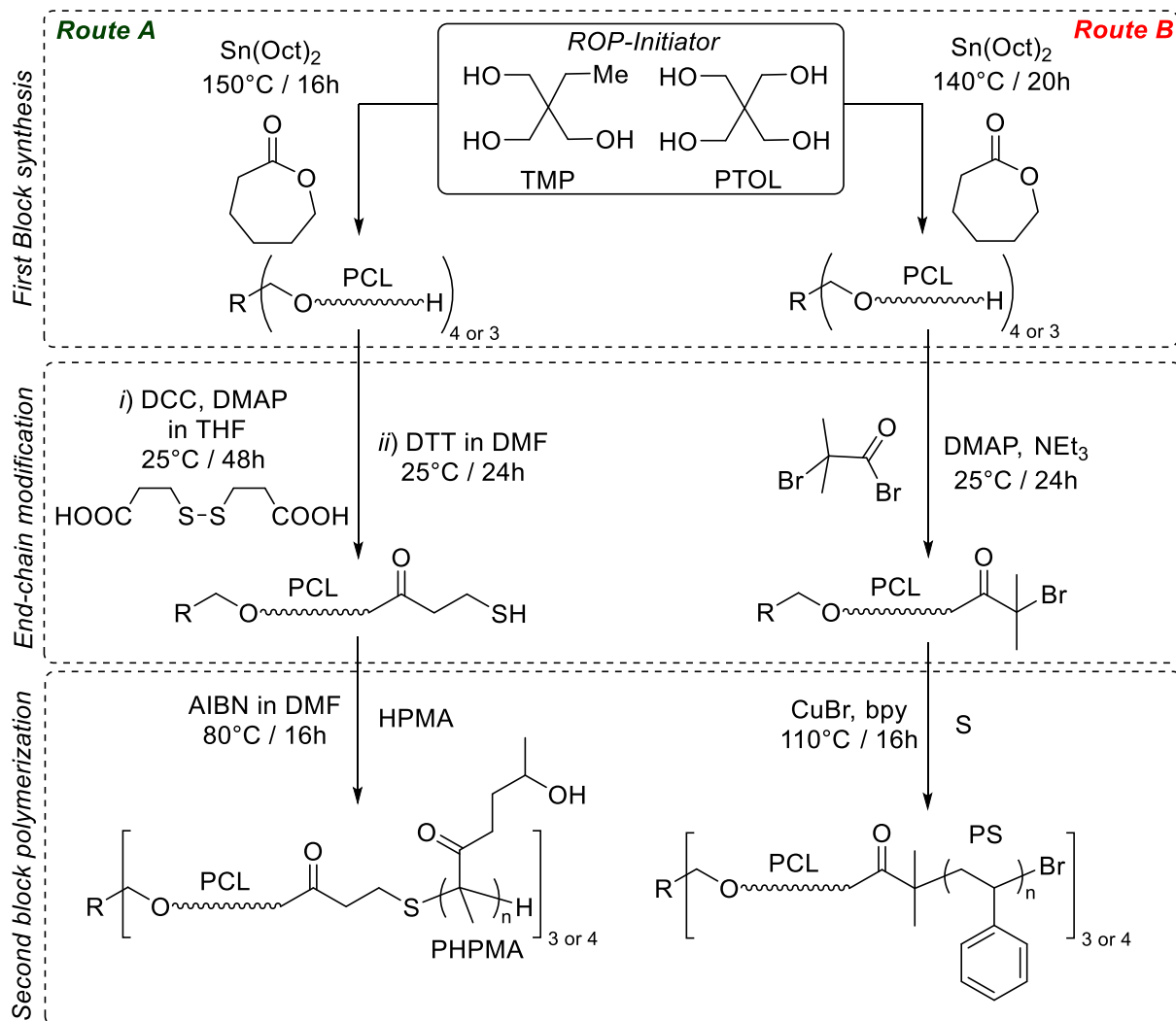


Figure IV-5: Multistep synthesis of PCL-*b*-PHPMA (route A) and PCL-*b*-PS (route B) star copolymers.

In 2002, Leroux and co-workers reported the *Route A* depicted in *Figure IV-5 (left)*.²⁹⁵ The first block was produced by the $\text{Sn}(\text{Oct})_2$ -catalyzed ROP of CL and the chain extension by RAFT of *N*-((2-hydroxypropyl)methacrylamide) (HPMA) as monomer. The ROP was carried out at 150 °C over 16 h using trimethylolpropane (TMP) or pentaerythritol (PTOL) as polyfunctional initiators, producing PCL 3- or 4-arm stars, respectively, with a dispersity around 1.35. Afterward, the hydroxyl group of the PCL chains was modified in two steps. First, by dicyclohexyl carbodiimide (DCC)-mediated coupling of the hydroxyl end functions with 3,3'-dithiobis(propionic acid) (DTPA). Then, dithiothreitol (DTT) treatment allowed reducing the disulfide bonds to thiols as chain-end functions. Thus, the polymer chains could be reactivated to mediate the radical polymerization of HPMA. This synthetic route finally produced star PCL-*b*-PHPMA copolymers, which exhibited molar masses of ca. 27 000 g mol⁻¹ and dispersities between 1.65 and 1.75.

The system presented in *Route B* of *Figure IV-5 (right)* was reported by Wang, Xiayu *et al.* in 2005.²⁹⁶ It is based on the same principles as that presented above, except that the treatment of the PCL first blocks with 2-bromoisobutyryl bromide led to bromine-

functionalized chain-ends, which could be further chain-extended by the Cu-mediated ATRP of styrene (CuBr/Bpy, 110°C, 16 h). The obtained copolymers revealed relatively narrow dispersities ($\mathcal{D} \geq 1.30$) and M_n values close to the theoretical ones.

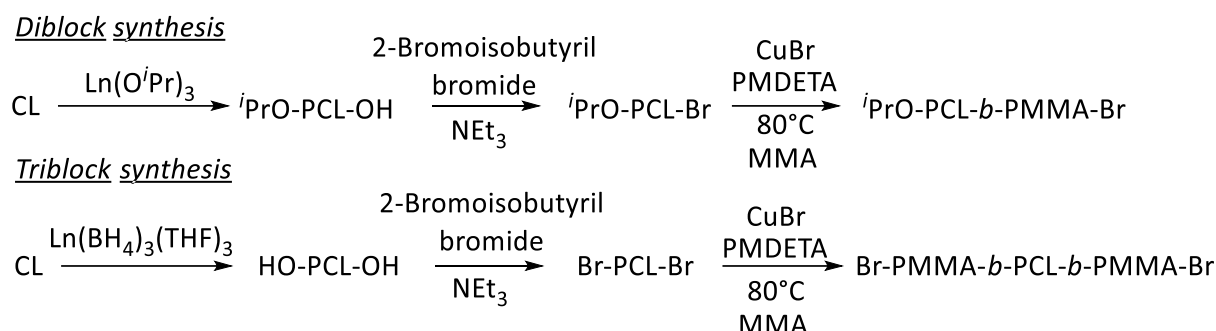


Figure IV-6: Syntheses of di- and tri-block copolymers by successive ROP and ATRP.²⁹⁷

In 2007, Guillaume *et al.* reported a method to produce di- and tri-block copolymers (AB and ABA) by successive well-controlled ROP and ATRP processes.²⁹⁷ As shown in Figure IV-6, the ROP of CL was mediated by $\text{Ln}(\text{O}^i\text{Pr})_3$ and provided a ${}^i\text{PrO-PCL-OH}$ macroinitiator. The alcohol function was modified with 2-bromoisobutyryl bromide to obtain a bromine-functionalized chain end suitable for the Cu-catalysed ATRP of MMA. Replacing $\text{Ln}(\text{O}^i\text{Pr})_3$ by $\text{Ln}(\text{BH}_4)_3(\text{THF})_3$ to modify the PCL chain-end with two alcohol function allowed to access a triblock ABA copolymer using the same strategy.

Wang, Poli *et al.* described the switch of polymerization mechanisms from OMRP to ROCoP and *vice versa* by reactions with O_2 or CO , respectively, as shown in Figure IV-7.²⁹⁸⁻³⁰⁰ For the OMRP to ROCoP switch, the Co-PVAc macroinitiator was synthesized following a classical Co-mediated OMRP of VAc using AIBN as thermal initiator. The macroinitiator was modified to be compatible to ROCoP by reaction with O_2 , leading to the insertion of one O atom into the Co-C_{PVAc} bond, *i.e.* affording a Co-O_{PVAc} macroinitiator. Then, the resulting cobalt(III)alkoxide species readily mediated the ROCoP of epoxides and CO_2 .²⁹⁸ For the reverse switch, the Co-O_{polycarbonate} chain-end was transformed into a Co-C(O)-O_{polycarbonate} bond by insertion of CO , which was suitable for the photoinitiation of the OMRP of various acrylates.²⁹⁹

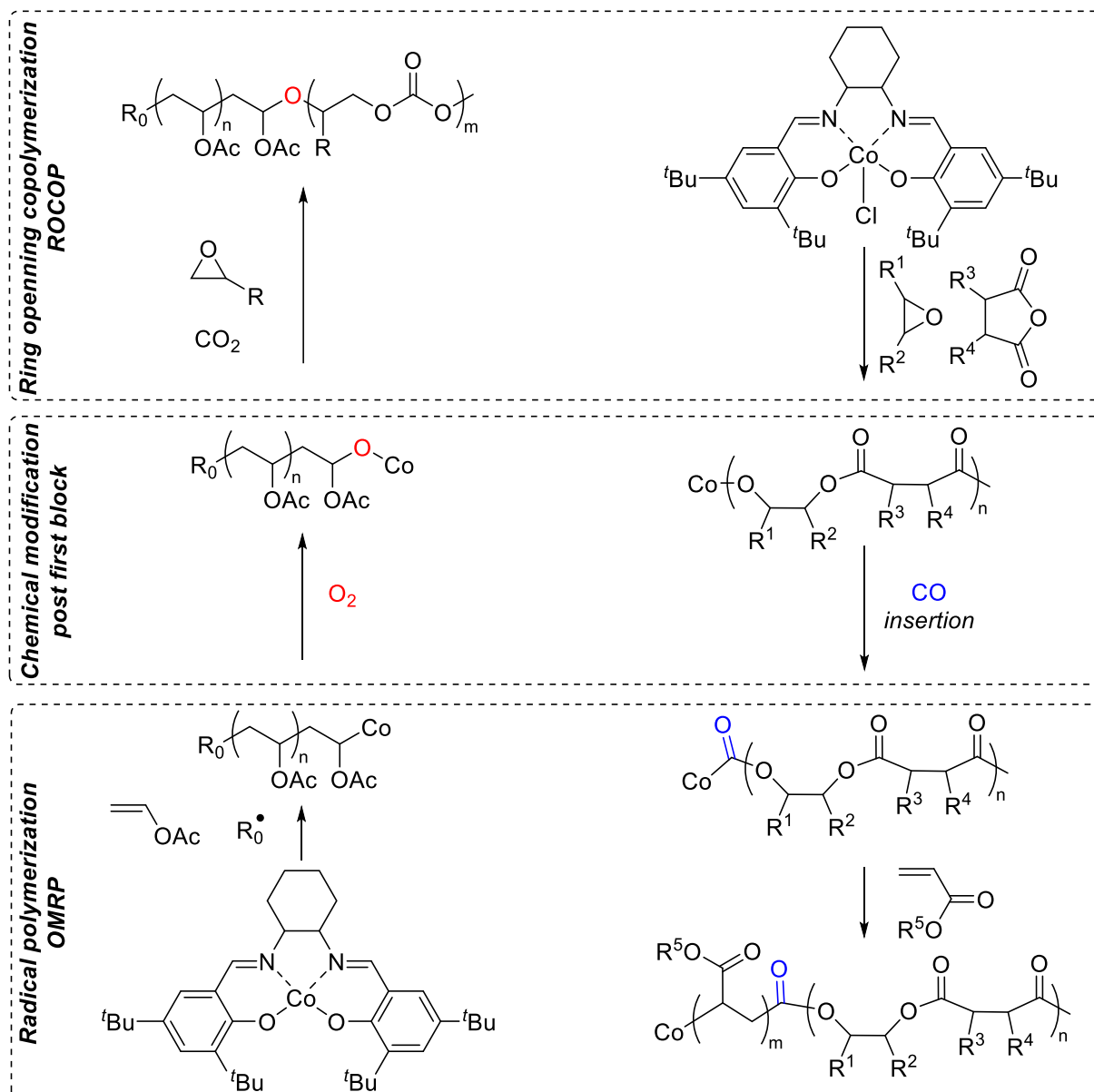


Figure IV-7: Polymerization switch from OMRP to ROCOP (left) and from ROCOP to OMRP (right).

More recently, Harth *et al.* reported a switch from an olefin polymerization by the coordination/insertion mechanism, using the Pd complex depicted in Figure IV-8 (left), to radical polymerization by photo-induced homolytic cleavage of the Pd–C_{polymer} bond in the dormant polyolefin chain obtained after insertion of one acrylate monomer.³⁰¹ While the polymerization of ethylene and 1-hexene were well-controlled (\bar{D} 1.05-1.17), the chain extension by radical polymerization of (meth)acrylates (MA, EA, n-BA or MMA) afforded polymeric materials with \bar{D} values ranging from 1.10 (MA) to 2.34 (n-BA). All of these copolymers were characterized by DOSY, MALDI-TOF and NMR analyses.

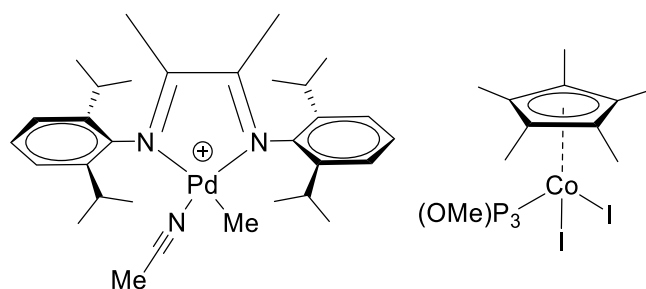


Figure IV-8: Recent examples of dual polymerization based on palladium³⁰¹ and cobalt³⁰² complexes.

In the same spirit, Nozaki *et al.*³⁰² reported that the system based on $(\text{Co}^{\text{III}}(\eta^5\text{-C}_5\text{H}_5)\text{P}(\text{OMe})_3\text{I}_2)$ and isobutyl modified methylaluminoxane (MMAO) could realize a self-switching copolymerization of MA by OMRP and ethylene by coordination/insertion polymerization, based on a thorough NMR study (1D, 2D, DOSY ...), which also allowed to characterize the one-pot produced multiblock PMA-*b*-PE-*b*-PMA-*b*-PE-*b*-PMA copolymers.³⁰³

4. Conclusion

The studies presented in this section, dealing with the synthesis of original di- or tri-block copolymers obtained by combination of radical polymerization (ATRP, RAFT, OMRP...) and by ring opening (co)polymerization (ROP, ROCoP) (or coordination/insertion polymerization), highlight the interest of the community in the development of such polymeric materials and in the methods to access them. However, most of these systems require a chemical modification of the macroinitiator obtained after the polymerization of a first monomer (*via* a first technique), to make the chain-end suitable for reactivation by a second technique and allow the polymerization of a second monomer. To the best to our knowledge, the only example of self-switching catalyst is the example of Nozaki (which still requires a co-catalyst). However, the switch is only possible after complete conversion (acrylate) or removal (ethylene) of the residual first monomer, to allow the polymerization of the second one, which limits the switch to the formation of block copolymers. A “real” self-switching catalyst, which does not require a co-catalyst and could work in a mixture of monomers, is still missing. Such compound would allow the synthesis of statistical or alternating copolymers that are not accessible to date. The development of such compounds is the main objective of the present thesis project.

V. References

1. Jakubowski, W.; Matyjaszewski, K., New Segmented Copolymers by Combination of Atom Transfer Radical Polymerization and Ring Opening Polymerization. *Macromolecular Symposia* **2006**, *240* (1), 213-223.
2. David Mecerreyes, G. M., Philippe Dubois, Robert Jerome*, James L. Hedrick,* Craig J. Hawker,* Eva E. Malmström, and Mikael Trollsas, Simultaneous Dual Living Polymerizations: A Novel One-Step Approach to Block and Graft Copolymers. *Angew. Chem. Int. Ed.* **1998**, *37*, 1275-1276.
3. Erdogan, T.; Ozyurek, Z.; Hizal, G.; Tunca, U., Facile synthesis of AB₂-type miktoarm star polymers through the combination of atom transfer radical polymerization and ring-opening polymerization. *Journal of Polymer Science Part A: Polymer Chemistry* **2004**, *42* (10), 2313-2320.
4. Jenkins, A. D.; Jones, R. G.; Moad, G., Terminology for reversible-deactivation radical polymerization previously called "controlled" radical or "living" radical polymerization (IUPAC Recommendations 2010). *Pure and Applied Chemistry* **2009**, *82* (2), 483-491.
5. Moad, G., Living and controlled RAP (reversible activation polymerization) on the way to RDRP (reversible deactivation radical polymerization). No chance for immortality. A mini-review on the terminological development of RDRP. *Polymer International* **2022**.
6. Charles H. J. Johnson, G. M., David H. Solomon, Thomas H. Spuvling and Davren J. veaving, The Application of Supercomputers in Modelling Chemical Reaction Kinetics: Kinetic Simulation of 'Quasi-Living' Radical Polymerization. *Aust. J. Chem.*, **1990**, *43*, 1215-30.
7. Moad, G.; Rizzardo, E., Alkoxyamine-Initiated Living Radical Polymerization: Factors Affecting Alkoxyamine Homolysis Rates. *Macromolecules* **2002**, *28* (26), 8722-8728.
8. Roshan T. A. Mayadunne, J. J., Graeme Moad and Ezio Rizzardo, Living Free Radical Polymerization with Reversible Addition-Fragmentation Chain Transfer (RAFT Polymerization): Approaches to Star Polymers. *Macromolecules* **2003**, *36*, 1505-1513.
9. Atsushi Goto, K. S., Yoshinobu Tsujii, Takeshi Fukuda,* , Graeme Moad, Ezio Rizzardo, and San H. Thang, Mechanism and Kinetics of RAFT-Based Living Radical Polymerizations of Styrene and Methyl Methacrylate. *Macromolecules* **2001**, *34*, 402-408.
10. Roshan T. A. Mayadunne, E. R., * John Chiefari, Yen Kwong Chong, Graeme Moad, and San H. Thang, Living Radical Polymerization with Reversible Addition-Fragmentation Chain Transfer (RAFT Polymerization) Using Dithiocarbamates as Chain Transfer Agents. *Macromolecules* **1999**, *32*, 6977-6980.
11. David G. Hawthorne, G. M., * Ezio Rizzardo,* and San H. Thang*, Living Radical Polymerization with Reversible Addition-Fragmentation Chain Transfer (RAFT): Direct ESR Observation of Intermediate Radicals. *Macromolecules* **1999**, *32*, 5457-5459.
12. Nothling, M. D.; Fu, Q.; Reyhani, A.; Allison-Logan, S.; Jung, K.; Zhu, J.; Kamigaito, M.; Boyer, C.; Qiao, G. G., Progress and Perspectives Beyond Traditional RAFT Polymerization. *Adv Sci (Weinh)* **2020**, *7* (20), 2001656.
13. Fliedel, C.; Poli, R., Homolytically weak metal-carbon bonds make robust controlled radical polymerizations systems for "less-activated monomers". *Journal of Organometallic Chemistry* **2019**, *880*, 241-252.
14. Fliedel, C.; Dagorne, S.; Le Roux, E., Metal Complexes as Catalysts/Moderators for Polymerization Reactions. In *Comprehensive Coordination Chemistry III*, 2021; pp 410-464.
15. Asandei, A. D.; Moran, I. W., TiCp₂Cl-catalyzed living radical polymerization of styrene initiated by oxirane radical ring opening. *Journal of the American Chemical Society* **2004**, *126* (49), 15932-15933.
16. Asandei, A. D.; Moran, I. W.; Castro, M. A., Ti(III)-catalyzed living radical polymerization of styrene initiated by benzoyl peroxide. *Polym. Prepr. (Am. Chem. Soc., Div. Polym. Chem.)* **2003**, *44* (1), 829-830.
17. Asandei, A. D.; Chen, Y., Ti(III)Cp₂Cl catalyzed living radical polymerization of styrene initiated from benzaldehydes. *Polym. Prepr. (Am. Chem. Soc., Div. Polym. Chem.)* **2004**, *45* (2), 766-767.

18. Asandei, A. D.; Moran, I. W., The ligand effect in Ti-mediated living radical styrene polymerizations initiated by epoxide radical ring opening. 2. Scorpionate and half-sandwich LTiCl_3 complexes. *Journal of Polymer Science, Part A: Polymer Chemistry* **2005**, *43* (23), 6039-6047.
19. Asandei, A. D.; Moran, I. W., Ligand effect in titanium-mediated living radical styrene polymerizations initiated by epoxide radical ring opening. III. Substituted sandwich metallocenes. *Journal of Polymer Science, Part A: Polymer Chemistry* **2006**, *44* (3), 1060-1070.
20. Asandei, A. D.; Moran, I. W.; Saha, G.; Chen, Y., Titanium-mediated living radical styrene polymerizations. VI. Cp_2TiCl -catalyzed initiation by epoxide radical ring opening: effect of the reducing agents, temperature, and titanium/epoxide and titanium/zinc ratios. *Journal of Polymer Science, Part A: Polymer Chemistry* **2006**, *44* (7), 2156-2165.
21. Asandei, A. D.; Saha, G., Peroxide initiated, Cp_2TiCl -catalyzed living radical polymerization of styrene. *PMSE Preprints* **2006**, *94*, 480-481.
22. Asandei, A. D.; Saha, G., Cp_2TiCl -catalyzed living radical polymerization of styrene initiated from peroxides. *Journal of Polymer Science, Part A: Polymer Chemistry* **2006**, *44* (3), 1106-1116.
23. Asandei, A. D.; Moran, I. W.; Saha, G.; Chen, Y., Ti-catalyzed living radical polymerization of styrene initiated by epoxide radical ring opening. *ACS Symp. Ser.* **2006**, *944* (Controlled/Living Radical Polymerization), 125-139.
24. Asandei, A. D.; Saha, G., Cp_2TiCl -catalyzed styrene living radical polymerization initiated from 4-methoxybenzenesulfonyl chloride. *Polym. Prepr. (Am. Chem. Soc., Div. Polym. Chem.)* **2007**, *48* (2), 272-273.
25. Asandei, A. D.; Chen, Y., Cp_2TiCl -catalyzed styrene living radical polymerizations initiated from (1-bromoethyl)benzene. *PMSE Preprints* **2007**, *97*, 450-451.
26. Asandei, A. D.; Chen, Y.; Moran, I. W.; Saha, G., Similarities and differences of epoxide, aldehyde and peroxide initiators for Cp_2TiCl -catalyzed styrene living radical polymerizations. *J. Organomet. Chem.* **2007**, *692* (15), 3174-3182.
27. Asandei, A. D.; Chen, Y.; Simpson, C.; Gilbert, M.; Moran, I. W., Halide effects in the Cp_2TiCl -catalyzed styrene living radical polymerization initiated from α,α' -dihalo-p-xylene. *Polym. Prepr. (Am. Chem. Soc., Div. Polym. Chem.)* **2008**, *49* (1), 489-490.
28. Asandei, A. D.; Chen, Y.; Saha, G.; Moran, I. W., Cp_2TiCl -catalyzed radical chemistry: living styrene polymerizations from epoxides, aldehydes, halides, and peroxides. *Tetrahedron* **2008**, *64* (52), 11831-11838.
29. Asandei, A. D.; Chen, Y.; Adebolu, O., Inactivated halide initiators for Cp_2TiCl -catalyzed styrene living radical polymerization: 1,10-dibromodecane. *PMSE Preprints* **2008**, *98*, 370-371.
30. Asandei, A. D.; Yu, H. S.; Adebolu, O., Butadiene controlled radical polymerizations from aldehydes and Cp_2TiCl_2 . *PMSE Preprints* **2009**, *101*, 1377-1378.
31. Asandei, A. D.; Yu, H. S.; Simpson, C. P., Controlled radical butadiene polymerization with Cp_2TiCl_2 and benzyl halides. *PMSE Preprints* **2009**, *101*, 1379-1380.
32. Asandei, A. D.; Yu, H. S., Cp_2TiCl -mediated radical polymerization of butadiene initiated by epoxide radical ring opening. *Polym. Prepr. (Am. Chem. Soc., Div. Polym. Chem.)* **2009**, *50* (2), 450-451.
33. Asandei, A. D.; Yu, H. S.; Simpson, C. P., Butadiene initiation with late and early transition metals from activated halides. *PMSE Preprints* **2010**, *103*, 511-512.
34. Asandei, A. D.; Yu, H. S.; Simpson, C. P., Activated halide redox initiation of butadiene with late and early transition metals. *PMSE Preprints* **2010**, *102*, 68-69.
35. Asandei, A. D.; Simpson, C. P.; Yu, H. S., Cp_2TiCl -catalyzed controlled radical polymerization of isoprene initiated from epoxides, aldehydes and halides. *Polym. Prepr. (Am. Chem. Soc., Div. Polym. Chem.)* **2008**, *49* (2), 73-74.
36. Asandei, A. D.; Simpson, C. P.; Yu, H. S.; Adebolu, O. I.; Saha, G.; Chen, Y., Cp_2TiCl -Mediated Controlled Radical Polymerization of Isoprene Initiated by Epoxide Radical Ring Opening. *ACS Symp. Ser.* **2009**, *1024*, 149-163.

37. Asandei, A. D.; Moran, I. W., The ligand effect in Ti-mediated living radical styrene polymerizations initiated by epoxide radical ring opening. 1. Alkoxide and bisketonate Ti complexes. *Journal of Polymer Science Part a-Polymer Chemistry* **2005**, *43* (23), 6028-6038.
38. Asandei, A. D.; Moran, I. W.; Saha, G.; Chen, Y. H., Titanium-mediated living radical styrene polymerizations. V. Cp₂TiCl-catalyzed initiation by epoxide radical ring opening: Effect of solvents and additives. *Journal of Polymer Science Part a-Polymer Chemistry* **2006**, *44* (6), 2015-2026.
39. Asandei, A. D.; Chen, Y., New initiators for living radical polymerization: Cp₂TiCl-catalyzed set reduction of aldehydes. *Polym. Prepr. (Am. Chem. Soc., Div. Polym. Chem.)* **2007**, *48* (1), 232-233.
40. Asandei, A.; Saha, G., Cp₂TiCl₂/Zn-Catalyzed Living Radical Polymerization of Styrene Initiated from Benzoyl Peroxide. *Polym. Mater.: Sci. Eng.* **2005**, *93*, 470-471.
41. Asandei, A. D.; Moran, I. W., Alkoxide and bisketonate titanium catalysts for the living radical polymerization of styrene initiated by epoxide radical ring opening. *Polym. Prepr. (Am. Chem. Soc., Div. Polym. Chem.)* **2005**, *46* (2), 136-137.
42. Coward, D. L.; Lake, B. R. M.; Poli, R.; Shaver, M. P., Radically initiated group transfer polymerization of methacrylates by titanium amino-phenolate complexes. *Macromolecules (Washington, DC, U. S.)* **2019**, *52*, 3252-3256.
43. Grishin, D.; Semyonycheva, L.; Telegina, E.; Smirnov, A.; Nevodchikov, V., Dicyclopentadienyl complexes of titanium, niobium, and tungsten in the controlled synthesis of poly(methyl methacrylate). *RUSSIAN CHEMICAL BULLETIN* **2003**, *52* (2), 505-507.
44. Grishin, D. F.; Ignatov, S. K.; Shchepalov, A. A.; Razuvaev, A. G., Mechanism of the controlled radical polymerization of styrene and methyl methacrylate in the presence of dicyclopentadienyltitanium dichloride. *Applied Organometallic Chemistry* **2004**, *18* (6), 271-276.
45. Ma, L. F.; Liu, W. J.; Sheng, Y. P.; Huang, Q. G.; Yang, W. T., Synthesis of Well-Defined Star-Shaped Organosiloxane-Functionalized Polymethylmethacrylate Promoted by Epoxide-Derived Titanocene Alkoxides via Radical Polymerization. *Journal of Applied Polymer Science* **2011**, *120* (3), 1652-1658.
46. Asandei, A. D.; Simpson, C. P.; Adebolu, O.; Chen, Y., Evaluation of epoxides, aldehydes halides and peroxides as initiators for the Cp₂TiCl₂-mediated radical polymerization of vinylidene fluoride. *Polym. Prepr. (Am. Chem. Soc., Div. Polym. Chem.)* **2011**, *52* (2), 554-555.
47. Asandei, A. D.; Moran, I. W.; Saha, G.; Chen, Y., Effect of Temperature and Stoichiometry in the Cp₂TiCl-Catalyzed Living Radical Polymerization of Styrene Initiated by Epoxide Radical Ring Opening. *Polym. Mater.: Sci. Eng.* **2006**, *94*, 597-598.
48. Asandei, A. D.; Chen, Y., Cp₂TiCl-Catalyzed SET Reduction of Aldehydes: A New Initiating Protocol for Living Radical Polymerization. *Macromolecules* **2006**, *39* (22), 7549-7554.
49. Asandei, A. D.; Simpson, C. P., Cp₂TiCl-catalyzed synthesis of styrene/isoprene copolymers by controlled radical polymerization. *Polym. Prepr. (Am. Chem. Soc., Div. Polym. Chem.)* **2008**, *49* (2), 75-76.
50. Reardon, D.; Conan, F.; Gambarotta, S.; Yap, G.; Wang, Q., Life and death of an active ethylene polymerization catalyst. Ligand involvement in catalyst activation and deactivation. Isolation and characterization of two unprecedented neutral and anionic vanadium(I) alkyls. *J. Am. Chem. Soc.* **1999**, *121*, 9318-9325.
51. Milione, S.; Cavallo, G.; Tedesco, C.; Grassi, A., Synthesis of α-diimine V(III) complexes and their role as ethylene polymerisation catalysts. *Journal of the Chemical Society, Dalton Transactions* **2002**, (8), 1839-1846.
52. Colamarco, E.; Milione, S.; Cuomo, C.; Grassi, A., Homo- and Copolymerization of Butadiene Catalyzed by an Bis(imino)pyridyl Vanadium Complex. *Macromol. Rapid Comm.* **2004**, *25* (2), 450-454.
53. Lang, J. R. V.; Denner, C. E.; Alt, H. G., Homogeneous catalytic dimerization of propylene with bis(imino)pyridine vanadium(III) complexes. *J. Mol. Catal. A* **2010**, *322* (1-2), 45-49.
54. Shaver, M. P.; Hanhan, M. E.; Jones, M. R., Controlled radical polymerization of vinyl acetate mediated by a vanadium complex. *Chemical Communications* **2010**, *46* (12), 2127-2129.

55. Allan, L. E. N.; Cross, E. D.; Francis-Pranger, T. W.; Hanhan, M. E.; Jones, M. R.; Pearson, J. K.; Perry, M. R.; Storr, T.; Shaver, M. P., Controlled Radical Polymerization of Vinyl Acetate Mediated by a Bis(imino)pyridine Vanadium Complex. *Macromolecules* **2011**, *44* (11), 4072-4081.
56. Perry, M. R.; Allan, L. E. N.; Decken, A.; Shaver, M. P., Organometallic mediated radical polymerization of vinyl acetate using bis(imino)pyridine vanadium trichloride complexes. *DALTON TRANSACTIONS* **2013**, *42* (25), 9157-9165.
57. Lee, M.; Minoura, Y., Polymerization of vinyl monomers initiated by chromium(II) acetate + organic peroxides. *J. Chem. Soc., Faraday Trans. 1* **1978**, *74* (7), 1726-1737.
58. Lee, M.; Morigami, T.; Minoura, Y., "Living" radical polymerizations of vinyl monomers initiated by aged "Cr²⁺ + BPO" in homogeneous solution. *J. Chem. Soc., Faraday Trans. 1* **1978**, *74* (7), 1738-1749.
59. Lee, M.; Utsumi, K.; Minoura, Y., Effect of hexamethylphosphoric triamide on the "living" radical polymerization initiated by aged Cr²⁺ + BPO. *J. Chem. Soc., Faraday Trans. 1* **1979**, *75* (8), 1821-1829.
60. Lee, M.; Ishida, Y.; Minoura, Y., Effects of Ligands on the "Living" Radical Polymerization Initiated by the Aged Cr²⁺ Plus Benzoyl Peroxide System. *Journal of Polymer Science Part a-Polymer Chemistry* **1982**, *20* (2), 457-465.
61. Grishin, D.; Semyonycheva, L.; Artemov, A.; Telegina, E.; Valetova, N.; Illichev, I., Vinylarenetricarbonyl complexes of chromium as chain propagation regulators for polymerization of acrylic monomers. *APPLIED ORGANOMETALLIC CHEMISTRY* **2003**, *17* (9), 717-722.
62. Grishin, D. F.; Valetova, N. B.; Il'ichev, I. S.; Semenycheva, L. L.; Artemov, A. N.; Sazonova, E. V., Free-radical polymerization of methyl methacrylate in the presence of stilbene(tricarbonyl)chromium and stilbene. *Polymer Science Series B* **2005**, *47* (5-6), 163-166.
63. Valetova, N. B.; Semyonycheva, L. L.; Illichev, I. S.; Artemov, A. N.; Grishin, D. F., Diphenylbutadiene chromium tricarbonyl in radical polymerization of methylmethacrylate. *Applied Organometallic Chemistry* **2005**, *19* (8), 971-974.
64. Valetova, N. B.; Semenycheva, L. L.; Il'ichev, I. S.; Artemov, A. N.; Grishin, D. F., Features of polystyrene synthesis in the presence of (diphenylbutadiene)tricarbonylchromium. *Russian Journal of Applied Chemistry* **2007**, *80* (5), 818-821.
65. Champouret, Y.; Baisch, U.; Poli, R.; Tang, L.; Conway, J. L.; Smith, K. M., Homolytic bond strengths and formation rates in half-sandwich chromium-alkyl complexes: relevance for controlled radical polymerization. *Angew. Chem., Int. Ed.* **2008**, *47*, 6069-6072.
66. Champouret, Y.; MacLeod, K. C.; Baisch, U.; Patrick, B. O.; Smith, K. M.; Poli, R., Cyclopentadienyl Chromium β -Diketiminato Complexes: Initiators, Ligand Steric Effects, and Deactivation Processes in the Controlled Radical Polymerization of Vinyl Acetate. *Organometallics* **2010**, *29* (1), 167-176.
67. Champouret, Y.; MacLeod, K. C.; Smith, K. M.; Poli, R., Controlled Radical Polymerization of Vinyl Acetate with Cyclopentadienyl Chromium β -Diketiminato Complexes: ATRP vs. OMRP. *Organometallics* **2010**, *29*, 3125-3132.
68. Le Grogne, E.; Claverie, J.; Poli, R., Radical Polymerization of Styrene controlled by Half-Sandwich Mo(III)/Mo(IV) Couples: all Basic Mechanisms are Possible. *J. Am. Chem. Soc.* **2001**, *123*, 9513-9524.
69. Stoffelbach, F.; Poli, R.; Richard, P., Half-sandwich Molybdenum(III) Compounds Containing Diazadiene Ligands and Their Use in the Controlled Radical Polymerization of Styrene. *J. Organometal. Chem.* **2002**, *663*, 269-276.
70. Stoffelbach, F.; Poli, R.; Maria, S.; Richard, P., How the interplay of different control mechanisms affects the initiator efficiency factor in controlled radical polymerization: an investigation using organometallic Mo^{III}-based catalysts. *J. Organomet. Chem.* **2007**, *692*, 3133-3143.
71. Stoffelbach, F.; Claverie, J.; Poli, R., Atom Transfer Radical Polymerization of Styrene Controlled by Phosphine-Containing Coordination Compounds of Mo(III)/Mo(IV). *C. R. Acad. Sci. Paris C* **2002**, *5*, 37-42.

72. Maria, S.; Stoffelbach, F.; Mata, J.; Daran, J.-C.; Richard, P.; Poli, R., The radical trap in atom transfer radical polymerization need not be thermodynamically stable. A study of the $\text{MoX}_3(\text{PMe}_3)_3$ ($\text{X} = \text{Cl}, \text{Br}, \text{I}$) catalysts. *J. Am. Chem. Soc.* **2005**, *127*, 5946-5956.
73. Aliwi, S. M.; Bamford, C. H.; Mullik, S. U., Recent studies in photoinitiated polymerization. *Journal of Polymer Science Part C-Polymer Symposium* **1975**, (50), 33-50.
74. Asandei, A. D.; Adebolu, O. I.; Simpson, C. P., Mild-Temperature $\text{Mn}_2(\text{CO})_{10}$ -Photomediated Controlled Radical Polymerization of Vinylidene Fluoride and Synthesis of Well-Defined Poly(vinylidene fluoride) Block Copolymers. *Journal of the American Chemical Society* **2012**, *134* (14), 6080-6083.
75. Simpson, C. P.; Adebolu, O. I.; Kim, J.-S.; Vasu, V.; Asandei, A. D., Metal and Ligand Effects of Photoactive Transition Metal Carbonyls in the Iodine Degenerative Transfer Controlled Radical Polymerization and Block Copolymerization of Vinylidene Fluoride. *Macromolecules* **2015**, *48* (18), 6404-6420.
76. Morales-Cerrada, R.; Fliedel, C.; Daran, J.-C.; Gayet, F.; Ladmiral, V.; Améduri, B.; Poli, R., Fluoroalkyl radical generation by homolytic bond dissociation in pentacarbonylmanganese derivatives. *Chem. Eur. J.* **2019**, *25*, 296-308.
77. Morales-Cerrada, R.; Ladmiral, V.; Gayet, F.; Fliedel, C.; Poli, R.; Améduri, B., Fluoroalkyl Pentacarbonylmanganese(I) Complexes as Initiators for the Radical (co)Polymerization of Fluoromonomers. *Polymers* **2020**, *12*, 384/1-17.
78. Morales-Cerrada, R.; Fliedel, C.; Gayet, F.; Ladmiral, V.; Améduri, B.; Poli, R., Homolytic bond strength and radical generation from (1-carbomethoxyethyl)pentacarbonylmanganese(I). *Eur. J. Inorg. Chem.* **2019**, 4228-4233.
79. Grishin, I. D.; Krivykh, V. V.; Shchepalov, A. A.; Taits, E. S.; Ustynyuk, N. A.; Grishin, D. F., Stable 17-electron manganese complexes in the synthesis of macromolecules. *Russian Chemical Bulletin* **2009**, *58* (9), 1866-1871.
80. Poli, R.; Allan, L. E. N.; Shaver, M. P., Iron-Mediated Reversible Deactivation Radical Polymerisation. *Prog. Polym. Sci.* **2014**, *39*, 1827-1845.
81. Kanagasabapathy, S.; Serero, D.; Silie, D.; Prost, S.; Ruiz-Guerrero, R.; Claverie, J., Controlled "Living" radical polymerization of styrene with iron complexes. *Res. Discl.* **1998**, P1595-P1604.
82. Xue, Z.; Poli, R., Organometallic Mediated Radical Polymerization of Vinyl Acetate with $\text{Fe}(\text{acac})_2$. *J. Polym. Sci. A Polym. Chem.* **2013**, *51*, 3494-3504.
83. Wang, J. R.; Zhou, J.; Sharif, H.; He, D.; Ye, Y. S.; Xue, Z. G.; Xie, X. L., Living radical polymerization of vinyl acetate mediated by iron(III) acetylacetonate in the presence of a reducing agent. *Rsc Advances* **2015**, *5* (117), 96345-96352.
84. Shaver, M. P.; Allan, L. E. N.; Gibson, V. C., Organometallic Intermediates in the Controlled Radical Polymerization of Styrene by α -Diimine Iron Catalysts. *Organometallics* **2007**, *26* (19), 4725-4730.
85. Poli, R.; Shaver, M. P., ATRP/OMRP/CCT Interplay in Styrene Polymerization Mediated by Iron(II) Complexes: a DFT Study of the α -Diimine System. *Chem. Eur. J.* **2014**, *20* (52), 17530-17540.
86. Allan, L. E. N.; MacDonald, J. P.; Reckling, A. M.; Kozak, C. M.; Shaver, M. P., Controlled Radical Polymerization Mediated by Amine-Bis(phenolate) Iron(III) Complexes. *Macromolecular Rapid Communications* **2012**, *33* (5), 414-418.
87. Allan, L. E. N.; MacDonald, J. P.; Nichol, G. S.; Shaver, M. P., Single Component Iron Catalysts for Atom Transfer and Organometallic Mediated Radical Polymerizations: Mechanistic Studies and Reaction Scope. *Macromolecules (Washington, DC, U. S.)* **2014**, *47* (4), 1249-1257.
88. Schroeder, H.; Lake, B. R. M.; Demeshko, S.; Shaver, M. P.; Buback, M., A Synthetic and Multispectroscopic Speciation Analysis of Controlled Radical Polymerization Mediated by Amine-Bis(phenolate)iron Complexes. *Macromolecules* **2015**, *48* (13), 4329-4338.
89. Coward, D. L.; Lake, B. R. M.; Shaver, M. P., Understanding Organometallic-Mediated Radical Polymerization with an Iron(II) Amine-Bis(phenolate). *Organometallics* **2017**, *36* (17), 3322-3328.

90. Poli, R.; Shaver, M. P., ATRP and OMRP of Styrene Mediated by Diaminobis(phenolato)iron(II) Complexes: A DFT Study. *Inorg. Chem.* **2014**, *53* (14), 7580–7590.
91. Kato, M.; Kamigaito, M.; Sawamoto, M.; Higashimura, T., Polymerization of methyl methacrylate with the $\text{CCl}_4/(\text{PPh}_3)_2\text{Cl}_2\text{Ru(II)}/\text{MeAl(ODBP)}_2$ initiating system: possibility of living radical polymerization. *Macromolecules* **1995**, *28*, 1721-1723.
92. Takahashi, H.; Ando, T.; Kamigaito, M.; Sawamoto, M., Half-metallocene-type ruthenium complexes as active catalysts for living radical polymerization of methyl methacrylate and styrene. *Macromolecules* **1999**, *32*, 3820-3823.
93. Braunecker, W. A.; Itami, Y.; Matyjaszewski, K., Osmium Mediated Radical Polymerization. *Macromolecules* **2005**, *38*, 9402-9404.
94. Braunecker, W. A.; Brown, W. C.; Morelli, B.; Tang, W.; Poli, R.; Matyjaszewski, K., Origin of Activity in Cu, Ru, and Os Mediated Radical Polymerization. *Macromolecules* **2007**, *40*, 8576-8585.
95. Wayland, B. B.; Poszmik, G.; Fryd, M., Metalloradical Reactions of Rhodium(II) Porphyrins with Acrylates - Reduction, Coupling, and Photopromoted Polymerization. *Organometallics* **1992**, *11* (11), 3534-3542.
96. Tang, W.; Tsarevsky, N. V.; Matyjaszewski, K., Determination of Equilibrium Constants for Atom Transfer Radical Polymerization. *Journal of the American Chemical Society* **2006**, *128* (5), 1598-1604.
97. Ribelli, T. G.; Fantin, M.; Daran, J.-C.; Augustine, K. F.; Poli, R.; Matyjaszewski, K., Synthesis and Characterization of the Most Active Copper-based ATRP Catalyst based on tris[(4-dimethylaminopyridyl)methyl]amine. *J. Am. Chem. Soc.* **2018**, *140*, 1525–1534.
98. Ribelli, T. G.; Matyjaszewski, K.; Poli, R., The interaction of carbon-centered radicals with copper(I) and copper(II) complexes. *J. Coord. Chem.* **2018**, *71*, 1641-1668.
99. Matyjaszewski, K.; Woodworth, B. E., Interaction of Propagating Radicals with Cu^I and Cu^{II} species. *Macromolecules* **1998**, *31*, 4718-4723.
100. Schröder, K.; Konkolewicz, D.; Poli, R.; Matyjaszewski, K., Formation and Possible Reactions of an Organometallic Intermediate with Active Copper(I) Catalysts in an ATRP. *Organometallics* **2012**, *31*, 7994-7999.
101. Ribelli, T. G.; Rahaman, S. M. W.; Daran, J.-C.; Kryszewski, P.; Matyjaszewski, K.; Poli, R., Effect of Ligand Structure on the Cu^{II} -R OMRP Dormant Species and its Consequences for Catalytic Radical Termination in ATRP. *Macromolecules* **2016**, *49*, 7749–7757.
102. Wang, Y.; Soerensen, N.; Zhong, M.; Schroeder, H.; Buback, M.; Matyjaszewski, K., Improving the "Livingness" of ATRP by Reducing Cu Catalyst Concentration. *Macromolecules* **2013**, *46* (3), 683-691.
103. Rahaman, S. M. W.; Matyjaszewski, K.; Poli, R., Cobalt(III) and copper(II) hydrides at the crossroad of catalyzed chain transfer and catalyzed radical termination: a DFT study. *Polym. Chem.* **2016**, *7*, 1079–1087.
104. Ribelli, T. G.; Augustine, K. F.; Fantin, M.; Kryszewski, P.; Poli, R.; Matyjaszewski, K., Disproportionation or Combination? The Termination of Acrylate Radicals in ATRP. *Macromolecules (Washington, DC, U. S.)* **2017**, *50*, 7920–7929.
105. Ribelli, T. G.; Rahaman, S. M. W.; Matyjaszewski, K.; Poli, R., Catalyzed radical termination (CRT) in the metal-mediated polymerization of acrylates: experimental and computational studies. In *Reversible Deactivation Radical Polymerization: Mechanisms and Synthetic Methodologies*, Tsarevsky, N.; Gao, H.; Matyjaszewski, K.; Sumerlin, B., Eds. American Chemical Society: Washington D.C., 2018; Vol. 1284, pp 135-159.
106. Thevenin, L.; Fliedel, C.; Matyjaszewski, K.; Poli, R., Impact of catalyzed radical termination (CRT) and reductive radical termination (RRT) in metal-mediated radical polymerization processes. *Eur. J. Inorg. Chem.* **2019**, 4489–4499.
107. Fantin, M.; Lorandi, F.; Ribelli, T. G.; Fliedel, C.; Thevenin, L.; Isse, A. A.; Poli, R.; Matyjaszewski, K., The Impact of Organometallic Intermediates on Copper-Catalyzed Atom Transfer Radical Polymerization. *Macromolecules (Washington, DC, U. S.)* **2019**, *52*, 4079-4090.

108. Ribelli, T. G.; Lorandi, F.; Fantin, M.; Matyjaszewski, K., Atom Transfer Radical Polymerization: Billion Times More Active Catalysts and New Initiation Systems. *Macromolecular Rapid Communications* **2019**, *40* (1), 1800616.
109. Enciso, A. E.; Lorandi, F.; Mehmood, A.; Fantin, M.; Szczepaniak, G.; Janesko, B. G.; Matyjaszewski, K., p-Substituted Tris(2-pyridylmethyl)amines as Ligands for Highly Active ATRP Catalysts: Facile Synthesis and Characterization. *Angewandte Chemie-International Edition* **2020**.
110. Debuigne, A.; Poli, R.; Jérôme, C.; Jérôme, R.; Detrembleur, C., Overview of cobalt-mediated radical polymerization: roots, state of the art and future prospects. *Prog. Polym. Sci.* **2009**, *34*, 211-239.
111. Peng, C.-H.; Yang, T.-Y.; Zhao, Y.; Fu, X., Reversible deactivation radical polymerization mediated by cobalt complexes: recent progress and perspectives. *Organic & Biomolecular Chemistry* **2014**, *12* (43), 8580-8587.
112. Wayland, B.; Poszmik, G.; Mukerjee, S., Living radical polymerization of acrylates by organocobalt porphyrin complexes. *J. Am. Chem. Soc.* **1994**, *116*, 7943-7944.
113. Arvanitopoulos, L. D.; Greuel, M. P.; Harwood, H. J., "Living" free radical photopolymerization using alkyl cobaloximes as photoinitiators. *Polym. Prepr.* **1994**, *35*, 549-550.
114. Arvanitopoulos, L. D.; Greuel, M. P.; King, B. M.; Shim, A. K.; Harwood, H. J., Photochemical polymerizations initiated and mediated by soluble organocobalt compounds. *ACS Symp. Ser.* **1998**, *685* (Controlled Radical Polymerization), 316-331.
115. Lu, Z.; Fryd, M.; Wayland, B. B., New life for living radical polymerization mediated by cobalt(II) metalloradicals. *Macromolecules* **2004**, *37* (8), 2686-2687.
116. Wayland, B. B.; Basickes, L.; Mukerjee, S.; Wei, M.; Fryd, M., Living radical polymerization of acrylates initiated and controlled by organocobalt porphyrin complexes. *Macromolecules* **1997**, *30*, 8109 - 8112.
117. Wayland, B.; Mukerjee, S.; Poszmik, G.; Woska, D.; Basickes, L.; Gridnev, A.; Fryd, M.; Ittel, S., Control of radical polymerizations by metalloradicals. *ACS Symp. Ser.* **1998**, *685* (Controlled Radical Polymerization), 305-315.
118. Wayland, B. B.; Peng, C.-H.; Fu, X.; Lu, Z.; Fryd, M., Degenerative Transfer and Reversible Termination Mechanisms for Living Radical Polymerizations Mediated by Cobalt Porphyrins. *Macromolecules* **2006**, *39* (24), 8219-8222.
119. Wayland, B. B.; Fu, X.; Peng, C.-H.; Lu, Z.; Fryd, M., Living Radical Polymerizations Mediated by Metallo Radical and Organo-Transition Metal Complexes. *ACS Symp. Ser.* **2006**, *944*, 358-371.
120. Peng, C.-H.; Fryd, M.; Wayland, B. B., Organocobalt Mediated Radical Polymerization of Acrylic Acid in Water. *Macromolecules* **2007**, *40* (19), 6814-6819.
121. Zhao, Y.; Dong, H.; Li, Y.; Fu, X., Living radical polymerization of acrylates and acrylamides mediated by a versatile cobalt porphyrin complex. *Chemical Communications* **2012**, *48* (29), 3506-3508.
122. Dong, H. L.; Hou, T. J.; Zhao, Y. G.; Fu, X. F.; Li, Y. Y., DFT study of cobalt porphyrin complex for living radical polymerization of olefins. *Computational and Theoretical Chemistry* **2012**, *1001*, 51-59.
123. Peng, C. H.; Scricco, J.; Li, S.; Fryd, M.; Wayland, B. B., Organo-cobalt mediated living radical polymerization of vinyl acetate. *Macromolecules* **2008**, *41* (7), 2368-2373.
124. Li, S.; de Bruin, B.; Peng, C. H.; Fryd, M.; Wayland, B. B., Exchange of organic radicals with organo-cobalt complexes formed in the living radical polymerization of vinyl acetate. *Journal of the American Chemical Society* **2008**, *130* (40), 13373-13381.
125. Hsu, C. S.; Yang, T. Y.; Peng, C. H., Vinyl acetate living radical polymerization mediated by cobalt porphyrins: kinetic-mechanistic studies. *Polymer Chemistry* **2014**, *5* (12), 3867-3875.
126. Maria, S.; Kaneyoshi, H.; Matyjaszewski, K.; Poli, R., Effect of Electron Donors on the Radical Polymerization of Vinyl Acetate Mediated by Co(acac)₂: degenerative transfer versus reversible homolytic cleavage of an organocobalt(III) complex. *Chem. Eur. J.* **2007**, *13*, 2480-2492.

127. Zhao, Y. G.; Yu, M. M.; Fu, X. F., Photo-cleavage of the cobalt-carbon bond: visible light-induced living radical polymerization mediated by organo-cobalt porphyrins. *Chemical Communications* **2013**, 49 (45), 5186-5188.
128. Zhao, Y.; Yu, M.; Zhang, S.; Liu, Y.; Fu, X., Visible Light Induced Living/Controlled Radical Polymerization of Acrylates Catalyzed by Cobalt Porphyrins. *Macromolecules* **2014**, 47 (18), 6238-6245.
129. Debuigne, A.; Caille, J. R.; Detrembleur, C.; Jerome, R., Effective cobalt mediation of the radical polymerization of vinyl acetate in suspension. *Angew. Chem., Int. Ed.* **2005**, 44 (22), 3439-3442.
130. Debuigne, A.; Caille, J. R.; Jérôme, R., Highly efficient cobalt-mediated radical polymerization of vinyl acetate. *Angew. Chem., Int. Ed.* **2005**, 44 (7), 1101-1104.
131. Bryaskova, R.; Detrembleur, C.; Debuigne, A.; Jerome, R., Cobalt-mediated radical polymerization (CMRP) of vinyl acetate initiated by redox systems: Toward the scale-up of CMRP. *Macromolecules* **2006**, 39 (24), 8263-8268.
132. Santhosh Kumar, K. S.; Gnanou, Y.; Champouret, Y.; Daran, J.-C.; Poli, R., Radical Polymerization of Vinyl Acetate with Bis(tetramethylheptadionato)cobalt(II): the Cohabitation of Three Different Mechanisms. *Chem. Eur. J.* **2009**, 15, 4874-4885.
133. Kaneyoshi, H.; Matyjaszewski, K., Effect of Ligand and n-Butyl Acrylate on Cobalt-Mediated Radical Polymerization of Vinyl Acetate. *Macromolecules* **2005**, 38 (20), 8163-8169.
134. Banerjee, S.; Bellan, E. V.; Gayet, F.; Debuigne, A.; Detrembleur, C.; Poli, R.; Améduri, B.; Ladmiral, V., Bis(formylphenolato)cobalt(II)-Mediated Alternating Radical Copolymerization of tert-Butyl-2-trifluoromethacrylate with Vinyl Acetate. *Polymers* **2017**, 9, 702.
135. Bellan, E. V.; Thevenin, L.; Gayet, F.; Fliedel, C.; Poli, R., Catalyzed Chain Transfer in Vinyl Acetate Polymerization mediated by 9-Oxyphenalenone Cobalt(II) complexes. *ACS Macro Letters* **2017**, 6, 959-962.
136. Kaneyoshi, H.; Matyjaszewski, K., Radical (Co)polymerization of vinyl chloroacetate and N-vinylpyrrolidone mediated by bis(acetylacetonate)cobalt derivatives. *Macromolecules* **2006**, 39 (8), 2757-2763.
137. Debuigne, A.; Willet, N.; Jerome, R.; Detrembleur, C., Amphiphilic Poly(vinyl acetate)-b-poly(N-vinylpyrrolidone) and Novel Double Hydrophilic Poly(vinyl alcohol)-b-poly(N-vinylpyrrolidone) Block Copolymers Prepared by Cobalt-Mediated Radical Polymerization. *Macromolecules* **2007**, 40 (20), 7111-7118.
138. Debuigne, A.; Schoumacher, M.; Willet, N.; Riva, R.; Zhu, X. M.; Rutten, S.; Jerome, C.; Detrembleur, C., New functional poly(N-vinylpyrrolidone) based (co)polymers via photoinitiated cobalt-mediated radical polymerization. *Chemical Communications* **2011**, 47 (47), 12703-12705.
139. Debuigne, A.; Morin, A. N.; Kermagoret, A.; Piette, Y.; Detrembleur, C.; Jérôme, C.; Poli, R., Key Role of Intramolecular Metal Chelation and Hydrogen Bonding in the Cobalt-Mediated Radical Polymerization of N-Vinyl amides. *Chem. Eur. J.* **2012**, 18, 12834-12844.
140. Hurtgen, M.; Liu, J.; Debuigne, A.; Jerome, C.; Detrembleur, C., Synthesis of Thermo-Responsive Poly(N-vinylcaprolactam)-Containing Block Copolymers by Cobalt-Mediated Radical Polymerization. *Journal of Polymer Science Part A-Polymer Chemistry* **2012**, 50 (2), 400-408.
141. Piette, Y.; Debuigne, A.; Jérôme, C.; Bodart, V.; Poli, R.; Detrembleur, C., Cobalt-Mediated Radical (Co)polymerization of Vinyl Chloride and Vinyl Acetate. *Polymer Chemistry* **2012**, 3, 2880-2891.
142. Banerjee, S.; Ladmiral, V.; Debuigne, A.; Detrembleur, C.; Poli, R.; Améduri, B., Organometallic Mediated Radical Polymerization of Vinylidene Fluoride. *Angew. Chem. Int. Ed.* **2018**, 57, 2934-2937.
143. Falireas, P. G.; Ladmiral, V.; Debuigne, A.; Detrembleur, C.; Poli, R.; Ameduri, B., Straightforward synthesis of well-defined poly(vinylidene fluoride) and its block copolymers by cobalt-mediated radical polymerization. *Macromolecules (Washington, DC, U. S.)* **2019**, 52, 1266-1276.

144. Kermagoret, A.; Debuigne, A.; Jerome, C.; Detrembleur, C., Precision design of ethylene- and polar-monomer-based copolymers by organometallic-mediated radical polymerization. *Nat. Chem.* **2014**, *6* (3), 179-187.
145. Bryaskova, R.; Willet, N.; Degee, P.; Dubois, P.; Jerome, R.; Detrembleur, C., Copolymerization of vinyl acetate with 1-octene and ethylene by cobalt-mediated radical polymerization. *J. Polym. Sci., Part A: Polym. Chem.* **2007**, *45* (12), 2532-2542.
146. Kermagoret, A.; Wenn, B.; Debuigne, A.; Jerome, C.; Junkers, T.; Detrembleur, C., Improved photo-induced cobalt-mediated radical polymerization in continuous flow photoreactors. *Polymer Chemistry* **2015**, *6* (20), 3847-3857.
147. Demarteaue, J.; Améduri, B.; Ladmiral, V.; Mees, M. A.; Hoogenboom, R.; Debuigne, A.; Detrembleur, C., Controlled Synthesis of Fluorinated Copolymers via Cobalt-Mediated Radical Copolymerization of Perfluorohexylethylene and Vinyl Acetate. *Macromolecules (Washington, DC, U. S.)* **2017**, *50* (10), 3750-3760.
148. Debuigne, A.; Warnant, J.; Jerome, R.; Voets, I.; de Keizer, A.; Stuart, M. A.; Detrembleur, C., Synthesis of novel well-defined poly(vinyl acetate)-b-poly(acrylonitrile) and derivatized water-soluble poly(vinyl alcohol)-b-poly(acrylic acid) block copolymers by cobalt-mediated radical polymerization. *Macromolecules* **2008**, *41* (7), 2353-2360.
149. Debuigne, A.; Michaux, C.; Jérôme, C.; Jérôme, R.; Poli, R.; Detrembleur, C., Cobalt Mediated Radical Polymerization (CMRP) of Acrylonitrile : Kinetic Investigations and DFT Calculations. *Chem. Eur. J.* **2008**, *14*, 7623-7637.
150. Detrembleur, C.; Versace, D. L.; Piette, Y.; Hurtgen, M.; Jerome, C.; Lalevee, J.; Debuigne, A., Synthetic and mechanistic inputs of photochemistry into the bis-acetylacetonatocobalt-mediated radical polymerization of n-butyl acrylate and vinyl acetate. *Polymer Chemistry* **2012**, *3* (7), 1856-1866.
151. Debuigne, A.; Jerome, C.; Detrembleur, C., Isoprene-Assisted Radical Coupling of (Co)polymers Prepared by Cobalt-Mediated Radical Polymerization. *Angew. Chem. Int. Ed.* **2009**, *48* (8), 1422-1424.
152. Debuigne, A.; Poli, R.; De Winter, J.; Laurent, P.; Gerbaux, P.; Dubois, P.; Wathélet, J.-P.; Jérôme, C.; Detrembleur, C., Cobalt-Mediated Radical Coupling (CMRC): An Unusual Route to Mid-chain-functionalized Symmetrical Macromolecules. *Chem. Eur. J.* **2010**, *16*, 1799-1811.
153. Debuigne, A.; Poli, R.; De Winter, J.; Laurent, P.; Gerbaux, P.; Wathélet, J.-P.; Jérôme, C.; Detrembleur, C., Effective Cobalt-Mediated Radical Coupling (CMRC) of Poly(vinyl acetate) and Poly(N-vinylpyrrolidone) (Co)polymers Precursors. *Macromolecules* **2010**, *43*, 2801-2813.
154. Debuigne, A.; Champouret, Y.; Jérôme, R.; Poli, R.; Detrembleur, C., Mechanistic Insights into Cobalt Mediated Radical Polymerization (CMRP) of Vinyl Acetate via Cobalt(III) Adducts as Initiators. *Chem. Eur. J.* **2008**, *14*, 4046-4059.
155. Debuigne, A.; Poli, R.; Jérôme, R.; Jérôme, C.; Detrembleur, C., Key Role of Metal-Coordination in Cobalt-Mediated Radical Polymerization of Vinyl Acetate. *ACS Symp. Ser.* **2009**, *1024*, 131-148.
156. Wang, F. S.; Yang, T. Y.; Hsu, C. C.; Chen, Y. J.; Li, M. H.; Hsu, Y. J.; Chuang, M. C.; Peng, C. H., The Mechanism and Thermodynamic Studies of CMRP: Different Control Mechanisms Demonstrated by Co-II(TMP), Co-II(salen*), and Co-II(acac)(2) Mediated Polymerization, and the Correlation of Reduction Potential, Equilibrium Constant, and Control Mechanism. *Macromolecular Chemistry and Physics* **2016**, *217* (3), 422-432.
157. Wang, Z.; Poli, R.; Detrembleur, C.; Debuigne, A., Organometallic-Mediated Radical (Co)Polymerization of γ -Methylene- γ -Butyrolactone: Access to pH-Responsive Poly(vinyl alcohol) Derivatives. *Macromolecules (Washington, DC, U. S.)* **2019**, *52*, 8976-8988.
158. Morin, A. N.; Detrembleur, C.; Jérôme, C.; Tullio, P. D.; Poli, R.; Debuigne, A., Effect of head-to-head addition in vinyl acetate reversible deactivation radical polymerization: why is Co(acac)₂-mediated polymerization so much better? *Macromolecules (Washington, DC, U. S.)* **2013**, *46*, 4303-4312.

159. Poli, R.; Rahaman, S. M. W.; Ladmiral, V.; Améduri, B., Effect of α - and β -H/F substitution on the homolytic bond strength in dormant species of controlled radical polymerization: OMRP vs. ITP and RAFT. *Journal of Organometallic Chemistry* **2018**, *864*, 12-18
160. Gridnev, A. A., Radical polymerization of methyl methacrylate in the presence of cobaloximes and benzoyl peroxide. *Polymer Journal* **1992**, *24* (7), 613-623.
161. Heuts, J. P. A.; Forster, D. J.; Davis, T. P., The role of monomer in the chain transfer reaction in cobaloxime-mediated free-radical polymerization. *Macromolecular Rapid Communications* **1999**, *20* (6), 299-302.
162. Roberts, G. E.; Davis, T. P.; Heuts, J. P. A.; Russell, G. T., Viscosity effects in cobaloxime-mediated catalytic chain-transfer polymerization of methacrylates. *Journal of Polymer Science Part A-Polymer Chemistry* **2002**, *40* (6), 782-792.
163. Engelis, N. G.; Anastasaki, A.; Whitfield, R.; Jones, G. R.; Liarou, E.; Nikolaou, V.; Nurumbetov, G.; Haddleton, D. M., Sequence-Controlled Methacrylic Multiblock Copolymers: Expanding the Scope of Sulfur-Free RAFT. *Macromolecules* **2018**, *51* (2), 336-342.
164. Ng, Y. H.; di Lena, F.; Chai, C. L. L., On the use of Cob(II)alamin as a spin trap in radical polymerization. *Macromolecular Research* **2012**, *20* (5), 473-476.
165. Sherwood, R. K.; Kent, C. L.; Patrick, B. O.; McNeil, W. S., Controlled radical polymerisation of methyl acrylate initiated by a well-defined cobalt alkyl complex. *Chemical Communications* **2010**, *46* (14), 2456-2458.
166. Liao, C.-M.; Hsu, C.-C.; Wang, F.-S.; Wayland, B. B.; Peng, C.-H., Living radical polymerization of vinyl acetate and methyl acrylate mediated by Co(Salen*) complexes. *Polymer Chemistry* **2013**, *4* (10), 3098-3104.
167. Zhao, Y.; Wang, Y.; Zhou, X.; Xue, Z.; Wang, X.; Xie, X.; Poli, R., Oxygen Triggered Switchable Polymerization for One-Pot Synthesis of CO₂-Based Block Copolymers from Monomer Mixtures. *Angew Chem Int Ed Engl* **2019**, *58*, 14311 – 14318.
168. Zhao, Y.; Yu, M.; Zhang, S.; Wu, Z.; Liu, Y.; Peng, C.-H.; Fu, X., A well-defined, versatile photoinitiator (salen)Co-CO₂CH₃ for visible light-initiated living/controlled radical polymerization. *Chemical Science* **2015**, *6* (5), 2979-2988.
169. Zhao, Y. G.; Zhang, S. L.; Wu, Z. Q.; Liu, X.; Zhao, X. Y.; Peng, C. H.; Fu, X. F., Visible-Light-Induced Living Radical Polymerization (LRP) Mediated by (salen)Co(II)/TPO at Ambient Temperature. *Macromolecules* **2015**, *48* (15), 5132-5139.
170. Wu, Z. Q.; Wang, Z. K.; Wang, B. W.; Peng, C. H.; Fu, X. F., Visible-Light-Induced Living/Controlled Radical Copolymerization of 1-Octene and Acrylic Monomers Mediated by Organocobalt Complexes. *Macromolecules* **2020**, *53* (1), 212-222.
171. Wang, Y.; Zhao, Y.; Zhu, S.; Zhou, X.; Xu, J.; Xie, X.; Poli, R., Switchable Polymerization Triggered by Fast and Quantitative Insertion of Carbon Monoxide into Cobalt–Oxygen Bonds. *Angew Chem Int Ed Engl* **2020**, *59* (15), 5988-5994.
172. Chiang, L.; Allan, L. E. N.; Alcantara, J.; Wang, M. C. P.; Storr, T.; Shaver, M. P., Tuning ligand electronics and peripheral substitution on cobalt salen complexes: structure and polymerisation activity. *DALTON TRANSACTIONS* **2014**, *43* (11), 4295-4304.
173. Langlotz, B. K.; Loret Fillol, J.; Gross, J. H.; Wadepohl, H.; Gade, L. H., Living radical polymerization of acrylates mediated by 1,3-Bis(2-pyridylimino)isoindolatocobalt(II) complexes: monitoring the chain growth at the metal. *Chem. Eur. J.* **2008**, *14*, 10267-10279.
174. Bagchi, V.; Raptopoulos, G.; Das, P.; Christodoulou, S.; Wang, Q. W.; Ai, L.; Choudhury, A.; Pitsikalis, M.; Paraskevopoulou, P.; Stavropoulos, P., Synthesis and characterization of a family of Co(II) triphenylamido-amine complexes and catalytic activity in controlled radical polymerization of olefins. *Polyhedron* **2013**, *52*, 78-90.
175. Santhosh Kumar, K. S.; Li, Y.; Gnanou, Y.; Baisch, U.; Champouret, Y.; Poli, R.; Robson, K. C. D.; McNeil, W. S., Electronic and Steric Ligand Effects in the Radical Polymerization of Vinyl Acetate Mediated by β -Ketoiminate Complexes of Cobalt(II). *Chem. Asian J.* **2009**, *4*, 1257-1265.
176. Chen, Y. H.; Chen, S. J.; Li, J. Q.; Wu, Z. Q.; Lee, G. H.; Liu, Y. H.; Cheng, W. T.; Yeh, C. Y.; Peng, C. H., Cobalt(II) phenoxy-imine complexes in radical polymerization of vinyl acetate: The

- interplay of catalytic chain transfer and controlled/living radical polymerization. *Journal of Polymer Science* **2020**, *58* (1), 101-113.
177. Auras, R.; Harte, B.; Selke, S., An overview of polylactides as packaging materials. *Macromol Biosci* **2004**, *4* (9), 835-64.
178. Zhu, Y.; Romain, C.; Williams, C. K., Sustainable polymers from renewable resources. *Nature* **2016**, *540* (7633), 354-362.
179. Shen, L.; Worrell, E.; Patel, M., Present and future development in plastics from biomass. *Biofuels, Bioproducts and Biorefining* **2010**, *4* (1), 25-40.
180. Degradable Aliphatic Polyesters. *Advances in Polymer Science* **2002**, *157*.
181. Gupta, A. P.; Kumar, V., New emerging trends in synthetic biodegradable polymers – Polylactide: A critique. *European Polymer Journal* **2007**, *43* (10), 4053-4074.
182. Odile Dechy-Cabaret, B. M.-V., and Didier Bourissou, Controlled Ring-Opening Polymerization of Lactide and Glycolide. *Chem. Rev.* **2004**, *104*, 6147–6176.
183. Thibault, M. H.; Fontaine, F. G., Aluminium complexes bearing functionalized trisamido ligands and their reactivity in the polymerization of epsilon-caprolactone and rac-lactide. *Dalton Trans* **2010**, *39* (24), 5688-97.
184. Shaheen Motala-Timol, A. B.-L., Dhanjay Jhurry, Kinetic Study of the Al-Schiff's Base Initiated Polymerization of epsilon-caprolactone and Synthesis of Graft Poly(methylmethacrylate-g-caprolactone). *Macromol. Symp.* **2006**, *231*, 69–80.
185. Dagonne, S.; Fliedel, C., Organoaluminum Species in Homogeneous Polymerization Catalysis. *Top Organometal Chem* **2013**, *41*, 125-171.
186. Hege, C. S.; Schiller, S. M., Non-toxic catalysts for ring-opening polymerizations of biodegradable polymers at room temperature for biohybrid materials. *Green Chem.* **2014**, *16* (3), 1410-1416.
187. Thomas, C. M., Stereocontrolled ring-opening polymerization of cyclic esters: synthesis of new polyester microstructures. *Chem Soc Rev* **2010**, *39* (1), 165-73.
188. Malcolm H. Chisholm*, J. C. G., and Hongfeng Yin, Cyclic esters and cyclodepsipeptides derived from lactide and 2,5-morpholinediones. *PNAS* **2006**, *103*, 15315–15320.
189. Buffet, J.-C.; Okuda, J., Initiators for the stereoselective ring-opening polymerization of meso-lactide. *Polymer Chemistry* **2011**, *2* (12).
190. Dagonne, S.; Fliedel, C.; de Frémont, P., Gallium and Indium Compounds in Homogeneous Catalysis. In *Encyclopedia of Inorganic and Bioinorganic Chemistry*, 2016; pp 1-27.
191. Sarazin, Y.; Carpentier, J.-F., Discrete Cationic Complexes for Ring-Opening Polymerization Catalysis of Cyclic Esters and Epoxides. *Chem. Rev.* **2015**, *115* (9), 3564-3614.
192. Wheaton, C. A.; Hayes, P. G.; Ireland, B. J., Complexes of Mg, Ca and Zn as homogeneous catalysts for lactide polymerization. *Dalton Trans.* **2009**, (25), 4832-4846.
193. Bhunora, S.; Mugo, J.; Bhaw-Luximon, A.; Mapolie, S.; Van Wyk, J.; Darkwa, J.; Nordlander, E., The use of Cu and Zn salicylaldimine complexes as catalyst precursors in ring opening polymerization of lactides: ligand effects on polymer characteristics. *Applied Organometallic Chemistry* **2011**, *25* (2), 133-145.
194. Bradley M. Chamberlain, B. A. J., Maren Pink, Marc A. Hillmyer,* and William B. Tolman*, Controlled Polymerization of DL-Lactide and epsilon-Caprolactone by Structurally Well-Defined Alkoxo-Bridged Di- and Triyttrium(III) Complexes. *Macromolecules* **2000**, *33*, 3970-3977.
195. Amgoune, A.; Thomas, C. M.; Roisnel, T.; Carpentier, J. F., Ring-opening polymerization of lactide with group 3 metal complexes supported by dianionic alkoxy-amino-bisphenolate ligands: combining high activity, productivity, and selectivity. *Chemistry* **2005**, *12* (1), 169-79.
196. Cai, C. X.; Amgoune, A.; Lehmann, C. W.; Carpentier, J. F., Stereoselective ring-opening polymerization of racemic lactide using alkoxy-amino-bis(phenolate) group 3 metal complexes. *Chem Commun (Camb)* **2004**, (3), 330-1.
197. Bouyahyi, M.; Ajellal, N.; Kirillov, E.; Thomas, C. M.; Carpentier, J. F., Exploring electronic versus steric effects in stereoselective ring-opening polymerization of lactide and beta-butyrolactone with amino-alkoxy-bis(phenolate)-yttrium complexes. *Chemistry* **2011**, *17* (6), 1872-83.

198. Ligny, R.; Hanninen, M. M.; Guillaume, S. M.; Carpentier, J. F., Steric vs. electronic stereocontrol in syndio- or iso-selective ROP of functional chiral beta-lactones mediated by achiral yttrium-bisphenolate complexes. *Chem Commun (Camb)* **2018**, 54 (58), 8024-8031.
199. Sauer, A.; Kapelski, A.; Fliedel, C.; Dagonne, S.; Kol, M.; Okuda, J., Structurally well-defined group 4 metal complexes as initiators for the ring-opening polymerization of lactide monomers. *Dalton Trans* **2013**, 42 (25), 9007-23.
200. Ejfler, J.; Kobyłka, M.; Jerzykiewicz, L. B.; Sobota, P., Titanium complexes supported by bis(aryloxo) ligand: Structure and lactide polymerization activities. *Journal of Molecular Catalysis A: Chemical* **2006**, 257 (1-2), 105-111.
201. Della Monica, F.; Luciano, E.; Roviello, G.; Grassi, A.; Milione, S.; Capacchione, C., Group 4 Metal Complexes Bearing Thioetherphenolate Ligands. Coordination Chemistry and Ring-Opening Polymerization Catalysis. *Macromolecules* **2014**, 47 (9), 2830-2841.
202. Chmura, A. J.; Cousins, D. M.; Davidson, M. G.; Jones, M. D.; Lunn, M. D.; Mahon, M. F., Robust chiral zirconium alkoxide initiators for the room-temperature stereoselective ring-opening polymerisation of rac-lactide. *Dalton Trans* **2008**, (11), 1437-43.
203. Whitelaw, E. L.; Jones, M. D.; Mahon, M. F., Group 4 salalen complexes and their application for the ring-opening polymerization of rac-lactide. *Inorg Chem* **2010**, 49 (15), 7176-81.
204. Saravanamoorthy, S.; Muneeswaran, M.; Giridharan, N.; Velmathi, S., Solvent-free ring opening polymerization of ϵ -caprolactone and electrical properties of polycaprolactone blended BiFeO₃ nanocomposites. *RSC Advances* **2015**, 5 (54), 43897-43905.
205. Durr, C. B.; Williams, C. K., New Coordination Modes for Modified Schiff Base Ti(IV) Complexes and Their Control over Lactone Ring-Opening Polymerization Activity. *Inorg Chem* **2018**, 57 (22), 14240-14248.
206. Mandal, D.; Chakraborty, D.; Ramkumar, V.; Chand, D. K., Group 4 alkoxide complexes containing [NNO]-type scaffold: synthesis, structural characterization and polymerization studies. *RSC Advances* **2016**, 6 (26), 21706-21718.
207. Ou, H.-W.; Lu, W.-Y.; Vandavasi, J. K.; Lin, Y.-F.; Chen, H.-Y.; Lin, C.-C., Improvement in titanium complexes supported by Schiff bases in ring-opening polymerization of cyclic esters: ONO-tridentate Schiff bases. *Polymer* **2018**, 140, 315-325.
208. Minggang Hu*, W. Z., Wenhui Ma, Fuzhong Han, Weiming Song, Preparation of titanium complexes containing unsymmetric N2O2-ligands and their catalytic properties for polymerization of rac-lactide. *Polymer* **2018**, 153, 445-452.
209. Hu, M.; Cao, Q.; Deng, Q.; Yan, H.; Ma, W.; Song, W.; Dong, G., Synthesis and structural characterization of a new tetranuclear Zr complex supported by unsymmetric N2O2 ligand and its catalytic behaviors for ring-opening polymerization of rac-lactide. *Polyhedron* **2015**, 102, 308-312.
210. Mandal, M.; Ramkumar, V.; Chakraborty, D., Salen complexes of zirconium and hafnium: synthesis, structural characterization and polymerization studies. *Polymer Chemistry* **2019**, 10 (25), 3444-3460.
211. Muhammad Yusuf¹, A. N. P., Rizki Dwi Irmala Sari, Dinda Prihatini Fitri Amne, Rahmayani Siregar, Mawaddatur Rahmah, Ring-opening Polymerization Reaction Mechanism of ϵ -Caprolactone Catalyzed by Bis(dibenzoylmethanato) zirconium(IV) Using PM3 Semi-Empirical Method. *Journal of Physics* **2021**.
212. Dai, R.; Diaconescu, P. L., Investigation of a zirconium compound for redox switchable ring opening polymerization. *Dalton Trans* **2019**, 48 (9), 2996-3002.
213. Broderick, E. M.; Guo, N.; Vogel, C. S.; Xu, C.; Sutter, J.; Miller, J. T.; Meyer, K.; Mehrkhodavandi, P.; Diaconescu, P. L., Redox control of a ring-opening polymerization catalyst. *J Am Chem Soc* **2011**, 133 (24), 9278-81.
214. Quan, S. M.; Wang, X.; Zhang, R.; Diaconescu, P. L., Redox Switchable Copolymerization of Cyclic Esters and Epoxides by a Zirconium Complex. *Macromolecules* **2016**, 49 (18), 6768-6778.
215. Ma, J.; Zhao, K. Q.; Walton, M.; Wright, J. A.; Hughes, D. L.; Elsegood, M. R.; Michiue, K.; Sun, X.; Redshaw, C., Tri- and tetra-dentate imine vanadyl complexes: synthesis, structure and

- ethylene polymerization/ring opening polymerization capability. *Dalton Trans* **2014**, 43 (44), 16698-706.
216. Ma, J.; Zhao, K. Q.; Walton, M. J.; Wright, J. A.; Frese, J. W.; Elsegood, M. R.; Xing, Q.; Sun, W. H.; Redshaw, C., Vanadyl complexes bearing bi-dentate phenoxyimine ligands: synthesis, structural studies and ethylene polymerization capability. *Dalton Trans* **2014**, 43 (22), 8300-10.
217. Nakayama, Y., Olefin polymerization behavior of bis(phenoxy-imine) Zr, Ti, and V complexes with MgCl₂-based cocatalysts. *Journal of Molecular Catalysis A: Chemical* **2004**, 213 (1), 141-150.
218. Nakayama, Y.; Bando, H.; Sonobe, Y.; Suzuki, Y.; Fujita, T., Highly Active, Thermally Robust V-based New Olefin Polymerization Catalyst System. *Chemistry Letters* **2003**, 32 (8), 766-767.
219. Wu, J.-Q.; Pan, L.; Hu, N.-H.; Li, Y.-S., Synthesis, Structural Characterization, and Ethylene Polymerization Behavior of the Vanadium(III) Complexes Bearing Salicylaldiminato Ligands. *Organometallics* **2008**, 27 (15), 3840-3848.
220. Yoshifumi Onishi, S. K., Michiya Fujiki, and Kotohiro Nomura, Synthesis and Structural Analysis of (Arylimido)vanadium(V) Complexes Containing Phenoxyimine Ligands: New, Efficient Catalyst Precursors for Ethylene Polymerization. *Organometallics* **2008**, 27, 2590-2596.
221. Ishikura, H.; Neven, R.; Lange, T.; Galetová, A.; Blom, B.; Romano, D., Developments in vanadium-catalysed polymerisation reactions: A review. *Inorganica Chimica Acta* **2021**, 515.
222. Santoro, O.; Zhang, X.; Redshaw, C., Synthesis of Biodegradable Polymers: A Review on the Use of Schiff-Base Metal Complexes as Catalysts for the Ring Opening Polymerization (ROP) of Cyclic Esters. *Catalysts* **2020**, 10 (7).
223. Arbaoui, A.; Redshaw, C., Metal catalysts for ϵ -caprolactone polymerisation. *Polymer Chemistry* **2010**, 1 (6).
224. Nomura, J. Y. a. K., A Stable Vanadium(V)-Methyl Complex Containing Arylimido and Bis(ketimide) Ligands That Exhibits Unique Reactivity with Alcohol. *Organometallics* **2005**, 24, 3621-3623.
225. Kaminsky, W.; Funck, A.; Hahnsen, H., New application for metallocene catalysts in olefin polymerization. *Dalton Trans* **2009**, (41), 8803-10.
226. Redshaw, C., Metallocene catalysts: alpha-olefin polymerization and ROP of cyclic esters. *Dalton Trans* **2016**, 45 (22), 9018-30.
227. Clowes, L.; Redshaw, C.; Hughes, D. L., Vanadium-based pro-catalysts bearing depleted 1,3-calix[4]arenes for ethylene or epsilon-caprolactone polymerization. *Inorg Chem* **2011**, 50 (16), 7838-45.
228. Clowes, L.; Walton, M.; Redshaw, C.; Chao, Y.; Walton, A.; Elo, P.; Sumerin, V.; Hughes, D. L., Vanadium(III) phenoxyimine complexes for ethylene or ϵ -caprolactone polymerization: mononuclear versus binuclear pre-catalysts. *Catal. Sci. Technol.* **2013**, 3 (1), 152-160.
229. Ge, F.; Dan, Y.; Al-Khafaji, Y.; Prior, T. J.; Jiang, L.; Elsegood, M. R. J.; Redshaw, C., Vanadium(V) phenolate complexes for ring opening homo- and co-polymerisation of ϵ -caprolactone, L-lactide and rac-lactide. *RSC Advances* **2016**, 6 (6), 4792-4802.
230. Sergei I. Vagin, R. R., Stephan Klaus, and Bernhard Rieger*, Conformationally Flexible Dimeric Salphen Complexes for Bifunctional Catalysis. *J. AM. CHEM. SOC.* **2010**, 132, 14367-14369.
231. Vagin, S.; Winnacker, M.; Kronast, A.; Altenbuchner, P. T.; Deglmann, P.; Sinkel, C.; Loos, R.; Rieger, B., New Insights into the Ring-Opening Polymerization of β -Butyrolactone Catalyzed by Chromium(III) Salphen Complexes. *ChemCatChem* **2015**, 7 (23), 3963-3971.
232. Kricheldorf, H. R.; Damrau, D.-O., Polylactones. 44. Polymerizations of L-Lactide Catalyzed by Manganese Salts. *Journal of Macromolecular Science, Part A* **1998**, 35 (11), 1875-1887.
233. Rajashekar, B.; Chakraborty, D., Co(II) and Mn(II) catalyzed bulk ring-opening polymerization of cyclic esters. *Polymer Bulletin* **2014**, 71 (9), 2185-2203.
234. Daneshmand, P.; Schaper, F., Exploring the reactivity of manganese(III) complexes with diphenolate-diamino ligands in rac-lactide polymerization. *Dalton Trans* **2015**, 44 (47), 20449-58.
235. Yang, W.; Zhao, K. Q.; Wang, B. Q.; Redshaw, C.; Elsegood, M. R.; Zhao, J. L.; Yamato, T., Manganese coordination chemistry of bis(imino)phenoxide derived [2 + 2] Schiff-base macrocyclic ligands. *Dalton Trans* **2016**, 45 (1), 226-36.

236. Fazekas, E.; Nichol, G. S.; Garden, J. A.; Shaver, M. P., Iron(III) Half Salen Catalysts for Atom Transfer Radical and Ring-Opening Polymerizations. *ACS Omega* **2018**, *3* (12), 16945-16953.
237. Duan, R.; Hu, C.; Li, X.; Pang, X.; Sun, Z.; Chen, X.; Wang, X., Air-Stable Salen-Iron Complexes: Stereoselective Catalysts for Lactide and ϵ -Caprolactone Polymerization through in Situ Initiation. *Macromolecules* **2017**, *50* (23), 9188-9195.
238. Cozzolino, M.; Leo, V.; Tedesco, C.; Mazzeo, M.; Lamberti, M., Salen, salen and salalen iron(III) complexes as catalysts for CO₂/epoxide reactions and ROP of cyclic esters. *Dalton Trans* **2018**, *47* (37), 13229-13238.
239. Driscoll, O. J.; Leung, C. K. C.; Mahon, M. F.; McKeown, P.; Jones, M. D., Iron(III) Salalen Complexes for the Polymerisation of Lactide. *European Journal of Inorganic Chemistry* **2018**, *2018* (47), 5129-5135.
240. Fazekas, E.; Nichol, G. S.; Garden, J. A.; Shaver, M. P., Iron(III) Half Salen Catalysts for Atom Transfer Radical and Ring-Opening Polymerizations. *ACS Omega* **2018**, *3* (12), 16945-16953.
241. Fazekas, E.; Nichol, G. S.; Shaver, M. P.; Garden, J. A., Stable Fe(III) phenoxyimines as selective and robust CO₂/epoxide coupling catalysts. *Dalton Trans* **2018**, *47* (37), 13106-13112.
242. Marin, P.; Tschan, M. J.; Isnard, F.; Robert, C.; Haquette, P.; Trivelli, X.; Chamoreau, L. M.; Guerineau, V.; Del Rosal, I.; Maron, L.; Venditto, V.; Thomas, C. M., Polymerization of rac-Lactide Using Achiral Iron Complexes: Access to Thermally Stable Stereocomplexes. *Angew Chem Int Ed Engl* **2019**, *58* (36), 12585-12589.
243. Xiaoying Wang, K. L., * Daping Quan, and Qing Wu, Bulk Ring-Opening Polymerization of Lactides Initiated by Ferric Alkoxides. *Macromolecules* **2005**, *38*, 4611-4617.
244. Brendan J. O'Keefe, S. M. M., Marc A. Hillmyer,* and William B. Tolman*, Rapid and Controlled Polymerization of Lactide by Structurally Characterized Ferric Alkoxides. *J. Am. Chem. Soc.* **2001**, *123*, 339-340.
245. Brendan J. O'Keefe, L. E. B., Marc A. Hillmyer,* and William B. Tolman*, Mechanistic Comparison of Cyclic Ester Polymerizations by Novel Iron(III)-Alkoxide Complexes: Single vs Multiple Site Catalysis. *J. AM. CHEM. SOC.* **2002**, *124*, 4384-4393.
246. Gibson, V. C.; Marshall, E. L.; Navarro-Llobet, D.; White, A. J. P.; Williams, D. J., A well-defined iron(II) alkoxide initiator for the controlled polymerisation of lactide. *Journal of the Chemical Society, Dalton Transactions* **2002**, (23), 4321-4322.
247. DAVID S. MCGUINNESS, E. L. M., VERNON C. GIBSON, JONATHAN W. STEED, Anionic Iron(II) Alkoxides as Initiators for the Controlled Ring-Opening Polymerization of Lactide. *3799-3803* **2003**.
248. Yurii K. Gun'ko, a. U. C., [a] and Vadim G. Kessler[b], Synthesis and Structure of the First Fell Heterometallic Alkoxide [(THF)NaFe(OtBu)₃]₂ η a Possible Precursor for New Materials. *Eur. J. Inorg. Chem.* **2002**, 1029-1031.
249. Biernesser, A. B.; Li, B.; Byers, J. A., Redox-controlled polymerization of lactide catalyzed by bis(imino)pyridine iron bis(alkoxide) complexes. *J Am Chem Soc* **2013**, *135* (44), 16553-60.
250. Delle Chiaie, K. R.; Biernesser, A. B.; Ortuno, M. A.; Dereli, B.; Iovan, D. A.; Wilding, M. J. T.; Li, B.; Cramer, C. J.; Byers, J. A., The role of ligand redox non-innocence in ring-opening polymerization reactions catalysed by bis(imino)pyridine iron alkoxide complexes. *Dalton Trans* **2017**, *46* (38), 12971-12980.
251. Manna, C. M.; Kaplan, H. Z.; Li, B.; Byers, J. A., High molecular weight poly(lactic acid) produced by an efficient iron catalyst bearing a bis(amidinato)-N-heterocyclic carbene ligand. *Polyhedron* **2014**, *84*, 160-167.
252. Kang, Y. Y.; Park, H.-R.; Lee, M. H.; An, J.; Kim, Y.; Lee, J., Dinuclear iron(III) complexes with different ligation for ring opening polymerization of lactide. *Polyhedron* **2015**, *95*, 24-29.
253. Silvino, A. C.; Rodrigues, A. L. C.; Resende, J. A. L. C., Synthesis, structure and application to lactide polymerization of a new phenoxy-imine iron(III) complex. *Inorganic Chemistry Communications* **2015**, *55*, 39-42.
254. Paul, S.; Zhu, Y.; Romain, C.; Brooks, R.; Saini, P. K.; Williams, C. K., Ring-opening copolymerization (ROCOP): synthesis and properties of polyesters and polycarbonates. *Chem Commun (Camb)* **2015**, *51* (30), 6459-79.

255. Wu, G. P.; Wei, S. H.; Ren, W. M.; Lu, X. B.; Xu, T. Q.; Darensbourg, D. J., Perfectly alternating copolymerization of CO₂ and epichlorohydrin using cobalt(III)-based catalyst systems. *J Am Chem Soc* **2011**, *133* (38), 15191-9.
256. Yuan, C.; Xu, X.; Zhang, Y.; Ji, S., Ring-opening Polymerization of L-Lactide by an Anionic Cobalt(II) Aryloxide. *Chinese Journal of Chemistry* **2012**, *30* (7), 1474-1478.
257. Marin, P.; Tschan, M. J. L.; Haquette, P.; Roisnel, T.; del Rosal, I.; Maron, L.; Thomas, C. M., Single-site cobalt and zinc catalysts for the ring-opening polymerization of lactide. *European Polymer Journal* **2019**, *120*.
258. Tschan, M. J.; Guo, J.; Raman, S. K.; Brule, E.; Roisnel, T.; Rager, M. N.; Legay, R.; Durieux, G.; Rigaud, B.; Thomas, C. M., Zinc and cobalt complexes based on tripodal ligands: synthesis, structure and reactivity toward lactide. *Dalton Trans* **2014**, *43* (11), 4550-64.
259. Wang, K.; Prior, T. J.; Redshaw, C., Turning on ROP activity in a bimetallic Co/Zn complex supported by a [2+2] Schiff-base macrocycle. *Chem Commun (Camb)* **2019**, *55* (75), 11279-11282.
260. Ruiz, A. C.; Damodaran, K. K.; Suman, S. G., Towards a selective synthetic route for cobalt amino acid complexes and their application in ring opening polymerization of rac-lactide. *RSC Adv* **2021**, *11* (27), 16326-16338.
261. John, A.; Katiyar, V.; Pang, K.; Shaikh, M. M.; Nanavati, H.; Ghosh, P., Ni(II) and Cu(II) complexes of phenoxy-ketimine ligands: Synthesis, structures and their utility in bulk ring-opening polymerization (ROP) of l-lactide. *Polyhedron* **2007**, *26* (15), 4033-4044.
262. Routaray, A.; Mantri, S.; Nath, N.; Sutar, A. K.; Maharana, T., Nickel(II) complex catalyzed ring-opening polymerization of lactide. *Polyhedron* **2016**, *119*, 335-341.
263. Ding, L.; Jin, W.; Chu, Z.; Chen, L.; Lü, X.; Yuan, G.; Song, J.; Fan, D.; Bao, F., Bulk solvent-free melt ring-opening polymerization (ROP) of L-lactide catalyzed by Ni(II) and Ni(II)-Ln(III) complexes based on the acyclic Salen-type Schiff-base ligand. *Inorganic Chemistry Communications* **2011**, *14* (8), 1274-1278.
264. Jin, W.-J.; Ding, L.-Q.; Chu, Z.; Chen, L.-L.; Lü, X.-Q.; Zheng, X.-Y.; Song, J.-R.; Fan, D.-D., Controllable bulk solvent-free melt ring-opening polymerization (ROP) of l-lactide catalyzed by Ni(II) and Ni(II)-Ln(III) complexes based on the Salen-type Schiff-base ligand. *Journal of Molecular Catalysis A: Chemical* **2011**, *337* (1-2), 25-32.
265. Xiao, G.; Yan, B.; Ma, R.; Jin, W. J.; Lü, X. Q.; Ding, L. Q.; Zeng, C.; Chen, L. L.; Bao, F., Bulk ring-opening polymerization (ROP) of L-lactide catalyzed by Ni(ii) and Ni(ii)-Sm(iii) complexes based on a salen-type schiff-base ligand. *Polym. Chem.* **2011**, *2* (3), 659-664.
266. Gowda, R. R.; Chakraborty, D., Copper acetate catalyzed bulk ring opening polymerization of lactides. *Journal of Molecular Catalysis A: Chemical* **2011**, *349* (1-2), 86-93.
267. Whitehorne, T. J.; Schaper, F., Square-planar Cu(II) diketiminate complexes in lactide polymerization. *Inorg Chem* **2013**, *52* (23), 13612-22.
268. Chen, L.-L.; Ding, L.-Q.; Zeng, C.; Long, Y.; Lü, X.-Q.; Song, J.-R.; Fan, D.-D.; Jin, W.-J., Bulk solvent-free melt ring-opening polymerization of L-lactide catalyzed by Cu(II) and Cu(II)-Nd(III) complexes of the Salen-type Schiff-base ligand. *Applied Organometallic Chemistry* **2011**, *25* (4), 310-316.
269. Whitehorne, T. J.; Schaper, F., Nacnac(Bn)CuOiPr: a strained geometry resulting in very high lactide polymerization activity. *Chem Commun (Camb)* **2012**, *48* (83), 10334-6.
270. Li, C.-Y.; Hsu, S.-J.; Lin, C.-I.; Tsai, C.-Y.; Wang, J.-H.; Ko, B.-T.; Lin, C.-H.; Huang, H.-Y., Air-stable copper derivatives as efficient catalysts for controlled lactide polymerization: Facile synthesis and characterization of well-defined benzotriazole phenoxide copper complexes. *Journal of Polymer Science Part A: Polymer Chemistry* **2013**, *51* (18), 3840-3849.
271. Fortun, S.; Daneshmand, P.; Schaper, F., Isotactic rac-Lactide Polymerization with Copper Complexes: The Influence of Complex Nuclearity. *Angew Chem Int Ed Engl* **2015**, *54* (46), 13669-72.
272. Daneshmand, P.; Pinon, L.; Schaper, F., Dinuclear iminophenoxide copper complexes in rac-lactide polymerisation. *Dalton Trans* **2018**, *47* (30), 10147-10161.

273. Fernández-G, J. M.; Xochitiotzi-Flores, J.; Hernández-Ortega, S.; Gómez-Vidales, V.; Del Rocío Patiño-Maya, M., Structures of o-hydroxy Schiff-base copper(II) complexes derived from p-benzylamines. *Journal of Coordination Chemistry* **2010**, *63* (12), 2132-2145.
274. Lee, J.; Yoon, M.; Lee, H.; Nayab, S., Stereoselective polymerization of methyl methacrylate and rac-lactide mediated by iminomethylpyridine based Cu(ii) complexes. *RSC Advances* **2020**, *10* (27), 16209-16220.
275. Bhattacharjee, A.; Halder, S.; Ghosh, K.; Rizzoli, C.; Roy, P., Mono-, tri- and polynuclear copper(ii) complexes of Schiff-base ligands: synthesis, characterization and catalytic activity towards alcohol oxidation. *New Journal of Chemistry* **2017**, *41* (13), 5696-5706.
276. Guerre, M.; Wahidur Rahaman, S. M.; Améduri, B.; Poli, R.; Ladmiral, V., RAFT synthesis of well-defined PVDF-b-PVAc block copolymers. *Polymer Chemistry* **2016**, *7* (45), 6918-6933.
277. Wang, Y.; Wang, M.; Bai, L.; Zhang, L.; Cheng, Z.; Zhu, X., Facile synthesis of poly(N-vinyl pyrrolidone) block copolymers with "more-activated" monomers by using photoinduced successive RAFT polymerization. *Polymer Chemistry* **2020**, *11* (12), 2080-2088.
278. Antoine Debuigne, J.-R. C., Nicolas Willet, and Robert Jerome, Synthesis of Poly(vinyl acetate) and Poly(vinyl alcohol) Containing Block Copolymers by Combination of Cobalt-Mediated Radical Polymerization and ATRP. *Macromolecules* **2005**, *35*, 9488-9496.
279. Haque, F. M.; Ishibashi, J. S. A.; Lidston, C. A. L.; Shao, H.; Bates, F. S.; Chang, A. B.; Coates, G. W.; Cramer, C. J.; Dauenhauer, P. J.; Dichtel, W. R.; Ellison, C. J.; Gormong, E. A.; Hamachi, L. S.; Hoyer, T. R.; Jin, M.; Kalow, J. A.; Kim, H. J.; Kumar, G.; LaSalle, C. J.; Liffland, S.; Lipinski, B. M.; Pang, Y.; Parveen, R.; Peng, X.; Popowski, Y.; Prebihalo, E. A.; Reddi, Y.; Reineke, T. M.; Sheppard, D. T.; Swartz, J. L.; Tolman, W. B.; Vlaisavljevich, B.; Wissinger, J.; Xu, S.; Hillmyer, M. A., Defining the Macromolecules of Tomorrow through Synergistic Sustainable Polymer Research. *Chemical Reviews* **2022**, *122* (6), 6322-6373.
280. Dirany, M.; Lacroix-Desmazes, P.; Vayer, M.; Erre, R.; Boutevin, B.; Sinturel, C., Polystyrene-block-poly(lactide) obtained by the combination of atom transfer radical polymerization and ring-opening polymerization with a commercial dual initiator. *Journal of Applied Polymer Science* **2011**, *122* (5), 2944-2951.
281. Wang, W.-W.; Ren, W.-Y.; Jiang, L.; Dan, Y., Synthesis and characterization of AB-type copolymers poly(L-lactide)-block-poly(methyl methacrylate) via a convenient route combining ROP and ATRP from a dual initiator. *Journal of Applied Polymer Science* **2010**, n/a-n/a.
282. Li, M.; Wang, S.; Li, F.; Zhou, L.; Lei, L., Iodine-mediated photo-controlled atom transfer radical polymerization (photo-ATRP) and block polymerization combined with ring-opening polymerization (ROP) via a superbase. *Polymer Chemistry* **2020**, *11* (41), 6591-6598.
283. Mao, J.; Ji, X.; Bo, S., Synthesis and pH/Temperature-Responsive Behavior of PLLA-b-PDMAEMA Block Polyelectrolytes Prepared via ROP and ATRP. *Macromolecular Chemistry and Physics* **2011**, *212* (7), 744-752.
284. Capasso Palmiero, U.; Sponchioni, M.; Manfredini, N.; Maraldi, M.; Moscatelli, D., Strategies to combine ROP with ATRP or RAFT polymerization for the synthesis of biodegradable polymeric nanoparticles for biomedical applications. *Polymer Chemistry* **2018**, *9* (30), 4084-4099.
285. Wolf, F. F.; Friedemann, N.; Frey, H., Poly(lactide)-block-Poly(HEMA) Block Copolymers: An Orthogonal One-Pot Combination of ROP and ATRP, Using a Bifunctional Initiator. *Macromolecules* **2009**, *42* (15), 5622-5628.
286. Amit Garle, U. O., Bridgette M. Budhlall, Combination of ROP and RAFT for synthesis of a novel biodegradable, stimuli responsive P(CL-ran-CCL)-b-PNIPAm-bP(CL-ran-CCL) triblock copolymer.
287. Yezi You, C. H., Wenping Wang, Weiqi Lu, and Caiyuan Pan, Preparation and Characterization of Thermally Responsive and Biodegradable Block Copolymer Comprised of PNIPAAm and PLA by Combination of ROP and RAFT Methods. *Macromolecules* **2004**, *37*, 9761-9767.
288. Öztürk, T.; Göktaş, M.; Hazer, B., One-step synthesis of triarm block copolymers via simultaneous reversible-addition fragmentation chain transfer and ring-opening polymerization. *Journal of Applied Polymer Science* **2010**, NA-NA.

289. Song, J.; Xu, J.; Pispas, S.; Zhang, G., One-pot synthesis of poly(l-lactide)-b-poly(methyl methacrylate) block copolymers. *RSC Advances* **2015**, *5* (48), 38243-38247.
290. Aydogan, C.; Kutahya, C.; Allushi, A.; Yilmaz, G.; Yagci, Y., Block copolymer synthesis in one shot: concurrent metal-free ATRP and ROP processes under sunlight. *Polymer Chemistry* **2017**, *8* (19), 2899-2903.
291. Kang, H. U.; Yu, Y. C.; Shin, S. J.; Youk, J. H., One-step synthesis of block copolymers using a hydroxyl-functionalized trithiocarbonate RAFT agent as a dual initiator for RAFT polymerization and ROP. *Journal of Polymer Science Part A: Polymer Chemistry* **2012**, *51* (4), 774-779.
292. Kryuchkov, M. A.; Detrembleur, C.; Bazuin, C. G., Linear amphiphilic diblock copolymers of lactide and 2-dimethylaminoethyl methacrylate using bifunctional-initiator and one-pot approaches. *Polymer* **2014**, *55* (10), 2316-2324.
293. Wang, Y.; Zhao, Y.; Ye, Y.; Peng, H.; Zhou, X.; Xie, X.; Wang, X.; Wang, F., A One-Step Route to CO₂-Based Block Copolymers by Simultaneous ROCOP of CO₂/Epoxides and RAFT Polymerization of Vinyl Monomers. *Angew Chem Int Ed Engl* **2018**, *57* (14), 3593-3597.
294. Fu, C.; Xu, J.; Boyer, C., Photoacid-mediated ring opening polymerization driven by visible light. *Chem Commun (Camb)* **2016**, *52* (44), 7126-9.
295. B.S. Lele, J.-C. L., Synthesis of novel amphiphilic star-shaped poly(1-caprolactone)-blockpoly(N-(2-hydroxypropyl)methacrylamide) by combination of ring-opening and chain transfer polymerization. *Polymer* **2002**, *43*, 5595-5606.
296. Chen, J.; Zhang, H.; Chen, J.; Wang, X.; Wang, X., Synthesis of Star-Shaped Poly(ϵ -caprolactone)-b-Poly(styrene) Block Copolymer by Combining Ring-Opening Polymerization and Atom Transfer Radical Polymerization. *Journal of Macromolecular Science, Part A* **2005**, *42* (9), 1247-1257.
297. Michele Schappacher, N. F., and Sophie M. Guillaume*, Poly(methyl methacrylate)-Poly(caprolactone) AB and ABA Block Copolymers by Combined Ring-Opening Polymerization and Atom Transfer Radical Polymerization. *Macromolecules* **2007**, *10*, 8887-8896.
298. Zhao, Y.; Wang, Y.; Zhou, X.; Xue, Z.; Wang, X.; Xie, X.; Poli, R., Oxygen-Triggered Switchable Polymerization for the One-Pot Synthesis of CO₂-Based Block Copolymers from Monomer Mixtures. *Angew Chem Int Ed Engl* **2019**, *58* (40), 14311-14318.
299. Wang, Y.; Zhao, Y.; Zhu, S.; Zhou, X.; Xu, J.; Xie, X.; Poli, R., Switchable Polymerization Triggered by Fast and Quantitative Insertion of Carbon Monoxide into Cobalt-Oxygen Bonds. *Angew Chem Int Ed Engl* **2020**, *59* (15), 5988-5994.
300. Zhao, Y.; Zhu, S.; Liao, C.; Wang, Y.; Lam, J. W. Y.; Zhou, X.; Wang, X.; Xie, X.; Tang, B. Z., Cobalt-Mediated Switchable Catalysis for the One-Pot Synthesis of Cyclic Polymers. *Angew Chem Int Ed Engl* **2021**, *60* (31), 16974-16979.
301. Dau, H.; Keyes, A.; Basbug Alhan, H. E.; Ordonez, E.; Tsogtgerel, E.; Gies, A. P.; Auyeung, E.; Zhou, Z.; Maity, A.; Das, A.; Powers, D. C.; Beezer, D. B.; Harth, E., Dual Polymerization Pathway for Polyolefin-Polar Block Copolymer Synthesis via MILRad: Mechanism and Scope. *J Am Chem Soc* **2020**, *142* (51), 21469-21483.
302. Zhao, Y.; Jung, J.; Nozaki, K., One-Pot Synthesis of Polyethylene-Based Block Copolymers via a Dual Polymerization Pathway. *J Am Chem Soc* **2021**, *143* (45), 18832-18837.
303. Brookhart, M.; DeSimone, J. M.; Grant, B. E.; Tanner, M. J., Cobalt(III)-Catalyzed Living Polymerization of Ethylene: Routes to End-Capped Polyethylene with a Narrow Molar Mass Distribution. *Macromolecules* **2002**, *28* (15), 5378-5380.
304. Olafs Daugulis, M. B., * and Peter S. White, Ethylene Polymerization Using Tetramethyl(2-methylthioethyl)cyclopentadienyl Complexes of Cobalt. *Organometallics* **2003**, *22*, 4699-4704.

Chapter II. Cobalt(III) carboxylate complexes

Chapter II is dedicated to the synthesis and characterization of cobalt(III) complexes that can potentially initiate and moderate a polymerization reaction, following either a radical (OMRP) or a coordination insertion (ROP) path. This chapter is restricted to the results belonging to the coordination chemistry, the polymerization results being discussed in **Chapter III**.

Table of contents

Chapter II. Cobalt(III) carboxylate complexes	77
I. Introduction and strategy targeting.....	80
II. Cobalt complexes with (N_2, O_2)-type ligands	82
1. Introduction	82
2. (N_2, O_2) ligand architectures	82
3. Cobalt(II) complexes with Schiff-base ligands	84
4. Cobalt(III) carboxylate complexes with (N_2, O_2)-type ligands	85
a. Cobalt(III) acetate complex with a Schiff-base ligand	85
b. Cobalt(III) acetate complex with a diamino-bis(phenolate) tetradentate tripodal ligand.....	88
c. Cobalt(III) carboxylate complexes with a Schiff-base ligand	91
5. Conclusion	95
III. Cobalt complexes with an (O_2, O_2)-type ligand.....	96
1. Introduction	96
2. (Acetylacetonato)-cobalt(III) carboxylate complexes	96
a. Bis(acetylacetonato)-cobalt(III) benzoate complex	96
b. Bis(acetylacetonato)-cobalt(III) complexes with substituted benzoates	102
c. Bis(acetylacetonato)-cobalt(III) complexes with alkyl carboxylates	107
d. Use of simple peroxide	109
IV. Conclusion and outlook.....	110
V. Experimental section.....	111
1. Materials	111
2. Characterizations	111
3. Methods	113
VI. References.....	118

I. Introduction and strategy targeting

To be used as a polymerization moderator, an organometallic complex must satisfy a few conditions. As shown in the Chapter I, the metal centre, the coordination sphere and the nature of the monomers have an impact on the polymerization. Ligand engineering permits, in theory, to modulate the reactivity of the coordination compound and to adapt it to a desired monomer or experimental condition. It is thus possible to imagine a complex capable to self-initiate and moderate either a radical polymerization (OMRP) or a ring opening polymerization (ROP) or both.

In terms of radical polymerization, several cobalt(II) or organocobalt(III) complexes were shown to control the OMRP of MAMs such as acrylates. For example, Peng *et al.*^{1, 2} described a cobalt Schiff-base system working at room temperature (*Figure I-1*, **1** and **2**). However, these systems require the simultaneous use of a co-initiator (AIBN or 2,4,6-trimethylbenzoyl diphenylphosphine oxide (TPO)).

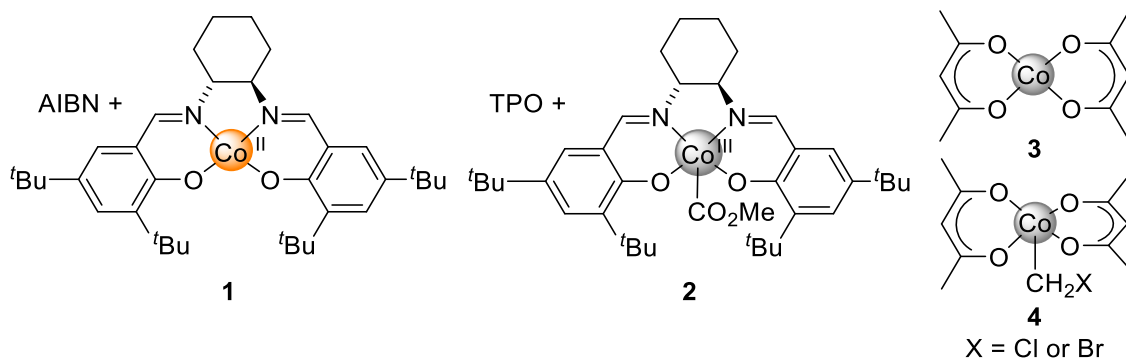
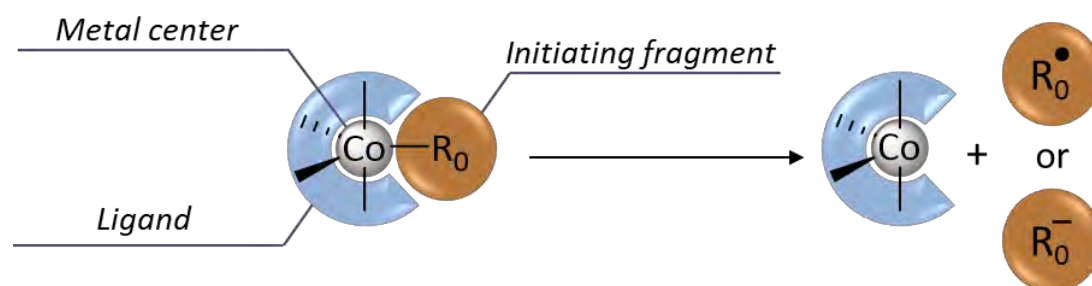


Figure I-1 : Reported systems for the OMRP of MAMs (1, 2) & LAMs (3, 4).

Concerning the controlled polymerization of LAMs such as vinyl esters and amides, a few performing systems have been described by Debuigne, Poli *et al.*^{3, 4}, notably cobalt(II) bisacetylacetonate (*Figure I-1*, **3**), which also requires the presence of an external radical source (*e.g.* AIBN, V70, *etc.*)⁵ Alternatively, organocobalt(III) complexes such as **4**⁴ (*Figure I-1*) or the short-chain [Co^{III}(acac)₂-VAc_xR₀] system, which feature weak metal-carbon bonds that are homolytically cleaved under mild conditions, can be used without additives to start the polymerization.⁶ Even though the halomethyl-cobalt(III) complexes **4** have suitably weak metal-carbon bonds, these derivatives were obtained in low yield (around 26%) and needed silica column purification. The synthesis of the short-chain [Co^{III}(acac)₂-VAc_xR₀] macroinitiator^{6, 7} needs a long reaction time (40 h), can only be carried out on a small scale, and also requires a tedious chromatographic separation and gives a low yield.⁶ In addition, these organocobalt(III) products are difficult to handle because of air sensitivity and must be stored at low temperatures because of thermal fragility. In summary, the available moderating systems either need to use a co-initiator, or their syntheses are difficult, low-yielding, and the products are delicate to handle.

On the other hand, as described in the previous chapter, the reported systems based on cobalt for ring opening polymerization are not abundant, contrary to the more abundant reports of Fe-catalysed ROP⁸ or ROCOP.^{9, 10} One of the few cobalt-based catalysts, complex **10.7** (cf. *Chapter I, Section 8, Figure III-19*), reported by Thomas *et al.*,¹¹ works well for the living polymerization of LA under the ROP mechanism. However, this type of architecture has not been shown capable to undergo homolytic bond cleavage and generate radicals.

Our objective is the design of complexes capable to simultaneously undergo two different processes as shown in *Scheme I-1*: self-initiate and moderate a radical polymerization (cf. *Chapter I, Figure II-4*) without the need of a co-initiator; coordinate and insert ROP monomers by nucleophilic attack (cf. *Chapter I, Figure III-1*). In addition, we also wish to optimize the synthesis procedure. In fact, our objective is to develop a new air-stable, easily synthesized and purified system that can function as a dual initiating tool without any chemical modification or co-agent.



Scheme I-1: New tool to self-initiate and control polymerization by radical or ring opening polymerization.

As depicted in *Scheme I-1*, the tool we propose to develop can be divided into three parts; the cobalt metal centre (the reasons of this choice were discussed in *Chapter I*), the supporting/stabilizing ligand, the stereo-electronic properties of which should be easily tuned, and a versatile initiating group. Based on the literature, we decided to focus our attention on tetradentate dianionic Schiff bases, on diamino-bis(phenolate) (N_2, O_2) ligands and on fully oxygenated (O_4) coordination spheres, *i.e.* the bis(acetylacetonate) system. From DFT calculations (see below), the latter coordination sphere should provide weaker Mt-R bonds and consequently better OMRP processes for LAMs,¹²⁻²⁹ whereas N - or mixed N, O -based ligands (*e.g.* porphyrin, Schiff bases, respectively) should give rise to a better control for MAMs (cf. *Chapter I*).^{17, 30, 31} Moreover, as highlighted in *Chapter I*, complexes of Schiff base were also successfully applied to the ROP of cyclic esters.^{11, 32} Concerning the initiating group, we decided to focus on O -based R_0 groups, *i.e.* alkoxides or carboxylates, because we expected better stability for the resulting initiators. Moreover, alkoxides are well-known as efficient initiating groups for ROP processes while peroxides, supposedly furnishing alkoxy radicals by thermal decomposition, are effective as initiators for radical polymerization processes.

This chapter will be divided in two parts according to the two ligand architectures studied: diamino-bis(phenolate) (N_2, O_2) and bis(acetylacetonate) (O_2, O_2), for which few R_0 groups were explored.

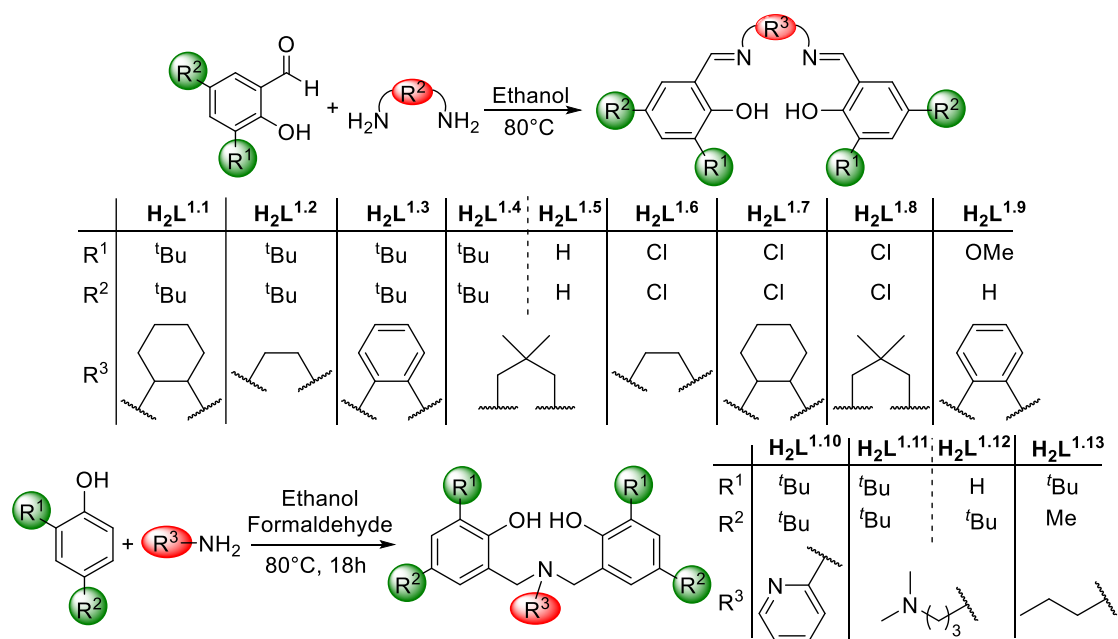
II. Cobalt complexes with (N_2, O_2)-type ligands

1. Introduction

As shown in the bibliographic chapter, Schiff bases were extensively studied in the fields of controlled radical polymerization³³⁻³⁸ and ring opening polymerization reactions.^{39, 40} Such a scaffold presents several interests such as a facile synthesis, which consists of the condensation of amines with salicylaldehyde derivatives, easy purification (precipitation/recrystallization) and a high level of tunability (substituents on the phenol ring or on the N atom). The first example of this kind of ligand was reported in 1933.⁴¹ The second class of ligands we aimed at studying, *i.e.* tetradentate tripodal diamino-bis(phenolates), are also readily accessible and highly tunable and already afforded efficient initiators/moderators for radical⁴² or ring opening polymerizations.¹¹ The following sections will describe the synthesis and characterization of the ligands, the corresponding neutral cobalt(II) complexes and their corresponding neutral cobalt(III) carboxylates.

2. (N_2, O_2) ligand architectures

As shown in *Scheme II-1*, we synthesized a large library of Schiff-base and amino-bis(phenol) pro-ligands with either electron-donating, electron-withdrawing, bulky or small substituents, because these substituents may be crucial for adjusting the Co- P_n bond strength (BDE) or the Lewis acidity of the metal, therefore affecting the performance of the corresponding systems in polymerizations.^{43, 44} Although all of these pro-ligands were already reported in the literature,^{32, 43, 45-54} we carefully characterized them (*i.e.* UV, IR, NMR and XRD) to assess their purity and to provide some missing experimental data.



Scheme II-1: Typical reactions to access Schiff-base and amino-bis(phenolate) pro-ligands.

As representative examples, the ^1H NMR spectra of pro-ligands $\text{H}_2\text{L}^{1.4}$ and $\text{H}_2\text{L}^{1.10}$ are depicted in *Figure II-1* and *Figure II-2*, respectively. That of $\text{H}_2\text{L}^{1.4}$ exhibits^{43, 44} a series of singlets at δ 1.09 (6H), 1.30 (18H), 1.45 (18H) ppm attributed to the CMe_2 and ^tBu groups, respectively, while the methylene group of the linker gives rise to a doublet at δ 3.50 (4H) ppm. The two *meta*-H of the phenol ring and the $\text{N}=\text{CH}$ group are observed at δ 7.14 (2H), 7.38 (2H) and 8.38 (2H) ppm, respectively.

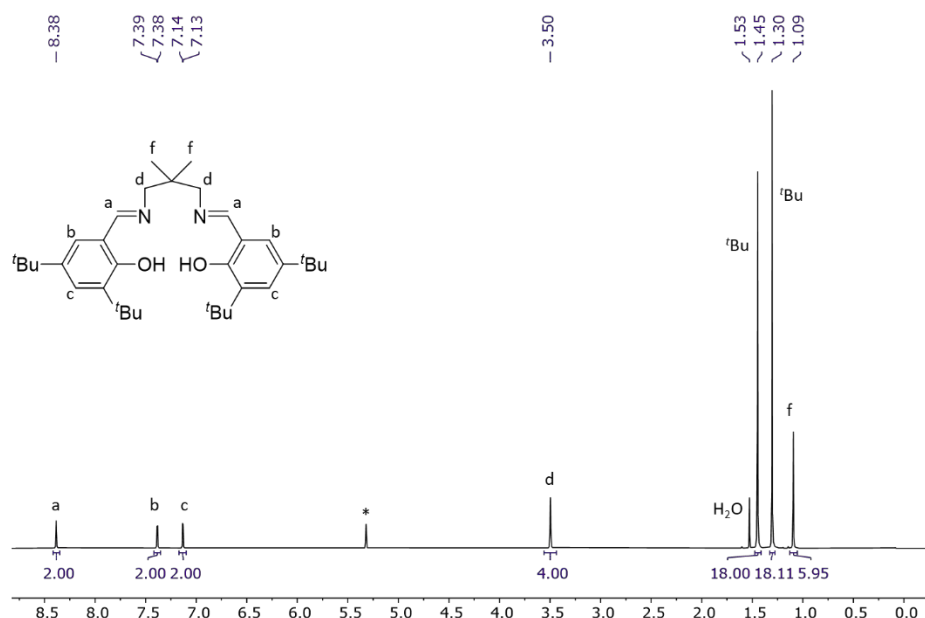


Figure II-1: ^1H NMR (400 MHz, 25°C) spectrum of pro-ligand **1.4** recorded in CD_2Cl_2 (*).

Pro-ligands $\text{H}_2\text{L}^{1.10-1.13}$ were prepared following a procedure reported by our team in 2019,³² and the ^1H NMR spectrum of $\text{H}_2\text{L}^{1.10}$ also exhibits the expected signals (*Figure II-2*).

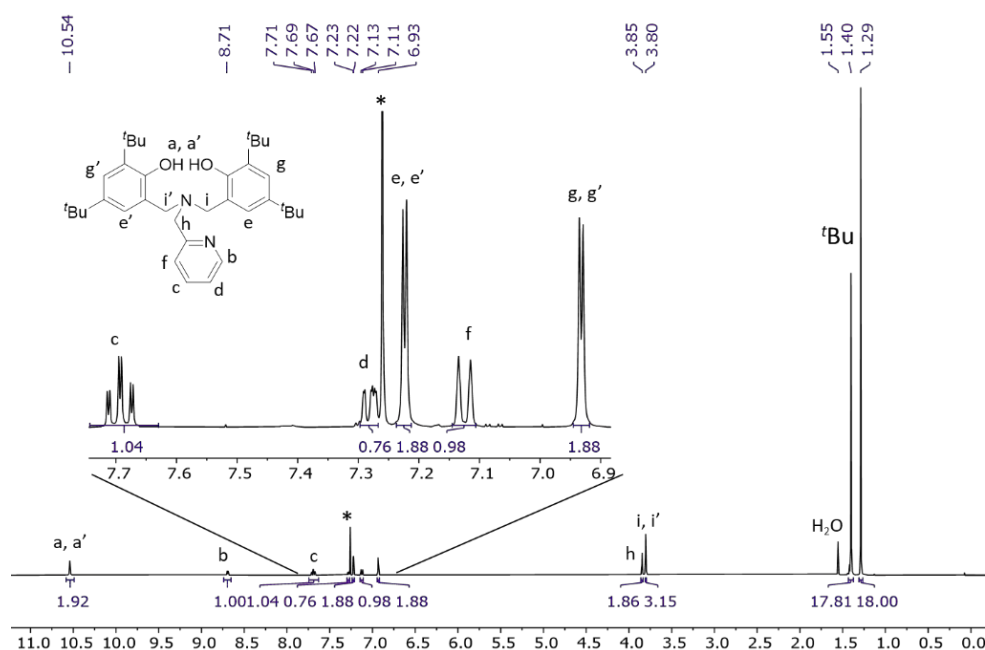
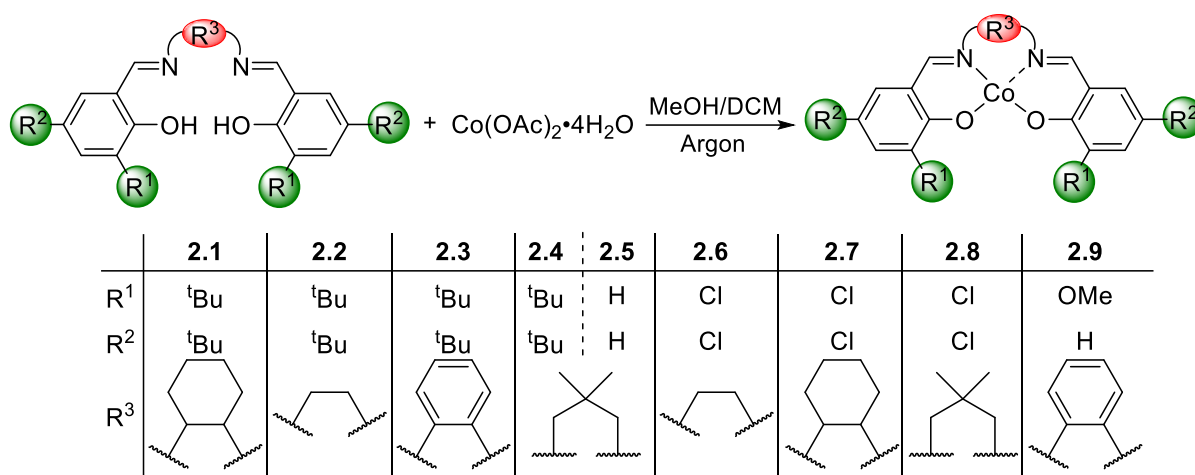


Figure II-2: ^1H NMR (400 MHz, 25°C) spectrum of pro-ligand $\text{H}_2\text{L}^{1.10}$ recorded in CD_2Cl_2 (*).

3. Cobalt(II) complexes with Schiff-base ligands

The neutral cobalt(II) complexes with the above-described salen-type ligands were synthesized according to a previously reported procedure^{55, 56} by mixing (nearly) equimolar amounts of cobalt(II) acetate tetrahydrate and the pro-ligand at room temperature under an inert atmosphere (*Scheme II-2*). As highlighted in *Chapter I*, such complexes may be further used as OMRP moderators following a reverse initiation (*e.g.* with AIBN or TPO as initiators),^{2, 57, 58} or as ROP catalysts in the presence of an alcohol (*e.g.* BnOH or *i*PrOH) to initiate polymerization.⁵⁹



Scheme II-2: Synthesis of cobalt(II) complexes of Schiff-base ligands.

The phenolate ring substituents (R¹ and R², *Scheme II-2*) allow modulating the steric hindrance around the cobalt(II) centre, in the order H < Cl < OMe < ^tBu, and the ligand donating power, due to their electron-donating (such as ^tBu) or electron-withdrawing (such as Cl) nature. Both steric and electronic parameters may affect the activity/reactivity of the complexes, by *e.g.* modifying the Mt-P_n BDE in the corresponding OMRP dormant species, or altering the Lewis acidity and/or accessibility of the Co centre, which are crucial for ROP processes. The length and flexibility/rigidity of the linker between the two N donors may also affect these parameters, therefore we synthesized compounds with a large panel of linkers, *i.e.* cyclohexane-1,2-diyl, 1,2-phenylene, ethane-1,2-diyl or 2,2-dimethyl-propane-1,3-diyl (*Schemes II-1 and II-2*). The cobalt(II) complexes being paramagnetic, they did not afford exploitable NMR spectra, therefore their formation and purity was assessed by elemental analysis (EA), mass spectrometry (MS) and electron paramagnetic resonance (EPR), as shown below for compound **2.4** (see experimental section for the spectroscopic characterization of the other complexes). The ESI-MS spectrum of complex **2.4** reveals as most intense peak the [M]⁺ ion (*m/z* = 591.3 g mol⁻¹), with the expected isotopic distribution (*Figure II-3*). The EPR spectrum exhibits eight lines of equivalent intensity, in accordance with a ⁵⁹Co (*I* = 7/2) hyperfine splitting (*Figure II-4*).^{56, 57}

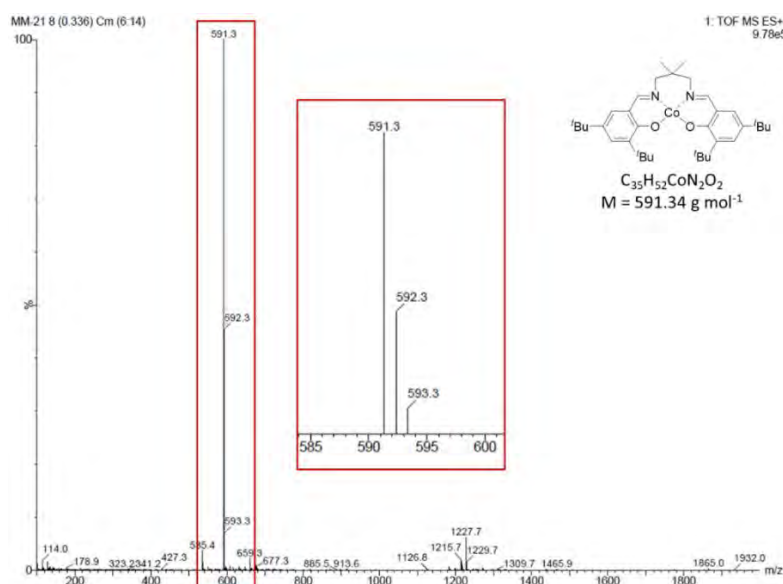


Figure II-3: ESI of the compound **2.4** in DCM/ACN.

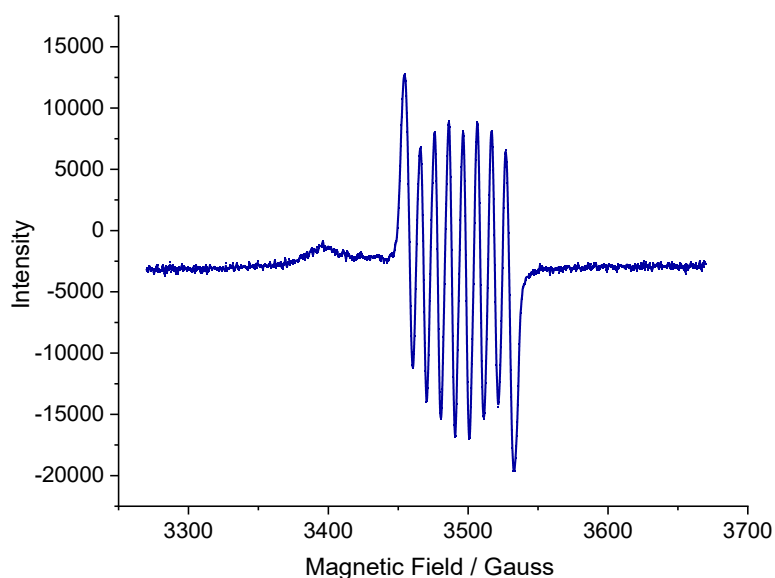


Figure II-4: EPR spectrum of complex **2.4** in toluene.

4. Cobalt(III) carboxylate complexes with (N_2, O_2)-type ligands

This section describes the two explored methods for the synthesis of cobalt(III) carboxylate complexes of (N_2, O_2)-type ligands, *i.e.* Schiff bases and diamino-bis(phenolates), as potential unimolecular air-stable initiators for OMRP and ROP processes.

a. Cobalt(III) acetate complex with a Schiff-base ligand

The Schiff base-cobalt(III) acetate complex $[Co^{III}(L^{1-1})(OAc)]$ **3.1** (Figure II-5) was prepared by reacting the $[Co(OAc)_2]$ precursor and the pro-ligand (1:1 ratio) in glacial acetic acid under aerobic oxidation, as described by Jabcosen and coll. in 2004 (*cf. experimental section*).^{43, 60}

This compound was part of a larger series, including salen-Co^{III}-OH, -Co^{III}-Cl and -Co^{III}-OTs derivatives, which were applied to the hydrolytic kinetic resolution of epoxides. In 2005, Coates and coll. applied complex **3.1** to the alternating copolymerization of propylene oxide and carbon dioxide.⁶¹ Complex **3.1** was properly characterized and further applied as unimolecular OMRP⁵⁸ and ROP initiator (see *Chapter III*). As anticipated, complex **3.1** is diamagnetic, suggesting an octahedral environment for the Co^{III} metal ion with a d⁶ electronic configuration. The recorded ¹H NMR spectrum compared well with the literature and, in particular, the singlet resonance at δ 1.52 (3H) confirmed the presence of the OAc group (Figure II-6).

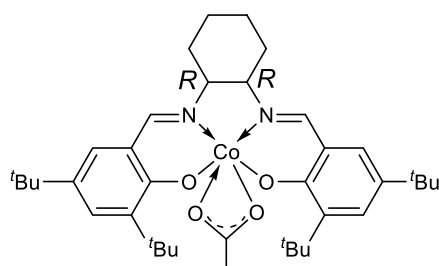


Figure II-5: Schiff base-cobalt(III) acetate complex [Co^{III}(L^{1.1})(OAc)] (**3.1**).

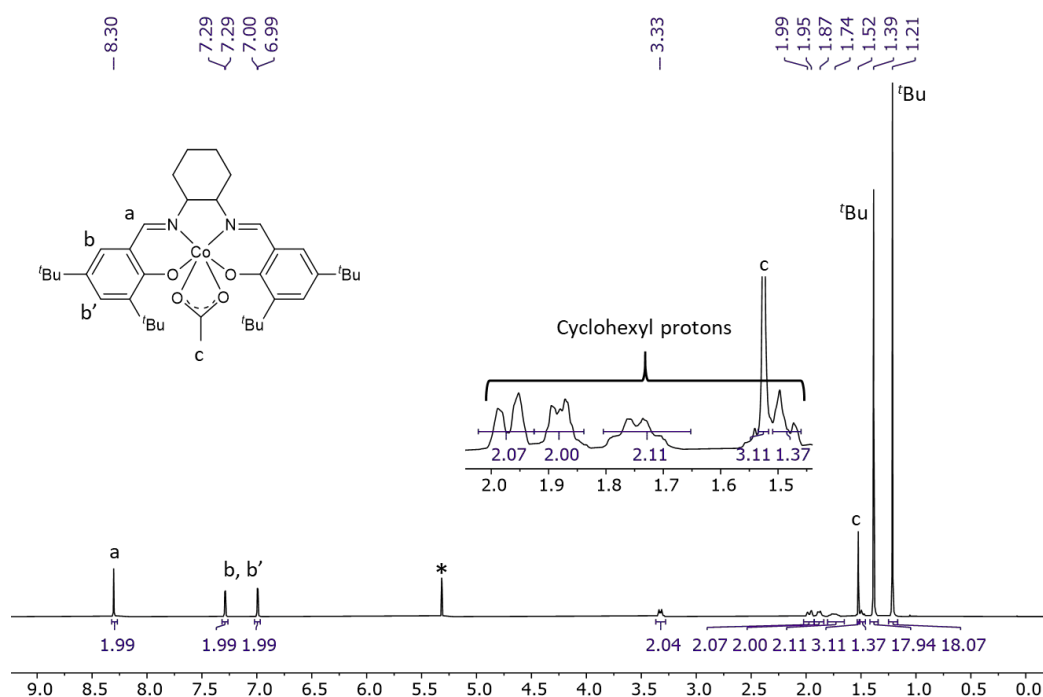
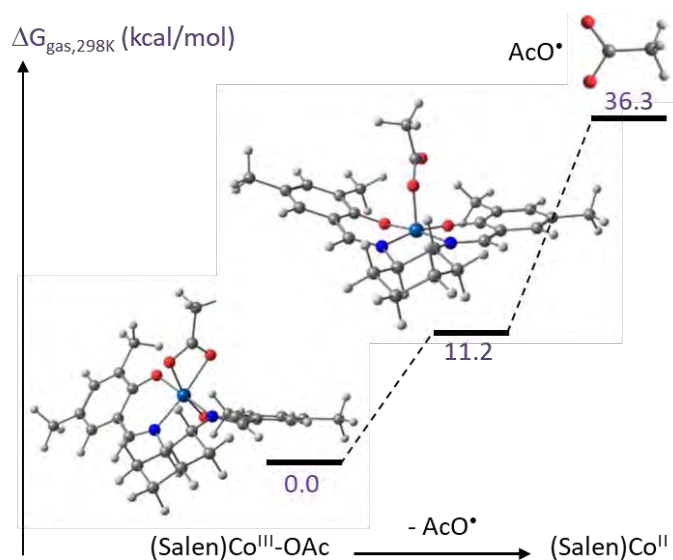


Figure II-6: ¹H NMR (400 MHz, 25°C) of complex **3.1** recorded in CD₂Cl₂ (*).

The aptitude of complex **3.1** to generate an AcO[•] radical by homolytic cleavage of the Co-OAc bond was studied by DFT calculations (Prof. Rinaldo Poli). As shown by the Gibbs energy profile depicted in Figure II-7, the release of the acetate radical follows a two-step mechanism. First, the acetate switches from a bidentate chelating to a monodentate coordination mode and, secondly, the Co-O_(OAc) bond homolysis occurs. The overall Gibbs energy for the AcO[•]

dissociation is $36.3 \text{ kcal mol}^{-1}$ under standard conditions (25°C), while the homolytic cleavage (from the 5-coordinate Co^{III} species) costs only $25.1 \text{ kcal mol}^{-1}$.

This calculated bond strength is consistent with the NMR study presented in *Figure II-8*, which consisted in heating at 70°C for 12 h a CDCl_3 solution of **3.1**. The thermal treatment led to a broadening of the signals of **3.1** and to the appearance of the signals of its paramagnetic Co^{II} counterpart.



*Figure II-7: Gibbs energy profiles for the dissociation of the AcO^\bullet radical from the $\text{Co}(\text{salen})\text{OAc}$ complex **3.1**, calculated with BPW91*.*

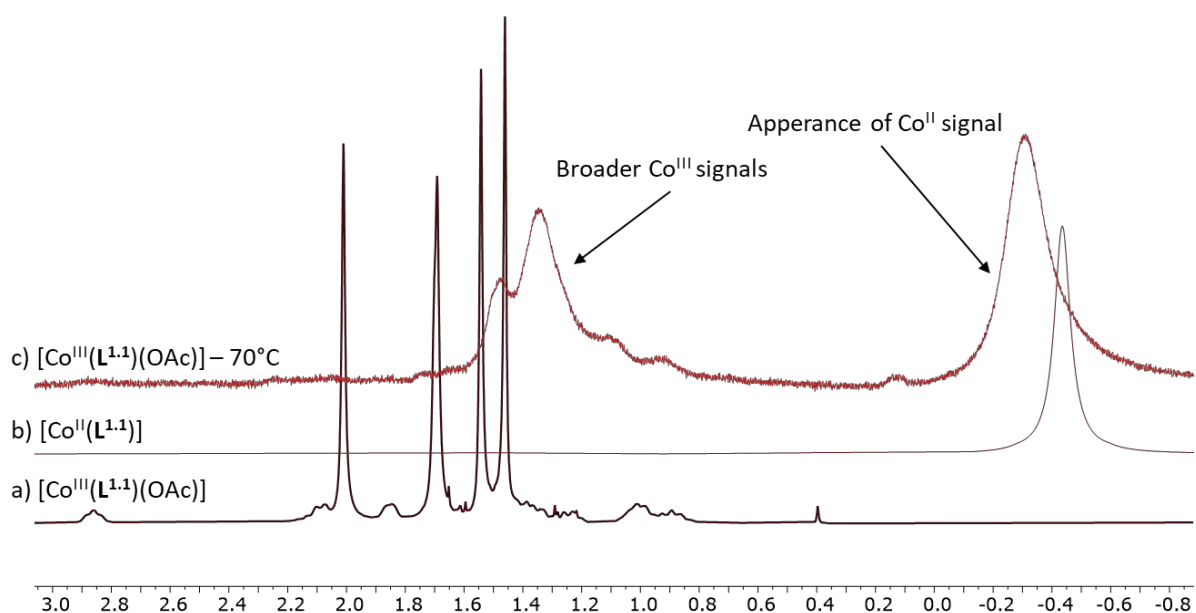


*Figure II-8: Stacking of the ^1H NMR (400 MHz) spectra of a) **3.1**, b) **2.1** and c) **3.1** after heating at 70°C in CDCl_3 for 12h.*

Based on the energy profile shown in *Figure II-9*, should a homolytic cleavage of the Co-O(OAc) bond take place for complex **3.1**, a polymerization of MA and MMA should proceed in the presence of these monomers, and a moderating effect by OMRP should occur, because the cobalt(III)-C bond strengths ($\Delta G^{\text{MA}} = 20.5 \text{ kcal mol}^{-1}$; $\Delta G^{\text{MMA}} = 15.1 \text{ kcal mol}^{-1}$) are sufficiently high to ensure reversible radical trapping. Moreover, the dormant species of the OMRP MMA should be more easily reactivated, because $\Delta G^{\text{MMA}} < \Delta G^{\text{MA}}$. However, and as anticipated, the OMRP of the less-activated VAc monomer, appears more difficult, due to a higher ΔG^{VAc} value (see *Chapter I*).^{57, 62, 63}

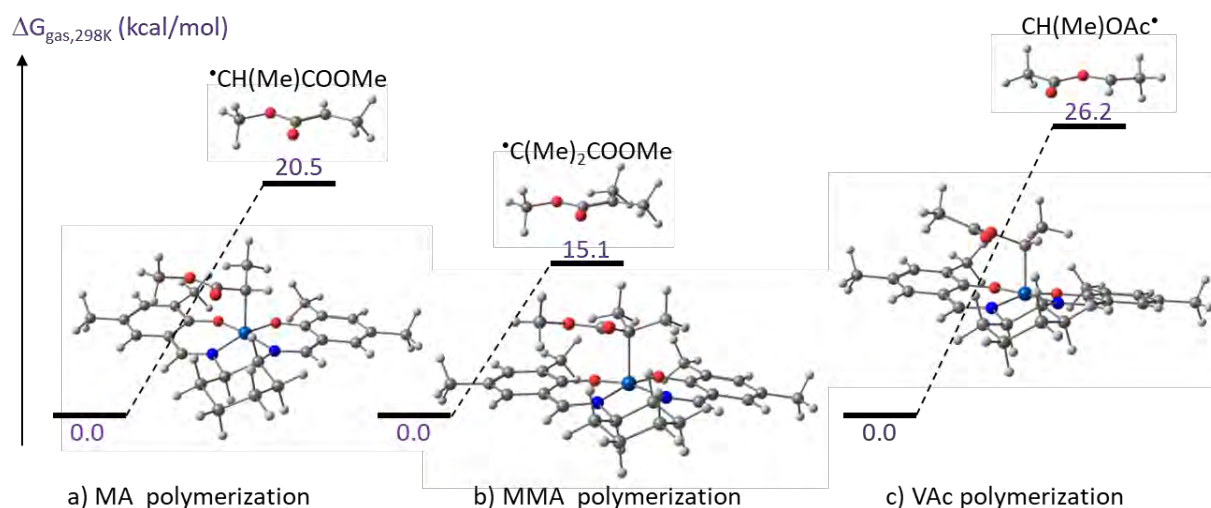


Figure II-9: Gibbs energy profiles for the dissociation of the dormant species a) Co-MA, b) Co-MMA and c) Co-VAc, calculated with BPW91.*

b. Cobalt(III) acetate complex with a diamino-bis(phenolate) tetradentate tripodal ligand

A few examples of cobalt complexes of tetradentate tripodal ligands were applied to polymerization reactions, including the radical polymerization of MAMs, the ROP of lactide and the copolymerization of epoxides with carbon dioxide.^{11, 64, 65} Our group recently reported the synthesis of (acetylacetonato)cobalt(III) and iron(III) complexes with such ligands.³² However, these species did not initiate radical polymerization under the studied conditions. It was concluded that the Co(acac) chelate is too stable to generate acac• radicals. Therefore, we switched target to its supposedly more fragile acetate analogue.

The (acetato)cobalt(III) complex $[\text{Co}(\text{L}^{1.10})(\text{OAc})]$ (**3.2**) with ligand $\text{H}_2\text{L}^{1.10}$ was synthesized in moderate yield (62%) under aerobic conditions, as described in the experimental section. Its ESI-MS spectrum only revealed the peak of the $[\text{M} - \text{OAc}]^+$ ion ($m/z = 601.3 \text{ g mol}^{-1}$), with the expected isotopic distribution, the OAc fragment being probably lost at the ionization step. The ^1H and ^{13}C NMR spectra recorded in CDCl_3 confirmed the formation of the diamagnetic cobalt(III) complex **3.2** (*Figure II-10* to *Figure II-12*). Concerning the ^1H NMR signals, four resonances at 8.56 (*d*, $J = 5.3 \text{ Hz}$), 7.39 (*t*, $J = 7.6 \text{ Hz}$), 7.00 (*t*, $J = 6.5 \text{ Hz}$) and 6.64 (*d*, $J = 8.2 \text{ Hz}$) ppm were attributed to the pyridine ring H atoms, whereas two mutually coupled ($J = 2.6 \text{ Hz}$)

doublets with the roof effect at 6.95 and 6.79 ppm were attributed to the *meta*-H atoms of the phenoxide group. In addition, the methylene protons of the phenolate arms gave rise to inequivalent doublets at δ 4.57 ($J = 12.2$ Hz) and 3.03 ($J = 12.9$ Hz) ppm, the methylene protons of the pyridine arm was characterized by a singlet at 3.97 ppm, and the ^tBu protons are observed as two singlets at 1.31 and 1.20 ppm (Figure II-10). Importantly, the singlet resonance at 1.95, absent in the spectrum of the pro-ligand (Figure II-11) and integrating for three protons, confirmed the quantitative formation of the acetate complex.

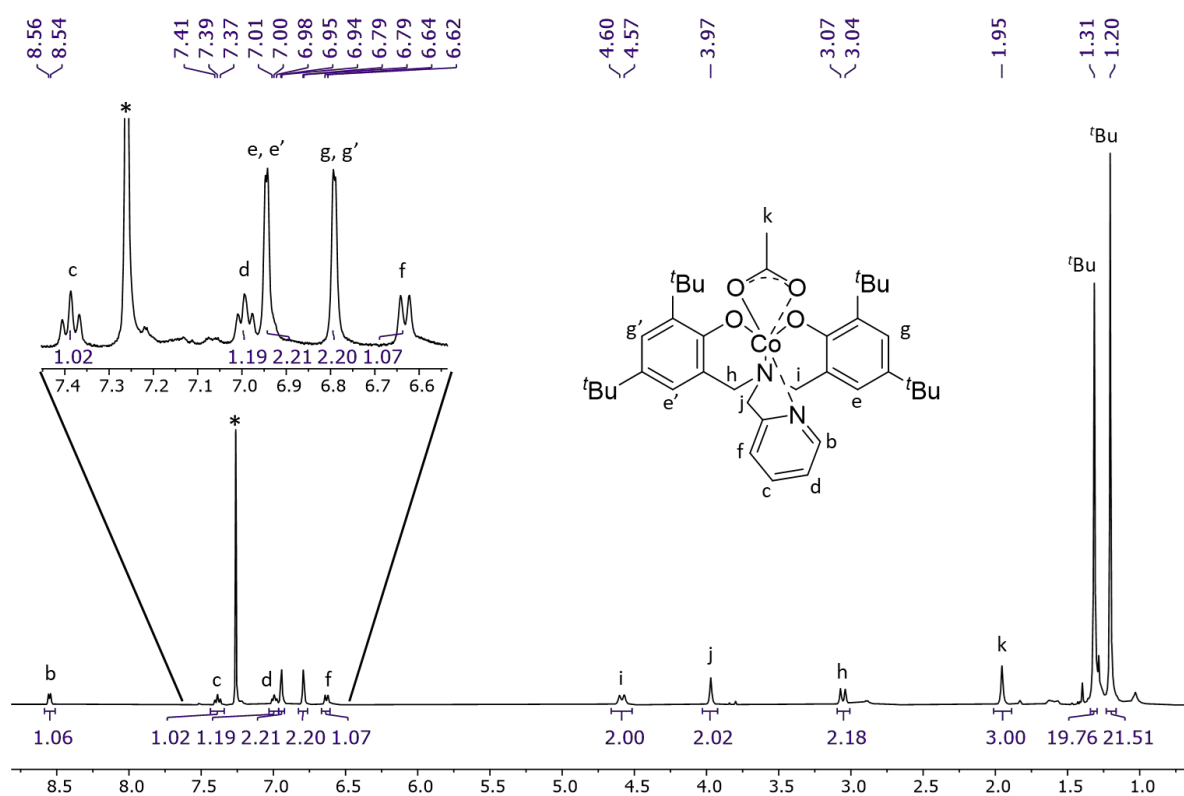


Figure II-10: ¹H NMR (400 MHz, 25°C) spectrum of complex **3.2** recorded in CDCl₃ (*).

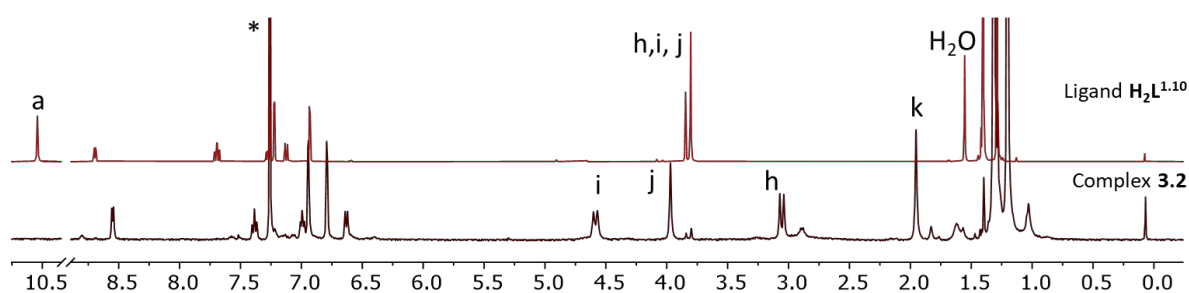


Figure II-11: Stacking of the ¹H NMR (400 MHz, 25°C) spectra of **3.2** and **H₂L^{1.10}**, in CDCl₃ (*).

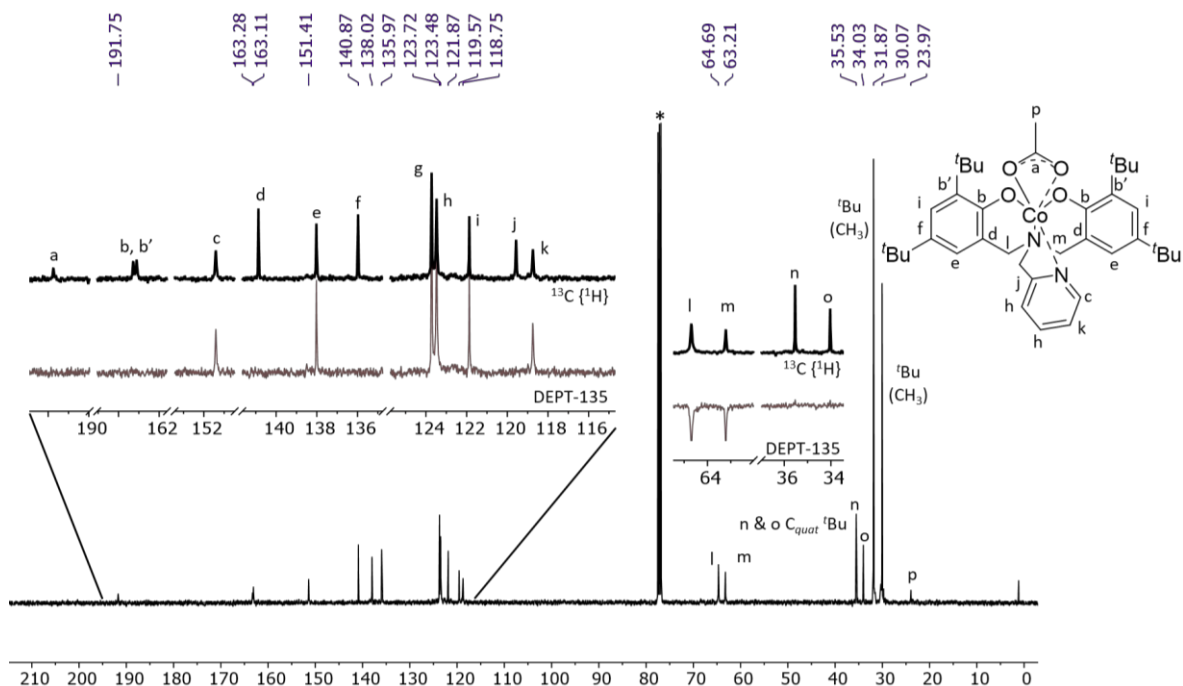


Figure II-12 : ^{13}C NMR (100 MHz, 25°C) and DEPT-135 spectra of the compound **3.2**, recorded in CDCl_3 (*).

The combination of the ^{13}C , DEPT-135, and JMOD spectra recorded for **3.2** allowed the complete assignment of the signals, particularly those corresponding to the OAc group, *i.e.* 191.75 (C_{quat} , $\text{OC}(\text{CH}_3)\text{O}$, a) and 23.97 (CH_3 , $\text{OC}(\text{CH}_3)\text{O}$, p) (Figure II-12).

Single crystals of $\text{H}_2\text{L}^{1.10}$, suitable for an XRD analysis, were grown by slow diffusion of pentane into a saturated CH_2Cl_2 solution of $\text{H}_2\text{L}^{1.10}$. The solid-state structure of $\text{H}_2\text{L}^{1.10}$, depicted in Figure II-13 (left), revealed the presence of H-bonds between the N atoms and the O-H groups, acting as proton acceptors and donors, respectively, with $\text{O2}(-\text{H2})\cdots\text{N1} = 2.7318(13)$ Å and $\text{O3}(-\text{H3})\cdots\text{N16} = 2.8637(14)$ Å. Similar crystallisation conditions led to crystals of **3.2** that were analysed by XRD and afforded the solid-state structure depicted in Figure II-13 (right). The Co^{III} centre is found in a distorted octahedral coordination geometry, with ligand $\text{H}_2\text{L}^{1.10}$ acting as a dianionic tetradentate chelating ligand and the coordination sphere is completed by the chelating OAc ligand. The $\text{Co}-\text{O}_{(\text{Phenoxy})}$ (1.875(4)-1.901(4) Å) and $\text{Co}-\text{N}$ distances (1.892(5)-1.942(5) Å) were found in the range of those measured in similar complexes (see ³² and references therein). The $\text{Co}-\text{O}_{(\text{OAc})}$ bond lengths, $\text{Co}(1)-\text{O}(3)$ (1.932(4) Å) and $\text{Co}(1)-\text{O}(4)$ (1.970(4) Å), are significantly longer than the $\text{Co}-\text{O}_{(\text{acac})}$ distances measured in the (acetylacetonato)-analogue of **3.2** (1.898(3)-1.906(2) Å).³² This property may highlight a weaker $\text{Co}-\text{O}_{(\text{OAc})}$ bond strengths and therefore a higher tendency to cleave homolytically and release an OAc^\bullet radical.

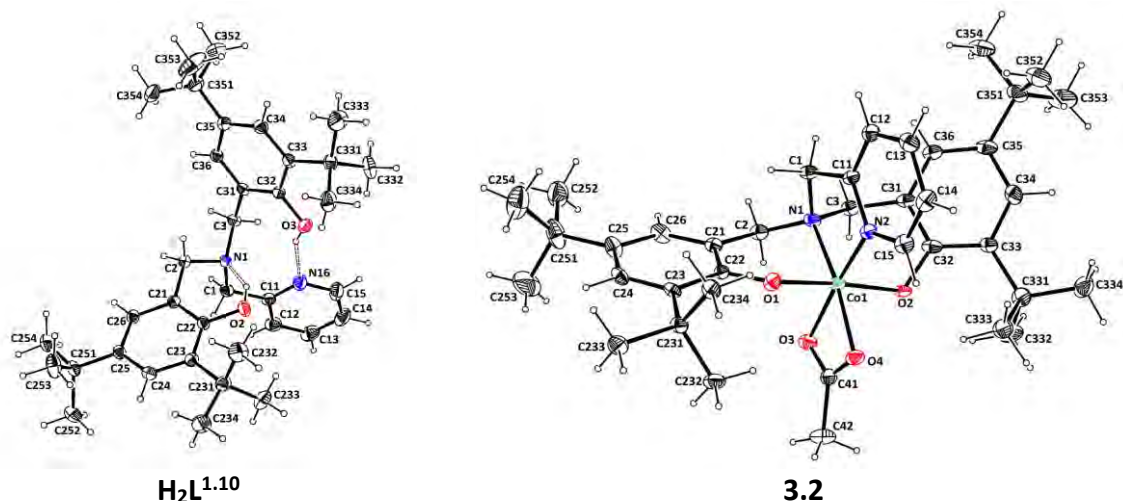
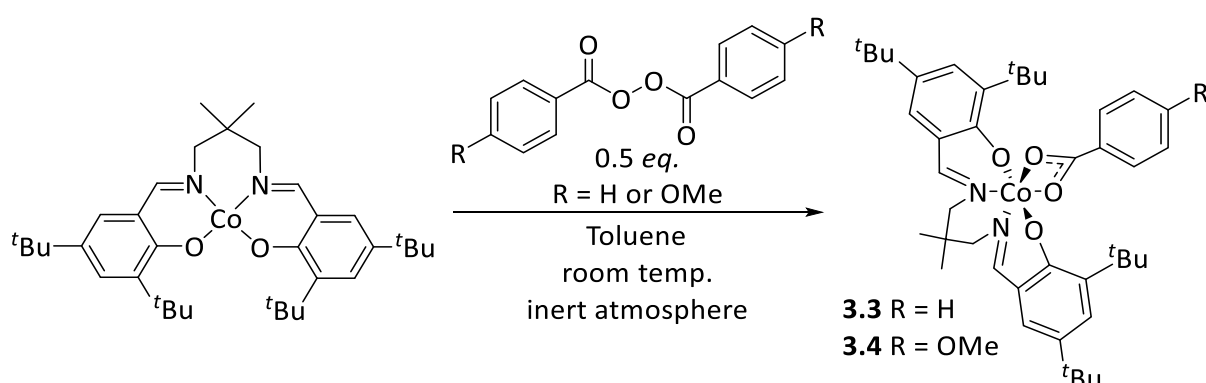


Figure II-13: ORTEP views of pro-ligand ($H_2L^{1.10}$) and (acetato)cobalt(III) complex (**3.2**) with ellipsoids are represented at the 50% probability level.

c. Cobalt(III) carboxylate complexes with a Schiff-base ligand

The synthetic pathways explored above were quite restrictive, because they only allowed the formation of acetato-cobalt(III) complexes, the acetate group originating from the cobalt precursor (or the solvent). With the aim of varying the potential R_0 initiating groups for the targeted applications, we explored another unprecedented approach, which consists in reacting the isolated salen-cobalt(II) complexes with half an equivalent of an acyl peroxide to form the corresponding carboxylates. Initial attempts, using *di**tert*butyl- or *di*cumyl-peroxide, which would afford alkoxide derivatives, were unfortunately unsuccessful. Moving to benzoyl peroxide (BPO), the Schiff base-cobalt(III) carboxylate complex $[Co^{III}(L^{1.4})(OBz)]$ **3.3** was isolated in good yield (76%, *Scheme II-3*). The method was also applied to the *para*-OMe-functionalized BPO derivate, affording the corresponding $[Co^{III}(L^{1.4})(O_2CC_6H_4-p-OMe)]$ complex **3.4** (45%).



*Scheme II-3: Synthesis of cobalt(III) carboxylate complexes of a Schiff base ligand (**3.3**, **3.4**).*

Due to their similarities, only the characterization data of **3.3** will be discussed here, and these of **3.4** are available in the *Experimental section*. *Figure II-14* shows the UV-Visible spectra

of ligand **H₂L^{1.4}**, of its cobalt(II) complex (**2.4**), and of the cobalt(III) carboxylate derivative (**3.3**) in toluene. Both coordination of the Schiff base ligand to the Co^{II} centre and oxidation of Co^{II} to Co^{III} modify the absorption properties. The λ_{max} value shifted from $\lambda_{\text{Ligand}} = 330 \text{ nm}$ to $\lambda_{\text{Co(II)}} = 375 \text{ nm}$ and $\lambda_{\text{Co(III)}} = 410 \text{ nm}$.

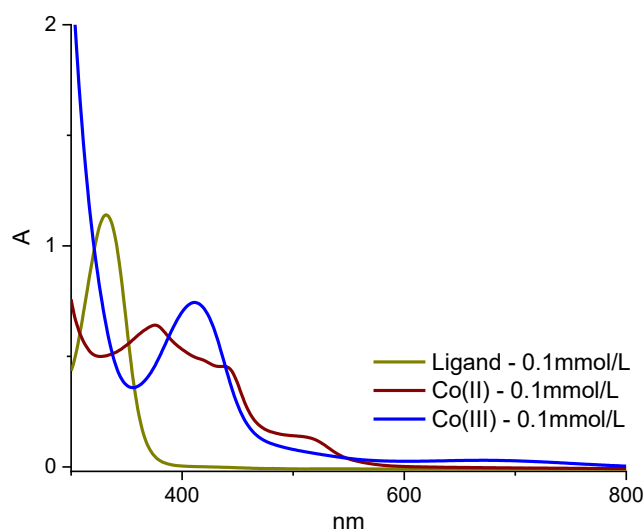


Figure II-14: UV-Vis spectra of ligand **1.4** (green line), $[\text{Co}^{\text{II}}(\text{L}^{1.4})]$ complex **2.4** (red line) and the $[\text{Co}^{\text{III}}(\text{L}^{1.4})(\text{OBz})]$ complex **3.3** (blue line) recorded in toluene at 0.01 mmol L^{-1} .

The diamagnetic nature of complex **3.3** was confirmed by the well-defined ¹H and ¹³C NMR spectra. In addition to the expected signals attributed to the Schiff base ligand, the ¹H NMR spectrum of **3.3** exhibits three resonances attributed to the benzoate fragment at δ (ppm) 6.94 (*t*, $J = 3.8 \text{ Hz}$, 2H, g), 6.86 (*t*, $J = 7.5 \text{ Hz}$, 2H, f), 6.64 (*s*, 1H, h) (Figure II-15). The ¹³C NMR spectrum of complex **3.3** exhibits the expected numbers of resonances and the DEPT-135 highlights the CH₂ and quaternary carbons of the complex, even though not all of them could be unambiguously assigned (Figure II-16).

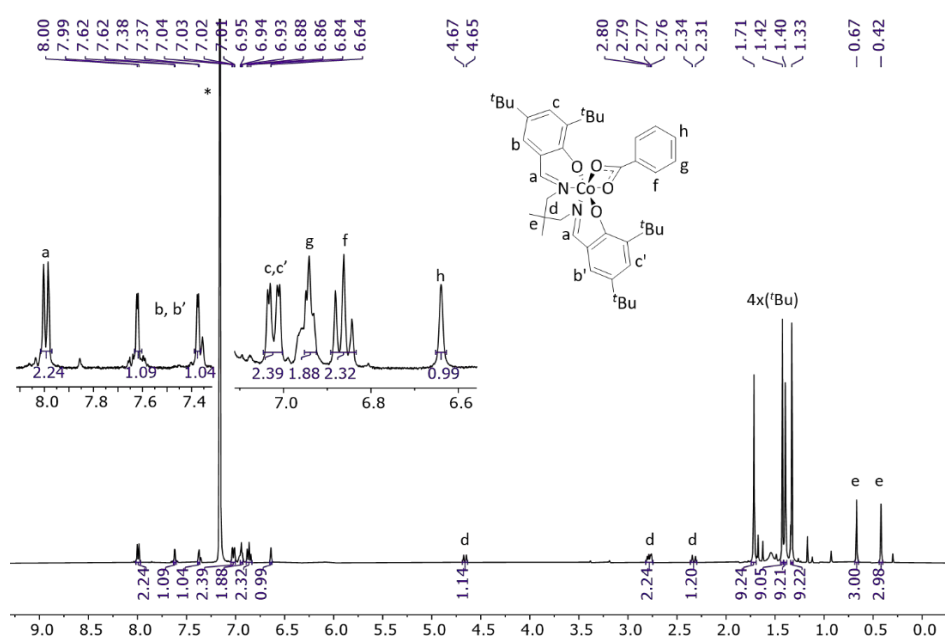


Figure II-15: ¹H NMR (400 MHz, 25°C) spectrum of complex **3.3** recorded in C₆D₆ (*).

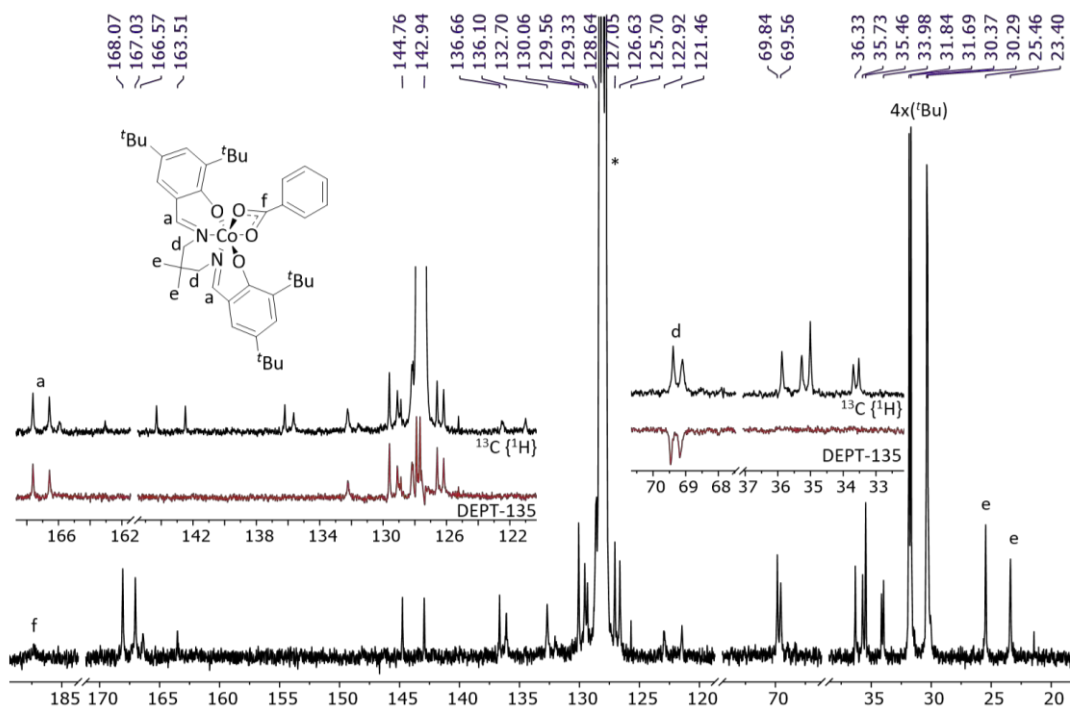


Figure II-16 : ^{13}C NMR spectrum of complex **3.3** recorded in C_6D_6 (*), 400 MHz.

The ESI-MS spectrum of **3.3** exhibited two peaks, the major one corresponding to the $[\text{M} - \text{O}(\text{CPh})\text{O}]^+$ ion ($m/z = 591.3 \text{ g mol}^{-1}$) and the second one to the molecular ion ($[\text{M}]^+$: $m/z = 712.4 \text{ g mol}^{-1}$), both with the expected isotopic distributions (Figure II-17). The lability of the benzoate group, following electrospray ionization, is not surprising, since the OAc group in **3.1** behaved similarly.

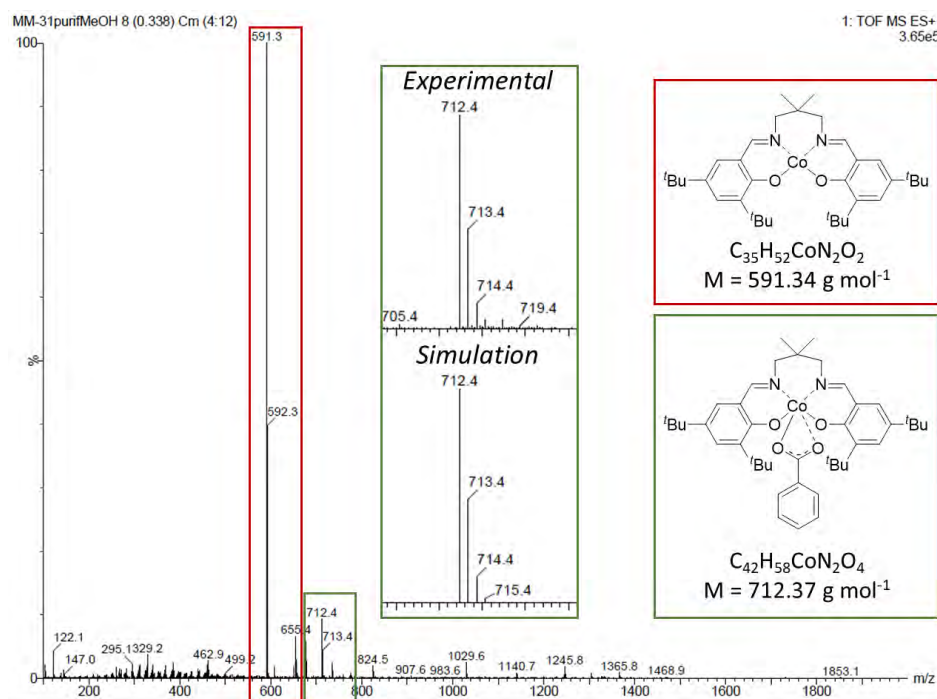
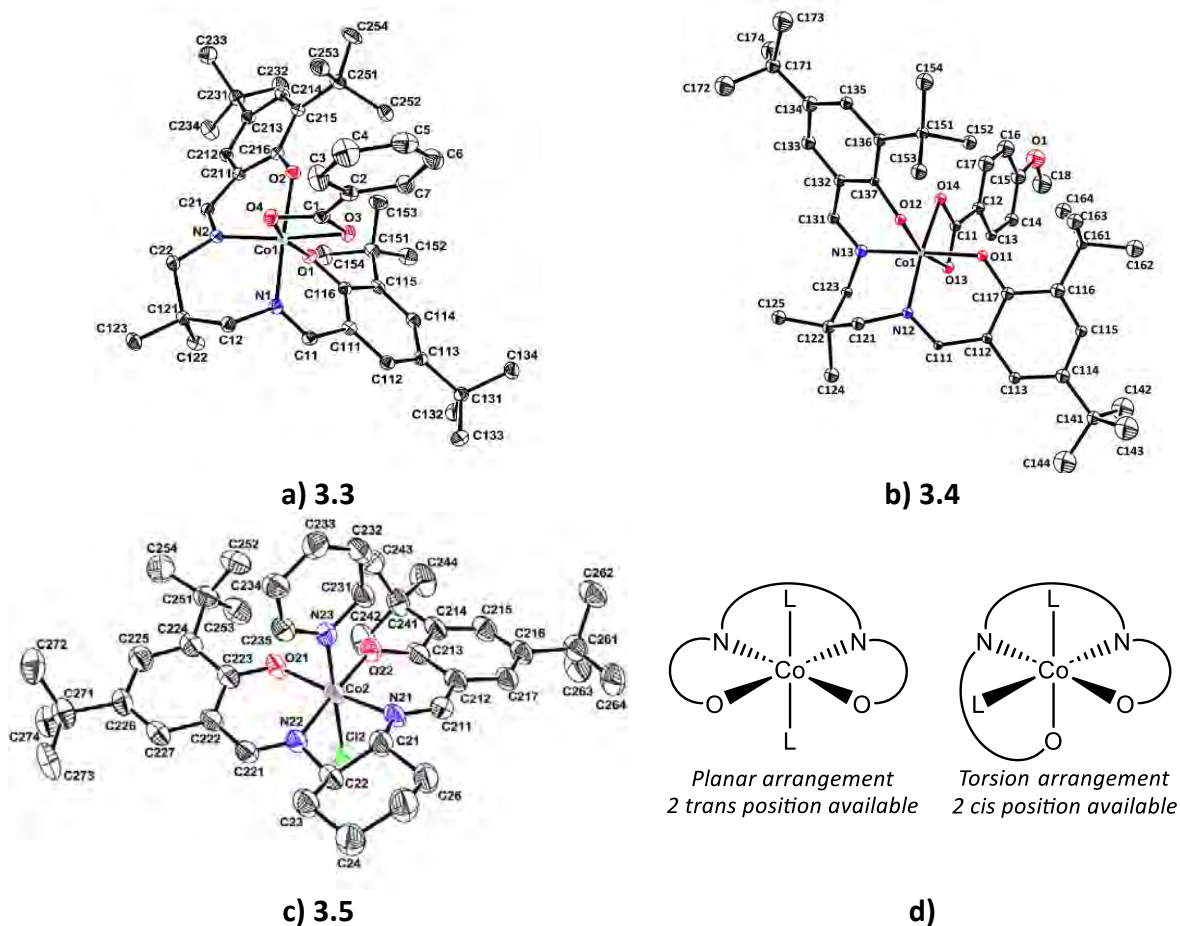


Figure II-17 : ESI of the complex **3.3** recorded in DCM/ACN .

The structures of complexes **3.3** and **3.4** were further confirmed by XRD studies (investigations carried out by Dr. Jean-Claude Daran, *Figure II-18*). In each complex, the Co^{III} is found in a slightly distorted octahedral geometry, composed of the tetradentate Schiff base ligand and the chelating benzoate ligand, which requires *cis*-coordination. And the structure **3.5** shown a planar Schiff base ligand with pyridine and chloride as *trans* position.



*Figure II-18: OTERP views of the Schiff base cobalt(III) benzoate complexes a) **3.3** and b) **3.4** and c) the [Co(L^{1.1})(Cl)(Pyr)] (**3.5**). Ellipsoids are drawn at the 30% probability level and d) possible arrangement of the Schiff-base ligand in coordination sphere.*

This prevents the supporting salen-type ligand to adopt the preferred planar coordination mode. Indeed, relative to the two N donors, one phenolate O atom is arranged in a *mer* fashion (O2 for **3.3** and O11 for **3.4**) while the second one is arranged in a *fac* fashion (O1 for **3.3** and O12 for **3.4**). This observation may rationalize the fact that a similar reactivity was not observed for salen-type ligands with more rigid *N,N*-spacer, such as ethylene, or cyclohexyl (**3.5**). The bond lengths and angles around the metal centre in complexes **3.3** and **3.4** are very similar (Table II-1). As stated above, the bidentate chelating coordination mode of the carboxylate group can only be *cis*, and therefore prevents the planar coordination mode of the supporting salen-type ligand (O,N,N,O torsion angles: **3.3** = -55.04°, **3.4** = -51,20° and **3.5** = -2.78°).

Table II-1. Characteristics bond length and angles of the species **3.3**, **3.4** and **3.5**.

[Co ^{III} (L ^{1.4})(OBz)] (3.3)		[Co ^{III} (L ^{1.4})(O ₂ CC ₆ H ₄ - <i>p</i> -OMe)] (3.4)		[Co(L ^{1.1})(Cl)(Pyr)] (3.5)	
<i>Schiff-base scaffold</i>					
Co(1)-O(1)	1.8758(12)	Co(1)-O(11)	1.896(6)	Co(2)-O(21)	1.899(4)
Co(1)-O(2)	1.8820(12)	Co(1)-O(12)	1.888(6)	Co(2)-O(22)	1.883(4)
Co(1)-N(1)	1.9023(15)	Co(1)-N(12)	1.896(7)	Co(2)-N(21)	1.877(5)
Co(1)-N(2)	1.9014(15)	Co(1)-N(13)	1.919(7)	Co(2)-N(22)	1.888(5)
O(2)-Co(1)-N(2)	91.33(6)	O(12)-Co(1)-N(13)	90.7(3)	N(21)-Co(2)-O(22)	93.4(2)
N(2)-Co(1)-N(1)	92.57(6)	N(12)-Co(1)-N(13)	88.2(3)	N(21)-Co(2)-N(22)	86.4(2)
O(1)-Co(1)-N(1)	90.78(6)	N(12)-Co(1)-O(11)	90.9(3)	N(22)-Co(2)-O(21)	94.7(19)
O(1)-Co(1)-O(2)	91.15(5)	O(12)-Co(1)-O(11)	90.0(2)	O(22)-Co(2)-O(21)	85.7(18)
<i>Carboxylate fragment</i>					
Co(1)-O(3)	1.9709(13)	Co(1)-O(13)	1.992(6)	-	-
Co(1)-O(4)	1.9764(13)	Co(1)-O(14)	1.963(6)	-	-
O(3)-C(1)-O(4)	117.16(16)	O(13)-C(11)-O(14)	116.3(8)	-	-

5. Conclusion

I have reported in this section one new cobalt(III) acetate complex (**3.2**) and two benzoate complexes (**3.3** and **3.4**) with (*N*₂,*O*₂)-supporting ligands, and evaluated the aptitude of an already known acetate complex (**3.1**) to generate acetate radicals. The benzoate derivatives were synthesized *via* an unprecedented redox route, by metal-mediated peroxide cleavage and radical trapping. All these species were developed with the aim of applying them as unimolecular initiators/moderators for polymerization processes and this will be discussed in *Chapter III*.

The library of salen-type cobalt(III) benzoate complexes could not be extended to analogues with a more rigid (two-carbon) spacer between the N donors, presumably because of insufficient flexibility to adopt a *cis*-octahedral coordination environment. As a perspective, it may be interesting to apply the redox route to half-salen complexes, *i.e.* cobalt complexes with two bidentate phenoxyimine (*N,O*) ligands, which could better accommodate to the *cis*-coordination geometry imposed by the chelating carboxylate group.⁶⁶⁻⁶⁸ Another possible perspective is to apply the chemistry developed with the salen-type (*N*₂,*O*₂) ligands to their softer (*S*₂,*O*₂) analogues, their coordination compounds being already reported as efficient ROP catalysts.^{40, 69, 70}

III. Cobalt complexes with an (O_2, O_2)-type ligand

1. Introduction

As discussed previously, the coordination chemistry of cobalt towards (N,O)-based ligands is very rich. In contrast, only few mononuclear cobalt(III) complexes with an entirely O -based coordination sphere have been isolated and characterized: $[Co(H_2O)_6]^{3+}$,⁷¹ $[Co(DMSO)_6]^{3+}$ (DMSO = dimethylsulfoxide),⁷² a trioxalate complex, $[Co(C_2O_4)_3]^{3-}$,⁷³ and a variety of tris(β -diketonates), amongst which the ubiquitous and commercially available tris(acetylacetonate), $[Co(acac)_3]$ ^{74, 75} (the literature references are restricted to the structural characterizations by X-ray diffraction). The carbonate $[Co(CO_3)_3]^{3-}$ has recently been generated electrochemically.⁷⁶

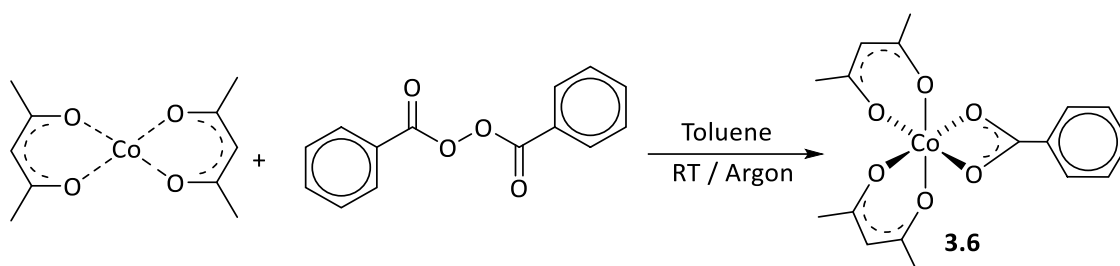
In the literature, compounds $[Co^{III}(acac)_3]$ and $[Co^{III}(salen)(acac)]$ were proposed to serve as radical polymerization initiators by UV photolytic or thermal activation, to generate an $acac^{\bullet}$ radical.⁷⁷⁻⁷⁹ On the other hand, no system based on the cobalt bis(acetylacetonate) scaffold were applied to ROP processes. Moreover, we envisioned to apply the redox route described in the previous section for (N_2, O_2)-based ligands to (O_2, O_2)-based systems.

2. (Acetylacetonato)-cobalt(III) carboxylate complexes

In 2006, Bryaskova *et al.* introduced the combination of benzoyl or lauryl peroxide and $[Co^{II}(acac)_2]$ as a redox-initiating system for the OMRP of vinyl acetate (VAc).⁸⁰ This system was also subsequently used for the polymerization of acrylic esters,⁸¹ other vinyl esters^{82, 83} and vinylidene fluoride.⁸⁴ A question came to us: "What is the initiation mechanism?". Does the peroxide undergo homolytic cleavage and initiate the polymerization, and the Co^{II} complex only installs the ORMP equilibrium? Or does the mixture generate an $(acac)_2-Co^{III}$ carboxylate intermediate? Namely, does the Co^{II} induce the peroxide cleavage and traps the corresponding radical, which further initiates the polymerization? To elucidate these questions, we explored the synthesis of the presumed $(acac)_2-Co^{III}$ carboxylate complexes. Furthermore, if the synthesis is successful, this type of compound could also be of interest for applications in the ROP of cyclic esters.

a. Bis(acetylacetonato)-cobalt(III) benzoate complex

The reaction between inexpensive and commercially available $[Co^{II}(acac)_2]$ and BPO, afforded the corresponding $[Co^{III}(acac)_2(O_2CPh)]$ complex **3.6** in 60% yield after 1 h of reaction at room temperature under an inert atmosphere (*Scheme III-1*).



Scheme III-1: Synthesis of the bis(acetylacetonato)-cobalt(III) benzoate complex 3.6.

While the reaction proceeds, the sparingly soluble pink $[\text{Co}^{\text{II}}(\text{acac})_2]$ disappears to produce a deep green solution of the corresponding cobalt(III) product, *Figure III-1*.

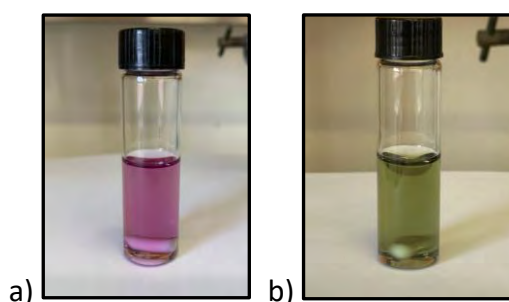


Figure III-1: Pictures of the reaction at a) T_0 and b) T_f .

The UV-Visible spectra shown in *Figure III-2* highlight the shift of λ_{max} from 545 nm ($[\text{Co}^{\text{II}}(\text{acac})_2]$) to 610 nm upon oxidation and benzoate coordination, and the absorption evolution vs. time shows the rapidity of the conversion.

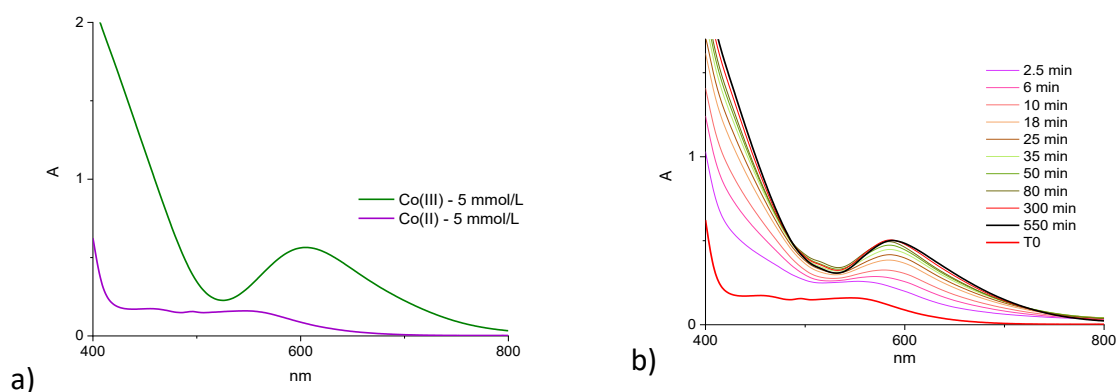
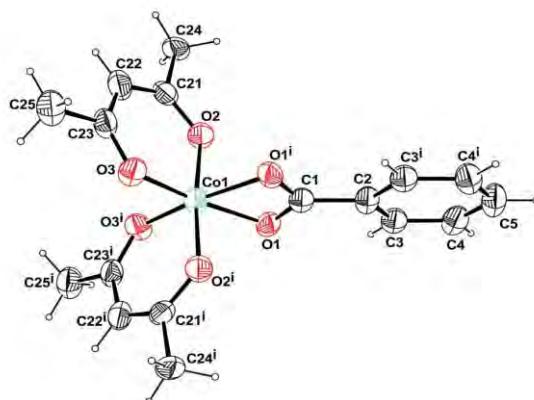


Figure III-2: a) UV spectra of $\text{Co}^{\text{II}}(\text{acac})_2$ in purple and $\text{Co}^{\text{III}}(\text{acac})_2(\text{O}_2\text{CPh})$ in green, b) monitoring of the cobalt(III) complex formation by UV-vis analysis (5 mM in toluene in all cases).

The diamagnetic nature of compound **3.6** allowed its characterization by multinuclear NMR spectroscopy. The ^1H and ^{13}C NMR spectra are shown below (*Figure III-* and *Figure III-*). The presence of three singlet ^1H resonances in a 2:6:6 ratio for the acac H (δ 5.29) and Me (δ 2.04 and 1.79) protons indicates asymmetry, consistent with the *cis* arrangement in a chiral

octahedral geometry, as confirmed by a single-crystal X-ray diffraction investigation carried out by Dr. Jean-Claude Daran (Figure III-3).



3.6

Figure III-3: a) ORTEP views of the complexes **3.6** with the atom labelling scheme. Ellipsoids are drawn at the 50% probability level. X-ray crystallographic data for complexes **3.6**, Co(1)-O(1) 1.948(2); Co(1)-O(1ⁱ) 1.948(2); Co(1)-O(2) 1.882(2); Co(1)-O(3) 1.869(2); Co(1)-O(2ⁱ) 1.882(2); Co(1)-O(3ⁱ) 1.869(2); O(1ⁱ)-Co(1)-O(1) 67.3°; 113.3°.

Moreover, the resonances belonging to the phenyl protons can be easily attributed due to their multiplicity and integration: δ 8.22 for the *ortho* protons (*dt*, $J = 7.3$ and 1.4 Hz, 2H, f), 6.94 for the *para* proton (*ddd*, $J = 7.5$, 6.0 and 1.4 Hz, 1H, e) and 6.84 for the *meta* protons (*dd*, $J = 8.5$ and 7.0 Hz, 2H, d).

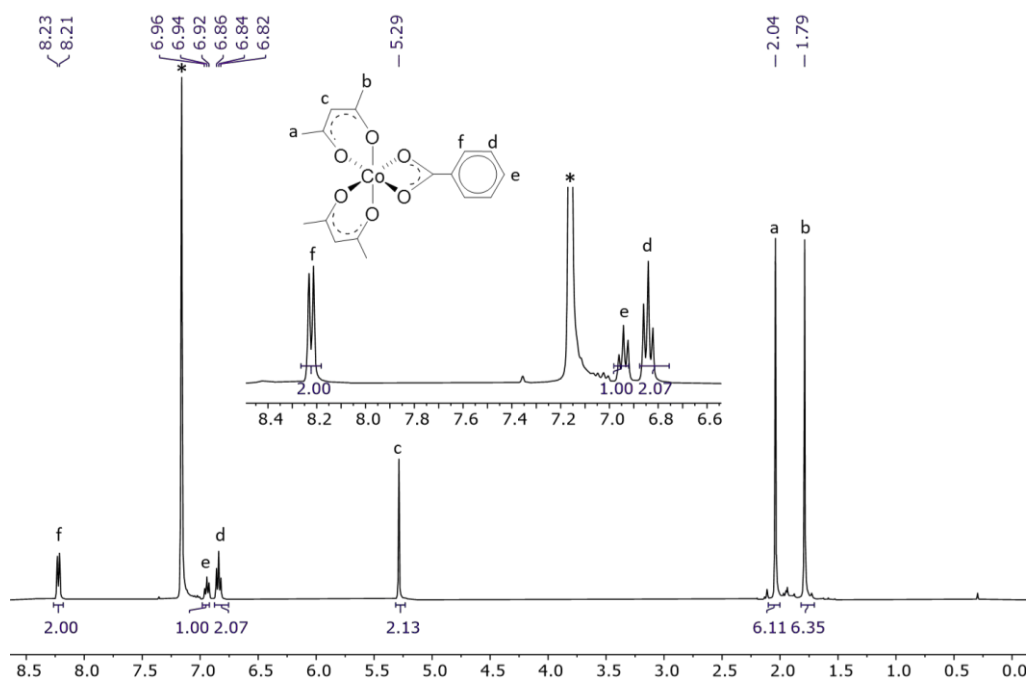


Figure III-4: ¹H NMR (400 MHz, 25°C) spectrum of **3.6** recorded in C₆D₆ (*).

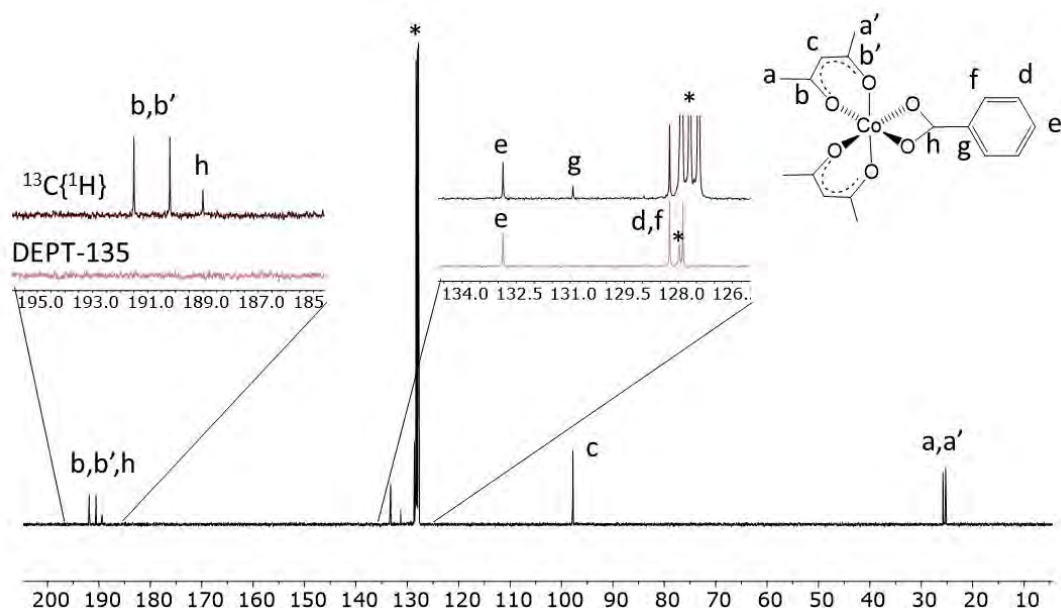


Figure III-5: ^{13}C NMR (100 MHz, 25°C) spectrum of **3.6** recorded in C_6D_6 (*).

Electrochemical measurements show that $[\text{Co}^{\text{III}}(\text{acac})_2(\text{O}_2\text{CPh})]$ is much more easily reduced ($E_{p,c} = -0.90$ V vs. Fc) than $[\text{Co}^{\text{III}}(\text{acac})_3]$ ($E_{p,c} = -1.33$ V vs. Fc) (Figure III-6, left). After reduction, a reoxidation wave at much higher potential ($E_{p,a} = 0.15$ V vs. Fc) becomes clearly visible only at the higher scan rate (Figure III-6, right).

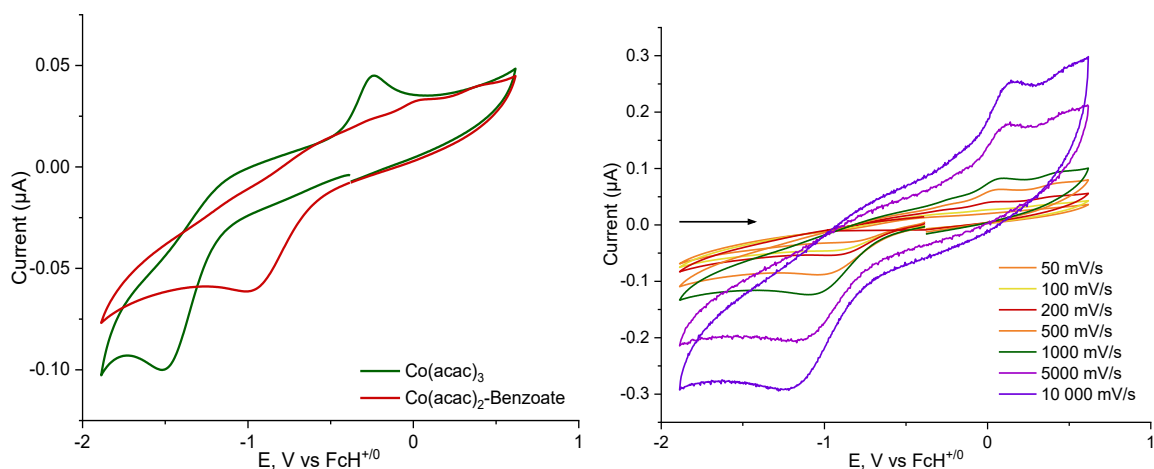


Figure III-6: Cyclic voltammograms of compounds $[\text{Co}(\text{acac})_2(\text{O}_2\text{CPh})]$ (red curve) and $[\text{Co}(\text{acac})_3]$ (green curve) in CH_2Cl_2 on a Pt working electrode at $v = 200$ mV s^{-1} (left) and at various scan rates (values in the legends in mV s^{-1}) (right). $[\text{Complex}] = 10^{-3}$ M; Supporting electrolyte: $n\text{Bu}_4\text{PF}_6$, 0.1 M).

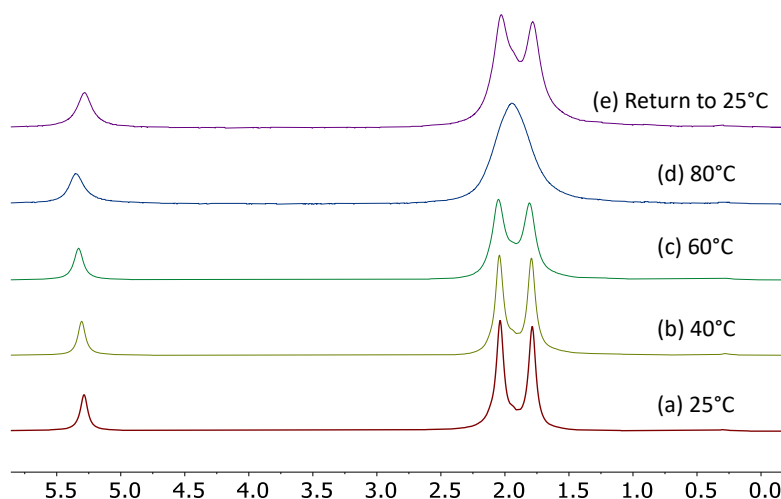


Figure III-7: Temperature dependence of the acac ^1H NMR (400 MHz) resonances for $[\text{Co}(\text{acac})_2(\text{O}_2\text{CPh})]$ (**3.6**) in C_6D_6 .

The thermal stability of complex **3.6** was evaluated at several temperatures and times. A variable-temperature ^1H NMR investigation in C_6D_6 revealed a line broadening phenomenon between 25 and 80 $^\circ\text{C}$ in the acac region, possibly consistent with a dynamic configuration inversion, *e.g.* via a Bailar twist. However, the line broadening is not fully reversible upon cooling, suggesting partial decomposition with generation of a paramagnetic species *Figure III-7*. This phenomenon suggests reversibility for the $\text{Co}^{\text{III}}\text{-O}$ bond formation and the generation of PhCOO^\bullet . Additional ^1H NMR investigations in C_6D_6 at constant temperature revealed slow decomposition overnight at 60 $^\circ\text{C}$, resulting in the deposition of $\text{Co}(\text{acac})_2$ crystals, whereas no decomposition was evident after 16 h at 40 $^\circ\text{C}$ or upon standing at room temperature for 3 days in daylight (*Figure III-8*).

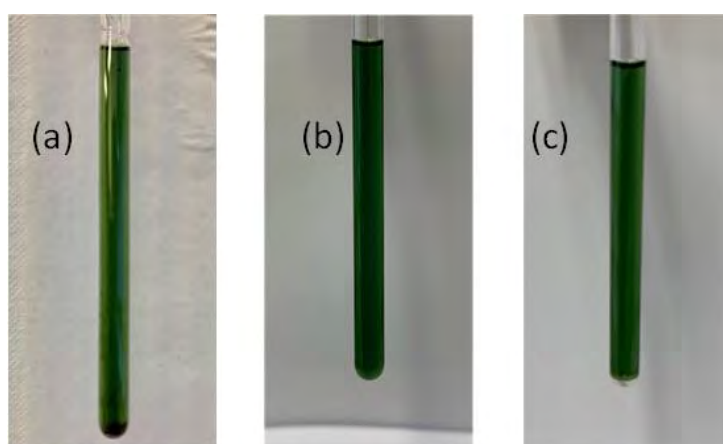


Figure III-8: Pictures of $[\text{Co}(\text{acac})_2(\text{O}_2\text{CPh})]$ solutions in C_6D_6 . (a) After 13 h at 60 $^\circ\text{C}$. (b) After 16 h at 40 $^\circ\text{C}$. (c) After 72 h at room temperature.

All of these observations were also rationalized by DFT calculations (Prof. Rinaldo Poli), which permit to show the aptitude of $[\text{Co}^{\text{III}}(\text{acac})(\text{O}_2\text{CPh})]$ to liberate PhCOO^\bullet . As already shown for the $[\text{Co}^{\text{III}}(\text{L}^{1.1})(\text{OAc})]$ complex (*Figure II-7*), the liberation of the radical was probed as a two-step reaction. The overall Gibbs energy cost is 28.8 kcal mol^{-1} under standard

conditions ($27.1 \text{ kcal mol}^{-1}$ at $60 \text{ }^\circ\text{C}$) (Figure III-9). These numbers are consistent with the relatively good thermal stability of the compound, but not inconsistent with a significant rate of radical production.^{85,86} However, the homolytic cleavage occurs only in the second step and costs $12.2 \text{ kcal mol}^{-1}$. For comparison, homolytic bond cleavage was experimentally observed and kinetically investigated for $\text{R-Cr}^{\text{III}}_{\text{aq}}$ complexes (ΔH_a^\ddagger up to 40 kcal mol^{-1})⁸⁷⁻⁹⁰ and for $[\text{R}_F\text{-Mn}^{\text{I}}(\text{CO})_5]$ complexes with $\text{R}_F =$ fluorinated alkyl ligands (ΔH_a^\ddagger up to $53.8 \text{ kcal mol}^{-1}$ for $\text{R}_F = \text{CF}_3$).⁹¹

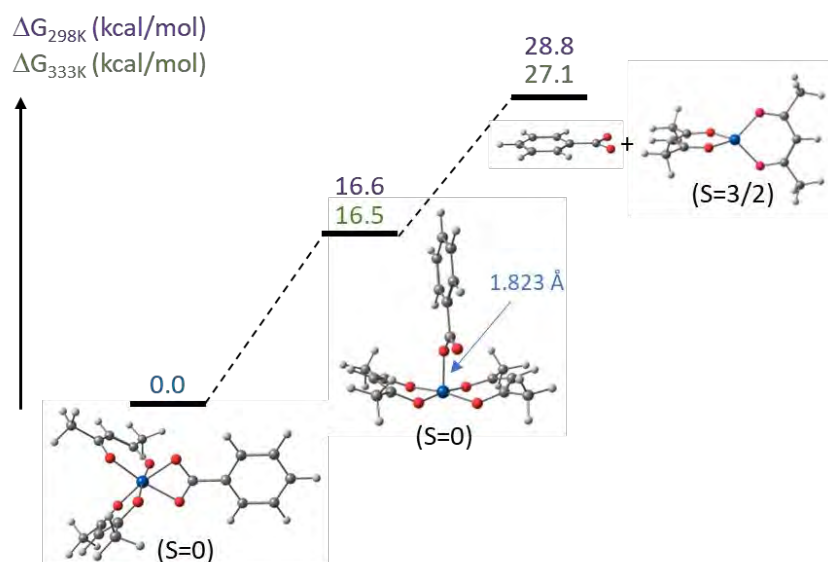
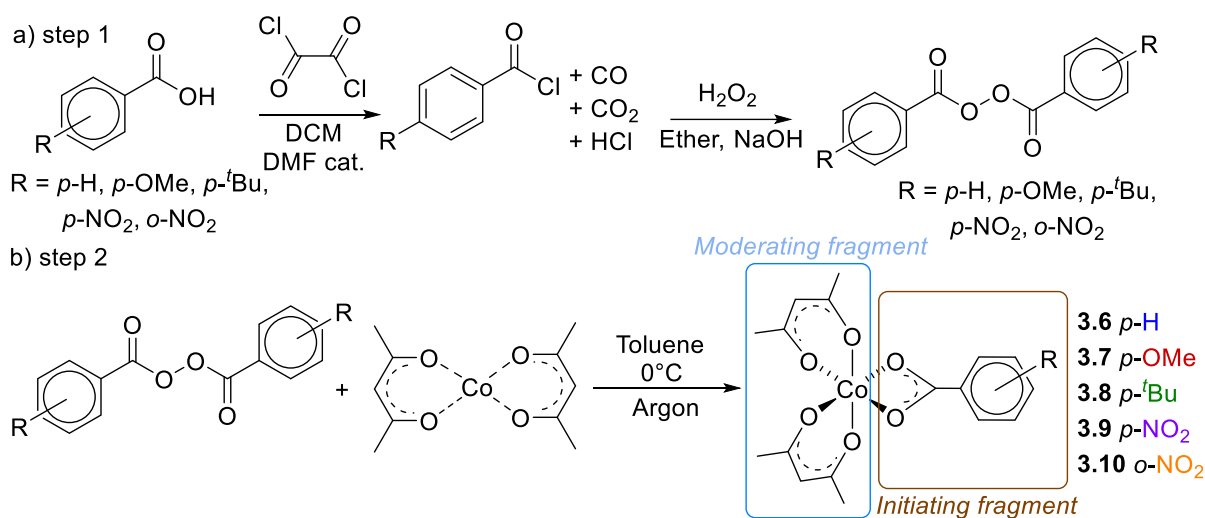


Figure III-9: Gibbs energy profile for the dissociation of a PhCOO^\bullet radical from $[\text{Co}(\text{acac})_2(\text{O}_2\text{CPh})]$.

The $[\text{Co}^{\text{III}}(\text{acac})_2(\text{O}_2\text{CPh})]$ complex **3.6** is, to the best of our knowledge, a unique example of a mononuclear heteroleptic Co^{III} carboxylate complex supported by a fully O-based coordination sphere, and this architecture could be very promising for the direct initiation of OMRP and ROP process. Therefore, we extended the scope of peroxides to (maybe) modulate the properties of the $\text{Co-O}_{(\text{carboxylate})}$ bond.

b. Bis(acetylacetonato)-cobalt(III) complexes with substituted benzoates

In addition to modulating the reactivity of the Mt-O_(carboxylate) bond, extending the peroxide scope may also allow the introduction of a functional group at the polymer chain-end and subsequent post-polymerization modifications. A series of substituted benzoyl peroxide derivatives were synthesized in good yields, according to previously reported procedures (Scheme III-2, a).⁹²



Scheme III-2: a) Synthesis of substituted benzoyl peroxide derivatives, b) synthesis of bis(acetylacetonato)cobalt(III) carboxylate complexes.

The bis(acetylacetonato)cobalt(III) complexes with substituted benzoate derivatives (**3.7-3.10**) were obtained in one step from commercially available [Co(acac)₂] and the corresponding peroxides in toluene at 0°C under an inert atmosphere (Scheme III-2, b).⁹² All of these new complexes were characterized by ¹H NMR (Figure III-3) and UV-Vis (Figure III-10). Figure III-3 shows a stacking of the ¹H NMR spectra of complexes **3.6-3.9** and highlights that the substitution of the aryl ring of the benzoate derivative has a negligible effect on the acac resonances.

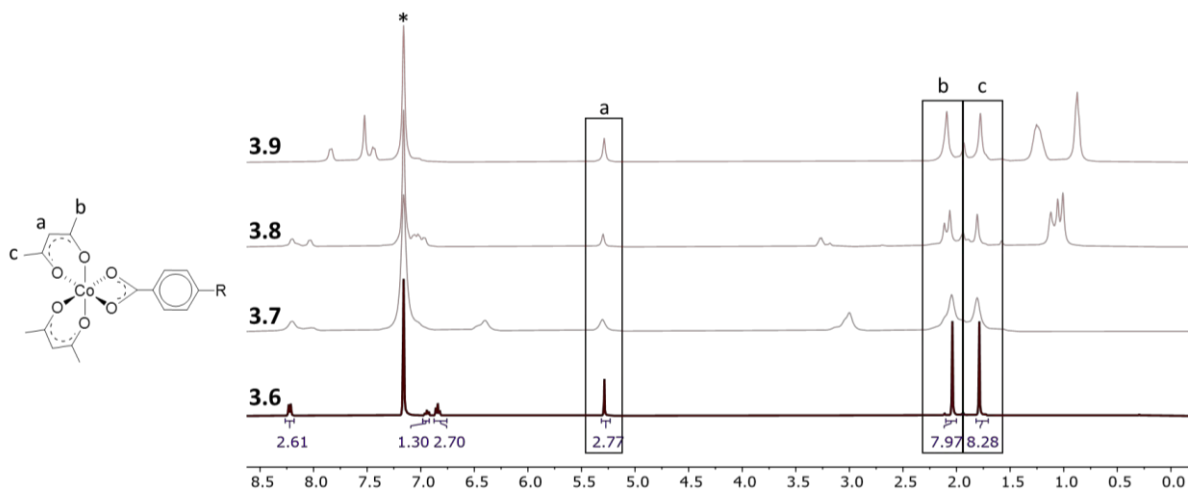
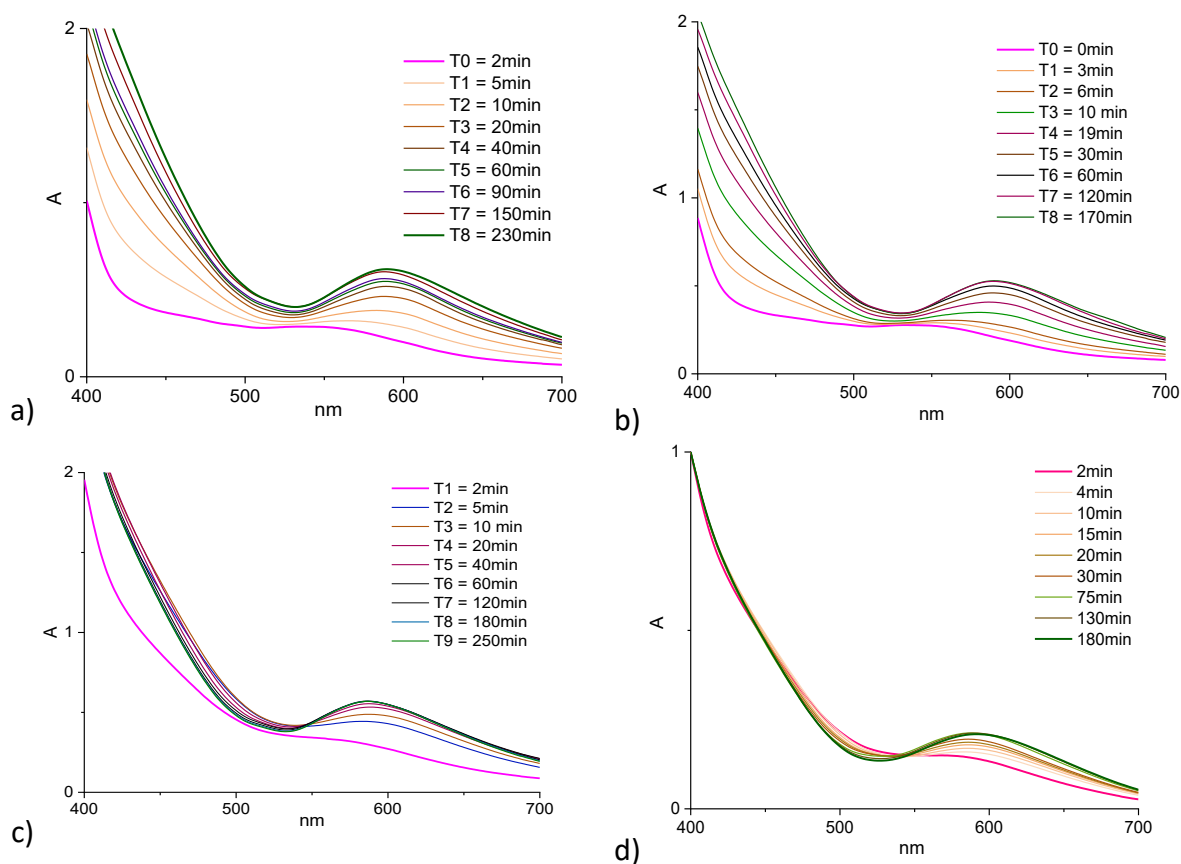


Figure III-3: Stacking of ¹H NMR (400 MHz, 25°C) spectra of **3.6 – 3.9** recorded in C₆D₆ (*).

Like for complex **3.6**, the formation of complexes **3.7-3.10** investigated by UV-Vis spectroscopy. First of all, the objective was to determine the λ_{\max} for a possible application as OMRP photoinitiators. These values are very similar for all compounds (**3.6**, 586 nm; **3.7**, 589 nm; **3.8**, 584 nm; **3.9**, 587 nm; **3.10**, 591 nm; *Figure III-10*). The rate of formation appeared qualitatively different for the various systems. Therefore, the evolution of the spectra was followed as a function of time during the formation of complexes **3.6-3.10** (*Figure III-10*) and the time dependence of the absorbance at λ_{\max} is reported in *Figure III-11*.



*Figure III-10: UV-visible monitoring of the complex formation: a) **3.7** $\text{Co}(\text{acac})_2\text{-ArOMe}$ (\blacktriangle), b) **3.8** $\text{Co}(\text{acac})_2\text{-Ar}^t\text{Bu}$ (\bullet), c) **3.9** $\text{Co}(\text{acac})_2\text{-Ar}^p\text{NO}_2$ (\blacklozenge), d) **3.10** $\text{Co}(\text{acac})_2\text{-Ar}^o\text{NO}_2$ (\star).*

Using a slight excess of peroxides allowed extracting a tendency of the kinetics of the reactions, as shown in the first-order plot of *Figure III-12*, which gives straight lines. The slope of these lines allows concluding that the formation of complexes **3.6-3.8** and **3.10** occur at similar rates, while the formation **3.9** is much faster. The faster formation of **3.9** may indicate a higher thermodynamic stability, which could alter/prevent the homolytic cleavage of the Co-O_{benzoate} bond, *i.e.* OMRP initiation.

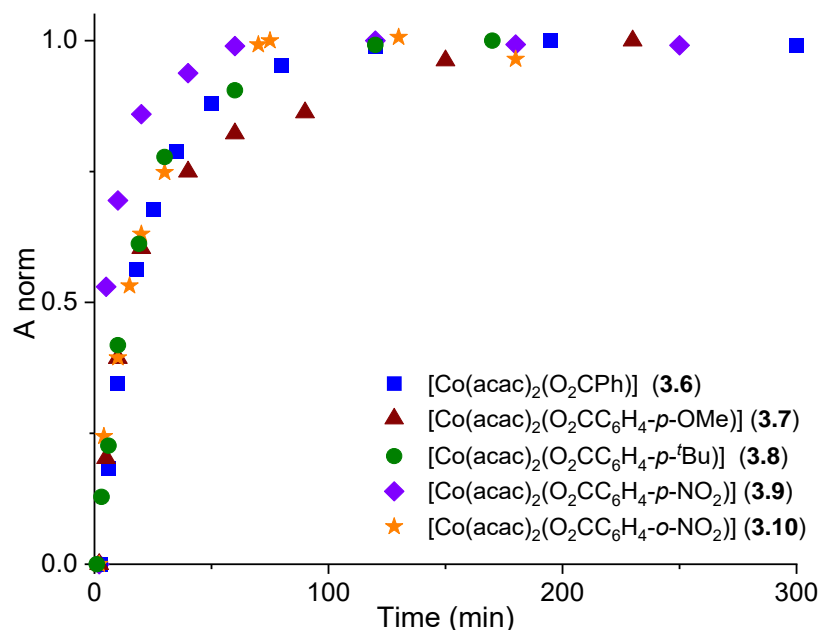


Figure III-11: Evolution of the absorbance at λ_{max} as a function of time during the formation of complexes **3.6** (■), **3.7** (▲), **3.8** (●), **3.9** (◆), **3.10** (★).

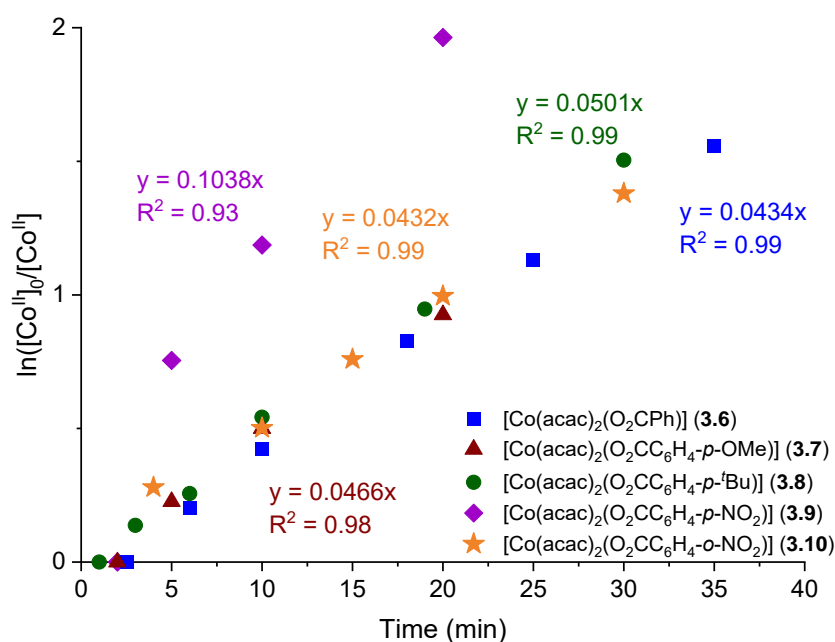


Figure III-124: First-order kinetic plot of the formation of complexes **3.6-3.10**.

An electrochemical study by cyclic voltammetry showed that the *para*-OMe derivative (**3.7**, Figure III-13a) is much more difficult to reduce ($E_{p,c} = -1.08$ V vs. Fc) than the *para*-NO₂ derivative (**3.9**, Figure III-13b) ($E_{p,c} = -0.29$ V vs. Fc). In addition, complex **3.9** also exhibits a second reduction potential ($E_{p,c} = -0.94$ V), indicating further reduction to Co^I. For both compounds, the reverse oxidation scan shows waves at much higher potentials ($E_{p,a} = 0.50$ V for **3.7**, 0.19 and 0.56 V for **3.9**, vs. Fc). The *ortho*-derivative **3.10** is the most difficult complex to reduced ($E_{p,c} = -1.92$ and -1.50 V vs. Fc).

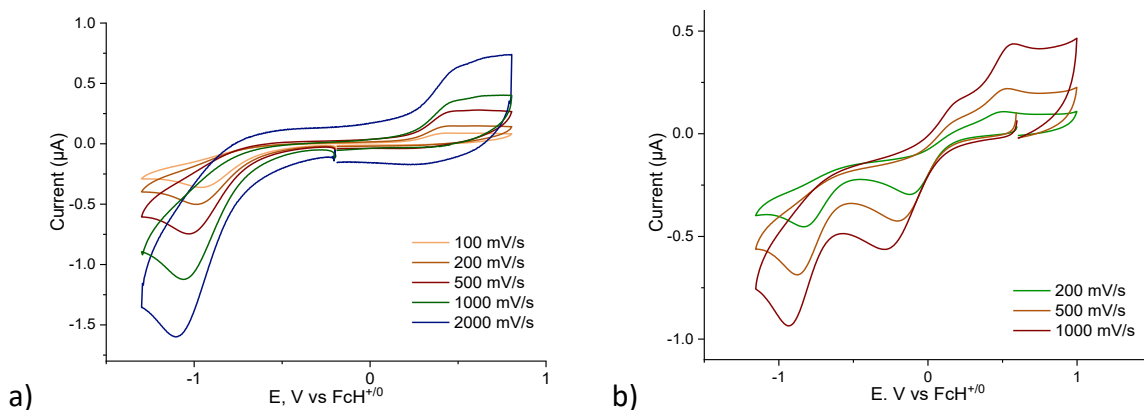


Figure III-53 : Cyclic voltammogram of compounds a) $[\text{Co}(\text{acac})_2(\text{O}_2\text{CC}_6\text{H}_4\text{-p-OMe})]$ (**3.7**), and b) $[\text{Co}(\text{acac})_2(\text{O}_2\text{CC}_6\text{H}_4\text{-p-NO}_2)]$ (**3.9**), in CH_2Cl_2 on a GC working electrode at various scan rates. $[\text{Complex}] = 10^{-3} \text{ M}$; supporting electrolyte: $n\text{Bu}_4\text{PF}_6 = 0.1 \text{ M}$.

Complexes **3.9** and **3.10** have also been investigated by single-crystal XRD (carried out by Dr. Jean-Claude Daran). The molecular structures are depicted in Figure III-3 for **3.6** and Figure III-14 for **3.9** and **3.10** and the most relevant bond distances and angles are reported in Table III-1.

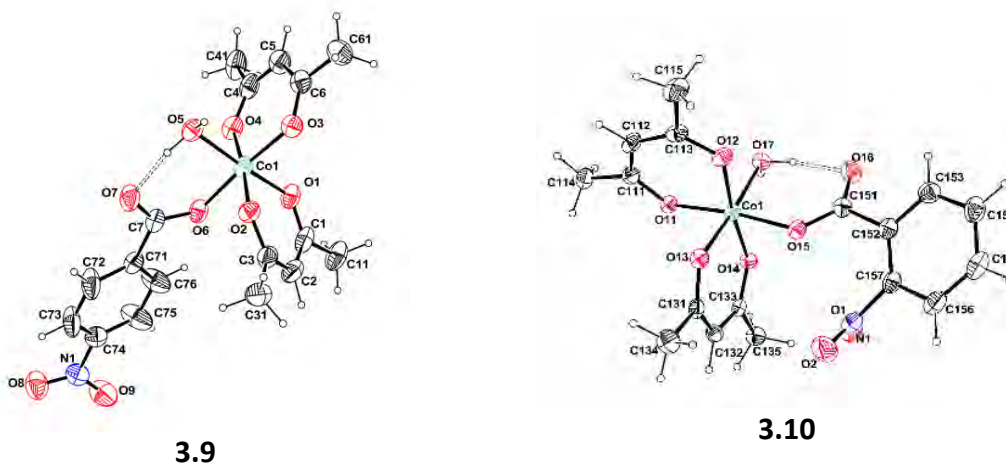


Figure III-14: ORTEP views of the complexes **3.6**, **3.9** and **3.10** with the atom labelling scheme. Ellipsoids are drawn at the 30% for **3.9** and 50% probability level for **3.6** and **3.10**.

The main difference between the structures of **3.9** and **3.10** and that of **3.6** is the presence of one water molecule (probably originating from the synthesis of the peroxide), which prevents the benzoate derivative to act as a bidentate (chelate) ligand and establishes an H-bond as proton donor with the uncoordinated benzoate carbonyl group. As a result, the O-C-O' (benzoate) angles (126.3° (**3.9**) and 127.0° (**3.10**)) and the $\text{O}_{(\text{H}_2\text{O})}\text{-Co-O}_{(\text{benzoate})}$ angles (94.1° (**3.9**) and 96.1° (**3.10**)) are closer to the ideal 120 and 90° values in **3.9** and **3.10**, whereas they significantly deviate from these ideal values in **3.6** (113.3° and 67.3° , respectively) (cf. Table III-1). Note: due to the low thermal stability of these derivatives, attempts to remove the coordinated water molecule by heating were not carried out.

Table III-1 : X-ray crystallographic data for complexes **3.6**, **3.9** and **3.10**.

[Co(acac) ₂ (O ₂ CPh)] 3.6		[Co(acac) ₂ (O ₂ CC ₆ H ₄ - <i>p</i> -NO ₂)] 3.9		[Co(acac) ₂ (O ₂ CC ₆ H ₄ - <i>o</i> -NO ₂)] 3.10	
Cobalt – carboxylate					
Co(1)-O(1)	1.948(2)	Co(1)-O(6)	1.9119(18)	Co(1)-O(15)	1.909(2)
Cobalt - Water molecule					
Co(1)-O(1 ⁱ)	1.948(2)	Co(1)-O(5)	1.9298(17)	Co(1)-O(17)	1.955(3)
Cobalt acac					
Co(1)-O(2)	1.882(2)	Co(1)-O(4)	1.8752(17)	Co(1)-O(12)	1.873(2)
Co(1)-O(3)	1.869(2)	Co(1)-O(3)	1.8768(18)	Co(1)-O(11)	1.883(2)
Co(1)-O(2i)	1.882(2)	Co(1)-O(2)	1.8914(17)	Co(1)-O(13)	1.856(2)
Co(1)-O(3i)	1.869(2)	Co(1)-O(1)	1.8659(17)	Co(1)-O(14)	1.869(2)
Angle carboxylate					
O(1 ⁱ)-Co(1)-O(1)	67.3°	O(6)-Co(1)-O(5)	94.10°	O(15)-Co(1)-O(17)	96.07°
O(1 ⁱ)-C(1)-O(1)	113.3°	O(6)-C(7)-O(7)	126.30°	O(15)-C(151)-O(16)	126.97°
Hydrogen bond					
-	-	O(5)-H(52)···O(7)	1.655(17)	O(17)-H(172)···O(16)	1.765(15)

The XRD analysis of crystals obtained from a solution of complex **3.8** [Co^{III}(acac)₂Ar-(*p*)^tBu] revealed the structure depicted in *Figure III-15*. The structure consists of a trinuclear complex of formula [Co_{3^{II,II,III}}(acac)₂(OOCAr)₄(OH)(H₂O)]·ArCOOH (**3.8'**), composed of two cobalt(II) centres (Co1 and Co2) and one cobalt(III) ion (Co3). Co3 presents the expected stoichiometry (highlighted in orange in *Figure III-12b*), *i.e.* two chelating acac ligands and one monodentate benzoate ligand. The coordination sphere of the Co3 centers is completed by a hydroxyl ligand, which is also bonded to Co1 and Co2. The coordination sphere of the Co1 is tetrahedral, with three benzoate O atoms, two of them bringing to the Co2 atom and one terminal, in addition to the triply bridging OH group. That of Co2 is octahedral and composed of three (*p*-*tert*-butylbenzoyl), the two bridging ones with Co1 and one bridging to Co3, the triply bridging hydroxyl group and one water molecule. The structure is completed by an external benzoic acid molecule, which is H-bonded as a proton acceptor to the triply bridging OH ligand and as a proton donor to the free carbonyl group of the monodentate benzoate bonded to Co1.

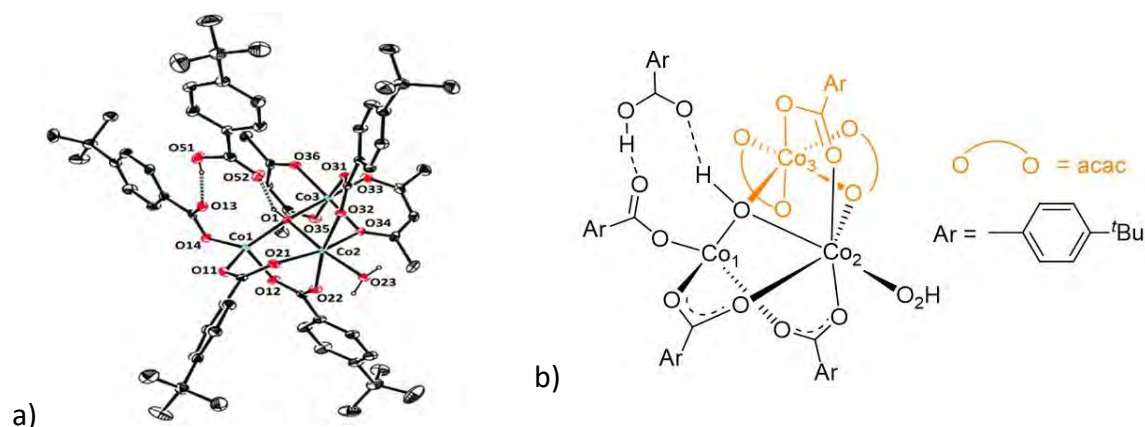
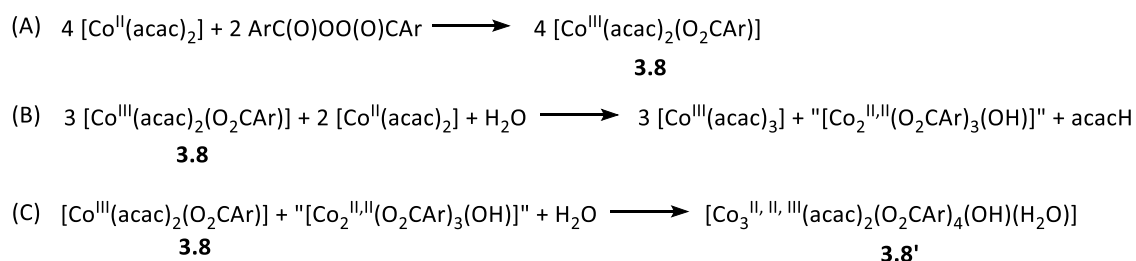
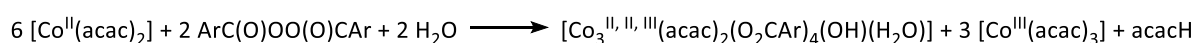


*Figure III-6: a) OTERP view of the polynuclear structure resulting from the crystallization of **3.8**, with the atom labelling scheme. Ellipsoids are drawn at the 30% probability level; b) simplified view of the compound.*

The formation of this polynuclear complex may be rationalized on the basis of the presence of residual water and $[\text{Co}^{\text{II}}(\text{acac})_2]$ in the reaction medium, as schematically illustrated in *Scheme Erreur ! Source du renvoi introuvable.III-3* (Ar = $\text{C}_6\text{H}_4\text{-}p\text{-}^t\text{Bu}$). The four carboxylate ligands in **3.8'** must all be originating from the acyl peroxide, requiring two peroxide molecules and the oxidation of four $[\text{Co}^{\text{II}}(\text{acac})_2]$ molecules (equation A). Out of the four produced molecules of **3.8**, one ends up in the final product while the other three are sacrificial, furnishing the carboxylate ligands to the two Co^{II} centers by ligand scrambling, with participation of one water molecule (equation B). This furnishes the dinuclear “[$\text{Co}_2(\text{O}_2\text{CAR})_3(\text{OH})$]” moiety that combines with one molecule of **3.8**, with participation of an additional water molecule, to yield the observed trinuclear product **3.8'** (equation C). This is, of course, only a stoichiometric rationalization of the product genesis, not a proposition of the reaction mechanism, which must be much more complex.



overall stoichiometry



Scheme III-3: Proposed reaction scheme for the formation of 3.8'.

The bond distances involving the Co^{III} ion (Co3) and the acac ligands (1.869(3) Å and 1.8914(17) Å) are in the range of the distances observed for complexes **3.6**, **3.9** and **3.10** (Table III-1). The Co(3)-O(31)_{Benzoate} bond length of 1.908(3) Å and the O(31)-Co(3)-O(1) and O(31)-C(31)-O(32) angles (94.10° and 125.95°, respectively) compare well with those in **3.9** and **3.10**, (Table III-1).

c. Bis(acetylacetonato)-cobalt(III) complexes with alkyl carboxylates

With the objective of varying the potential carboxylate R₀ initiating groups, we further extended the strategy presented above (*Scheme III-1* and *Scheme III-2, b*) to alkyl peroxide derivatives. First of all, the bis(acetylacetonato) cobalt(III) acetate complex, $[\text{Co}(\text{acac})_2(\text{OAc})]$ (**3.11**) was synthesized by reaction between $[\text{Co}(\text{acac})_2]$ and diacetyl peroxide (APO), prepared according to the literature procedure⁹³⁻⁹⁵ (*Figure III-16, top*). The success of the reaction could be assessed by; 1) a rapid (10 min) color change from pink (Co^{II}) to green (Co^{III}) and, 2) the recording of a diamagnetic ^1H NMR spectrum that revealed the presence of the characteristic OC(CH₃)O resonance (δ 1.90 ppm, *Figure III-17*). However, complex **3.11** turned out to be very sensitive, degrading rapidly upon attempted purifications. Therefore, it was used “as synthesized” for the polymerization tests. Since the polymerization results were not

promising, further efforts were focused on the more promising benzoate derivatives (*Chapter III*). Complex $[\text{Co}(\text{acac})_2(\text{O}_2\text{C}(\text{CH}_2)_{10}\text{CH}_3)]$ (**3.12**) was similarly synthesized from $[\text{Co}(\text{acac})_2]$ and the commercially available dilauroyl peroxide (*Figure III-16, bottom*). The presence of the long aliphatic chain was expected to increase the stability of the resulting Co^{III} complex (inductive donor effect). However, the ^1H NMR spectrum of the crude product exhibited several set of signals that were attributed to the formation of two or three types of complexes, possibly differing by the coordination mode of the carboxylate ligand, *i.e.* monodentate, bidentate chelating or bidentate bridging, as observed in the above-described solid-state structures of **3.6** (chelating), **3.9** and **3.10** (monodentate), and **3.8'** (bridging). Purification/separation tests were unsuccessful, therefore we focused our attention on the most promising benzoate derivatives (*Chapter III*).

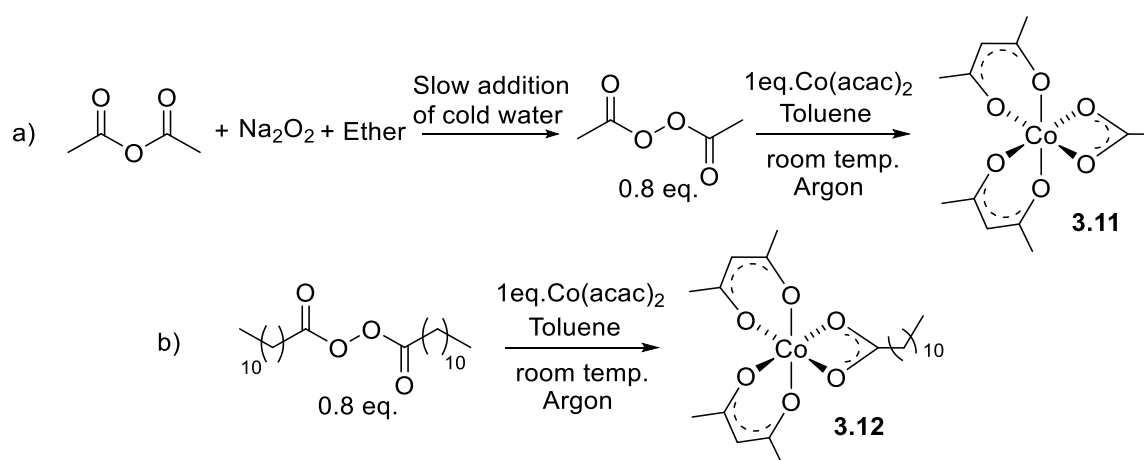


Figure III-7: Synthesis of bis(acetylacetonato)-cobalt(III) complexes of alkyl carboxylates, a) $[\text{Co}(\text{acac})_2(\text{OAc})]$ and b) $[\text{Co}(\text{acac})_2(\text{O}_2\text{C}(\text{CH}_2)_{10}\text{CH}_3)]$.

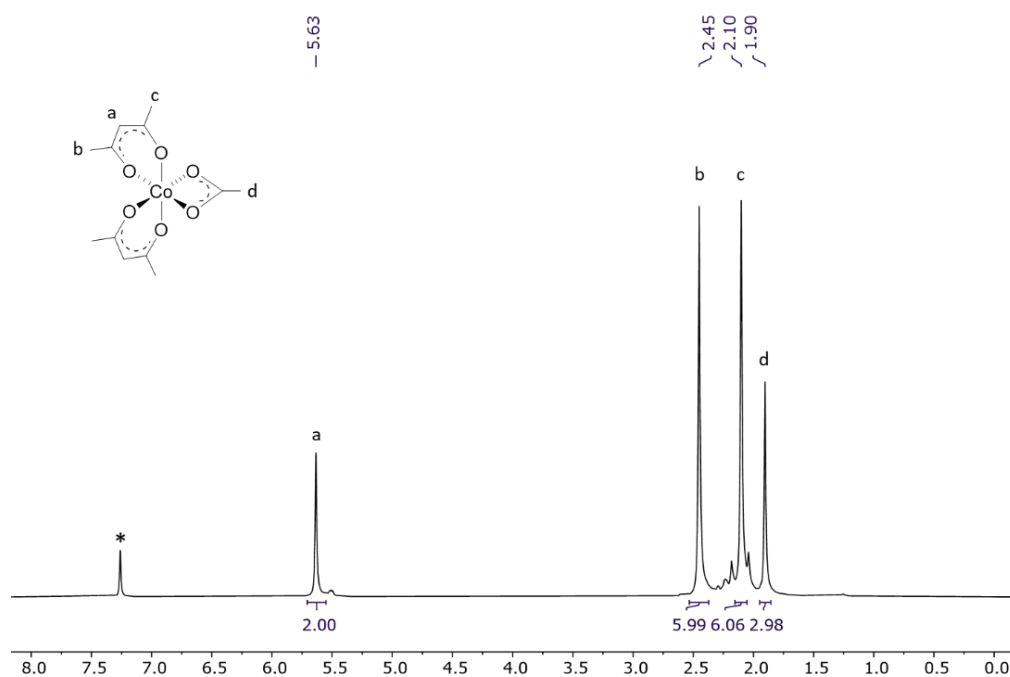


Figure III-8: ^1H NMR of the compound $[\text{Co}(\text{acac})_2(\text{OAc})]$ (**3.11**) recorded in CDCl_3 , 400MHz.

d. Use of simple peroxide

The simplicity and efficiency of the synthetic route to access carboxylate complexes from acyl peroxides led us to investigate its potential extension to the synthesis of alkoxide derivatives from “simple” alkyl peroxides (namely, R-O-O-R vs. R'-C(O)-O-O-(O)C-R'). Therefore, [Co(acac)₂] was reacted with the commercially available *di-tert*butyl peroxide (TBPO). However, the typical colour change associated to the Co^{II} to Co^{III} transformation was not observed, indicating that no reaction occurred (several reaction temperatures were explored). The choice of TBPO, as peroxide, was motivated by the low value of the DFT-calculated (acac)₂Co-O^tBu bond dissociation Gibbs energy (5.8 kcal mol⁻¹ at room temperature, *Figure III-*), which should make it an effective OMRP initiator (low barrier for the production of the corresponding *t*BuO• radical).

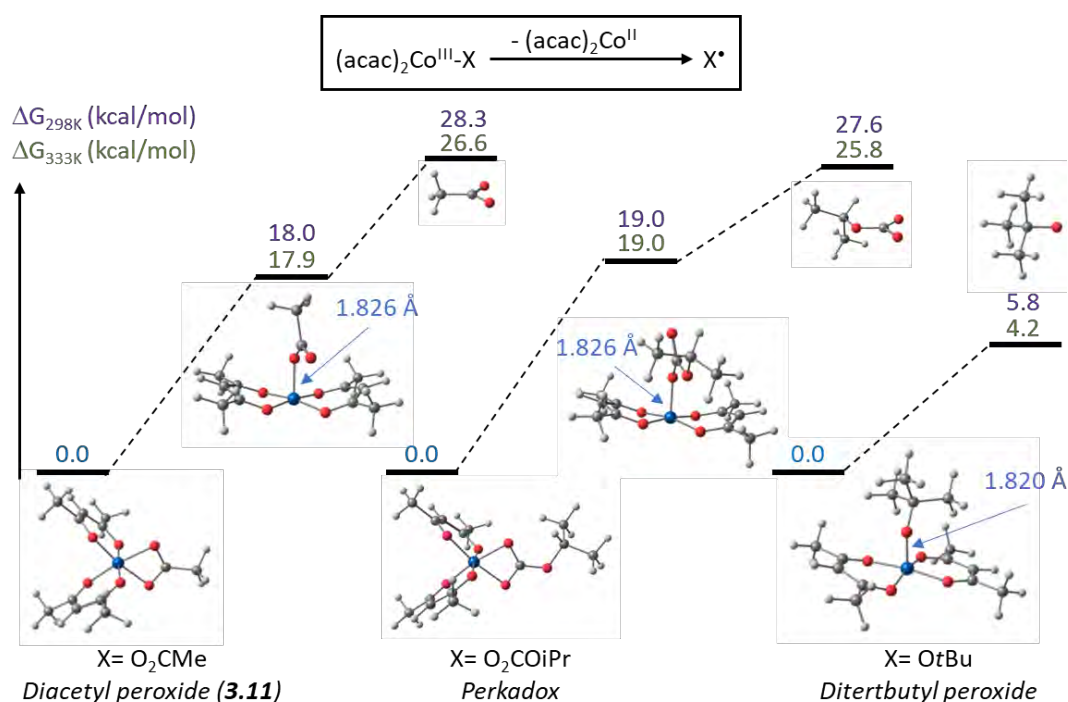


Figure III-9: DFT-calculated (acac)₂Co^{III}-R₀ BDEs.

IV. Conclusion and outlook

The present chapter summarized the synthetic work in the fields of ligands synthesis and coordination chemistry, realized along this thesis project. Two cobalt(III) acetate complexes of a $[\text{Co}^{\text{III}}(\text{L}^{1.1})(\text{OAc})]$ (**3.1**) and $[\text{Co}^{\text{III}}(\text{L}^{1.10})(\text{OAc})]$ (**3.2**) were obtained following previously reported methods. An original pathway to access cobalt(III) carboxylate complexes, by reaction between their cobalt(II) analogues and peroxides, was developed and allowed to isolate a series potential initiators of polymerization processes (see *Chapter III*). This method was feasible for both cobalt(II) complexes with Schiff bases and acac as supporting ligands. A summary of the developed architectures is depicted in *Figure IV-1*.

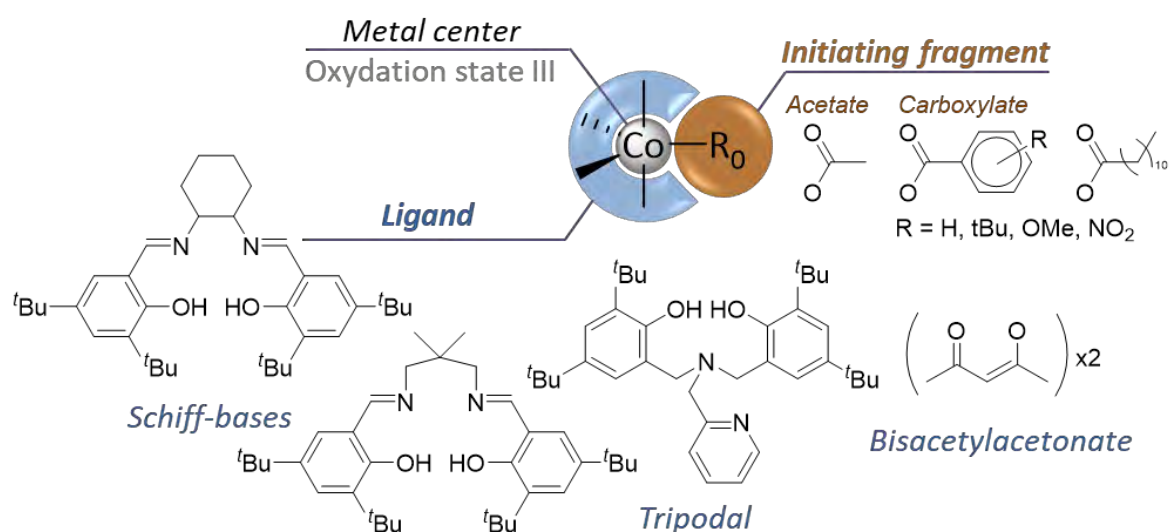


Figure IV-1: Summary of the architectures described in this chapter, to be tested as polymerization initiators and controlling agents.

The systems developed in the present chapter have been evaluated as initiators for radical (OMRP) and ring-opening polymerization (ROP) processes. The results of these investigations are presented and discussed in *Chapter III*.

V. Experimental section

1. Materials

The following compounds were all purchased from Sigma-Aldrich and used as received: cobalt acetate ($\text{Co}(\text{OAc})_2$, 99.99%), (1*R*,2*R*)-(-)-1,2-diaminocyclohexane (98%), 3,5-di-*tert*-butyl-2-hydroxybenzaldehyde (99%), 3-(dimethylamino)-1-propylamine (99%), *p*-toluenesulfonic acid monohydrate ($\geq 98.5\%$), ethylenediamine (99%), *o*-phenylenediamine (99.5%), 2,2-dimethyl-1,3-propanediamine (99%), 3,5-dichlorosalicylaldehyde (99%), salicylaldehyde (98%), propylamine ($\geq 99\%$) and sodium peroxide (Na_2O_2 , 97%, Sigma Aldrich). Bis(acetylacetonate)cobalt(II), $[\text{Co}(\text{acac})_2]$ (97%, Sigma Aldrich), benzoyl peroxide (Luperox A70S, 70% in water, Sigma Aldrich), *tert*-butyl peroxide (Luperox DI, 99%, Sigma Aldrich), TEMPO (2,2,6,6-tetramethylpiperidine-1-oxyl, Apollo Scientific), and the deuterated solvents C_6D_6 , CD_2Cl_2 and CDCl_3 (99.8% D, Eurisotop) were also used as received. Benzoyl peroxide (BPO) was purchased from Sigma-Aldrich and recrystallized from acetone/ethanol at -80°C . After filtration and washings (3 times with cold ethanol), the white solid was dried under vacuum. Vinyl acetate (Sigma-Aldrich) was dried on CaH_2 overnight, distilled under static vacuum and stored under argon. Reagent grade (99.5%) acetone, ethanol, pentane and diethylether were purchased from Sigma-Aldrich and tetrahydrofuran ($\geq 99.9\%$) was purchased from Carlo Erba. All solvents were purified by standard methods and distilled under argon prior to use except toluene, which was degassed and stored on molecular sieves (4 Å) from Fluka. Schiff-base cobalt(II) complexes **2.1-2.8** were synthesized according to the literature procedure.^{60, 96} The complex **3.1** was produced based on the paper published by Jacobsen *et al.*⁶⁰ All of the aromatics peroxides precursors⁹² and the diacetyl peroxide⁹³⁻⁹⁵ were prepared according to the literature.

2. Characterizations

NMR. The spectra were recorded on a Bruker Avance III 300 or 400 MHz spectrometer at ambient temperature. ^1H and ^{13}C chemical shifts (δ) are reported in ppm vs. SiMe_4 and were determined with respect to the residual ^1H solvent peaks as internal standard.

UV-Visible. The analyses were made with a Perkin Elmer Lambda 950 spectrophotometer equipped with tungsten and deuterium sources, a double beam with double monochromator and a photodiode detector.

EPR. The EPR spectrum was obtained at 4.13 K on an Elexsys E 500 Bruker spectrometer, operating at a microwave frequency of approximately 9.5 GHz, using a microwave power of 20 mW across a sweep width of 150 mT (centered at 310 mT) with modulation amplitude of 0.5 mT.

Cyclic voltammetry (CV) and square-wave voltammetry (SQW). experiments were carried out with an Autolab PGSTAT100 potentiostat (Metrohm) controlled by GPES 4.09 software. Experiments were carried out at room temperature in a homemade airtight three-electrode cell connected to a vacuum/argon line. The reference electrode consisted of a saturated calomel electrode (SCE) separated from the solution by a bridge compartment. The counter electrode was a platinum wire of *ca.* 1 cm² apparent surface. The working electrode was a platinum microdisk (0.5 mm diameter). The supporting electrolyte [n-Bu₄N][PF₆] (Sigma-Aldrich, 99 % electrochemical grade) was dried and degassed under argon. CH₂Cl₂ was freshly purified on an Innovative PURESOLV system equipped with 4 Å MS columns prior to use. The solutions used during the electrochemical studies were typically 10⁻³ M in analyte and 0.1 M in supporting electrolyte. Before each measurement, the solutions were degassed by bubbling Ar and the working electrode was polished with a polishing machine (Presi P230). All electrochemical data are referenced versus ferrocenium/ferrocene (FcH⁺/FcH) couple by adding ferrocene (10⁻³ M) at the end of the experiments.

GC-MS. The GC-MS investigation were carried out with a Shimadzu QP2010 Ultra equipped with a Phenomenex ZB-5MSplus column (0.25µm x 0.25mm x 30m). The experiments were conducted with the injection chamber at 250 °C at the ramp programme set at 50°C (constant for 1 min), then heating 20 °/min until 250 °C (then kept constant for 19 min).

X-ray structure. A single crystal was mounted under inert perfluoropolyether on the tip of a glass fiber and cooled in the cryostream of a Rigaku Oxford Diffraction GEMINI EOS diffractometer. The structure was solved by the integrated space-group and crystal-structure determination SHELXt software and refined by least-squares procedures on F₂ using SHELXL. All H atoms attached to carbon were introduced in the calculations at idealized positions and treated with the riding model. The drawing of the molecules was realized with the help of ORTEP32. Crystal data and refinement parameters are shown on the following part (Dr. Jean-Claude DARAN).

Calculation. The computational work was carried out using the Gaussian09 suite of programs. The geometry optimizations were performed without any symmetry constraint using BPW91* functional, which is a reparametrized version of B3PW91 with the same parameters previously optimized for B3LYP. This functional was chosen because it has provided the best results in our previous work on the energetics of Co^{III}-R bond cleavage processes. The 6-311G(d,p) basis functions was employed for all light atoms (H, C, N), whereas the Co atom was treated with the SDD basis set augmented by an f polarization function ($\alpha = 2.780$). The effect of dispersion forces was considered by using Grimme's D3 empirical method during the optimization process. The thermal corrections leading to the Gibbs energy (zero-point vibrational energy or ZPVE, PV, and TS) were obtained from the solution of the nuclear equation using the standard ideal gas and harmonic approximations at T = 298.15 K (25 °C) and 333.15 K (60 °C), which also verified the nature of all optimised geometries as local minima or first-order saddle

points. A correction of 1.95 kcal/mol was applied to all G values to change the standard state from the gas phase (1 atm) to solution (1 M) (Prof. Rinaldo POLI).

3. Methods

Schiff-base pro-ligands. The pro-ligands $\text{H}_2\text{L}^{1.1-1.9}$ were synthesized on the basis of the literature procedure^{43,44} The procedure is described in detail here only for $\text{H}_2\text{L}^{1.1}$. In a 250 mL two-neck round bottom flask with reflux condenser, (1*R*,2*R*)-(-)-1,2-diaminocyclohexane (0.975 g, 8.5 mmol, 1eq) was dissolved in 100 mL of absolute ethanol. The solution was heated at 80°C (reflux condition), and then a solution of 3,5-di-*tert*-butyl-2-hydroxybenzaldehyde (4 g, 17.1 mmol, 2 eq), previously dissolved in 50 mL of absolute ethanol, was added dropwise. The mixture was stirred 2 hours at 80°C, then cooled down to room temperature and then further to 0 °C with stirring for an additional 2 h. The formed yellow precipitate was isolated by filtration and dried under vacuum overnight, giving a yellow solid (3.94g, 85%). ¹H NMR (400 MHz, CD₂Cl₂): δ (ppm) = 8.29 (2H, *s*, N=CH), 7.29 (2H, *d*, *J* = 2.5 Hz, H_{aromatic}), 6.99 (2H, *d*, *J* = 2.5 Hz, H_{aromatic}), 3.37-3.28 (2H, *m*, CH₂), 1.97 (2H, *d*, *J* = 14.3 Hz, CH₂), 1.88 (2H, *d*, *J* = 10.2 Hz, CH₂), 1.80-1.65 (2H, *m*, CH₂), 1.52 residual water, 1.48 (2H, *d*, ³*J* = 9.8 Hz, CH₂), 1.39 (18H, *s*, ^{*t*}Bu), 1.28 (18H, *s*, ^{*t*}Bu) (Figure S1).

The other ligands were obtained following the same procedure from the appropriate diamine and aldehyde precursor.

$\text{H}_2\text{L}^{1.2}$: Yield 85%. ¹H NMR (400 MHz, CD₂Cl₂): δ (ppm) = 8.40 (2H, *s*, N=CH), 7.36 (2H, *d*, *J* = 2.5 Hz, CH aromatic), 7.09 (2H, *d*, *J* = 2.5 Hz, H_{aromatic}), 3.92 (4H, *s*, 2xCH₂), 1.52 residual water, 1.41 (18H, *s*, ^{*t*}Bu), 1.27 (18H, *s*, ^{*t*}Bu) (Figure S2).

$\text{H}_2\text{L}^{1.3}$: Yield 76%. ¹H NMR (400 MHz, CD₂Cl₂): δ (ppm) = 8.66 (*s*, 2H), 7.46 (*m*, 2H), 7.26 (*m*, 2H), 7.07 (*d*, *J* = 7.6 Hz, 2H), 6.79 (*d*, *J* = 7.7 Hz, 2H), 1.52 (*s*, 9H), 1.46 (*s*, 9H), 1.33 (*d*, *J* = 4.2 Hz, 18H) (Figure S3).

$\text{H}_2\text{L}^{1.5}$: Yield 84%. ¹H NMR (400 MHz, CD₂Cl₂): δ (ppm) = 8.36 (*s*, 2H, a), from 7.33 to 6.87 (*m*, 8H, H_{aromatic}), 3.50 (*s*, 4H, b), 1.54 residual water, 1.45 (*s*, 6H, c) (Figure S4).

$\text{H}_2\text{L}^{1.6}$: Yield 83%. ¹H NMR (400 MHz, CD₂Cl₂): δ (ppm) = 8.32 (*s*, 2H, a), 7.41 (*d*, 2H, ⁴*J* = 2.5 Hz, b), 7.20 (*d*, 2H, ⁴*J* = 2.5 Hz, c), 4.00 (*s*, 4H, d), 1.54 residual water (Figure S5).

$\text{H}_2\text{L}^{1.7}$: Yield 75%. ¹H NMR (400 MHz, CDCl₃): δ (ppm) = 8.18 (*s*, 2H, a), 7.36 (*d*, *J* = 2.5 Hz, 2H, b), 7.08 (*d*, *J* = 2.5 Hz, 2H, c), 3.44 – 3.25 (*m*, 2H, d), 1.93 (*tt*, *J* = 12.4, 2.9 Hz, 4H, e), 1.82 – 1.62 (*m*, 2H, f), 1.59 – 1.41 (*m*, 2H, g), 1.56 residual water (Figure S6).

$\text{H}_2\text{L}^{1.8}$: Yield 86%. ¹H NMR (400 MHz, CD₂Cl₂): δ (ppm) = 8.30 (*s*, 2H, a), 7.42 (*d*, *J* = 2.5 Hz, 2H, b), 7.22 (*d*, *J* = 2.5 Hz, 2H, c), 3.59 – 3.53 (*m*, 4H, d), 1.09 (*s*, 6H, e) (Figure S7).

$\text{H}_2\text{L}^{1.9}$: Yield 71%. ¹H NMR (400 MHz, C₆D₆): δ (ppm) = 8.62 (*s*, 2H, a), 7.32 (*m*, 2H, b), 7.20 (*m*, 2H, c), 6.69 (*m*, 4H, d), 6.86 (*d*, 2H, e), 3.90 (*s*, 6H, f) (Figure S8).

Tripodal pro-ligand. The desired amine (0.048 mol, 1 eq) was added to a mixture of the phenol (0.096 mol, 2 eq) and formaldehyde (37% in H₂O, 10 mL, 0.12 mol) in water/ethanol (70 + 30 mL, respectively) at room temperature. The resulting reaction mixture was stirred for 18 h at

70 °C. After cooling the homogenous solution to 0 °C, a white solid corresponding to the desired pro-ligand precipitated. The white precipitate was filtered off, washed with cold ethanol (3 x 20 mL) and dried under vacuum.^{32,97} Characterization data:

H₂L¹⁻¹⁰: Yield 59%. ¹H NMR (400 MHz, CDCl₃): δ (ppm) 10.54 (s, 2H, OH), 8.71 (d, 1H, b), 7.69 (td, 1H, c), 7.23 (m, 1H), 7.13 (d, 2H), 7.11 (d, 1H, f), 6.93 (d, 2H), 3.85 (s, 2H), 3.80 (d, 2H), 1.40 (s, 18H), 1.29 (s, 18H).

H₂L¹⁻¹¹: Yield 58%. ¹H NMR (400 MHz, CDCl₃): δ (ppm) = 7.19 (d, J = 2.5 Hz, 2H), 6.86 (d, J = 6.0 Hz, 2H), 3.63 (s, 4H), 2.59 (t, J = 6.0 Hz, 2H), 2.44 (t, J = 6.0 Hz, 2H), 2.35 (s, 6H), 1.77 (p, J = 5.7 Hz, 2H), 1.39 (s, 18H), 1.27 (s, 18H) (Figure S9).

H₂L¹⁻¹²: Yield 56%. ¹H NMR (400 MHz, CDCl₃) δ (ppm) = 7.19 (dd, J = 8.5, 2.5 Hz, 2H), 7.03 (d, J = 2.5 Hz, 2H), 6.80 (d, J = 8.5 Hz, 2H), 3.64 (s, 4H), 2.62 (t, J = 6.2 Hz, 2H), 2.51 – 2.47 (m, 2H), 2.36 (s, 6H), 1.86 – 1.79 (m, 2H), 1.29 (s, 18H) (Figure S10).

H₂L¹⁻¹³: Yield 61%. ¹H NMR (400 MHz, CDCl₃) δ 7.01 (d, J = 2.2 Hz, 2H), 6.73 (d, J = 2.3 Hz, 2H), 3.63 (s, 4H), 2.51 – 2.45 (m, 2H), 2.24 (s, 6H), 1.62 (q, J = 7.4 Hz, 2H), 1.39 (s, 24H), 0.86 (t, J = 7.3 Hz, 3H) (Figure S11).

General procedure for the synthesis of Cobalt(II) Schiff bases complexes. A solution of cobalt acetate tetrahydrate (597 mg, 2.4 mmol) in methanol (8 mL) was prepared under argon (purple solution). Separately, the pro-ligand (2 mmol) was dissolved in 8 mL of DCM (yellow solution). The solution of the cobalt complex was added dropwise to the ligand solution *via* a purged syringe. The resulting mixture was stirred at room temperature for 15 min, followed by stirring for an additional 30 min at 0°C. The red precipitate was collected by filtration and washed twice with cold methanol.

2.1: Red powder, yield 80%. MS (ESI, pos., m/z): found, 603.3; calculated, 603.34 g mol⁻¹, (Figure S12-S13).

2.2: Red powder, yield 94%. MS (ESI, pos., m/z): found, 549.3; calculated, 549.29 g mol⁻¹, (Figure S14-S15).

2.3: Dark brown powder, yield 18%. MS (ESI, pos., m/z): found, 597.3; calculated, 597.29 g mol⁻¹, (Figure S16).

2.5: Dark red powder, yield 93%. MS (ESI, pos., m/z): found, 367.1; calculated, 367.09 g mol⁻¹, (Figure S17).

2.6: Light brown powder: yield 77%. MS (ESI, pos., m/z): found, 460.9; calculated, 460.88 g mol⁻¹, (Figure S18-S19).

2.7: Red powder, yield 97%. MS (ESI, pos., m/z): found, 514.9; calculated, 514.93 g mol⁻¹, (Figure S20).

2.8: Red powder, yield 92%. MS (ESI, pos., m/z): found, 502.9; calculated, 502.93 g mol⁻¹, (Figure S21).

Synthesis of [Co^{III}(L¹⁻¹)(OAc)] (3.1). Based on paper published by Jacobsen *et al.*⁶⁰ in 2004, the cobalt II acetate (177.08 g mol⁻¹, 0.647g, 3.6 mmol, 1eq) and glacial acid acetic (60.05 g/mol, 25 mL) was introduced in round bottom flask followed by addition of ligand (R,R)-Salen

previously synthesis ($546.42 \text{ g mol}^{-1}$, 2g, 3.6mmol, 1eq) at room temperature. The yellow, brown suspension turned to the dark brown solution after few minutes of stirring. After 30min, air was bubbled into the solution during 3 hours and stirred under air atmosphere overnight. The acid acetic was removed under vacuum. The crude product obtained was then solubilised in methanol (10 mL) followed by drop wise addition of water (same amount as methanol). A brown precipitate formed was collected by filtration and washed 3 times with water before dried under vacuum (12h). The pure product (R,R)-SalenCoOAc was collected as brown powder (2.16g).

3.1. Yield 89 %. Chemical formula: $\text{C}_{38}\text{H}_{55}\text{CoN}_2\text{O}_4$. Molar mass: $662.35 \text{ g mol}^{-1}$. Elemental analysis: calculated data (%): C 68.86, H 8.36, N 4.23; Found: C 65.79, H 8.22, N 3.95. $^1\text{H NMR}$ (400 MHz, CD_2Cl_2): δ (ppm) = 7.47 (1H, s, N=CH), 7.34, 7.30, 7.25 (4H aromatics), 6.52 (1H, s, N=CH), 4.65 (1H, m, CH Cyclohexyl), 3.42 (residual MeOH and second CH cyclohexyl), 2.79 (2H, d, CH_2 of Cy), 2.12 (residual acid acetic), 1.92 (2H, second CH_2 of Cy), 1.68 (3H, s, CH_3 of OAc), 1.49-1.36-1.32-1.25 (36H, s, 4x ^tBu), 1.56 and 1.61 (2x CH_2 of Cy).

Synthesis of $[\text{Co}^{\text{III}}(\text{L}^{1.10})\text{(OAc)}]$ (3.2). Solid $[\text{Co}(\text{OAc})_2]$ (32.5 mg, 0.18 mmol) was added in one portion to a solution of pro-ligand $\text{H}_2\text{L}^{1.10}$ (100 mg, 0.18 mmol) and excess of NEt_3 (0.5 mL) in a 2:1 mixture of MeOH/ CHCl_3 (30 mL) at room temperature. The resulting mixture was stirred at room temperature in air during 24 h. The crude product obtained after removal of the volatiles was recrystallized from CHCl_3 , leading to complex **3.2** as a dark red powder (75.2 mg, 62%). Suitable crystals for the X-ray diffraction analysis were grown by slow diffusion of pentane into a saturated CHCl_3 solution of **3.2** over a week at room temperature. Anal. Calcd. for $\text{C}_{38}\text{H}_{53}\text{CoN}_2\text{O}_4$ (660.79): C, 69.07; H, 8.08; N, 4.24. Found: 68.79; H, 8.30; N, 4.34. FTIR: $\nu_{\text{max}}(\text{solid})/\text{cm}^{-1}$: 2950br, 1602w, 1515w, 1470vs, 1443s, 1411s, 1361m, 1277s, 1238m, 1203m, 1167m, 1130w, 1059w, 950w, 914w, 875w, 835m, 805w, 763s, 748m, 688vs, 625m, 554m, 496s, 438m. MS (ESI): m/z 601.3 $[\text{M} - \text{OAc}]^+$. UV-Vis: $\lambda_{\text{max}}(\text{toluene})/\text{nm}$: 428 ($\epsilon/\text{dm}^3 \text{ mol}^{-1} \text{ cm}^{-1}$: 2687). $^1\text{H NMR}$ (400 MHz, CDCl_3): δ (ppm) 8.55 (d, $^3J = 5.7 \text{ Hz}$, 1H, H_{arom} , Py), 7.39 (t, $^3J = 7.7 \text{ Hz}$, 1H, H_{arom} , Py), 6.99 (t, $^3J = 6.7 \text{ Hz}$, 1H, H_{arom} , Py), 6.94 (d, $^4J = 2.5 \text{ Hz}$, 2H, H_{arom} , Phenol), 6.79 (d, $^4J = 2.5 \text{ Hz}$, 2H, H_{arom} , Phenol), 6.63 (d, $^3J = 7.9 \text{ Hz}$, 1H, H_{arom} , Py), 4.59 (d, $^2J = 13.3 \text{ Hz}$, 2H, CH_2), 3.97 (s, 2H, CH_2), 3.06 (d, $^2J = 13.2 \text{ Hz}$, 2H, CH_2), 1.95 (s, 3H, $\text{OC}(\text{CH}_3)\text{O}$), 1.31 (s, 18H, ^tBu), 1.20 (s, 18H, ^tBu). $^{13}\text{C}^{98} \text{NMR}$ (101 MHz, CDCl_3): δ (ppm) 191.75 ($\text{OC}(\text{CH}_3)\text{O}$), 163.28 (C_{quat}), 163.11 (C_{quat}), 151.41 (CH_{arom} , Py), 140.87 (C_{quat}), 138.02 (CH_{arom} , Py), 135.97 (C_{quat}), 123.72 (CH_{arom} , Phenol), 123.48 (CH_{arom} , Phenol), 121.87 (CH_{arom} , Py), 119.57 (C_{quat}), 118.75 (CH_{arom} , Py), 64.69 ($\text{NCH}_2\text{Phenol}$), 63.21 (NCH_2Py), 35.53 ($\text{C}(\text{CH}_3)_3$), 34.03 ($\text{C}(\text{CH}_3)_3$), 31.87 ($\text{C}(\text{CH}_3)_3$), 30.06 ($\text{C}(\text{CH}_3)_3$), 23.97 ($\text{OC}(\text{CH}_3)\text{O}$).

Synthesis of $[\text{Co}^{\text{III}}(\text{L}^{1.4})\text{(OBz)}]$ (3.3). In the glove box, 651 mg (1 mmol) of complex **2.4** was dissolved in 70 mL of toluene. The solution was placed in the ice bath and 200 mg (0.826 mmol L^{-1}) of BPO was added. The resulting solution was stirred for two hours and the volatiles were then evaporated to dryness under vacuum. The dark brown solid was washed 2 times with pentane and dried overnight under vacuum and collect the resulting brown powder. Yield

76%. Elemental analysis: Calcd. C, 70.77; H, 8.06; N, 3.98. Found: C, 70.90; H, 8.53; N, 3.79. ^1H NMR (400 MHz, CDCl_3): δ (ppm): 7.99 (*d*, $J = 6.8$ Hz, 2H, a), 7.62 and 7.37 (*d*, $J = 2.6$ Hz, 1H, b and b'), 7.02 (*dd*, $J = 8.7, 2.6$ Hz, 2H, c), 1.71, 1.42, 1.40 and 1.33 (*s*, 9H, $4\times^t\text{Bu}$), 6.94 (*t*, $J = 3.8$ Hz, 2H, g), 6.86 (*t*, $J = 7.5$ Hz, 2H, f), 6.64 (*s*, 1H, h), 4.67 (*d*, 1H, $J=11.1\text{Hz}$, d), 2.77 (*m*, 2H, d), 2.33 (*d*, 1H, $J=13.2\text{Hz}$, d), 0.67 (*s*, 3H, e), 0.42 (*s*, 3H, e). ^{13}C NMR (400 MHz, C_6D_6): δ (ppm) 187.37 (C_{quat} of the carboxylate, f), 168.07 and 167.03 ($-\text{CH}=\text{N}$, a), the signals at 166.57, 163.51, 144.76, 142.94, 136.66, 125.70, 122.92, 121.46 and 136.10 (C_{quat}), 132.70, 130.06, 129.56, 129.33, 128.64, 127.05 and 126.63 ($\text{CH}_{\text{aromatic}}$), 69.84 and 69.56 ($-\text{CH}_2-\text{N}$, d), 36.33, 35.73, 35.46, 34.15 and 33.98 (C_{quat} of ^tBu), 31.84, 31.69, 30.37 and 30.29 (C_{methyl} ^tBu), 25.46 ($-\text{CH}_3$, e), 23.40 ($-\text{CH}_3$ amine bridge), 21.44 (C_{quat} of amine bridge).

Synthesis of $\text{Co}^{\text{III}}(\text{L}^{1.4})(\text{O}_2\text{CC}_6\text{H}_4\text{-p-OMe})$ (3.4). The procedure used to obtain this compound was identical to that described in the previous section for **3.3**. The product, however, was obtained in low yields (12%) and was not very pure. ^1H NMR (400 MHz, C_6D_6), δ (ppm) = 8.00 (*d*, $J = 8.9$ Hz, 2H), 7.63 (*d*, $J = 2.6$ Hz, 1H), 7.37 (*d*, $J = 2.6$ Hz, 1H), 7.04 (*d*, $J = 2.6$ Hz, 1H), 7.02 (*dd*, $J = 5.5, 1.9$ Hz, 1H), 6.95 (*d*, $J = 4.2$ Hz, 1H), 6.68 (*s*, 1H), 6.46 (*d*, $J = 9.0$ Hz, 2H), 4.71 (*d*, $J = 10.5$ Hz, 1H), 2.98 (*s*, 3H), 2.81 (*s*, 2H), 2.38 (*s*, 1H), 1.75 (*s*, 8H), 1.43 (*s*, 8H), 1.40 (*s*, 8H), 1.34 (*s*, 10H), 0.68 (*s*, 3H), 0.43 (*s*, 3H).

General procedure for the synthesis of substituted Benzoyl peroxides.⁹² In a round bottom flask, the desired carboxylic acid (32.8 mmol) was dissolved in dichloromethane (100 mL) and the resulting solution was placed in ice bath. A few drops of DMF were added, followed by the dropwise addition of oxalyl chloride (34.5 mmol). The resulting mixture was stirred until no more gas evolved, then the solvent was completely removed by evaporation under reduced pressure. The produced acid chloride was dissolved in diethyl ether (10 mL) and the resulting solution was placed in an ice bath. A hydrogen peroxide solution (35 wt. % in H_2O , 15 mmol) was added dropwise over 10 min. This was followed by the dropwise addition of an aqueous solution of NaOH (32.8 mmol) over 20 min. The resulting white precipitate was collected by filtration. After washing with water (2×10 mL) and diethyl ether (2×10 mL), the solid was crystallized first from a cold acetone / water mixture (1:3 v/v), then recrystallized from acetone/ethanol (^1H NMR spectra in Figure S26-S29).

Bis(*p*-nitrobenzoyl) peroxide. was obtained as white powder (Yield 81%). ^1H NMR (400MHz, CD_2Cl_2): δ 8.40 (*d*, $J = 9.0$ Hz, 2H), 8.28 (*d*, $J = 9.0$ Hz, 2H) (Figure S26).

Bis(*p*-tert-butylbenzoyl) peroxide. The product was obtained as white powder (Yield 72%). ^1H NMR (400MHz, CD_2Cl_2): δ 8.00 (*d*, $J = 9.1$ Hz, 2H), 7.57 (*d*, $J = 9.0$ Hz, 2H), 3.89 (*s*, 9H) (Figure S27).

Bis(*o*-nitrobenzoyl) peroxide. The product was obtained as with powder (Yield 78%). ^1H NMR (400MHz, CD_2Cl_2): δ 8.23 (*d*, $J = 8.1$ Hz, 1H), 7.87 (*m*, 3H) (Figure S28).

Bis(*p*-methoxybenzoyl) peroxide. The product was obtained as with powder (Yield 80%). ^1H NMR (400MHz, CD_2Cl_2): δ 8.00 (*d*, $J = 9.1$ Hz, 2H), 7.00 (*d*, $J = 9.0$ Hz, 2H), 3.89 (*s*, 3H) (Figure S28).

Synthesis of diacetyl peroxide. Based on the literature of 60's,⁹³⁻⁹⁵ In round bottom flask the 5g (0.0489mol) of anhydride acetic, 2.54g (0.0326mol) of sodium peroxide and 50mL of cold ether were added. Under stirring in ice bath, the cold water was added dropwise until full decomposition of sodium peroxide. Stirred vigorously over 10min after the end of water addition. After that, using separating funnel to isolate the organic phase. Dried under vacuum and collect a pure white powder (1.447g), yield = 37% (Figure S30)

Synthesis of [Co(acac)₂(O₂CPh)] (3.6). In a round-bottom flask under argon, [Co(acac)₂] (0.5 g, 1.94 mmol) was dissolved in 30 mL of toluene to yield a pink solution. A separately prepared solution of BPO (0.351 g, 1.45 mmol) in 2 mL of toluene was then injected into the complex solution, resulting in an instantaneous colour change to dark green. After 2 hours of stirring at room temperature, the solvent was removed by evaporation under reduced pressure. The resulting crude product was washed with diethyl ether (25 mL) and pentane (2x25 mL), then filtered and dried. Yield 0.44 g (60 %). Elemental analysis: theoretical values for C₁₇H₁₉CoO₆ (378.27 g mol⁻¹): C, 53.98; H, 5.06 %. Found: C, 53.22; H, 4.39 %. ¹H NMR (δ/ppm, 400 MHz, C₆D₆): 8.22 (2H, *d*, CH *ortho*), 6.94 (1H, *tt*, CH *para*), 6.84 (2H, *t*, CH *meta*) aromatic protons, 5.28 (2H, *s*, 2xCH acetylacetonate), 2.04 (6H, *s*, 2xCH₃ acetylacetonate) and 1.78 (6H, *s*, 2xCH₃ acetylacetonate).

Synthesis of [Co^{III}(acac)₂(O₂C*Ar*)] (3.7-3.12). These complexes were prepared following the same procedure presented before for **3.6**, except that the reaction was carried out in cold toluene (ice bath).

Characterization data:

3.7: Yield 45%. ¹H NMR (400 MHz, C₆D₆) δ (ppm) = 8.20 (*s*, 2H, *a*), 6.40 (*s*, 3H, *b*), 5.30 (*s*, 2H, *c*), 2.99 (*s*, 4H, *d*), 2.04 and 1.81 (*s*, 6H, *e*, *e'*) (Figure S31).

3.8: Yield 45%. ¹H NMR (400 MHz, C₆D₆) δ (ppm) = 8.19 (*s*, 2H, *a*), 8.04 (*s*, 2H, *b*), 5.30 (*s*, 2H, *c*), 2.06 and 1.81 (*s*, 2x6H, *d* and *d'*), 1.06 (*s*, 6H, *?*), 1.01 (*s*, 8H, *t*Bu) (Figure S32).

3.9: Yield 45%. ¹H NMR (400 MHz, CDCl₃) δ (ppm) = 7.41 (*s*, 2H), 6.28 (*s*, 2H), 4.71 (*s*, 2H), 1.48 (*s*, 6H), 1.17 (*s*, 7H) (Figure S33).

3.10: Yield 45%. ¹H NMR (300 MHz, CDCl₃): δ (ppm) = 8.00 (*s*, 1H), 7.90 (*s*, 1H), 7.73 (*s*, 2H), 5.73 (*s*, 1H), 5.53 (*s*, 1H), 2.36 (*s*, 6H), 2.19 (*s*, 3H), 2.02 (*s*, 3H) (Figure S34).

3.11: Yield 5%. ¹H NMR (400 MHz, C₆D₆): δ (ppm) = 5.27 (*s*, 2H), 2.13 (*s*, 6H), 1.73 (*s*, 6H), 1.53 (*s*, 3H).

3.12. Yield 47%. ¹H NMR (400 MHz, C₆D₆): δ (ppm) = 5.29 (*s*, 1H), 2.17 (*s*, 3H), 2.07 (*s*, 2H), 2.04 (*d*, *J* = 4.7 Hz, 2H), 1.95 (*s*, 4H), 1.75 (*s*, 2H), 1.58 (*s*, 3H), 1.29 (*s*, 18H), 0.94 (*s*, 3H) (Figure S36).

VI. References

1. Zhao, Y.; Yu, M.; Zhang, S.; Wu, Z.; Liu, Y.; Peng, C. H.; Fu, X., A well-defined, versatile photoinitiator (salen)Co-CO₂CH₃ for visible light-initiated living/controlled radical polymerization. *Chem Sci* **2015**, *6* (5), 2979-2988.
2. Zhao, Y.; Zhang, S.; Wu, Z.; Liu, X.; Zhao, X.; Peng, C.-H.; Fu, X., Visible-Light-Induced Living Radical Polymerization (LRP) Mediated by (salen)Co(II)/TPO at Ambient Temperature. *Macromolecules* **2015**, *48* (15), 5132-5139.
3. Fliedel, C.; Poli, R., Homolytically weak metal-carbon bonds make robust controlled radical polymerizations systems for "less-activated monomers". *Journal of Organometallic Chemistry* **2019**, *880*, 241-252.
4. Demarteau, J.; Kermagoret, A.; German, I.; Cordella, D.; Robeyns, K.; De Winter, J.; Gerbaux, P.; Jerome, C.; Debuigne, A.; Detrembleur, C., Halomethyl-cobalt(bis-acetylacetonate) for the controlled synthesis of functional polymers. *Chem Commun (Camb)* **2015**, *51* (76), 14334-7.
5. Debuigne, A.; Champouret, Y.; Jerome, R.; Poli, R.; Detrembleur, C., Mechanistic insights into the cobalt-mediated radical polymerization (CMRP) of vinyl acetate with cobalt(III) adducts as initiators. *Chemistry* **2008**, *14* (13), 4046-59.
6. Antoine Debuigne, J.-R. C., Nicolas Willet, and Robert Jerome, Synthesis of Poly(vinyl acetate) and Poly(vinyl alcohol) Containing Block Copolymers by Combination of Cobalt-Mediated Radical Polymerization and ATRP. *Macromolecules* **2005**, *35*, 9488-9496.
7. Antoine Debuigne, J.-R. C., and Robert Jerome, Synthesis of End-Functional Poly(vinyl acetate) by Cobalt-Mediated Radical Polymerization. *Macromolecules* **2005**, *38*, 5452-5458.
8. Duan, R.; Hu, C.; Li, X.; Pang, X.; Sun, Z.; Chen, X.; Wang, X., Air-Stable Salen-Iron Complexes: Stereoselective Catalysts for Lactide and ϵ -Caprolactone Polymerization through in Situ Initiation. *Macromolecules* **2017**, *50* (23), 9188-9195.
9. Longo, J. M.; Sanford, M. J.; Coates, G. W., Ring-Opening Copolymerization of Epoxides and Cyclic Anhydrides with Discrete Metal Complexes: Structure-Property Relationships. *Chemical Reviews* **2016**, *116* (24), 15167-15197.
10. Sanford, M. J.; Van Zee, N. J.; Coates, Geoffrey W., Reversible-deactivation anionic alternating ring-opening copolymerization of epoxides and cyclic anhydrides: access to orthogonally functionalizable multiblock aliphatic polyesters. *Chemical Science* **2018**, *9* (1), 134-142.
11. Tschan, M. J.; Guo, J.; Raman, S. K.; Brule, E.; Roisnel, T.; Rager, M. N.; Legay, R.; Durieux, G.; Rigaud, B.; Thomas, C. M., Zinc and cobalt complexes based on tripodal ligands: synthesis, structure and reactivity toward lactide. *Dalton Trans* **2014**, *43* (11), 4550-64.
12. Poli, R., Relationship between one-electron transition metal reactivity and radical polymerization processes. *Angew. Chem., Int. Ed.* **2006**, *45*, 5058-5070.
13. Smith, K. M.; McNeil, W. S.; Abd-El-Aziz, A. S., Organometallic-Mediated Radical Polymerization: Developing Well-Defined Complexes for Reversible Transition Metal-Alkyl Bond Homolysis. *Macromol. Chem. Phys.* **2010**, *211* (1), 10-16.
14. Allan, L. E. N.; Perry, M. R.; Shaver, M. P., Organometallic mediated radical polymerization. *Progress in Polymer Science* **2012**, *37* (1), 127-156.
15. Poli, R., Organometallic Mediated Radical Polymerization. In *Polymer Science: A Comprehensive Reference*, Matyjaszewski, K.; Möller, M., Eds. Elsevier BV: Amsterdam, 2012; Vol. 3, pp 351-375.

16. Demarteau, J.; Debuigne, A.; Detrembleur, C., Organocobalt Complexes as Sources of Carbon-Centered Radicals for Organic and Polymer Chemistries. *Chem. Rev.* **2019**, *119* (12), 6906-6955.
17. Debuigne, A.; Poli, R.; Jérôme, C.; Jérôme, R.; Detrembleur, C., Overview of cobalt-mediated radical polymerization: roots, state of the art and future prospects. *Prog. Polym. Sci.* **2009**, *34*, 211-239.
18. Debuigne, A.; Caille, J. R.; Jérôme, R., Highly efficient cobalt-mediated radical polymerization of vinyl acetate. *Angew. Chem., Int. Ed.* **2005**, *44* (7), 1101-1104.
19. Maria, S.; Kaneyoshi, H.; Matyjaszewski, K.; Poli, R., Effect of Electron Donors on the Radical Polymerization of Vinyl Acetate Mediated by Co(acac)₂: degenerative transfer versus reversible homolytic cleavage of an organocobalt(III) complex. *Chem. Eur. J.* **2007**, *13*, 2480-2492.
20. Debuigne, A.; Michaux, C.; Jérôme, C.; Jérôme, R.; Poli, R.; Detrembleur, C., Cobalt Mediated Radical Polymerization (CMRP) of Acrylonitrile : Kinetic Investigations and DFT Calculations. *Chem. Eur. J.* **2008**, *14*, 7623-7637.
21. Debuigne, A.; Poli, R.; Jérôme, R.; Jérôme, C.; Detrembleur, C., Key Role of Metal-Coordination in Cobalt-Mediated Radical Polymerization of Vinyl Acetate. *ACS Symp. Ser.* **2009**, *1024*, 131-148.
22. Debuigne, A.; Poli, R.; De Winter, J.; Laurent, P.; Gerbaux, P.; Wathélet, J.-P.; Jérôme, C.; Detrembleur, C., Effective Cobalt-Mediated Radical Coupling (CMRC) of Poly(vinyl acetate) and Poly(N-vinylpyrrolidone) (Co)polymers Precursors. *Macromolecules* **2010**, *43*, 2801-2813.
23. Debuigne, A.; Morin, A. N.; Kermagoret, A.; Piette, Y.; Detrembleur, C.; Jérôme, C.; Poli, R., Key Role of Intramolecular Metal Chelation and Hydrogen Bonding in the Cobalt-Mediated Radical Polymerization of N-Vinyl amides. *Chem. Eur. J.* **2012**, *18*, 12834–12844.
24. Piette, Y.; Debuigne, A.; Jérôme, C.; Bodart, V.; Poli, R.; Detrembleur, C., Cobalt-Mediated Radical (Co)polymerization of Vinyl Chloride and Vinyl Acetate. *Polymer Chemistry* **2012**, *3*, 2880-2891.
25. Morin, A. N.; Detrembleur, C.; Jérôme, C.; Tullio, P. D.; Poli, R.; Debuigne, A., Effect of head-to-head addition in vinyl acetate reversible deactivation radical polymerization: why is Co(acac)₂-mediated polymerization so much better? *Macromolecules (Washington, DC, U. S.)* **2013**, *46*, 4303–4312.
26. Kermagoret, A.; Debuigne, A.; Jerome, C.; Detrembleur, C., Precision design of ethylene- and polar-monomer-based copolymers by organometallic-mediated radical polymerization. *Nat. Chem.* **2014**, *6* (3), 179-187.
27. Wang, Z.; Poli, R.; Detrembleur, C.; Debuigne, A., Organometallic-Mediated Radical (Co)Polymerization of γ -Methylene- γ -Butyrolactone: Access to pH-Responsive Poly(vinyl alcohol) Derivatives. *Macromolecules (Washington, DC, U. S.)* **2019**, *52*, 8976-8988.
28. Banerjee, S.; Ladmiral, V.; Debuigne, A.; Detrembleur, C.; Poli, R.; Améduri, B., Organometallic Mediated Radical Polymerization of Vinylidene Fluoride. *Angew. Chem. Int. Ed.* **2018**, *57*, 2934–2937.
29. Falireas, P. G.; Ladmiral, V.; Debuigne, A.; Detrembleur, C.; Poli, R.; Ameduri, B., Straightforward synthesis of well-defined poly(vinylidene fluoride) and its block copolymers by cobalt-mediated radical polymerization. *Macromolecules (Washington, DC, U. S.)* **2019**, *52*, 1266-1276.
30. Wayland, B.; Poszmik, G.; Mukerjee, S., Living radical polymerization of acrylates by organocobalt porphyrin complexes. *J. Am. Chem. Soc.* **1994**, *116*, 7943-7944.

31. Wayland, B.; Mukerjee, S.; Poszmik, G.; Woska, D.; Basicckes, L.; Gridnev, A.; Fryd, M.; Ittel, S., Control of radical polymerizations by metalloradicals. *ACS Symp. Ser.* **1998**, *685* (Controlled Radical Polymerization), 305-315.
32. Redjel, Y. K.; Thevenin, L.; Daran, J.-C.; Benslimane, M.; Poli, R.; Fliedel, C., Acetylacetonato cobalt(III) and iron(III) complexes of picolylamine- and aminopropylamine-bis(phenolate) ligands: Synthesis, characterization and crystal structures. *Polyhedron* **2019**, *158*, 83-90.
33. Liao, C.-M.; Hsu, C.-C.; Wang, F.-S.; Wayland, B.; Peng, C.-H., Living radical polymerization of vinyl acetate and methyl acrylate mediated by Co(Salen*) complexes. *Polymer Chemistry* **2013**, *4* (10).
34. Zhao, Y.; Wang, Y.; Zhou, X.; Xue, Z.; Wang, X.; Xie, X.; Poli, R., Oxygen-Triggered Switchable Polymerization for the One-Pot Synthesis of CO₂-Based Block Copolymers from Monomer Mixtures. *Angew Chem Int Ed Engl* **2019**, *58* (40), 14311-14318.
35. Poli, R.; Allan, L. E. N.; Shaver, M. P., Iron-mediated reversible deactivation controlled radical polymerization. *Progress in Polymer Science* **2014**, *39* (10), 1827-1845.
36. Kanagasabapathy, S.; Serero, D.; Silie, D.; Prost, S.; Ruiz-Guerrero, R.; Claverie, J., Controlled "Living" radical polymerization of styrene with iron complexes. *Res. Discl.* **1998**, P1595-P1604.
37. Kermagoret, A.; Jerome, C.; Detrembleur, C.; Debuigne, A., In situ bidentate to tetradentate ligand exchange reaction in cobalt-mediated radical polymerization. *Eur. Polym. J.* **2015**, *62*, 312-321.
38. Sherwood, R. K.; Kent, C. L.; Patrick, B. O.; McNeil, W. S., Controlled radical polymerisation of methyl acrylate initiated by a well-defined cobalt alkyl complex. *Chem Commun (Camb)* **2010**, *46* (14), 2456-8.
39. Santoro, O.; Zhang, X.; Redshaw, C., Synthesis of Biodegradable Polymers: A Review on the Use of Schiff-Base Metal Complexes as Catalysts for the Ring Opening Polymerization (ROP) of Cyclic Esters. *Catalysts* **2020**, *10* (7).
40. Buffet, J.-C.; Okuda, J., Initiators for the stereoselective ring-opening polymerization of meso-lactide. *Polymer Chemistry* **2011**, *2* (12).
41. P. Pfeiffer, E. B., E. Lибbe und T. Tsumaki, Tricy clische or thokondensier t e Neb envalenzringe. **1932**, 84-130.
42. Fazekas, E.; Nichol, G. S.; Garden, J. A.; Shaver, M. P., Iron(III) Half Salen Catalysts for Atom Transfer Radical and Ring-Opening Polymerizations. *ACS Omega* **2018**, *3* (12), 16945-16953.
43. Cozzi, P. G., Metal-Salen Schiff base complexes in catalysis: practical aspects. *Chem Soc Rev* **2004**, *33* (7), 410-21.
44. Muldoon, M. J., Modern multiphase catalysis: new developments in the separation of homogeneous catalysts. *Dalton Trans* **2010**, (2), 337-48.
45. Donald J. Darensbourg, J. C. Y., Mechanistic Aspects of the Copolymerization Reaction of Carbon Dioxide and Epoxides, Using a Chiral Salen Chromium Chloride Catalyst. *J. Am. Chem. Soc.* **2002**, *124*, 6335-6342.
46. Pratt, C. C., P.; Errington, W.; Moore, P.; Malcom, G., N,N'-Bis(2-hydroxybenzylidene)-2,2-dimethyl-1,3-propanediamine. *Acta Cryst.* **1996**, 125-127.
47. Azam, M.; Al-Resayes, S. I.; Soliman, S. M.; Kruszynska, A. T.; Kruszynski, R., Synthesis, structural characterization, crystal structure and theoretical study of a Pd(II)-salen complex with propylene linkage. *Journal of Molecular Structure* **2017**, *1137*, 310-319.

48. Ergun, E.; Ergun, U.; Ileri, O.; Kucukmuzevir, M. F., An investigation of some Schiff base derivatives as chemosensors for Zn(II): The performance characteristics and potential applications. *Spectrochim Acta A Mol Biomol Spectrosc* **2018**, *203*, 273-286.
49. G. R. J. Artus, W. A. H., Crystal structure of 1,3-bis[N',N'-(3,5-di-tert-butyl)salicylideneimine]-2,2dimethylpropane. **1997**.
50. Kargar, H.; Kia, R.; Abbasian, S.; Tahir, M. N., 4,6-Dichloro-2-[(E)-(3-[(E)-3,5-dichloro-2-hydroxy-benzylidene]amino)-2,2-dimethylpropyl]imino]-methylphenol. *Acta Crystallogr Sect E Struct Rep Online* **2012**, *68* (Pt 1), o142.
51. Ourari, A.; Baameur, L.; Bouacida, S.; Gilles, B.; Magali, A., 2,4-Dichloro-6-([2-[(3,5-dichloro-2-hydroxy-benzylidene)amino]-ethyl]imino-methyl)phenol. *Acta Crystallogr Sect E Struct Rep Online* **2012**, *68* (Pt 6), o1700.
52. Zhang, G.; Li, Q.; Proni, G., One-pot diastereoselective assembly of helicates based on a chiral salen scaffold. *Inorganic Chemistry Communications* **2014**, *40*, 47-50.
53. Marin, P.; Tschan, M. J.; Isnard, F.; Robert, C.; Haquette, P.; Trivelli, X.; Chamoreau, L. M.; Guerineau, V.; Del Rosal, I.; Maron, L.; Venditto, V.; Thomas, C. M., Polymerization of rac-Lactide Using Achiral Iron Complexes: Access to Thermally Stable Stereocomplexes. *Angew Chem Int Ed Engl* **2019**, *58* (36), 12585-12589.
54. Marin, P.; Tschan, M. J. L.; Haquette, P.; Roisnel, T.; del Rosal, I.; Maron, L.; Thomas, C. M., Single-site cobalt and zinc catalysts for the ring-opening polymerization of lactide. *European Polymer Journal* **2019**, *120*.
55. Chen, D.; Martell, A. E., Dioxygen affinities of synthetic cobalt Schiff base complexes. *Inorganic Chemistry* **1987**, *26* (7), 1026-1030.
56. Pui, A.; Policar, C.; Mahy, J.-P., Electronic and steric effects in cobalt Schiff bases complexes: Synthesis, characterization and catalytic activity of some cobalt(II) tetra-halogen-dimethyl salen complexes. *Inorganica Chimica Acta* **2007**, *360* (6), 2139-2144.
57. Chiang, L.; Allan, L. E.; Alcantara, J.; Wang, M. C.; Storr, T.; Shaver, M. P., Tuning ligand electronics and peripheral substitution on cobalt salen complexes: structure and polymerisation activity. *Dalton Trans* **2014**, *43* (11), 4295-304.
58. Wang, F. S.; Yang, T. Y.; Hsu, C. C.; Chen, Y. J.; Li, M. H.; Hsu, Y. J.; Chuang, M. C.; Peng, C. H., The Mechanism and Thermodynamic Studies of CMRP: Different Control Mechanisms Demonstrated by Co-II(TMP), Co-II(salen*), and Co-II(acac)(2) Mediated Polymerization, and the Correlation of Reduction Potential, Equilibrium Constant, and Control Mechanism. *Macromolecular Chemistry and Physics* **2016**, *217* (3), 422-432.
59. Pradhan, H. C.; Mantri, S.; Routaray, A.; Maharana, T.; Sutar, A. K., Cobalt (II) complex catalyzed polymerization of lactide and coupling of CO₂ and styrene oxide into cyclic styrene carbonate. *Journal of Chemical Sciences* **2020**, *132* (1).
60. Lars P. C. Nielsen, C. P. S., Donna G. Blackmond,* and Eric N. Jacobsen*, Mechanistic Investigation Leads to a Synthetic Improvement in the Hydrolytic Kinetic Resolution of Terminal Epoxides. *J. AM. CHEM. SOC.* **2004**, *126*, 1360-1362.
61. Claire T. Cohen, T. C., and Geoffrey W. Coates*, Cobalt Catalysts for the Alternating Copolymerization of Propylene Oxide and Carbon Dioxide: Combining High Activity and Selectivity. *J. AM. CHEM. SOC.* **2005**, *127*, 10869-10878.
62. Tsung-Ting Tsou, M. L., and Jack Halpern*, Kinetic Determination of Transition-Metal-Alky Bond Dissociation Energies: Application to Organocobalt Compounds Related to B12 Coenzymes. *J. Am. Chem. Soc.* **1982**, *104*, 623-624.
63. Li, G.; Zhang, F. F.; Chen, H.; Yin, H. F.; Chen, H. L.; Zhang, S. Y., Determination of Co-C bond dissociation energies for organocobalt complexes related to coenzyme B12 using

- photoacoustic calorimetry. *Journal of the Chemical Society, Dalton Transactions* **2002**, (1), 105-110.
64. Zhang, J.; Wang, B.; Wang, L.; Sun, J.; Zhang, Y.; Cao, Z.; Wu, Z., Versatile cobalt complexes for initiating immortal ring-opening polymerization (ROP) of lactide (LA), mediating living radical polymerization of *t*-butyl acrylate (*t*BA) and catalyzing copolymerization of LA and *t*BA by combination of ROP and organometallic-mediated radical polymerization. *Applied Organometallic Chemistry* **2017**, 32 (2).
65. Ambrose, K.; Robertson, K. N.; Kozak, C. M., Cobalt amino-bis(phenolate) complexes for coupling and copolymerization of epoxides with carbon dioxide. *Dalton Trans* **2019**, 48 (18), 6248-6260.
66. Kinoshita, S.; Kawamura, K.; Fujita, T., Early-Transition-Metal Catalysts with Phenoxy-Imine-Type Ligands for the Oligomerization of Ethylene. *Chemistry - An Asian Journal* **2011**, 6 (2), 284-290.
67. Matsugi, T.; Fujita, T., High-performance olefin polymerization catalysts discovered on the basis of a new catalyst design concept. *Chemical Society Reviews* **2008**, 37 (6).
68. Fazekas, E.; Nichol, G. S.; Shaver, M. P.; Garden, J. A., Stable Fe(III) phenoxyimines as selective and robust CO₂/epoxide coupling catalysts. *Dalton Trans* **2018**, 47 (37), 13106-13112.
69. Thomas, C. M., Stereocontrolled ring-opening polymerization of cyclic esters: synthesis of new polyester microstructures. *Chem Soc Rev* **2010**, 39 (1), 165-73.
70. Haiyan Ma, T. P. S., and Jun Okuda, Rare-Earth Metal Complexes Supported by 1,ω-Dithiaalkanediy-Bridged Bis(phenolato) Ligands: Synthesis, Structure, and Heteroselective Ring-Opening Polymerization of *rac*-Lactide. *Inorganic Chemistry* **2008**, 47, 3328-3339.
71. I. Stein, U. R., Z. Natuforsch. B, Drei neue Koordinationsverbindungen mit komplexen Metallkationen [M(X)₆]ⁿ⁺ (M=Co: X =H₂O, NH₃ und n =3; M=Ni: X =H₂O und n = 2) und Hydrogenacetylendicarboxylat als Anion. **2011**, 66, 471-478.
72. Li, Q.; Ng, S. W., Hexakis(dimethyl sulfoxide-κO)cobalt(III) trinitrate. *Acta Crystallographica Section E Structure Reports Online* **2009**, 66 (1), m21-m21.
73. Lee Martin, S. S. T., Peter Day, Philippe Guionneau, Judith A. K. Howard, Dai E. Hibbs, Mark E. Light, Michael B. Hursthouse, Mikio Uruichi, and Kyuyo Yakush, Crystal Chemistry and Physical Properties of Superconducting and Semiconducting Charge Transfer Salts *Inorg. Chem.* **2001**, 40, 1363-1371.
74. Hon, P. K.; Pfluger, C. E., The Crystal and Molecular Structure of Tris (Acetylacetonato)-Aluminum(III) and -Cobalt(III). *Journal of Coordination Chemistry* **2006**, 3 (1), 67-76.
75. Krüger, G. J.; Reynhardt, E. C., New investigation of the structure of trisacetylacetonatocobalt(III). *Acta Crystallographica Section B Structural Crystallography and Crystal Chemistry* **1974**, 30 (3), 822-824.
76. Patra, S. G.; Illés, E.; Mizrahi, A.; Meyerstein, D., Cobalt Carbonate as an Electrocatalyst for Water Oxidation. *Chemistry – A European Journal* **2019**, 26 (3), 711-720.
77. Kastning, E. G.; Naarmann, H.; Reis, H.; Berding, C., Metal Chelates as Polymerization Initiators. *Angewandte Chemie International Edition in English* **1965**, 4 (4), 322-327.
78. Thiagarajan, R.; Kalpagam, V.; Nandi, U. S., Mixed ligand complexes in vinyl polymerization. I. [N,N'-ethylenebis (salicylideneiminato)](acetylacetonato)cobalt(III) as an initiator. *Journal of Polymer Science: Polymer Chemistry Edition* **1982**, 20 (3), 675-681.
79. P. Grutsh, C. K., Mechanistic Photochemistry of Transition Metal PDiketonate Complexes. 3. Detection of a New Reaction Pathway in the Ultraviolet Photochemistry of

trans-Tris(1,1,1-trifluoro-2,4-pentanedionato)cobalt(III). *Inorganica Chimica Acta*, **1982**, *59*, 249-253.

80. Rayna Bryaskova, C. D., Antoine Debuigne, and Robert Jerome, Cobalt-Mediated Radical Polymerization (CMRP) of Vinyl Acetate Initiated by Redox Systems: Toward the Scale-Up of CMRP. *Macromolecules* **2006**, *39*, 8263-8268.
81. Hurtgen, M.; Debuigne, A.; Jérôme, C.; Detrembleur, C., Solving the Problem of Bis(acetylacetonato)cobalt(II)-Mediated Radical Polymerization (CMRP) of Acrylic Esters. *Macromolecules* **2010**, *43* (2), 886-894.
82. Bunck, D. N.; Sorenson, G. P.; Mahanthappa, M. K., Cobalt-mediated radical polymerization routes to poly(vinyl ester) block copolymers. *Journal of Polymer Science Part A: Polymer Chemistry* **2011**, *49* (1), 242-249.
83. Nzé, R.-P.; Colombani, O.; Nicol, E., Synthesis of poly(vinyl laurate)-b-poly(vinyl stearate) diblock copolymers by cobalt-mediated radical polymerization in solution. *Journal of Polymer Science Part A: Polymer Chemistry* **2012**, *50* (19), 4046-4054.
84. Falireas, P. G.; Ladmiral, V.; Debuigne, A.; Detrembleur, C.; Poli, R.; Ameduri, B., Straightforward Synthesis of Well-Defined Poly(vinylidene fluoride) and Its Block Copolymers by Cobalt-Mediated Radical Polymerization. *Macromolecules* **2019**, *52* (3), 1266-1276.
85. Michelas, M.; Fliedel, C.; Poli, R., Reversible Homolysis of Metal-Carbon Bonds. In *Comprehensive Organometallic Chemistry IV*, Elsevier: 2021; Vol. 1, pp 31-85.
86. Poli, R., A journey into metal-carbon bond homolysis. *C. R. Chimie* **2021**, *24*, 147-175.
87. Coombes, R. G.; Johnson, M. D., σ -Bonded organotransition-metal ions. Part II. Kinetics and mechanism of the aerobic acidolysis of penta-aquo(pyridiomethyl)chromium(III). *J. Chem. Soc. (A)* **1966**, 177-182.
88. Schmidt, A. R.; Swaddle, T. W., Homolysis versus heterolysis in the decomposition of chromium(III) complexes in acidic solution. *J. Chem. Soc. (A)* **1970**, 1927-1932.
89. Nohr, R. S.; Espenson, J. H., Acidolysis and oxidative cleavage reactions of benzylchromium cations. *J. Am. Chem. Soc.* **1975**, *97*, 3392-3396.
90. Kirker, G. W.; Bakac, A.; Espenson, J. H., Homolysis and Acidolysis Reactions of (Alpha-Hydroxyalkyl)-Chromium(III) and (Alpha-Alkoxyalkyl)Chromium(III) Complexes - Kinetics, Steric Effects, and Bond-Energies. *Journal of the American Chemical Society* **1982**, *104* (5), 1249-1255.
91. Morales-Cerrada, R.; Fliedel, C.; Daran, J.-C.; Gayet, F.; Ladmiral, V.; Améduri, B.; Poli, R., Fluoroalkyl radical generation by homolytic bond dissociation in pentacarbonylmanganese derivatives. *Chem. Eur. J.* **2019**, *25*, 296-308.
92. Wing-Yiu Yu, W. N. S., Zhongyuan Zhou, and Albert S.-C. Chan, Palladium-Catalyzed Decarboxylative Arylation of C-H Bonds by Aryl Acylperoxides. *Organic Letters* **2009**, *11*, 3174-3177.
93. Herk, L.; Feld, M.; Szwarc, M., Studies of "Cage" Reactions. *Journal of the American Chemical Society* **1960**, *83* (14), 2998-3005.
94. Martin, J. C.; Drew, E. H., Molecule-induced Homolytic Decompositions. I. Oxygen-18 Labeling Studies on the Reaction Yielding Cyclohexyl Acetate from Cyclohexene and Acetyl Peroxide. *Journal of the American Chemical Society* **1960**, *83* (5), 1232-1237.
95. Slagle, J.; Shine, H., Notes. Improved Yields in the Preparation of Diacetyl Peroxide. *The Journal of Organic Chemistry* **1958**, *24* (1), 107-107.
96. Pui, A.; Dobrota, C.; Mahy, J.-P., Electrochemical and spectroscopic characterization and catalytic activity of Co(II) complexes of tetra-chloro-R-Salen ([tClSalen= bis(3,5-dichloro- α -R salicylidene)ethylenediamine]) and tetra-chloro-R-Salophen ([tClSalophen= bis

(3,5-di-chloro- α -R salicylidene)-1,2-phenylenediamine]), R=H, CH₃, CH₂-CH₃. *Journal of Coordination Chemistry* **2007**, *60* (5), 581-595.

97. Saunders, L. N.; Pratt, M. E.; Hann, S. E.; Dawe, L. N.; Decken, A.; Kerton, F. M.; Kozak, C. M., Structural variations in the coordination chemistry of amine-bis(phenolate) cobalt(II/III) complexes. *Polyhedron* **2012**, *46* (1), 53-65.

98. Chmura, A. J.; Cousins, D. M.; Davidson, M. G.; Jones, M. D.; Lunn, M. D.; Mahon, M. F., Robust chiral zirconium alkoxide initiators for the room-temperature stereoselective ring-opening polymerisation of rac-lactide. *Dalton Trans* **2008**, (11), 1437-43.

Chapter III. Polymerization processes

Chapter 3 collects the results of the polymerizations carried out under the OMRP or ROP approaches with both the already known and the new complexes. A few tests of the polymerization switch from OMRP to ROP and from ROP to OMRP, without chemical modification between the first and second block synthesis, are also presented.

Table of contents

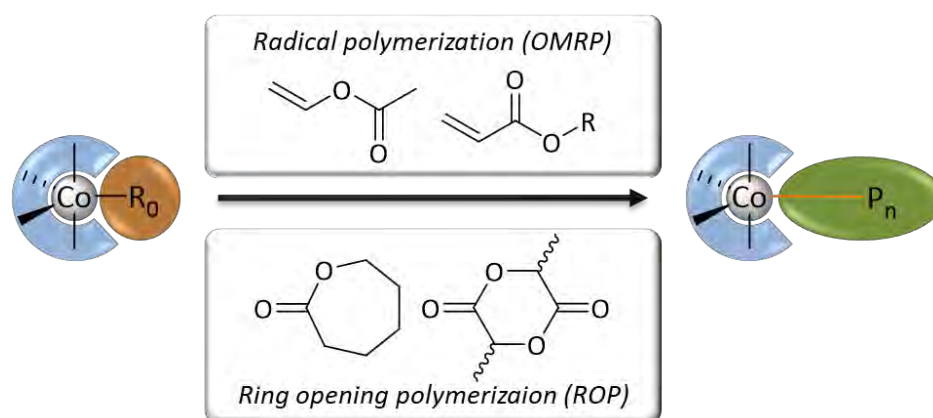
Chapter III. Polymerization processes	125
I. Introduction and strategy	129
II. Radical polymerization (OMRP).....	131
1. (N₂,O₂)-Cobalt(III) complexes for the polymerization of MAMs	131
a. Complex [Co ^{III} (L ^{1.1})(OAc)]	131
i. Methyl methacrylate polymerization (previous work)	131
ii. Methyl acrylate polymerization	133
iii. Chain end investigation	135
b. Complex [Co ^{III} (L ^{1.10})(OAc)].....	137
c. Complex [Co ^{III} (L ^{1.4})(OBz)]	138
2. Conclusion on the use of (N₂,O₂)-based complexes as initiating systems	140
3. (O₂,O₂)-Cobalt(III) carboxylate complexes	141
a. Complex [Co ^{III} (acac) ₂ (O ₂ Ph)]	141
i. Radical polymerization of MAMs	141
ii. Radical polymerization of LAMs.....	143
iii. Chain end investigation	146
iv. Efficiency factor improvement.....	151
v. Photoinitiation test	153
b. Polymerizations initiated by the other [Co(acac) ₂ -O(O)CAr] complexes	154
c. Carboxylate alkyl – [Co(acac) ₂ -O(O)C-Alkyl]	157
i. Bis(acetylacetonate) cobalt acetate, [Co(acac) ₂ (OAc)]	157
ii. Lauroyl derivative, [Co(acac) ₂ (O ₂ C(CH ₂) ₁₀ CH ₃)].....	158
4. Conclusion	160
III. Ring opening polymerization (ROP)	161
1. Introduction	161
2. (N₂,O₂)-Cobalt complex (3.1).....	162
a. Polymerization without alcohol transfer agent.....	162
b. Polymerization initiated by complex 3.1 in the presence of benzyl alcohol as chain transfer agent.....	165
c. Polymerization initiated by complex (3.3).....	168

3.	(O₂,O₂)-Cobalt carboxylate complexes	169
a.	Polymerizations initiated by [Co(acac) ₂ (O ₂ CPh)].....	169
b.	Polymerizations initiated by [Co(acac) ₂ OAc].....	170
4.	Conclusion	171
IV.	Polymerization switch	173
1.	Sequential polymerization processes (Block copolymers)	174
a.	Switch from OMRP to ROP	174
b.	Switch from ROP to OMRP	178
2.	One pot procedure (Mixture of PVAc & PCL)	180
3.	Selective degradation of copolymer (OMRP-<i>b</i>-ROP)	183
V.	Conclusion and outlook.....	185
VI.	Experimental section	186
1.	Materials	186
2.	Characterizations	186
3.	Methods	187
	General conclusion and perspectives.....	190
	References.....	193

I. Introduction and strategy

This chapter highlights polymerization processes carried out in the presence of cobalt complexes that follow either a radical pathway or a coordination/insertion mechanism (ROP). The concept and mechanism of both polymerization techniques have already been described in the bibliographic chapter. The aim, here, is to show the diverse reactivity of the various complexes that we have synthesized and described in *Chapter II* and to discuss the efficiency of these complexes for the initiation and moderation of polymerizations that proceed by both the radical and the coordination/insertion mechanisms.

As a reminder, the complexes highlighted in *Chapter II* were designed to fulfil the various objectives of this thesis work, namely to unite in the same metal complex the ability to directly initiate and control both OMRP and ROP processes, as well as to be able to switch from one mechanism to the other one (*Scheme I-1*).

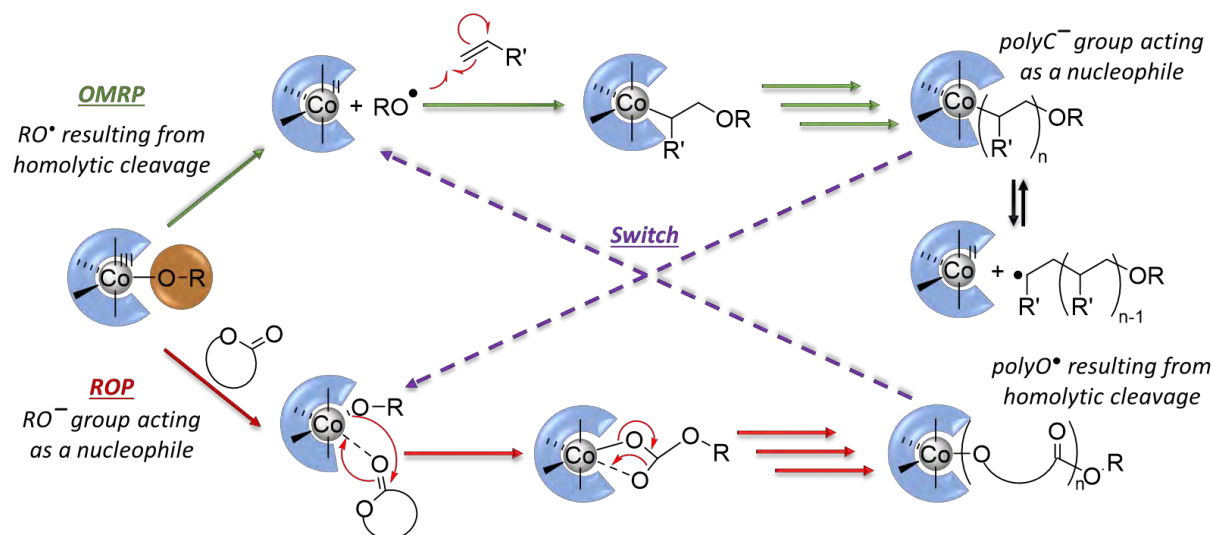


Scheme I-1: Use of cobalt alkoxide for direct initiation and controlled polymerization of vinyl monomers (OMRP) and cyclic esters (ROP).

The present chapter will be divided into three major parts. The first one deals with the direct initiation of the controlled radical polymerization of vinyl monomers. Cobalt complexes designed for more and less activated monomers (MAMs and LAMs) will be highlighted in separate subsections. In this part, we will debate about the initiation efficiency, the control and also the potential generation of block copolymers where each block is produced by a radical pathway. Then, a second part will be dedicated to the ring opening polymerization of cyclic ester (mostly L-LA and ϵ -CL) by the coordination/insertion mechanism. The aim of this study is to learn whether the polarizability of the cobalt-alkoxide bond is sufficient to induce a nucleophilic attack.

In the last part of this chapter, attempts to achieve a mechanism switch in a one-pot polymerization process, aimed at developing original polymer architectures such as block copolymer, will be described. Namely, these cobalt complexes will be used as initiators and moderators for the polymerization of a first monomer to provide the first block by either OMRP or ROP, then a reactivity switch of the cobalt chain end in the macroinitiator will be probed, aiming at the formation of the second block and achieving original polymers of type

OMRP-*b*-ROP or ROP-*b*-OMRP. In comparison to previously reported block copolymers that were obtained by a mechanistic switch,¹⁻⁵ the processes described here should permit to achieve this target without any chemical modification between the two polymerizations and without the need of additional co-agents.



Scheme 1-2: Strategy targeting for the unique metal complex perform both OMRP (green), ROP (red) and switch (purple) from one to the other.

The species that enable the switch in each direction (*i.e.* OMRP to ROP and ROP to OMRP) are different. In fact, the chain end produced by OMRP (green in *Scheme 1-2*) is a cobalt-alkyl species. In order to switch to a ROP process, a vacant site is required for the carbonyl approach and the alkyl chain must be sufficiently nucleophilic to undergo the migratory insertion process. In the opposite direction, the chain end produced by ROP (red in *Scheme 1-2*) is a cobalt-alkoxide species, which must be able to homolytically cleave for the switch (purple). As an outlook, we will debate about biodegradability, which represents an important environmental and societal issue, and about possible new directions for this project.

II. Radical polymerization (OMRP)

This section will feature radical polymerizations carried out in the presence of the complexes synthesized and characterized in *Chapter I*. The section is organized on the basis of the ligand architecture. A first part deals with the complexes supported by a (N₂,O₂) ligand and the second one reports processes carried out with complexes supported by a fully O-based coordination sphere. The aim is to probe the ability of these compounds to generate a primary radical and start the polymerization and to see whether we they can successfully moderate the polymerization of a variety of monomers.

1. (N₂,O₂)-Cobalt(III) complexes for the polymerization of MAMs

This part will be subdivided into three part, corresponding to each (N₂,O₂)-cobalt complex described in the previous chapter. The first two sections are dedicated to the acetate complexes (**3.1** and **3.2**) with, respectively, the 1,2-diaminocyclohexane Schiff base ligand (**H₂L^{1.1}**) and the aminopyridinebis(phenolate) tripodal ligand (**H₂L^{1.10}**). The last part deals with the Schiff base (**H₂L^{1.4}**) benzoate complex (**3.3**).

a. Complex [Co^{III}(L^{1.1})(OAc)]

The radical polymerization tests with complex **3.1** were initiated by Jirong Wang, PhD student in our team (2018/2019) and by Sophie McGee-Renedo, master 2 internship, 2020.

i. Methyl methacrylate polymerization (previous work)

The polymerization of MMA was carried out at 60°C in bulk. *Figure II-1-a* highlights the monomer conversion as a function of time. As is quite evident, a rapid polymerization occurred, reaching over 70% monomer conversion in about 6 h, proving that this cobalt complex is able to produce primary radicals that initiate the MMA polymerization. The radical character of the reaction was shown by a parallel TEMPO quenching experiment: the conversion stopped after TEMPO (a radical trap) was added 2 h after the start of the reaction.

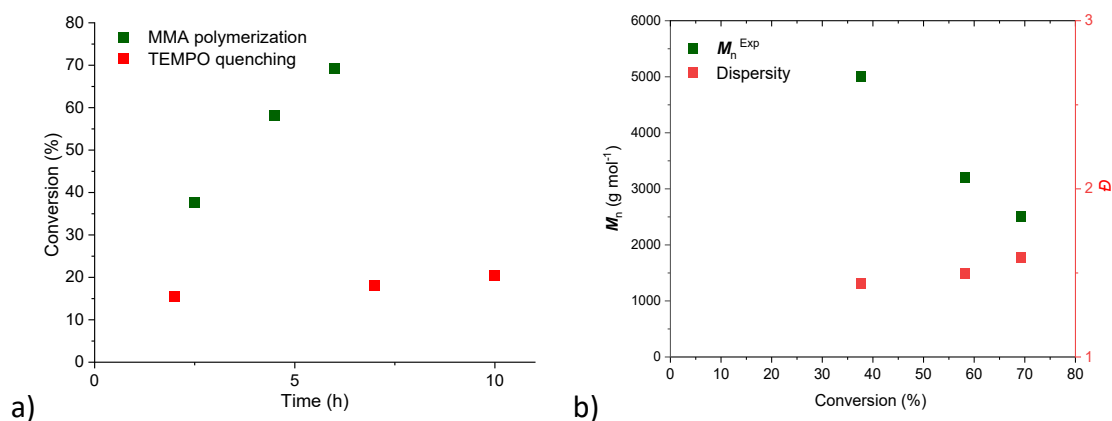


Figure II-1: MMA polymerization: a) Progression of the conversion as function of time and TEMPO quenching; b) Evolution of the molar masses and dispersity vs. conversion. Conditions: $[Co]/[M]=1/200$, in bulk at 60°C.

However, as shown in Figure II-1-b, the M_n decreases when the conversion increases and the dispersity increases, perhaps because of catalytic chain transfer (CCT) as an interfering process.⁶ The polymerization was also tested at lower temperature (40°C), but the same phenomena were observed as shown in Figure S1. Indeed, a MALDI-TOF-MS analysis of the polymer confirmed that the dominant family of macromolecules have the expected chain ends for catalytic chain transfer (Figure II-2).

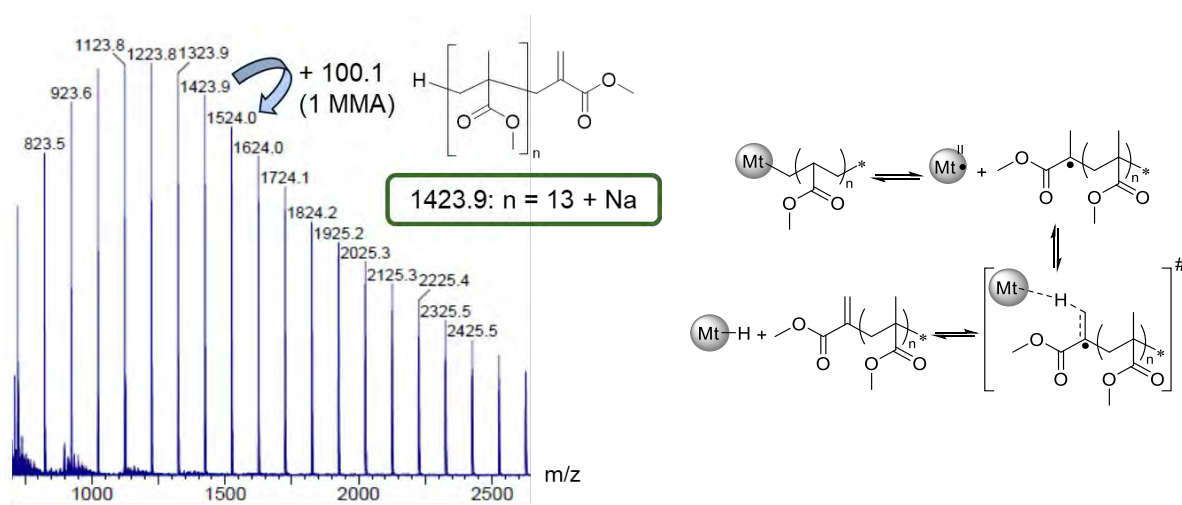
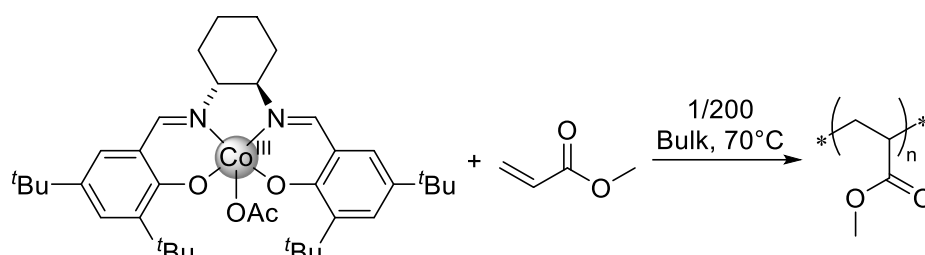


Figure II-2: MALDI-TOF mass spectrum recorded for the PMMA obtained by the **3.1**-initiated polymerization, using a dithranol/NaI matrix (left), CTT process (right).

These results highlight the ability of complex **3.1** to generate primary radicals and start the polymerization. However, in the case of MMA, the tertiary radical has a strong tendency to undergo the CCT reaction. It is useful to underline that, although CCT is an unwanted side reaction for our objectives, it is useful for specific applications.⁷

ii. Methyl acrylate polymerization

Although MMA shows a strong interference of the CCT reaction, an investigation was also carried out using MA, which gives a secondary radical, for which the CCT process is well-known to be less favoured. Interestingly, no bulk polymerization occurred at the same temperatures where MMA is polymerized rapidly, e.g. 40°C. On the other hand, a slow polymerization process occurred at 70°C, see *Figure II-3-a*.



Scheme II-1: Methyl acrylate radical polymerization mediated with 3.1.

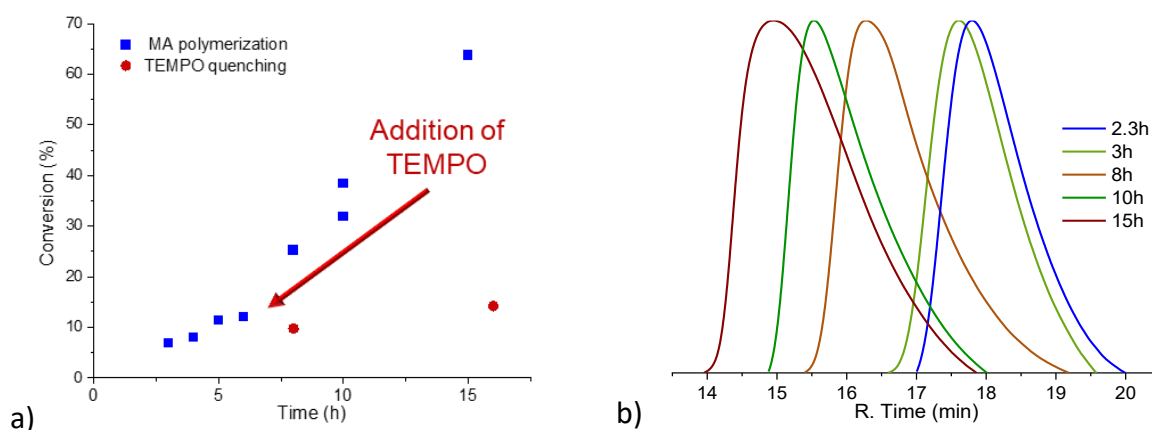


Figure II-3: a) Conversion vs. time, b) GPC traces.

The MA polymerization started rather slowly but then increased in rate after ca. 6 h and achieved 60% of conversion in 15 hours. The TEMPO quenching experiment highlighted once again the radical nature of the reaction, as for the polymerization of MMA. In this case, the molar mass distribution shown by the GPC analysis (*Figure II-3-b*) shifts toward higher M_n at higher conversions, suggesting a moderating role of the metal complex in OMRP.

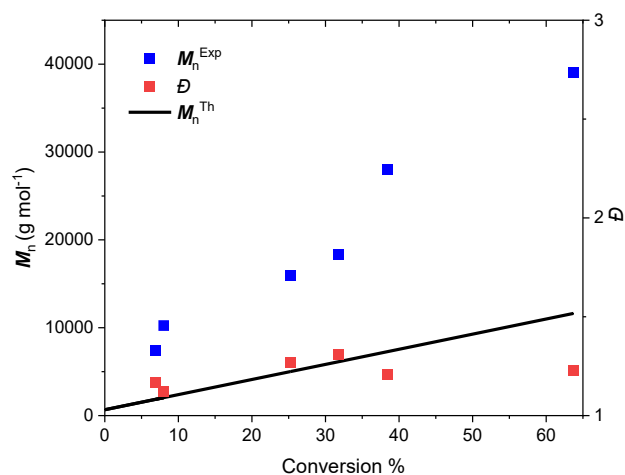


Figure II-4: Evolution of the M_n and \bar{D} Vs. Conv.

The plot of M_n as a function of conversion (Figure II-4) shows an approximately linear increase, while the polymer dispersity remains relatively narrow (≤ 1.31). However, the experimental molar masses are higher than the theoretical values shown by the straight black line. This deviation reflects a low efficiency factor (*ca.* 30%) for the initiation by complex **3.2**. Thus, only *ca.* 30% of the complex present in the medium undergoes the homolytic cleavage required to start the macromolecular chain growth.

These experimental observations confirm the prediction of the DFT calculations described in *chapter II, Figure II-9*. As a reminder, the computed Co^{III}-X homolytic bond strengths (ΔG) are 20.5 kcal mol⁻¹ (X = carbomethoxyethyl, PMA model) and 15.1 kcal mol⁻¹ (X = carbomethoxyisopropyl, PMMA model). Both values are lower than the computed strength of the Co^{III}-OAc bond ($\Delta G^{\text{Co-OAc}} = 25.1$ kcal mol⁻¹). This confirms the stronger aptitude of the metal complex to trap the PMA radicals and control the chain growth, whereas the bond with the PMMA radical is too weak, opening the way to a greater impact of CCT. On the other hand, the greater strength of the Co^{III}-OAc bond results in slow initiation and thus in a low efficiency factor. The initiation rate must obviously be the same, at the same temperature, for the two polymerizations, but the MA polymerization does not significantly occur at a lower temperature because, after converting complex **3.1** to $[(L^{1.1})\text{Co}^{\text{III}}\text{CH}(\text{COOMe})\text{CH}_2\text{OAc}]$ by the first monomer insertion, the homolytic bond cleavage of this bond requires greater thermal activation to observe a significant polymerization rate.

The polymerization of styrene was also tested. While a polymerization did take place, the control of this reaction appears quite bad, with polymer dispersities above 1.5 (Figure S2) and M_n decreased with conversion, suggesting a possible intervention of CCT. Finally, a polymerization test with vinyl acetate (VAc) did not lead to any polymer (Table II-1), even at high temperatures, as expected because the Co^{III}-CH(OAc)CH₂X product of the first monomer insertion (X = primary radical generated from complex **3.2**) is too strong ($\Delta G^{\text{VAc}} = 26.2$ kcal mol⁻¹ > $\Delta G^{\text{Co-OAc}} = 25.1$ kcal mol⁻¹).

Table II-1: Summaries of the MAMs polymerization reaction mediated with 3.1.^a

Monomer	T. (°C)	Time (h)	Conv. (%) ^b	M_n^{Exp} (g/mol) ^c	M_n^{Th} (g mol ⁻¹) ^d	\bar{D}^c
MMA	40	24	22	4 535	4650	1.41
	60	6	70	2 500	14 000	1.59
	70	4	74	1 700	13 200	1.15
MA	60	20	0	No polymerization occurs		
	70	15	63	39 000	12 000	1.23
	80	19	77	29 000	13 000	2.05
St	60	17	14	7 291	3 400	1.61
	70	63	28	6 827	14 000	1.50
VAc	70	50	0	No polymerization occurs		
	70	40	0	No polymerization occurs		

^aConditions: $[M]/[Co] = 200/1$ in bulk, under argon. ^bConversion calculated by gravimetry, ^cDetermined from the GPC analysis with THF as eluent by using polystyrene standards. ^dCalculated according to the conversion and molar masses of the monomers.

iii. Chain end investigation

Mechanistic considerations bring us to the question of the primary radical structure. To confirm that AcO^{\bullet} is the primary radical initiating the polymerization, its presence at the chain-end position must be demonstrated. To this end, the recovered polymer sample was quenched with tributyl tin (TBT), which is able to replace the metal complex at the chain-end position with a hydrogen atom (in red in Figure II-5).

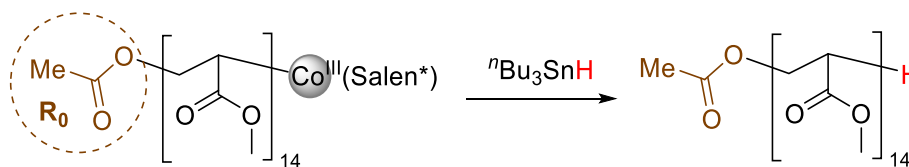


Figure II-5: tributyl tin (TBT) quenching reaction.

The MALDI-ToF mass spectrum of the resulting sample highlights two isotopic envelopes with 86.1 g mol^{-1} between subsequent peaks, which confirms the PMA production (Figure II-6). The most abundant envelope (highlighted in blue in the expansion of the spectrum) has m/z values consistent with the presence of a hydrogen atom at each terminal position and sodium as cationizing agent from the matrix. There is a good match between the experimental and simulated isotopic distributions, showing that this envelope corresponds to a single population. The minor envelope (highlighted in orange) is in fact the overlap of two populations, one of which has again H atoms at both chain end and potassium as cationizing agent, whereas the second one has an H atom at one chain end and a methyl group at the other one. For all populations, the presence of one H chain-end is expected to result from the TBT quenching process. The presence of a second H chain end suggests that the MA polymerization, like that of MMA, is also affected by a significant contribution of CCT. The Me group at the second chain-end for one minor population suggests rapid decarboxylation of the acetate radical before addition to the first monomer to start the chain propagation. This result

permits us to confirm that the polymerization is initiated by the $\text{Co}^{\text{III}}\text{-OAc}$ bond homolytic cleavage.

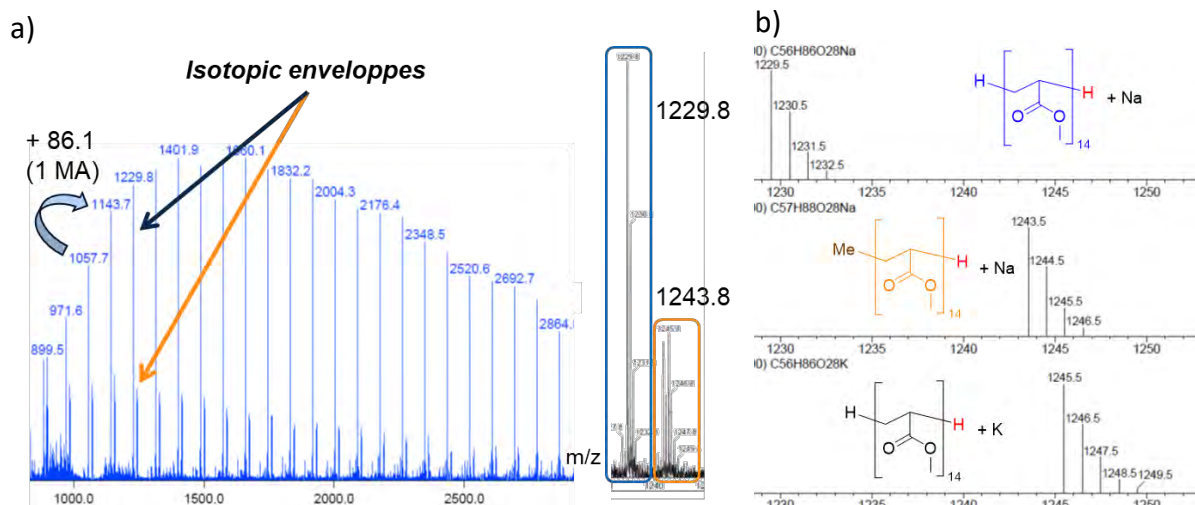


Figure II-6: Chain-end investigation for the PMA obtained by initiation with complex **3.1**: a) Maldi-ToF spectrum (left) and b) simulation of the different populations (right).

A chain extension experiment was also carried out to confirm the presence of the metal complex at one chain end. To that end, a PMA macroinitiator was first prepared as described above and then reactivated at 70 °C in the presence of butyl acrylate (BA) with a molar BA/macroinitiator ratio of 200/1 to yield the PMA-*b*-PBA block copolymer (Figure II-7).

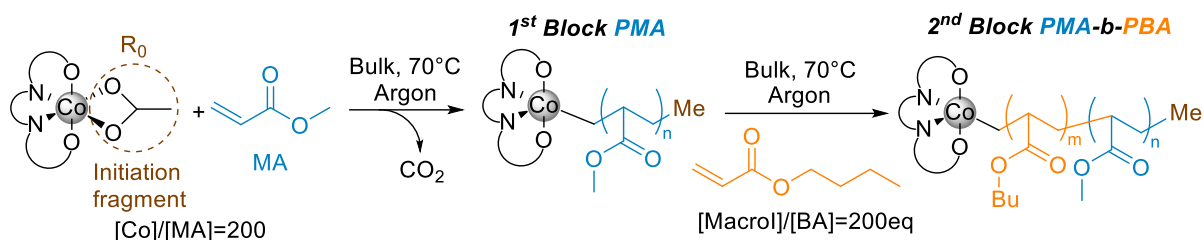


Figure II-7: Block copolymer synthesis (Co-PBA-*b*-PMA-Me).

The polymer synthesis was followed by GPC, as shown in Figure II-8. The PMA- $\text{Co}^{\text{III}}(\text{L}^{1.1})$ macroinitiator shows a monomodal distribution (blue signal) with $M_n = 5\,100\text{ g mol}^{-1}$. After chain extension, the molar mass distribution shifts to $29\,200\text{ g mol}^{-1}$ (orange signal) and remains monomodal, although with an evident tailing at low molar masses, while the signal of the starting PMA macroinitiator disappears. This result confirms the occurrence of chain extension, rather than homopolymerization of BA.

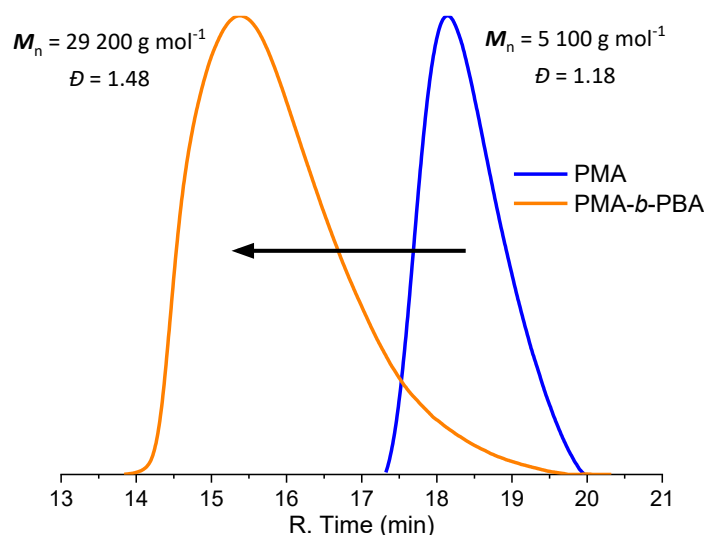


Figure II-8: GPC investigation of the PMA- $\text{Co}^{\text{III}}(\text{L}^{1.1})$ chain extension with BA.

To conclude about this system, it is possible to use the acetate complex **3.2** as a unimolecular initiator for the polymerization of MAMs (MMA, MA and St), but the polymerization of LAMs is inhibited (as expected). Although polymerizations occur with MMA and St, they are not controlled and the polymer analyses suggest the contribution of CCT. The polymerization of MA, on the other hand, follows an OMRP mechanism of controlled chain growth, even though the efficiency factor of the initiation step is low.

b. Complex $[\text{Co}^{\text{III}}(\text{L}^{1.10})(\text{OAc})]$

Based on previous work in our team, as highlighted in previous chapters, we have extended the library of tripodal cobalt complexes to install acetate in place of acetylacetonate (complex **3.2**), hoping to improve the initiation system.⁸

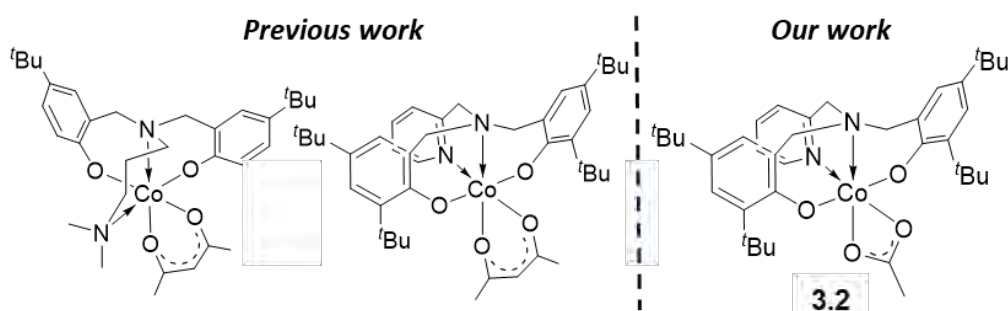


Figure II-9: Tripodal cobalt (III) acac or acetate (R_0 fragment) structures.⁸

Unfortunately, after several polymerization tests at various temperatures, no polymerization was ever observed in the presence of either MA or MMA. Consequently, this system was abandoned to concentrate on other complexes, for which preliminary tests were much more promising.

c. Complex $[\text{Co}^{\text{III}}(\text{L}^{1.4})(\text{OBz})]$

As shown in section a, it is possible to initiate a radical polymerization using the cobalt acetate complex **3.1**, and the MA polymerization is relatively well-controlled by the moderating action of the associated $[\text{Co}^{\text{II}}(\text{L}^{1.4})]$ complex released in the medium. It was thus of interest to verify the potential of other Schiff-base cobalt systems as unimolecular initiators/moderating agents. In the present section, the results obtained by using the new cobalt(III) benzoate complex **3.3** are reported and discussed.

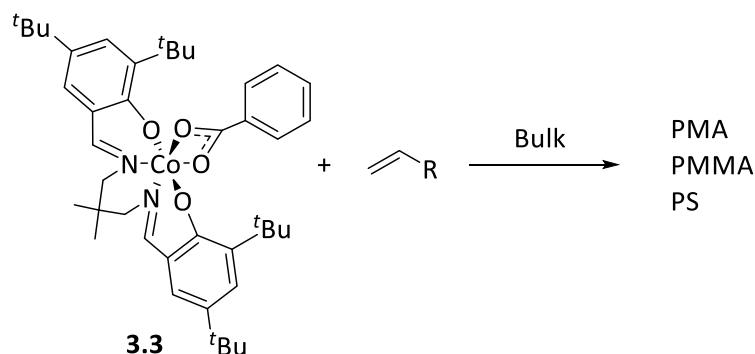


Figure II-10: Radical polymerization test initiated and mediated with complex **3.3**.

A polymerization test with MA was initially carried out at the same temperature (70°C) as with complex **3.1** (Table II-2, entry 1). However, no significant polymerization was observed. The same outcome was given after raising the temperature to 80 °C (entry 2). A slow polymerization, on the other hand, occurred, at 90 °C, yielding a 19% conversion in 20 h. The polymerization of MMA, which yields a chain radical that forms a weaker bond with the metal, is also slow at 90°C (Table II-2, entry 4), with only 5% conversion after 16 h. In addition, the control appears bad, because much higher molar masses (260 and 76 kg mol⁻¹) than the theoretical values and broad dispersities (1.57 and 1.84) were obtained for MA and MMA, respectively (Figure II-11).

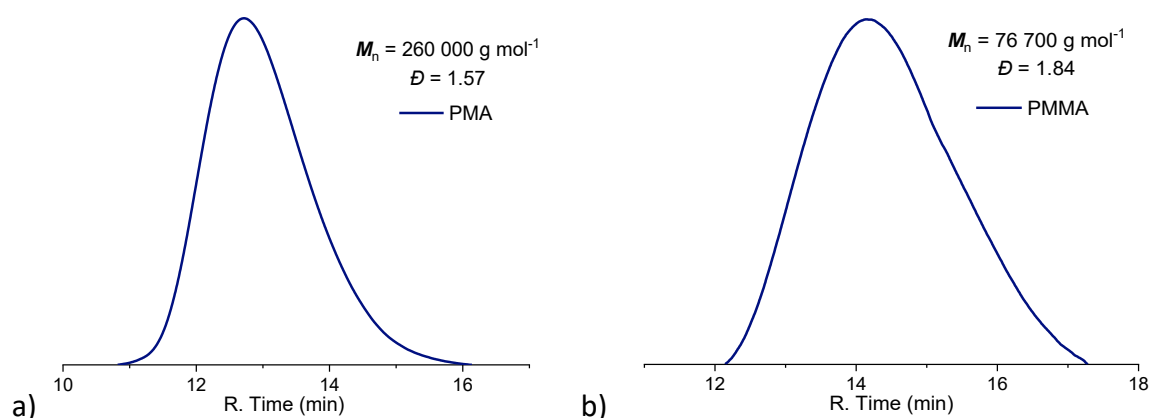


Figure II-11: GPC analyses of the polymers obtained with initiation by complex **3.3** at 90°C: a) PMA (20 h), b) PMMA (16 h).

These results suggest two things. First, the initiation step is very slow, namely the Co^{III}-benzoate bond in **3.3** is stronger than the Co^{III}-acetate bond in **3.1**. Secondly, the generated Co^{II} complex from **3.3**, containing the 2,2-dimethyl-1,3-propanediamine-tethered Schiff-base, is less able to trap the growing radical chain to exert the desired control, relative to the Co^{II} complex with the *trans*-1,2-cyclohexanediamine-tethered Schiff-base generated from **3.1**, although the temperature difference between the two polymerizations (70°C with **3.1**, 90°C with **3.3**) may also rationalize the decreased moderating ability in the present system.

Table II-2: Summaries of MAMs radical polymerization test with **3.3**.^a

Entry	Monomer	Ratio [Co]/[M]	Temp. (°C)	Time (h)	Conv (%) ^b	M_n^{Exp} (g mol ⁻¹) ^c	M_n^{Th} (g mol ⁻¹) ^d	\mathcal{D}^c
1	MA	1/400	70	65	-	-	-	-
2	MA	1/300	80	20	-	-	-	-
3	MA	1/400	90	20	19	260 000	3 900	1.57
4	MMA	1/300	90	16	5	76 700	1 700	1.84
4	St	1/300	90	16	47	396 600	10 100	1.59
5	St	1/300	80	2	3	300 000	900	1.76
6	St	1/300	60	3	8	351 0000	2 400	1.54
7	St	1/300	40	0	-	-	-	-
8	VAc	1/400	90	24	-	-	-	-

^aConditions: bulk polymerization under argon. ^bConversion calculated by gravimetry, ^cDetermined by GPC analysis with THF as eluent, by using polystyrene standards. ^dCalculated according to the conversion and molar masses of the monomers.

For styrene, the polymerization is a bit faster, but it also seems uncontrolled because, once again, much higher molar masses and broad dispersities were obtained under different conditions (Table II-2, entries 5-7). Moreover, the kinetic polymerization at 80°C revealed that the molar masses decrease with time and the dispersity increases, suggesting a possible contribution of CCT (Figure II-12-b). Another test carried out at 40°C did not produce any polymer (Table II-2, entry 6).

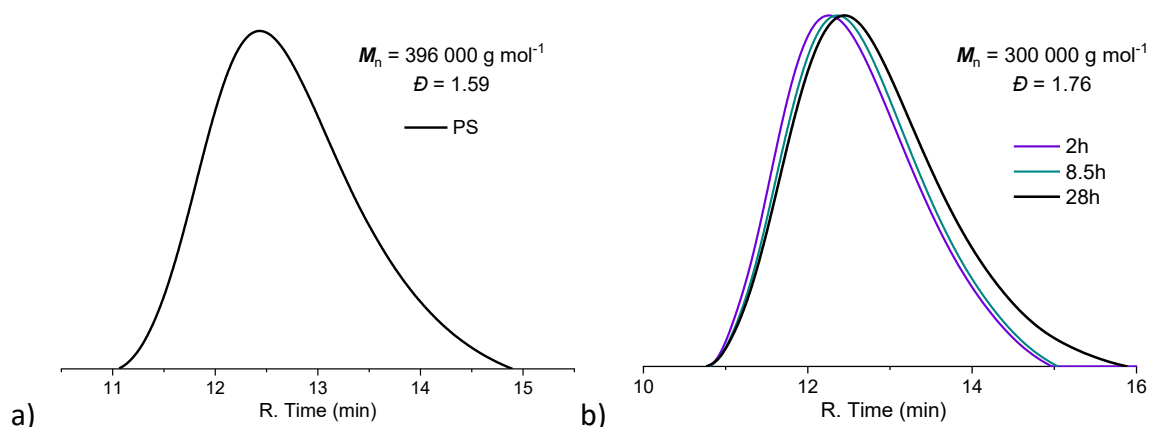


Figure II-12: Chromatograms of St polymerization obtained a) at 90°C and b) 80°C.

Finally, no polymerization was observed for VAc, as might have been anticipated on the basis of the literature and of the previous results with **3.1**. All these results suggest that complex **3.3** is indeed able to generate a primary radical by homolytic cleavage. However, there is no control for the investigated monomers under the employed conditions, which suggest that the trapping efficiency of the generated Co^{II} species is insufficient under these conditions.

The polymerization control should in principle be improved when a certain molar fraction of the moderating system (*i.e.* the $[\text{Co}^{\text{II}}(\text{L}^{1.4})]$ complex in the presence case) is already present in the reaction mixture at the beginning of the polymerization. To check this, a new polymerization of styrene was run at 80°C in the presence of 0.25 equivalent of the corresponding cobalt(II) complex. However, *Figure II-13* reveals that high molar masses were again achieved very quickly, and M_n decreased while the dispersity increased at higher conversions.

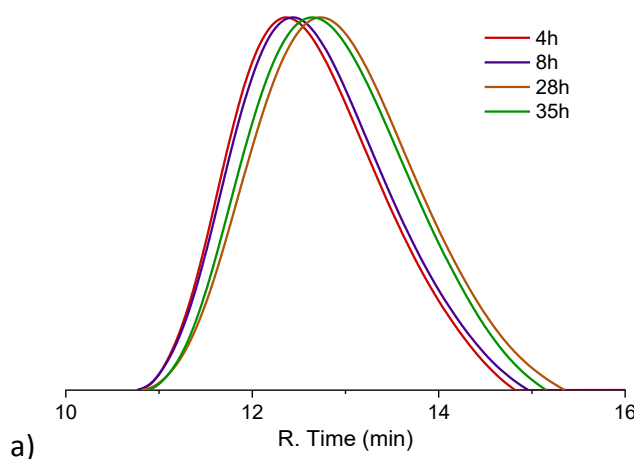


Figure II-13: a) Chromatograms of the St bulk polymerization (80°C) obtained with $[\text{Co}^{\text{III}}]/[\text{Co}^{\text{II}}]/[\text{St}]=1/0.25/300$.

2. Conclusion on the use of (N_2, O_2)-based complexes as initiating systems

The cobalt(III) acetate complex **3.1** could be used to control the MA polymerization and also for a PMA-*b*-PBA block copolymer synthesis. Provided it is also efficient in ROP, this compound could be promising for the polymerization switch. Complex **3.2** based on the tripodal aminopyridinebis(phenolato) ligand was abandoned because no polymerization occurs under the tested conditions. Concerning **3.3**, the investigations were limited because the primary radical generation by homolytic Co^{III} -benzoate bond cleavage proved more difficult, leading to poor results.

3. (O₂,O₂)-Cobalt(III) carboxylate complexes

The cobalt(III) complexes with a fully O-based coordination sphere that have been used in this thesis for radical homopolymerization are based essentially on the new synthesis route described in chapter II from peroxides and bis(acetylacetonato)cobalt(II). These compounds are the most convenient initiation/moderation systems in terms of facile accessibility, number of synthesis step and price. The polymerization tests with these aryl and alkyl carboxylate complexes are reported in this section.

a. Complex [Co^{III}(acac)₂(O₂Ph)]

First of all, a study based on complex [Co^{III}(acac)₂(O₂Ph)] (**3.6**) (*chapter II, Scheme III-1*) was carried out, because this complex is easily synthesized and available in gram scale, allowing a large number of reaction and condition tests. To begin with, it is useful to see whether this species is capable to generate radicals in polymerization tests with MAMs. The [Co^{II}(acac)₂] complex, which is the putative moderator generated by the homolytic cleavage of the Co^{III}-benzoate bond in **3.6**, is an efficient moderator for the controlled polymerization of LAMs.⁹⁻¹² This means that the [(acac)₂Co^{III}-polymer] bonds are weaker than the corresponding [(L)Co^{III}-polymer] bonds (L = N₂O₂-based ligand such as a Schiff base). Therefore, a rapid polymerization of MAMs (*e.g.* St or MA), even if uncontrolled, would demonstrate the ability of **3.6** to rapidly generate primary radicals.

i. Radical polymerization of MAMs

As shown in Table II-3, the bulk polymerization of MA, BA and styrene is rapid at 30 °C. The conversions were 55% in 4 h for MA (entry 1), 90% in just 2 h for BA (entry 3) and 42% in 24 h for styrene (entry 5). The high rate of the BA polymerization is striking, considering that this test was conducted in the presence of a 25% molar fraction of [Co^{II}(acac)₂], which should slow down the process by displacing the activation/deactivation equilibrium. All these polymerizations occurred without any control, as shown by the high molar masses relative to the theoretical values and dispersities around 2, see the GPC traces in *Figure II-14*. The BA polymerization gave rise to a bimodal distribution.

Table II-3: Summary of the polymerization of MAMs initiated by 3.6.^a

Entry	M	[Co]/[M]	Temp. (°C)	Time (h)	Conv (%) ^b	M_n^{Exp} (g mol ⁻¹) ^c	M_n^{Th} (g mol ⁻¹) ^e	\mathcal{D}^c
1	MA	1/200	30	4	55	375 800	9 800	1.94
2	MA	1/20	5	6	11	1 100 000	560	1.41
3 ^d	BA	1/0.25/126	30	2	90	Bimodale (780 000, 13 500)	15 000	1.33 2.08
4	St	1/200	30	24	42	220 000	9 100	2.37
5	NVP	1/200	30	4	76	300 000	17 200	11.1

^aConditions: bulk polymerization under argon. ^bConversion calculated by gravimetry, ^cDetermined by GPC analysis with THF as eluent by using polystyrene standards. ^d[Co^{III}]/[Co^{II}]/[BA]=1/0.25/126. ^eCalculated according to the monomer molar masses.

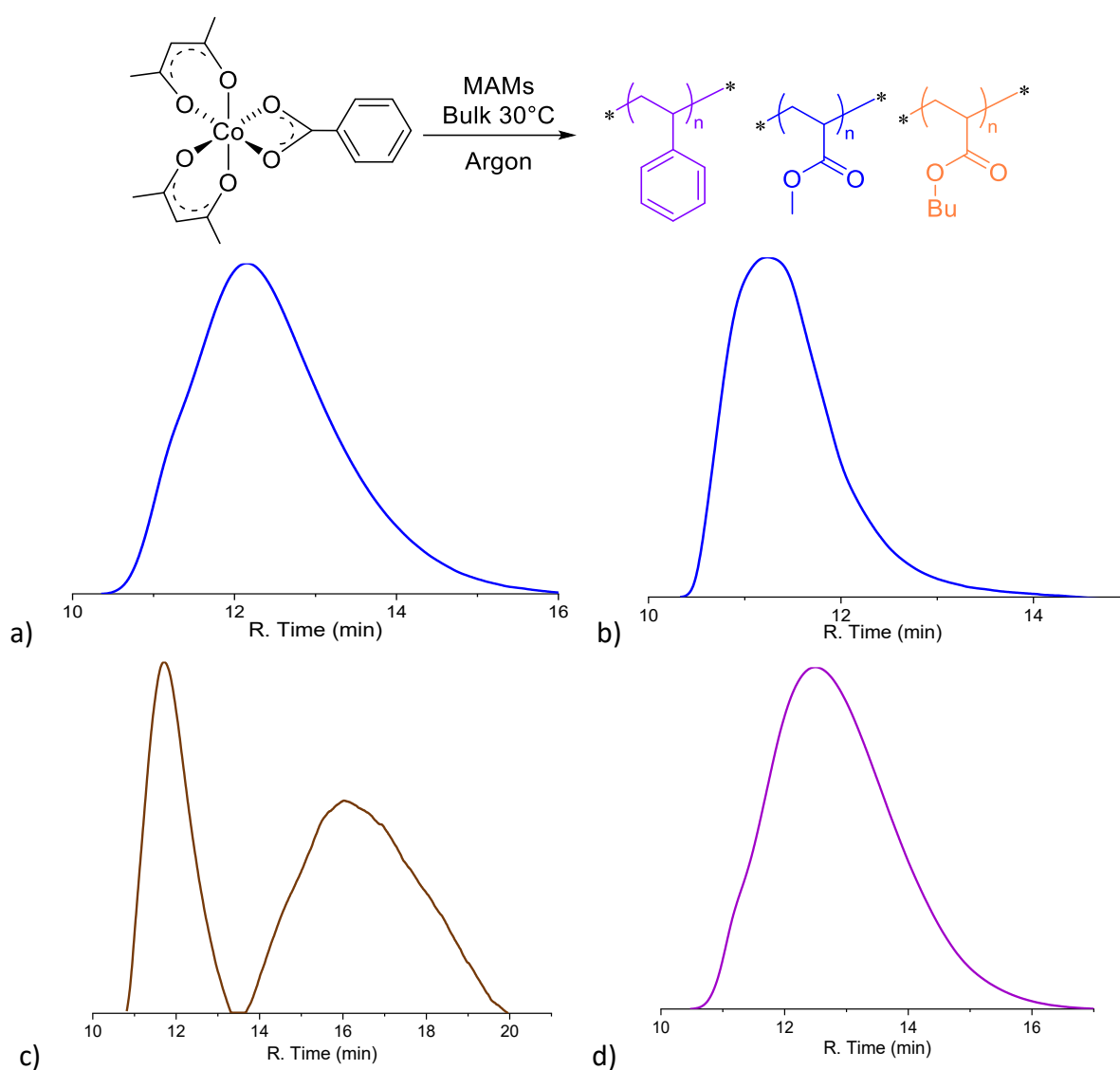


Figure II-14: GPC traces of the polymers of Table II-3 obtained with 3.6 as initiator: a) PMA (entry 1); b) PMA (entry 2); c) PBA (entry 3); d) PS (entry 4).

The MA polymerization was repeated at a lower temperature (5°C), aiming at slowing down the process and possibly improving its control (Table III-3, entry 2). The GPC result (*Figure II-14b*) reveals that the polymerization is uncontrolled even under these conditions, because the molar mass was even higher (over 1 million g mol⁻¹) with a dispersity around 1.5. All these results suggest that complex **3.6** should be efficient for the initiation of a controlled polymerization of LAMs, because the initiation and the uncontrolled polymerization of MAMs demonstrates the efficient production of primary radicals at 30°C. We can therefore expect promising results for the controlled polymerization of vinyl acetate, as described in the literature.⁹⁻¹²

ii. Radical polymerization of LAMs

Before investigating the most promising monomer (VAc), a polymerization test was also conducted for 1-vinyl-2-pyrrolidinone (NVP), which yields a non-stabilized radical and is generally considered within the LAM family. A previous report shows that NVP can be reasonably well controlled by [Co^{II}(acac)₂] upon direct initiation by the organocobalt(III) complex [Co(acac)₂-(CH(OAc)CH₂)_x-R₀] with a short oligomeric PVAc chain (x ~ 4).¹³ However, the NVP polymerization with initiation by complex **3.6**, like those described above for the MAMs, took place rapidly at 30 °C (Table II-3, entry 5) and was not controlled, see the GP trace in *Figure II-15*.

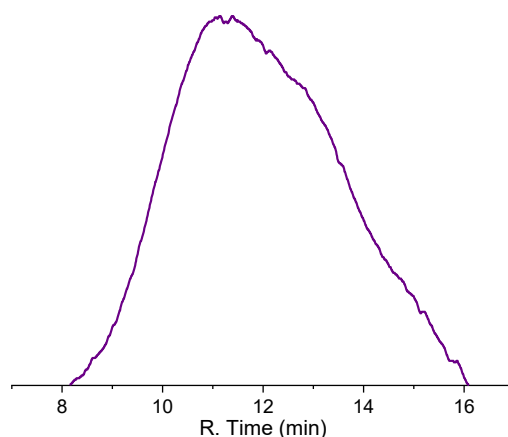


Figure II-15: GPC trace of PNVP (Table II-3, entry 5) obtained with 3.6 as initiator.

Finally, a homopolymerization was carried out with vinyl acetate in bulk at 30°C, see *Figure II-16*. The polymerization rate for this monomer is slower than polymerization rate of the MAMs and of NVP, and also slower than that reported by Debuigne *et al.*¹⁴ for the same monomer, based on the reverse initiation system composed as the [Co^{II}(acac)₂] moderating complex with BPO as an external source of radicals. Nevertheless, a sustained polymerization occurs to reach a 60% conversion over 120 h, while a controlled chain growth is suggested by the shift of the GPC signal to higher molar masses at higher conversions (*Figure II-16d*) and the relatively low dispersities, at least initially. However, the molar masses versus conversion

plot (Figure II-16c) reveals the existence of three regimes during the polymerization process. During the first one, lasting for ca. 5 h, the average molar mass increases very quickly and takes much greater values than the theoretical ones, suggesting a low initiation efficiency. During the second regime (between ca. 5 and 40 h), the molar mass continues to increase with conversion, but at a much lower rate, while the dispersity increases. Finally, at very long reaction times the molar mass shows a tendency to decrease and to further broaden the distribution, as has also been previously observed for the $[\text{Co}^{\text{II}}(\text{acac})_2]$ -mediated VAc polymerization in bulk beyond 40% conversion, due to high viscosity. The observed low efficiency for the initiation process means that only a low fraction of the complex generates the primary radicals able to start the polymerization and turns into metal-capped growing chains, hence explaining the slow polymerization process.

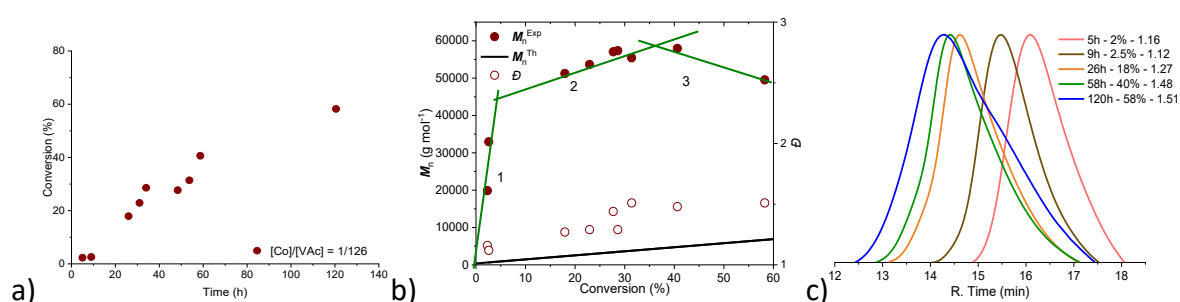


Figure II-16: Homopolymerization of vinyl acetate (VAc) initiated with **3.6** in bulk at 30°C, $[\text{Co}]/[\text{M}] = 1/126$, a) Kinetic plot, b) plot of conversion vs. M_n vs. \bar{D} . and c) Chromatograms obtained by GPC-THF with polystyrene calibration.

Subsequent investigations aimed to optimize the system. First, a certain fraction of $[\text{Co}^{\text{II}}(\text{acac})_2]$ was added at the beginning of the polymerization (Figure II-17) to improve the control from the start of the reaction. Various $[\text{Co}^{\text{III}}]/[\text{Co}^{\text{II}}]$ ratios were tested from 0.1 to 1 (see Table II-4).

Table II-4: Radical bulk homopolymerization of VAc initiated by complex **3.6** with various amount of $[\text{Co}^{\text{II}}(\text{acac})_2]^a$.

Entry	$[\text{Co}^{\text{III}}]/[\text{Co}^{\text{II}}]$	Time (h)	Conv (%) ^b	M_n^{Exp} (g mol^{-1}) ^c	M_n^{th} (g mol^{-1}) ^d	\bar{D}^c
1	1/0	58.7	40	57 957	4863	1.48
2	1/0.1	55.6	38	46 727	4 568	1.22
3	1/0.25	62.0	53	54 122	6 131	1.25
4	1/0.5	48.0	39	52 804	4 646	1.24
5	1/1	85.5	48	42 590	5002	1.22

^a $[\text{Co}^{\text{III}}]/[\text{Co}^{\text{II}}]/[\text{VAc}] = 1/\text{X}/126$, bulk, 30°C, under argon. ^bDetermined by gravimetry. ^cDetermined by GPC with THF as eluent by using polystyrene standards.

As presented in *Figure II-17*, the addition of $[\text{Co}^{\text{II}}(\text{acac})_2]$ had an impact on the polymerization control, because, in its presence, the molar masses increased linearly with conversion along the same straight line throughout the polymerization process. Moreover, *Table II-4* highlights a tendency to decrease M_n and especially \mathcal{D} as the $[\text{Co}^{\text{II}}(\text{acac})_2]$ fraction increases, although the M_n values remain largely superior to the theoretical ones. Thus, the initiator efficiency remains low.

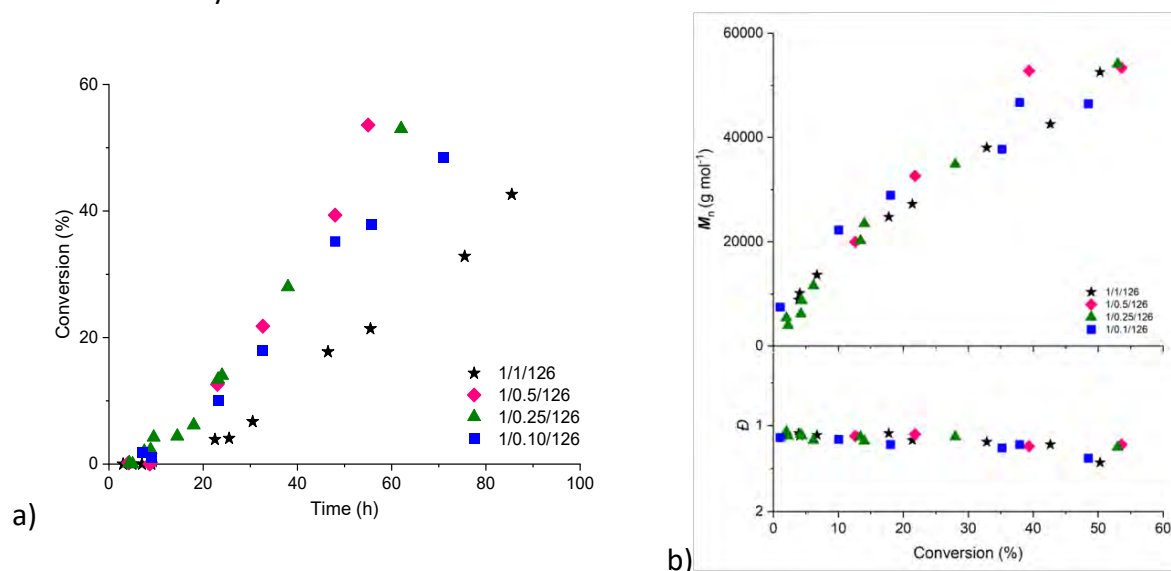


Figure II-17: Homopolymerization of vinylacetate (VAc) initiated by cobalt(III) complex in bulk at 30°C, with X equivalent of cobalt(II): $[\text{Co}^{\text{III}}]/[\text{Co}^{\text{II}}]/[\text{VAc}] = 1/X/126$, (a) Kinetic of VAc polymerization with $X = 0$ (●), 0.10 (■), 0.25 (▲), 0.5 (◆) or 1 (★), (b) The corresponding plot of conversion vs. M_n vs. \mathcal{D} .

The polymerization carried out with 1 equivalent of $[\text{Co}^{\text{II}}(\text{acac})_2]$ (*Table II-4*, entry 5 and *Figure II-17*) reveals a significant impact on the polymerization kinetics, probably because the high concentration of the trapping agent significantly shifts the activation/deactivation equilibrium toward the dormant species. On the other hand, the experiments with 0.1, 0.25 and 0.5 equivalent of $[\text{Co}^{\text{II}}(\text{acac})_2]$ (*Table II-4*, entries 2-4) provide similar polymerization rates. However, the effect on the molar mass evolution (*Figure II-17b*) is minor. The GPC traces of the polymer samples withdrawn from the reaction carried out with a $[\text{Co}^{\text{III}}]/[\text{Co}^{\text{II}}]/[\text{VAc}]$ ratio of 1/0.25/126 are shown in *Figure II-18* (chromatograms and kinetic results with other $[\text{Co}^{\text{II}}(\text{acac})_2]$ fractions are presented in the *Figures S3-4* and *Table S1*). The figure demonstrates the regular progression and narrow shape of the molecular weight distribution as the conversion increases. The bimodal shape of the signals is the result of the workup, because the same unquenched samples were used for the conversion determination by gravimetry, which was done in air, and for the GPC analyses. Thus, a certain fraction of terminations by coupling occurs during this work-up and lead to the appearance of the second distribution at double molar masses. The radical character of this reaction was demonstrated by a TEMPO quenching experiment, as shown in *Figure II-18c*. The conversion was stopped after the addition of the radical scavenger (black curve) while the GPC signal did not further evolve (*Figure II-18d*).

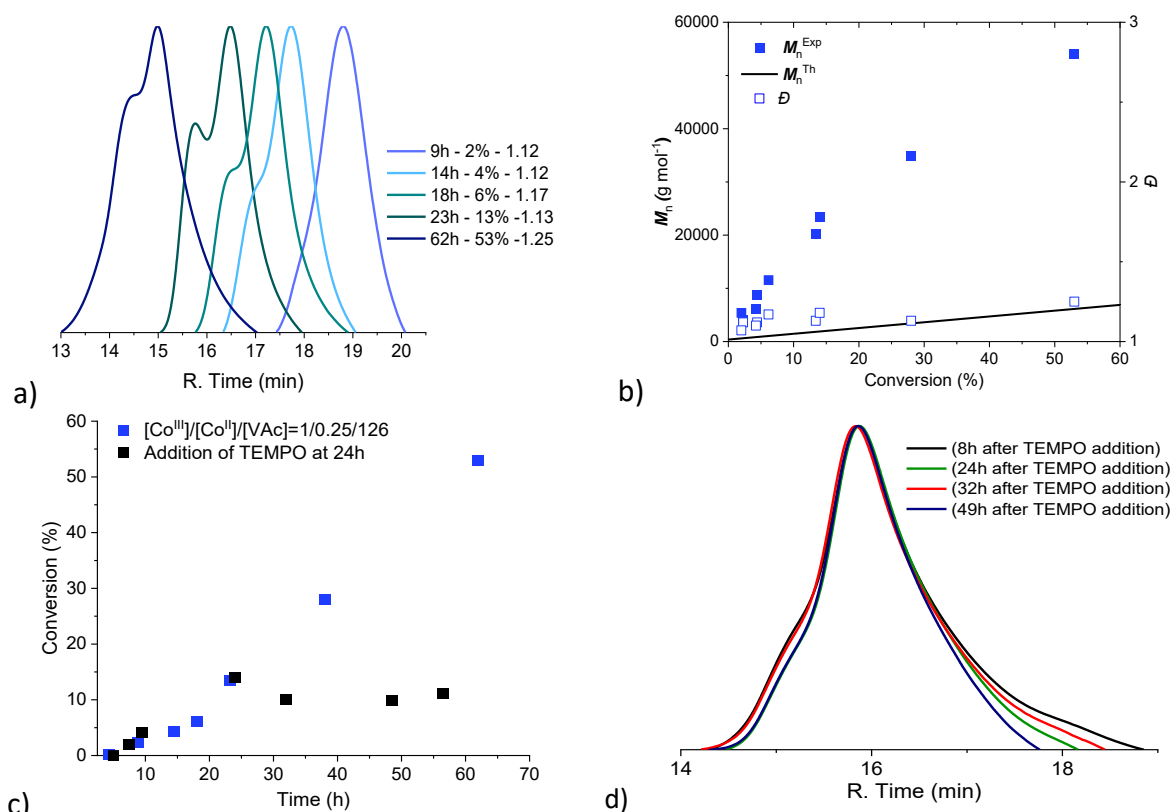


Figure II-18: $[Co^{III}]/[Co^{II}]/[VAc] = 1/0.25/126$ (\blacktriangle), (a) Chromatograms obtained by GPC (b) Plot of conversion vs. M_n vs. \bar{D} . (c) TEMPO quenching after 24h of reaction (\blacksquare), d) GPC traces obtained after addition of TEMPO in the polymerization medium.

iii. Chain end investigation

All our attempts to detect the compounds resulting from the benzoate radical decomposition (*i.e.* biphenyl and phenyl benzoate) by either NMR, or by the $CaOH_2$ test for the rejection of CO_2 were unsuccessful. However, the GC-MS experiment highlight the decomposition of the $[Co^{III}(acac)_2(O_2CPh)]$ in C_6D_6 (Figure 19a) and reveals the formation of benzoic acid from $PhC(O)O^\bullet$. Conversely, the formation of phenyl radicals is evidenced by the formation of large amounts of toluene. This presumably results from abstraction of a methyl group from an acac ligand within the $\{[Co(acac)_2], Ph^\bullet\}$ radical pair. The other major peak in the GC is due to acetylacetone.

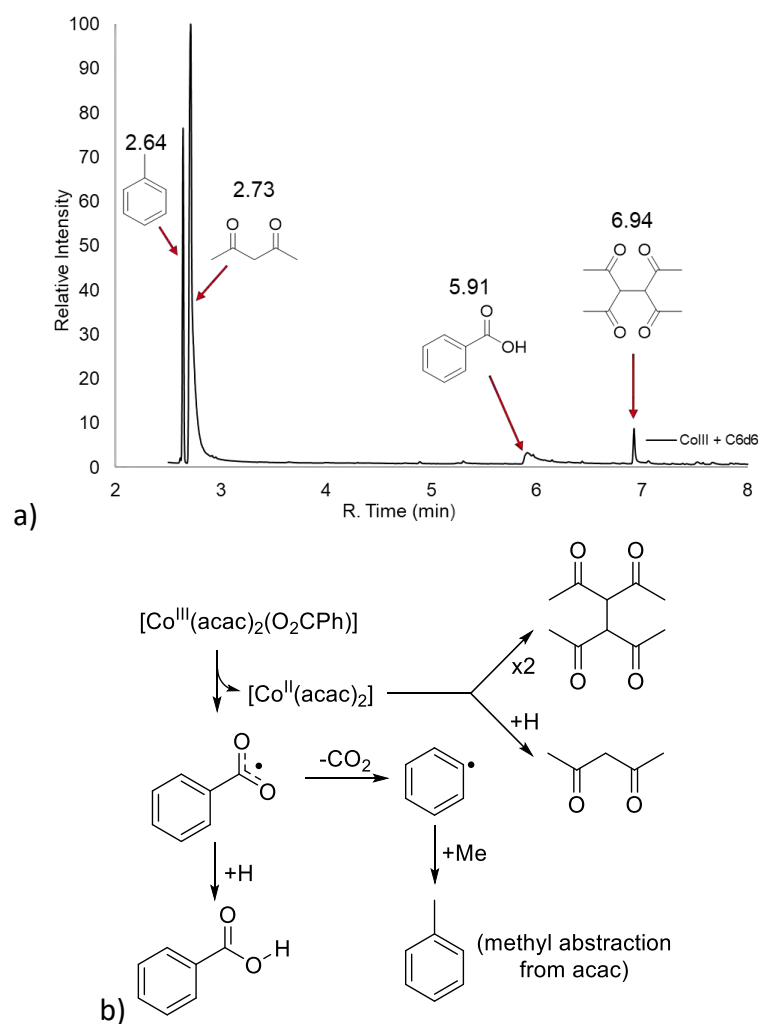


Figure II-19: a) GC-MS investigation of the decomposition of complex $[\text{Co}^{\text{III}}(\text{acac})_2(\text{O}_2\text{CPh})]$ in C_6D_6 : GC trace (for the MS characterization, see *Figure S5*, b) decomposition mechanism of $[\text{Co}^{\text{III}}(\text{acac})_2(\text{O}_2\text{CPh})]$ in C_6D_6 .

In order to confirm the initiation mechanism, the chain ends of a PVAc sample obtained as shown in same condition as Table II-4, entry 3, with lower time of reaction (5h) were investigated by an ESI mass spectrometry experiment. The polymer sample was recovered without quenching in order to preserve the cobalt complex at the ω chain end the ESI technique was privileged for the analysis, because the MALDI-TOF injection mode results in metal loss. The presence of several populations is evident in the spectrum (*Figure II-20*), all of which are repeated at intervals of $86.09 \text{ g mol}^{-1} \text{ m/z}$ units, permitting to validate the presence of VAc repeating units.

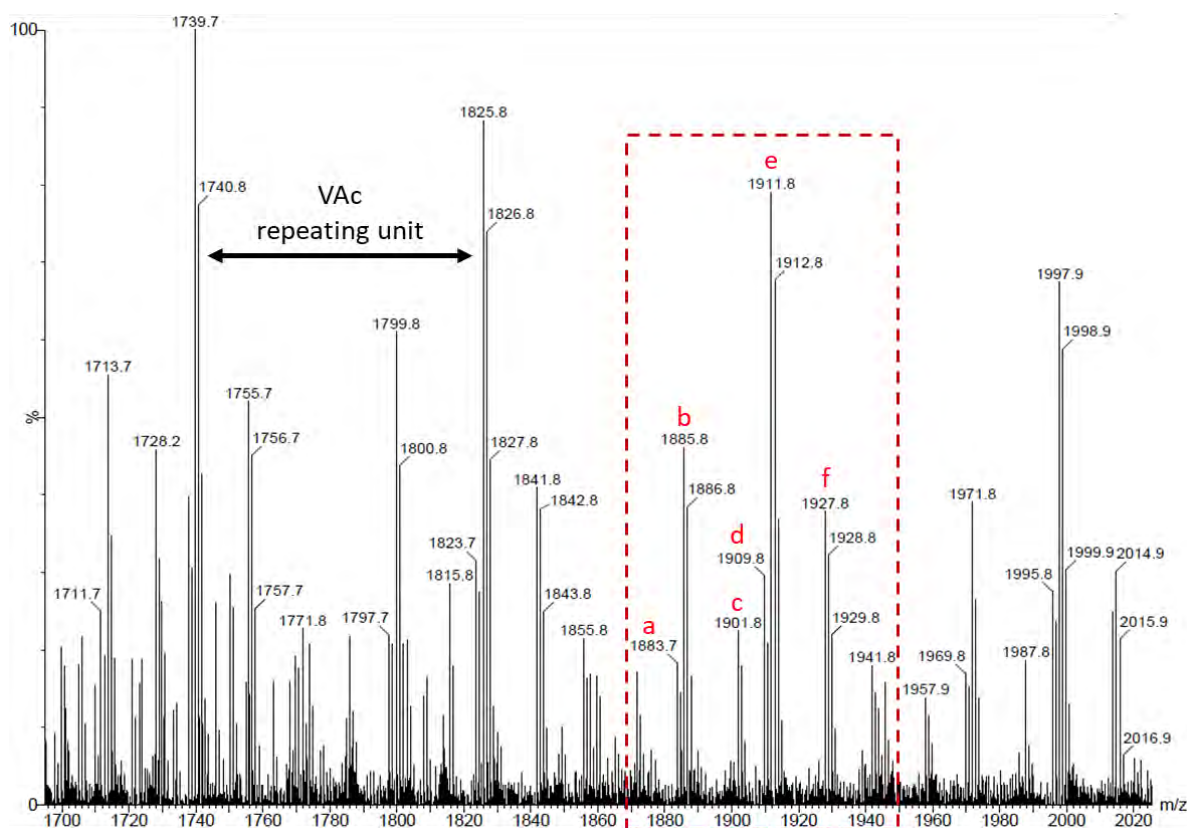
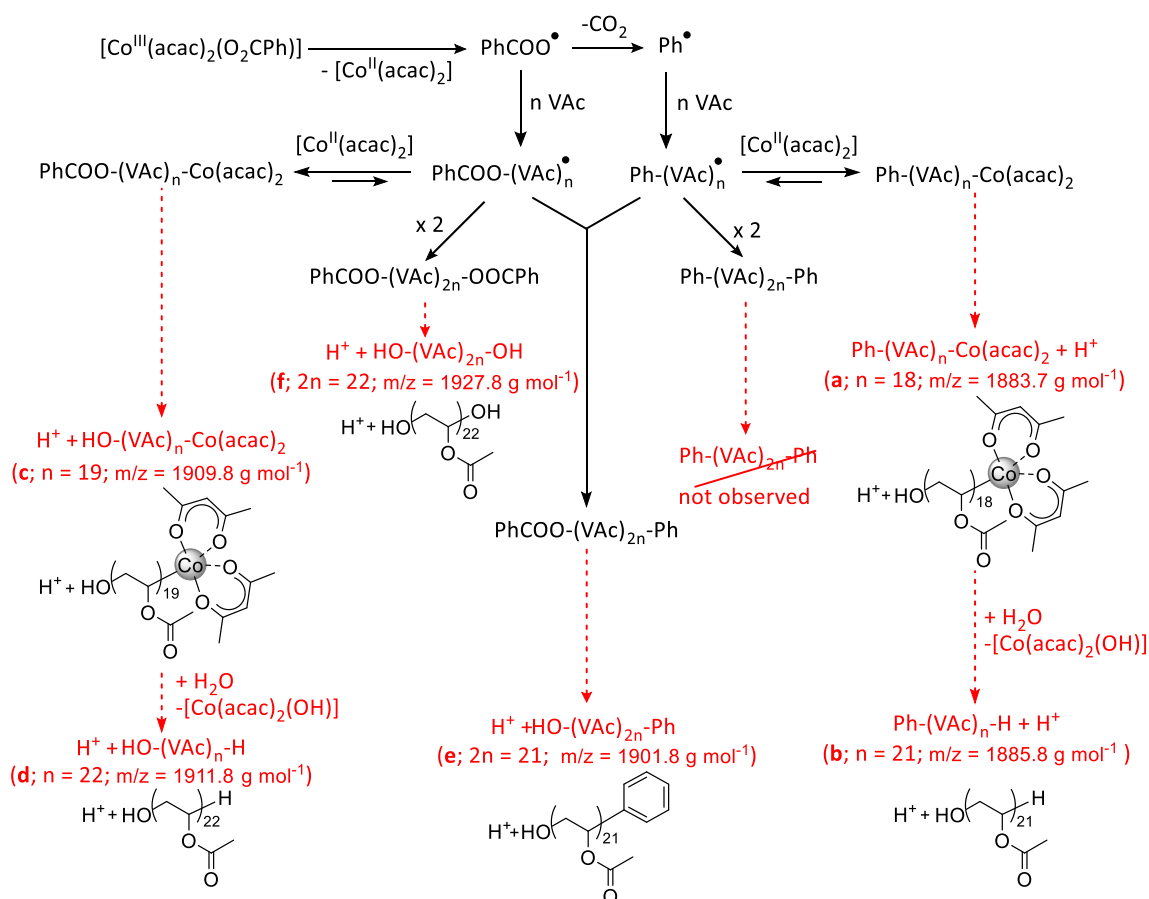


Figure II-20: Expansion of the ESI-MS spectrum (positive mode, QToF – NaI) in the 1700-2020 m/z range of polyvinylacetate (PVAc) obtained by initiation with complex 3.6.

The six highest-intensity populations of the ESI-MS spectrum in Figure II-20 can be rationalized on the basis of the initiation and polymerization mechanism shown in Scheme II-2. The simulation of the isotopic distribution for each population is given in Figure S6. The polymer chains are initiated by both phenyl and benzoate radicals. The Ph-initiated dormant chains are detected directly ($\text{Co}(\text{acac})_2$ ω -end with cationization by proton addition, population **a**). However, a more abundant population from these chains results from the hydrolytic cleavage (H ω -end, population **b**). The chains with a PhCOO α -end are hydrolysed under the ESI-MS analytical conditions, resulting in OH α -chain ends. Hence, after cationization by proton addition, chains with both $\text{Co}(\text{acac})_2$ (population **c**) and H (population **d**) at the ω -end are detected. The homolytic weakness of the PVAc- $\text{Co}(\text{acac})_2$ bond favours radical production during the polymer works up procedure, leading to terminated chains by combination, as also illustrated by the GPC results in Figure II-18. Thus, coupling of two PhCOO-initiated chains leads to population **f**; coupling of one PhCOO-initiated chain with one Ph-initiated chain leads to population **e**. Finally, coupling of two Ph-initiated chains should lead to a Ph- VAc_{2n} -Ph population, which is not visible in the ESI-MA spectrum. We presume that this results from the reluctance of these chains to be cationized, presumably because of the more hydrophobic chain ends.



Scheme II-2: Initiation mechanism of the VAc polymerization, and relationship with the chains observed by ESI-MS.

In order to further substantiate the cobalt presence at the ω chain-end position and probe its possible reactivation, a chain extension reaction was carried out. Thus, a short PVAc chain (Table II-5, entry 1) was produced using the standard conditions described above, followed by isolation and drying to remove the excess monomer.

Table II-5: Block copolymer synthesis.

Entry	Monomer	Time (h)	Conv (%) ^c	$M_n^{\text{Exp}} (\text{g mol}^{-1})$ ^d	$M_n^{\text{Th}} (\text{g mol}^{-1})$ ^e	\bar{D}^d
1 ^a	VAc	10	4	5400	900	1.07
2 ^b	VAc	42	5	8 246	6 260	1.20
3 ^b	St	26	8	32 227	7 060	1.41
4 ^b	MA	18	81	58 395	19 346	1.52
5 ^b	BA	9	3	42687	6 169	5.46

^a $[\text{Co}^{\text{III}}]/[\text{Co}^{\text{II}}]/[\text{VAc}] = 1/0.25/126$, bulk, 30°C , under argon. ^b $[\text{Macroinitiator}]/[\text{M}] = 1/500$. ^cDetermined by gravimetry. ^dDetermined by GPC analysis with THF as eluent by using polystyrene standards. ^eCalculated according to the monomer molar masses.

Then, recovered PVAc was used as macroinitiator for the chain extension reaction of several monomers (VAc, S, MA and BA; Table II-5, entries 2-5). As shown in *Figure II-19-b*, the macroinitiator GPC signal (green trace) shifted to a greater or smaller extent, depending on the new monomer. In all cases, there is no significant residual intensity at the mass of the macroinitiator. The VAc chain extension was slow, yielding only a 5% conversion after 42 h. Conversely, styrene and MA added quite rapidly, yielding very viscous media in less than one day and very large shifts on the chromatogram.

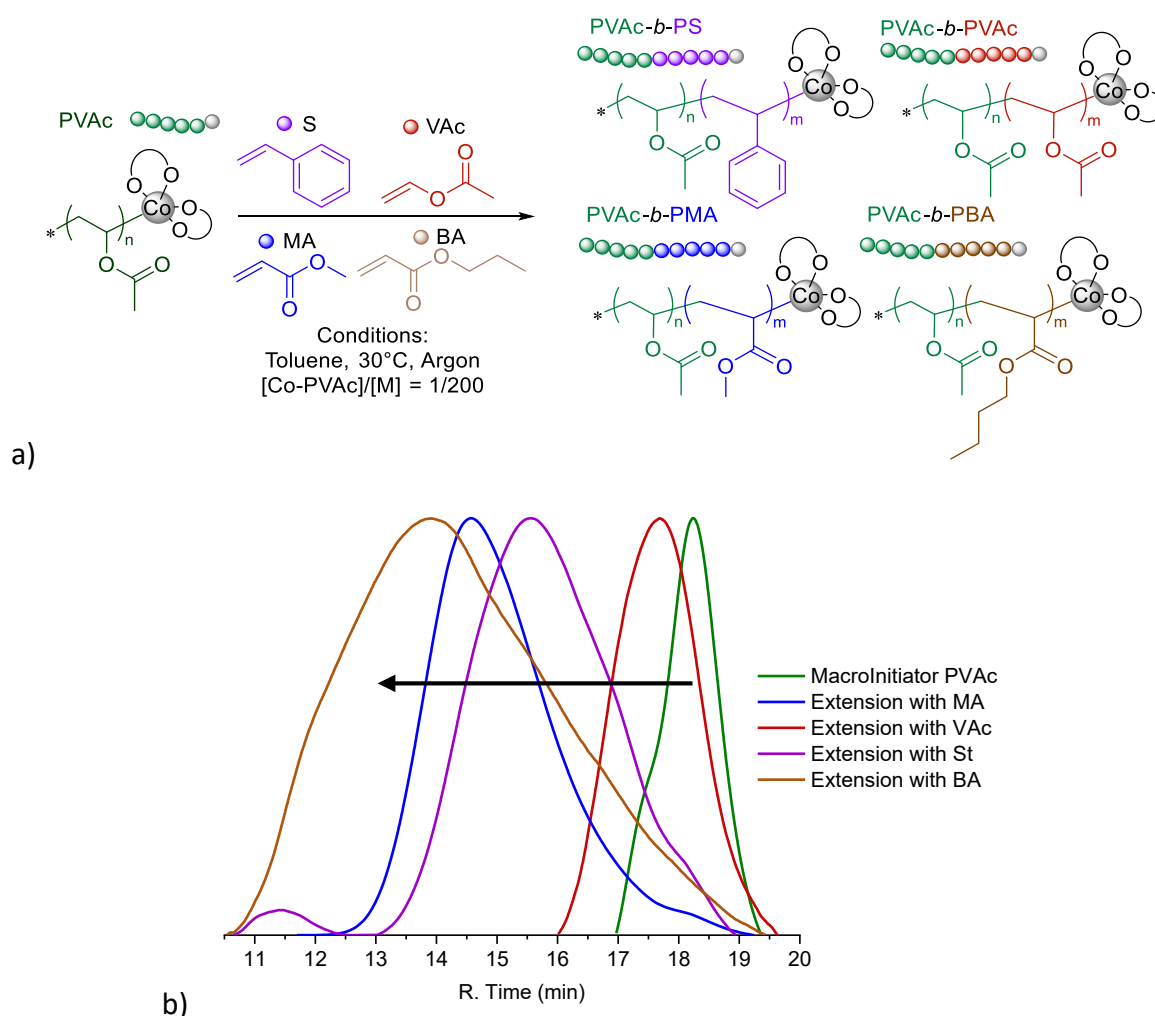


Figure II-19: (a) Chain extension reaction of the [PVAc-Co(acac)₂] macroinitiator with vinyl acetate (VAc), styrene (S), methyl acrylate (MA) and butyl acrylate (BA). (b) GPC traces of the PVAc macroinitiator and of the PVAc-b-PVAc, PVAc-b-PS, PVAc-b-PMA, PVAc-b-PBA final products.

To conclude, the investigation has revealed a controlled radical polymerization of VAc, but the polymer molar masses were always higher than expected, indicating a low initiation efficiency of complex **3.6**.

iv. Efficiency factor improvement

The efficiency factor found in the above investigations, expressed by the ratio between the theoretical and experimental values, is around 10%, which means that only 10% of the complex undergoes homolytic bond cleavage to generate the primary radical and start the chain propagation. To improve the efficiency factor, the polymerization was carried out at higher temperatures, as highlighted in Table II-6.

Table II-6: Polymerization at various temperatures.^a

Entry	T. (°C)	Time (h)	Conv (%) ^b	M_n^{Exp} (g mol ⁻¹) ^c	M_n^{Th} (g mol ⁻¹) ^d	M_n^{Th}/M_n^{Exp}	\mathcal{D}^c
1	30	62.0	53	54 122	6 131	0.11	1.25
2	40	15.5	60	53 800	6 925	0.13	1.23
3	50	3.5	47	37 800	5 547	0.14	1.15
4	60	0.5	70	39 382	7 987	0.20	1.44

^a[Co^{III}]/[Co^I]/[VAc] = 1/0.25/126, bulk, under argon. ^bDetermined by gravimetry. ^cDetermined by GPC with THF eluent analysis by using polystyrene standards. ^dCalculated according to the conversion ($M(VAc)=86.09$ g mol⁻¹).

As expected, the polymerization rate increased at higher temperatures (see the kinetic monitoring in Figure II-20a). For example, the reaction is 10 times faster at 50 °C relative to 30 °C: a 50% conversion was achieved in 5 hours, against 60 hours at 30 °C. The level of control remained acceptable at all temperatures (linear molar mass increase with the conversion and low dispersities, except for a slight \mathcal{D} increase at 60 °C, Figure II-20b). The GPC traces showing the shift of the molar mass distribution are available in the supporting information, Figure S8. The polymer molar masses remained higher than expected (black straight line in Figure II-20b). However, the efficiency factor steadily increased from 11% at 30 °C to 20% at 60 °C, in line with the expected greater activation of the Co^{III}-benzoate bond at higher temperatures.

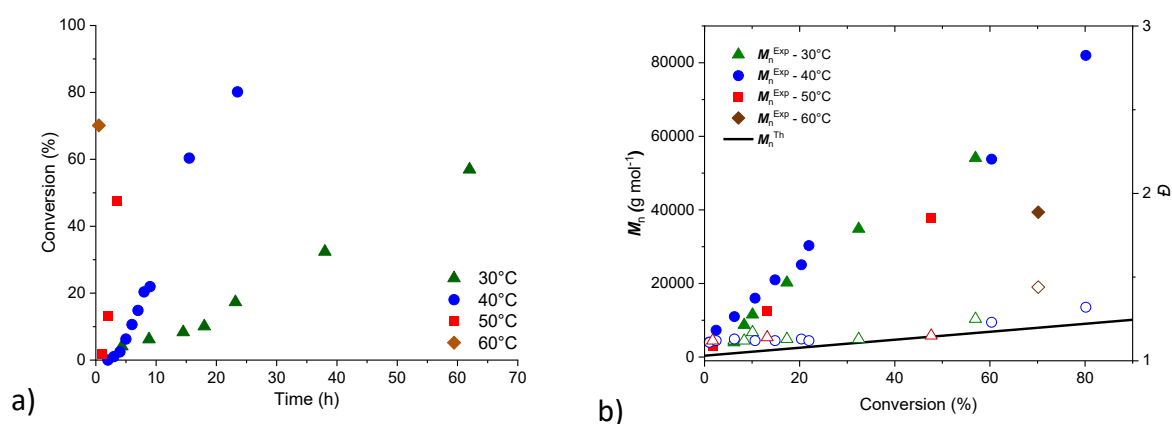


Figure II-20: Influence of the temperature on the controlled polymerization of VAc; [Co^{III}]/[Co^I]/[VAc] = 1/0.25/126 at 30 °C (▲), 40 °C (●), 50 °C (■), 60 °C (◆) and corresponding hollow symbols for dispersity.

A few polymerizations were also carried out in toluene. The first test at 30°C gave no polymer after two days of reaction. On the other hand, a polymerization occurred at 40 °C. The time evolution of this polymerization is shown in *Figure II-21*, in comparison with that of the bulk process.

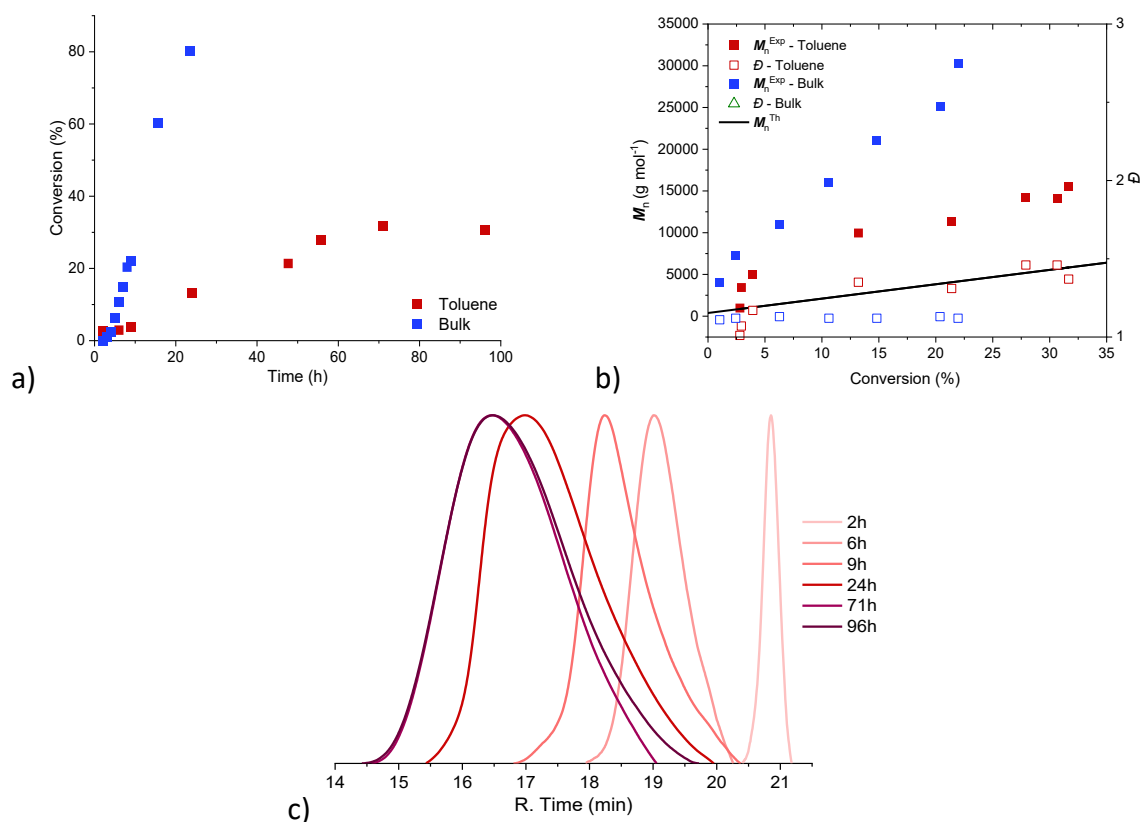


Figure II-21: Comparison of the VAC polymerization initiated by complex 3.6 in bulk and in toluene ([VAC] = 4 M): a) kinetics; b) M_n and \bar{D} vs. conversion; c) GPC traces with THF as eluent and polystyrene calibration.

As we can be seen in *Figure II-21*, the polymerization is slower in solution relative to the bulk, as expected. Like for the bulk polymerization, the molar masses increased linearly with the conversion. In addition, they are closer to the theoretical values, which means that the initiator efficiency factor is greater, in the 20-40% range (Table II-7). After 60 h of reaction, the molar mass distribution becomes broader and the conversion stops.

Table II-7: Polymerization of VAc at 40°C in Toluene.^a

Entry	Time (h)	Conv (%) ^b	M_n^{Exp} (g mol ⁻¹) ^c	M_n^{Th} (g mol ⁻¹) ^d	M_n^{Th}/M_n^{Exp}	\bar{D}^c
1	6	3	3432	883	0.26	1.07
2	9	4	4981	1055	0.21	1.17
3	24	13	9969	2651	0.26	1.35
4	48	21	11387	4062	0.35	1.31
5	56	28	14175	5183	0.36	1.46
6	71	31	15520	5830	0.37	1.37
7	96	30	14081	5655	0.40	1.46

^a[Co^{III}]/[Co^{II}]/[VAc] = 1/0.25/126, toluene, under argon. ^bDetermined by gravimetry. ^cDetermined from GPC analysis by using polystyrene standards. ^dCalculated according to the conversion ($M(VAc)=86.09$ g mol⁻¹).

v. Photoinitiation test

Still with the objective of improving the initiation efficiency, another activation mode, namely with light assistance for a bond photocleavage, was also attempted. The UV-Vis spectrum of complex **3.6** reveals a band with λ_{max} around 600 nm (*Chapter II, Figure II-2*). In collaboration with the “Institut Charles Gerhardt” in Montpellier, the possible photocleavage process was explored using a few LEDs working at different wavelengths (see Table II-8) to irradiate a solution of the complex at 4 mmol L⁻¹ in toluene. The presence of photocleavage should induce an absorbance decrease. However, all the experiments gave no indication of any absorbance decrease (Table II-8), demonstrating the photostability of complex **3.6**.

Table II-8: Photocleavage tests of complex [Co(acac)₂(O₂CPh)] (**3.6**) at various λ .^a

	Time (min)	A^a
irradiation at $\lambda = 590$ nm (Strength 3.1W/cm ²) ^b	0	0.5035
	30	0.5196
	80	0.5221
irradiation at $\lambda = 625$ nm (Strength 2.6.W/cm ²) ^b	0	0.4789
	75	0.4915
	250	0.5116
irradiation at $\lambda = 400$ nm (Strength 3.1W/cm ²) ^b	0	0.4789
	60	0.5268

Tests carried out under nitrogen. ^aAbsorbance recorded at the λ_{max} of the complex absorption spectrum (605 nm). ^bStrength of the irradiation measured with a radiometer.

Following that, it was decided to run the photoactivation test in the presence of VAc in bulk, but no polymerization occurred after 5 hours of irradiation ($\lambda = 590$ nm) at room temperature (around 23°C), and less than 10% of conversion was achieved after 22 hours of irradiation. These results suggest that irradiation has no effect, because the polymerization is also thermally initiated at room temperature.

In summary, the new complex **3.6** was demonstrated to possess the dual role of thermal initiator and moderator for the radical polymerization of vinyl acetate. The polymerization study has shown a relatively well-controlled polymerization in bulk and in solution in the low temperature 30-60 °C range. The main drawback of this system comes from the low initiation efficiency. The temperature increase has a positive but minor effect, whereas photoactivation was unsuccessful. Therefore, other complexes based on cobalt bis(acetylacetonate) were synthesized and described in chapter II. The aim was to extend the scope of the complexes capable to initiate and moderate the polymerization of VAc and to improve the initiation efficiency by chemical modification of the benzoyl radical (R_0) with electron-withdrawing or -donating or sterically encumbering groups, hoping to promote the homolytic cleavage of the Co^{III} - R_0 bond at low temperatures.

b. Polymerizations initiated by the other $[Co(acac)_2-O(O)CAR]$ complexes

The same conditions highlighted above for the VAc polymerization initiated by $[Co(acac)_2(O_2CPh)]$ were also applied to the others bis(acetylacetonato)cobalt(III) carboxylate complexes (**3.7-3.10**). All experiments were carried out in bulk monomer under argon using a $[Co^{III}]/[Co^{II}]/[VAc]$ ratio of 1/0.25/200. The results are collected in Table II-9.

Table II-9: Results of the VAc polymerizations initiated by $[Co(acac)_2(O_2CAR)]$ (**3.6-3.10**).^a

Complex	Temp (°C)	Conv. (%) ^a	M_n^{Exp} (g mol ⁻¹) ^b	M_n^{Th}/M_n^{Exp}	\mathcal{D}^b
$[Co(acac)_2(O_2CPh)]$ (3.6)	30	14	20 232	0.16	1.12
$[Co(acac)_2(O_2CC_6H_4-p-OMe)]$ (3.7)	30	6	10 192	0.17	1.24
$[Co(acac)_2(O_2CC_6H_4-p-tBu)]$ (3.8)	30	-	No polymerization		
	40	4	9 228	0.12	1.23
$[Co(acac)_2(O_2CC_6H_4-p-NO_2)]$ (3.9)	30-40-60	-	No polymerization		
$[Co(acac)_2(O_2CC_6H_4-o-NO_2)]$ (3.10)	30-40-60	-	No polymerization		

Conditions: Bulk polymerization $Co^{III}/Co^{II}/VAc = 1/0.25/200$ during 24h. ^aDetermined by gravimetry. ^bDetermined from GPC with THF as eluent by using polystyrene standards.

For the polymerizations initiated by the *tert*-butyl and methoxy *para*-substituted derivatives (**3.7** and **3.8**), the evolution of the molar mass distributions shown by GPC (*Figure II-24a* and *b*) and the linear increase of the number-average molar masses as function of conversion (*Figure II-24d*) indicate controlled processes. However, the polymerization rates are lower than for the **3.6**-initiated polymerization. In fact, after one day of reaction at 30 °C, the **3.7**-initiated polymerization gave only a 6% conversion, vs. 14% for **3.6**. The kinetics for the two complexes is compared in *Figure II-24c*.

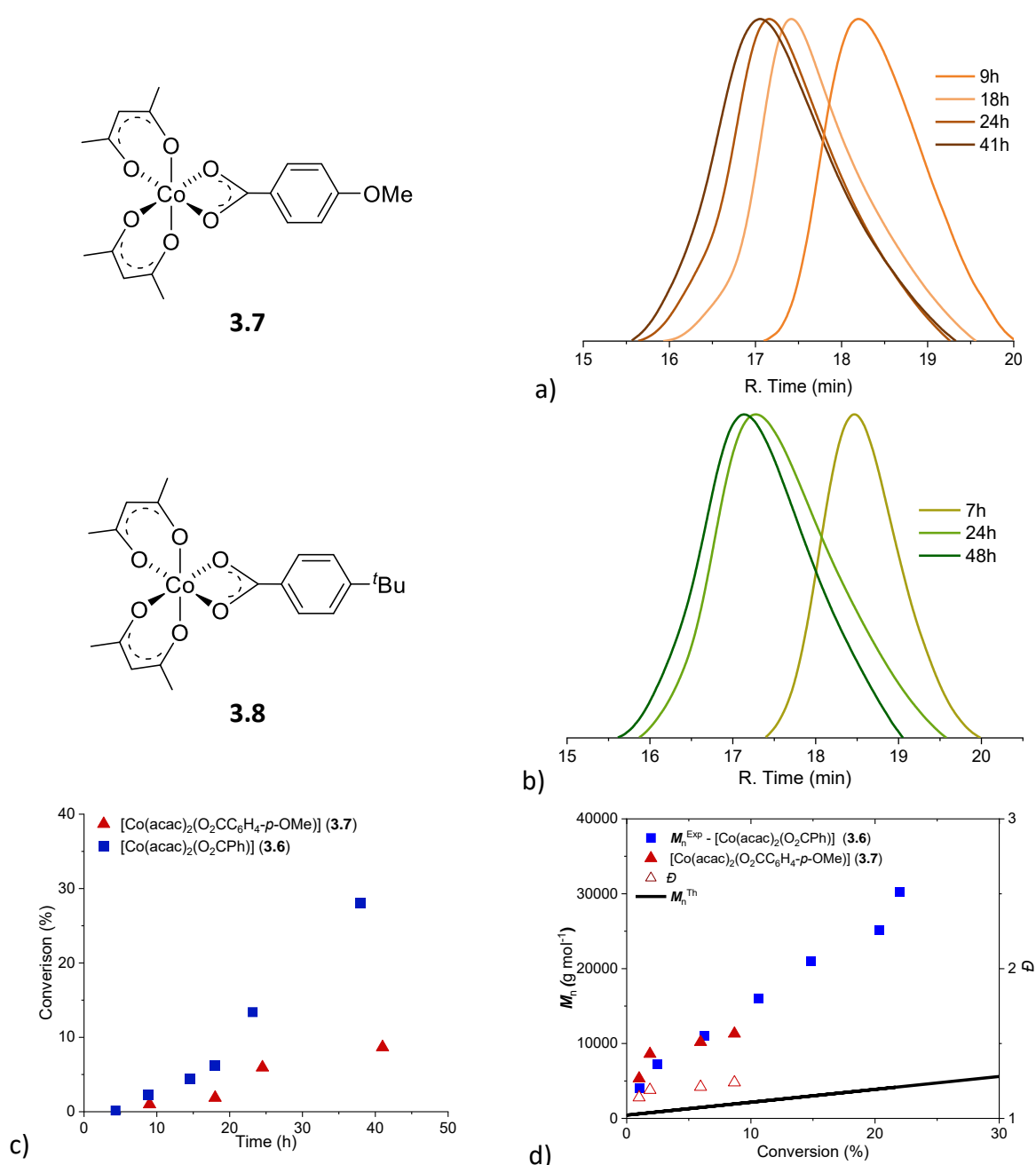


Figure II-22: GPC analyses of the PVAc obtained by bulk polymerization of VAc at 30 °C with initiation by a) **3.7**, b) **3.8**, using THF as eluent and polystyrene standards for calibration. Comparison of conversion vs. time (c) and M_n and \bar{D} vs. conversion **3.6** and **3.7**.

On the other hand, the polymerization initiated by **3.8** gave no polymer after one day at 30°C, but a small conversion (4%) was obtained at 40°C. Figure II-25 compares the kinetics and the M_n evolution with conversion for the polymerizations initiated by **3.6** and **3.8** at 40°C. The molar mass evolution as a function of conversion suggests a similar efficiency factor for **3.7** and a lower one for **3.8**.

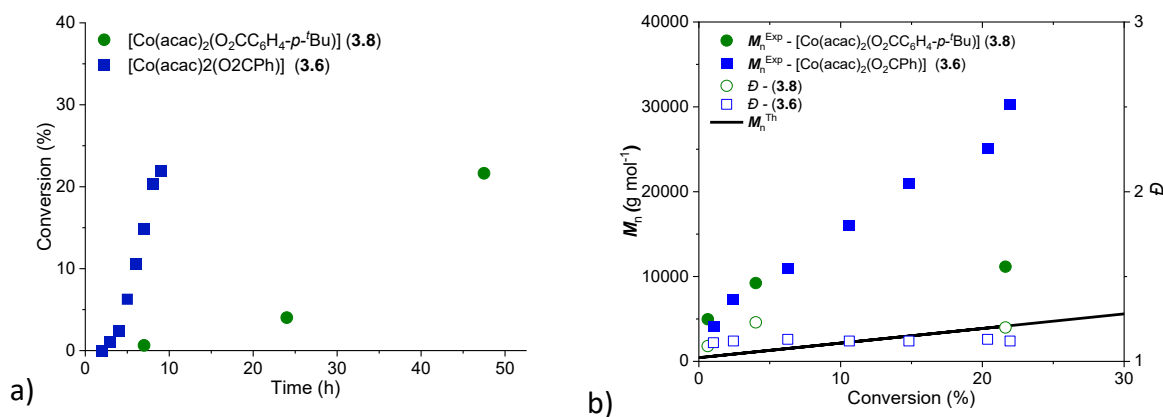


Figure II-23: Comparison between **3.6** and **3.8**, obtained at 40°C. a) Plot of conversion as function of time and b) plot of conversion vs. M_n vs. \bar{D} .

These results suggest that both **3.7** and **3.8** feature stronger Co^{III}-carboxylate bonds than **3.6**. In fact, given the electron donating power of the *tert*-butyl and methoxy groups (by inductive and mesomeric effect, respectively), the higher oxidation state [Co^{III}(acac)₂(O₂CAR)] complex is better stabilized relative to the sum of [Co^{II}(acac)₂] and the ArCO₂[•] radical, contributing to the Co^{III}-O bond strengthening and consequently to increase the BDE.

On the other hand, the polymerization test with the *para*-nitro derivative (**3.9**) reveals no polymerization even at 60°C. This result may seem surprising, because being electron-withdrawing by mesomeric effect, the nitro group should have a destabilizing effect on the higher oxidation state Co^{III} carboxylate complex and thus favour its reduction by radical expulsion. On the other hand, it is also possible to envisage that the major effect is to make the metal electron poorer and thus increase the heterolytic strength of the Co^{III}-O bond. This is also highlighted by the impact on the reduction potential shown by the electrochemical study. Moreover, this result is also consistent with the observed formation rate of these compounds, as presented and discussed in Chapter II. In fact, species **3.9** was formed faster than the other complexes, which suggests its greater thermodynamic stability (*Chapter II, Figure III-15*).

The analogous *ortho*-NO₂ derivative **3.10** similarly yields no polymer at 30, 40°C and even at 60°C. In addition to the same considerations outlined for the *para*-nitro analogue, this compound may also establish a hydrogen bond, as shown in the solid-state structure, between one oxygen atom of the nitro group and a hydrogen atom of an acac ligand, due to the spatial proximity (*Figure III-11, chapter II*).

To conclude about the series of substituted cobalt benzoate complexes, new compounds capable to thermally initiate and control the VAc polymerization have been highlighted. However, the main drawback is the low initiation efficiency factor. Hypotheses about the possible reasons for this low efficiency were made and additional investigations were carried out aiming to improve it by modification of the R₀ group. However, no significant improvement could be achieved so far and the impact of the aryl substituent on the reactivity is still under investigation. On the other hand, the investigation of the chain ends revealed the presence of both benzoate and phenyl functions, giving precious information on the initiation mechanism,

because that means that the direct addition of the benzoyl radical to the VAc monomer competes with the decarboxylation reaction. For that reason, it was decided to test another carboxylate architecture, with an alkyl substituent.

c. Carboxylate alkyl – $[\text{Co}(\text{acac})_2\text{-O(O)C-Alkyl}]$

Two alkyl carboxylate species (**3.11** and **3.12**), structurally analogous to **3.6-10**, were synthesized with a short and a long carbon chain, respectively (1 carbon atom for **3.11** or 10 for **3.12**), as detailed in Chapter II.

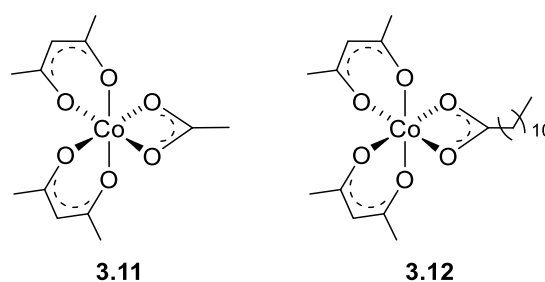


Figure II-24: Structures of complexes $[\text{Co}(\text{acac})_2\text{-OAc}]$ (**3.11**) and $[\text{Co}(\text{acac})_2\text{-O(O)C(CH}_2\text{)}_{10}\text{CH}_3]$ (**3.12**).

i. Bis(acetylacetonate) cobalt acetate, $[\text{Co}(\text{acac})_2(\text{OAc})]$

This complex is related to **3.1** by having the same acetate ligand as target primary radical to initiate the polymerization, but has a fully *O*-based coordination sphere. The ability of the acetate radical to initiate the polymerization of VAc was probed by using diacetyl peroxide (APO) as a thermal initiator. A blank reaction without any complex was carried out in bulk at 30°C in presence of 250 equivalent of monomer, producing a high molecular weight (460 000 g mol⁻¹) polymer product with high dispersity (around 2) in 2 hours (Figure S9). This shows an uncontrolled polymerization process, as expected. Subsequently, the polymerization was repeated in the presence of $[\text{Co}^{\text{II}}(\text{acac})_2]$ at 30°C (same conditions used for the corresponding reaction with BPO).¹⁴ As shown in Figure II-27, the polymerization starts after an induction period (4 hours), the molar mass distribution in the GPC trace gradually shifts to lower retention times and the number average molar mass increases linearly with the conversion and \mathcal{D} remains always low, highlighting a controlled polymerization. The large gap between the experimental values and the theoretical line shows that the initiator efficiency factor of this system is similar (0.15 vs. \approx 0.19) to that of the related BPO/ $[\text{Co}^{\text{II}}(\text{acac})_2]$ initiating system.

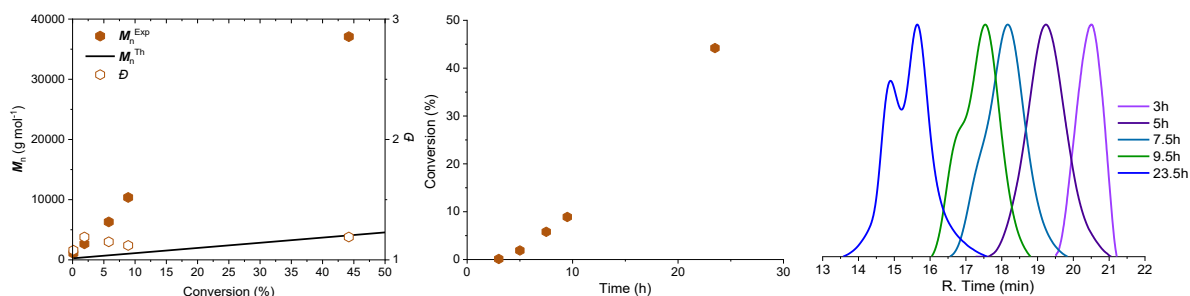


Figure II-25: Homopolymerization of VAc initiated by diacetyl peroxide in the presence of $[\text{Co}^{\text{II}}(\text{acac})_2]$ at 30°C under argon.

Using $[\text{Co}(\text{acac})_2(\text{OAc})]$ (**3.11**) as unimolecular initiator under the same conditions optimized for the benzoate system ($\text{Co}^{\text{III}}/\text{Co}^{\text{II}}/\text{VAc} = 1/0.25/126$ in bulk at 30 °C under argon), the polymerization was very slow, yielding only 5% of conversion in 3 days. When the temperature was raised to 50 °C, a 20% conversion was obtained in 5 hours. However, in the GPC traces only one signal was observed mixed with the solvent feature. Therefore, the investigation of this initiator was abandoned, because of the explosion hazard of the diacetyl peroxide precursor and the low yield of the synthesis of complex **3.11**. That is why our attention shifted toward using a longer aliphatic chain with dilauryl peroxide (LPO) (11 carbons), which is a commercially available compound.

ii. Lauroyl derivative, $[\text{Co}(\text{acac})_2(\text{O}_2\text{C}(\text{CH}_2)_{10}\text{CH}_3)]$

An initial polymerization test with the **3.12** initiator was carried out for methyl acrylate bulk polymerization at 30°C for 255 equivalents of monomer vs. cobalt. As expected, this polymerization was uncontrolled, producing a very high molar mass product, (around 10^6 g mol⁻¹), see the GPC analysis in Figure II-26.

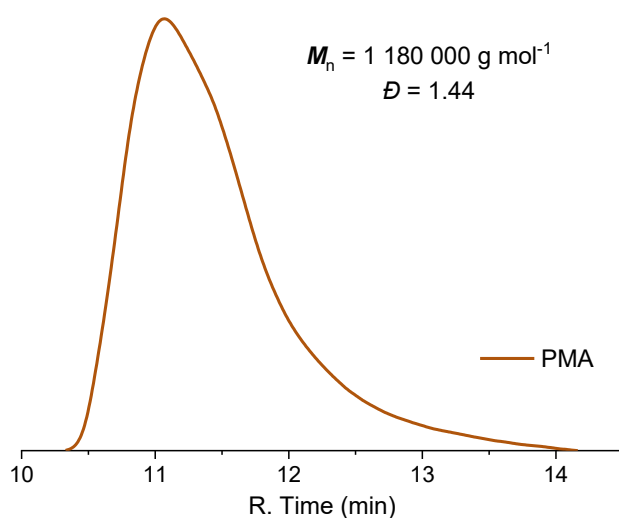


Figure II-26: Homopolymerization of methyl acrylate initiated by complex **3.12** (30°C in bulk).

Concerning the VAc polymerization, direct initiation with complex **3.12** yielded no polymerization at 30 and 40°C. On the other hand, the corresponding reverse initiation strategy with LPO/[Co^{II}(acac)₂] gave controlled polymerizations at 30 and 40°C, yielding similar results to the initiation by APO/[Co^{II}(acac)₂], as shown in *Figure II-27*.

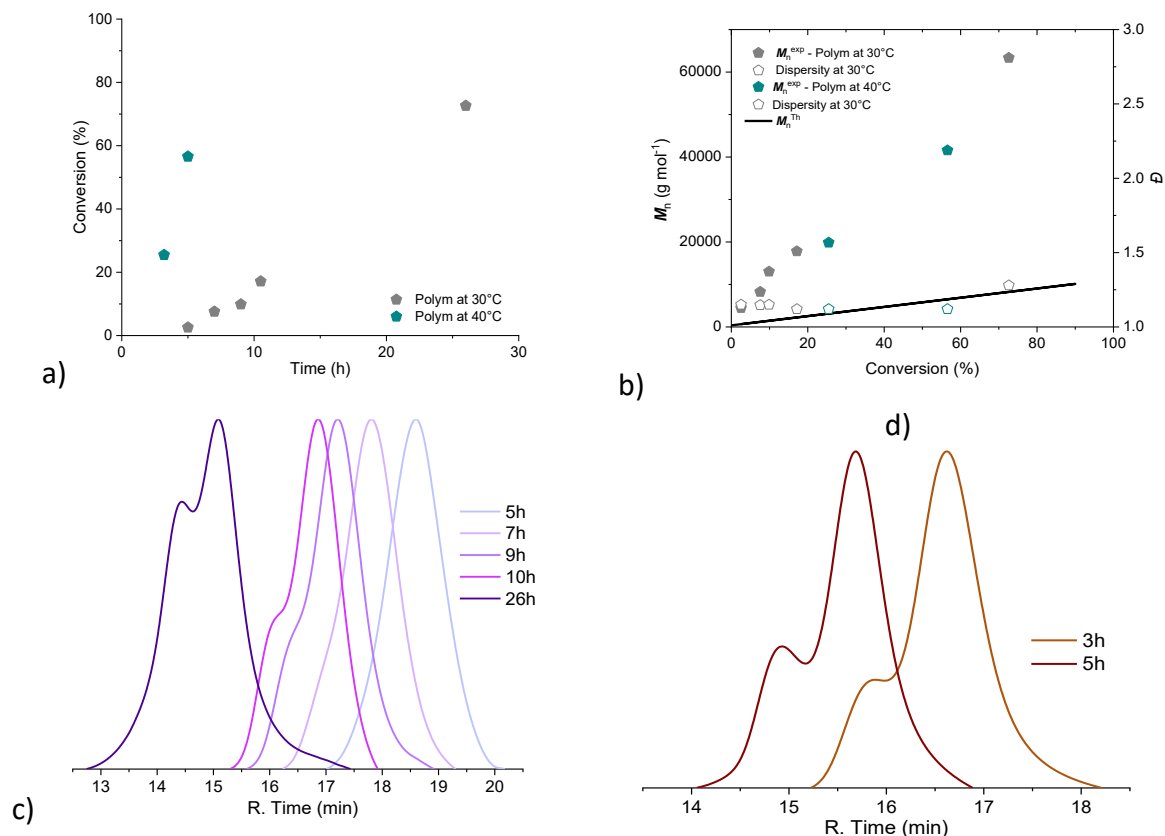


Figure II-27: Homopolymerization of vinyl acetate with reverse initiation by LPO/[Co^{II}(acac)₂]. Conditions: [Co^{II}]/[LPO]/[VAc] = 1/0.5/126, in bulk under argon at 30°C (●) and 40°C (■). a) Conversion vs. time; b) M_n and \bar{D} vs. conversion; c) GPC traces at 30°C and d) at 40°C, obtained using THF as eluent and polystyrene standards for calibration.

To conclude on this work on the cobalt alkyl carboxylates, the polymerization tests reveal no or low polymer production by direct initiation at low temperature, even though the generation of primary radicals is demonstrated by the initiation of the methyl acrylate polymerization.

4. Conclusion

Within the family of cobalt(III) complexes supported by (*N*2,*O*2) ligands for the controlled radical polymerization of MAMs, the tripodal (*N*2,*O*2) systems with either acac (previously published results)¹⁴ or acetate (**3.2**, this work) as *R*₀ fragment did not give rise to any polymer production, unlike the Schiff-base cobalt acetate complex **3.1**, which is able to initiate and moderate the polymerization of MA. The polymerization of MMA with direct initiation by **3.1**, on the other, gives rise to catalytic chain transfer.

Concerning the family of cobalt(III) complexes supported by (*O*2,*O*2) ligands for the polymerization of VAc, the most readily accessed complex [Co(acac)₂(O₂CPh)] (**3.6**) also gave the best results in terms of polymerization. The methoxy and *tert*-butyl derivatives (**3.7** and **3.8**) were also efficient for the controlled polymerization of VAc. On the other hand, the nitro derivatives **3.9** and **3.10** did not produce any polymer even at 60 °C, giving useful information about the impact of this substituent on the Co^{III}-O bond strength. *Figure II-30* summarizes the efficiencies of the various systems for the direct initiation and control of the polymerization of vinyl monomers.

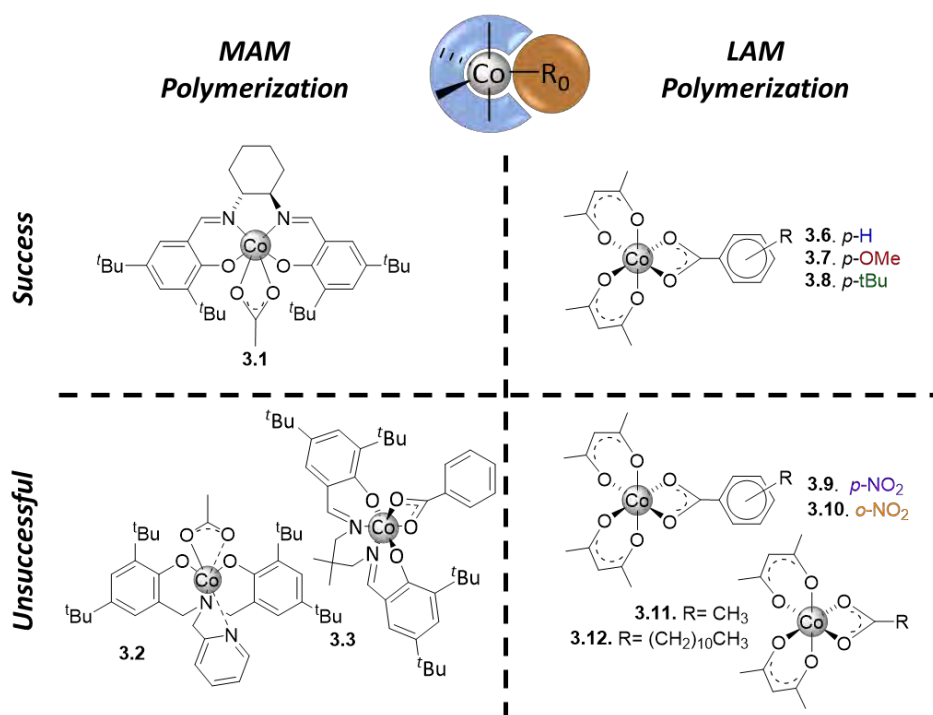
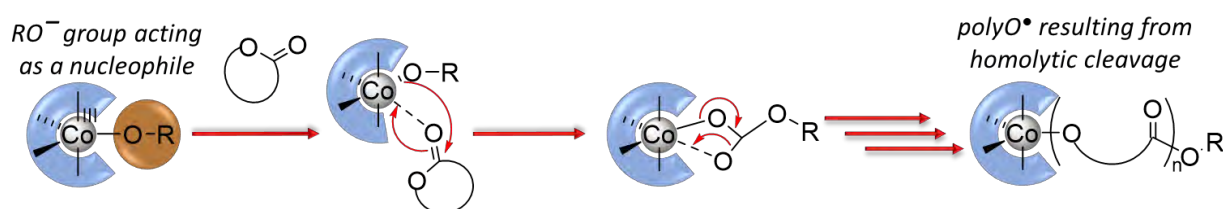


Figure II-28: Summary of the investigated complex architectures and of their efficiency.

III. Ring opening polymerization (ROP)

1. Introduction

The polymers produced by Ring Opening Polymerization (ROP) are more and more investigated due to their biodegradability and biocompatibility. In fact, they are promising in the medicinal, pharmaceutical and agricultural fields.^{15, 16} Historically, the pioneers of this chemistry were Klein *et al.*,¹⁷⁻¹⁹ who reported the catalytic action of complexes based on tin and aluminium in the 50's.²⁰ Concerning transition metals, several iron complexes have shown high activity in ROP.²¹⁻²⁴ Copper-based systems constitute the second largest group of investigated catalysts.²⁵⁻²⁸ The absence of cobalt alkoxide architectures amongst the ROP catalysts in the literature pushed us to investigate our cobalt carboxylate complexes. Given the $\text{Co}^{\text{III}}\text{-O}$ bond polarity, the main question is whether the alkoxide ligand is nucleophilic enough to open cyclic esters, as illustrated in *Scheme III-1*.



Scheme III-1: Cobalt alkoxide for ROP of cyclic ester.

The second question concerns the polymerization mechanistic switch. For instance, to switch from ROP to OMRP the cobalt-alkoxide polymer chain end must undergo homolytic cleavage for radical production.

This section will be divided in two major parts, each one based on the previously presented complex that gave the best results for the controlled polymerization of a MAM (*i.e.* MA, **3.1**) and a LAM (*i.e.* VAc, **3.6**), respectively. These complexes have been tested for the homopolymerization of cyclic esters by the ROP mechanism. The goal here was to probe the existence of a unique metal complex that could be used for two different applications, namely OMRP as already shown and ROP. The final objective is to apply this complex in a sequential block copolymerization by two different polymerization mechanisms.

2. (N₂,O₂)-Cobalt complex (3.1)

A ROP process may follow either one of two mechanisms to produce polymer: the classical coordination/insertion pathway and a Lewis acid activation also called the activated monomer mechanism (*Chapter 1, Figure III-1*).²¹ We set out to investigate the polymerization of ϵ -caprolactone (CL) and L-lactide (LA).

a. Polymerization without alcohol transfer agent

First of all, the polymerization has been investigated in the absence of transfer agent. In addition to thermally produce radicals, complex **3.1** may also have sufficient nucleophilic reactivity to act as a ROP initiator for cyclic esters. The polymerization of CL was tested at 120°C in bulk under argon, as illustrated in *Figure III-1-a*.

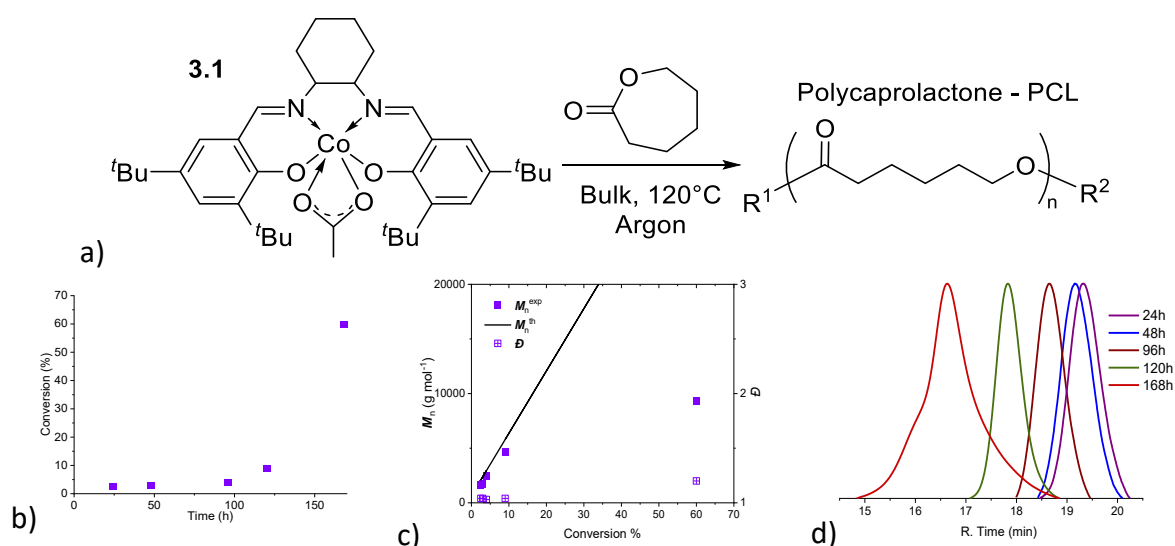


Figure III-1: a) Ring Opening Polymerization of ϵ -caprolactone initiated by the cobalt Schiff base acetate complex **3.1**; condition: $[\text{Co}]/[\text{CL}] = 1/500$, under argon in bulk at 120°C. (b) Conversion vs. time (c) M_n and \bar{D} vs. conversion. (d) GPC traces showing the evolution of the PCL molar mass distribution.

The conversion data in *Figure III-1-b* reveal an initially slow polymerization, reaching ca. 10% conversion after 120 h, followed by rapid monomer consumption. The GPC analysis (*Figure III-1-d*) indicates that the polymerization starts with the characteristics of a living chain growth, with narrow molar mass distributions and number average molar masses in close agreement with the theoretical values, as also shown by the data in Table III-1. In the fast polymerization regime, the molar mass deviates from the theoretical line towards lower values and the GPC signal becomes broader (*Figure III-1-d*). This suggests the intervention of chain transfer phenomena.

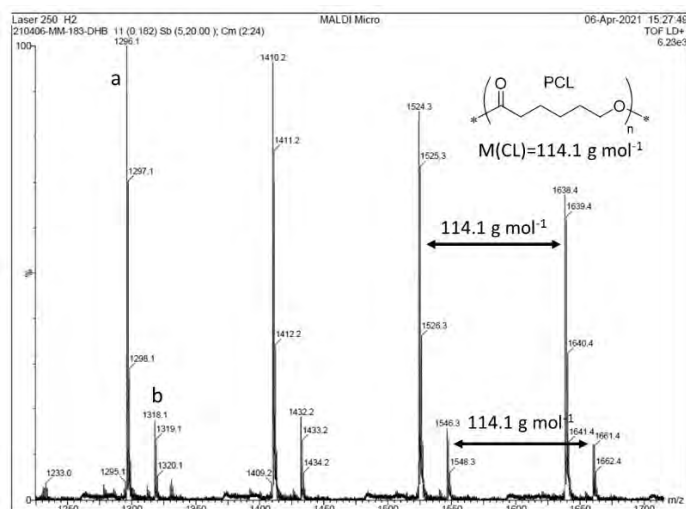
Table III-1: ROP of ϵ -caprolactone initiated by the $[(L^{1.1}Co(OAc))]^a$

Entry	Time (h)	Conv. (%) ^b	M_n^{corr} (g mol ⁻¹) ^c	M_n^{th} (g mol ⁻¹) ^d	\bar{D}^c
1	24	2	1 600	2 089	1.04
2	48	3	1 700	2 374	1.04
3	96	4	2 500	2 945	1.03
4	120	9	4 600	5 798	1.04
5	160	60	9 336	34 904	1.20

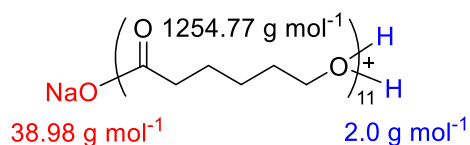
^aReaction condition: $[Co]/[M] = 1/500$ at $120^\circ C$ in bulk, ^bDetermined by 1H NMR analysis, ^cDetermined from GPC analysis by using THF as eluent and polystyrene standards and applying a correction factor of 0.56 for PCL.

^dCalculated according to the conversion ($M(CL)=114.14$ g mol⁻¹).

The polymer chain ends were investigated by MALDI-TOF mass spectrometry (Figure III-2) on a low molar mass PCL sample produced during the living polymerization regime (below 10% conversion). Two populations, one major and one minor, were observed and each of them shows the expected spacing of 114.1 g mol⁻¹ between subsequent members, which corresponds to the CL repeating unit. The highest peak of population a) at $m/z = 1296.1$ g mol⁻¹ corresponds to 11 monomer units ($11 \times 114.07 = 1254.77$ g mol⁻¹) plus 41.33 g mol⁻¹ for the two chain ends that correspond to 2H and NaO. The peak at $m/z = 1318.1$ g mol⁻¹ for the second population corresponds to the same polymer with one more sodium in place of the H atom in the OH terminus.



Population a) 1296.1 g mol⁻¹



Population b) 1318.1 g mol⁻¹

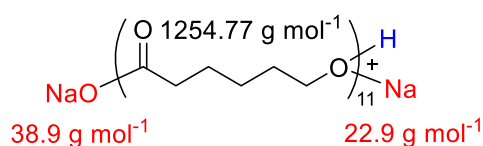


Figure III-2: MALDI-TOF mass spectrum of PCL. Matrix: Polymer/DHB/NaI = 1/3/1 (left). Proposed molecular formula (right).

The polymerization of lactide (LA) was also investigated, because this is also an important monomer for the fabrication of biodegradable polymeric materials. The tests were carried out under the same conditions of the above-described experiments with ϵ -caprolactone (Figure III-3a). The results, shown in Table III-2 and Figure III-3, are quite similar to those observed for CL: the number average molar mass shows a more or less linear increase with conversion, with values in agreement with the theoretical ones, until 10%, after which they deviate toward smaller values relative to theory, probably because of chain transfer reactions. In addition, at

the highest conversions, M_n showed a decrease and a large increase of dispersity. In addition to chain transfer process, the presence of intra/inter transesterification reactions may also account for this dispersity increase.

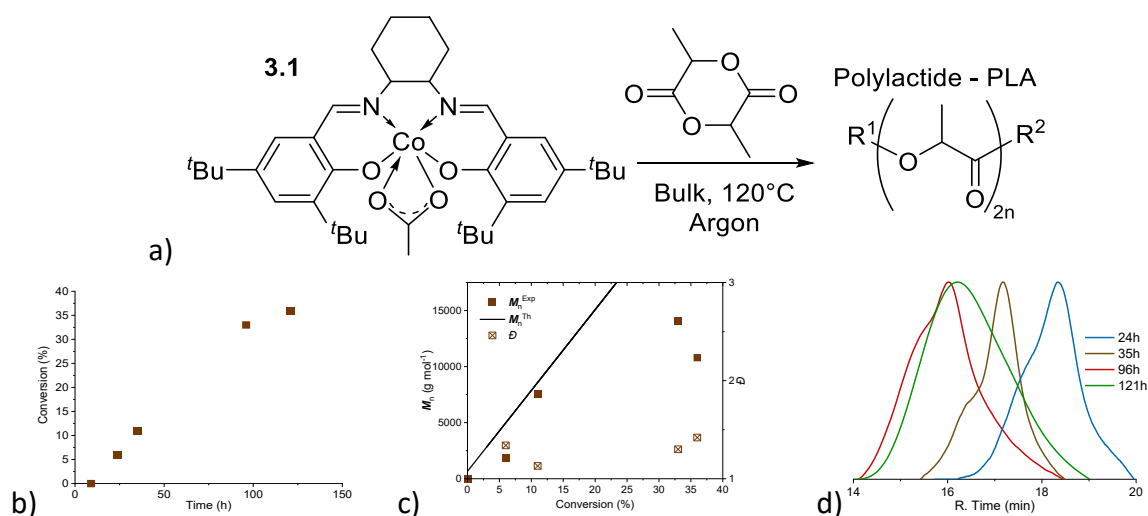


Figure III-3: a) Ring Opening Polymerization of LA initiated by **3.1**; conditions: $[Co]/[L-LA] = 1/500$, under argon in bulk at 120°C. b) Conversion vs. time. c) M_n and \bar{D} vs. conversion. d) GPC traces showing the evolution of the PLA molar mass distribution.

Table III-2: ROP of L-lactide initiated with the $[(L^{1.1})Co(OAc)]^a$.

Entry	Time (h)	Conv. (%) ^b	M_n^{corr} (g mol ⁻¹) ^c	M_n^{th} (g mol ⁻¹) ^d	\bar{D}^c
1	24	6	1897	4986	1.34
2	35	11	7596	8589	1.13
3	96	33	14068	24443	1.30
4	121	36	10800	26605	1.42

^aReaction conditions: $Co/M = 1/500$ at 120°C in bulk, ^bDetermined by ¹H NMR analysis, ^cDetermined from GPC analysis by using polystyrene standards and applying a correction factor of 0.58. ^dCalculated according to the conversion ($M(LA) = 144.13$ g mol⁻¹).

The MALDI-TOF mass spectrum was different depending on the selected matrix. Using either a dithranol/NaI matrix (Figure S10) or a DHB/NaI matrix (Figure III-4), the same two populations are observed with inversed relative intensities. The population with a peak at $m/z = 1287.8$ g mol⁻¹ (major when using dithranol/NaI) does not contain sodium and the positive charge is provided by addition of a proton, while the population with a peak at $m/z = 1265.9$ g mol⁻¹ (major when using DHB/NaI) corresponds to chains ionized by the addition of sodium cations. The two populations are interpreted as shown in Figure III-4. In all cases, the peaks are spaced by the mass of $\frac{1}{2}$ monomer unit, confirming the polymer nature as PLA.

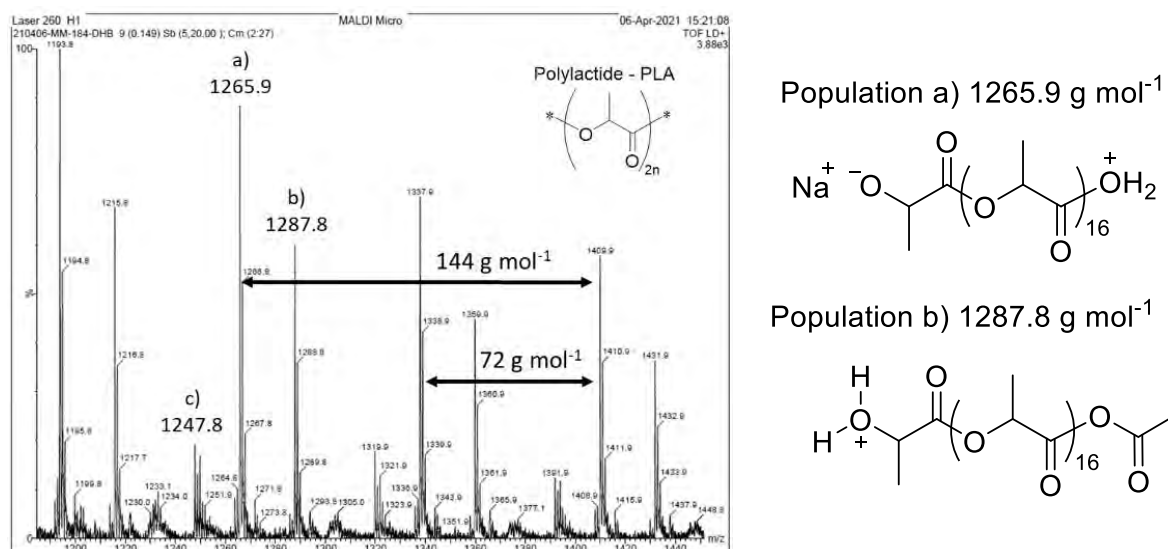


Figure III-4: Zoom of the MALDI-TOF mass spectrum of PLA obtained from a DHB-NaI 3/1 matrix (left) proposed polymer formulas (right).

Moreover, these analyses reveal three different populations. In fact, the $m/z = 1265.9 \text{ g mol}^{-1}$ peak corresponds to 8 monomer units ($1153.0 \text{ g mol}^{-1}$), which means that the chain end represents 112.9 g mol^{-1} , which corresponds to $\frac{1}{2}$ LA, Na and OH functions as described in Figure III-4. The second population with a peak at $m/z = 1287.9 \text{ g mol}^{-1}$ corresponds to the same polymer with an oxonium and the acetate fragment. For the third population, we were unable to make a reasonable hypothesis to fit the observed m/z values. To conclude, complex **3.1** is able to control the ROP of L-actide, but only for low molecular weights under classical conditions (no added alcohol). For that reason, the addition of alcohol (BnOH) was investigated in an attempt to improve the initiation mechanism (Chapter 1, Figure III-1).

b. Polymerization initiated by complex **3.1** in the presence of benzyl alcohol as chain transfer agent

To improve the system of the polymerization, alcohol was added to turn the living polymerization into an immortal polymerization, in the hope maintain the polymerization control up to greater conversion. The results obtained for LA and CL are presented in Table 3.

Table III-3: ROP of CL and LA initiated with $[(L^{1-1}\text{Co}(\text{OAc}))]$ in the presence of 0, 2 or 5 equivalent of BnOH.^a

Entry	Time (h)	M	Eq BnOH	Conv. (%) ^b	M_n^{corr} (g mol^{-1}) ^c	M_n^{th} (g mol^{-1}) ^d	\bar{D}^c
1			0	3	1690	2374 ^d	1.04
2	48	CL	2	9	2170	1820 ^e	1.10
3			5	16	1920	1630 ^f	1.10
4			0	16	10788	12192 ^d	1.34
5	48	LA	2	28	3862	6954 ^e	1.33
6			5	36	5275	4332 ^f	1.22

^aReaction conditions: $[Co]/[BnOH]/[M] = 1/X/500$ at $120^{\circ}C$ in bulk where X corresponding to the number of BnOH equivalents, ^bDetermined by 1H NMR analysis, ^cDetermined from GPC analysis by using polystyrene standards and applying a correction factor of 0.56 or 0.58 for PCL and PLA respectively. Calculated according to the number of transfer agents here ^d1, ^e3 or ^f6.

The addition of BnOH results in higher conversions, while the dispersities remain essentially unchanged. The conversion monitorings (Figure III-5a for CL and Figure III-5c for LA) clearly shows the increase of the polymerization rate with the increasing number of BnOH equivalents. Moreover, the molar masses increase linearly with the conversion (Figure III-5b for CL and Figure III-5d for LA). The decrease of the M_n vs. conversion slope as the number of BnOH equivalent is increased shows that a greater number of polymer chains are produced. This is fully consistent with the action of BnOH as a transfer agent in immortal polymerization. For the CL polymerization, the presence of BnOH allowed maintaining control up to higher conversions, because the molar mass continued to increase linearly, in relatively good agreement with the theoretical values, up to conversions of 15% or 22% for 2 and 5 equivalents, respectively, whereas M_n deviates from the theoretical line after a 10% conversion in the absence of benzyl alcohol. The same trend was observed for the PLA polymerization, although the higher dispersities indicate a lower level of control.

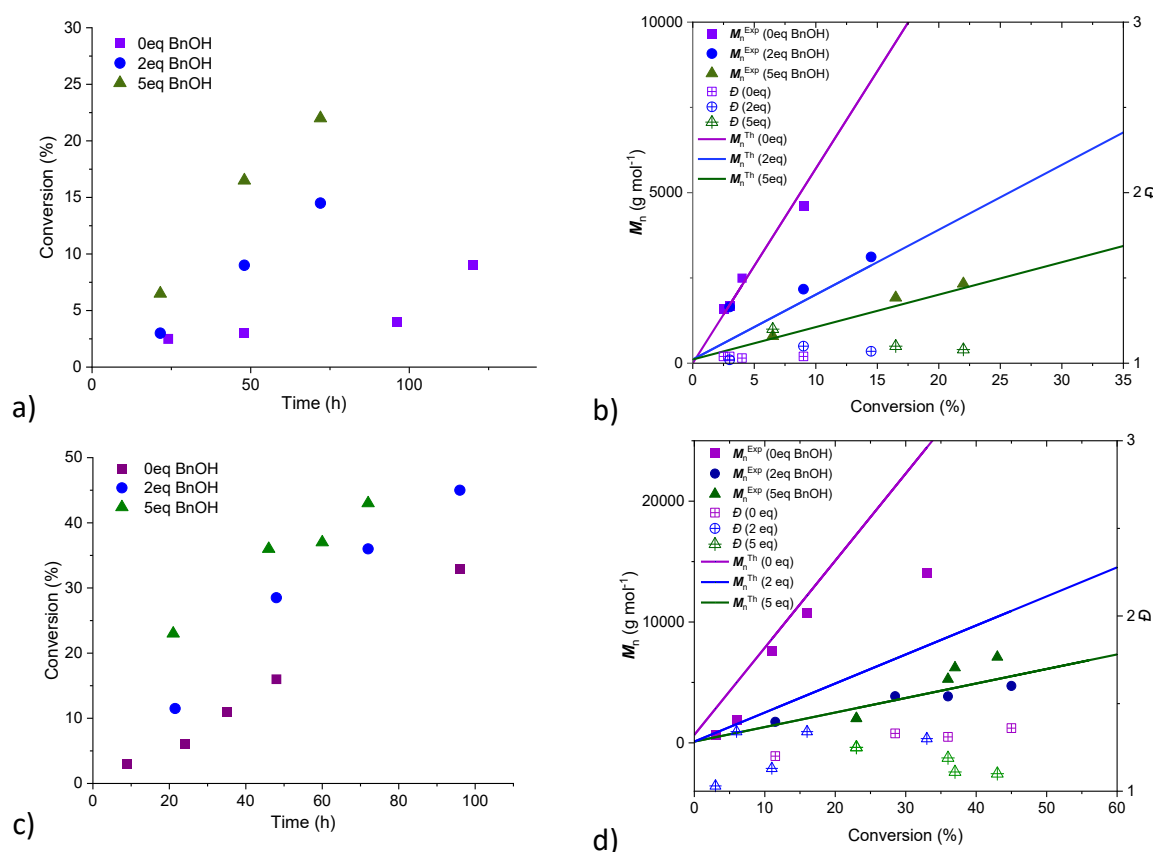


Figure III-5: (a) Kinetic of ϵ -caprolactone polymerization with conditions: $[Co]/X/[CL] = 1/X/500$ and 0 (■), 2 (●) or 5 (▲) equivalent of benzyl alcohol (BnOH) as function of cobalt (b) The plot of conversion vs. M_n vs. \bar{D} . (c) Kinetic of L-lactide polymerization with conditions: $[Co]/X/[LA] = 1/X/500$ and 0 (■), 2 (●) or 5 (▲) equivalent of benzyl alcohol (BnOH) as function of cobalt (d) The plot of conversion vs. M_n vs. \bar{D} .

The GPC analyses of both PCL and PLA products reveal bimodal shapes (*Figure III-6*). This could result from the occurrence of transesterification processes, especially considering the high reaction temperature.

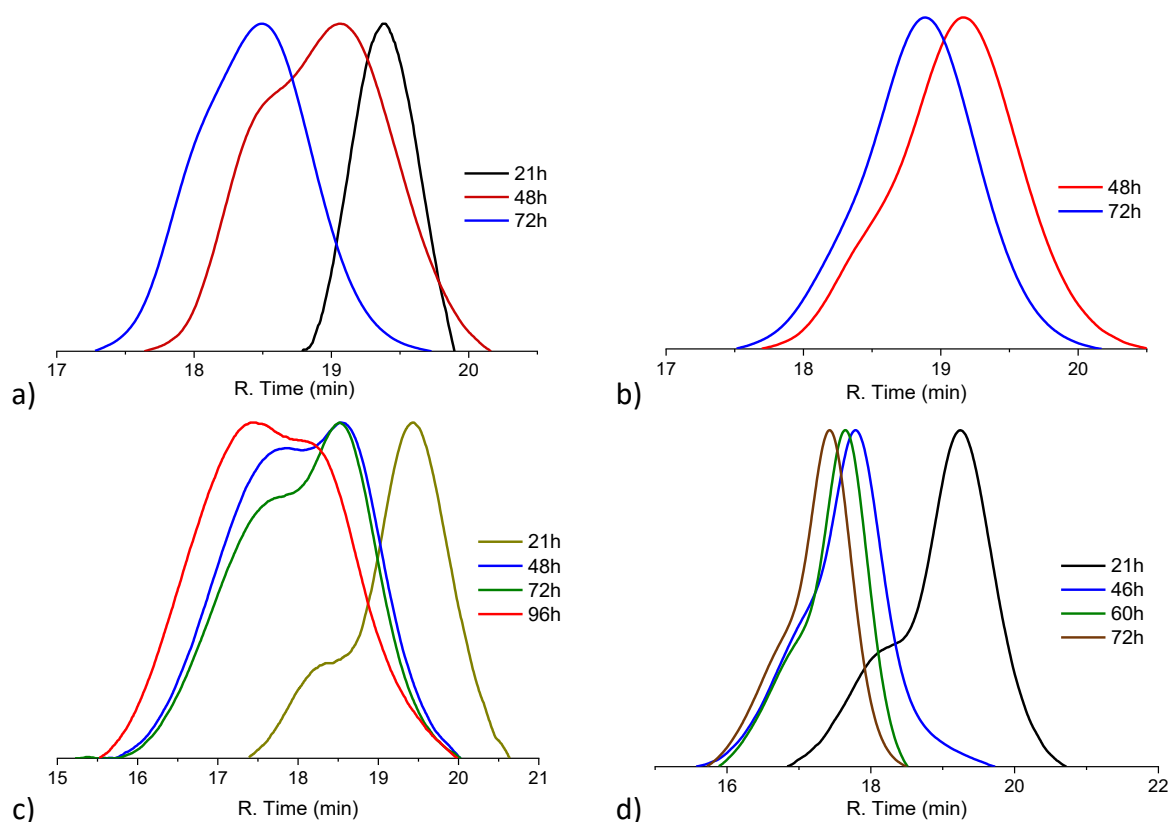


Figure III-6: GPC traces of the polymers (PCL, a and b; PLA, c and d) obtained by initiation with compound 3.1 and x equivalents of BnOH (x = 2, a and c; x = 5, b and d).

In conclusion, complex **3.1** can be used for the ROP of ϵ -caprolactone and L-lactide. However, the catalytic activity of this complex is quite low and the process is affected by side reactions, which take place at long reaction times, providing an unsuitable system if high conversions are desired. The addition of alcohol has allowed to improve the system by speeding up the polymerization and to reach higher conversions through the instalment of reversible chain transfer (immortal conditions). Nevertheless, this system is much less efficient than the best one reported in the literature by Thomas *et al.* in 2019, which is based on cobalt(II) complexes with tetradentate tripodal ligands and $N(\text{SiMe}_3)_2$ as reactive function.²⁹ For the ROP of LA carried out in toluene at room temperature (with one equivalent of *i*PrOH), the measured TOFs values was $2\,430\text{ h}^{-1}$ and the dispersity of the high molecular weights PLA samples were narrow (\mathcal{D} 1.06-1.09). (*cf. Chapter I, part III, section 8, Figure III-19*).²⁹

However, the objectives of this thesis work require the presence of the cobalt complex at the end of each chain for the polymerization mechanism switch, which means working under classical conditions with no added transfer agent.

c. Polymerization initiated by complex (3.3)

Due to the low efficiency of this complex in radical polymerization, only two polymerization tests were done with LA and CL to learn about the possible action of this complex as ROP initiator. As shown in Table III-4, after 72 h (48 h) at 100 °C (110 °C) a low conversion of LA (CL) produced a polymer M_n relatively close to the target value and narrow dispersity. The ROP of CL is slower and the produced PCL has M_n closer to the theoretical value. The GPC traces of both polymers (Figure III-7) are monomodal.

Table III-4: Polymerization test with 3.3.^a

Entry	M	Time (h)	Ratio [Co]/[M]	Temp. (°C)	Conv. (%) ^b	M_n^{corr} (g mol ⁻¹) ^c	M_n^{th} (g mol ⁻¹) ^c	\mathcal{D}^c
1	LA	72	1/200	100	18	10 500	5 900	1.14
2	CL	48	1/300	110	5	1 700	2 400	1.08

^aReaction condition: bulk under argon, ^bDetermined by ¹H NMR analysis, ^cDetermined from GPC analysis by using polystyrene standards and applying a correction factor of 0.56 or 0.58 for PCL and PLA respectively.

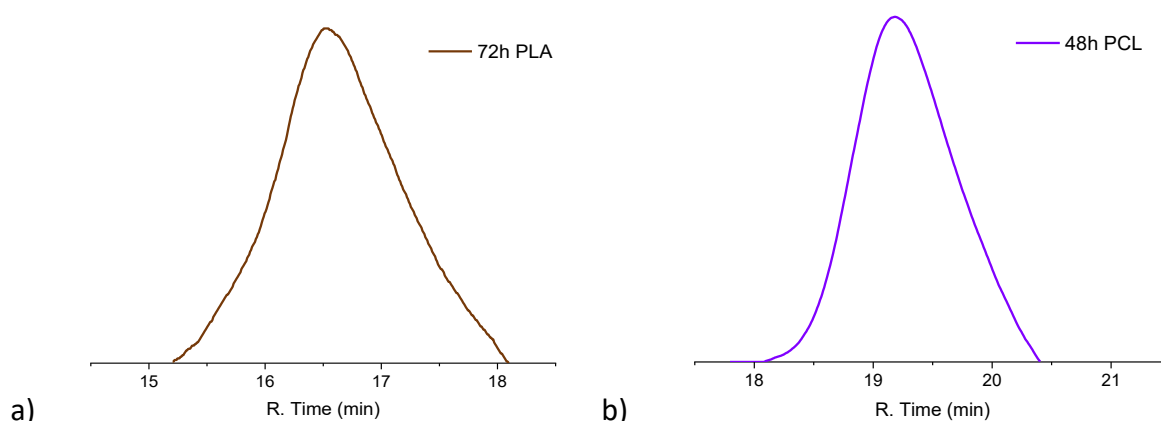


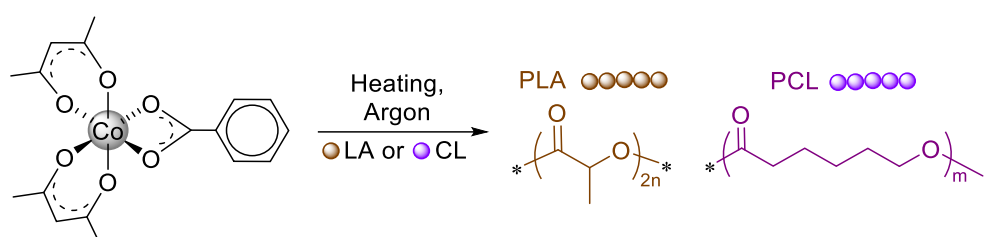
Figure III-7: Chromatograms of the polymers obtained with complex 3.3 (Table III-4): a) PLA; b) PCL.

This presented work with complex 3.3 is only a preliminary investigation. In the context of this thesis work, this complex was not further investigated because of its low efficiency in radical polymerization (radical production but uncontrolled polymerization). However, it would be interesting to carry out a deeper investigation in the presence of BnOH, independent of the mechanism switching objective.

3. (O₂,O₂)-Cobalt carboxylate complexes

a. Polymerizations initiated by [Co(acac)₂(O₂CPh)]

Complex [Co(acac)₂(O₂CPh)] (**3.6**) has been tested, like **3.1** and **3.3**, as an initiator and catalyst for the ROP of CL and LA (*Scheme III-2*).



Scheme III-2: Ring Opening Polymerization of LA and CL using (3.6).

The lactide polymerization was carried out at 100°C in bulk and at 90°C in toluene solution (2.5 mol L⁻¹). In each case, a shift of the molar mass distribution toward lower retention times in the GPC trace, a linear increase of the number average molar mass as a function of conversion and narrow dispersities in *Figure III-8* were observed, indicating the controlled nature of the polymerization. However, the measured molar masses are higher than the expected theoretical values, consistent with low initiation efficiency.

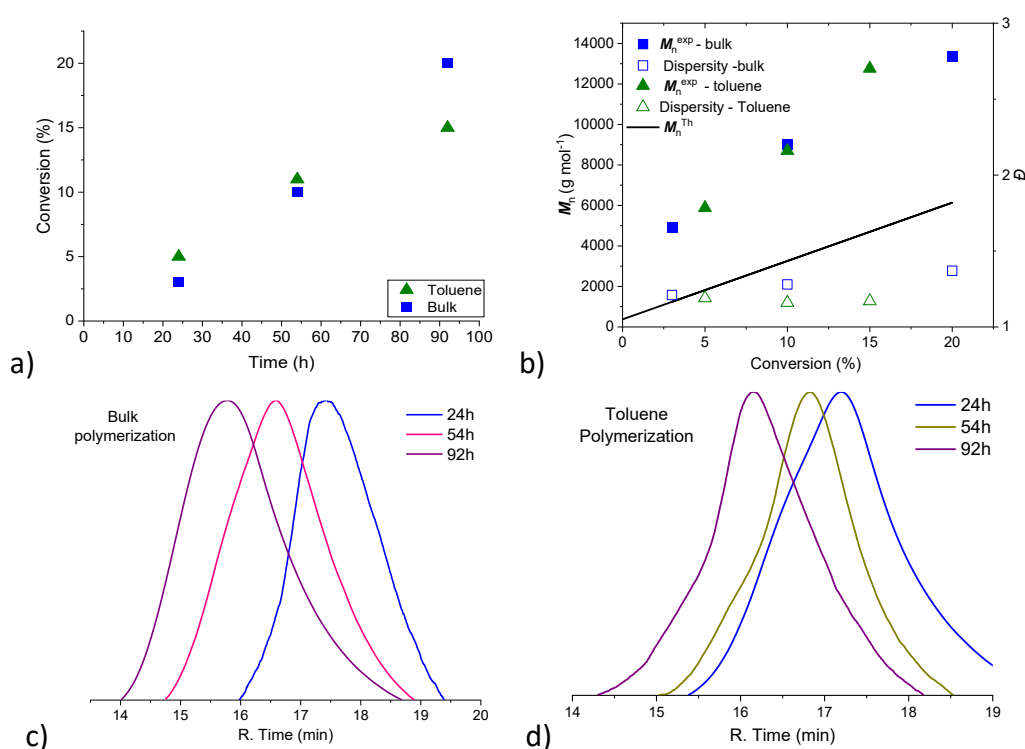


Figure III-8: LA polymerization at 100 °C in bulk and at 90 °C in toluene (LA/toluene = 2.5M), under argon, [Co]/[CL]=1/200: a) conversion vs. time; b) M_n and \bar{D} vs. conversion; c) GPC traces of the PLA obtained in bulk; d) GPC traces of the PLA obtained in toluene.

The polymerization of CL was carried out at 100°C in bulk in the presence of various equivalents of BnOH (0 to 5), *Figure III-9*. Like for the polymerization of LA and CL initiated by **3.1** (section III.2.b), the polymerization rate increased and the experimental molar masses decreased as the number of BnOH equivalent was increased, while the molar mass evolution remained linear. Like for the polymerization of LA initiated by **3.6**, the experimental M_n values are greater than the theoretical ones. Therefore, **3.6** is also able, like **3.1** to operate an immortal polymerization. We can conclude that this complex is promising for the thesis objective, because it can control both the radical polymerization of VAc and the ring opening polymerization of LA and CL.

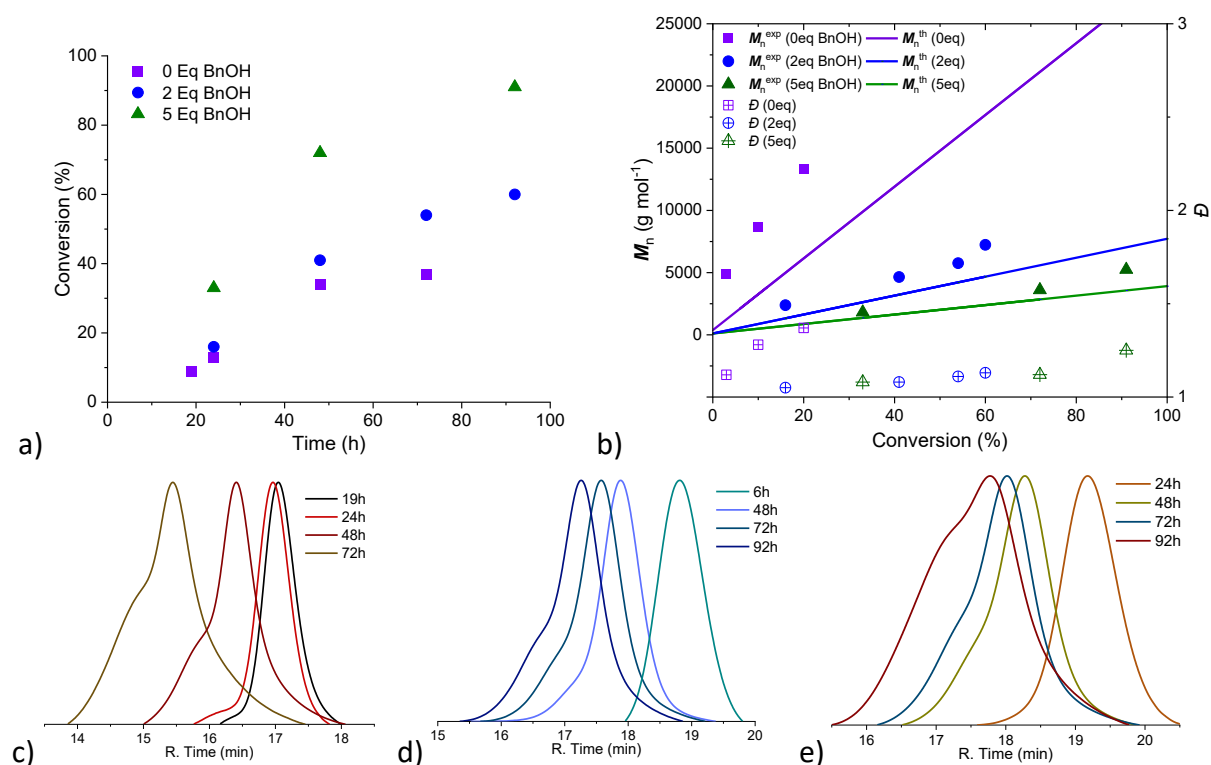


Figure III-9: CL polymerization initiated by complex 3.1 at 100°C in bulk, under argon, [Co]/[CL] = 1/200. a) Conversion vs. time. b) M_n and \bar{D} vs. conversion. c-e) GPC traces of the polymers obtained with X equivalents of BnOH (X = 0 (c); 2 (d); 5 (e)).

b. Polymerizations initiated by [Co(acac)₂OAc]

Due to its low stability, to the hazard of the diacetyl peroxide precursor used for its synthesis, and to the bad results obtained in radical polymerization (part II-3-c-i), the cobalt acetate complex **3.11** was not well investigated. A single polymerization test was carried out, for both CL and LA, at 120 °C in bulk. The recovered polymers showed the properties highlighted in Table III-5. Like the polymer obtained in the presence of complex **3.6**, the molar masses were higher than expected and dispersity was narrow, particularly for PCL (see GPC traces in *Figure III-10*).

Table III-5: ROP of CL and LA initiated by the $\text{Co}(\text{acac})_2(\text{OAc})$.^a

Entry	Time (h)	M	Conv. (%) ^b	M_n^{corr} (g mol^{-1}) ^c	M_n^{th} (g mol^{-1}) ^d	\bar{D} ^c
1	31	CL	10	6 300	2 600	1.02
2	24	LA	37	20 200	11 000	1.29

^aReaction conditions: $[\text{Co}]/[\text{M}] = 1/200$ at 120°C in bulk. ^bDetermined by ^1H NMR analysis. ^cDetermined by GPC analysis. ^dCalculated according to the conversion ($M(\text{CL}) = 114.14 \text{ g mol}^{-1}$ and $M(\text{LA}) = 144.12 \text{ g mol}^{-1}$).

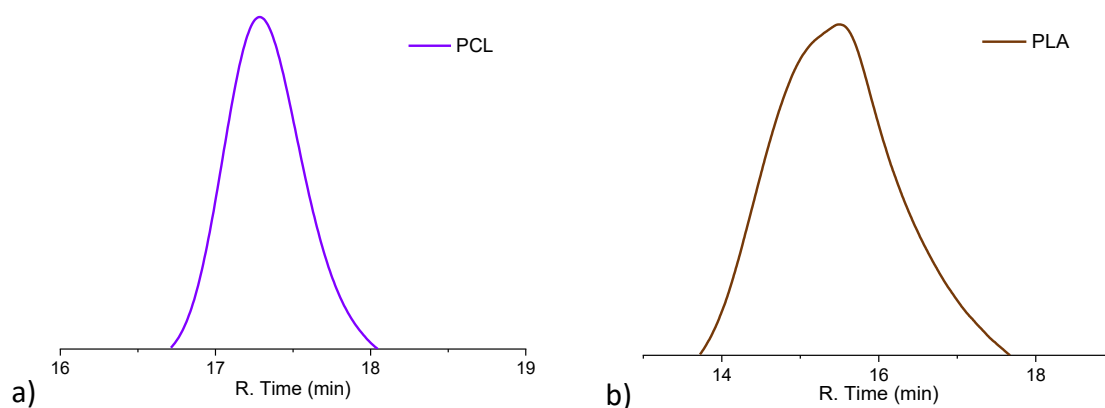


Figure III-10: Chromatogram of the resulting polymers a) PCL and b) PLA obtained with condition $[\mathbf{3.11}]/[\text{M}] = 1/200$, 120°C in bulk.

The ROP polymerization tests with complex **3.11** closes the discussion of this chapter on the efficiency of cobalt(III) carboxylate complexes for the direct initiation of the cyclic esters.

4. Conclusion

Even though, in this thesis work, the homopolymer production by ROP was less investigated than the radical polymerization processes, based on the various results highlighted in this section, it is possible to conclude that the cobalt(III) carboxylate complexes are able to induce a nucleophilic attack to start the ROP of LA and CL. Complex $[\text{Co}(\text{acac})_2(\text{O}_2\text{CPh})]$ (**3.6**) seems the most efficient catalyst for the production of polyesters, whereas complex $[\text{Co}(\text{L}^{1.1})\text{OAc}]$ (**3.1**) yields well-defined living polymers only at very low monomer conversions (less than 10%).

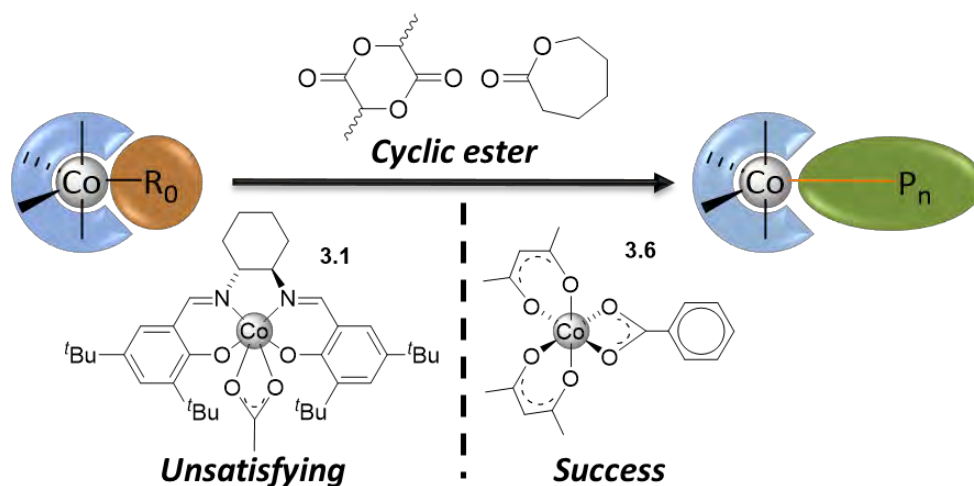
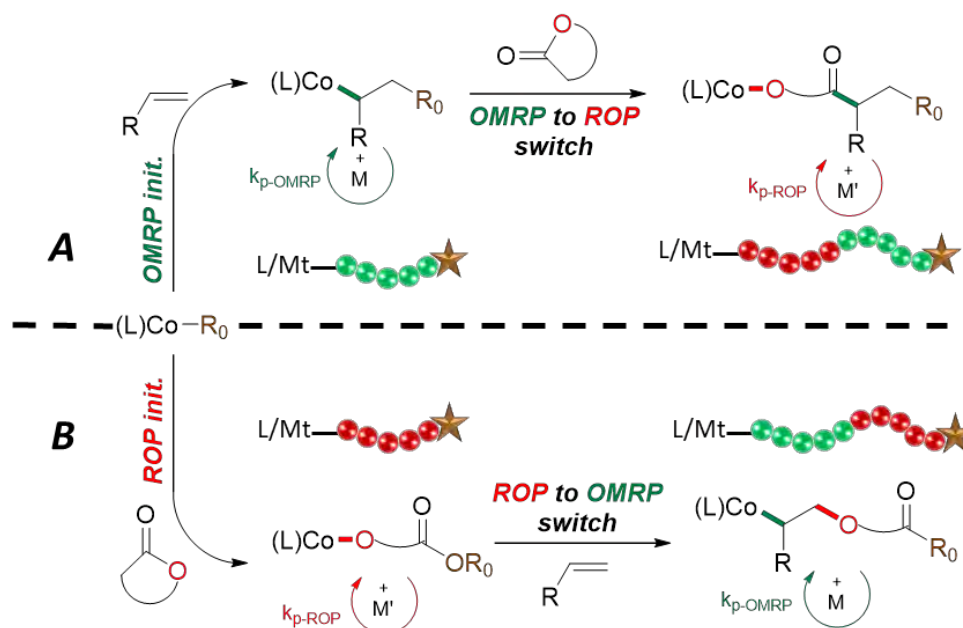


Figure III-71: Cobalt system involve ROP of LA and CL, which will be investigate for the polymerization switch.

No information could be obtained so far on the nature of the macromolecule chain ends; this is an important point that will require future investigations. Consequently, the question now is around the capacity of the putative $\text{Co}-\text{O}$ chain end to induce the required homolytic cleavage for the generation of radicals able to add to a vinyl monomer for chain extension with the OMRP technique. Another question is whether the $\text{Co}-\text{C}$ bond in the OMRP dormant species is nucleophilic enough to attack and ring-open the cyclic ester monomers, for chain extension with the ROP technique. The next section highlights the polymerization switch tests carried out so far with the most promising complexes (**3.1** and **3.6**) from OMRP to ROP and in the reverse direction (from ROP to OMRP).

IV. Polymerization switch

As mentioned throughout this manuscript, the objective of this thesis project is to design a metallic complex able to act as a single-molecule (additive-free) moderator and initiator of both the radical polymerization of vinyl monomers and the ring opening polymerization of cyclic esters, which are based on different mechanisms and reactivities. As a reminder, the principal issues of the two first parts were to highlight whether the cobalt-carboxylate architecture, which is relatively new, is capable to initiate the polymerization of vinyl monomers by homolytic Co^{III}-O bond cleavage and that of cyclic ester monomers by nucleophilic attack and ring opening. Both goals were and successfully achieved. The present final and most challenging part is to use these systems for block copolymers syntheses with the first block produced by one reactivity mode (radical or coordination/insertion) and switch the polymerization mechanism to generate the second block by the second mechanism, without chemical modification of the chain end. In fact, as described in the bibliographic chapter, this kind of original block copolymers were already achieved with various methods³ such as the use of difunctional initiator^{1, 30-33} or with chemical modification of the end-chain^{4, 5, 34} after the first block synthesis.



Scheme IV-1: Strategy for the mechanistic switch between radical (green) and ring opening (red) polymerizations.

Scheme IV-1 describes the polymerization switch strategy. Route A uses a cobalt(III) carboxylate complex to initiate radical polymerization, as described in the present chapter (section II) and yielding a dormant species with a cobalt-alkyl bond at the ω chain end. The remaining question is whether this cobalt-alkyl bond is nucleophilic enough, even though the presence of a vacant site permits, in theory, the coordination of the LA or CL monomer.

In the case of route B, the efficiency of the various cobalt(III) carboxylate complexes as ROP initiators, generating living chains with a cobalt-alkoxide bond at the ω chain end have been demonstrated in section III. However, this new chain end is different from that of the OMRP-initiating carboxylate complex and the potential homolytic cleavage of this kind of bond is still unexplored. In the literature, a few systems were shown to need CO insertion to modify the cobalt-alkoxide bond into a cobalt-acyl bond, making it possible to trigger the homolytic cleavage and start the radical polymerization.⁴

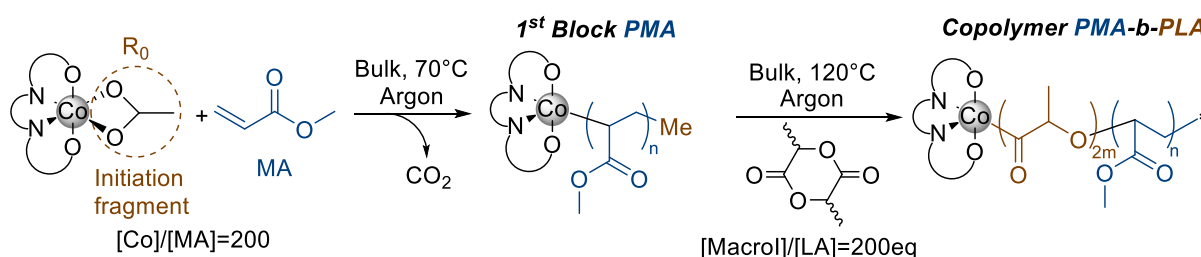
In the first part of this section, tests aimed at synthesizing block copolymers by sequential homopolymerization, with a switch from OMRP to ROP (*Scheme IV-1*, route A) and in the opposite direction (*Scheme IV-1*, route B) will be presented. Subsequently, a brief exploration of a one-pot procedure and perspectives in terms of the potential degradability of the polymers formed will be discussed.

1. Sequential polymerization processes (Block copolymers)

Based on the results previously presented in this thesis, only complexes **3.1** and **3.6** were used to explore this strategy.

a. Switch from OMRP to ROP

The first polymerization test was conducted using $[\text{Co}(\text{L}^{1.1})\text{OAc}]$ (**3.1**), which was found able to control the radical polymerization of MA to produce $[\text{PMA-Co}(\text{L})]$. This product was then tested as a macroinitiator for the ROP of LA *Figure II-8*.



Scheme IV-2: Sequential block copolymer PMA-b-PLA synthesis mediated with 3.1.

A macroinitiator of 19 000 g mol⁻¹, made as previously described (section II-1.b), was placed in presence of L-lactide for the chain extension reaction in bulk at 120°C. However, as highlighted in the GPC traces of *Figure IV-1*, no chain extension occurred after 24 h. The molar mass distribution of the macroinitiator did not shift, suggesting that the PMA chains were not extended, while a shoulder appeared at higher retention times (lower molar masses), suggesting the formation of PLA homopolymer chains.

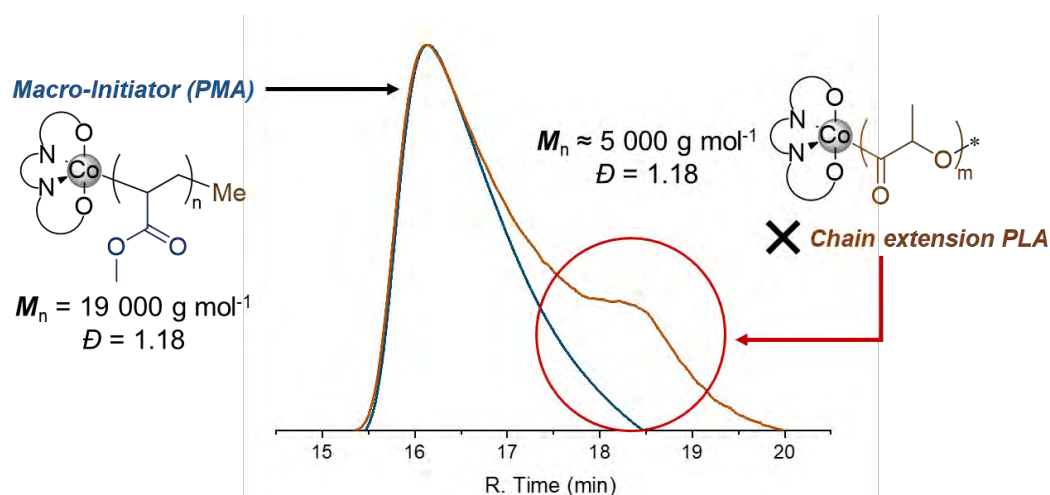
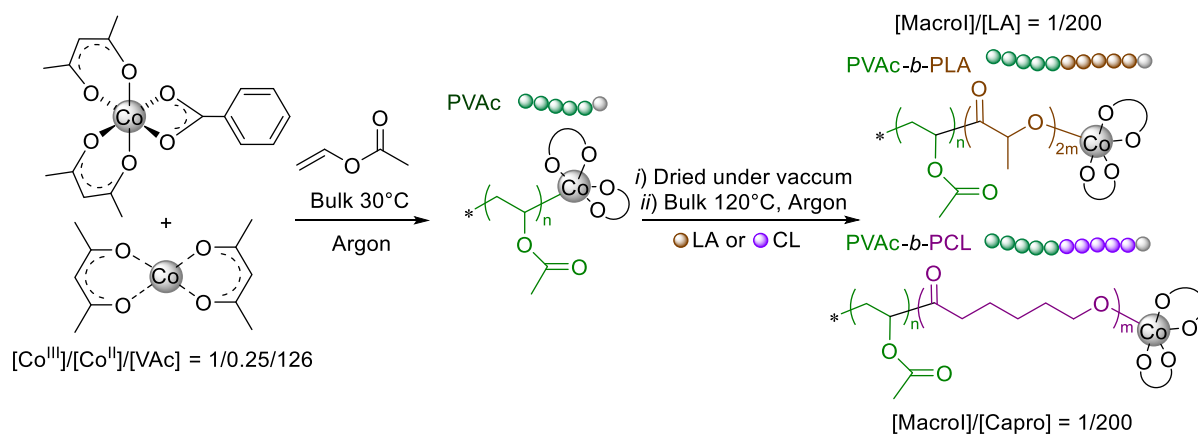


Figure IV-1: GPC of the polymer resulting from the LA polymerization in the presence of a $[(L)Co-PMA]$ macro-initiator in bulk at $120\text{ }^{\circ}C$; $[(L)Co-PMA]/[LA] = 1/200$.

Unfortunately, this approach could not be more deeply explored due to the lack of time. It would be interesting to test the same reaction with a smaller amount of macroinitiator or using ϵ -caprolactone (CL) or propylene oxide (PO) as ROP monomers.

Deeper investigations were carried out using the new benzoate complex developed in this thesis, $[Co^{III}(acac)_2(O_2CPh)]$ (**3.6**), and the resulting $[PVAc-Co^{III}(acac)_2]$ macroinitiator. Samples of this macroinitiator with M_n around 4000 g mol^{-1} , prepared as described above (section II-3.a), were used to re-initiate the polymerization of LA and CL in bulk at $120\text{ }^{\circ}C$, Scheme IV-3. The polymerization experiments and reaction conditions are summarized in Table IV-1.



Scheme IV-3: Sequential copolymerization of VAc by OMRP and LA or CL by ROP.

Table IV-1: Block copolymer syntheses.

Entry	Polymer	Temp. (°C)	Time (h)	Conv (%)	M_n^{Exp} ($g\ mol^{-1}$) ^f	\bar{D}^f	Diffusion Coeff. (m^2/s)
1 ^a	PVAc	30	7.2	3.0 ^d	4 012	1.11	3.1×10^{-10}
2 ^a	PVAc	30	7.0	2.8 ^d	3 635	1.11	-
3 ^b	PVAc- <i>b</i> -PLA	120	19.0	26.0 ^e	17 980	1.25	5.0×10^{-11}
4 ^c	PVAc- <i>b</i> -PCL	120	19.0	17.0 ^e	8 400	1.07	1.1×10^{-10}
5 ^c	PVAc- <i>b</i> -PCL	100	42.0	12.0 ^e	6 110	1.07	-

^a $[Co^{III}]/[Co^I]/[VAc] = 1/0.25/200$, bulk, under argon. ^b $[MacroInitiator-1]/[M]=1/500$. ^c $[MacroInitiator-2]/[M]=1/500$, conversion Determined by ^dgravimetry, ^eNMR. ^fDetermined from GPC analysis by using polystyrene standards and applying a correction factor of 0.56 or 0.58 for PCL and PLA extension, respectively.

The GPC analysis of the macroinitiator and final products are presented in Figure IV-2. For both chain extension reactions, the molar mass distribution of the PVAc macroinitiator in green shifts to lower retention time, while remaining narrow and monomodal, for the block copolymers products ($18\ 000\ g\ mol^{-1}$ and $8\ 400\ g\ mol^{-1}$ for PVAc-*b*-PLA and PVAc-*b*-PCL, respectively). Moreover, the signal of the initial PVAc macroinitiator disappears. These results strongly suggest the success of the chain extension reactions and thus support the nucleophilic reactivity of the Co^{III} -PVAc chain to attack the first coordinated cyclic ester molecule (LA or CL) and switch the polymerization mechanism from OMRP to ROP without any chemical modification.

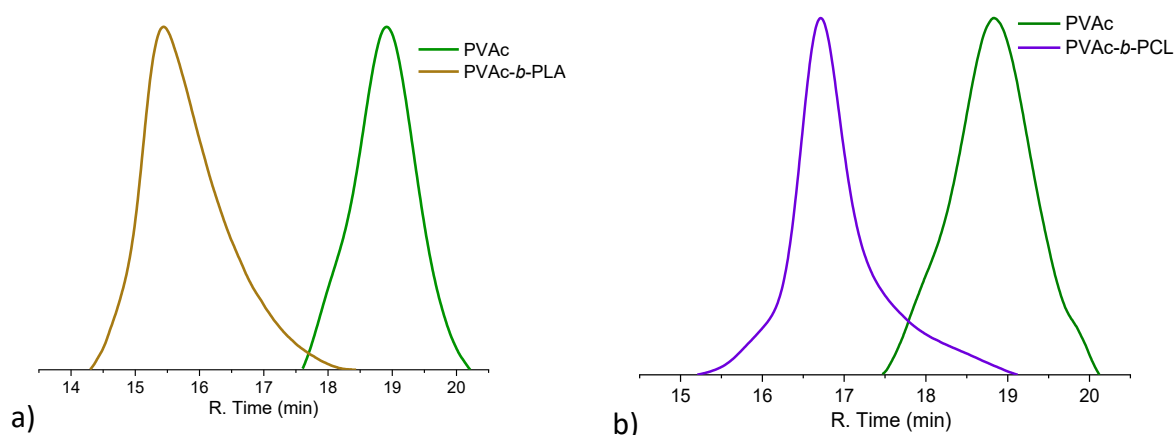
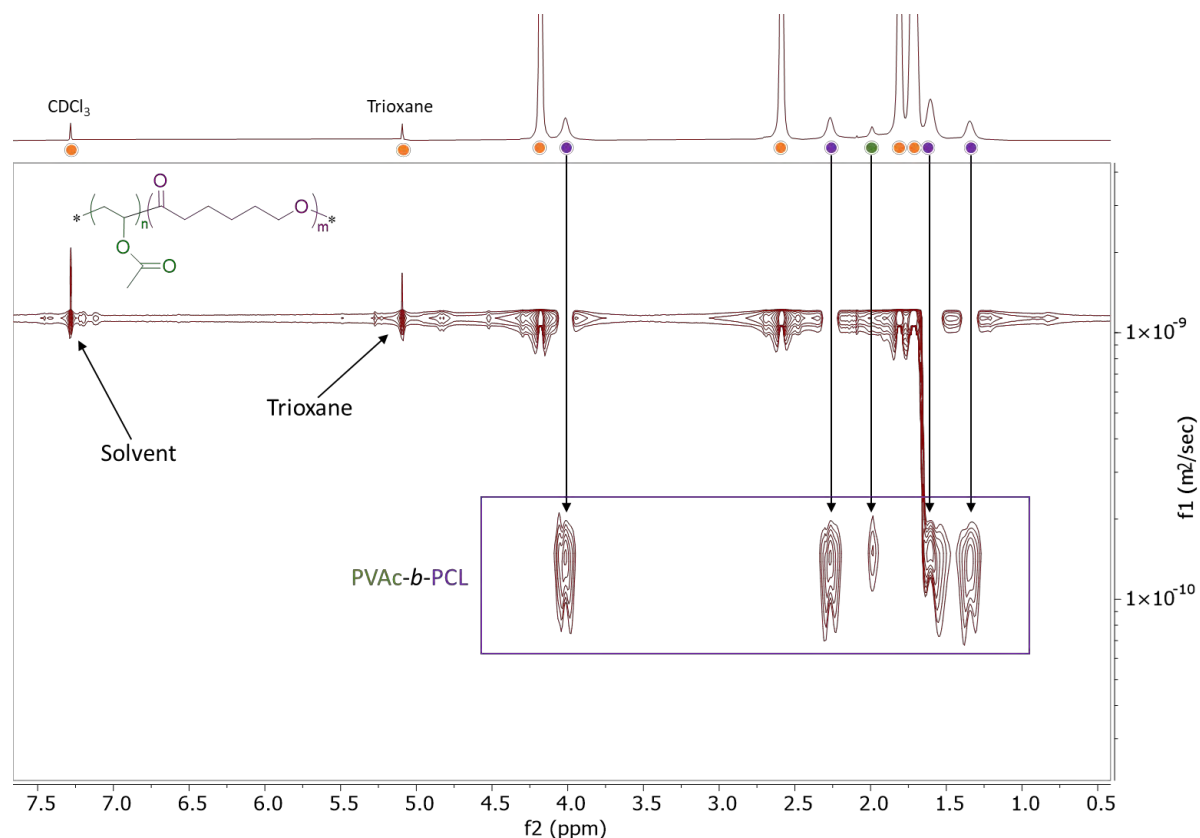


Figure IV-2: Chromatogram obtained of chain extension of macroinitiator PVAc (green) with a) lactide and b) caprolactone recorded with GPC-THF polystyrene calibration.

In order to validate the formation of block copolymer chains, the products were analysed by ¹H DOSY-NMR. This technique is a 2D experiment, consisting of a correlation of the ¹H NMR signals with the diffusion coefficient (D) of the molecule that generates that signal. Thus, signals of protons that are located on the same macromolecules will correspond to the same D value. The DOSY-NMR spectrum of the PVAc-*b*-PCL product is shown in Figure IV-3. The signals are clearly aligned along two D values. Those with greater D (ca. $10^{-9}\ m^2/s$) correspond

to the small molecules, namely residual monomer (CL), trioxane and solvent (CDCl_3) that are still present in the reaction medium at the end of the polymerization, represented with an orange dot in *Figure IV-3*. The signals with $D = 1.1 \times 10^{-10} \text{ m}^2/\text{s}$ correspond to the PVAc-*b*-PCL product. The characteristic signals of both PCL (purple dots) and PVAc (methyl group at δ 2.00 ppm, green dot) have the same diffusion coefficient, as expected if they are located on the same diblock macromolecule.



*Figure IV-3: DOSY-NMR of the PVAc-*b*-PCL block copolymer, recorded in CDCl_3 .*

The DOSY NMR spectrum of the $[\text{PVAc-Co}^{\text{III}}(\text{acac})_2]$ macroinitiator (*Figure S11*) shows all polymer resonances with a higher diffusion coefficient of $3.1 \times 10^{-10} \text{ m}^2/\text{s}$. Note that no signals are present in the *Figure IV-3* at this D value, demonstrating the successful chain extension. The PVAc-*b*-PLA product was also characterized by DOSY-NMR (*Figure S14*). Like for PVAc-*b*-PCL, all copolymer resonances are clearly aligned at the same D value, which is smaller than that of the macroinitiator and no intensity is observed in correspondence to the macroinitiator D value.

Another polymerization test was carried out to optimize the synthesis. Notably, the polymerization of the second block was carried out at a lower temperature. This experiment was carried out only for the extension with PCL, because the CL monomer is liquid (m.p. -1°C), whereas LA is solid (m.p. ca. 95°C) and needs high temperatures to operate under melt condition for a bulk polymerization. At 100°C , the chain extension was slower, yielding a very low conversion after 19 h and only a small shift for the GPC signal (*Figure IV-4*). Continuation

of the polymerization gave a 12% conversion after 41 h and yielded a PVAc-*b*-PCL product with a very narrow and monomodal molar mass distribution (*Table IV-1*).

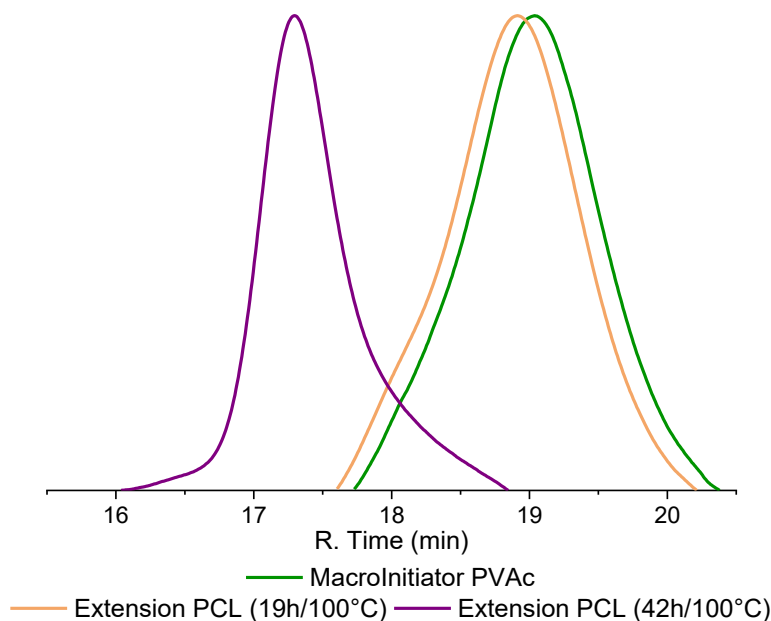


*Figure IV-4: Chromatograms of the chain extension reaction PVAc-*b*-PCL at 100°C, recorded with GPC-THF polystyrene calibration.*

Additional characterization of these copolymers, for instance by DSC and TGA, could not yet be accomplished because of time limitations. It will be interesting to compare the properties (T_g , T_m , degradation temperature) with those of the homopolymers.

b. Switch from ROP to OMRP

In order to operate the switch from ROP to OMRP, which is represented by route B in *Scheme IV-1*, a short [PLA-Co(L)] (2000 g mol^{-1}) was first synthesized using complex **3.1** and then used as macroinitiator for the chain extension in the presence of MA under bulk condition at 40°C. However, no monomer conversion was observed by gravimetry or ^1H NMR and the GPC analysis of the recovered polymer (*Figure S15*) showed no change with respect to the macroinitiator signal. Therefore, further efforts were focused on the bis(acetylacetonato) system.

For practical reasons (limited availability of the [PLA-Co^{III}(acac)₂] and [PCL-Co^{III}(acac)₂] living polymers), this extension trial used the living [PVAc-*b*-PCL-Co^{III}(acac)₂] copolymer described in the previous section as macroinitiator, which contains the same potentially reactivable Co-alkoxide chain end.

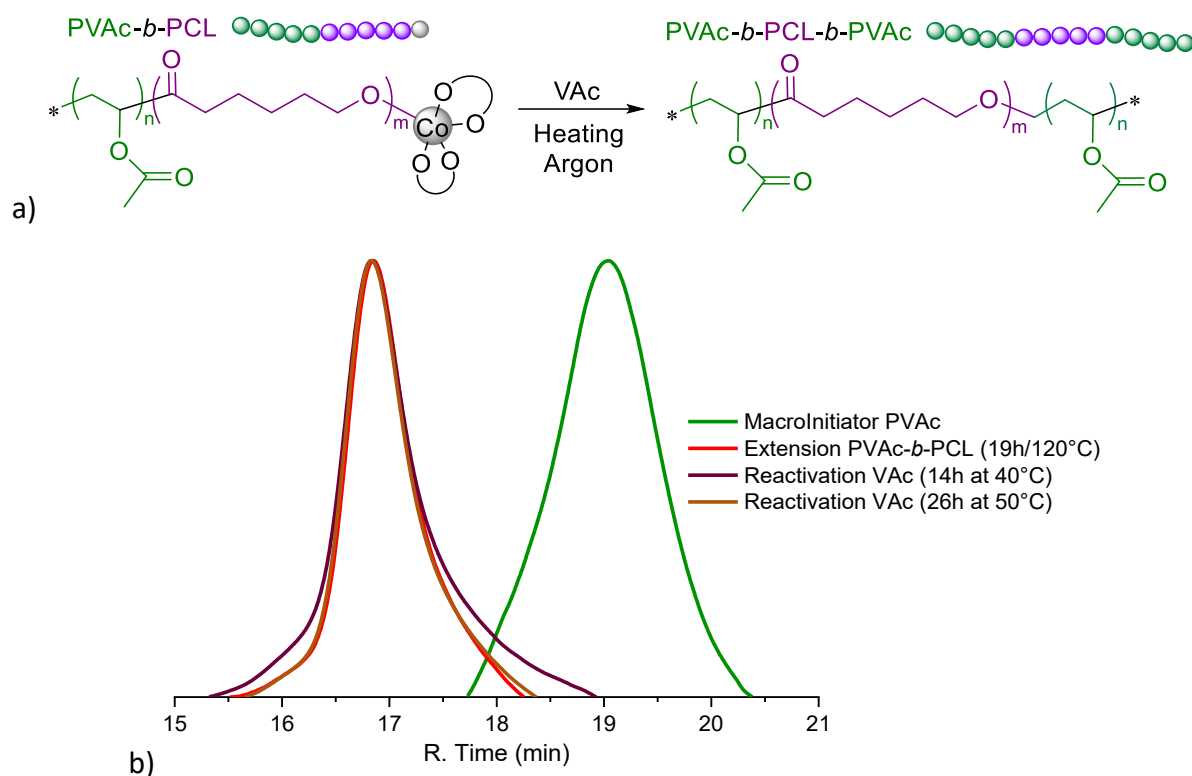


Figure IV-5: a) Chain extension reaction of the diblock PVAc-b-PCL, b) Chromatograms of the chain extension test of the diblock with VAc, recorded with GPC-THF polystyrene calibration.

However, as highlighted by the invariance of the GPC signal (Figure IV-5), the macroinitiator was not reactivated by VAc at 40 or 50°C. Another test was carried out using the $[\text{PCL-Co}^{\text{III}}(\text{acac})_2]$ macroinitiator, produced as described in section III-3.a, in the presence of a large excess of either MA or VAc at 50°C during 24 h. In these cases, a small shift of the molar mass distribution is revealed by the GPC analysis of the recovered polymer, which suggests chain extension. However, no further evolution of the GPC trace occurred after 50 h of reaction.

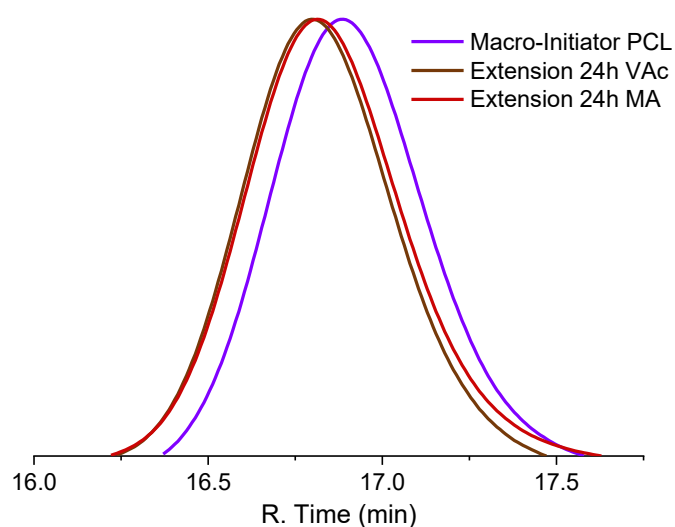
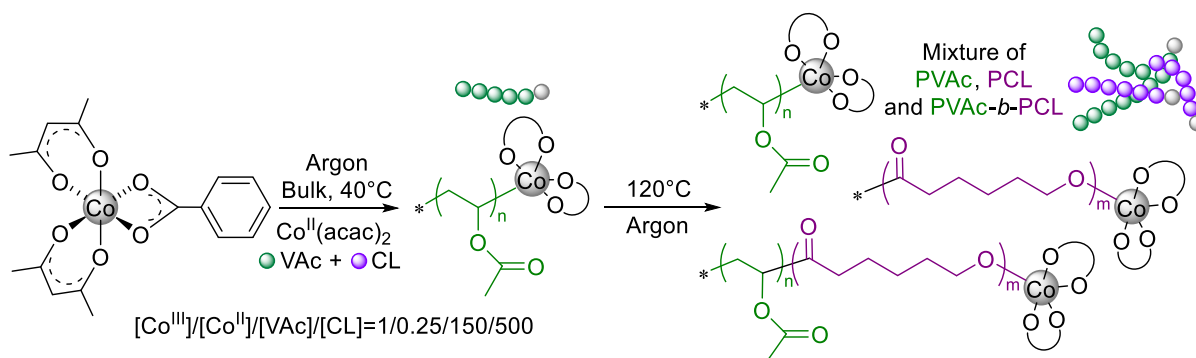


Figure IV-6: Chain extension reaction of the macro-initiator PCL with VAc and MA.

Moreover, the DOSY NMR (*Figure S16*) of the recovered polymer revealed only the PCL signals with coefficient diffusion of $1.3 \times 10^{-10} \text{ m}^2/\text{s}$. This means that the cobalt-alkoxide chain end cannot be reactivated by homolytic cleavage for radical generation. As of this moment, we have not found conditions that allow a polymerization switch from ROP to OMRP. In perspective, the chain extension may perhaps be tested with macroinitiators built from other cyclic esters.

2. One pot procedure (Mixture of PVAc & PCL)

As described in section II.3.a, the efficiency factor of complex **3.6** as a radical polymerization initiator is low (less than 20%). However, this property may be turned into an advantage. In fact, **3.6** was shown capable to initiate and control both the radical polymerization of VAc (at 30°C) and the ROP of CL (at 100°C or higher). Therefore, using a VAc/CL comonomer mixture in one pot at low temperature, only [PVAc-Co^{III}(acac)₂] homopolymer chains should grow by OMRP, while the CL monomer should not be polymerized. Subsequently, a temperature increase to 100 °C and the presence of a large fraction of unreacted **3.6** should induce the generation of [PCL-Co^{III}(acac)₂] homopolymer chains by ROP, but also the chain extension of the [PVAc-Co^{III}(acac)₂] chains to generate [PVAc-*b*-PCL-Co^{III}(acac)₂], as shown in section IV-1.a. This one-pot strategy is highlighted in *Scheme IV-4* below. This method cannot be applied to lactide, because this monomer is solid at 40°C. It may be possible to use a solvent such as toluene to solubilize the lactide monomer. However, this possible extension could not be explored due to time limitation and may be the subject of future work.



Scheme IV-4: One pot polymerization process.

Experimentally, caprolactone served as the solvent for the VAc polymerization at low temperature. After 45 hours the temperature was increased to 120°C and the CL was also polymerized. After a few tests to optimize the conditions, a polymer blend was prepared using the optimized ratio $[\text{Co}^{\text{III}}]/[\text{Co}^{\text{II}}]/[\text{VAc}]/[\text{CL}] = 1/0.25/150/500$. The GPC analysis (*Figure IV-7*) shows a broader molar mass distribution for the final polymer blend (purple trace) relative to the [PVAc-Co^{III}(acac)₂] homopolymer intermediate (analyzed prior to the second step at higher temperature, green trace), indicating the formation of low molar-mass [PCL-Co^{III}(acac)₂] homopolymer chains. A broadening of the distribution towards lower retention times suggests

that the extension of the $[\text{PVAc-Co}^{\text{III}}(\text{acac})_2]$ macroinitiator to yield $[\text{PVAc-}b\text{-PCL-Co}^{\text{III}}(\text{acac})_2]$ diblock chains may also have occurred.

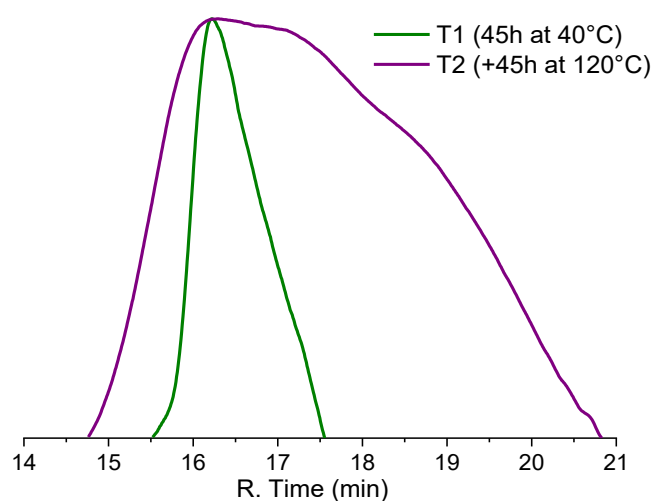


Figure IV-7: GPC analysis of the intermediate $[\text{PVAc-Co}^{\text{III}}(\text{acac})_2]$ and final polymer blend for the **3.6**-initiated one-pot copolymerization process.

The ^1H NMR monitoring of the polymerization process (Figure IV-8) provides further evidence in favor of the stepwise polymerization. Initially (T_0) no polymers resonances are visible. After 40 hours at 40°C (T_1), the PVAc formation (22% of conversion) is evident from the OMe resonance at ca. 5.1 ppm in the green box, while no PCL (OCH_2 resonance at ca. 3.95 ppm) is visible in the purple box. This confirms that VAc polymerizes at 40°C while CL does not. After heating at 120°C for an additional 45 h (T_2), the PVAc signal has increased (70% of conversion) and the PCL signal has appeared (5% of conversion purple box).

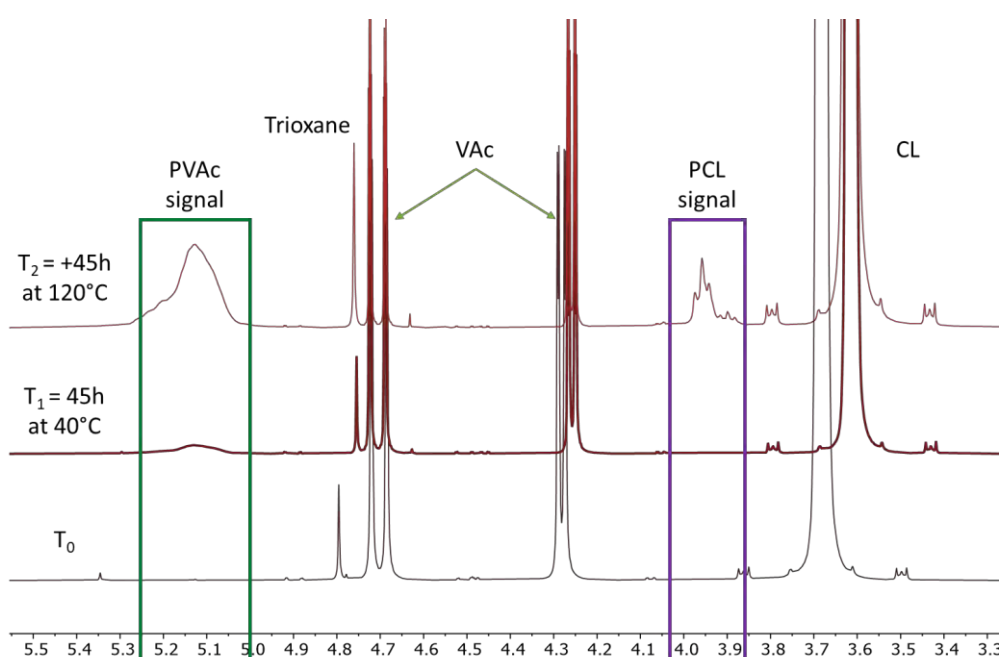


Figure IV-8: ^1H NMR monitoring of the one-pot copolymerization processes of VAc and CL initiated by complex **3.6**, recorded in CDCl_3 , 400 MHz.

The ^1H DOSY-NMR spectrum of the recovered final polymer blend is shown in *Figure IV-9*. In addition to the resonances of the small molecules (residual monomers, solvent) at a high D value (ca. $1 \times 10^{-9} \text{ m}^2/\text{s}$), the polymer resonances are essentially grouped around two different and lower D values.

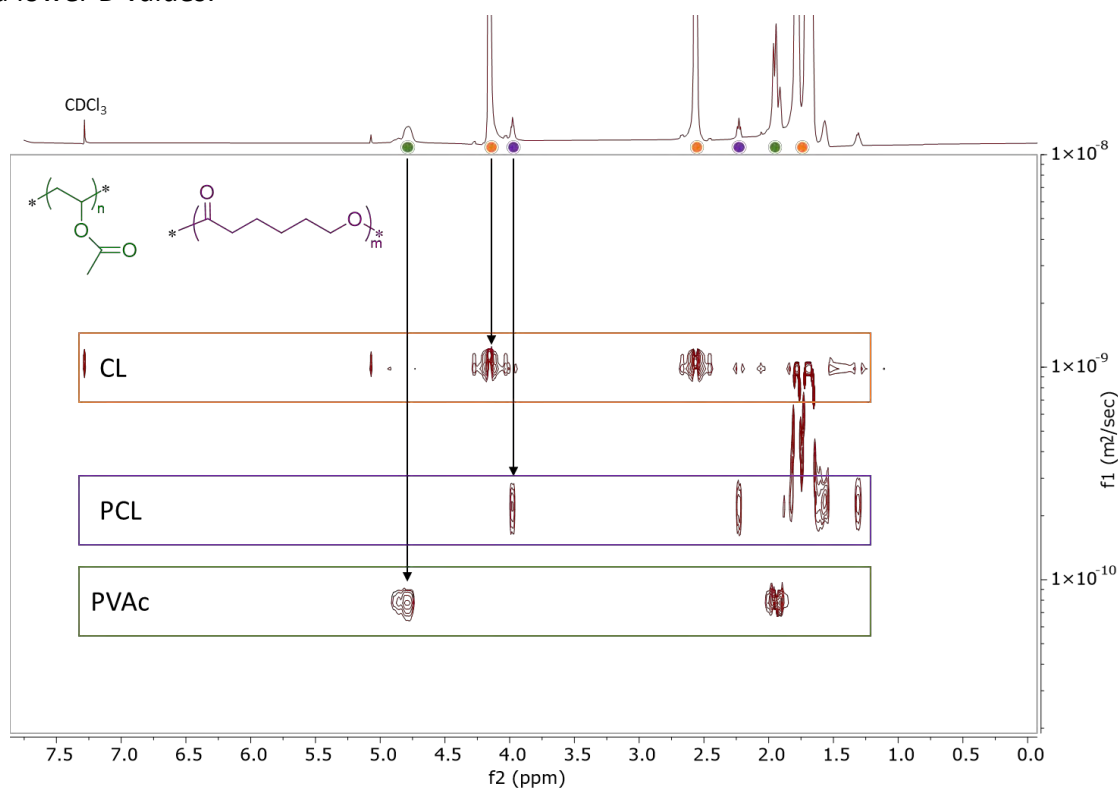


Figure IV-9: ^1H DOSY-NMR spectrum of the final polymer blend for the 3.6-initiated one-pot copolymerization process of VAc and CL, in CDCl_3 , 400 MHz.

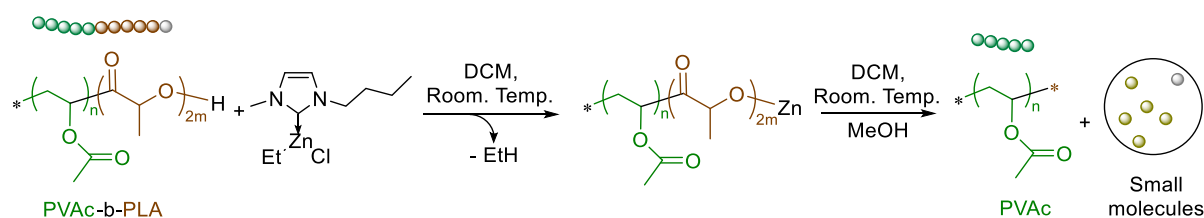
The resonances associated to the intermediate diffusion coefficient ($2.3 \times 10^{-10} \text{ m}^2/\text{s}$) correspond to PCL (purple dots). No PVAc resonances (green dots) are visible for this D value. This is consistent with the generation of $[\text{PCL-Co}^{\text{III}}(\text{acac})_2]$ homopolymer chains during the higher-temperature step of the polymerization. The PVAc resonances are visible, on the other hand, in correspondence with the lower D value ($7.2 \times 10^{-11} \text{ m}^2/\text{s}$), in agreement with the higher molar mass of the $[\text{PVAc-Co}^{\text{III}}(\text{acac})_2]$ product of the low-temperature step, as suggested by the GPC in *Figure IV-7*. No resonances at the chemical shift of PVCL are visible at this diffusion coefficient. This suggests that these macromolecules have either remained $[\text{PVAc-Co}^{\text{III}}(\text{acac})_2]$ homopolymers, or that they have extended with a small amount of PCL blocs, too small to afford visible signals. Consequently, this one-pot process allows the production of a polymer blend, of which one component is a PCL homopolymer and the second one is either a PVAc homopolymer or a PVAc-*b*-PCL diblock with a short PCL block, using two different mechanisms (radical and coordination/insertion).

One point that remains obscure is whether the resulting mixture is a simple blend or an interpenetrating polymer network (IPN). A material of this type was obtained, for instance, in a recent contribution by Gígenes, Broggi *et al.*,³⁵ through the simultaneous initiation of radical and anionic propagation processes. An IPN can be simply defined as a system consisting of

two polymer networks (3D) that are physically entangled but not chemically linked.³⁶ A simple polymers blend, on the other hand, is a mixture of two or more chemically different thermoplastic (1D) polymers. The answer to this question may be provided by the measurement of certain physical properties. For instance, polymer blends should give rise to two (or more) glass transitions, at the same T_g values specific for each polymer component, whereas interpenetrating polymers should yield only one broad glass transition. This point will be clarified through future work.

3. Selective degradation of copolymer (OMRP-*b*-ROP)

One of the major interests of this research comes from the environmental and societal pressure. In fact, the biodegradability of the usual polymers presents a great challenge for the scientific community. That is why a selective degradation experiment of the PVAc-*b*-PLA was carried out as a proof of concept. This experiment was based on a report of the use of zinc complexes for the controlled polymerization of lactide and also for the depolymerization of the PLA product in the presence of methanol.^{37, 38} In our case, as shown in *Scheme IV-5*, we wish to first remove the cobalt complex from the chain end, then install the NHC-zinc complex $[(I^{Me,Bu})ZnCl(Et)]$ ($I^{Me,Bu}$ = *N*-methyl-*N'*-butylimidazolydene, 1H NMR in Figure S17)^{37, 38} at the chain end and finally degrade the PLA block by transesterification with methanol ($[polymer]/[Zn]/[MeOH] = 1/1/100$ in CD_2Cl_2 , 24 h at room temperature) to release methyl lactate (*Figure IV-10*).



*Scheme IV-5: PVAc-*b*-PLA degradation catalyzed by the $[(I^{Me,Bu})ZnCl(Et)]$ complex.*

As can be observed from the 1H NMR monitoring of the degradation reaction (*Figure IV-10*), the methanol/Zn treatment degraded the PLA as proven by the appearance of the methyl lactate signals. The occurrence of polymer degradation is confirmed by the GPC analysis (*Figure IV-11*). The PVAc macroinitiator PVAc (green trace) was extended with LA to give the PVAc-*b*-PLA diblock copolymer (brown signal). After degradation, the molar masses distribution shifts to lower values (dashed brown line).

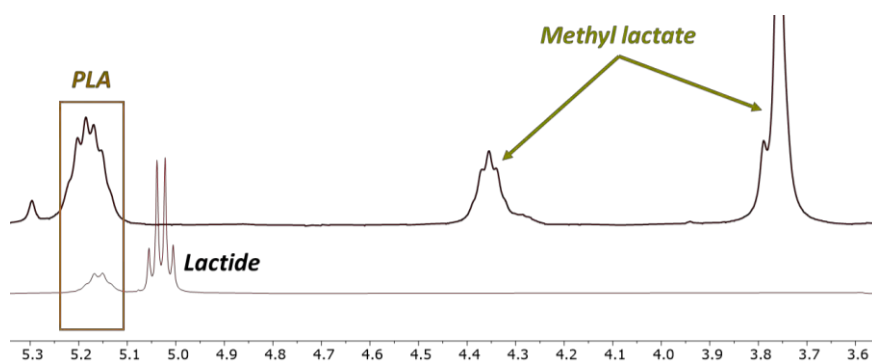


Figure IV-10: ^1H NMR spectra of the PVAc-*b*-PCV before (bottom) and after (top) treatment with MeOH and reaction with the Zn complex, recorded in CD_2Cl_2 .

As we can observe with the ^1H NMR above (Figure IV-10), the methanol/Zn treatment, which allows for the removal of the lactide, did not react and degraded the PLA due to the methyl lactate signals appearance. Moreover, this result is also well illustrated by the GPC analysis (Figure IV-11). The macro-initiator PVAc (green trace) is extended with a PLA block to give the brown signal. The degradation then induces a decrease of the molar masses, as highlighted by the dashed brown line.

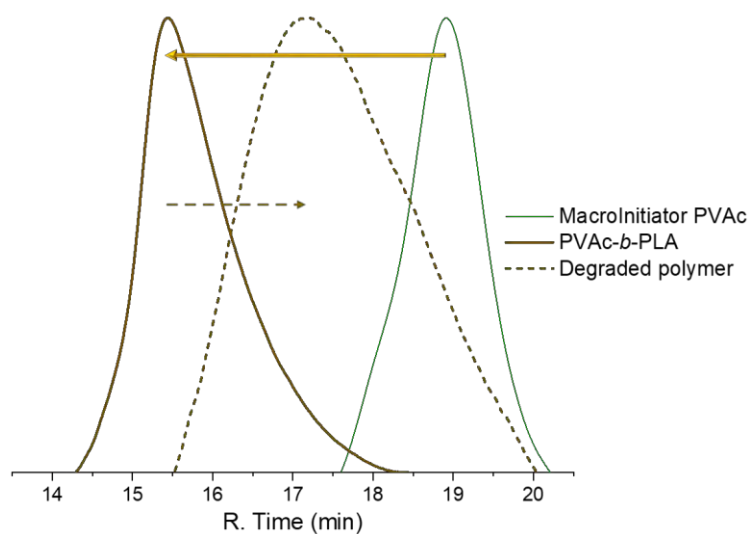


Figure IV-11: GPC analysis of the PVAc macroinitiator (green), chain-extended PVAc-*b*-PLA (brown) and degraded polymer after 24 h at room temperature (dashed brown).

Even though this is only a proof of concept, these results highlight a promising system. We can also imagine other degradation pathways such as an acid- or enzyme-catalyzed hydrolysis.³⁹ To conclude, a polymerization switch was clearly shown from OMRP to ROP. However, the reverse switch from ROP to OMRP could not be observed under the conditions used so far.

V. Conclusion and outlook

Several cobalt(III) carboxylate systems able to undergo the homolytic cleavage of the $\text{Co}^{\text{III}}\text{-O}_2\text{CR}$ bond and generate carboxyl radical (**3.1**, **3.3**, **3.6**, **3.7**, **3.8**, **3.12**) have been highlighted. Among these, complex **3.1** is the best initiator/moderator for the OMRP of methyl acrylate, whereas **3.6** gives the best results for vinyl acetate. For these reasons, the subsequent ROP investigation was essentially limited to these two complexes, revealing that the most efficient system is $[\text{Co}(\text{acac})_2(\text{O}_2\text{CPh})]$ (**3.6**). The combined OMRP and ROP investigations made this complex the most promising candidate for the target mechanistic switch between ROP and OMRP. This system proved indeed successful for the sequential block copolymerization (*Figure V-1-B*) of VAc by OMRP, switching to LA or CL by ROP. Unfortunately, the reverse switch from ROP to OMRP was unsuccessful under the experimental conditions tested so far. New block copolymers, synthesized by the sequential process with OMRP/ROP switch without chemical modification between blocks, have been characterized. The main drawback of this system is the low initiator efficiency. This drawback, however, could be turned into an advantage for the development of an original polymer blend produced in a one-pot process (*Figure V-1-C*).

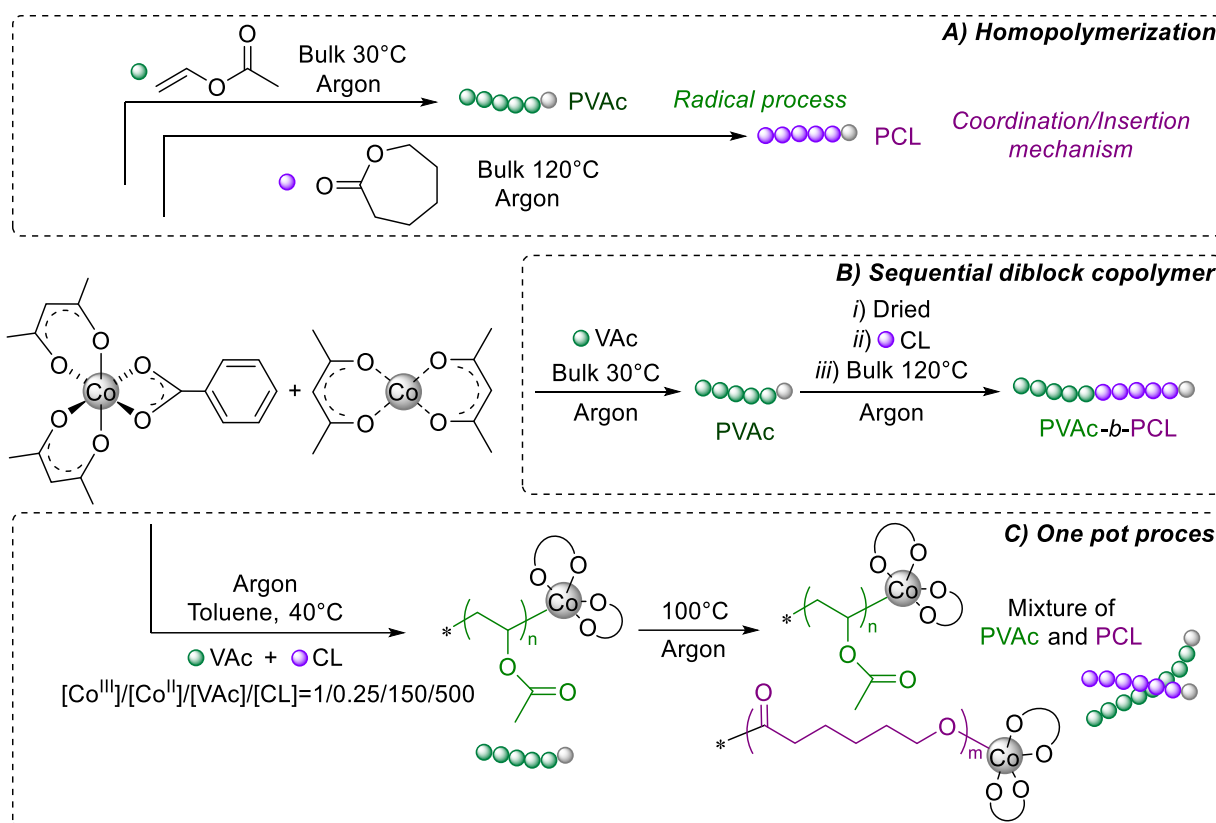


Figure V-1: Various applications of the $[\text{Co}(\text{acac})_2(\text{O}_2\text{CPh})]$ complex for polymer synthesis: A) homo-polymerization by OMRP or ROP; B) sequential copolymerization with switch from OMRP to ROP; C) one-pot process for polymer blend production.

VI. Experimental section

1. Materials

Cobalt(II) bisacetylacetonate ($\text{Co}(\text{acac})_2$, $\geq 99\%$, Sigma Aldrich) 1,3,5-trioxane ($\geq 99\%$, Sigma Aldrich), BnOH (Benzyl alcohol, Sigma Aldrich), 2,2,6,6-tetramethyl-1-piperidinyloxy (TEMPO, 98%, Sigma Aldrich), diethylzinc (ZnEt_2 , 1M in hexane, Sigma Aldrich), 1-methylimidazole (99%, Sigma Aldrich), 1-chlorobutane ($\geq 99.8\%$, Sigma Aldrich) and the deuterated solvents C_6D_6 , CD_2Cl_2 and CDCl_3 (99.8%D, Euriso-top) were purchased and used as received. L-lactide (purchased from Corbion) was recrystallized from toluene. ϵ -Caprolactone ($>99\%$, Sigma Aldrich) was dried over, distilled under static vacuum and stored under argon at 0°C .

2. Characterizations

NMR. All spectra were recorded on a Bruker Avance III 300 or 400 MHz spectrometer at ambient temperature. The ^1H and ^{13}C chemical shifts (δ) were determined using the residual ^1H solvent peaks as internal standard and reported in ppm vs. SiMe_4 .

GPC. analyses were carried out at 35°C with a Shimadzu DGU-20A3R equipped with Shim-pack GPC-801 and -805 columns (each having a length of 300 mm and an inner diameter of 8 mm) and a refractive index detector, using THF as mobile phase at a flow rate of 1 mL min^{-1} .

DOSY-NMR. The DOSY-NMR spectra were measured by the technical staff of the NMR platform of the Laboratoire de Chimie de Coordination. They were recorded on a Bruker Ascend 600 spectrometer equipped with a 5 mm triple resonance inverse Z-gradient probe (TBI 1H, 31P, BB) and acquired at 300K with the *stebpgp1s* pulse program from Bruker topspin software. All spectra were recorded with 16K time domain data point in the t_2 dimension and 16 t_1 increments. The gradients strength was linearly incremented in 16 steps from 2% up to 95% of the maximum gradient strength. All measurements were performed with a compromise diffusion delay Δ between 200 and 350 ms and a gradient pulse length δ between 3.2 and 4.0 ms.

^1H spin-lattice relaxation times (T_1). These T_1 parameters were measured using the excitation sculpting inversion-recovery pulse sequence *t1iresgp*. The relaxation delay was 6 s and the acquisition time was 1 s. For each measurement, the recovery times were from 50 ms to 6 s and 8 points were collected.

ESI. The electrospray ionization mass spectra (ESI-MS) were recorded by the technical staff of the mass spectrometry platform of the Toulouse Institute of Chemistry on a Q-ToF Premier (Waters) instrument using nitrogen as drying agent and nebulizing gas and MeCN as solvent.

3. Methods

OMRP tests with complex 3.1. In the glove box, complex $[\text{Co}(\text{L}^{1.1})\text{OAc}]$ (50 mg, 0.75 mmol) was added into the Schlenk. Methyl acrylate (200 eq) was then added by syringe and the tube was sealed with a rubber septum. The green mixture was stirred and heated at 70°C in the dark. The monomer conversion was determined by gravimetry from aliquots withdrawn from the reaction mixture at the desired times. The same aliquots were treated with pentane to precipitate the polymer products, which were dried under vacuum to remove the unreacted monomer. The dried polymers were then dissolved in THF (at concentrations between 3 and 5 mg mL⁻¹) for the GPC analysis.

OMRP tests with complex 3.2. In the glove box, a glass tube was charged with the previously synthesized cobalt complex (5.7 mg, 8.63x10⁻⁶ mol), trioxane as NMR standard (ca. 5 mg), methyl acrylate was then added by syringe (0.23 mL, 2.6 x10⁻³ mol, 300 eq), and the tube was sealed with a rubber septum. For methyl methacrylate, the same procedure was adopted with the cobalt complex (11.4 mg, 1.72x10⁻⁵ mol), trioxane (ca. 5 mg) and the monomer (0.54 mL, 5.1x10⁻³ mol, 300 eq). In each case, the dark brown mixture was stirred and heated at 60°C. The monomer conversion was determined by withdrawing aliquots of the reaction mixture for the gravimetric analysis and also followed by ¹H NMR. The polymer was precipitated by addition of pentane and dried under vacuum to remove the unreacted monomer.

OMRP bulk polymerizations of vinyl acetate with complex 3.6. In the glove box, complex $[\text{Co}^{\text{III}}(\text{acac})_2(\text{O}_2\text{CPh})]$ (128.9 mg, 0.34 mmol) and X equivalents of $[\text{Co}^{\text{II}}(\text{acac})_2]$ (0.1 eq, 8.74 mg, 0.03 mmol; 0.25 eq, 21.85 mg, 0.08 mmol; 0.5 eq, 43.7 mg, 0.17 mmol; 1 eq, 87.43 mg, 0.34 mmol) were added into a glass tube. Vinyl acetate was then added by syringe and the tube was sealed with a rubber septum. The green mixture was stirred and heated at 30°C, 40°C, 50°C or 60°C in the dark. The monomer conversion was determined by withdrawing aliquots of the reaction mixture for a gravimetric and/or ¹H NMR analysis. The polymer was precipitated by addition of pentane and dried under vacuum to remove the unreacted monomer. The dried polymer was then dissolved in THF (3-5 mg mL⁻¹) for the GPC analysis.

Quenched TEMPO reactions. 100 mg of TEMPO was dissolved in 1 mL of dry toluene under argon and the resulting solution was injected in the polymerization reaction mixture at the desired time.

OMRP of vinyl acetate in solution. In the glove box, complex $[\text{Co}^{\text{III}}(\text{acac})_2(\text{O}_2\text{CPh})]$ (20 mg, 0.053 mmol), $[\text{Co}^{\text{II}}(\text{acac})_2]$ (3.4 mg, 0.013 mmol, 0.25 eq) and 2.64 mL of toluene were added into a glass tube. Vinyl acetate (1 mL) was then added by syringe ($[\text{VAc}] = 4 \text{ mol L}^{-1}$) and the tube was sealed with a rubber septum. The green mixture was stirred and heated at 40°C in the dark. The monomer conversion was determined by withdrawing aliquots of the reaction mixture for a gravimetric and/or ¹H NMR analysis. The polymer was precipitated by addition

of pentane and dried under vacuum to remove the unreacted monomer. The dried polymer was then dissolved in THF (3-5 mg mL⁻¹) for the GPC analysis.

Ring opening polymerization reactions. All polymerizations followed the same procedure. A glass tube was charged with the complex, the monomer (and BnOH when necessary) in the desired molar ratio. The tube was then sealed with a rubber septum under inert atmosphere in the glove box. It was then placed in a thermostatic oil bath at 100°C with magnetic stirring and the reaction was stopped at the desired time by cooling to room temperature. For all of experiments, the monomer conversion determination and the polymer isolation and characterization by ¹H and GPC followed the same procedure already described in the previous sections.

OMRP sequential block copolymerizations. A green cobalt-terminated poly(vinyl acetate) macroinitiator ($M_n^{\text{GPC}} = 5400 \text{ g mol}^{-1}$, $\mathcal{D} = 1.07$) was prepared according the procedure described above with a [Co^{III}]/[Co^{II}] ratio of 1/0.25. Then, 50 mg of dried polymer was added to the bulk monomers (VAc, S, MA, BA; 1.8 mmol, 200 eq) in a glass tube. The tube was then sealed with a rubber septum and placed in a thermostatic bath at 30°C in the dark with magnetic stirring. The conversions were recorded by gravimetric analysis on an aliquot after 24 h or after the stirring was stopped by the increased viscosity. After precipitation by addition of pentane and recovery, the dried polymers were then dissolved in THF (3-5 mg mL⁻¹) for the GPC analysis.

Polymerization switch from OMRP to ROP with complex 3.6. A green cobalt-terminated poly(vinyl acetate) macroinitiator ($M_n^{\text{GPC}} = 3635 \text{ g mol}^{-1}$, $\mathcal{D} = 1.11$) was prepared according the procedure described above with a [Co^{III}]/[Co^{II}] ratio of 1/0.25. Then, LA or CL and trioxane (internal standard) were added to the dried polymer in a glass tube working in the glove box ([Macroinitiator]/[M] = 1/500). After sealing with a rubber septum, the tube was placed in a thermostatic bath at 120°C in the dark with magnetic stirring. The conversions were recorded by ¹H NMR analysis on aliquots withdrawn at the desired time. The polymers were precipitated by addition of pentane, dried and dissolved in THF (3-5 mg mL⁻¹) for the GPC analysis.

Triblock extension test. The cobalt-terminated PVAc-b-PCL diblock macroinitiator ($M_n^{\text{GPC}} = 8400 \text{ g mol}^{-1}$, $\mathcal{D} = 1.07$) prepared as described in the previous section was added to 400 equivalents of VAc in bulk and heated at 40°C for 14 h, then for 26 h at 50°C. The withdrawn aliquots were analyzed by ¹H NMR for conversion and the polymer was analyzed by GPC after precipitation, drying and redissolution in THF.

One pot copolymerization process. In the glove box, [Co^{III}(acac)₂(O₂CPh)] (20 mg, 0.0528 mmol), [Co^{II}(acac)₂] (3.4 mg, 0.0135 mmol, 0.25 eq) and trioxane (10 mg) were added into a glass tube. Vinyl acetate (0.68 g, 150 eq) and ε-caprolactone (3 g, 500 eq) were then added by

syringe and the tube was sealed with a rubber septum. The green mixture was stirred and heated at 40°C for 45 hours. The temperature was then increased to 120°C and stirred for an additional 45 hours. The monomer conversions were determined by withdrawing aliquots of the reaction mixture and ^1H NMR analysis. The polymer was precipitated by addition of pentane and dried under vacuum to remove the unreacted monomers. The dried polymer was then diluted in THF (3-5 mg mL⁻¹) for the GPC analysis.

General conclusion and perspectives

During the search for a unique metal complex for the initiation and moderation of both OMRP and ROP, and also for a switch between these two-polymerization mechanisms, we focused on various steps, which are summaries in the research roadmap of *Figure 1*.

Several cobalt(III) complexes were synthesized, a few of which such as Co(salen)OAc (**3.1**) were based on literature analogues. Other new complexes were inspired by previous work in our group, such as [Co(L^{1.10})OAc] (**3.2**). Other new mononuclear heteroleptic architectures containing one carboxylate ligand were synthesized and characterized, notably based on the new synthesis route from diacyl peroxides implemented for the first time in this work. This method has provided carboxylate cobalt(III) complexes supported by an (N2,O2) (**3.3-3.4**) and by an (O2,O2) (**3.6-3.10**) coordination sphere.

The first step of our study was to highlight the radical production from the carboxylate cobalt(III) complexes, to verify their ability for the direct initiation and control of an OMRP process. After that, the control of this reaction and the nature of the chain end were investigated for a potential reactivation of the well-defined polymers for ROP. Only complexes **3.1** (with MA) and **3.6-3.8** (with VAc) revealed a sufficiently well-controlled OMRP.

Therefore, only complexes **3.1** and **3.6** were used for the next step of this work. This step consisted in tests of initiation efficiency and control of ROP processes. These investigations could confirm that both complexes are efficient for the ROP of ϵ -caprolactone and L-lactide.

Consequently, these systems were used for tests of switch from OMRP to ROP. Success was achieved only with **3.6**, as clearly shown by the GPC and DOSY analyses. These new block copolymers were synthesized without any chemical modification or co-agents when moving from one mechanism to the next one. However, no suitable conditions have been found so far to provide a switch in the reverse direction (from ROP to OMRP). The main drawback of this system is the low initiator efficiency in the initial OMRP step. However, this drawback was turned into an opportunity for the parallel development of polymer blends produced in a one-pot process.

In the immediate future, the mechanical properties of these new polymers will be investigated. This new methodology of a single-molecule initiation by a carboxylate cobalt(III) complex could also be extended to other LAMs that could be controlled by OMRP in past work only by using either the reverse initiating [Co^{II}(acac)₂]/peroxide system or the oligoinitiator [PVAc-Co^{III}(acac)₂], which is rather tedious to synthesize, such as, for instance, VDF.^{9, 40}

In addition, this work could also be extended to the ring opening copolymerization of CO₂/epoxide for another type of polymerization switch (from OMRP to ROCOP, or viceversa).

Moreover, peroxide precursor design could open the way to different kinds of chain-end functionalization, for instance by introducing amine or alcohol functions, allowing the subsequent facile polymer grafting on surfaces through the use of click chemistry.

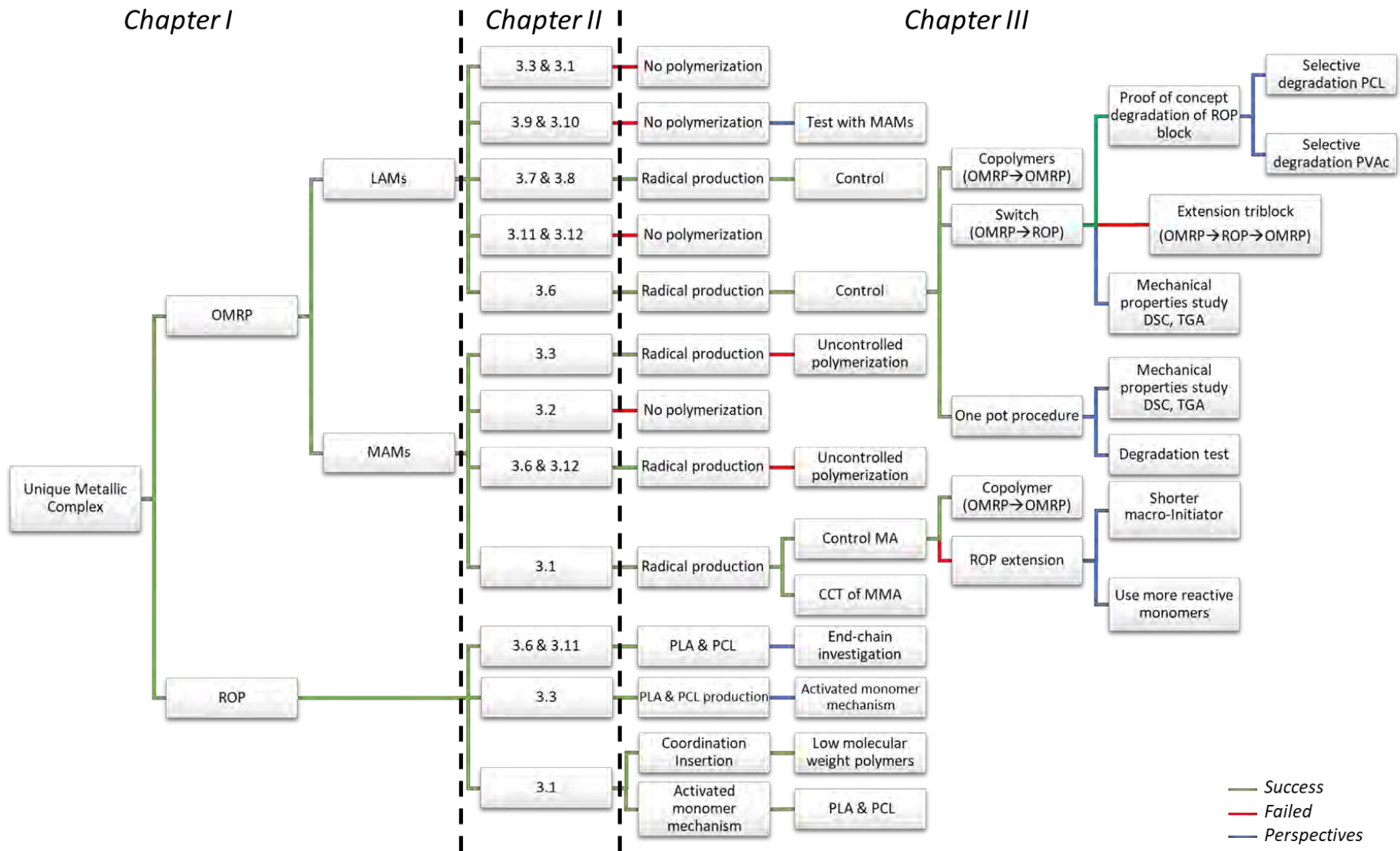


Figure 1: Road map of the thesis work.

References

1. Aydogan, C.; Kutahya, C.; Allushi, A.; Yilmaz, G.; Yagci, Y., Block copolymer synthesis in one shot: concurrent metal-free ATRP and ROP processes under sunlight. *Polymer Chemistry* **2017**, *8* (19), 2899-2903.
2. David Mecerreyes, G. M., Philippe Dubois, Robert Jerome*, James L. Hedrick,* Craig J. Hawker,* Eva E. Malmström, and Mikael Trollsas, Simultaneous Dual Living Polymerizations: A Novel One-Step Approach to Block and Graft Copolymers. *Angew. Chem. Int. Ed.* **1998**, *37*, 1275-1276.
3. Jakubowski, W.; Matyjaszewski, K., New Segmented Copolymers by Combination of Atom Transfer Radical Polymerization and Ring Opening Polymerization. *Macromolecular Symposia* **2006**, *240* (1), 213-223.
4. Wang, Y.; Zhao, Y.; Zhu, S.; Zhou, X.; Xu, J.; Xie, X.; Poli, R., Switchable Polymerization Triggered by Fast and Quantitative Insertion of Carbon Monoxide into Cobalt-Oxygen Bonds. *Angew Chem Int Ed Engl* **2020**, *59* (15), 5988-5994.
5. Zhao, Y.; Jung, J.; Nozaki, K., One-Pot Synthesis of Polyethylene-Based Block Copolymers via a Dual Polymerization Pathway. *J Am Chem Soc* **2021**, *143* (45), 18832-18837.
6. Poli, R., New Phenomena in Organometallic-Mediated Radical Polymerization (OMRP) and Perspectives for Control of Less Active Monomers. *Chemistry* **2015**, *21* (19), 6988-7001.
7. Gridnev, A. A., Catalytic Chain Transfer in Free-Radical Polymerizations. *Chem. Rev.* **2001**, *101*, 3611-3659.
8. Redjel, Y. K.; Thevenin, L.; Daran, J.-C.; Benslimane, M.; Poli, R.; Flidel, C., Acetylacetonato cobalt(III) and iron(III) complexes of picolylamine- and aminopropylamine-bis(phenolate) ligands: Synthesis, characterization and crystal structures. *Polyhedron* **2019**, *158*, 83-90.
9. Banerjee, S.; Ladmiral, V.; Debuigne, A.; Detrembleur, C.; Poli, R.; Améduri, B., Organometallic-Mediated Radical Polymerization of Vinylidene Fluoride. *Angewandte Chemie International Edition* **2018**, *57* (11), 2934-2937.
10. Debuigne, A.; Caille, J. R.; Detrembleur, C.; Jerome, R., Effective cobalt mediation of the radical polymerization of vinyl acetate in suspension. *Angew Chem Int Ed Engl* **2005**, *44* (22), 3439-42.
11. Debuigne, A.; Caille, J. R.; Jerome, R., Highly efficient cobalt-mediated radical polymerization of vinyl acetate. *Angew Chem Int Ed Engl* **2005**, *44* (7), 1101-4.
12. Debuigne, A.; Champouret, Y.; Jerome, R.; Poli, R.; Detrembleur, C., Mechanistic insights into the cobalt-mediated radical polymerization (CMRP) of vinyl acetate with cobalt(III) adducts as initiators. *Chemistry* **2008**, *14* (13), 4046-59.
13. Debuigne, A.; Morin, A. N.; Kermagoret, A.; Piette, Y.; Detrembleur, C.; Jérôme, C.; Poli, R., Key Role of Intramolecular Metal Chelation and Hydrogen Bonding in the Cobalt-Mediated Radical Polymerization of N-Vinyl amides. *Chem. Eur. J.* **2012**, *18*, 12834-12844.
14. Rayna Bryaskova, C. D., Antoine Debuigne, and Robert Jerome, Cobalt-Mediated Radical Polymerization (CMRP) of Vinyl Acetate Initiated by Redox Systems: Toward the Scale-Up of CMRP. *Macromolecules* **2006**, *39*, 8263-8268.
15. Auras, R.; Harte, B.; Selke, S., An overview of polylactides as packaging materials. *Macromol Biosci* **2004**, *4* (9), 835-64.
16. Haque, F. M.; Ishibashi, J. S. A.; Lidston, C. A. L.; Shao, H.; Bates, F. S.; Chang, A. B.; Coates, G. W.; Cramer, C. J.; Dauenhauer, P. J.; Dichtel, W. R.; Ellison, C. J.; Gormong, E. A.; Hamachi, L. S.; Hoyer, T. R.; Jin, M.; Kalow, J. A.; Kim, H. J.; Kumar, G.; LaSalle, C. J.; Liffland, S.; Lipinski, B. M.; Pang, Y.; Parveen, R.; Peng, X.; Popowski, Y.; Prebihalo, E. A.; Reddi, Y.; Reineke, T. M.; Sheppard, D. T.; Swartz, J. L.; Tolman, W. B.; Vlasisavljevich, B.; Wissinger, J.; Xu, S.; Hillmyer, M. A., Defining the Macromolecules of Tomorrow through Synergistic Sustainable Polymer Research. *Chemical Reviews* **2022**, *122* (6), 6322-6373.
17. Philippe Degée, P. D., Robert Jerome, Sven Jacobsen and HansGerhard Fritz, New catalysis for fast bulk ring-opening polymerization of lactide monomers. *Macromol. Symp.* **1999**, *144*, 289-302

18. Löfgren, A.; Albertsson, A.-C.; Dubois, P.; Jérôme, R., Recent Advances in Ring-Opening Polymerization of Lactones and Related Compounds. *Journal of Macromolecular Science, Part C: Polymer Reviews* **1995**, *35* (3), 379-418.
19. Odile Dechy-Cabaret, B. M.-V., and Didier Bourissou, Controlled Ring-Opening Polymerization of Lactide and Glycolide. *Chem. Rev.* **2004**, *104*, 6147–6176.
20. Sarazin, Y.; Carpentier, J. F., Discrete cationic complexes for ring-opening polymerization catalysis of cyclic esters and epoxides. *Chem Rev* **2015**, *115* (9), 3564-614.
21. Champouret, Y.; Hashmi, O. H.; Visseaux, M., Discrete iron-based complexes: Applications in homogeneous coordination-insertion polymerization catalysis. *Coordination Chemistry Reviews* **2019**, *390*, 127-170.
22. Biernesser, A. B.; Li, B.; Byers, J. A., Redox-controlled polymerization of lactide catalyzed by bis(imino)pyridine iron bis(alkoxide) complexes. *J Am Chem Soc* **2013**, *135* (44), 16553-60.
23. Brendan J. O’Keefe, S. M. M., Marc A. Hillmyer,* and William B. Tolman*, Rapid and Controlled Polymerization of Lactide by Structurally Characterized Ferric Alkoxides. *J. Am. Chem. Soc.* **2001**, *123*, 339-340.
24. Duan, R.; Hu, C.; Li, X.; Pang, X.; Sun, Z.; Chen, X.; Wang, X., Air-Stable Salen–Iron Complexes: Stereoselective Catalysts for Lactide and ϵ -Caprolactone Polymerization through in Situ Initiation. *Macromolecules* **2017**, *50* (23), 9188-9195.
25. Chen, L.-L.; Ding, L.-Q.; Zeng, C.; Long, Y.; Lü, X.-Q.; Song, J.-R.; Fan, D.-D.; Jin, W.-J., Bulk solvent-free melt ring-opening polymerization of L-lactide catalyzed by Cu(II) and Cu(II)-Nd(III) complexes of the Salen-type Schiff-base ligand. *Applied Organometallic Chemistry* **2011**, *25* (4), 310-316.
26. Gowda, R. R.; Chakraborty, D., Copper acetate catalyzed bulk ring opening polymerization of lactides. *Journal of Molecular Catalysis A: Chemical* **2011**, *349* (1-2), 86-93.
27. Fortun, S.; Daneshmand, P.; Schaper, F., Isotactic rac-Lactide Polymerization with Copper Complexes: The Influence of Complex Nuclearity. *Angew Chem Int Ed Engl* **2015**, *54* (46), 13669-72.
28. Whitehorne, T. J.; Schaper, F., Square-planar Cu(II) diketiminate complexes in lactide polymerization. *Inorg Chem* **2013**, *52* (23), 13612-22.
29. Marin, P.; Tschan, M. J. L.; Haquette, P.; Roisnel, T.; del Rosal, I.; Maron, L.; Thomas, C. M., Single-site cobalt and zinc catalysts for the ring-opening polymerization of lactide. *European Polymer Journal* **2019**, *120*.
30. Wang, W.-W.; Ren, W.-Y.; Jiang, L.; Dan, Y., Synthesis and characterization of AB-type copolymers poly(L-lactide)-block-poly(methyl methacrylate) via a convenient route combining ROP and ATRP from a dual initiator. *Journal of Applied Polymer Science* **2010**, n/a-n/a.
31. Erdogan, T.; Ozyurek, Z.; Hizal, G.; Tunca, U., Facile synthesis of AB₂-type miktoarm star polymers through the combination of atom transfer radical polymerization and ring-opening polymerization. *Journal of Polymer Science Part A: Polymer Chemistry* **2004**, *42* (10), 2313-2320.
32. Öztürk, T.; Gökteş, M.; Hazer, B., One-step synthesis of triarm block copolymers via simultaneous reversible-addition fragmentation chain transfer and ring-opening polymerization. *Journal of Applied Polymer Science* **2010**, NA-NA.
33. Kang, H. U.; Yu, Y. C.; Shin, S. J.; Youk, J. H., One-step synthesis of block copolymers using a hydroxyl-functionalized trithiocarbonate RAFT agent as a dual initiator for RAFT polymerization and ROP. *Journal of Polymer Science Part A: Polymer Chemistry* **2012**, *51* (4), 774-779.
34. Michele Schappacher, N. F., and Sophie M. Guillaume*, Poly(methyl methacrylate)-Poly(caprolactone) AB and ABA Block Copolymers by Combined Ring-Opening Polymerization and Atom Transfer Radical Polymerization. *Macromolecules* **2007**, *10*, 8887-8896.
35. Zhao, Y.; Rollet, M.; Charles, L.; Canard, G.; Gimes, D.; Vanelle, P.; Broggi, J., Switching from Single to Simultaneous Free-Radical and Anionic Polymerization with Enamine-Based Organic Electron Donors. *Angewandte Chemie International Edition* **2021**, *60* (35), 19389-19396.
36. Silverstein, M. S., Interpenetrating polymer networks: So happy together? *Polymer* **2020**, *207*.

37. Fliedel, C.; Mameri, S.; Dagonne, S.; Avilés, T., Controlled ring-opening polymerization of trimethylene carbonate and access to PTMC-PLA block copolymers mediated by well-defined N-heterocyclic carbene zinc alkoxides. *Applied Organometallic Chemistry* **2014**, *28* (7), 504-511.
38. Fliedel, C.; Vila-Viçosa, D.; Calhorda, M. J.; Dagonne, S.; Avilés, T., Dinuclear Zinc-N-Heterocyclic Carbene Complexes for Either the Controlled Ring-Opening Polymerization of Lactide or the Controlled Degradation of Polylactide Under Mild Conditions. *ChemCatChem* **2014**, n/a-n/a.
39. Zaaba, N. F.; Jaafar, M., A review on degradation mechanisms of polylactic acid: Hydrolytic, photodegradative, microbial, and enzymatic degradation. *Polymer Engineering & Science* **2020**, *60* (9), 2061-2075.
40. Falireas, P. G.; Ladmiral, V.; Debuigne, A.; Detrembleur, C.; Poli, R.; Ameduri, B., Straightforward Synthesis of Well-Defined Poly(vinylidene fluoride) and Its Block Copolymers by Cobalt-Mediated Radical Polymerization. *Macromolecules* **2019**, *52* (3), 1266-1276.

Documents Annexes

Maxime Michelas

“Design of cobalt(III) carboxylate complexes for switching between radical and ring opening polymerization mechanism”

Ecole doctorale : SDM – Sciences De la Matière – Toulouse

Spécialité : Chimie Organométallique et de Coordination

LCC – Laboratoire de Chimie de Coordination

Encadrés par Christophe Fliedel et Rinaldo Poli



Université
de Toulouse

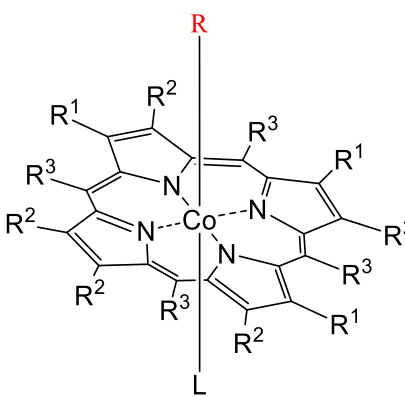
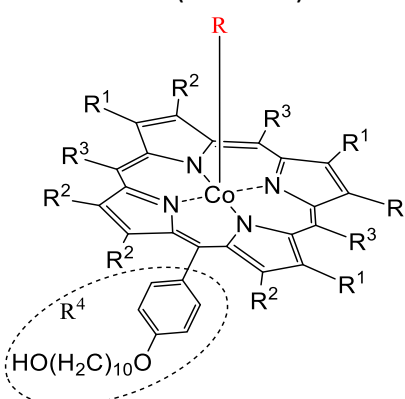
Annexes Chapter I

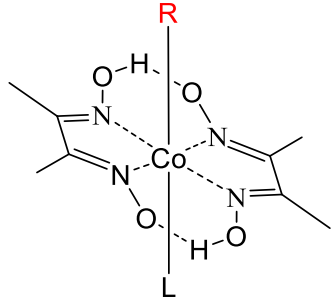
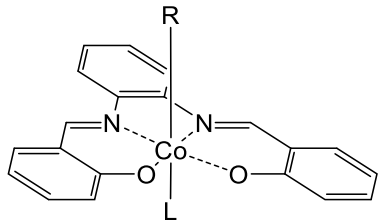
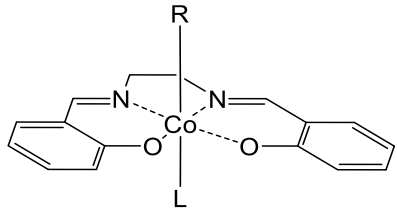
Table S 1: Summary of Cobalt complexes for OMRP polymerization with Bond Dissociation Energies.200

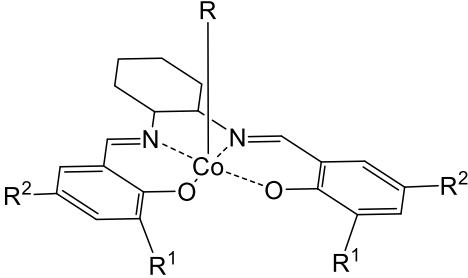
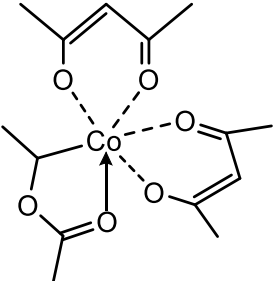
Table S 2: Summaries of polymerization result by Cobalt Mediated Radical Polymerization (OMRP).204

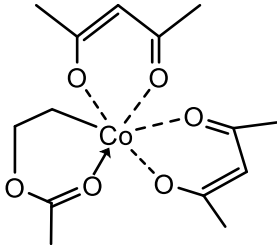
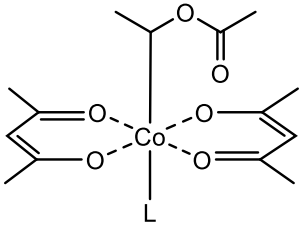
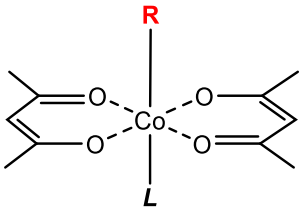
Table S 3: Summaries of polymerization results obtained with each complex presented in the ROP section.207

Table S 1: Summary of Cobalt complexes for OMRP polymerization with Bond Dissociation Energies.

Complex	Substituents			BDE Co-R (kcal.mol ⁻¹)	Method of BDE determination
	R	L	R ¹ , R ² , R ³		
<p>R-Co(por)-L</p> 	CH ₂ Ph	L = PBU ₃	R ¹ , R ² = Et, R ³ = H	29.1	Kinetic of trapping radicals with TEMPO
	CH ₂ Ph	L = PPH ₃	R ¹ , R ² = Et, R ³ = H	24.0	
	CH(CH ₃)CN	-	R ¹ , R ² = H, R ³ = C ₆ F ₅	22.0	DFT (B3LYP)
	CH(CH ₃)CN	-	R ¹ , R ² = H, R ³ = Ph(Me) ₃	24.0	
	CH(CH ₃)OAc	-	R ¹ , R ² = H, R ³ = PhMe ₃	24.0	
	CH(CH ₃)O ^t Bu	-	R ¹ , R ² = H, R ³ = PhMe ₃	14.0	
	CH(CH ₃)OMe	-	R ¹ , R ² = H, R ³ = PhMe ₃	18.0	
	CH(CH ₃)Ph	-	R ¹ , R ² = H, R ³ = Anisyl	20.0	
	C ₅ H ₉	-	R ¹ , R ² = H, R ³ = Anisyl	31.0	NMR
<p>R-Co(TMP-OH)</p> 	VAc	-	R ¹ , R ² = H R ³ = PhMe ₃ R ⁴ = Ph-O(CH ₂) ₁₀ OH	25.0	DFT
	MA	-		18.6	
	HEA	-		17.8	
	^t Ba	-		15.3	
	NIPAM	-		18.3	

<p><i>R</i>-Co(dmgH)₂-L</p> 	CH(CH ₃)Ph	4-NH ₂ -py		21.0	Kinetic of trapping radicals with R-SH
	CH(CH ₃)Ph	4-CN-py		18.0	
	CH ₂ Ph	P(CH ₃) ₂ Ph		30.0	Kinetic of trapping radicals with TEMPO
	CH ₂ Ph	PPh ₃		26.0	
	CH ₃	Py		31.0	DFT (B3LYP)
CH(CH ₃) ₂	Py	21.0			
<p><i>R</i>-Co(Saloph)-L</p> 	CH ₂ CH ₂ CH ₃	Py		25.0	Kinetic of trapping radicals with R-SH
	CH(CH ₃) ₂	Py		20.0	
<p><i>R</i>-Co(salen)-L</p> 	CH ₃	H ₂ O		49.0	Kinetic of trapping radicals with TEMPO
	CH(CH ₃) ₂	H ₂ O		19.0	

<p>R-Co(salen)</p> 	1-Phenyl-ethane		<p>$R^1 = {}^t\text{Bu}$ $R^2 = \text{NO}_2$ 15.4</p> <p>$R^1 = {}^t\text{Bu}$ $R^2 = \text{OMe}$ 13.7</p> <p>$R^1 = {}^t\text{Bu}$ $R^2 = {}^t\text{Bu}$ 14.1</p> <p>$R^1 = {}^t\text{Bu}$ $R^2 = \text{NMe}_2$ 13.3</p>	DFT (BP86)
<p>$\text{CH}_3(\text{CH}_3\text{COO})\text{CH-Co}(\text{acac})_2$</p> 		5-membered ring chelation	17.3	DFT (B3LYP)

<p>$\text{CH}_3\text{COOCH}_2\text{CH}_2\text{-Co(acac)}_2$</p> 		<p>6- membered ring chelation</p>		<p>18.3</p>	<p>DFT (B3LYP)</p>
<p>$\text{CH}_3(\text{CH}_3\text{COO})\text{CH-Co(acac)}_2\text{-L}$</p> 		<p>DMSO DMF</p>		<p>9.9 14.1</p>	<p>DFT (B3LYP) DFT (B3LYP)</p>
<p>$\text{R-Co(acac)}_2\text{-L}$</p> 	<p>CH_3 CH_3 CH_3 CH_3 CH_3 $\text{CH}(\text{OCH}_3)\text{CH}_3$ $\text{CH}(\text{OOCCH}_3)\text{CH}_3$ $\text{CH}(\text{OOCCH}_3)\text{CH}_3$ $\text{CH}(\text{OOCCH}_3)\text{CH}_3$ $\text{CH}(\text{OOCCH}_3)\text{CH}_3$ $\text{CH}(\text{CN})\text{CH}_3$ $\text{CH}(\text{CN})\text{CH}_3$ $\text{CH}(\text{CN})\text{CH}_3$</p>	<p>- Py NMe₃ NH₃ H₂O - - AN DMF DMSO - AN DMF</p>		<p>14.6 17.9 17.2 17.8 18.8 8.4 5.7 10.1 8.2 4.5 1.3 7.7 6.0</p>	<p>DFT (B3LYP)</p>

<p>R-Co(acac)₂-L</p>	CH(CN)CH ₃	DMSO		2.9
	CH(COOCH ₃)CH ₃	-		-1.5
	CH(CH ₃) ₂ CN	-		-5.5

Table S 2: Summaries of polymerization result by Cobalt Mediated Radical Polymerization (OMRP).

	Monomer	Solvent	Ratio [M]/[Co]/[I]	Eternal initiator	Temp (°C)	Time (h)	Conversion (%)	\bar{D}
Organocobalt porphyrins								
9.1	MA	Bulk	2083/1/1	V-70	60	2	10	1.13
	VAc	Bulk	1000/1/8	AIBN	60	8.5	70	1.34
9.3b	MA	Bulk	2083/1/0.75	V-70	60	-	55	1.8-2.2
9.3c	MA	C ₆ D ₆	2600/1	-	25	-	83	1.11
9.3d	AA	D ₂ O	3630/1/1.29	V-70	60	0.5	82	1.20
9.3e	AA	D ₂ O	3800	V-70	60	0.5	57	1.37
9.4	MA	C ₆ D ₆	2000/1/10	AIBN	53	9.5	30	1.21
	nBa	C ₆ D ₆	1000/1/10	AIBN	53	9	57	1.18
	^t Ba	MeOH	1000/1/10	AIBN	53	9	40	1.28
	DMA	MeOH	700/1/7	AIBN	50	18.5	94	1.21
	HEA	MeOH	2000/1/10	AIBN	53	9	28	1.32
	NIPAM	MeOH	1500/1/10	AIBN	53	5	23	1.29
	AA	MeOH	700/1/7	AIBN	50	21	28	1.33
Cobalt Bis(acetylacetonate)								
9.5a	VAc	Bulk	2168/1/6.5	V-70	30	14	60	1.33

9.5a	VAc	Bulk	813/1/6.5	V-70	30	13	16	1.10
	VAc	Bulk	542/1/3.25	V-70	30	28	50	1.20
	nBA	Bulk	348/1/1	V-70	30	5	8	2.10
	VAc	Water suspension	542/1/3.25	V-70	30	240	95	1.30
	VAc	Bulk	255/1.3/1	LPO	30	10	56	1.30
	VAc	Bulk	255/1.3/1	BPO	30	29	79	1.55
	VAc	Bulk	250/2/1	LPO/CA	30	3.25	79	1.40
9.5b	VAc	Bulk	500/1/2	V-70	30	524	76	1.32
9.5c	VAc	Bulk	500/1/1	V-70	30	60	62	1.30
9.6	VAc	Bulk	500/1/1	V-70	30	1	55	1.20
	VAc	Bulk	2010/1	-	40	10	28	1.17
9.7	VAc	Bulk	500/1/2	V-70	30	5	22	1.62
	VAc/MA (1/1)	Bulk	537/1/3	V-70	40	30	76	1.55
Cobalt Schiff-Base ligand								
9.10a	St	Bulk	100/1/0.6	AIBN	120	1	61	1.78
	VAc	Bulk	100/1/0.6		120	3	49	1.61
	MA	Bulk	100/1/0.6		120	0.16	95	1.56
	MMA	Bulk	100/1/0.6		120	0.25	70	1.24
	VAc	Bulk	984/1/6.5		60	8	85	1.25
	MA	C ₆ H ₆	500/1/10	60	2.8	77	1.30	
	VAc	C ₆ H ₆	600/1/1	3 mW/cm ²	95	46	1.25	
	MA	C ₆ H ₆	600/1/1	TPO	3 mW/cm ²	25	65	1.17
	nBa	C ₆ H ₆	600/1/1	3 mW/cm ²	29	77	1.19	
9.10b	St	Bulk	100/1/0.6	AIBN	120	1	55	2.23
	VAc					3	17	1.81
9.10c	St	Bulk	100/1/0.6	AIBN	120	1	72	2.38
	VAc					3	48	1.29

9.10d	St	Bulk	100/1/0.6	AIBN	120	1	85	2.65
	VAc					3	50	1.60
9.10e	St	Bulk	100/1/0.6	AIBN	120	1	58	1.35
1,3-bis(2-pyridylimino)isoindolato cobalt								
9.11a	MA						61	2.83
9.11b	MA						63	1.64
9.11d	MA						63	1.12
9.11e	MA						63	1.11
9.11f	MA						65	1.14
9.11g	MA						60	1.14
9.11h	MA	Benzene	600/1/1	V-70	60	-	63	1.15
9.11i	MA						69	1.40
9.11c	MA						70	1.09
9.11j	MA						69	1.10
9.11k	MA						68	1.10
9.11k	BA						66	1.13
9.11k	MA/BA						66	1.15
9.12a						20	5	1.26
9.12b						21	13	1.26
9.12c	MMA	Tol	1000/1	-	110	15	12	1.29
9.12d						17	70	1.52
9.12e						15	72	2.00
9.12f						15	40	1.58
Cobalt β-ketoiminates								
9.13a	VAc	Tol/VAc 50%	500/1/0.8	V-70	30	160	25	1.36
9.13b	VAc	Tol/VAc 50%	500/1/0.8	V-70	30	114	49	1.30

9.13c	VAc	Tol/VAc 50%	500/1/0.8	V-70	30	303	23	1.22
9.14a						0.5	18	1.27
9.14b						2.5	37	1.57
9.14c	VAc	Bulk	700/1/10	AIBN	60	2	32	1.70
9.14d						6	44	1.47
9.14e						8	24	1.83
9.14f						8	30	1.70

Table S 3: Summaries of polymerization results obtained with each complex presented in the ROP section.

Complex	[M]	[M]/[Complex]/[Additive]	Solvent	Additive	T°C	Time (min or h)	Conv. (%)	M_n^{Exp} (g/mol)	M_n^{th} (g/mol)	\bar{D}
Yttrium										
2.1		200/1				10h		36 000	28 800	1.25
2.2		500/1				20h		87 000	72 100	1.24
2.3		100/1				5h		19 000	14 400	1.28
2.4		100/1				5h		20 400	14 400	1.34
2.5		200/1				10h		38 500	28 800	1.28
2.6		100/1				5h		17 300	14 400	1.07
2.7		200/1				10h	complete	39 400	28 800	1.29
2.8	LA	100/1	THF	-	20	5h		22 000	14 400	1.18
2.9		200/1				10h		37 800	28 800	1.22
2.10		100/1				10h		26 300	14 400	1.19
2.11		100/1				5h		20 900	14 400	1.17
2.12		100/1				20h		26 300	14 400	1.19
2.13		100/1				60h		23 800	14 400	1.22
2.14		200/1				1h	79	32 500	22 700	1.15
2.15		200/1				2h	74	31 100	21 300	1.32
2.16		100/1				2h	60	15 300	8 600	1.66

Titanium										
3.1	CL	653/1	Bulk	-	150	24h	96	31660	-	1.33
3.2						24h	99	9460	11300	1.13
3.3						24h	99	8780	11300	1.20
3.4						9h	90	8890	10300	1.27
3.5						4h	99	13100	11300	1.27
3.6	CL	200/1	Tol	-	80	4h	73	10900	8330	1.10
3.7						2h	99	16100	11300	1.41
3.8						2h	99	13100	11300	1.09
3.9						2h	99	12200	11300	1.44
3.10						10min	93	20450	22900	1.19
3.11	CL	200/1	Bulk	-	100	9min	96	20980	22900	1.15
3.12						4min	97	21180	22900	1.12
3.10						21min	92	25420	28900	1.17
3.11	LA	200/1	Bulk	-	140	15min	96	25060	28900	1.15
3.12						8c	98	28150	28900	1.14
3.13							75	5500	4300	1.16
3.14							70	5100	4100	1.13
3.15							69	5100	4000	1.25
3.16	CL	200/1	Tol	-	30	12h	67	5400	3900	1.14
3.17							88	6000	5100	1.29
3.18							77	5800	4400	1.15
3.19							75	6100	4300	1.13
3.13							90	5900	6500	1.30
3.14							73	4100	5300	1.16
3.15							74	5700	5400	1.17
3.16	LA	200/1	Tol	-	70	20h	74	5700	5400	1.17
3.17							76	6400	5500	1.13
3.18							62	5000	4500	1.10
3.19							51	2900	3700	1.13

3.20						8h	87	10 100	-	1.19
3.21	LA	100/1	Bulk	-	130	8h	57	6 700	-	1.17
3.22						5h	94	5 200	-	1.11
3.23	LA	1800/1	Bulk	-	160	16h	96	99 000	-	1.14
Zirconium										
3.24	LA	300/1	Bulk	-	130	0.25h	98	42400	-	1.19
3.25						0.25h	52	8700	-	1.07
3.29					80	30min	42	11000	-	1.23
3.30							43	14000	-	1.23
3.31	LA	100/1	Tol	-			69	13400	-	1.08
3.32					20	24h	54	11300	-	1.12
3.33							63	10700	-	1.11
3.34							51	9000	-	1.15
3.35	LA	200/1	Tol	-	75	26h	91	7100	-	1.27
3.36a						7min	91	18360	22900	1.20
3.36b	CL	200/1	Bulk	-	100	6min	95	18050	22900	1.19
3.36c						4min	96	19450	22900	1.16
3.36a						17min	88	21980	28900	1.20
3.36b	LA	200/1	Bulk	-	140	12min	95	24760	28900	1.19
3.36c						6min	98	25030	28900	1.16
3.38	LA				140	36min	98	30100	28300	1.13
3.38	CL	200/1	Bulk	-	80	43min	97	23600	22200	1.15
3.39	LA				140	31min	96	34000	27700	1.10
3.39	CL				80	38min	95	26600	21700	1.11
	LA						71	6400		1.02
3.42	TMC	200/1	C ₆ D ₆	-	100	24h	92	10000	-	1.29
	VL						64	10800		1.13
	CHO					0.2h	100	28000		1.23
3.43	PO	200/1	C ₆ D ₆	-	25	24h	88	1800	-	1.62

Hafnium											
3.26						130	48h	75	24400	-	1.32
3.27	LA	300/1	Bulk	-		130	24h	96	46600	-	1.49
3.28						130	0.25h	99	7700	-	1.45
3.37a							6	90	16650	22900	1.23
3.37b	CL	200/1	Bulk	-	100		5	97	17890	22900	1.21
3.37c							3	98	17340	22900	1.18
3.37a							15	89	22330	28900	1.21
3.37b	LA	200/1	Bulk	-	140		10	93	22900	28900	1.20
3.37c							5	97	23430	28900	1.17
3.40	LA	200/1	Bulk	-		140	47min	97	26800	28000	1.12
3.40	CL					80	58min	98	20900	22400	1.17
Vanadium											
4.2a		500/1/1						13	4390	7440	1.10
4.2b		500/1/1						-	-	-	-
4.2c		500/1/1						25	8460	14300	1.10
4.3a		500/1/1						64	7830	36610	1.10
4.3b		500/1/1						53	8110	30320	1.30
4.3c		500/1/1				40	24h	60	8050	34320	1.10
4.3d		500/1/1						41	5510	23450	1.10
4.3e		500/1/1						65	10940	37180	1.10
4.3f	CL	500/1/1	Tol	BnOH				78	7920	44620	1.20
4.3g		500/1/1						74	15040	42330	1.30
4.3h		500/1/1						73	11860	41760	1.10
4.4		400/1/5						94	3100	45700	1.10
4.5a		400/1/5						46	3900	12300	1.10
4.5b		400/1/5				80	72h	20	5400	23700	1.30
4.6a		400/1/1						57	10751	26024	1.40
4.6b		400/1/1						47	8640	21458	1.40

4.7a								24	7977	10960	1.20
4.7b								33	9242	15070	1.20
4.8a								48	10080	21900	1.40
4.8b								70	11010	31960	2.30
4.9a								72	4973	32870	1.20
4.9b								100	4060	45660	1.10
4.10a	CL	400/1/1	Tol	BnOH	80	72h		87	13670	39720	1.30
4.10b								93	14260	42460	1.10
4.9c								97	21340	44290	1.10
4.9d								19	-	8670	-
4.11								93	13290	42460	1.20
4.12								94	4790	42920	1.10
4.13								3	4560	1370	1.40
4.14a	CL	200/1/0	Bulk	BnOH	80	30min	96	7130	21910	1.50	
	I-LA		Tol			24h	15	1340	4320	1.11	
4.14b	CL	200/1/0	Bulk	BnOH	80	40min	98	2600	22370	1.20	
	I-LA		Tol			24h	20	1930	5760	1.01	
4.15	CL	200/1/1	Bulk	BnOH	80	30min	97	1450	22250	1.49	
	I-LA		Tol			24h	53	3400	15380	1.29	
4.16	CL	200/1/0	Bulk	BnOH	80	30min	97	7200	22140	1.34	
	I-LA		Tol			24h	50	2120	14410	1.34	
4.17	CL	200/1/0	Bulk	BnOH	80	20min	99	16270	22600	1.45	
	I-LA		Tol			24h	54	2310	15570	1.24	
Chrome											
5.1								6	20000	-	2.00
5.2	B-BL	1000/1	Bulk	-	100	5h		35	71000	-	1.90
5.3								28	61000	-	2.20
5.4								31	70000	-	2.10
5.5	CHO	500/1	Bulk	-	60	27min	-	93100	-	1.60	
5.6					22	18min	-	46400	-	1.80	

5.7					22	34min		32300		2.10
5.8					22	34min		80800		1.60
Manganese										
6.1		100/1				2h	49	3500	1500	1.10
6.2		100/1		-	130	4h	71	10500	11000	1.30
6.3	CL	100/1	Bulk			4h	90	6500	5000	1.50
6.4		250/1/1		BnOH	110	24h	9	280	2565	1.02
6.5		250/1/1					12	450	3420	1.03
Iron										
7.1	LA	100/1	PO	PO	60	24h	90	19400	13100	1.58
7.2	LA	100/1	PO	PO	60	24h	91	18100	13200	1.46
7.3	LA	100/1	PO	PO	60	4h	91	24500	13200	1.54
7.4	LA	100/1	PO	PO	100	17h	93	9000	13500	2.36
7.5	LA	100/1	PO	PO	60	18h	96	8600	13900	1.61
7.6	LA	100/1	PO	PO	100	5h	89	10500	12900	1.63
7.7	LA	100/1	PO	PO	100	2h	94	14000	13600	1.72
7.8	LA	100/1	PO	PO	100	2h	90	11800	13100	1.78
7.9	CL	100/1/1	PO	PPNCl	RT	8h	83	10900	9400	1.12
7.10						24h	90	15500	10300	1.19
7.10					60	3d	76	10800		1.18
7.10					80	1d	72	9400		1.11
7.11					60	0.25d	76	10300		1.30
7.12	LA	100/1	PO	-	60	0.25d	80	7650	-	1.11
7.13					80	1d	93	11850		1.35
7.14					80	2d	92	12700		1.17
7.15					80	4d	92	8750		1.22
7.16					80	0.67	95	12150		1.09
7.19							95	8800	13700	1.40
7.20	LA	100/1/50	Tol	PO	120	24h	95	1500	13700	1.70
7.21							95	3300	13700	1.40

7.22								95	9000	13700	1.60
7.23								93	2100	13400	1.60
7.24								95	2100	13700	4.00
7.25								93	12600	13400	1.80
7.26								89	17200	12800	1.50
7.32		200/1/1					20min	82	24800	-	1.04
7.33		200/1/1					1min	75	16700	-	1.20
7.34	LA	800/1/1	Tol	iPrOH	RT		1.5min	82	79900	-	1.38
7.35		400/1/1					0.5min	48	29900	-	1.09
7.36		200/1/1					7min	93	21300	-	1.14
7.37					130		32h	97	14000	-	1.55
7.38	LA	1000/1	Bulk	-	130		32h	95	10000	-	1.63
7.39					130		32h	92	6310	-	1.74
7.40					130		32h	95	4000	-	1.87
7.41b	LA	1000/1		-	70		77min	88	39500	-	1.88
7.41c	LA	1000/1		-	70		37min	94	54400	-	1.25
7.41b	CL	100/1	Tol	-	25		190min	100	18600	-	1.81
7.41c	CL	50/1		-	25		20min	100	7500	-	1.19
7.42	LA	100/1	Tol	-	RT		20min	94	37500	-	1.12
7.42	CL	100/1	Tol	-	RT		20min	95	86200	-	1.38
7.43		230/1	DCM	-	RT		120min	99	21400	-	1.57
7.44		210/1	DCM	-	RT		60min	83	25200	-	1.89
7.45		50/1	DCM	-	RT		24h	14	15600	-	1.45
7.46a		50/1	DCM	-	RT		3h	93	6800	-	1.16
7.46a	LA	50/1/2	DCM	4-methoxyphenol	RT		3h	88	7200	-	1.18
7.46b		50/1/2	DCM	4-terbutylphenol	RT		24h	93	7500	-	1.21
7.46c		50/1/2	DCM	Neopentyl alcohol	RT		2h	96	4000	-	1.27
7.47a		50/1	Chloro benzene	-	RT		20min	86	16000	6200	1.14

7.47c		50/1	Tol	-	RT	10min	91	9600	6600	1.12
7.49		100/1	Bulk	-	130	1h	47	4900	6800	1.23
7.50		100/1	Bulk	-	130	1h	97	12500	14000	1.40
7.51		500/1	Bulk	-	120	48h	48	4700	-	1.50
Cobalt										
8.1	LA	100/1	Tol	-	25	72h	93	-	-	1.24
8.1					70	4h	92	-	-	1.19
8.2							13	-	-	-
8.3							45	5000	6400	1.21
8.4	LA	1000/1/10	Bulk	BnOH	130	3h	26	2300	3700	1.07
8.5							10	-	-	-
8.6							60	7300	8600	1.08
8.9							-	-	-	-
8.7	LA	200/1/1	Tol	<i>i</i> PrOH	RT	20min	82	25000	-	1.06
8.8						2min	81	23600	-	1.09
8.10	CL	500/1/1	Bulk	BnOH	130	24h	99	6 500	5 050	1.34
8.11a							94	12390	13540	1.11
8.11b	LA	100/1	Tol	-	130	60min	73	15330	10520	1.13
8.11c							91	19520	13110	1.22
Nickel										
9.3							90	10200	6600	1.10
9.4	LA	100/1/1	DCM	BnOH	RT	20h	88	10300	6500	1.07
9.5							85	9600	6200	1.09
9.3a					160	12h	-	30154	-	1.13
9.3b								30702	-	1.14
9.3c					130	24h	65	26940	-	1.12
9.3d	LA	1000/1	Bulk	-				28962		1.19
9.3e					160	12h	-	31555	-	1.13
9.3f								30035		1.15
9.3g								30695		1.16

9.4a							74	31507		1.08
9.4b							73	32109		1.12
9.4c							68	33183		1.13
9.4d	LA	1000/1	Bulk	-	130	24h	65	33661	-	1.09
9.4e							64	33555		1.05
9.4f							62	34032		1.10
9.4g							61	34834		1.14
Copper										
10.1							66	18500	-	1.43
10.2	LA	50/1	Bulk	-	160	4h	70	10400	-	1.43
10.3							55	15900	-	1.58
10.4						24h	18	-	-	-
10.5	LA	50/1	Tol	-	70	-	-	-	-	-
10.6							-	-	-	-
10.7			Dioxane	-	100	68h	10	-	-	-
10.8					70	35h	55	-	-	-
10.9	LA	50/1	Tol	-	-	-	-	-	-	-
10.10					70	35h	80	-	-	-
10.11		200/1	Bulk	-	145	1440	96	28800	-	1.08
10.11		200/1/5	Water	<i>i</i> PrOH	145	1140	98	5780	-	1.04
10.11		200/1/5	<i>i</i> PrOH	<i>i</i> PrOH	145	1080	98	5820	-	1.08
10.12		300/1/1	DCM	BnOH	RT	60min	95	35300	-	1.07
10.13		300/1/1	DCM	BnOH	RT	60min	95	4300	-	1.08
10.14	LA	300/1/2	DCM	BnOH	RT	60min	95	4300	-	1.53
10.15		1000/1	Bulk	-	130	24h	51	14100	-	1.38
10.16		1000/1	Bulk	-	130	24h	35	21800	-	1.19
10.17		300/1	DCM	-	RT	3	80	34600	-	1.03
10.17		300/1/1	DCM	<i>i</i> PrOH	RT	0.75	96	20800	-	1.04
10.17		300/1/5	DCM	<i>i</i> PrOH	RT	0.75	97	7000	-	1.07
10.18		300/1	DCM	-	RT	3-11 min	95-98	29400	-	1.04

10.19								10	1500	1600	1.10
10.20	LA	200/1/2	Tol	9-AnOH	110	6h		92	10800	13500	1.75
10.21								93	12600	13600	1.13
10.22	LA	200/1	C ₆ D ₆	-	RT	1440		84	21000	-	1.10
10.23								86	45000	-	1.00
10.24	LA	100/1	C ₆ D ₆	-	RT	≤5h		97	4300	1400	1.7
10.24	LA	100/1/1	C ₆ D ₆	PyCH ₂ OH	RT	≤5h		99	2400	14100	2.6
10.25	LA	100/1	C ₆ D ₆	-	50	≤5h		24	800	3500	1.3
10.28A	LA	100/1	C ₆ D ₆	-	RT	≤5h		98	7500	14100	1.1
10.29A	LA	100/1	C ₆ D ₆	-	RT	≤5h		96	7700	13800	1.2
10.31B	LA	100/1	C ₆ D ₆	-	RT	≤5h		97	14500	14000	1.2
10.32A	LA	100/1	C ₆ D ₆	-	RT	≤5h		99	5500	14300	1.5
10.33A	LA	100/1	C ₆ D ₆	-	RT	≤5h		36	6900	5200	1.3
10.33B	LA	100/1	C ₆ D ₆	-	RT	≤5h		26	1400	3700	1.3
10.26								15	-	-	-
10.27	LA	100/1	C ₆ D ₆	-	RT	≤5h		3	-	-	-
10.34B								98	15300	14100	1.3
10.35B								13	-	-	-
10.36								100	33000	14400	1.53
10.37								100	30000	14400	1.54
10.38	LA	100/1	DCM	MeLi	-25	2h		100	17500	14400	1.50
10.39								97	10400	14000	1.25
10.40								100	24800	14400	1.54
10.41								99	23500	14200	1.54

Annexes Chapter II

Figure S 1: ^1H NMR spectrum of the Ligand 1.1 in CD_2Cl_2 (*), 400MHz.....	218
Figure S 2 : ^1H NMR spectrum of the Ligand H₂L^{1.2} recorded in CD_2Cl_2 (*), 400 MHz.	218
Figure S 3 : ^1H NMR spectrum of the Ligand H₂L^{1.3} recorded in CD_2Cl_2 (*), 400 MHz.	219
Figure S 4 : ^1H NMR spectrum of the Ligand H₂L^{1.5} recorded in CD_2Cl_2 (*), 400 MHz.	219
Figure S 5 : ^1H NMR spectrum of the Ligand H₂L^{1.6} recorded in CD_2Cl_2 (*), 400 MHz.....	220
Figure S 6: ^1H NMR spectrum of the Ligand H₂L^{1.7} recorded in CDCl_3 (*), 400 MHz.....	220
Figure S 7: ^1H NMR spectrum of the Ligand H₂L^{1.8} recorded in CD_2Cl_2 (*), 400 MHz.	221
Figure S 8 : ^1H NMR spectrum of the Ligand H₂L^{1.9} recorded in CDCl_3 (*), 400 MHz.....	221
Figure S 9 : ^1H NMR spectrum of the Tripodal ligand H₂L^{1.11} recorded in CDCl_3 (*), 400 MHz.	222
Figure S 10 : ^1H NMR spectrum of the Tripodal ligand H₂L^{1.12} recorded in CDCl_3 (*), 400 MHz.	222
Figure S 11 : ^1H NMR spectrum of the Tripodal ligand H₂L^{1.13} in C_6D_6 (*), 400MHz.	223
Figure S 12 : ESI of complex 2.1	223
Figure S 13: EPR spectrum of complex 2.1 in toluene.	224
Figure S 14: ESI of complex 2.2	224
Figure S 15: EPR spectrum of complex 2.2 in toluene.	225
Figure S 16: ESI of complex 2.3	225
Figure S 17: ESI of complex 2.5	226
Figure S 18: ESI of complex 2.6	226
Figure S 19: Zoom and simulation ESI of complex 2.6	227
Figure S 20: ESI of complex 2.7	227
Figure S 21: ESI of complex 2.8	228
Figure S 22: UV-Vis analysis made in toluene 3.2	228
Figure S 23: ^1H NMR spectrum of 3.4 recorded in C_6D_6 (*), 400MHz.	229
Figure S 24 : Time dependence of the <i>acac</i> ^1H NMR resonances for $[\text{Co}(\text{acac})_2(\text{O}_2\text{CPh})]$ at 40°C . The starred resonance is the residual peak of the C_6D_6 solvent.	229
Figure S 25 : Time dependence of the <i>acac</i> ^1H NMR resonances for $[\text{Co}(\text{acac})_2(\text{O}_2\text{CPh})]$ at 60°C . The starred resonance is the residual peak of the C_6D_6 solvent.	230
Figure S 26: ^1H NMR spectrum of bis(<i>p</i> -nitrobenzoyl) peroxide recorded in CDCl_3 , 400MHz.	230
Figure S 27: ^1H NMR spectrum of bis(<i>p</i> -tert-benzoyl) peroxide recorded in CDCl_3 , 400MHz.....	231
Figure S 28 : ^1H NMR spectrum of bis(<i>o</i> -nitrobenzoyl) peroxide recorded in CDCl_3 , 400MHz.	231
Figure S 29 : ^1H NMR spectrum of bis(<i>p</i> -methoxybenzoyl) peroxide recorded in CDCl_3 , 400MHz.	232
Figure S 30: ^1H NMR spectrum of diacetyl peroxide recorded in CDCl_3 , 400MHz.....	232
Figure S 31: ^1H NMR spectrum of 3.7 in C_6D_6 (*), 400MHz.	233
Figure S 32: ^1H NMR spectrum of 3.8 in C_6D_6 (*), 400MHz.	233
Figure S 33: ^1H NMR spectrum of 3.9 in CDCl_3 (*), 300MHz.	234
Figure S 34 : ^1H NMR spectrum of 3.10 in CDCl_3 (*), 400MHz.	234
Figure S 35 : Cyclic voltammogram of compounds $\text{Co}^{\text{III}}(\text{acac})_2\text{O}(\text{O})\text{C}(\text{Ar})-\text{O}_2$ (3.10), in CH_2Cl_2 on a GC working electrode at various scan rates. [Complex] = 10^{-3} M; supporting electrolyte = $n\text{Bu}_4\text{PF}_6$ 0.1 M).	235
Figure S 36: ^1H NMR spectrum of 3.12 in C_6D_6 (*), 400MHz.	235
Table S 1 : Crystal data and structure refinement for ligand 1.10 and tripodal complex 3.2	236
Table S 2 : Crystal data and structure refinement for Schiff-base complexes 3.3 , 3.4 , 3.5	238
Table S 3 : Crystal data and structure refinement for (O ₂ ,O ₂)-based cobalt III complexes 3.6 , 3.8 , 3.9 , 3.10 . ..	239

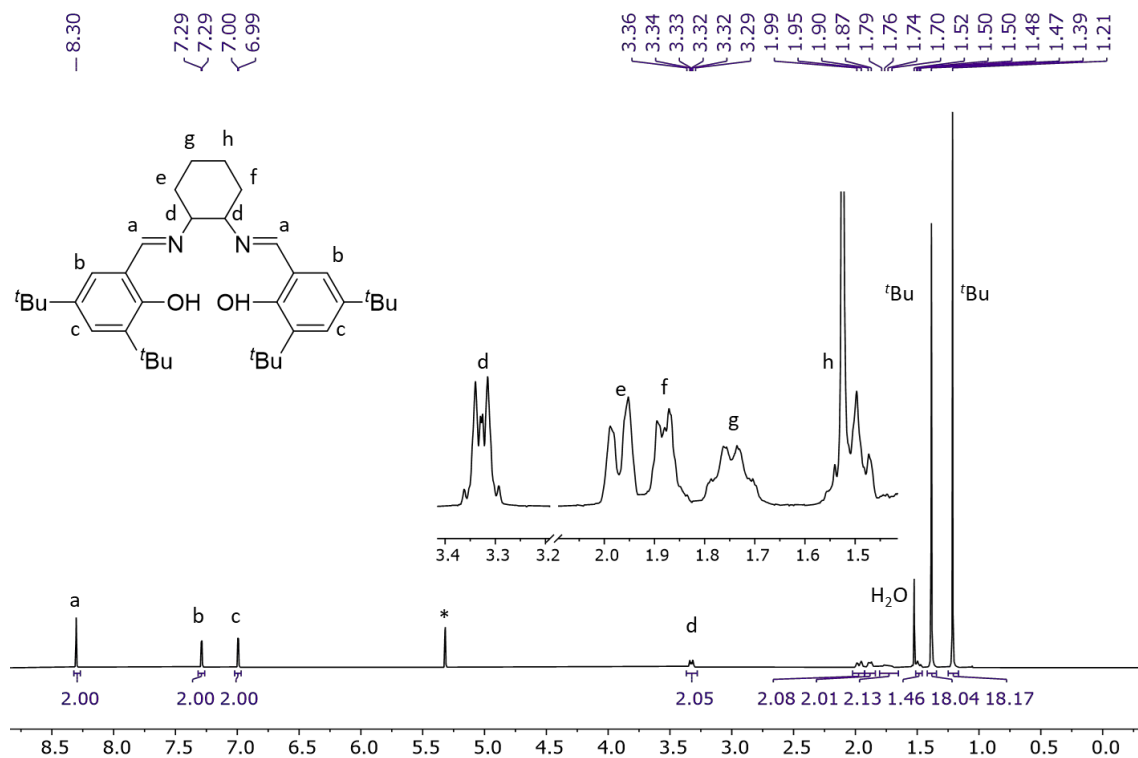


Figure S 1: ¹H NMR spectrum of the Ligand **1.1** in CD₂Cl₂ (*), 400MHz.

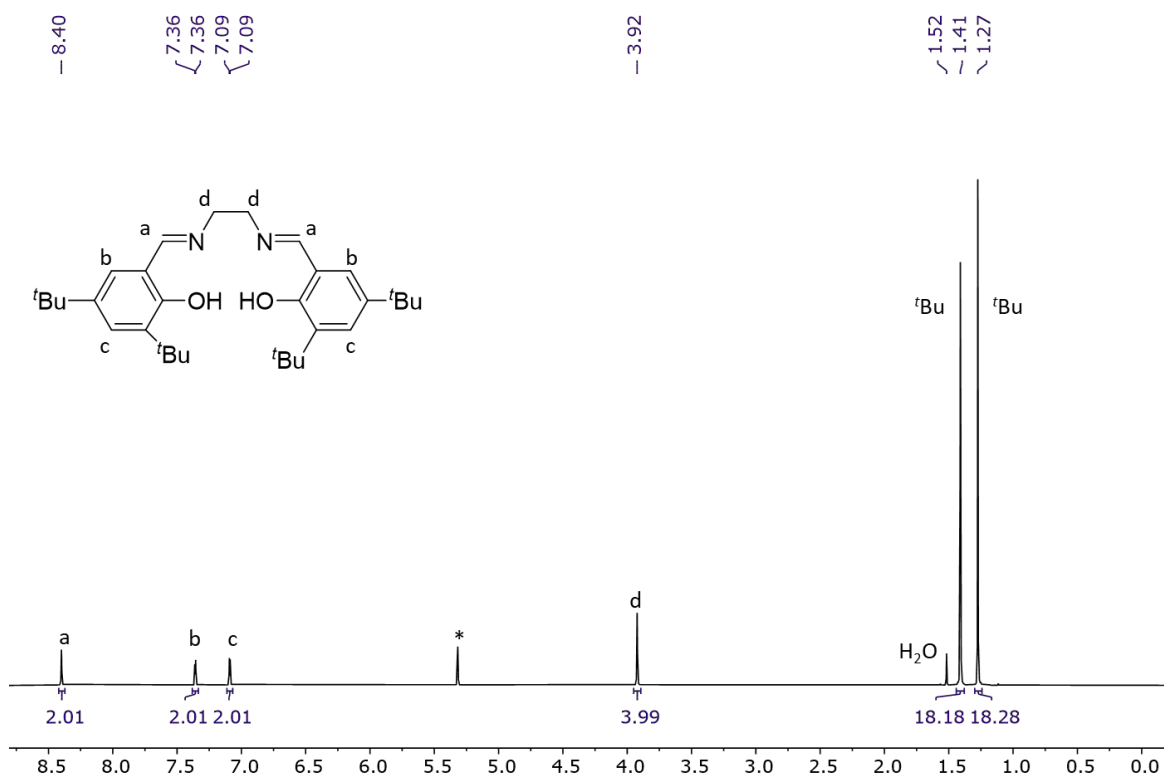
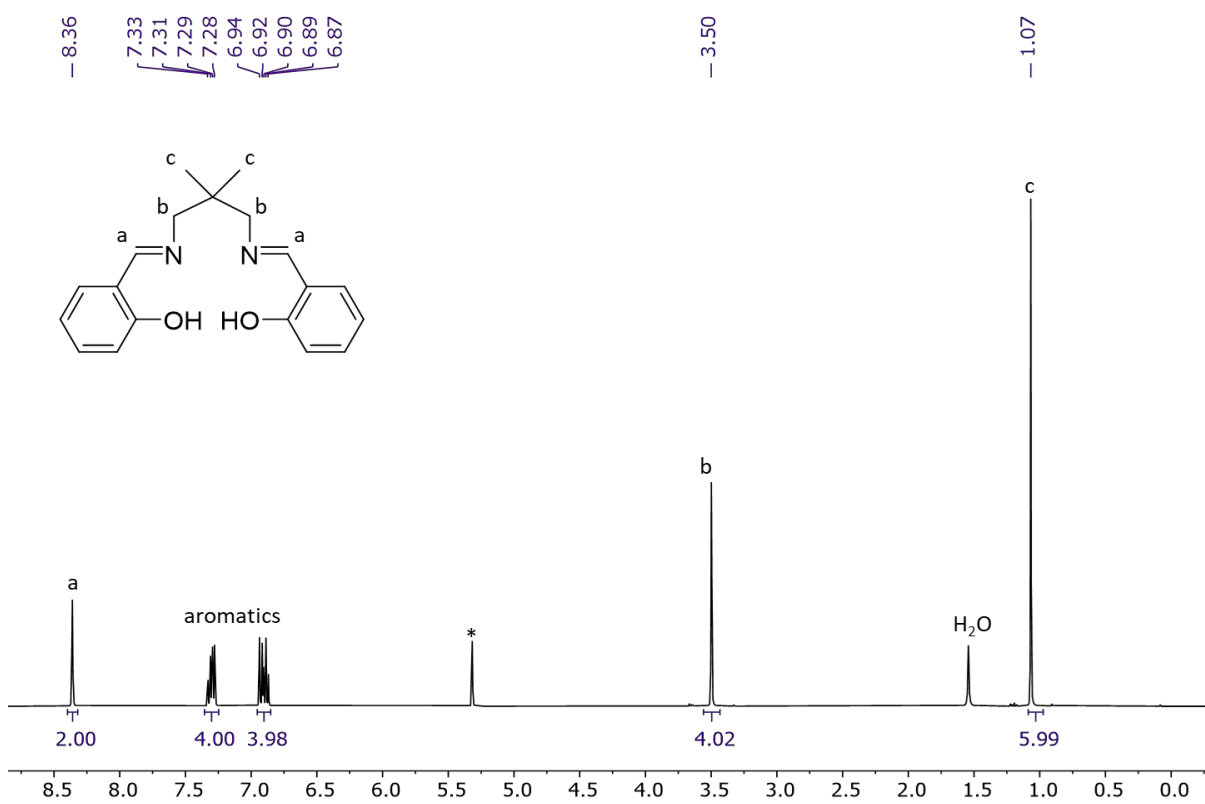
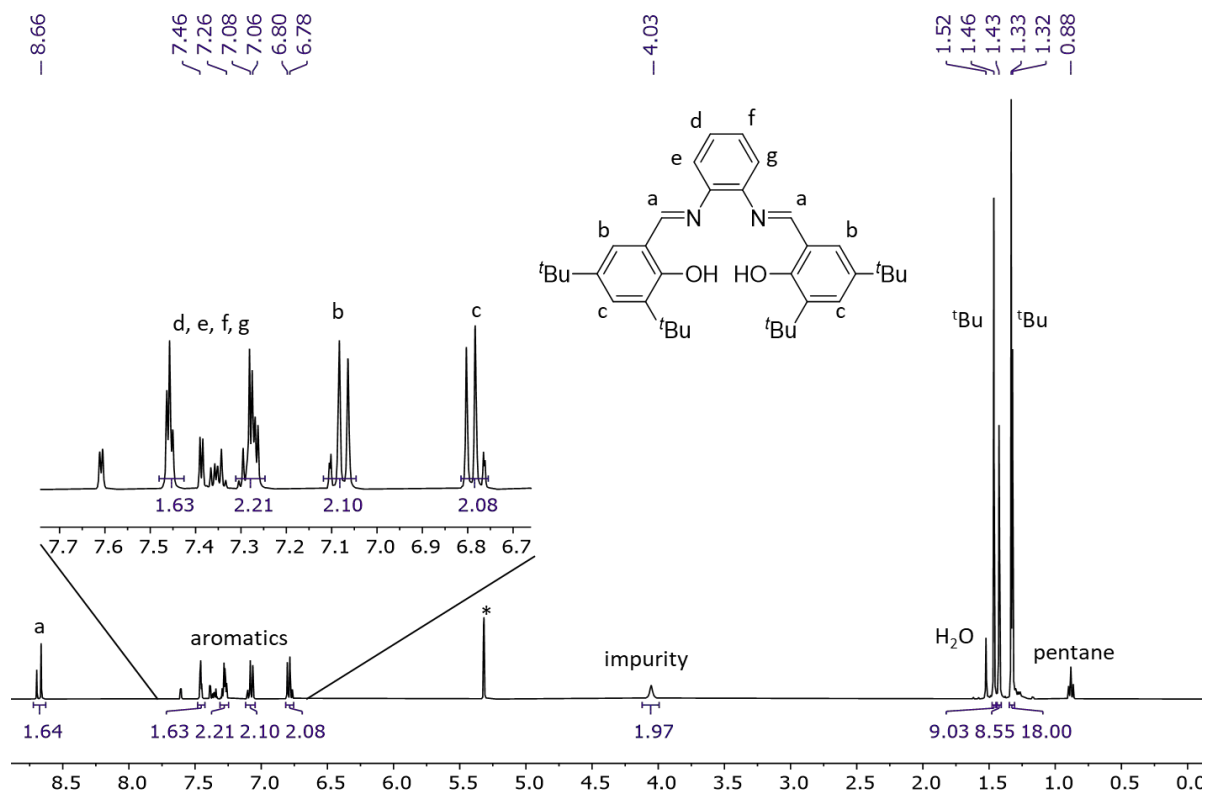


Figure S 2 : ¹H NMR spectrum of the Ligand **H₂L^{1.2}** recorded in CD₂Cl₂ (*), 400 MHz.



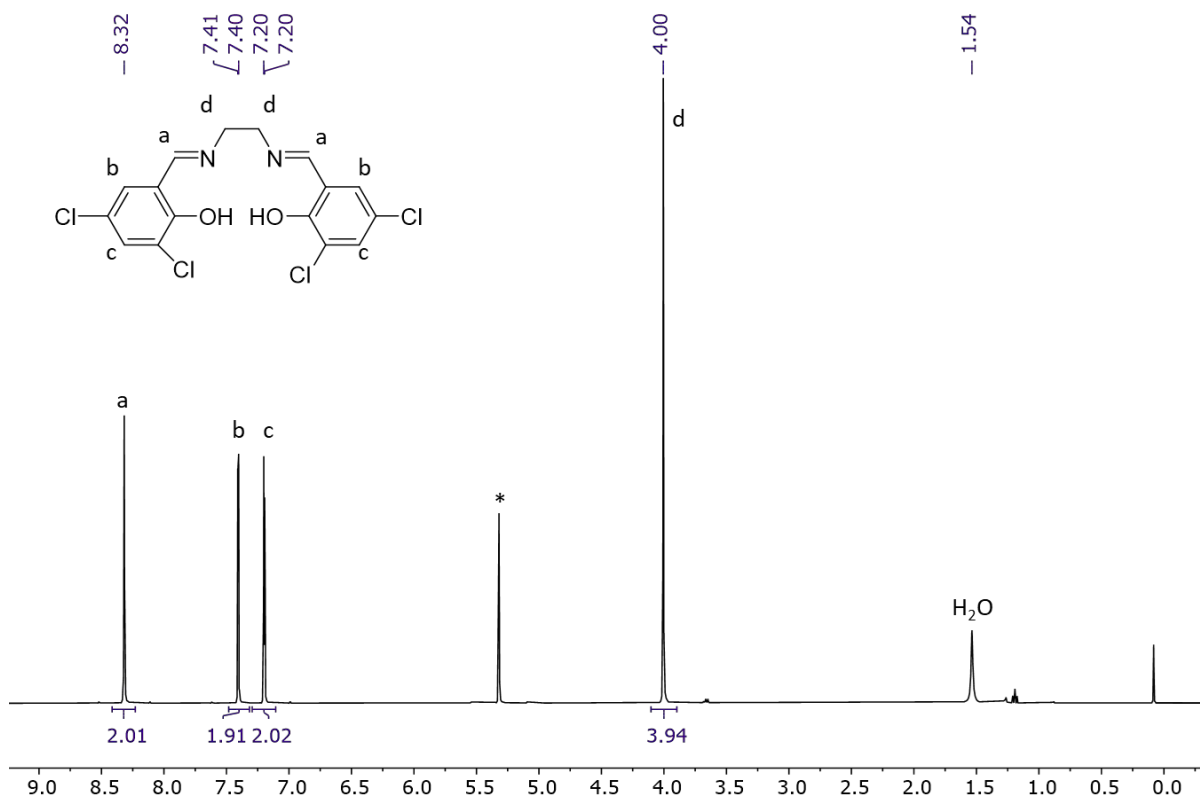


Figure S 5 : 1H NMR spectrum of the Ligand $H_2L^{1.6}$ recorded in CD_2Cl_2 (*), 400 MHz

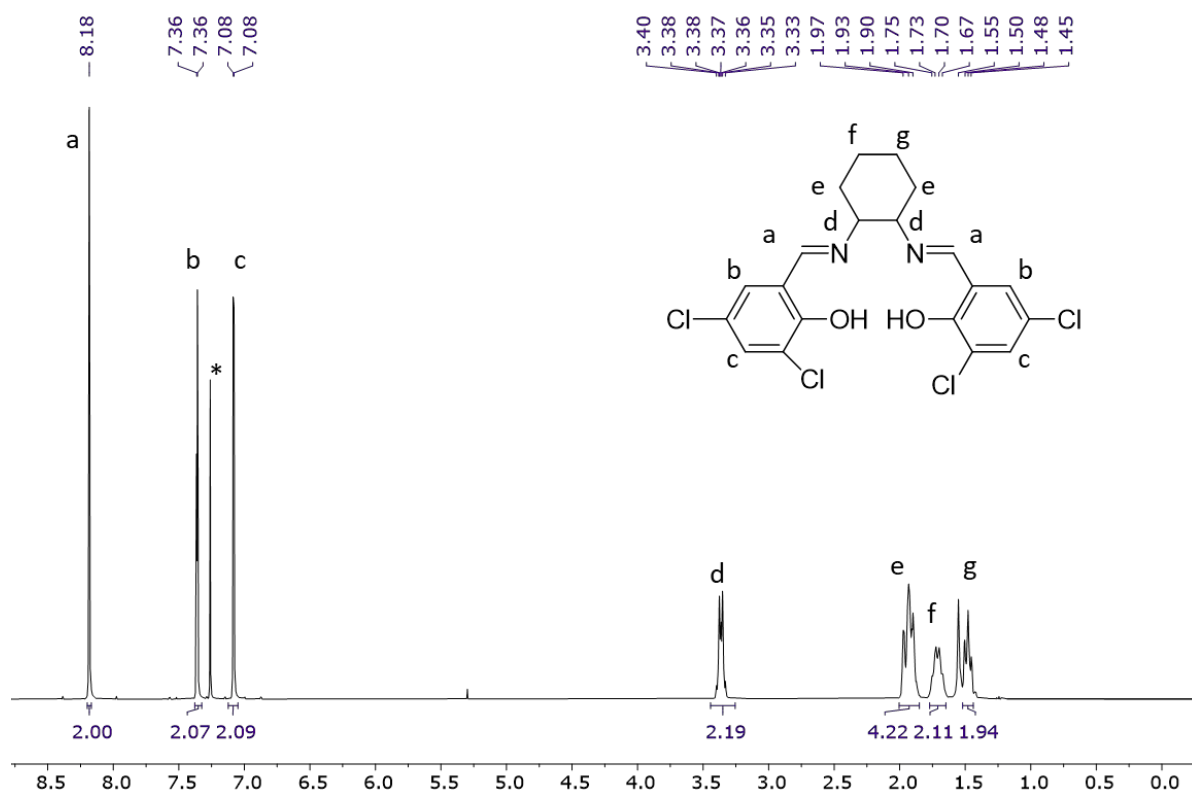


Figure S 6 : 1H NMR spectrum of the Ligand $H_2L^{1.7}$ recorded in $CDCl_3$ (*), 400 MHz.

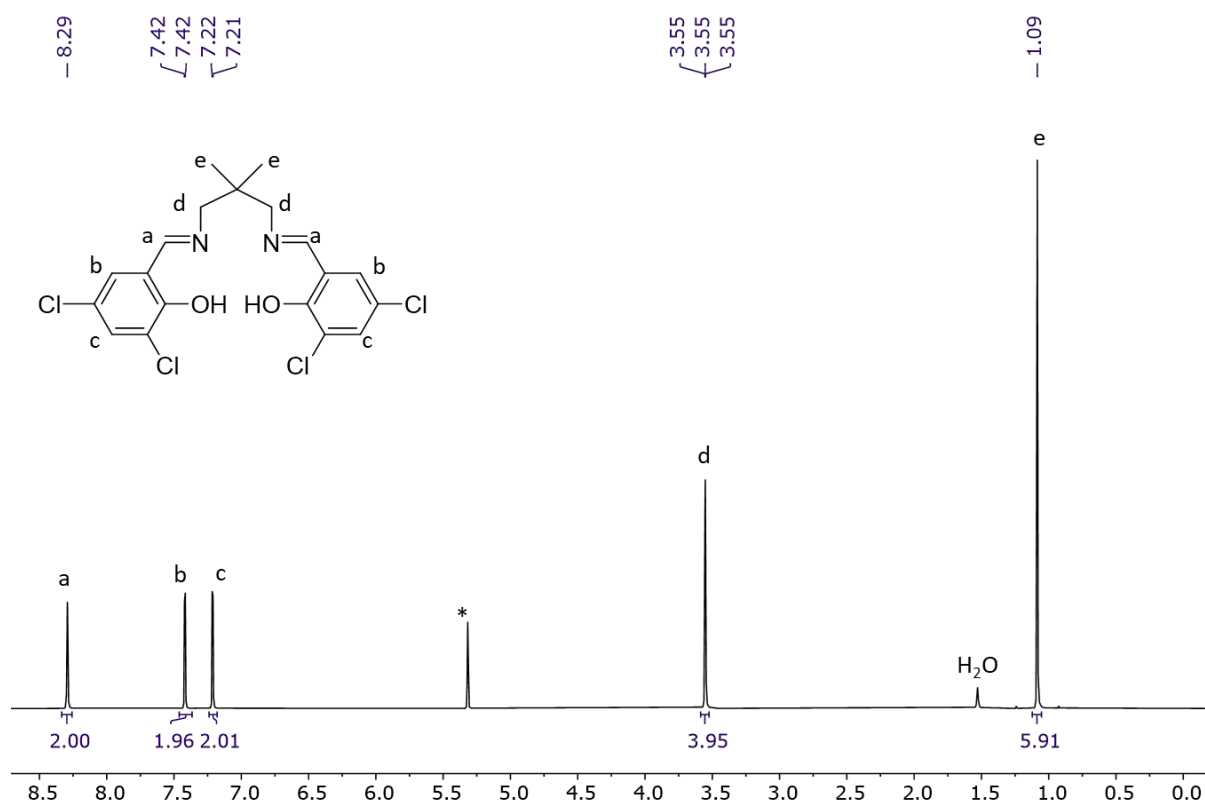


Figure S 7: 1H NMR spectrum of the Ligand $H_2L^{1.8}$ recorded in CD_2Cl_2 (*), 400 MHz.

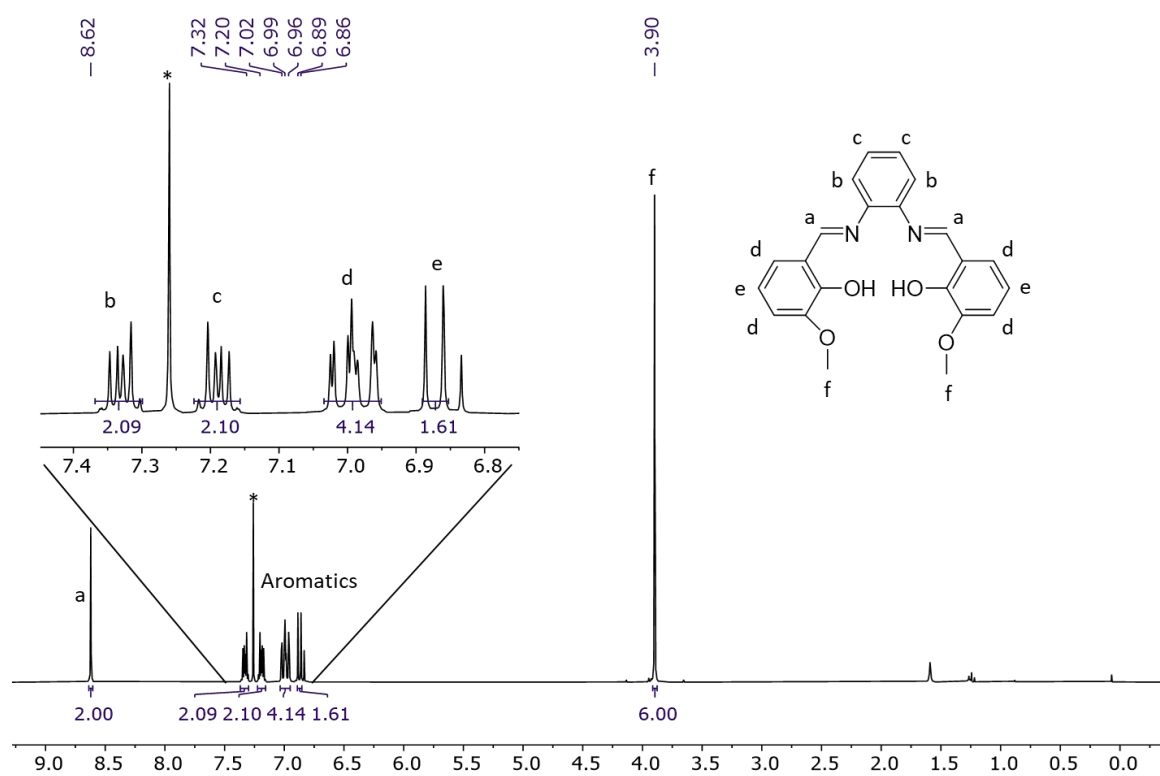


Figure S 8: 1H NMR spectrum of the Ligand $H_2L^{1.9}$ recorded in $CDCl_3$ (*), 400 MHz.

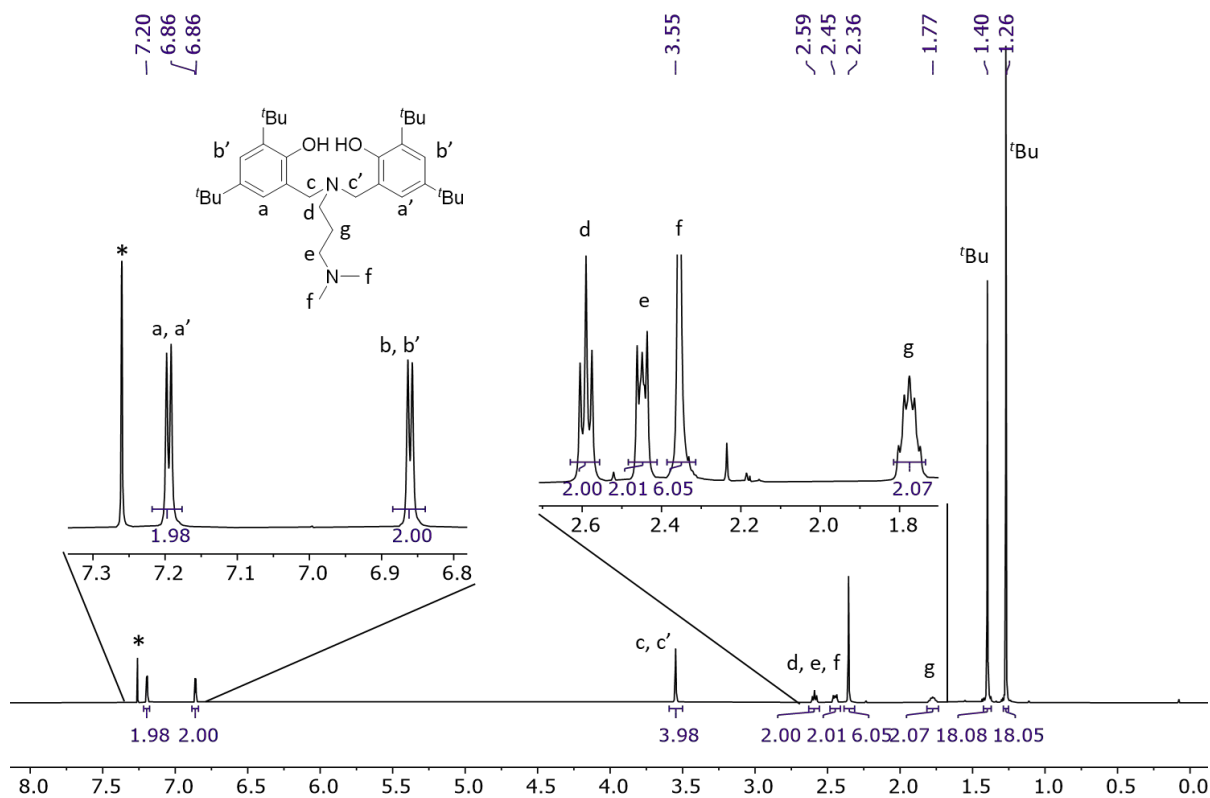


Figure S 9 : ^1H NMR spectrum of the Tripodal ligand $\text{H}_2\text{L}^{1.11}$ recorded in CDCl_3 (*), 400 MHz.

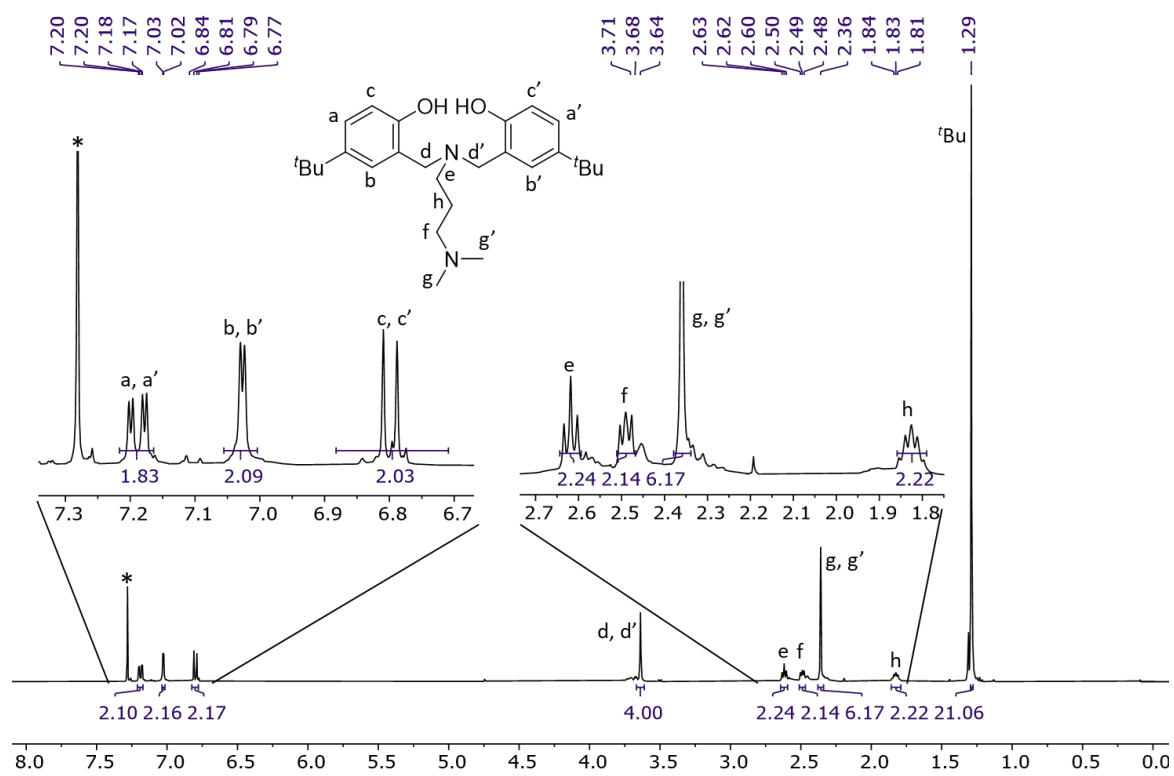


Figure S 10 : ^1H NMR spectrum of the Tripodal ligand $\text{H}_2\text{L}^{1.12}$ recorded in CDCl_3 (*), 400 MHz.

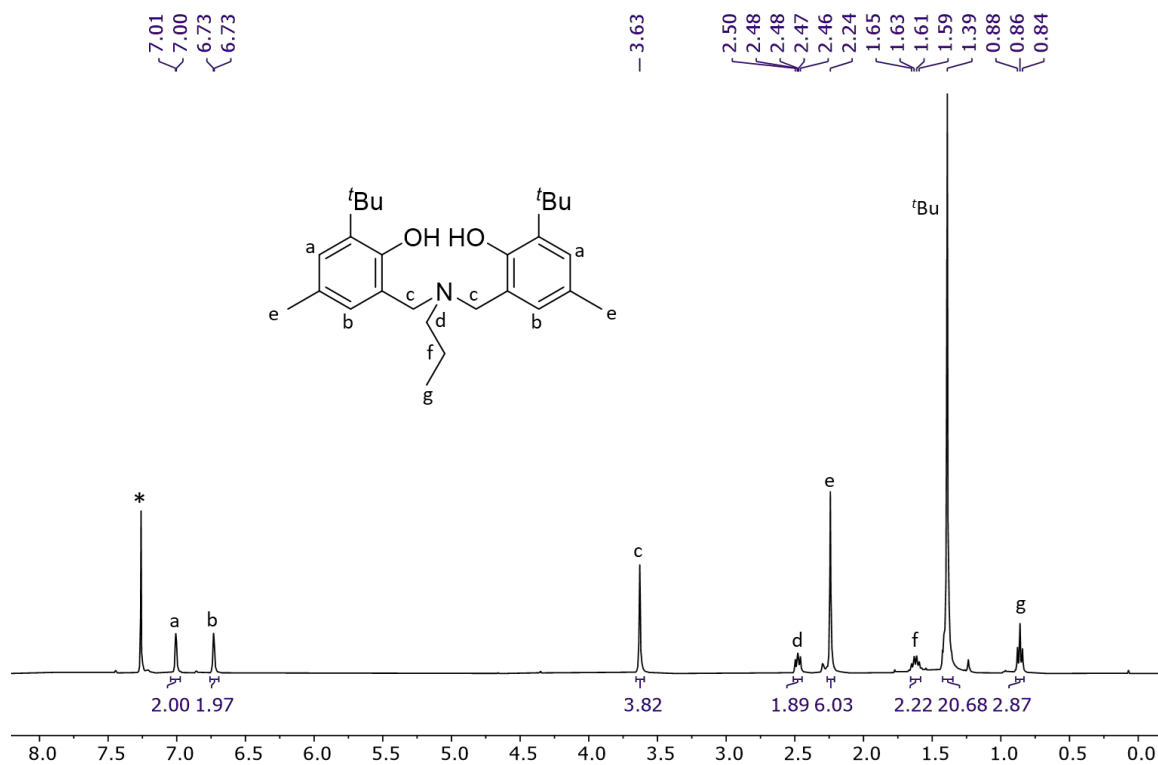


Figure S 11 : 1H NMR spectrum of the Tripodal ligand $H_2L^{1.13}$ in C_6D_6 (*), 400MHz.

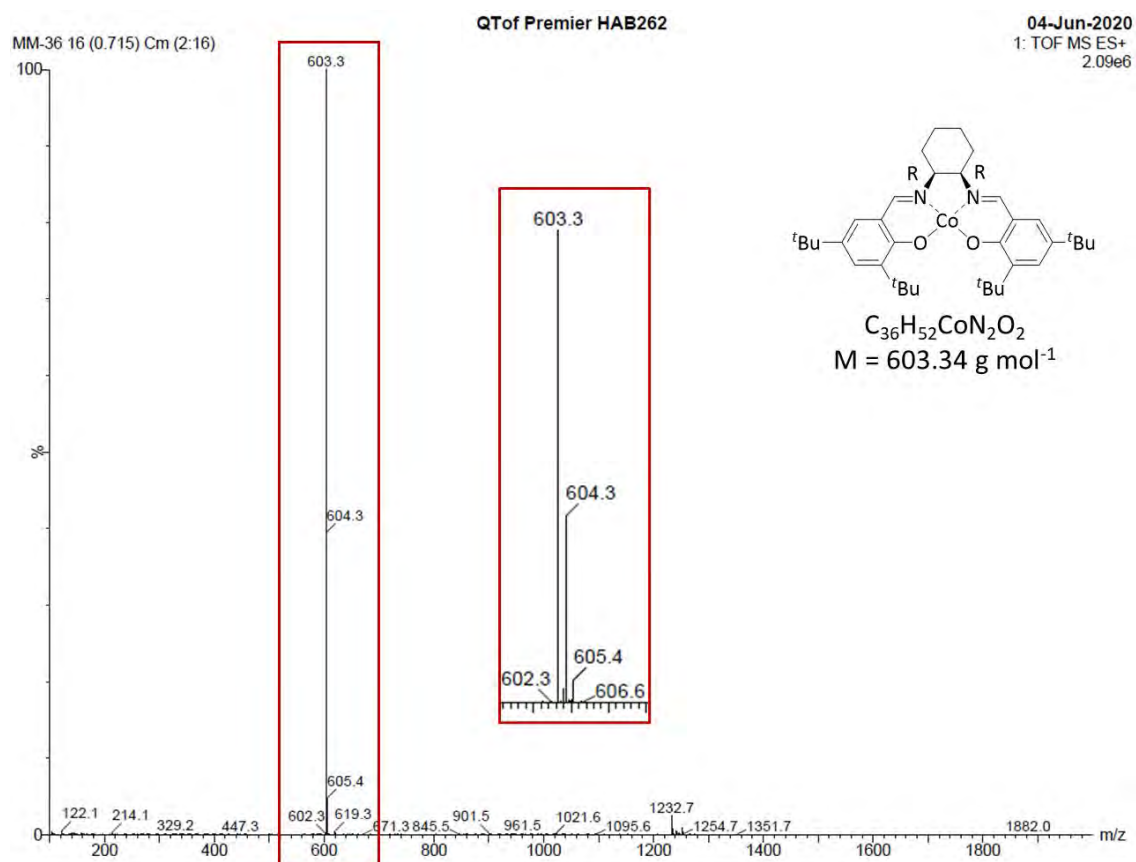


Figure S 12 : ESI of complex **2.1**.

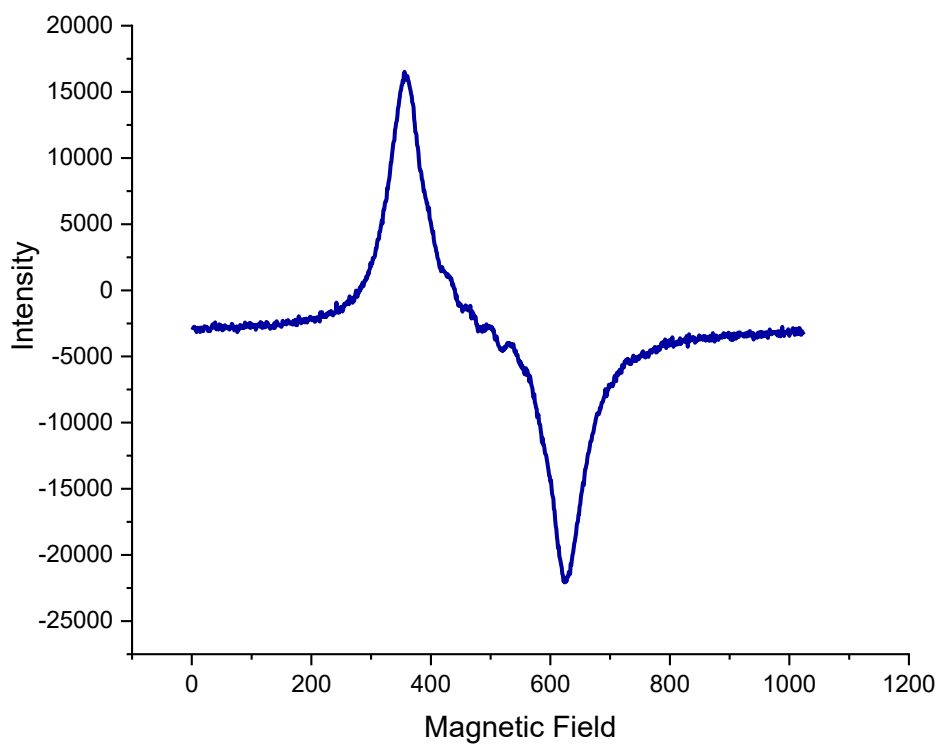


Figure S 13: EPR spectrum of complex **2.1** in toluene.

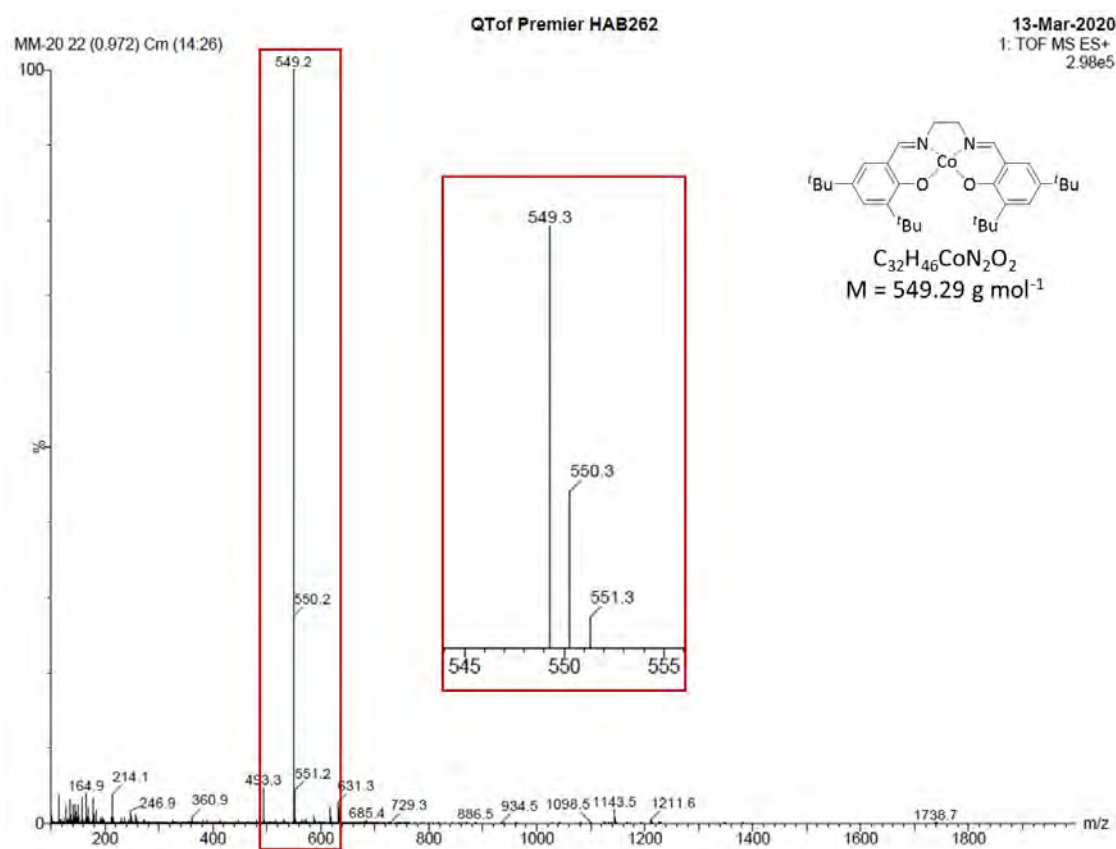


Figure S 14: ESI of complex **2.2**.

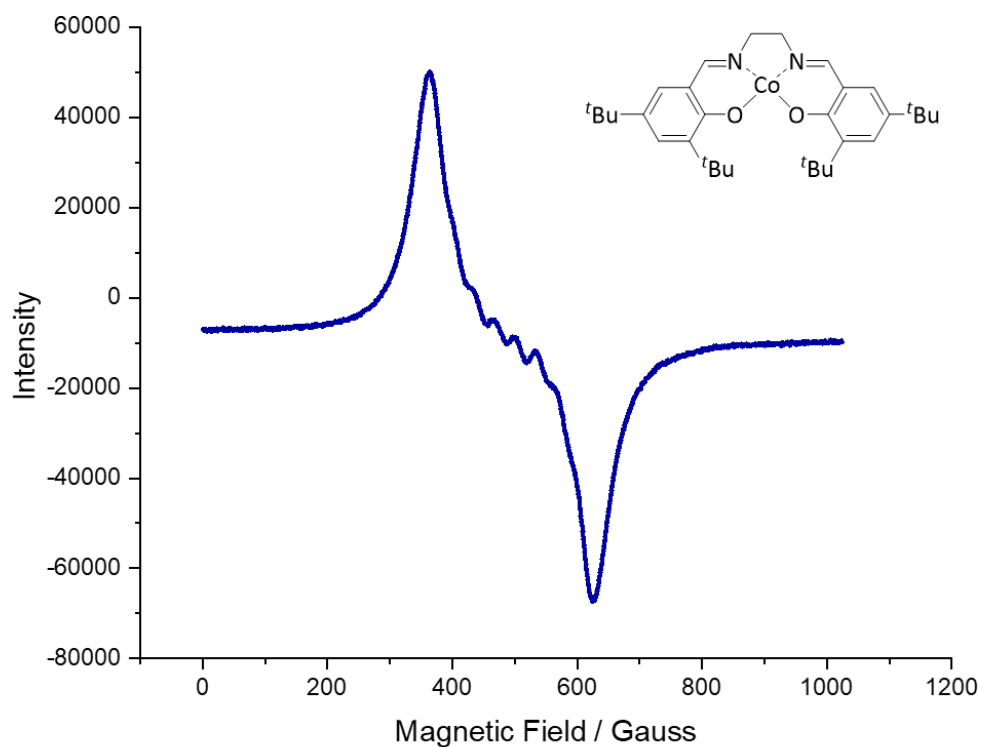


Figure S 15: EPR spectrum of complex **2.2** in toluene.

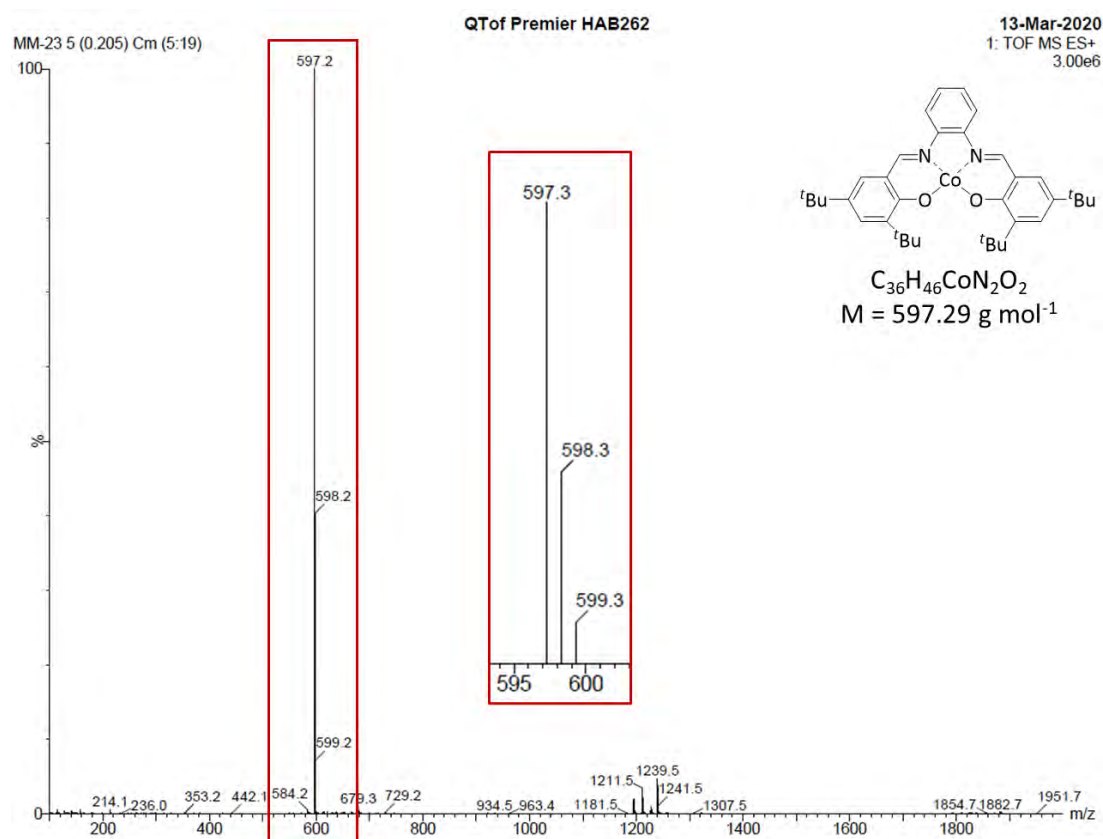


Figure S 16: ESI of complex **2.3**.

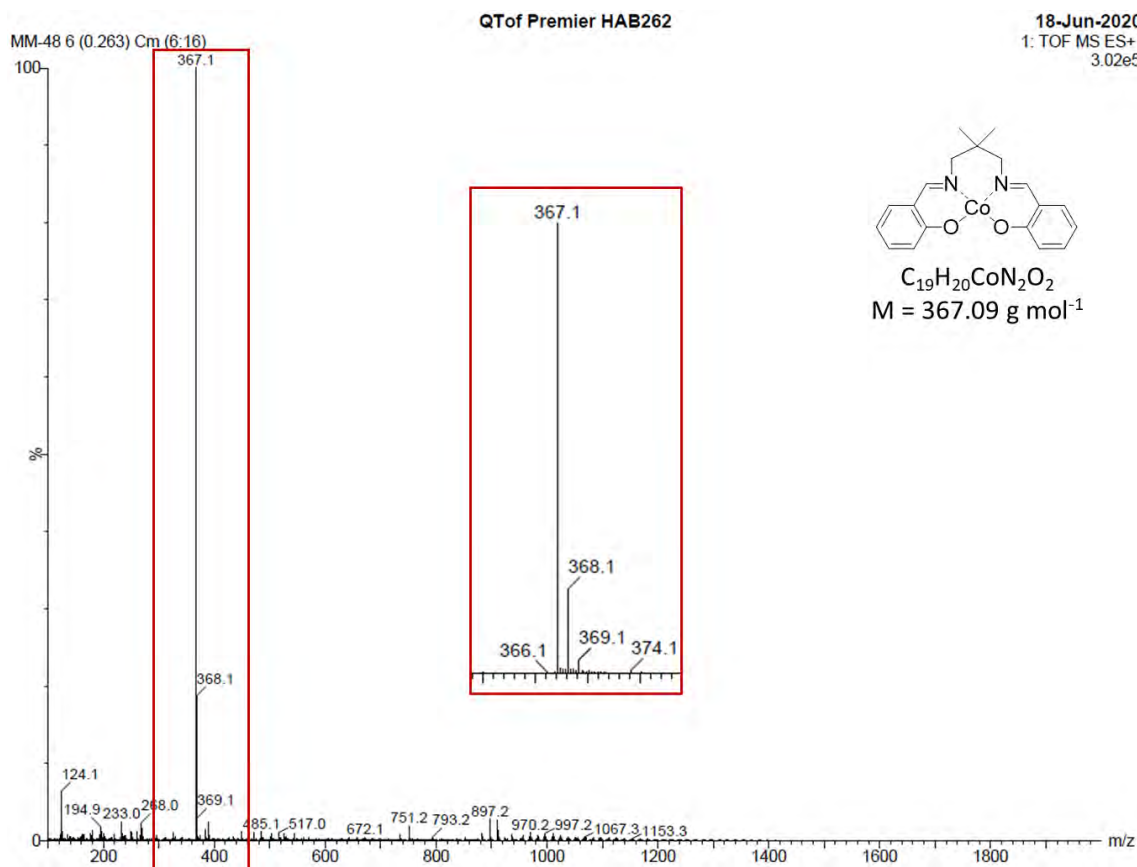


Figure S 17: ESI of complex 2.5.

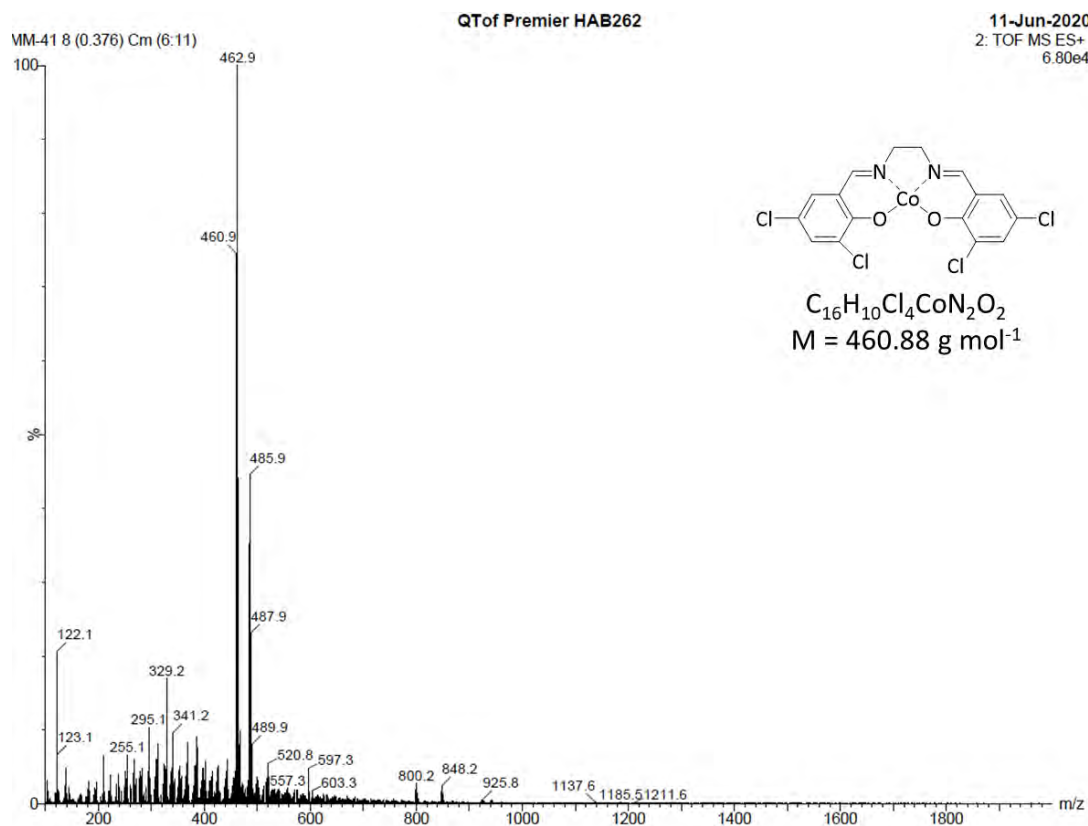


Figure S 18: ESI of complex 2.6.

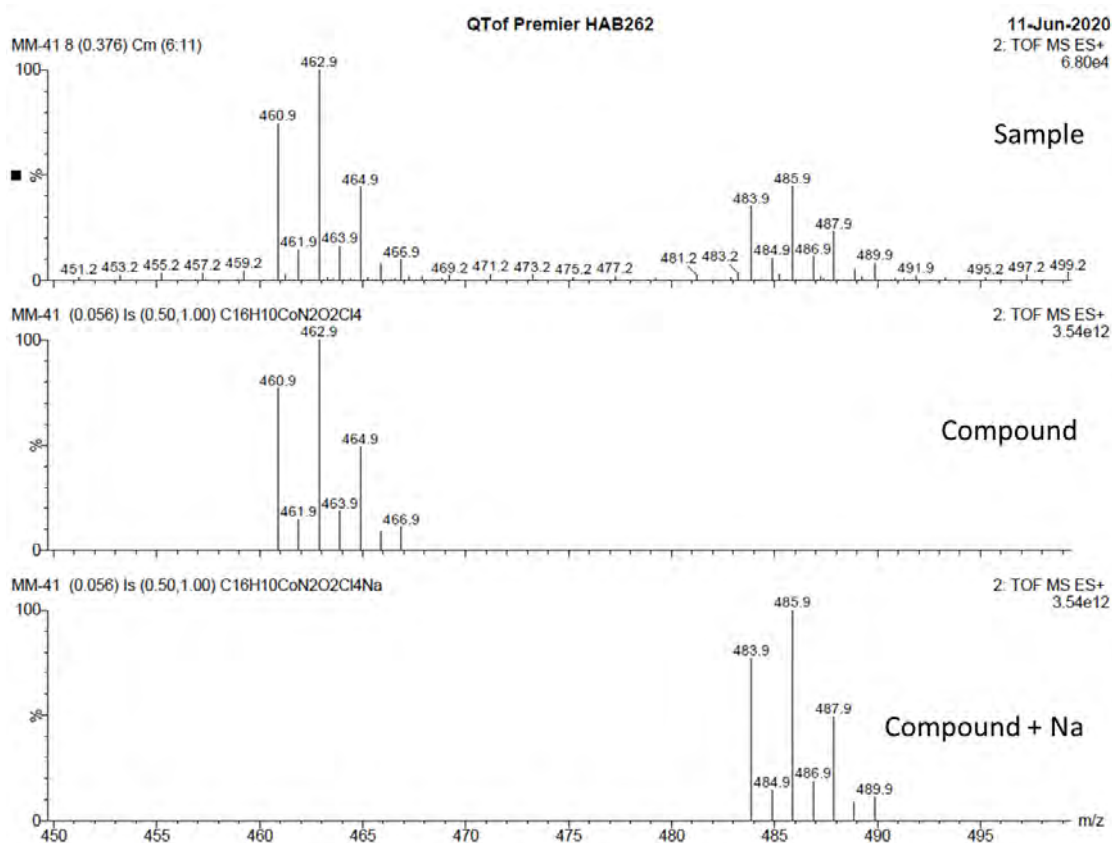


Figure S 19: Zoom and simulation ESI of complex 2.6.

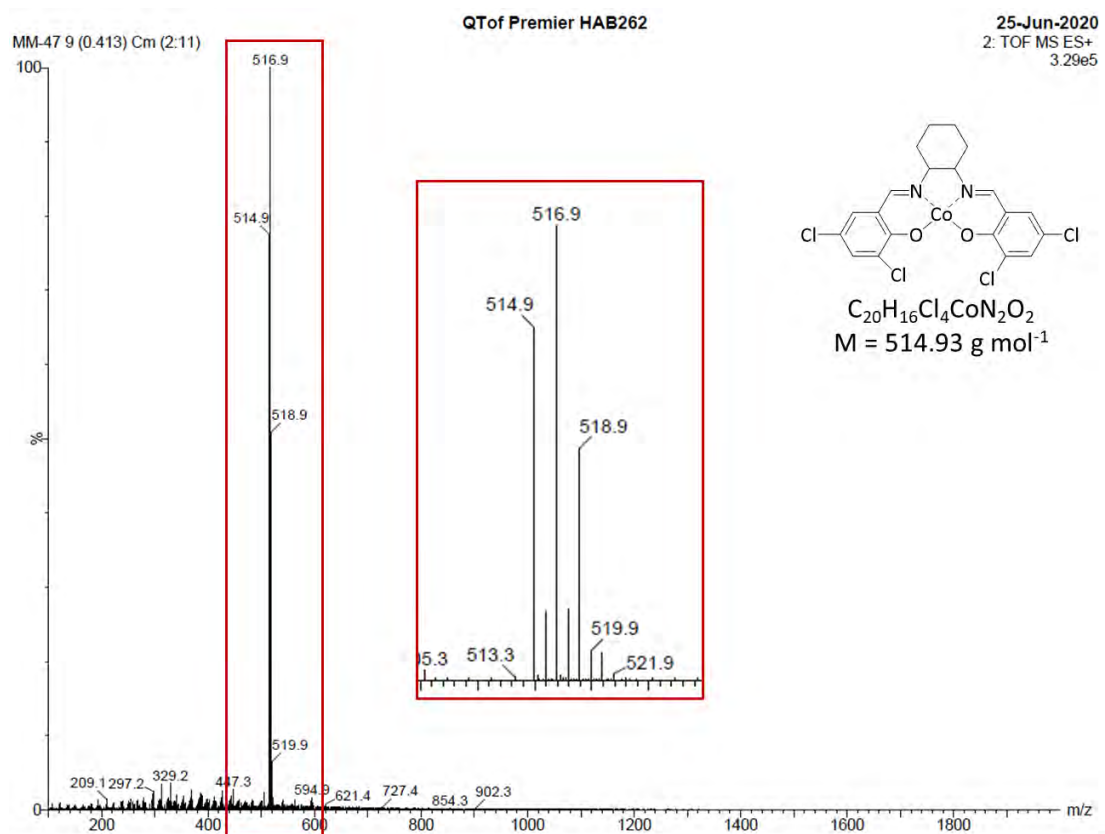
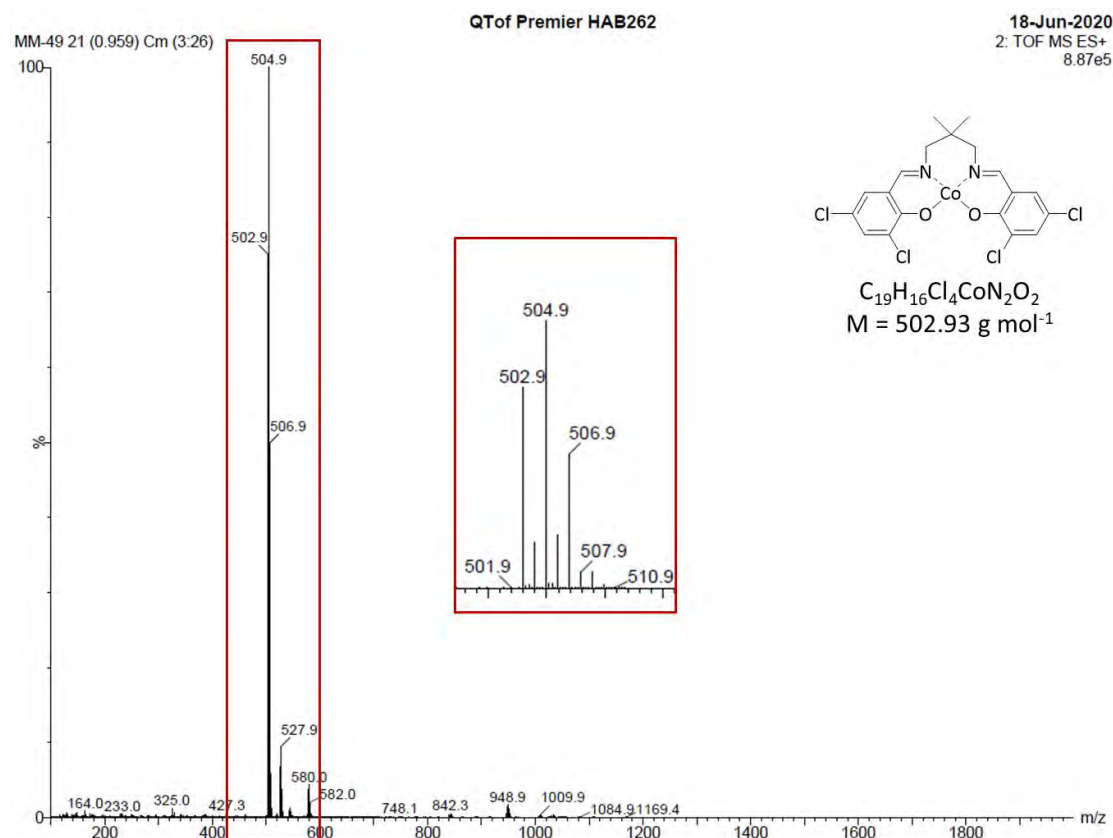
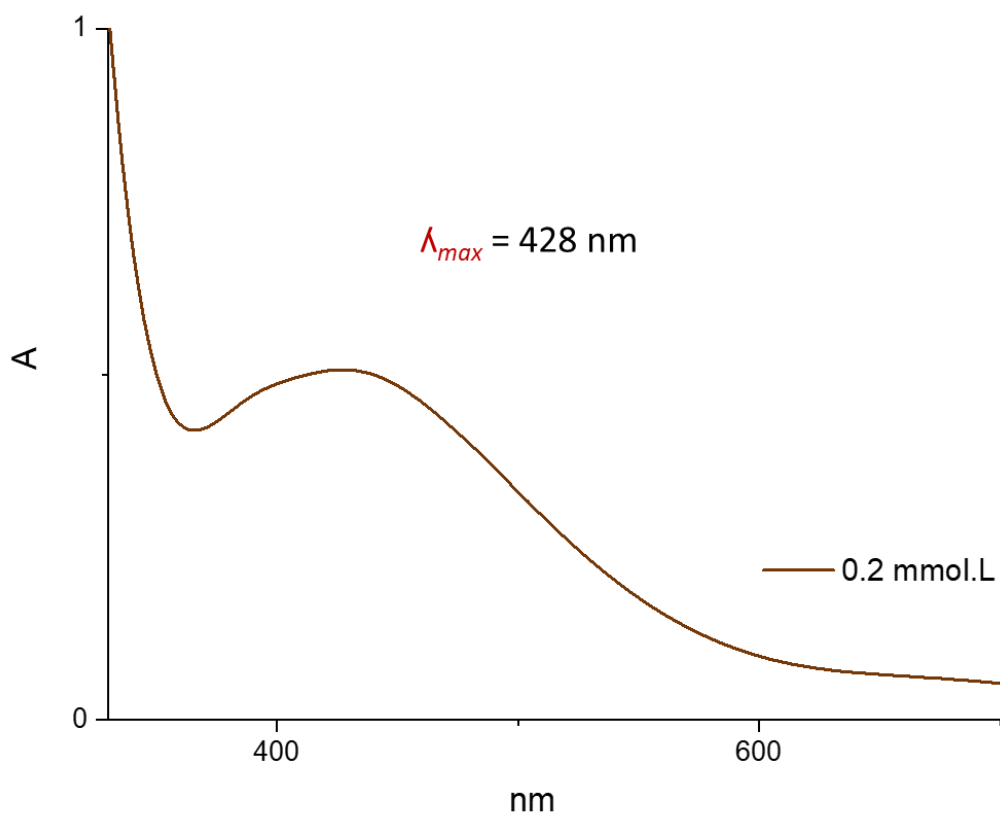


Figure S 20: ESI of complex 2.7.

Figure S 21: ESI of complex **2.8**.Figure S 22: UV-Vis analysis made in toluene **3.2**.

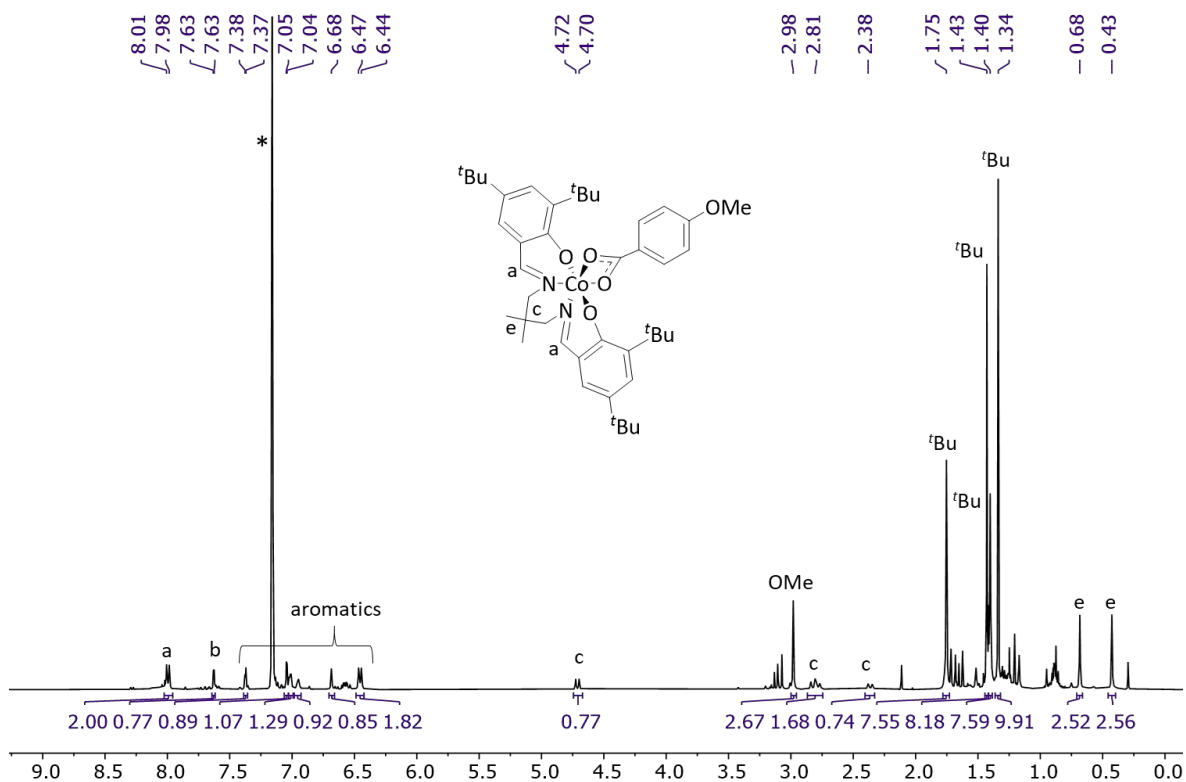


Figure S 23: ^1H NMR spectrum of 3.4 recorded in C_6D_6 (*), 400MHz.

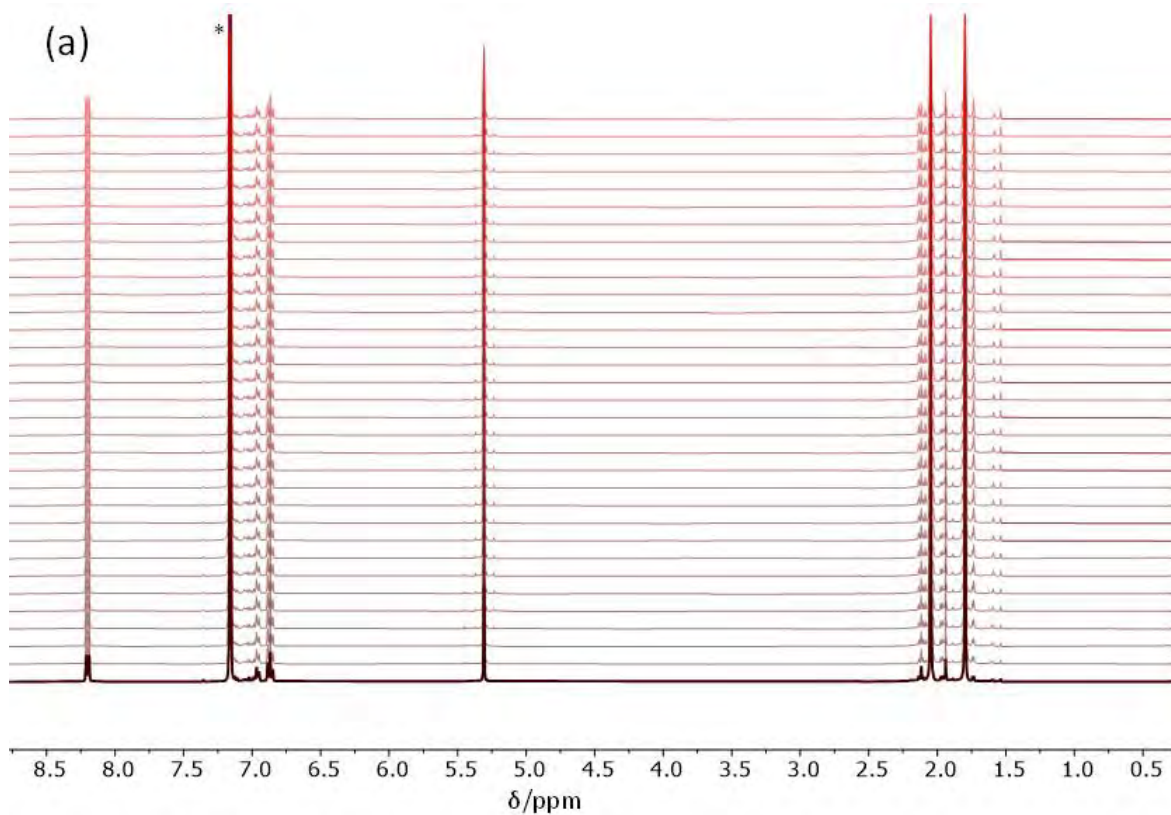


Figure S 24 : Time dependence of the acac ^1H NMR resonances for $[\text{Co}(\text{acac})_2(\text{O}_2\text{CPh})]$ at 40°C . The starred resonance is the residual peak of the C_6D_6 solvent.

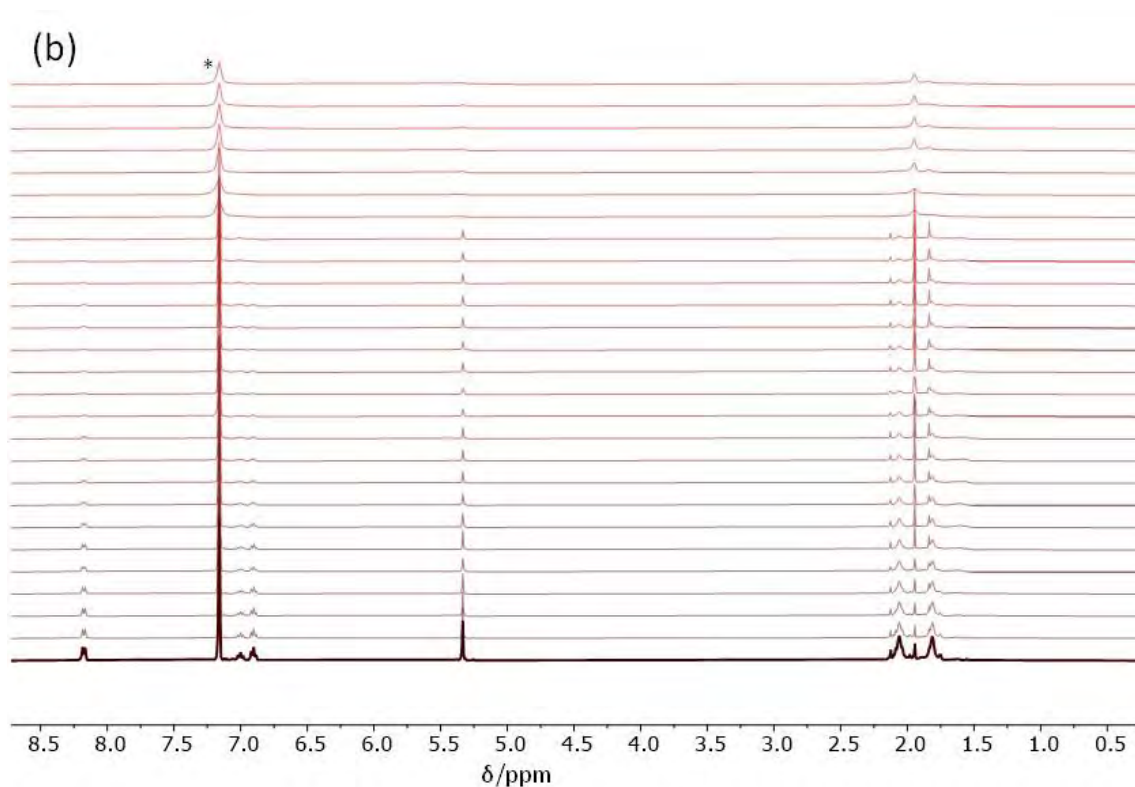
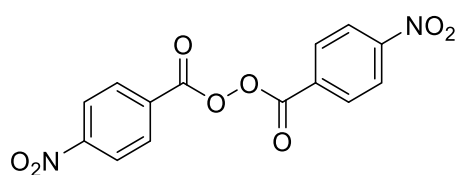


Figure S 25 : Time dependence of the acac ^1H NMR resonances for $[\text{Co}(\text{acac})_2(\text{O}_2\text{CPh})]$ at 60°C . The starred resonance is the residual peak of the C_6D_6 solvent.



Bis(p-nitrobenzoyl) peroxide. The product was obtained as powder (Yield 81%). ^1H NMR (400MHz, CD_2Cl_2): δ 8.40 (d, $J = 9.0$ Hz, 2H), 8.28 (d, $J = 9.0$ Hz, 2H).

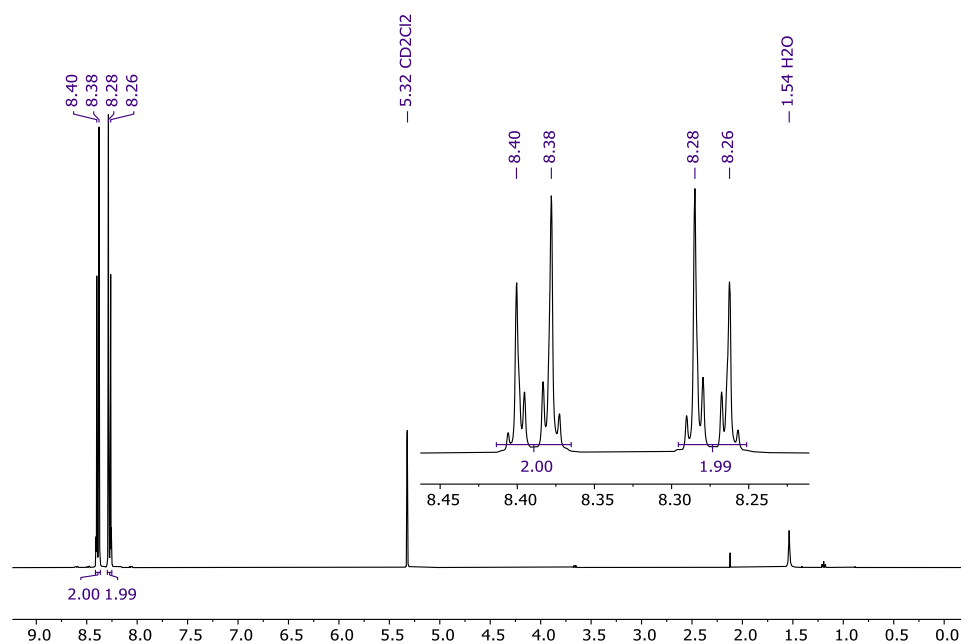
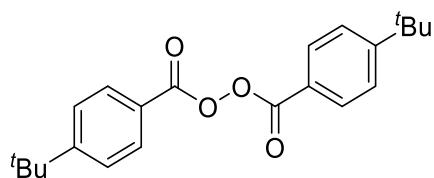


Figure S 26: ^1H NMR spectrum of bis(p-nitrobenzoyl) peroxide recorded in CDCl_3 , 400MHz.



Bis(p-tert-butylbenzoyl) peroxide. The product was obtained as with powder (Yield 72%). ^1H NMR (400MHz, CD_2Cl_2): δ 8.00 (d, $J = 9.1$ Hz, 2H), 7.57 (d, $J = 9.0$ Hz, 2H), 3.89 (s, 9H).

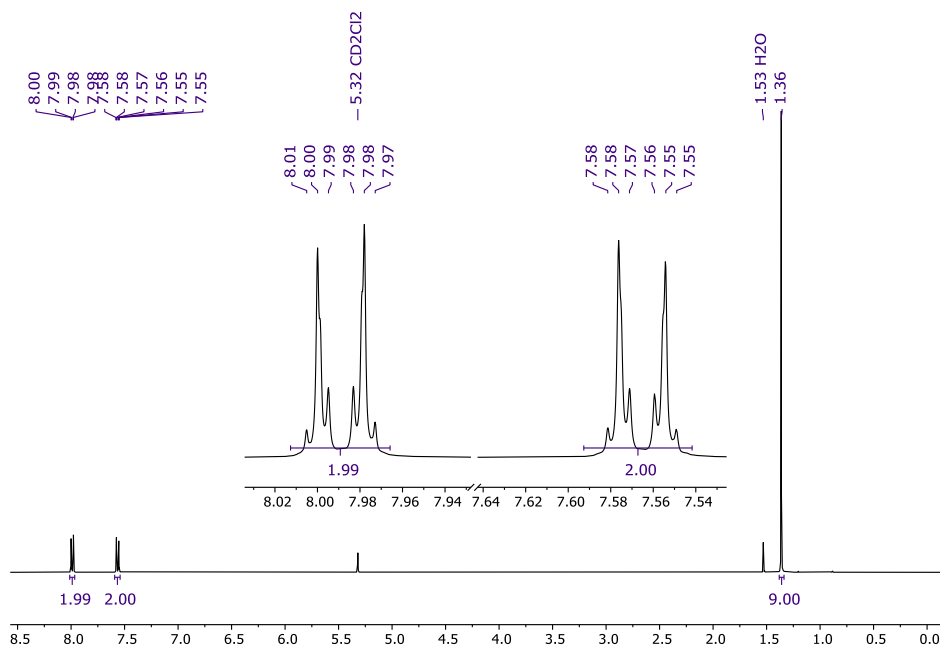
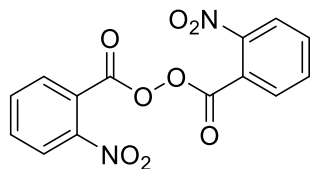


Figure S 27: ^1H NMR spectrum of bis(p-tert-benzoyl) peroxide recorded in CDCl_3 , 400MHz.



Bis(o-nitrobenzoyl) peroxide. The product was obtained as with powder (Yield 78%). ^1H NMR (400MHz, CD_2Cl_2): δ 8.23 (d, $J = 8.1$ Hz, 1H), 7.87 (m, 3H).

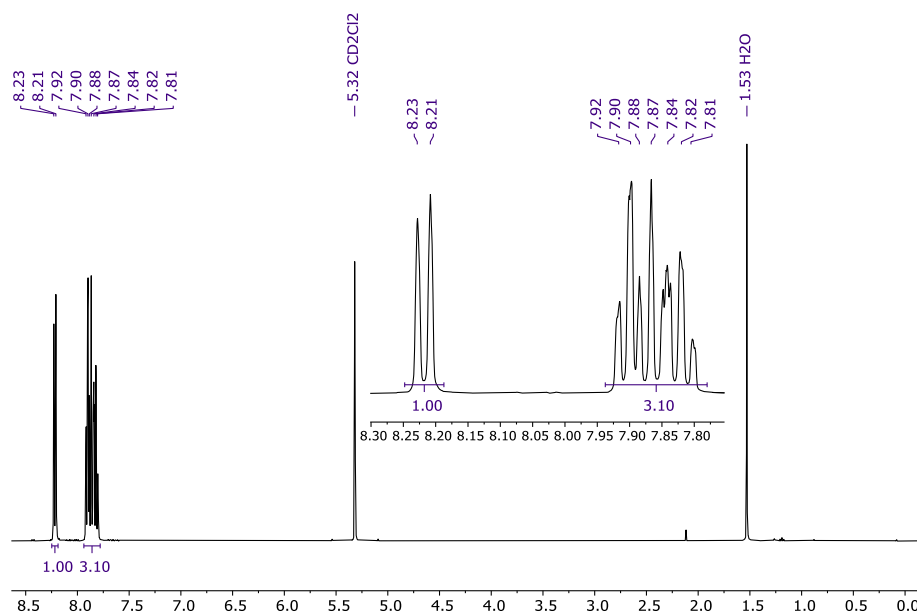
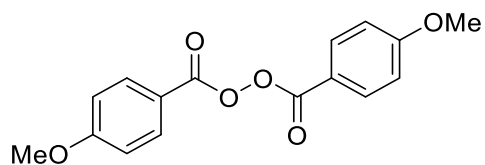


Figure S 28 : ^1H NMR spectrum of bis(o-nitrobenzoyl) peroxide recorded in CDCl_3 , 400MHz.



Bis(p-methoxybenzoyl) peroxide. The product was obtained as with powder (Yield 80%). ^1H NMR (400MHz, CD_2Cl_2): δ 8.00 (d, $J = 9.1$ Hz, 2H), 7.00 (d, $J = 9.0$ Hz, 2H), 3.89 (s, 3H).

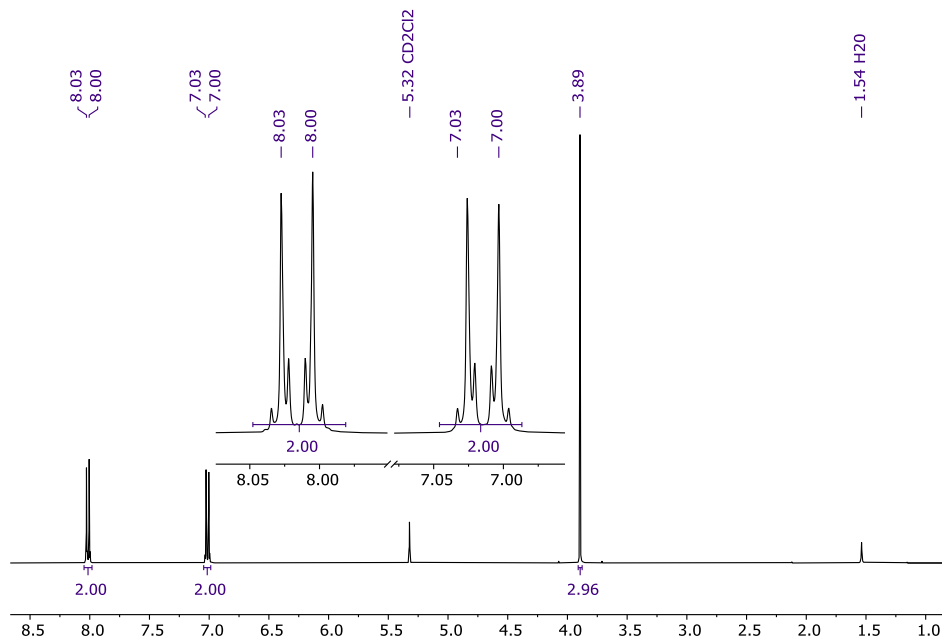


Figure S 29 : ^1H NMR spectrum of bis(p-methoxybenzoyl) peroxide recorded in CDCl_3 , 400MHz.

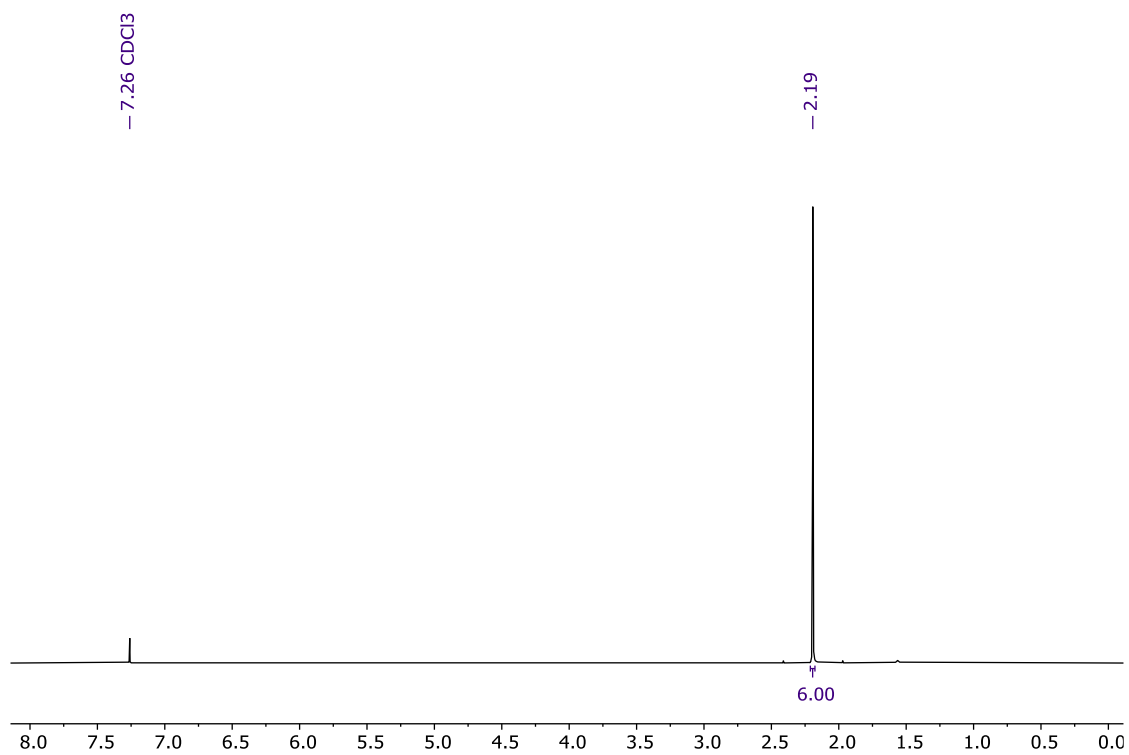
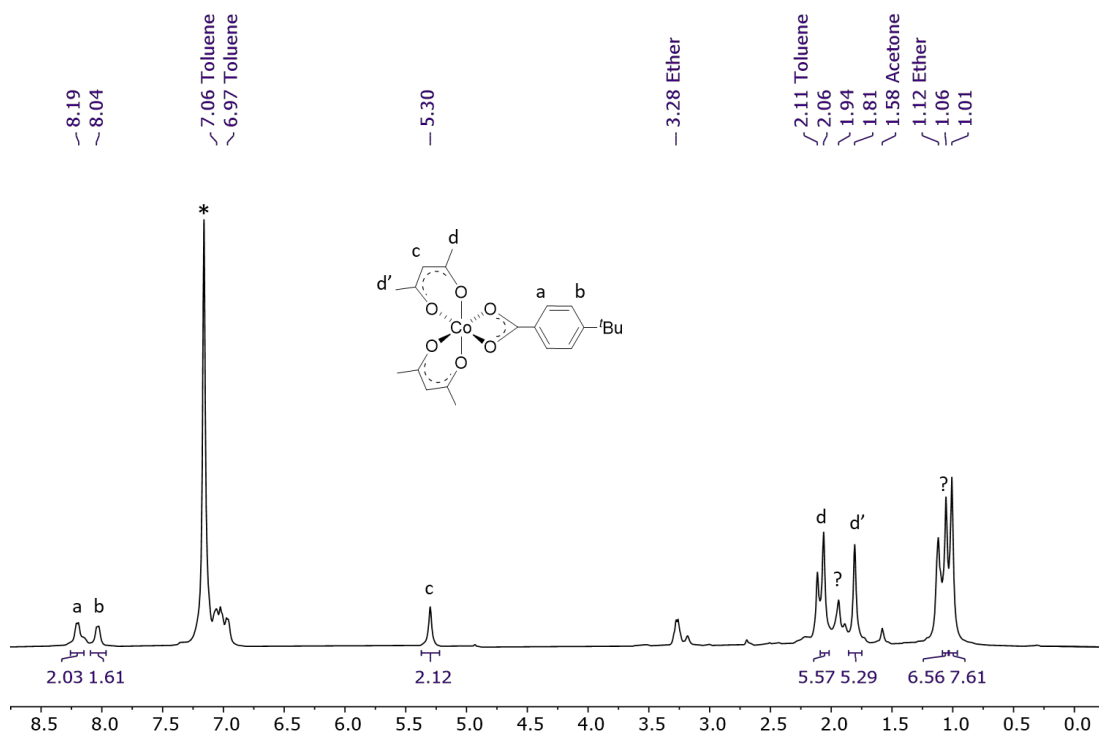
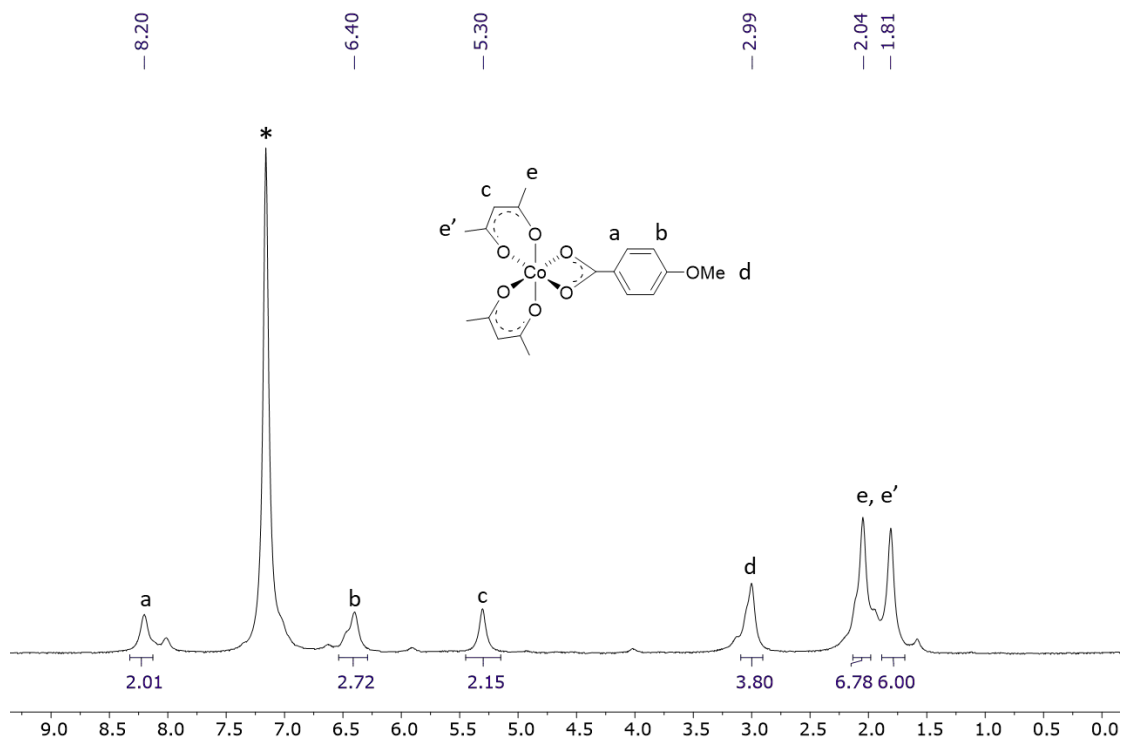


Figure S 30: ^1H NMR spectrum of diacetyl peroxide recorded in CDCl_3 , 400MHz.



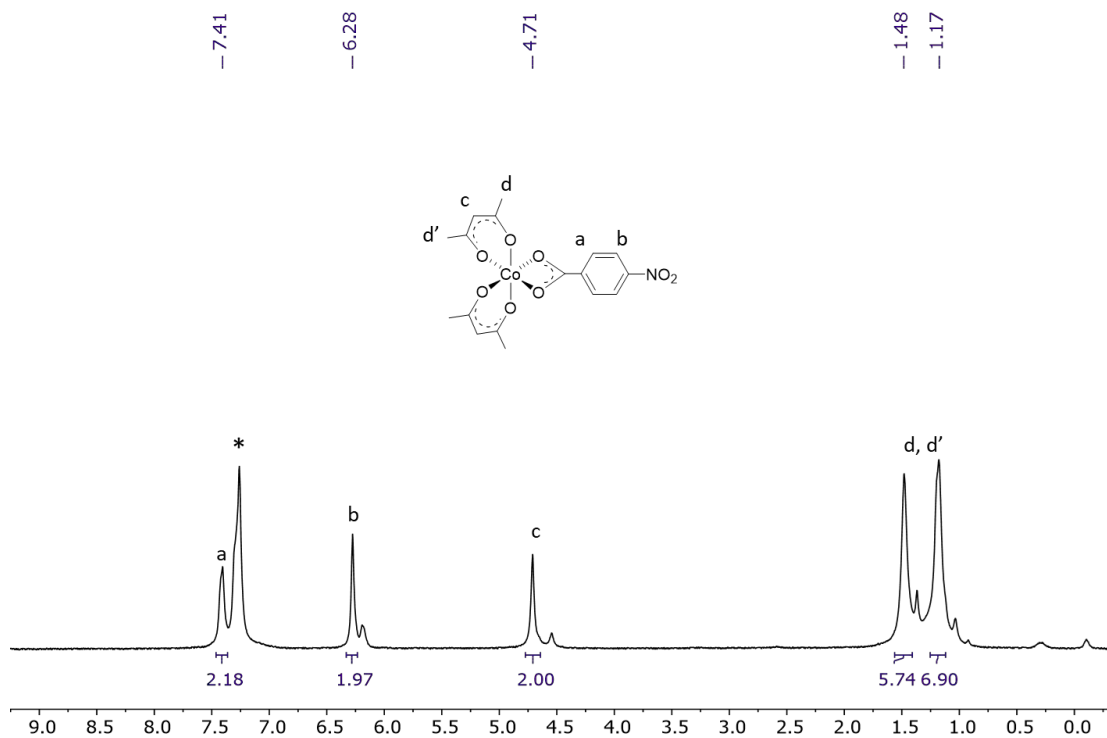


Figure S 33: ^1H NMR spectrum of **3.9** in CDCl_3 (*), 300MHz.

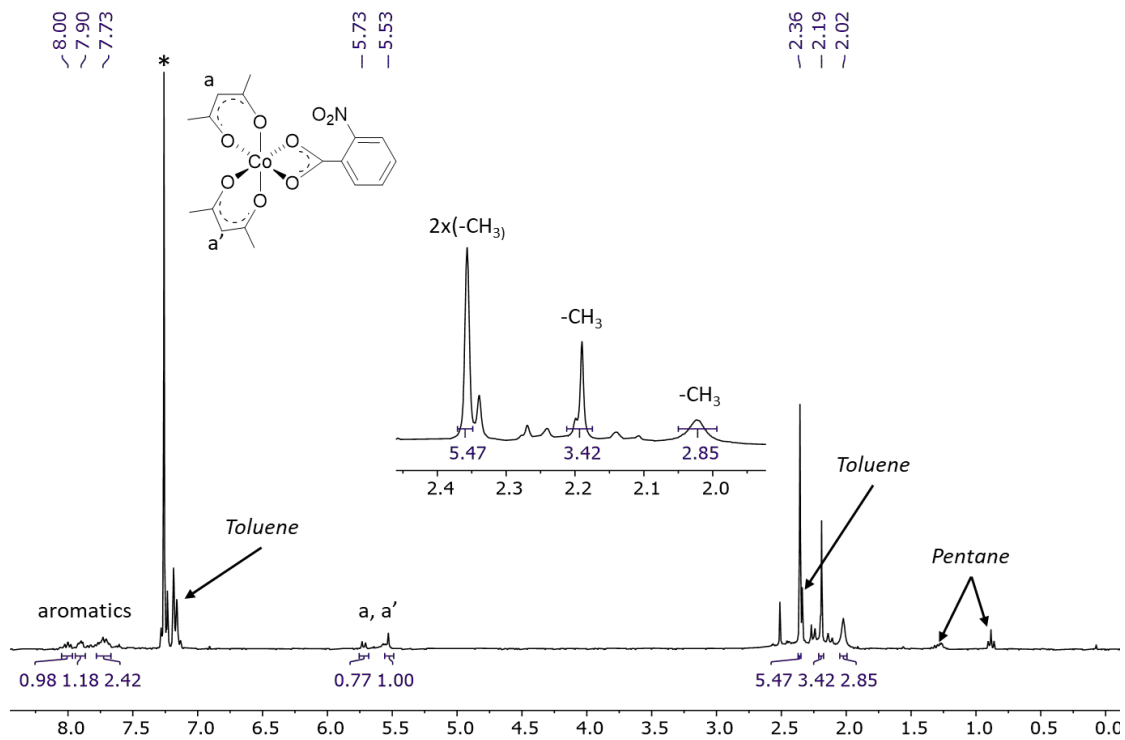


Figure S 34 : ^1H NMR spectrum of **3.10** in CDCl_3 (*), 400MHz.

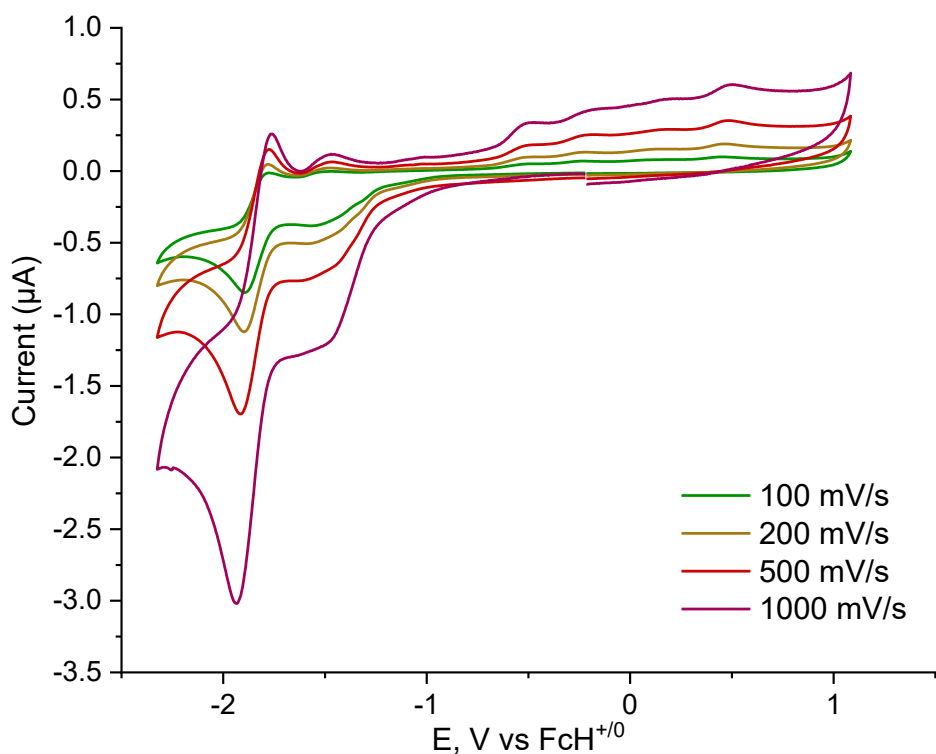


Figure S 35 : Cyclic voltammogram of compounds $\text{Co}^{\text{III}}(\text{acac})_2\text{O}(\text{O})\text{CAR}^{\text{o}}\text{NO}_2$ (**3.10**), in CH_2Cl_2 on a GC working electrode at various scan rates. [Complex] = 10^{-3} M; supporting electrolyte = $n\text{Bu}_4\text{PF}_6$ 0.1 M).

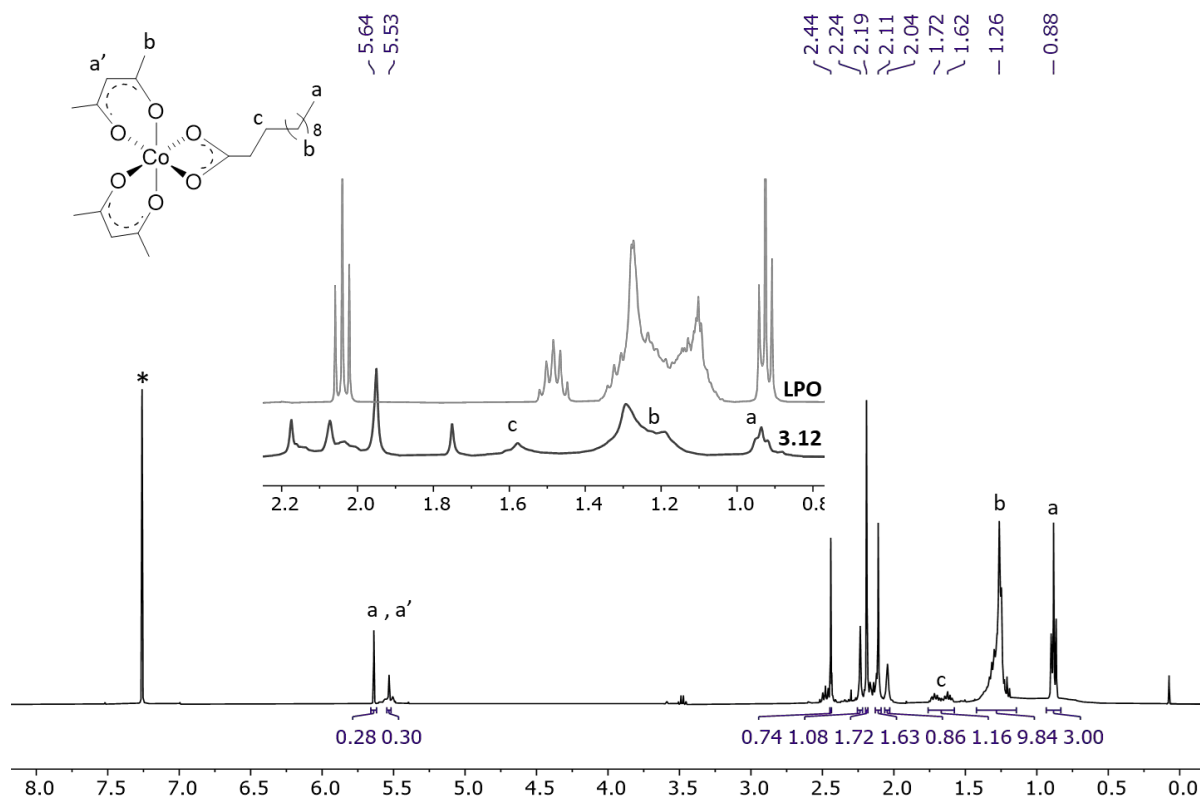


Figure S 36: ^1H NMR spectrum of **3.12** in CD_6D_6 (*), 400MHz.

Table S 1 : Crystal data and structure refinement for ligand **1.10** and tripodal complex **3.2**.

Identification code	1.10	3.2
Empirical formula	C ₃₆ H ₅₂ N ₂ O ₂	C ₃₈ H ₅₃ CoN ₂ O ₄
Formula weight	544.79	660,75
Temperature, K	173(2)	113(2)
Wavelength, Å	1.54184	0,71073
Crystal system	Monoclinic	Monoclinic
Groupe d'espace	P 2 ₁ /c	C 2/c
Unit cell parameters		
a, Å	16.23240(10)	29,704(4)
b, Å	8.764	17,917(3)
c, Å	23.3993(2)	14,5301(19)
α, °	90.0	90,0
β, °	103.4480(10)	94,423(4)
γ, °	90.0	90,0
Volume, Å ³	3237.35(4)	7709,7(19)
Z	4	8
Density (calc), Mg/m ³	1.118	1,139
Abs. coefficient, mm ⁻¹	0.522	0,482
F(000)	1192	2832
Crystal size, mm ³	0.250 x 0.200 x 0.150	0,100 x 0,080 x 0,020
Diffractometer	Rigaku. Oxford-Diffraction. XtaLAB Synergy. Dualflex. HyPix	Bruker, APEXII CCD
Theta range, °	2.799 à 71.433	1,895 à 25,060°,

Reflections collected	61043	69569
Indpt reflections (R_{int})	6285 (0.0379)	6830 (0,2454)
Absorption correction	Multi-scan	Multi-scan
Max. / min. transmission	1.0 et 0.78295	0,7466 et 0,7156
Refinement method	Moindres carrés sur F^2	Moindres carrés sur F^2
Data /restraints/parameters	6285 / 0 / 374	6830 / 0 / 419
Goodness-of-fit on F^2	1.045	1,030
R1, wR2 [$I > 2\sigma(I)$]	0.0416. 0.1088	0,0859, 0,1642
R1, wR2 (all data)	0.0443. 0.1118	0,1864, 0,2048
$\Delta\rho_{min}/\Delta\rho_{max}$, e,$\text{\AA}^{-3}$	0.450 / -0.363	0,948 / -0,501

Table S 2 : Crystal data and structure refinement for Schiff-base complexes 3.3, 3.4, 3.5.

Identification code	3.3	3.4	3.5
Empirical formula	C ₄₂ H ₅₇ Co N ₂ O ₄	(C ₄₃ H ₆₁ CoN ₂ O ₅) ₂	(C ₄₁ H ₅₇ ClCo N ₃ O ₄) ₂
Formula weight	712.82	1489.73	1436.55
Temperature, K	110(2)	100(2)	173.0(4)
Wavelength, Å	0.71073 Å	0.71073	1.54184
Crystal system	Monoclinic	Monoclinic	Tetragonal
Groupe d'espace	P 21/n	P 21/n	P 43 21 2
Unit cell parameters			
a, Å	11.6131(14)	18.6468(8)	25.9056(2)
b, Å	15.482(2)	20.2170(7)	25.9056(2)
c, Å	22.288(3)	25.5792(11)	26.2569(3)
α, °	90.0	90.0	90.0
β, °	101.284(4)	92.602(4)	90.0
γ, °	90.0	90.0	90.0
Volume, Å ³	3929.9(8)	9633.0(7)	17621.0(3)
Z	4	4	8
Density (calc), Mg/m ³	1.205 Mg/m ³	1.027	1.083
Abs. coefficient, mm ⁻¹	0.478	0.394	3.858
F(000)	1528	3200	6144
Crystal size, mm ³	0.16 x 0.12 x 0.09	0.11 x 0.08 x 0.04	0.16 x 0.13 x 0.12
Diffractometer	Bruker APEX II, CCD	Bruker APEX II. CCD	Xcalibur. Eos. Gemini ultra
Theta range, °	1.612 à 30.696	1.594 à 25.028	2.941 a 72.031

Reflections collected	108529	176527	54826
Indpt reflections (Rint)	11886 (0.0988)	17006 (0.3317)	16519 (0.0710)
Absorption correction	Multi-scan	Multi-scan	Multi-scan
Max. / min. transmission	0.7461 et 0.6899	0.7403 et 0.6960	1.0 et 0.8586
Refinement method	Moindres carrés sur F2	Moindres carrés sur F2	Moindres carrés sur F2
Data /restraints/parameters	11886 / 0 / 456	17006 / 0 / 419	16519 / 0 / 886
Goodness-of-fit on F2	1.041	1.132	1.017
R1, wR2 [I>2σ(I)]	0.0485, 0.0871	0.1567, 0.3078	0.0560, 0.1246
R1, wR2 (all data)	0.0918, 0.1005	0.2077, 0.3356	0.0948, 0.1464
Δρmin/Δρmax, e,Å⁻³	0.476 / -0.744	0.926 / -0.886	-0.031(2)/0.584/-0.390

Table S 3 : Crystal data and structure refinement for (O2,O2)-based cobalt III complexes 3.6, 3.8, 3.9, 3.10.

Identification code	3.6	3.8	3.9	3.10
Empirical formula	C ₁₇ H ₁₉ CoO ₆	C ₆₅ H ₈₃ Co ₃ O ₁₆	C ₁₇ H ₂₀ CoNO ₉	C ₃₄ H ₄₀ Co ₂ N ₂ O ₁₈
Formula weight	378.25	1297,10	441.27	882.54
Temperature. K	130(2)	100(2) K	100(2)	100(2)
Wavelength. Å	1.54184	0,71073 Å	1.54184	0.71073
Crystal system	Monoclinic	Triclinic	Monoclinic	Monoclinic
Groupe d'espace	C 2/c	P -1	P 2 ₁ /n	P 2 ₁ /c
Unit cell parameters				
a. Å	10.8167(9)	11,447(4)	8.10720(10)	15.242(7)
b. Å	12.0499(11)	16,393(5)	15.1580(2)	11.956(6)

c. Å	13.5182(11)	20,350(7)	15.2833(2)	21.477(9)
α. °	90.0	105,566(10)	90.0	90.0
β. °	103.533(9)	91,918(10)	100.7510(10)	98.246(16)
γ. °	90.0	100,402(9)	90.0	90.0
Volume. Å³	1713.0(3)	3605(2)	1845.18(4)	3873(3)
Z	4	2	4	4
Density (calc). Mg/m³	1.467	1,195	1.588	1.513
Abs. coefficient. mm⁻¹	8.118	0,741	7.772	0.936
F(000)	784	1364	912	1824
Crystal size. mm³	0.220 x 0.100 x 0.030	0,100 x 0,100 x 0,010	0.090 x 0.050 x 0.020	0.200 x 0.150 x 0.100
Diffractomètre	Xcalibur. Eos. Gemini ultra	Bruker APEX II, CCD	Rigaku. Oxford- Diffraction. XtaLAB Synergy. Dualflex. HyPix	Bruker APEX II. CCD
Theta range. °	5.583 à 71.292	1,043 à 25,065	4.144 to 80.237	1.350 to 28.642
Reflections collected	6407	81293	41453	88615
Indpt reflections (R_{int})	1655 (0.1133)	12769 (0,1296)	4024 (0.0427)	9909 (0.1351)
Absorption correction	Multi-scan	Multi-scan	Multi-scan	Multi-scan
Max. / min. transmission	1.0 et 0.4248	0,7403 - 0,6960	1.0 and 0.8041	0.7457 et 0.6389
Refinement method	Moindres carrés sur F ²	Moindres carrés sur F ²	Moindres carrés sur F ²	Moindres carrés sur F ²
Data	1655 / 0 / 114	12769 / 3 /	4024 / 3 / 263	9909 / 6 / 525

/restraints/parameters		785		
Goodness-of-fit on F²	1.827	1,015	1.068	1.002
R1. wR2 [I>2σ(I)]	0.1552. 0.4498	0,0533, 0,1162	0.0440. 0.1172	0.0540. 0.0991
R1. wR2 (all data)	0.2088. 0.5302	0,1064, 0,1365	0.0466. 0.1192	0.1160. 0.1196
Δρ_{min}/Δρ_{max}. e.Å⁻³	1.366 / -2.292	0,375 / -0,441	0.311 / -0.483	0.432 /-0.513

Annexes Chapter III

Figure S 1: Result of the MMA polymerization at 40°C, in bulk for [Co]/[MMA]=1/200 a) Kinetics, b) M_n and \bar{D} Vs. Conv. and c) MALDI-TOF result.....	244
Figure S 2: Styrene radical polymerization mediated by 3.1 , [Co]/[St]=1/200 at 70°C in bulk, a) Molar masses as function of conversion and evolution of the conversion as function of time.	244
Figure S 3: Kinetics of polymerization $[Co^{III}]/[Co^{II}]/[VAc] = 1/X/126$, under argon in bulk at 120°C. With $X = 0.10$ (■), 0.25 (▲), 0.50 (◆) and 1 (★) and the corresponding plot of conversion vs. M_n vs. \bar{D}	246
Figure S 4: GPC traces of polymerization $[Co^{III}]/[Co^{II}]/[VAc] = 1/X/126$ with $X =$ (a) 0.10 (■), (b) 0.50 (◆) and 1 (★).	247
Figure S 5: Comparison of observed (left) and library (right) mass spectra for the compounds indicated in Figure II-19.....	247
Figure S 6 : Simulations of the isotopic envelopes for the six highest-intensity populations (a-f) observed in the ESI-MS spectrum of PVAc shown in Figure II-19.	248
Figure S 7: DOSY experiment of the PVAc-b-PMA copolymer, $CDCl_3$	249
Figure S 8: GPC traces of VAc homopolymerization at (a) 40°C, (b) 50°C and (c) 60°C.	249
Figure S 9: Control polymerization VAc + diacylperoxide.	250
Figure S 10: Zoom of Polylactide MALDI-TOF analysis (a) matrix Dithranol-NaI 3/1	250
Figure S 11: DOSY homopolymer PVAc Diffusion coefficient $3.1 \times 10^{-01} m^2/s$	251
Figure S 12: DOSY homopolymer PCL ($M=12\ 000g/mol$) Diffusion coefficient $7.4 \times 10^{-11} m^2/s$	251
Figure S 13: Zoom DOSY experiment PVAc-b-PCL recorded in $CDCl_3$	252
Figure S 14: DOSY experiment of PVAc-b-PLA, $CDCl_3$	252
Figure S 15: Chromatogram of the Macro-Initiator PLA (Blue line) and result of the chain extension reaction in presence of MA obtained with GPC-THF polystyrene calibration.	253
Figure S 16: DOSY analysis of the chain extension reaction of short PCL with VAc. ($M= 8400 g mol^{-1}$)	253
Figure S 17: 1H NMR spectrum of NHC-Zinc ethyl chloride complex, recorded in CD_2Cl_2 , 400MHz.	254
 Table S 1: Value of kinetics reaction at various equivalent of cobalt(II). $[Co^{III}]/[Co^{II}]/[VAc] = 1/X/126$	244

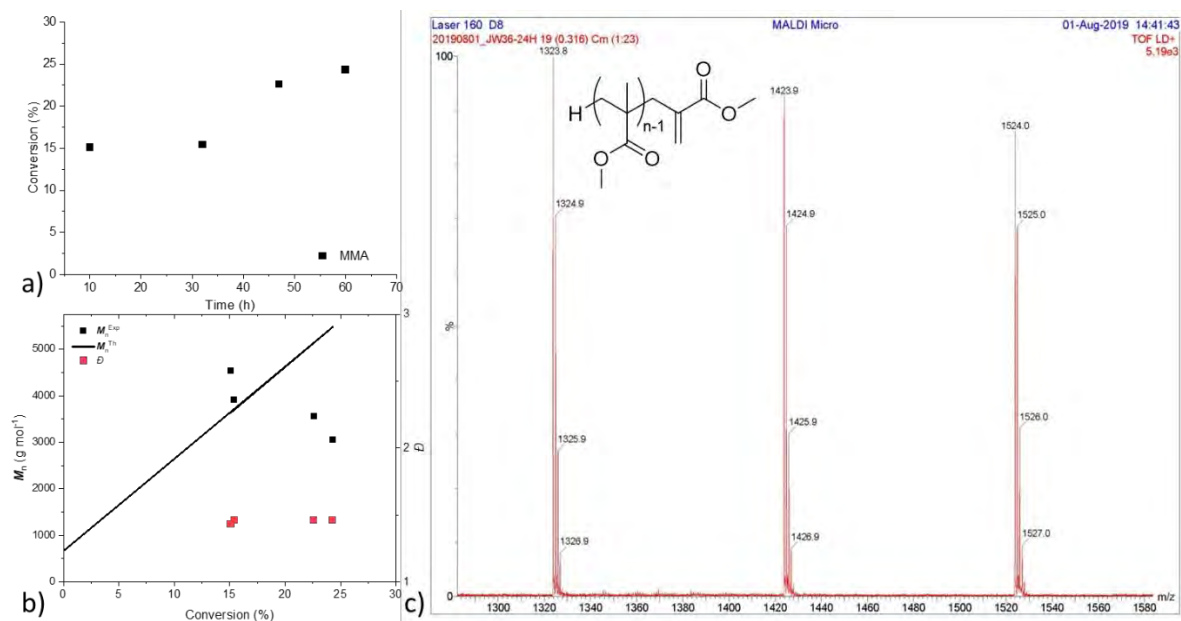


Figure S 1: Result of the MMA polymerization at 40°C, in bulk for $[Co]/[MMA]=1/200$ a) Kinetics, b) M_n and \bar{D} Vs. Conv. and c) MALDI-TOF result.

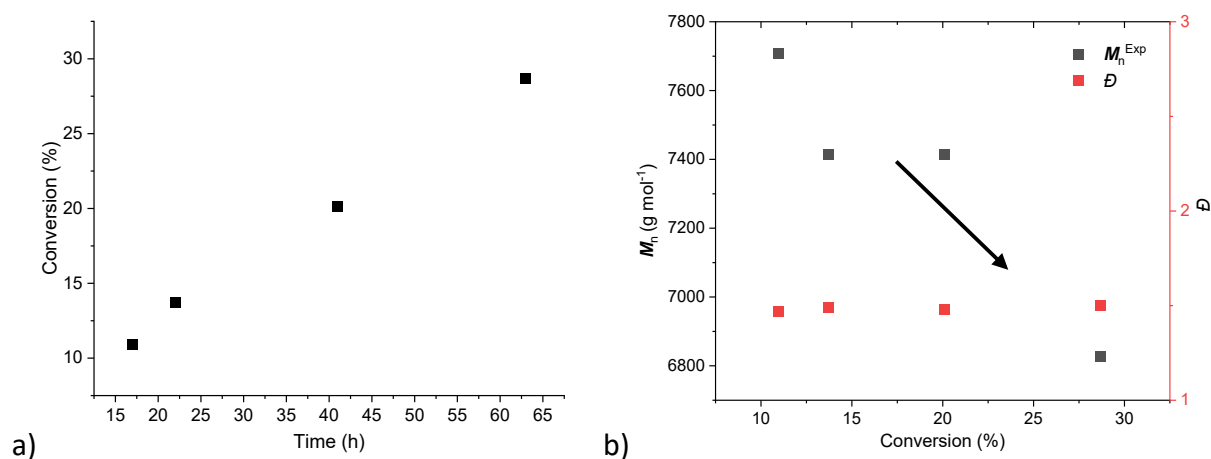


Figure S 2: Styrene radical polymerization mediated by **3.1**, $[Co]/[St]=1/200$ at 70°C in bulk, a) Molar masses as function of conversion and evolution of the conversion as function of time.

Table S 1: Value of kinetics reaction at various equivalent of cobalt(III). $[Co^{III}]/[Co^{II}]/[VAc] = 1/X/126$

Time (h)	Conv. (%) ^b	M_n^{PS} (g mol ⁻¹) ^c	\bar{D} ^d
$[Co^{III}]/[Co^{II}]/[VAc] = 1/0/126$			
5.0	2.3	19872	1.16
9.0	2.6	32957	1.12
26.0	17.9	51244	1.27
31.0	22.9	53658	1.29
34.0	28.6	57344	1.29
48.4	27.7	57050	1.44
53.7	31.4	55441	1.51
58.7	40.6	57957	1.48
120.5	58.2	49532	1.51

$[\text{Co}^{\text{III}}]/[\text{Co}^{\text{II}}]/[\text{VAc}] = 1/0.1/126$			
7.2	1.8		
9.0	1.1	7488	1.14
23.2	10.0	22231	1.16
32.6	18.0	28911	1.22
48.0	35.2	37782	1.26
55.6	37.9	46727	1.22
71.0	48.6	46500	1.38
$[\text{Co}^{\text{III}}]/[\text{Co}^{\text{II}}]/[\text{VAc}] = 1/0.25/126$			
4.3	0.2		
8.8	2.3	3982	1.12
23.2	13.4	20232	1.13
14.5	4.4	8720	1.12
18.0	6.2	11557	1.17
38.0	28.5	34865	1.13
62.0	53.0	54122	1.25
$[\text{Co}^{\text{III}}]/[\text{Co}^{\text{II}}]/[\text{VAc}] = 1/0.5/126$			
4.2	0.2	-	-
8.6	0.1	-	-
23.0	12.6	19969	1.12
32.6	21.8	32643	1.10
48.0	39.3	52804	1.24
55.0	53.7	53372	1.22
$[\text{Co}^{\text{III}}]/[\text{Co}^{\text{II}}]/[\text{VAc}] = 1/1/126$			
7.0	0	-	-
9.0	0	-	-
22.5	3.9	8879	1.09
25.5	4.1	10152	1.12
30.5	6.7	13644	1.11
46.5	17.7	24763	1.09
55.5	21.4	27250	1.17
75.5	32.8	38066	1.19
85.5	42.6	42590	1.22
142.5	50.3	52544	1.43

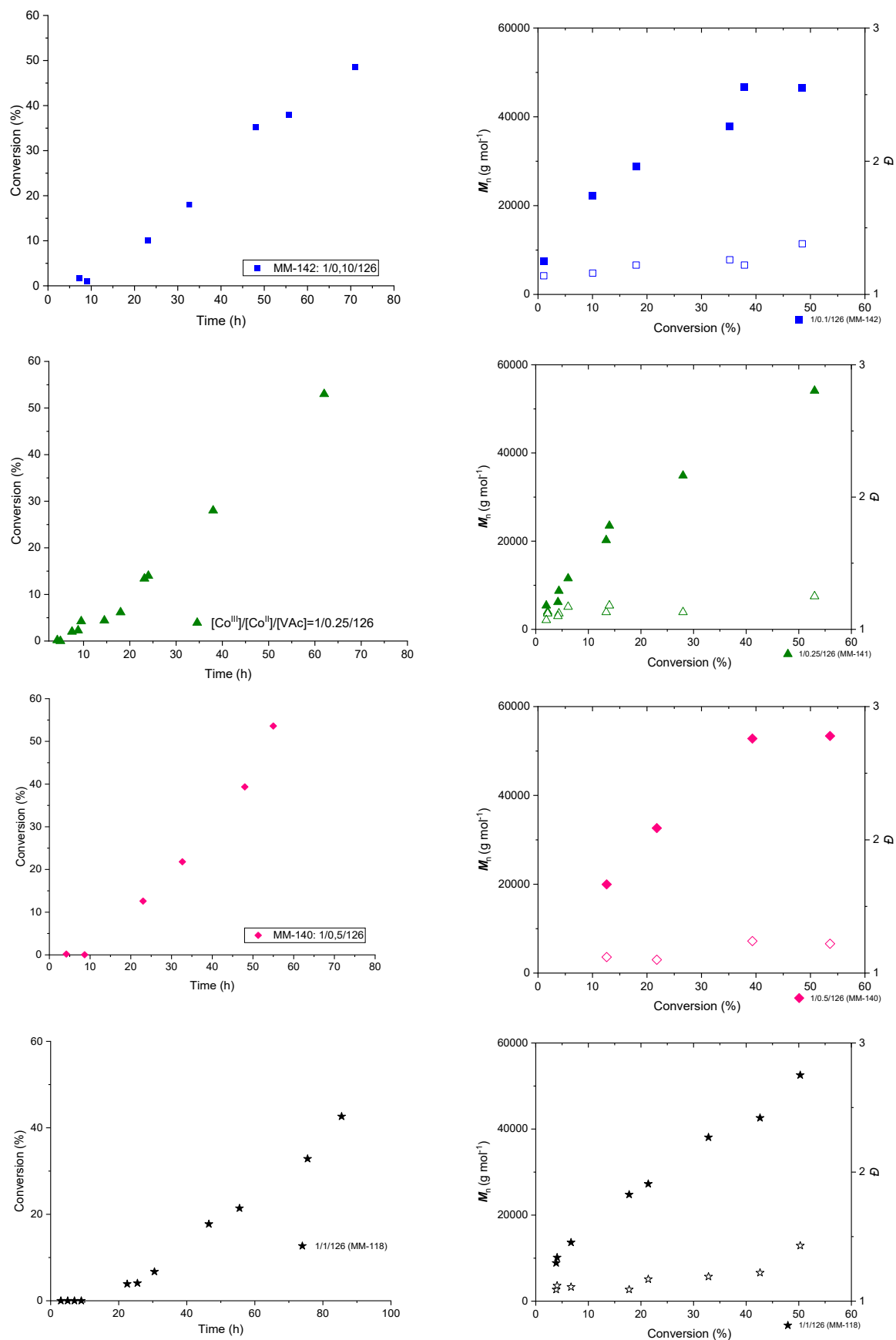


Figure S 3: Kinetics of polymerization $[Co^{III}]/[Co^{II}]/[VAc] = 1/X/126$, under argon in bulk at 120°C. With $X = 0.10$ (■), 0.25 (▲), 0.50 (◆) and 1 (★) and the corresponding plot of conversion vs. M_n vs. \bar{D} .

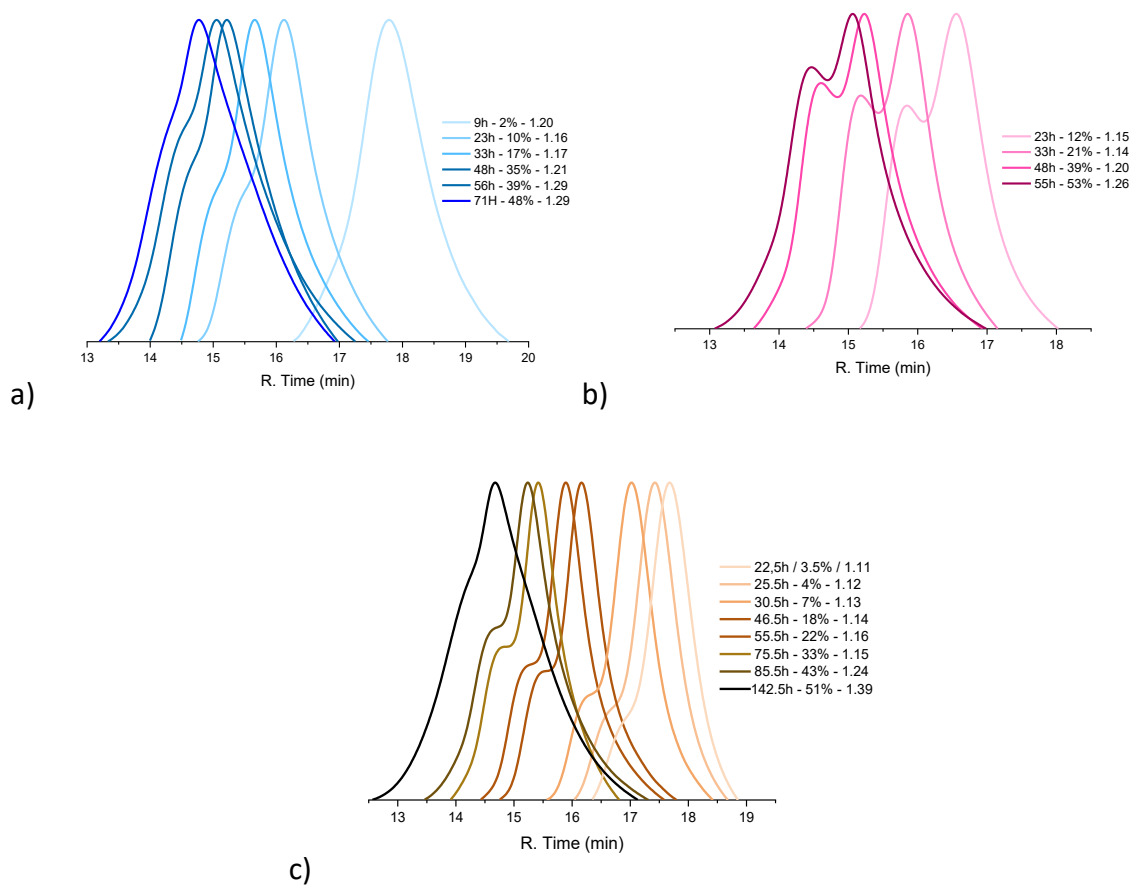


Figure S 4: GPC traces of polymerization $[Co^{III}]/[Co^{II}]/[VAc] = 1/X/126$ with $X = (a) 0.10$ (■), (b) 0.50 (◆) and 1 (★).

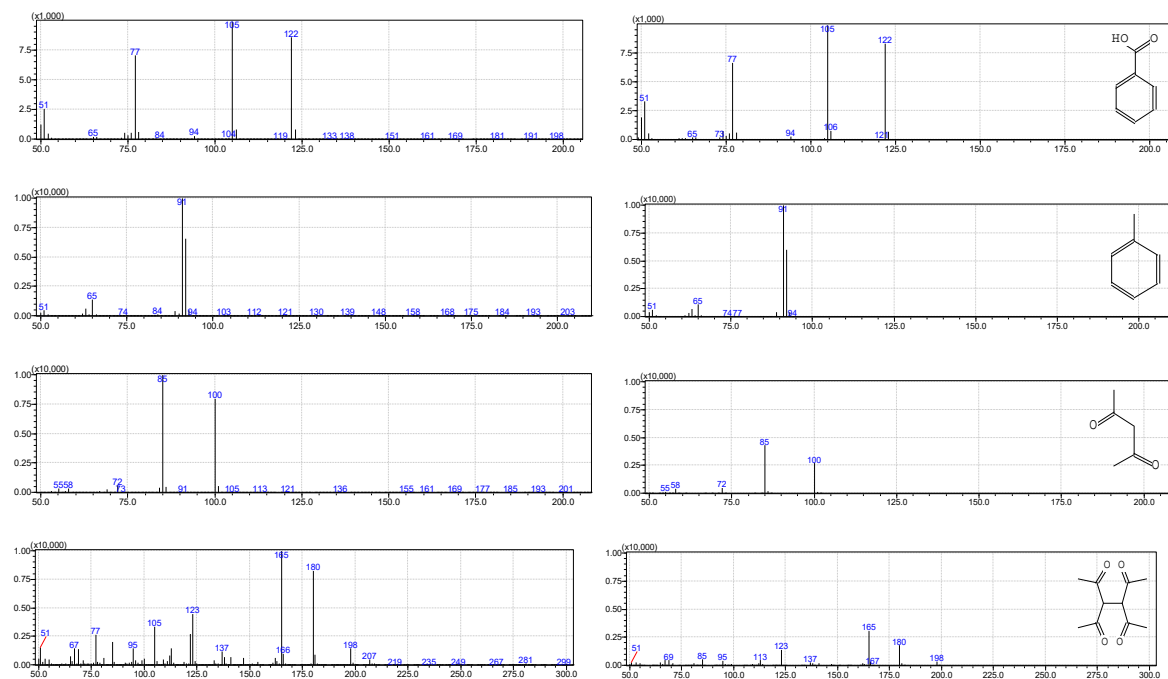


Figure S 5: Comparison of observed (left) and library (right) mass spectra for the compounds indicated in Figure II-19.

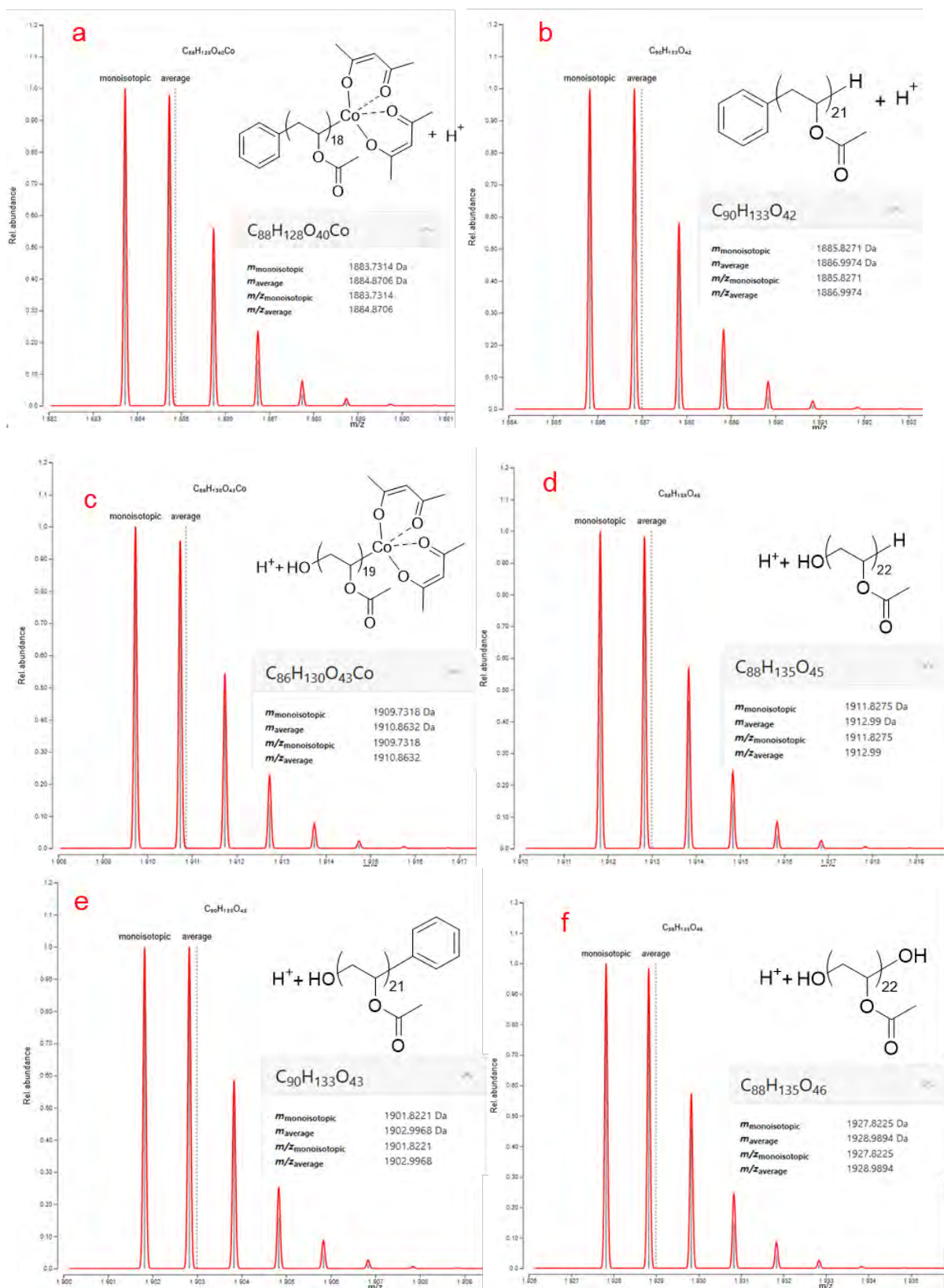


Figure S 6 : Simulations of the isotopic envelopes for the six highest-intensity populations (a-f) observed in the ESI-MS spectrum of PVAc shown in Figure II-19.

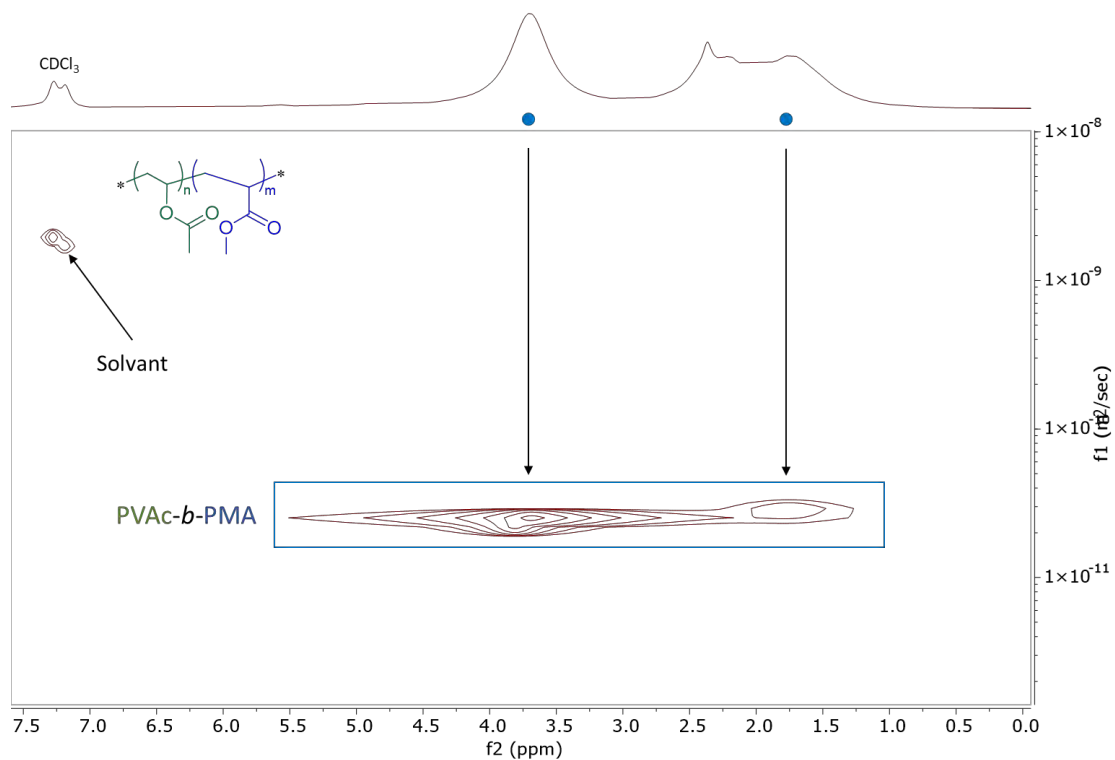


Figure S 7: DOSY experiment of the PVAc-*b*-PMA copolymer, CDCl_3 .

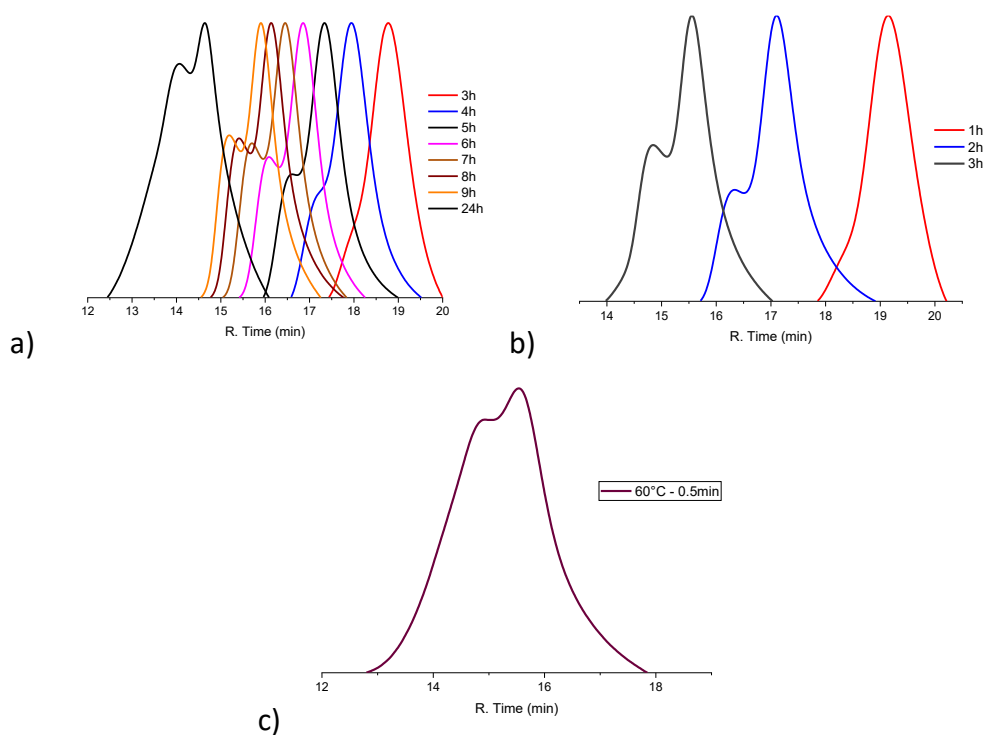


Figure S 8: GPC traces of VAc homopolymerization at (a) 40°C , (b) 50°C and (c) 60°C .

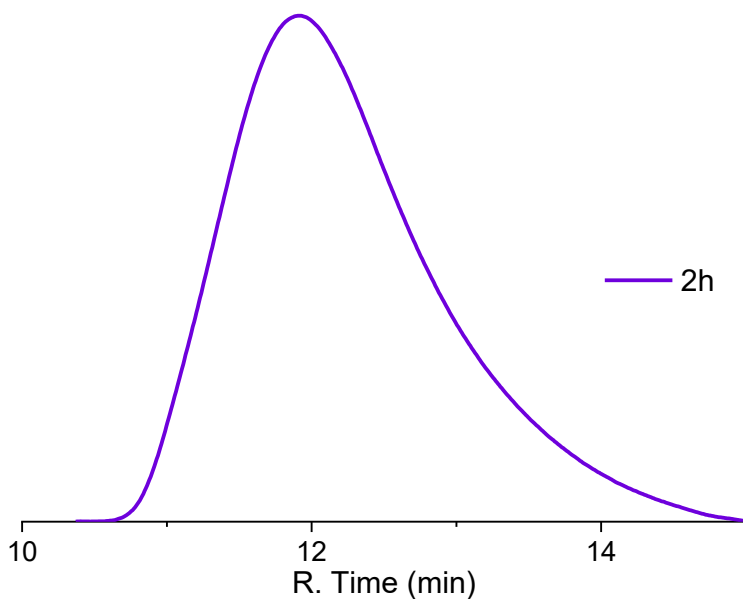


Figure S 9: Control polymerization VAc + diacetylperoxide.

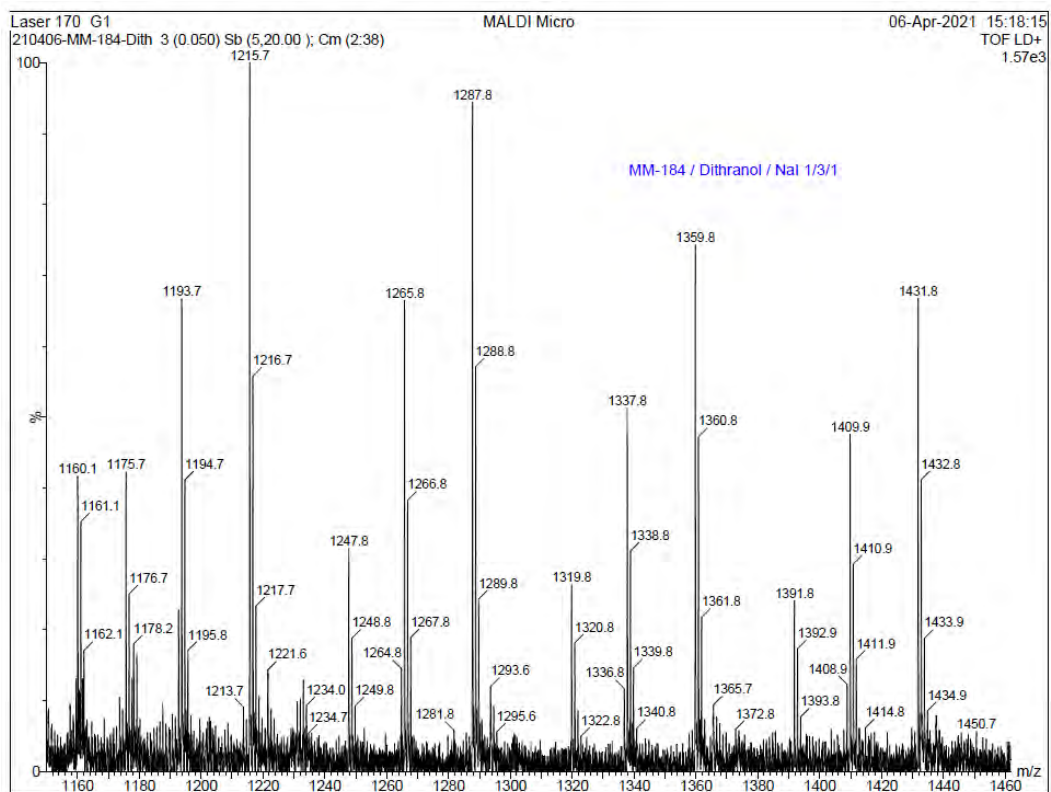


Figure S 10: Zoom of Polylactide MALDI-TOF analysis (a) matrix Dithranol-Nal 3/1

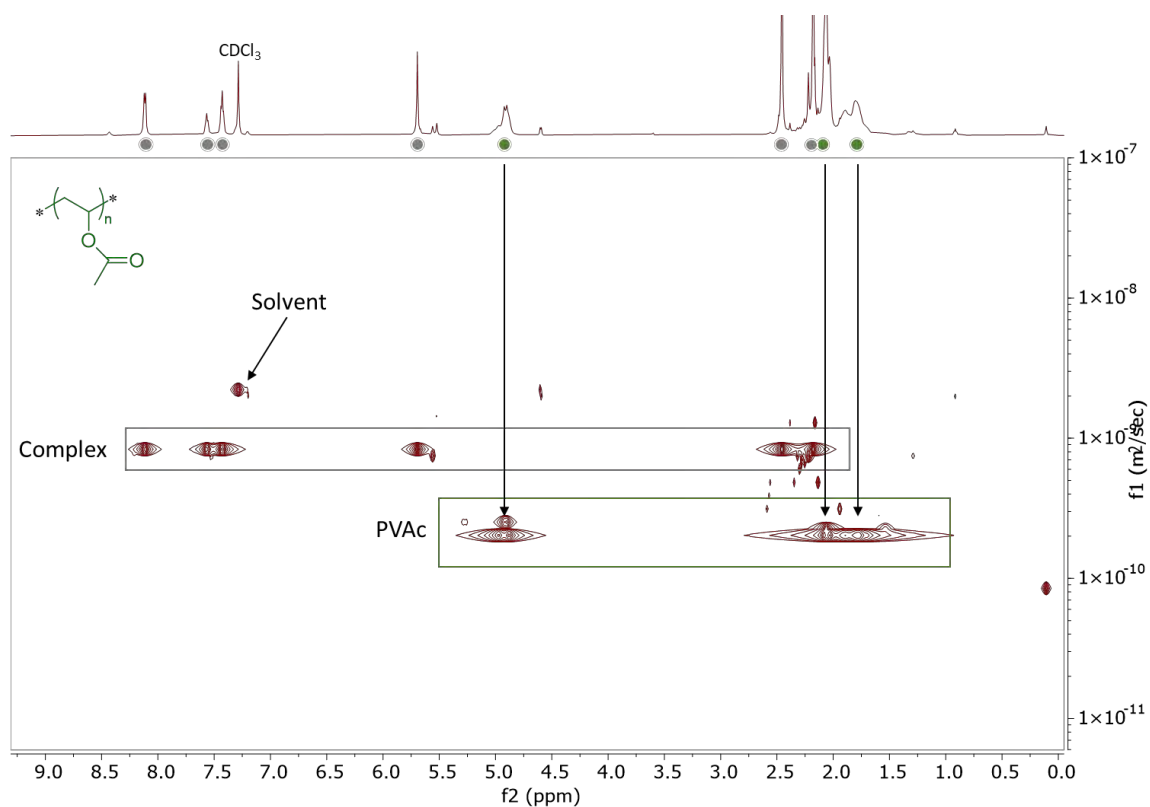


Figure S 11: DOSY homopolymer PVAc Diffusion coefficient $3.1 \times 10^{-10} \text{ m}^2/\text{s}$.

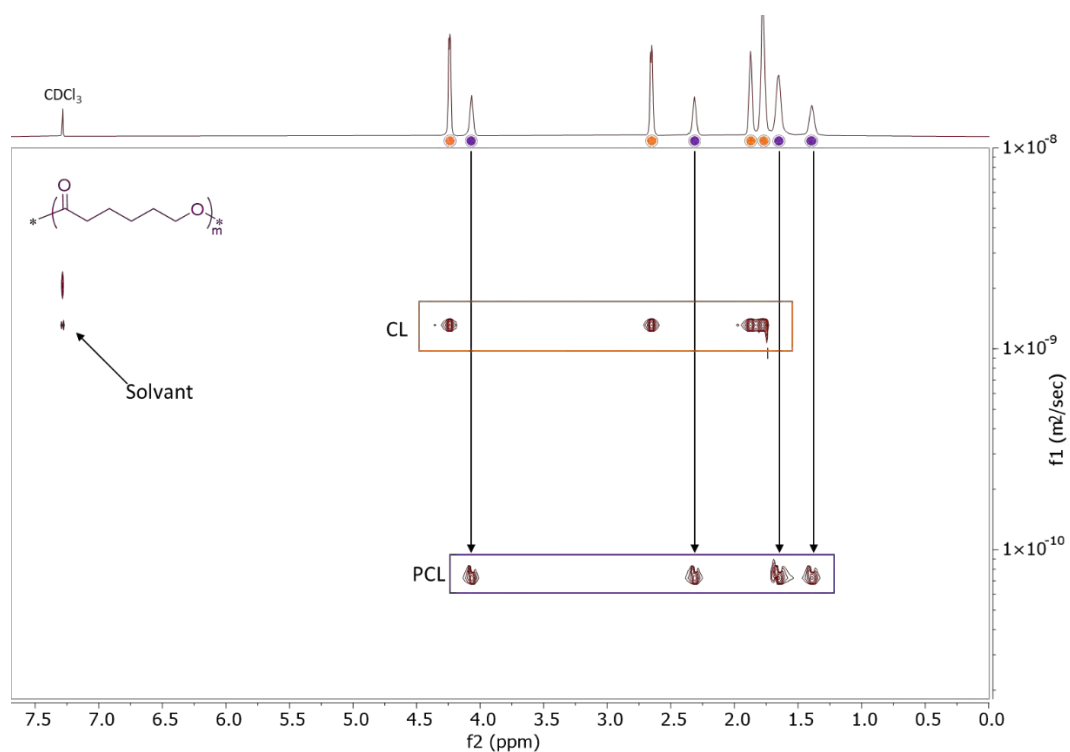


Figure S 12: DOSY homopolymer PCL ($M=12\ 000\text{g/mol}$) Diffusion coefficient $7.4 \times 10^{-11} \text{ m}^2/\text{s}$.

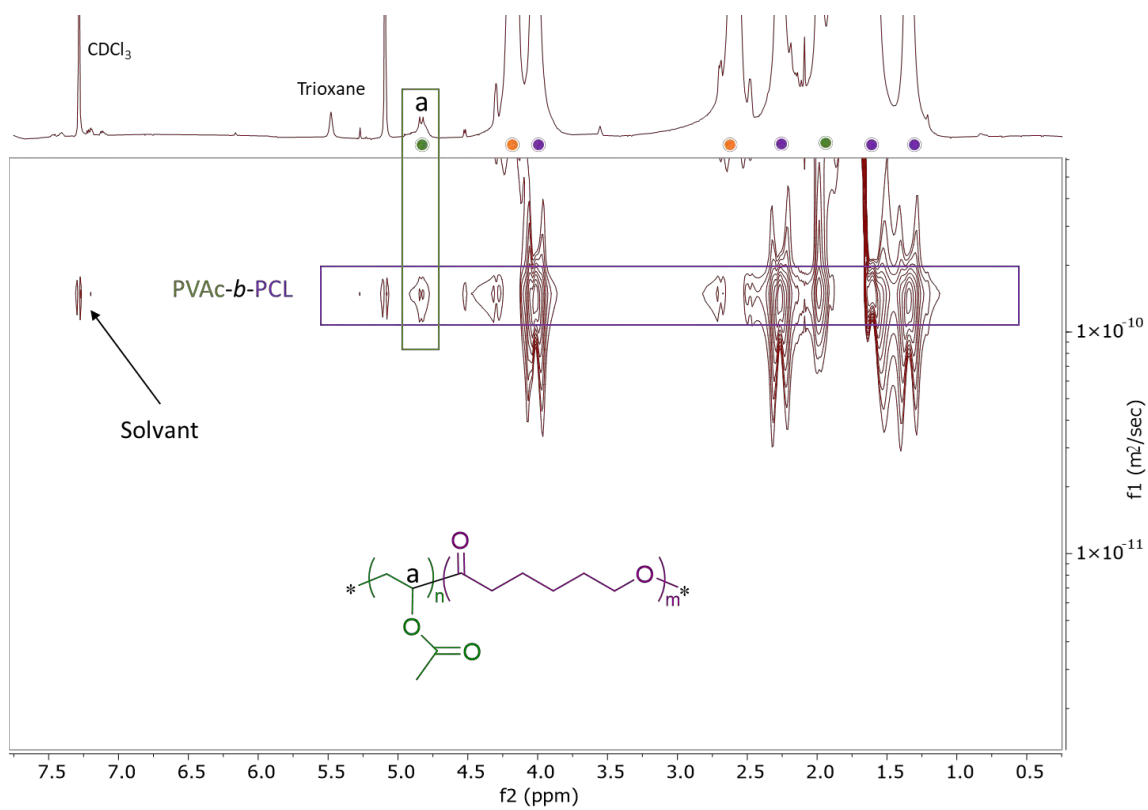


Figure S 13: Zoom DOSY experiment PVAc-b-PCL recorded in CDCl₃.

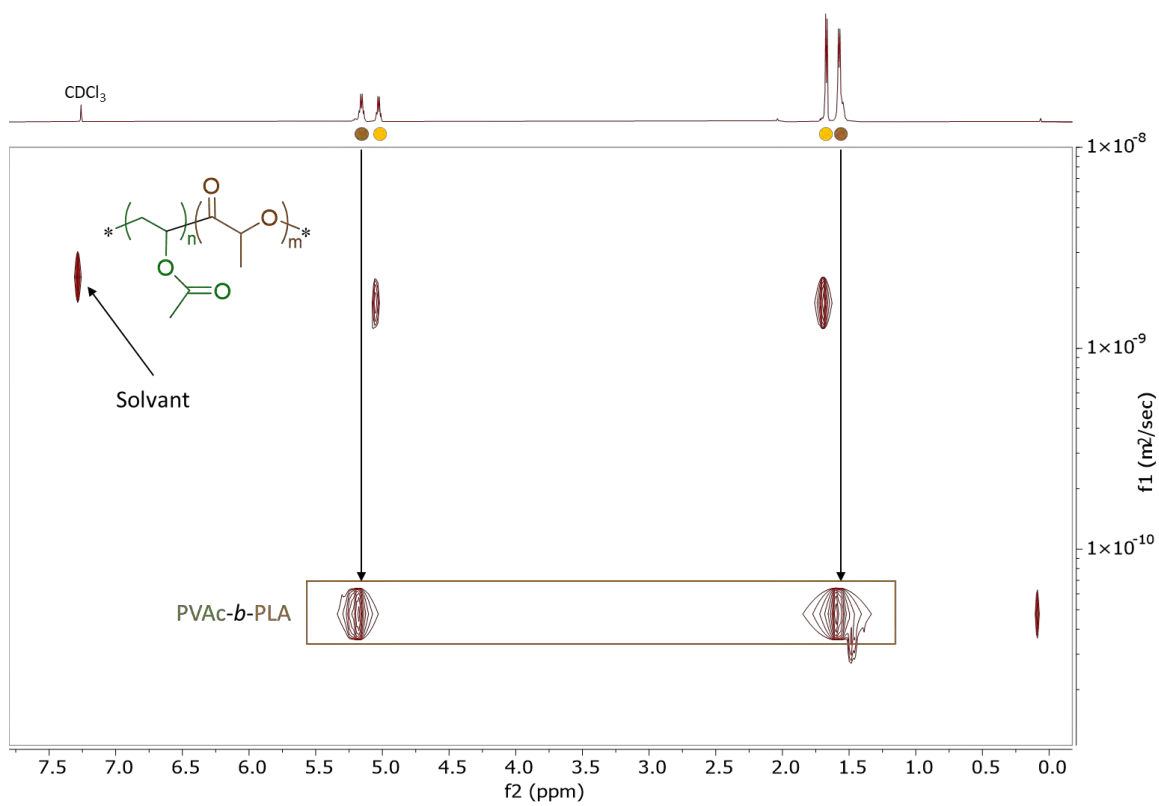


Figure S 14: DOSY experiment of PVAc-b-PLA, CDCl₃.

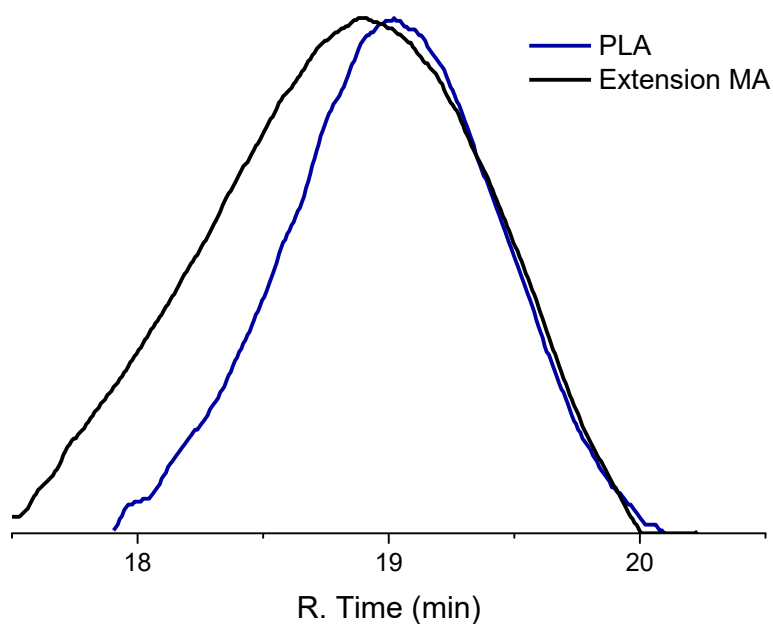


Figure S 15: Chromatogram of the Macro-Initiator PLA (Blue line) and result of the chain extension reaction in presence of MA obtained with GPC-THF polystyrene calibration.

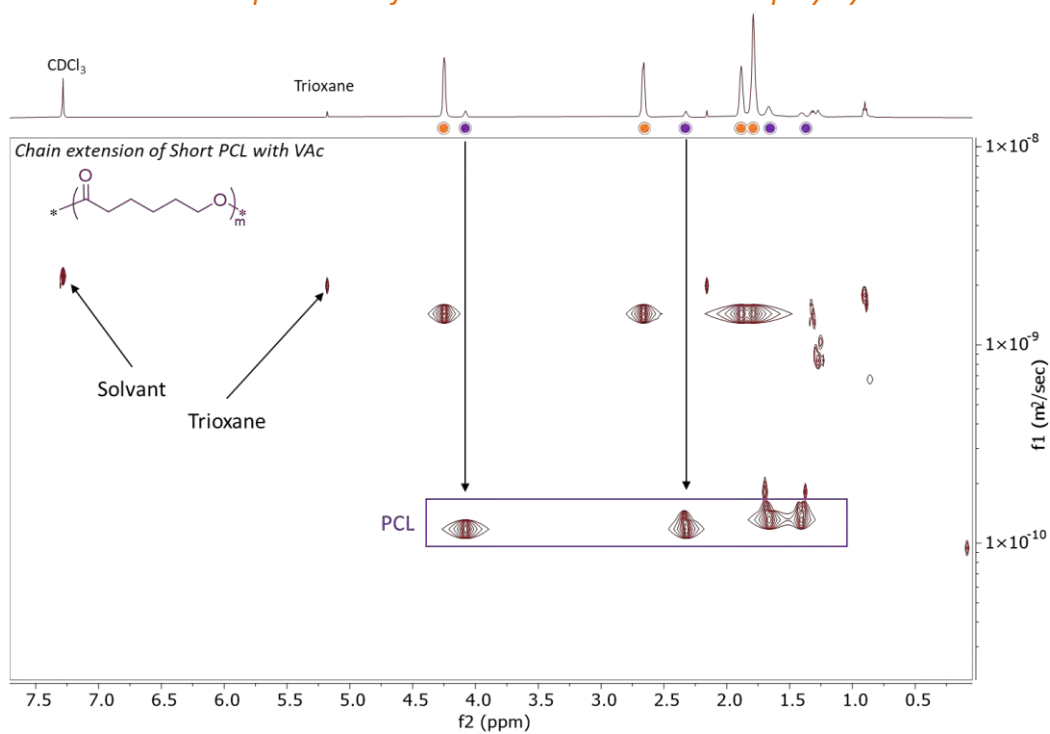


Figure S 16: DOSY analysis of the chain extension reaction of short PCL with VAc. ($M = 8400 \text{ g mol}^{-1}$)

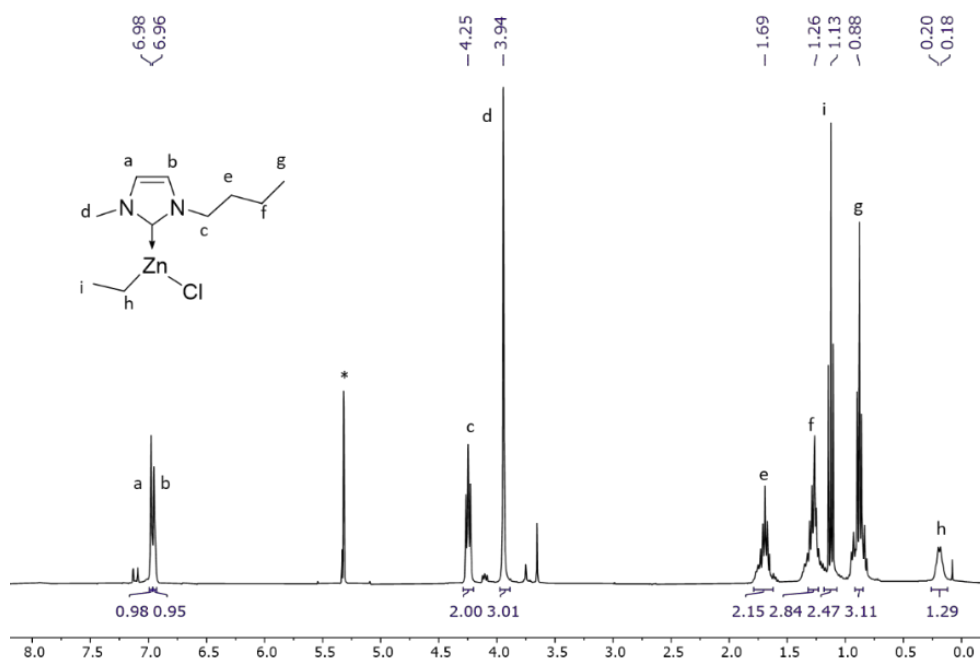


Figure S 17: ^1H NMR spectrum of NHC-Zinc ethyl chloride complex, recorded in CD_2Cl_2 , 400MHz.

Résumé en Français

Maxime Michelas

“Design of cobalt(III) carboxylate complexes for switching between radical and ring opening polymerization mechanism”

Ecole doctorale : SDM – Sciences De la Matière – Toulouse

Spécialité : Chimie Organométallique et de Coordination

LCC – Laboratoire de Chimie de Coordination

Encadrés par Christophe Fliedel et Rinaldo Poli



Université
de Toulouse

Les polymères communément appelés « plastiques », sont les matériaux les plus utilisés au monde. Ils remplacent bon nombre de matériaux traditionnels tels que le bois, l'acier ou le verre. En effet, ces polymères ont apporté une large gamme de propriétés intéressantes utiles à la vie de l'Homme comme celle de barrière aux gaz pour les emballages alimentaires, ou encore, permettent la constitution de matériaux plus légers pour l'automobile, réduisant ainsi les émissions de CO₂. De plus, les besoins en polymères bien définis, avec un contrôle sur l'architecture (*c-à-d.* masse molaire prédictible, dispersité contrôlée, ou des bouts de chaînes fonctionnalisés), ne cessent d'augmenter avec le temps pour le développement de nouveaux matériaux de hautes performances. Il faut savoir que tous les polymères sont composés d'unités de base que l'on appelle monomère, et que le choix du monomère, ainsi que de la méthode de polymérisation (fabrication), vont influencer les propriétés finales.

Bien qu'il existe une myriade de techniques de polymérisation, notre étude est focalisée sur les méthodes impliquant l'utilisation de complexes de coordination (ou catalyseurs). En effet, l'utilisation de métal pour la production de polymères est bien représentée dans l'industrie depuis plus de soixante ans. Le premier, et peut-être l'exemple le plus connu est le complexe de titane de Ziegler Natta dans les années 50.¹ Après cela, la polymérisation radicalaire par transfert d'atome (ATRP) a été développée dans les années 90, notamment par le groupe de Matyjaszewski, ce qui a remis sur le devant de la scène les techniques de polymérisation basées sur les métaux. Ici, ce sont des complexes de cuivre halogéné, qui, en présence de monomère vinylique, vont piéger de manière réversible le radical de la chaîne polymère en croissance. Les avantages de cette technique sont nombreux, comme le fait qu'elle nécessite seulement quelques *ppm* de catalyseur pour fonctionner, elle est facile à mettre en œuvre et permet d'obtenir des polymères bien définis. C'est pourquoi cette technique est de plus en plus utilisée dans l'industrie pour la fabrication de matériaux de haute performance.^{2,3}

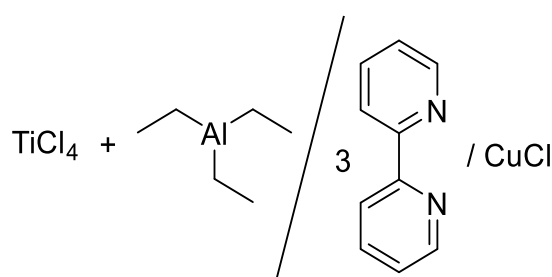


Figure 1 : Ziegler-Natta (à gauche) et ATRP (à droite) complexes utilisés industriellement pour la production de polymères.^{1,4,5}

L'ATRP fait partie des techniques de polymérisation radicalaire contrôlées (CRP), qui permet la production d'une large gamme de matériaux polymères. Ces techniques sont basées sur les monomères vinyliques et comme exposé sur le schéma 1, toutes ces techniques suivent le même principe. Après une étape d'amorçage, soit par la voie directe ou indirecte, le radical primaire va se propager sur le monomère qui va ensuite être piégé de manière réversible par

le modérateur ou l'agent de contrôle, ici noté T. Cette phase de propagation peut se faire selon deux mécanismes : la terminaison réversible (RT en vert) comme pour l'ATRP et la NMP^{6,7}, ou par transfert dégénéré (DT en rouge), comme pour la RAFT ou l'ITP.⁸⁻¹²

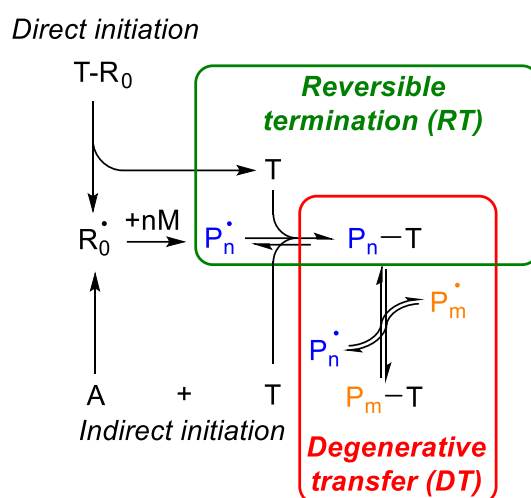


Schéma 1 : Mécanisme général de la polymérisation radicalaire contrôlée (CRP).

Cependant, le contrôle de la polymérisation dépend aussi beaucoup du monomère que l'on souhaite utiliser, du fait de leur réactivité respective. En effet, chez les monomères vinyliques, on peut distinguer deux classes : les monomères dit « plus actifs » (MAMs), comme l'acrylate de méthyle (MA), et « moins actifs » (LAMs), comme l'acétate de vinyle (VAc), qui représentent encore aujourd'hui un challenge. En effet, les moins actifs génèrent des radicaux très réactifs mais, *a contrario* des espèces dormantes, très difficiles à réactiver. Plus simplement, la stabilité du monomère est inversement proportionnelle à celle de l'espèce active. Au sein de notre groupe, on se propose de développer des complexes de coordinations, qui vont jouer ce rôle d'agent de contrôle (noté T dans le schéma 1). Cette technique de polymérisation est aussi appelée polymérisation radicalaire modérée par voie organométallique (OMRP - Organometallic Mediated Radical Polymerization).¹³ Cette méthode est décrite dans le schéma 2a, dans le cas d'un amorçage direct avec un mode RT. Cependant, bien que non détaillée ici, cette méthode peut aussi être utilisée sous un mode de DT avec un amorçage indirect, auquel cas on place dans le milieu le métal au degré d'oxydation X et un amorceur externe comme l'AIBN. Pour ce projet, nous avons fait appel à un système unimoléculaire (métal au degré d'oxydation X+1), qui, sous l'effet de la température, va pouvoir réaliser la rupture homolytique de la liaison Mt-R₀, afin de générer un radical primaire qui amorcera la polymérisation mais aussi, relarguera dans le milieu un métal au degré d'oxydation X. L'équilibre OMRP est donc géré par la force de la liaison métal-polymère (représentée en orange), qui est illustrée par la « Bond Dissociation Energy » (BDE, schéma 2b), traduisant la force nécessaire pour casser cette liaison métal-polymère. Comme illustré sur le schéma 2b, si elle est trop forte, le radical ne sera pas piégé de manière efficace et l'espèce active sera favorisée, ce qui entraînera une polymérisation non contrôlée. Ou à l'inverse, si elle est trop forte les radicaux seront piégés de façon irréversible et la

polymérisation sera stoppée. Cette BDE peut être modulée par le choix du centre métallique, ainsi que par le choix des ligands, qui vont avoir un impact de par leurs effets électroniques et/ou stériques. C'est ce qui rend cette méthode, en théorie, adaptable à tout type de monomère vinylique.

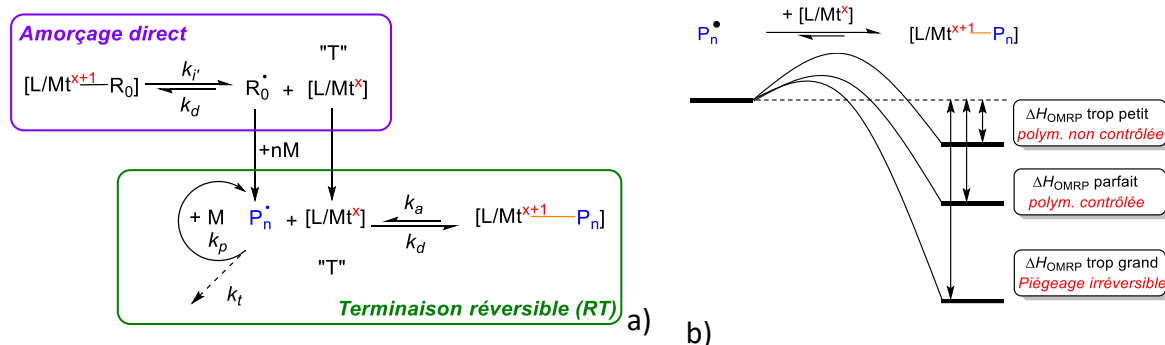


Schéma 2 : a) Mécanisme de l'OMRP par amorçage direct, b) Illustration du concept de contrôle de la polymérisation par la « Bond Dissociation Energy » (BDE).

D'un autre côté, depuis plusieurs décennies, en raison de l'émergence des problèmes environnementaux et des pressions sociétales, l'amélioration de nos matériaux usuels s'inscrit dans une stratégie de développement durable visant à remplacer ceux issus de la pétrochimie par des matériaux biosourcés et/ou biodégradables.¹⁴ L'approche la plus utilisée est la méthode de polymérisation par ouverture de cycle (ROP), et notamment d'esters cycliques comme le lactide, qui est obtenu à partir d'amidon. Le poly lactide obtenu à partir de cette technique est beaucoup étudié pour des applications de fabrication d'emballages ou dans le domaine biomédical pour des implants ou de la délivrance de principes actifs.¹⁵⁻¹⁷ Les précurseurs de cette chimie ont développé des complexes à base d'étain, d'aluminium et de zinc, qui sont encore utilisés aujourd'hui (figure 2).

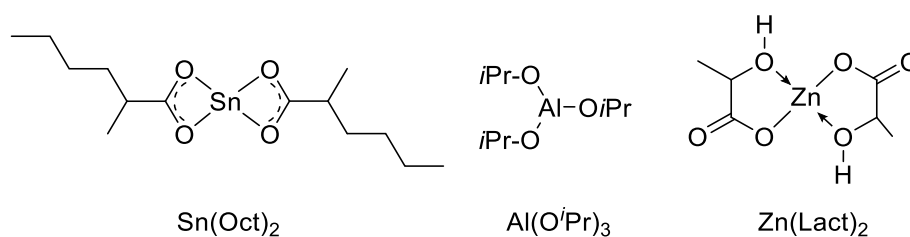


Figure 2 : Premier complexe reportés pour la ROP industriel. 18-20

Contrairement à la CRP, cette technique de polymérisation repose sur la polarisation des liaisons qui permettra la coordination du métal au monomère (schéma 3), puis, une attaque nucléophile induira l'insertion du monomère.

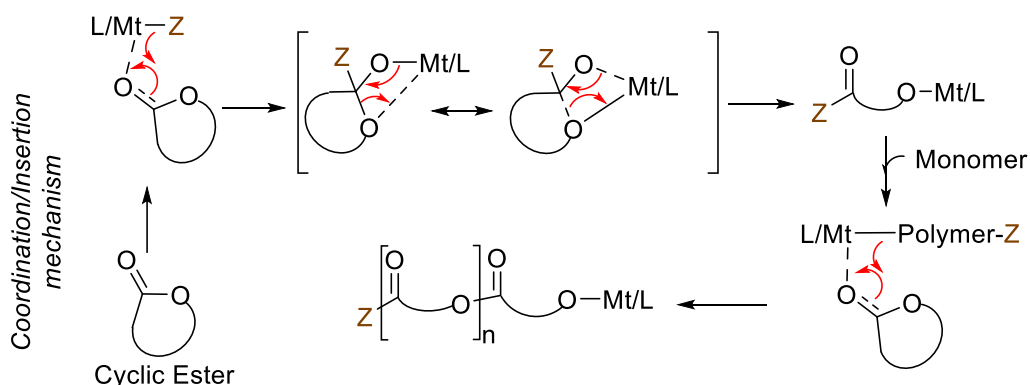


Schéma 3 : Mécanisme de la polymérisation par ouverture de cycle (ROP).

C'est à partir de ce postulat que notre projet s'inspire, car l'enthousiasme autour de ces méthodes de polymérisation, permettant de contrôler l'architecture des polymères, a motivé la communauté scientifique à mélanger, soit les monomères, soit les méthodes de polymérisation, pour obtenir des matériaux polymères avec de nouvelles propriétés originales.

C'est pourquoi, le but de ce projet était de développer des complexes de coordination à base de Cobalt, qui devaient à la fois jouer le rôle d'amorceur (amorçage direct) et d'agent de control (modérateur, T) dans deux types de polymérisation distincts : la polymérisation par ouverture de cycle (ROP - Ring Opening Polymerization) et la polymérisation radicalaire modérée par voie organométallique (OMRP). De plus, ces mêmes complexes devaient permettre la commutation entre ces deux mécanismes de polymérisation sans modification chimique pour produire des copolymères à blocs originaux (*schéma 4*). L'architecture des complexes de coordination est basée sur une étude bibliographique poussée et l'utilisation de nos compétences, qui a mis en lumière le Cobalt comme centre métallique, parce qu'il est très abondant, peu chère et moins toxique que les métaux utilisés aujourd'hui dans l'industrie (ex : étain). De plus, il fait partie des métaux de transition les plus reportés pour la polymérisation radicalaire mais très peu pour la ROP, ce qui en fait un très bon point de départ. Pour le choix des ligands, nous avons pu mettre en lumière des bases de Schiff (N_2, O_2), pour le contrôle de la polymérisation des MAMs^{21, 22}, et le bisacétylacetonate (O_2, O_2), pour les LAMs.²³⁻²⁵ D'autre part, comme énoncé dans le *schéma 2a*, il nous faut un complexe bien défini qui porte un fragment amorceur (R_0), pour fournir le radical primaire dans un cas et un nucléophile dans un autre. C'est sur ce point que reposait le principal challenge et que nous avons décidé de développer des complexes de Cobalt-alkoxide (Co-Oxygène), à ce jour encore peu reportés dans la littérature.

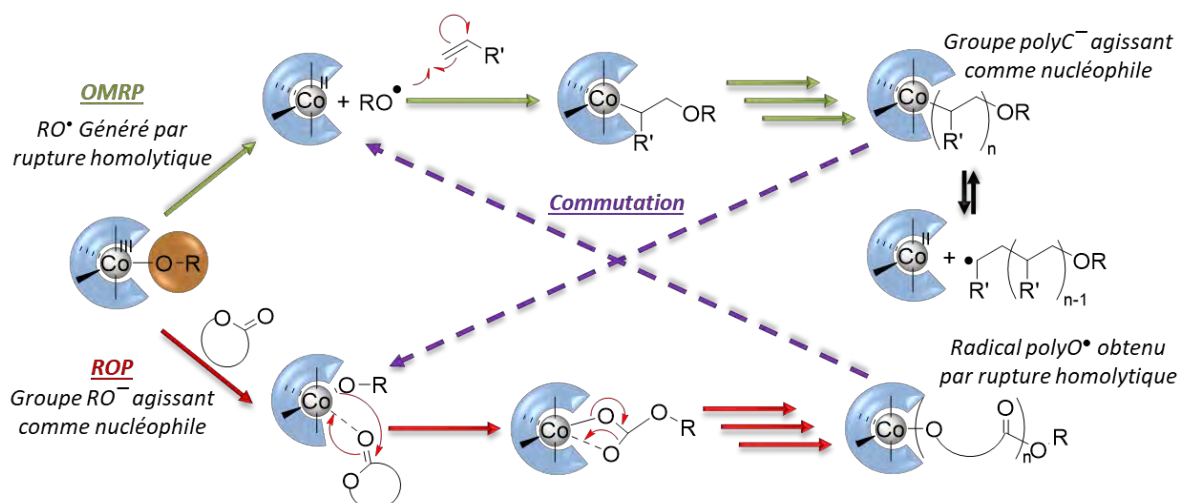


Schéma 4 : Schéma général représentant l'objectif du projet avec les deux mécanismes de polymérisations OMRP et ROP ainsi que les Commutation.

Comme illustré sur le schéma 3, nos complexes de Cobalt devaient être capable de réaliser la rupture homolytique métal-oxygène pour générer un radical oxygéné, qui pourra s'additionner sur un monomère vinylique (ex : VAc) dans des conditions d'OMRP (chemin vert schéma 3). Mais aussi, pouvoir fournir un nucléophile du fait de la possible polarisabilité de la liaison Mt-Oxygène, pour l'attaque de l'ester cyclique (ex : Lactone) dans des conditions de ROP (chemin rouge schéma 3). Et si possible, permettre une commutation entre les blocs (chemin violet), c'est-à-dire, faire la synthèse d'un premier bloc par OMRP, qui puisse être ensuite réactivé, et fournir un polyC^- pour une extension par ROP (et vice versa). Si le « switch » entre les deux techniques est possible et efficace sans modification du bout de chaîne, cela devait nous permettre un accès facile à des copolymères (aléatoires / à blocs / alternés / di-blocs / tri-blocs ...) totalement inédits et aux propriétés variables et originales.

Pour démarrer ces travaux, nous avons commencé par la synthèse du complexe $[\text{Co}^{\text{III}}(\text{L}^{1.1})(\text{OAc})]$ (**3.1**), qui remplissait toutes les caractéristiques souhaitées pour l'amorçage et le contrôle des MAMs, mais qui n'avait jamais été reporté pour ce type d'application.²⁶ Ainsi, que le complexe $[\text{Co}(\text{L}^{1.10})(\text{OAc})]$ (**3.2**), qui est dérivé de précédents travaux menés dans l'équipe, où un fragment acetylacetonate remplaçait notre acetate (figure 3).²⁷

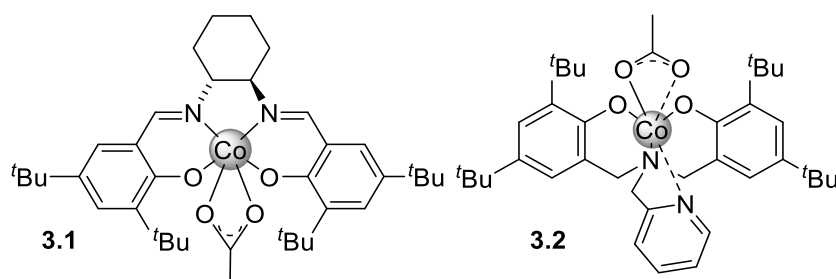


Figure 3 : Complexes de ligands (N2,O2) cobalt acetate.

Après avoir fait la synthèse des complexes présentés ci-dessus, les premiers tests de polymérisation ont été menés, pour savoir si, sous l'effet de la température, on avait bien rupture homolytique et production de radicaux, qui sont essentiels à l'ammorçage direct. Les divers tests ont révélés que le complexe **3.1** générant des radicaux à 40°C en présence de MMA et à 70°C avec le MA. Ce qui est venu appuyer les résultats obtenus par calcul DFT, qui ont montrés un $\Delta G^{\text{MA}} > \Delta G^{\text{MMA}}$ (20.5 contre 15.1 kcal mol⁻¹). Ainsi, qu'une absence de polymérisation en présence de VAc dû au $\Delta G^{\text{VAc}} = 26.2$ kcal mol⁻¹ trop élevé. De plus, ce complexe a montré de bons résultats pour le contrôle de la polymérisation par OMRP du MA, et un mécanisme de transfert de chaîne avec le MMA et le St, qui sont des monomères avec un radical plus stabilisé, favorisant ce type de processus. D'autre part, la synthèse de copolymères à blocs (PMA-*b*-PBA) a été faite avec succès, ce qui nous a permis de mettre en évidence la présence d'un Cobalt ré-activable en bout de chaîne (*figure 4*). Du fait de ces résultats encourageants, nous avons décidé de poursuivre l'investigation en ouverture de cycle (ROP), et là aussi, il a montré un bon contrôle pour la ROP du l-lactide et de la ϵ -caprolactone, mais seulement pour former des polymères de petite masse molaire. Ce qui met en évidence qu'un complexe portant la fonction carboxylate peut amorcer par voie radicalaire et par coordination/insertion.

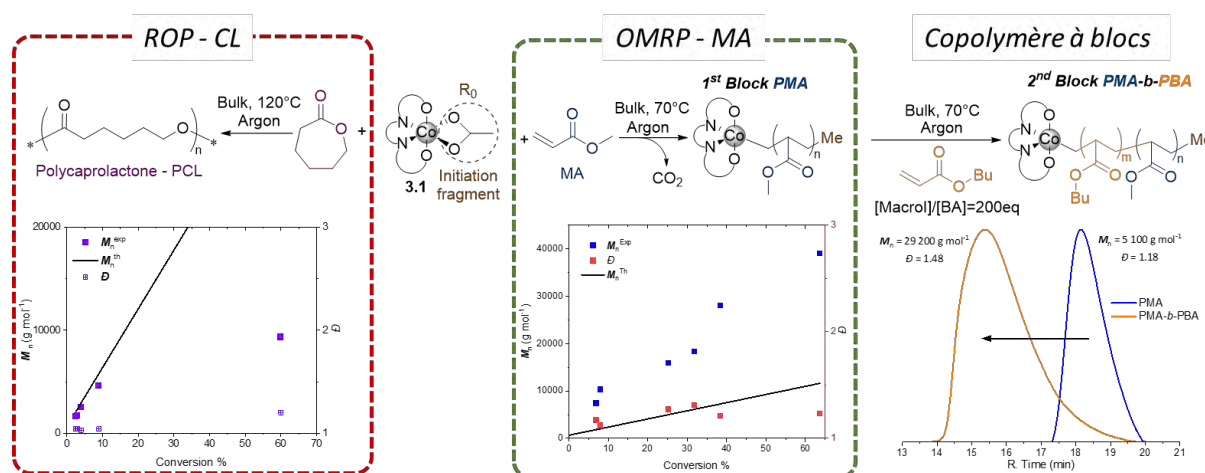


Figure 4 : Résultats obtenu en OMRP et ROP avec le complexe **3.1**.

Malheureusement, les travaux menés sur le complexe $[\text{Co}(\text{L}^{1.10})(\text{OAc})]$ (**3.2**) n'ont pas été concluants, en effet, après plusieurs tests de polymérisation avec divers monomères, nous n'avons pas observé de production de polymères, comme c'était le cas pour ses homologues déjà publié par notre groupe.²⁷

En parallèle, une voie de synthèse « rédox » originale a été mise en place. Cette dernière est présentée dans le schéma 5 et permet d'obtenir en une étape un complexe de Cobalt carboxylate $[\text{Co}(\text{acac})_2(\text{O}_2\text{CPh})]$ (**3.6**) à partir du précurseur Cobalt(II) bisacetylacetonate ($\text{Co}(\text{acac})_2$) et le benzoyl peroxide (BPO). Il est intéressant de noter que cette réaction se fait à température ambiante, à partir de deux réactifs commerciaux et peu coûteux.

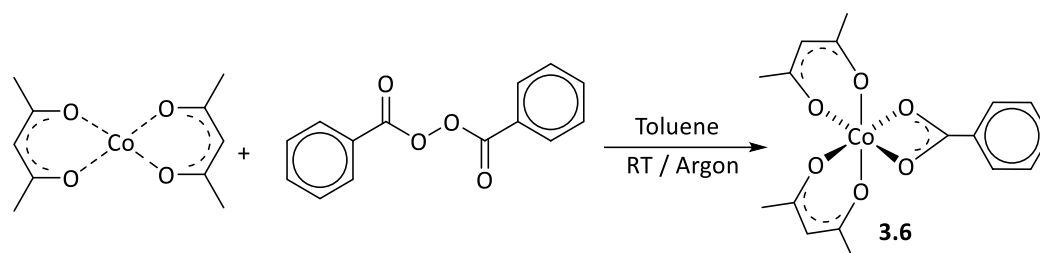


Schéma 5 : Synthèse du complexe de Cobalt hexa-coordinés par des oxygènes (**3.6**).

Après avoir bien caractérisé ce nouveau complexe (RMN, UV-Vis, électrochimie et X-rays), qui, à notre connaissance, est le premier complexe de Cobalt hétéroleptique avec une sphère de coordination entièrement oxygénée reporté à ce jour. Nous l'avons testé en polymérisation et contrairement au précédent, ce complexe amorce mais ne contrôle pas la polymérisation des MAMs. Ce qui n'est pas surprenant, car dans la littérature le Cobalt bisacetylacetonate est connu pour modérer la polymérisation de l'acétate de vinyle (LAMs). Cependant, le premier test de polymérisation avec le VAc montre bien l'amorçage radicalaire attendu mais seulement un contrôle partiel, qui a été relié au facteur d'efficacité du complexe. En effet, seulement 10% du complexe présent dans le milieu faisait la rupture homolytique, ce qui induit une trop faible concentration de modérateur relargué dans le milieu pour prendre le contrôle de la polymérisation. C'est pourquoi, en vue d'avoir un contrôle sur la polymérisation dès le début de la réaction, nous avons décidé dans un premier temps d'ajouter une quantité catalytique de Cobalt (II), comme illustré dans le schéma 6.

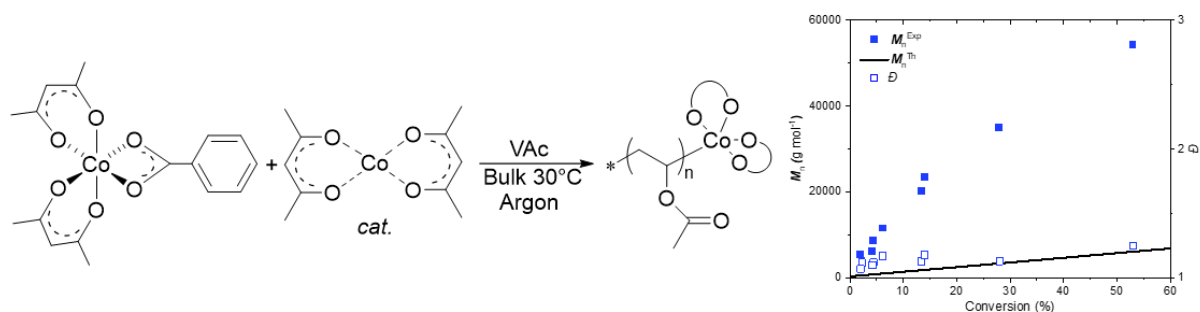


Schéma 6 : Polymérisation contrôlée du VAc avec le complexe 3.6 et une quantité catalytique de Cobalt (II) en masse à 30°C.

Ensuite, l'étude des bouts de chaîne a été entrepris, en vue d'expliquer ce faible facteur d'efficacité. Pour ce faire, des études ESI-MS (figure 5) ont mis en évidence plusieurs population, toutes séparés avec un intervalle de 86.09 g mol⁻¹, ce qui valide la présence d'unité de répétition VAc.

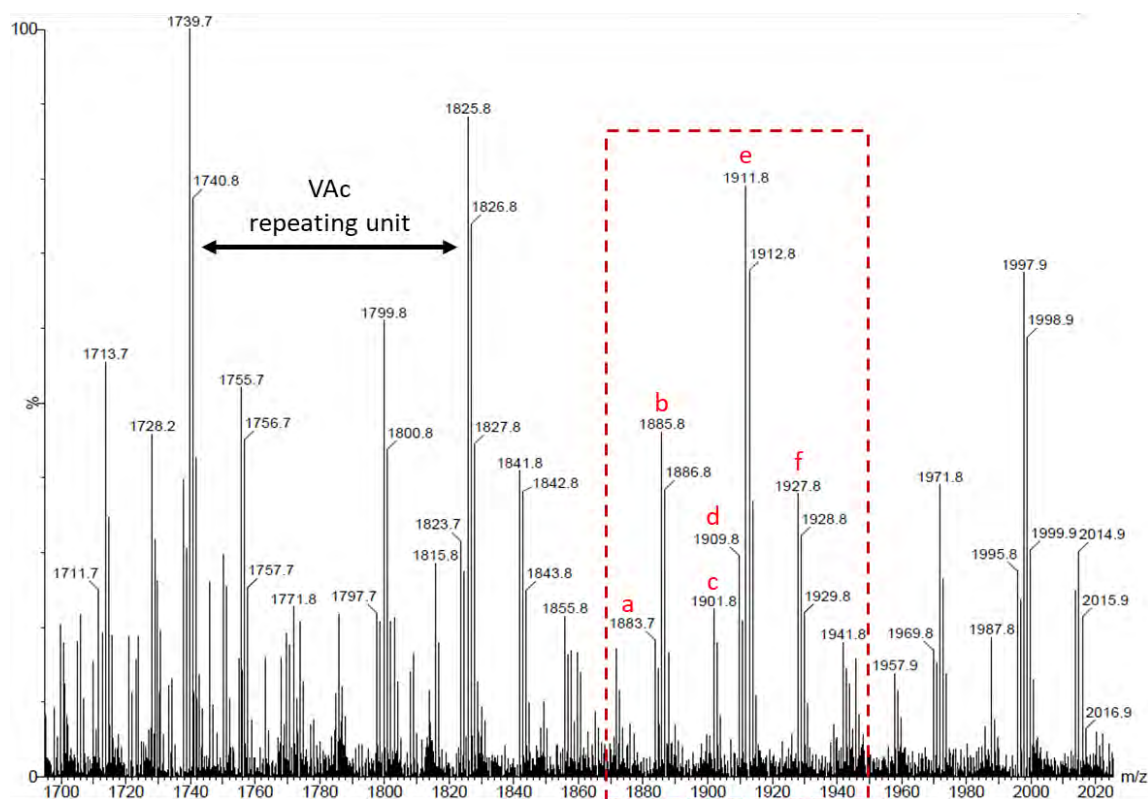


Figure 5 : Expansion du spectre ESI-MS (mode positif, QToF-NaI) entre 1700 - 2020 m/z du polyacétate de vinyle (PVAc) obtenue avec le complexe **3.6**.

Les six populations présentées dans la *figure 5* ont été rationalisé sur la base du mécanisme d'amorçage présenté dans le *schéma 7* où le radical phenyl, mais aussi avec le radical benzoate font l'amorçage de la polymérisation.

Les chaînes amorcées par le radical phenyl avec le $[Co(acac)_2]$ en bout de chaîne (position ω) a été directement détecté (population **a**). Cependant, la population résultante de ces chaînes provienne de la dissociation hydrolytique du cobalt (H en position ω , population **b**). Les chaînes amorcées avec le benzoate (PhCOO) en position α sont hydrolyser dans les conditions d'analyse de l'ESI-MS pour laisser apparaitre une fonction alcool et le cobalt en bout de chaîne, correspondant à la population **c**. Ainsi que la population **d** sans ce cobalt en bout de chaîne. La faible force de la liaison Co-PVAc favorise la production de radicaux au cours du traitement ce qui peut entrainer du couplage bimoléculaire, comme observé en GPC. Et, ces couplages soient entre une chaîne amorcée par un phenyl et un benzoate radical, soit par deux benzoate radical sont illustrés respectivement par les populations **f** et **e**. Cependant, le couplage entre deux chaînes amorcées par le phenyl n'a pas été observé. Cette observation montre bien une compétition entre la décarboxylation et le démarrage de la polymérisation radicalaire.

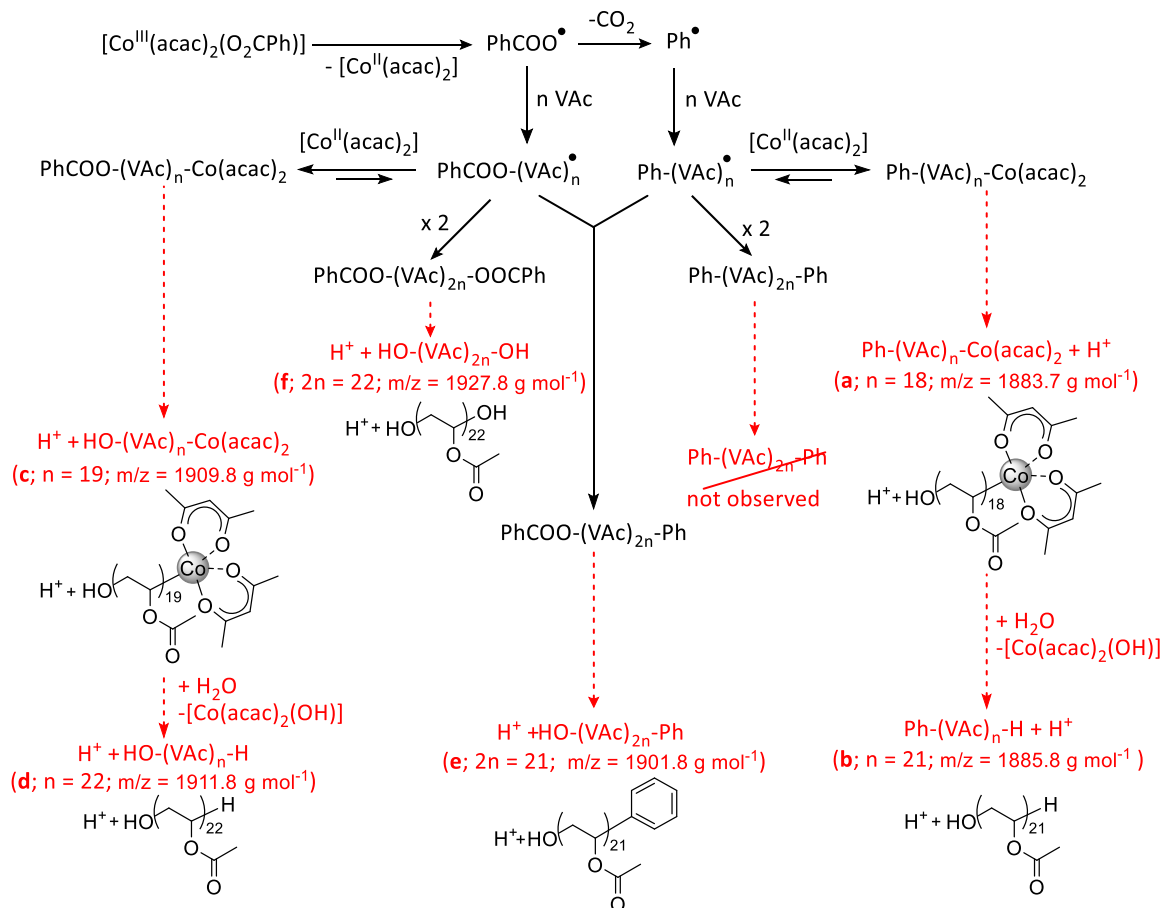


Schéma 7 : Mécanisme d'amorçage de polymérisation du VAc et leur relation avec les chaînes observées par ESI-MS.

Pour le second bout de chaîne, des expériences d'extensions de chaînes ont été réalisées pour mettre en lumière le Cobalt ré-activable en bout de chaîne polymère. C'est ainsi que nous avons obtenu des copolymères à blocs (PVAc-*b*-PSt, PVAc-*b*-PVAc, PVAc-*b*-PMA, PVAc-*b*-PBA, *figure 6*). De plus, l'analyse GPC (*figure 6*) montre bien un déplacement clair du signal en GPC vers des temps de rétention plus faibles (et donc des masses molaires plus élevées), suggérant la croissance des polymères avec une disparition totale du signal du macro-amorceur de départ, qui traduit l'extension de celui-ci et non la croissance d'une deuxième chaîne.

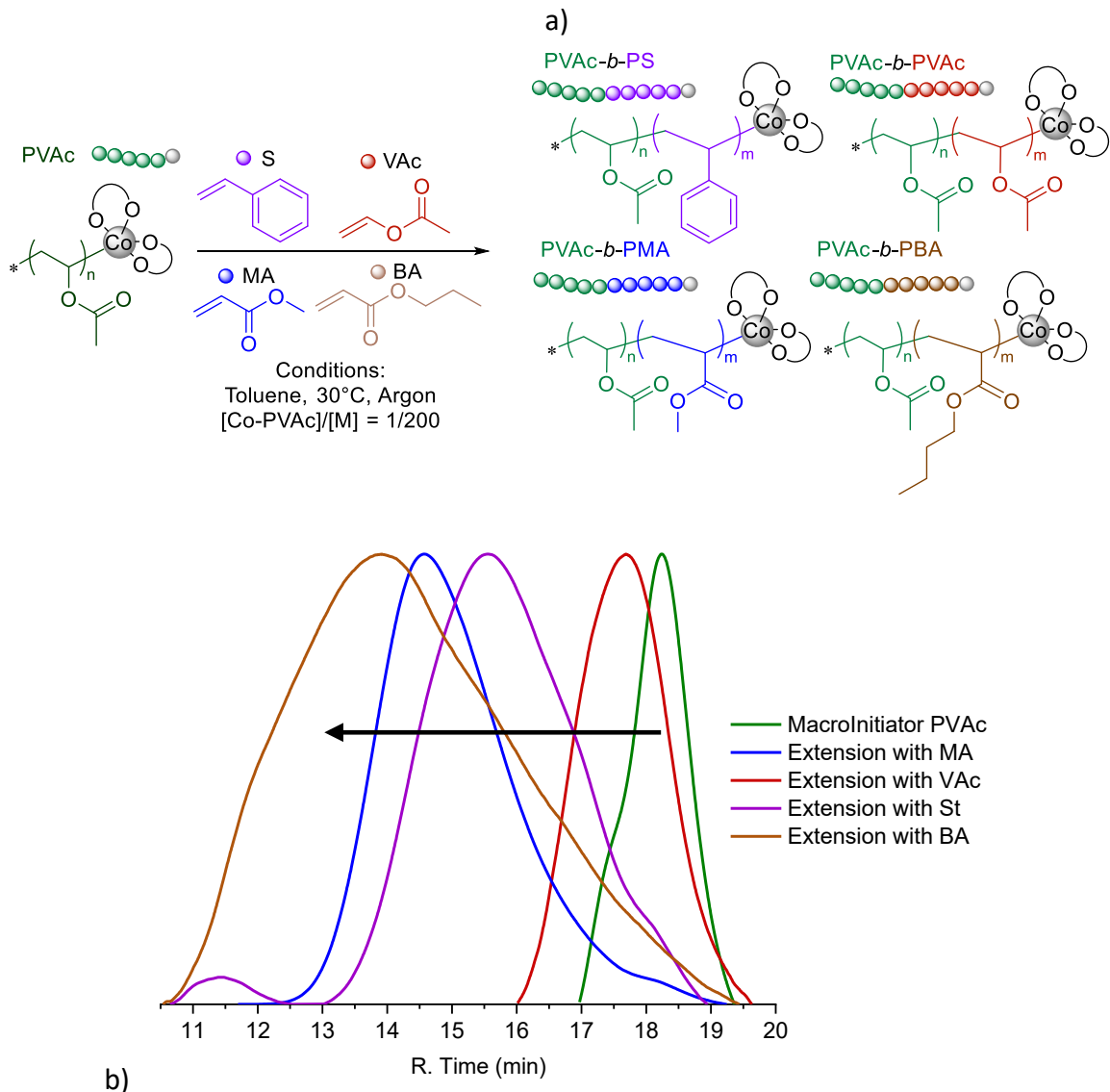


Figure 6 : a) Macro-amorceur (PVAc) pour des extensions de chaînes avec du VAc (rouge), St (violet), MA (en bleu) et du BA (en marron), b) Chromatogrammes GPC obtenue du macro-amorceur PVAc et des copolymères : PVAc-*b*-PVAc, PVAc-*b*-PS, PVAc-*b*-PMA, PVAc-*b*-PBA.

D'autre part, une rapide étude a montré que ce complexe pouvait aussi amorcer la polymérisation par ouverture de cycle ϵ -lactide et de la ϵ -caprolactone, comme on peut le voir sur la *figure 7*. En effet, des tests avec à 100°C en masse et à 90°C en solution ont montré que le poly lactide se formait, et l'évolution des masses molaires en fonction de la conversion suggère une croissance de chaîne contrôlée, bien qu'un peu écartée des valeurs théoriques attendues. Il en est de même pour les résultats obtenus lors des polymérisations avec la caprolactone. Mais dans ce cas, avec un ajout de différents équivalents de BnOH nous avons vu la vitesse de polymérisation s'accélérer ainsi que les masses molaires diminuer, tout en observant une évolution linéaire. En outre, nous avons observé dans tous les cas des dispersités étroites et bien plus faibles pour les PCL (<1.2) comparativement au PLA (<1.5).

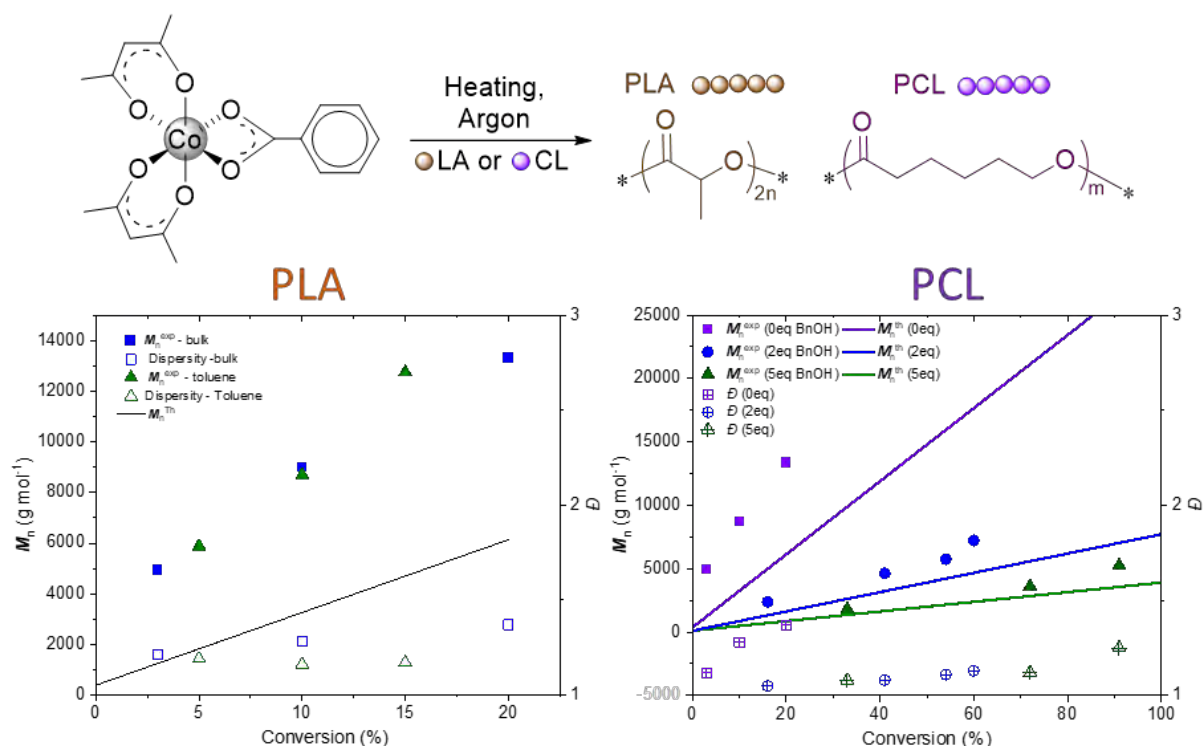


Figure 7 : Polymérisation par ROP du LA et CL, résultats PLA : M_n and \bar{D} vs. Conversion en masse à 100°C et en solution à 90°C et résultats PCL : M_n and \bar{D} vs. Conversion, en masse à 100°C avec plusieurs équivalents de BnOH (0eq, 2eq, 5eq).

L'ensemble des résultats obtenus en radicalaire et en ouverture de cycle en faisait un bon candidat pour la commutation de mécanisme de polymérisation. Mais avant d'étudier cette piste, nous avons exploré d'autres axes de recherche pour tenter d'améliorer ce système, qui présentait un facteur d'efficacité faible (autour de 10%) semblable à celui reporté dans la littérature.²⁸ Pour rappel, ce facteur correspond à la proportion de catalyseur qui, sous l'effet de la température, vient à se casser et à générer le radical primaire nécessaire à l'amorçage de la polymérisation. Pour ce faire, nous avons dans un premier temps augmenté la température (de 30°C jusqu'à 60°C). Ce qui nous a permis d'améliorer ce facteur jusqu'à 15-20% et de mettre en lumière une vitesse de polymérisation allant jusqu'à 10 fois plus vite avec le même contrôle (*figure 8a*). Après ça, nous avons transposé ces réactions en solution pour ralentir la phase d'amorçage et ainsi laisser plus de temps pour l'activation du complexe à 30°C. Nous avons pu remarquer une amélioration du facteur d'efficacité dans ces conditions, en effet, l'évolution des masses molaires est bien plus proche de la droite théorique (*figure 8b*). En parallèle de l'amorçage thermique, un photo-amorçage a aussi été envisagé du fait de la signature en UV-Vis mais sans aucun succès.

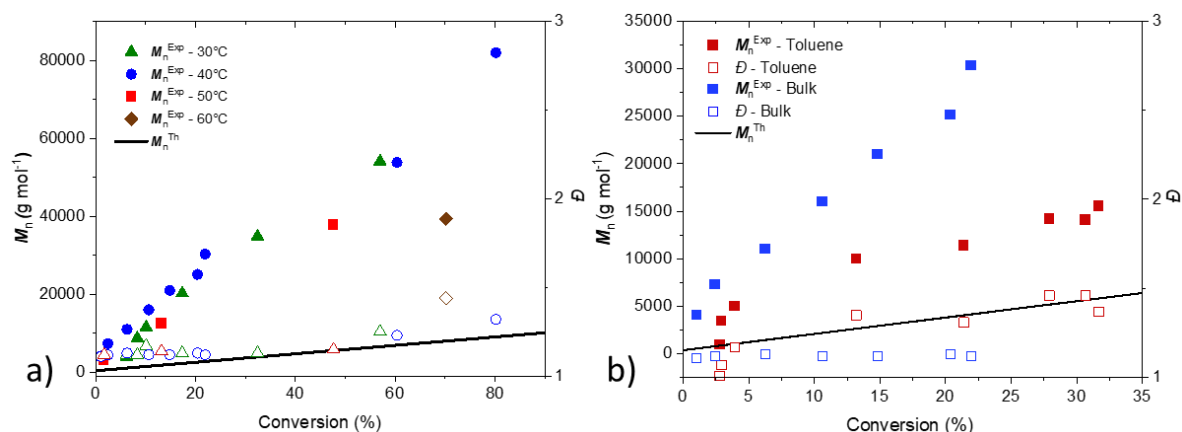


Figure 8 : Graphique représentant l'évolution des masses molaires et dispersité en fonction de la conversion initié avec **3.6 a)** à différentes températures et conditions $[Co^{III}]/[Co^{II}]/[VAc] = 1/0.25/126$, **b)** à 40°C en solution ($[VAc] = 4 M$) comparé à l'expérience fait en masse.

C'est ce qui nous a poussé à réfléchir à la modification du complexe et notamment la modification du fragment amorceur (R_0). En effet, ce complexe est produit à partir du Cobalt (II) et de benzoyl peroxyde, on a donc fait la synthèse d'autres peroxydes avec des substituants en *para* ou *ortho* du cycle aromatique. Le but de la manœuvre était d'élargir la bibliothèque des composés synthétisés avec cette nouvelle voie de synthèse et de voir s'il était possible de fragiliser la liaison Mt-Oxygène par effet électronique, avec l'ajout de groupement donneur ou attracteur (inductif ou mésomère) en *para*. Ou, par des effets stériques avec la modification en position *ortho* du cycle, pour ainsi améliorer significativement le facteur d'efficacité. Cette étude nous a permis de développer la librairie des complexes de Cobalt avec une sphère de coordination entièrement oxygénée avec huit nouveaux composés supplémentaires, présentés sur la *figure 9*, qui ont été isolés et caractérisés par RMN, X-Rays et UV-Vis. Il y a les dérivés du complexe **3.6**, qui sont issus de la modification du peroxyde aromatique (**3.7-3.10**). Et en parallèle, étendu aussi au peroxyde non aromatique, tel que le diacetyl peroxyde (**3.11**) et le dilauroyl peroxyde (**3.12**). Mais aussi, de transposer cette stratégie au complexe (N_2,O_2) base de Schiff, qui nous a permis de développer les complexes (**3.3** et **3.4**).

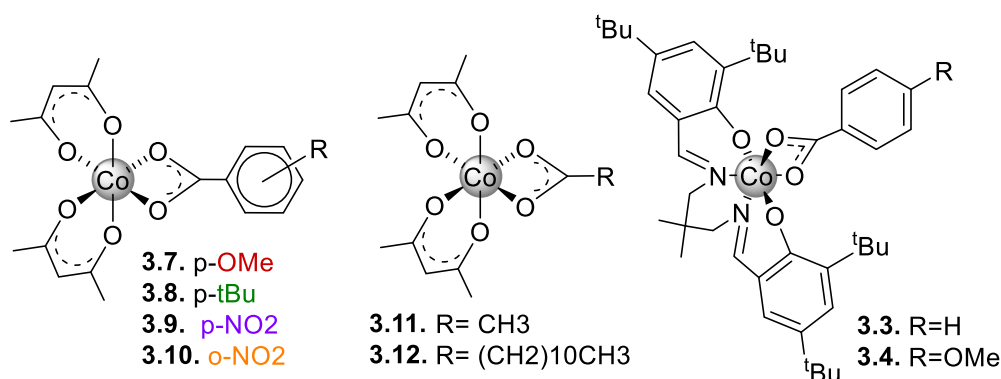


Figure 9 : Complexes de cobalt issu de la réaction red/ox avec des peroxydes.

Pour comparer avec le complexe de base **3.6**, on a suivi la formation des complexes **3.6** à **3.10** en UV-Visible dans des conditions de pseudo premier ordre (en excès de l'un des réactifs, ici le peroxyde), qui nous ont permis d'extrapoler des cinétiques de formation et ainsi émettre des hypothèses sur la stabilité thermodynamique de chaque complexe. En effet, comme on peut le voir sur le graphique ci-dessous où la pente traduit la vitesse de formation pour chaque complexe. Ils suivent la même tendance que le complexe **3.6**, hormis le **3.9** avec le groupement nitro en *para*, qui semble se former beaucoup plus vite que les autres. Ce qui voudrait dire qu'il est thermodynamiquement plus stable et donc que l'amorçage serait plus difficile.

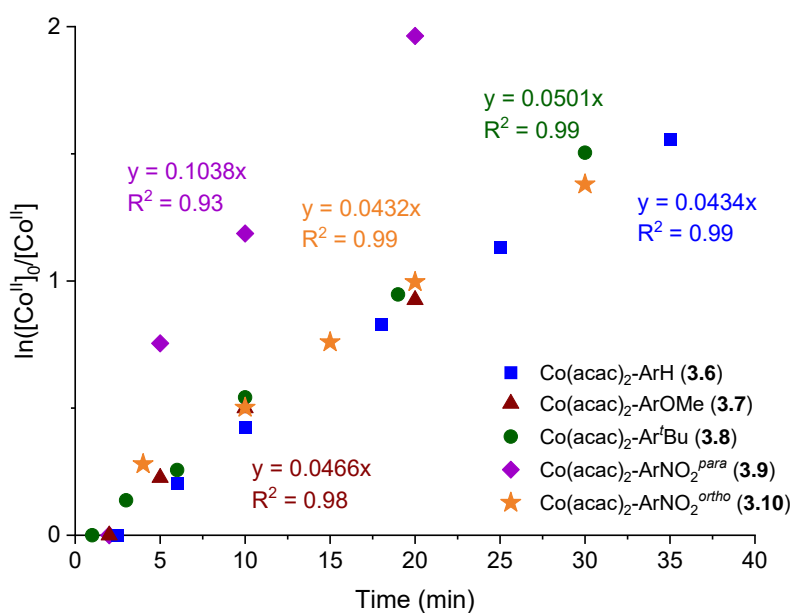


Figure 10 : Cinétiques de formation des complexes **3.6-3.10**.

Ces hypothèses ont pu ensuite être vérifiées par les tests expérimentaux de polymérisation en présence de VAc. Comme attendu, le complexe **3.9** n'amorce pas la polymérisation à 30°C, ni à 40 °C ou même 60°C, ce qui conforte l'hypothèse que ce complexe est thermodynamiquement plus stable que les autres. D'autre part, la même observation expérimentale a été faite avec le dérivé nitro en *ortho*, bien que la cinétique de formation soit dans la même tendance que le complexe **3.6**. Probablement, dû au fait de potentielles liaisons hydrogènes entre les oxygènes du groupement nitro (NO₂) et des H des ligands acetylacetonates. En outre, nous avons pu observer une polymérisation radicalaire contrôlée avec les deux autres **3.7** et **3.8**. Cependant, le dérivé tertbutyl (**3.8**) n'amorce pas à 30°C mais à 40°C contrairement au dérivé méthoxy (**3.7**) qui a généré avec succès des radicaux à cette température. Cette observation a été rationalisée par les effets électroniques de ces substituants : inductif donneur pour le tertbutyl et mésomère donneur pour le méthoxy. Le métal s'en trouve plus enrichi en électrons et de ce fait, défavorise la rupture homolytique (BDE plus grande). Cette étude recelle encore bon nombre de mystères, qui mériteraient d'être investigués plus en profondeur.

Comme mentionné plus haut, nous avons appliqué la même stratégie pour des peroxyde alkyl tels que le dilauryl peroxyde, qui est commercial, et le diacetyl peroxyde. Bien que nouvelle et prometteuse, cette voie fut vite abandonnée du fait des difficultés de caractérisation et de synthèse rencontrées. En effet, le diacetyl peroxyde est un composé hautement explosif et le di lauryl peroxyde comporte une chaîne alkyl de 11 carbones, rendant les cristallisations et les purifications impossibles. Concernant les composés basés sur des ligands (*N2,O2*)-base de Schiff (**3.3** et **3.4**), nous avons remarqué qu'ils pouvaient générer des radicaux et amorcer la polymérisation du MA, mais sans aucun contrôle malheureusement. Cependant, ces nouveaux complexes de coordination, ayant été bien caractérisés, restent peu étudiés du fait des résultats préliminaires peu encourageants.

Bien que plusieurs des complexes développés pendant ces travaux de thèse ne sont pas efficaces pour l'OMRP ou la ROP, ils restent tout de mêmes très intéressants et peuvent potentiellement servir pour d'autres applications. De ces travaux préliminaires nous avons donc pu dégager deux candidats (**3.1** et **3.6**) potentiels pour la production de copolymères à blocs *via* la comutation de mécanisme entre l'OMRP et la ROP. Le premier switch étudié a été celui de l'OMRP vers la ROP, des premiers tests ont été faits avec le système **3.1**, mais se sont révélés peu concluants comparativement au deuxième système **3.6** qui ayant montré de bons résultats, ce qui nous a amené à nous concentrer sur celui-ci. En effet, une chaîne courte PVAc, synthétisée en masse à 40°C et remise en présence d'un ester cyclique pour une extension de chaîne, a permis de mettre en place (après optimisation) une procédure séquentielle de polymérisation (Schéma 8).

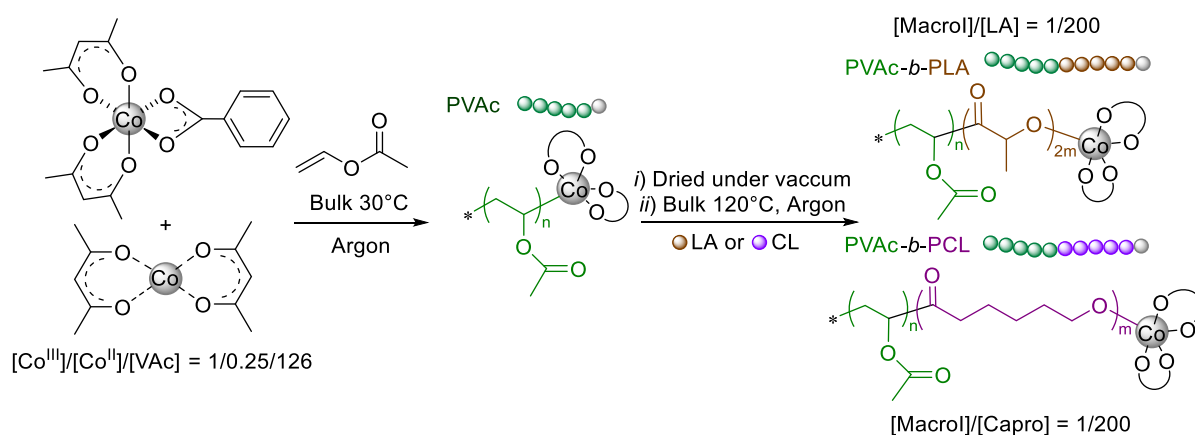


Schéma 8 : Séquentielle copolymérisation du VAc par OMRP et LA ou CL par ROP avec le système **3.6**.

Le résultat exposé sur la *figure 11* montre un déplacement clair du signal en GPC vers des temps de rétention plus faibles (et donc des masses molaires plus élevées), suggérant la croissance du polymère avec une disparition totale du signal du macroamorceur de départ qui traduit l'extension de celui-ci et non la croissance d'une deuxième chaîne.

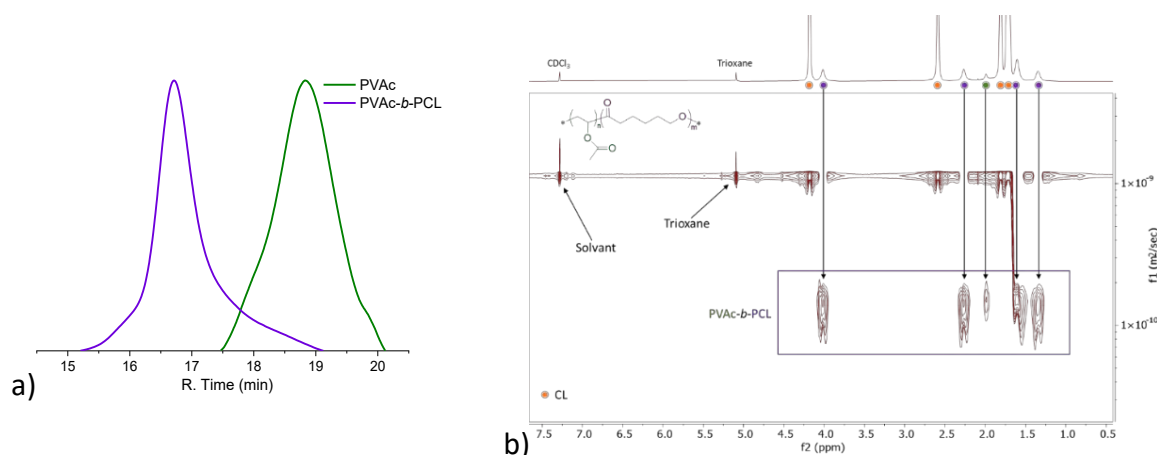


Figure 11 : a) Chromatogrammes obtenue en GPC-THF avec la calibration polystyrène, b) Spectre RMN DOSY du copolymère à blocs PVAc-b-PCL formé, dans le CDCl_3 .

Comme seconde preuve de la production d'un copolymère à blocs et non d'un mélange d'homopolymères, la RMN DOSY présentée dans la *figure 11b* allie le spectre du proton au coefficient de diffusion des espèces. Ce qui nous a permis de caractériser une espèce avec les signaux caractéristiques du polycaprolactone et du polyacetate de vinyle. Et d'autres signaux correspondant au solvant ou au monomère présent dans le milieu.

Pour promouvoir la commutation depuis la ROP vers l'OMRP, nous avons tout d'abord essayé de réactiver le copolymère formé précédemment pour faire un tribloc mais sans succès. Mais aussi, de suivre le même protocole que pour la commutation précédente (*Schéma 8*), c'est-à-dire commencer par la synthèse d'un macro-amorceur (PCL) de petite masse, que l'on a isolé et caractérisé puis remis en présence d'un monomère vinylique pour faire l'extension (ROP \rightarrow OMRP) mais sans succès.

C'est pourquoi, un autre axe de developement basé sur ce système a ensuite été mis en place et consiste à utiliser le faible facteur d'efficacité de notre complexe **3.6** pour mettre en place un procédé one-pot qui permettait la production d'un mélange de polymères.

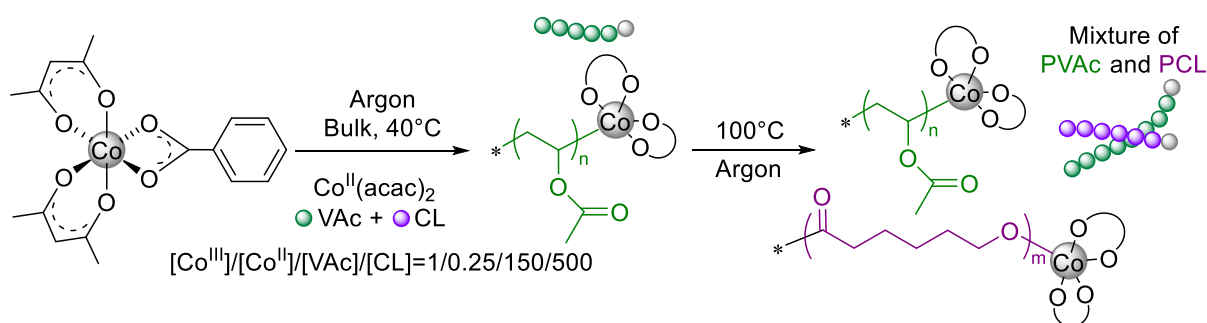


Schéma 9 : Procédé « one-pot » pour la polymérisation du VAc et CL.

C'est-à-dire, comme illustré dans le *schéma 9*, nous avons polymérisé de l'acetate de vinyle à 40°C en présence de caprolactone, qui, ici, a joué le rôle de solvant, en effet, il a été précédemment observé que la ROP de ce composé ne se fait qu'à partir de 100°C. Après un

temps approprié, la température est augmentée pour démarrer la ROP. Comme on peut le voir sur les RMN de la *figure 12a*, dans un premier temps, seule une production de PVAc est observée puis, dans un second temps, celle du PCL. Pour savoir s'il s'agissait bien d'un mélange de deux polymères, la DOSY a été faite et comme montré ci-dessous (*figure 12b*) nous avons bien deux coefficients de diffusion, qui correspondent aux signaux caractéristiques de chaque polymère.

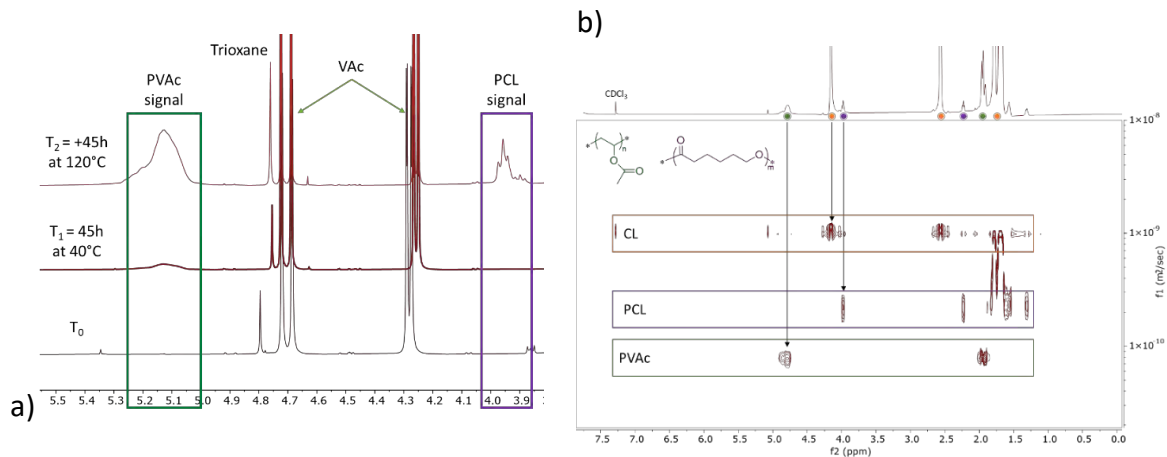


Figure 12 : a) ¹H RMN et b) DOSY RMN de la stratégie de polymérisation one-pot VAc + CL, dans CDCl₃.

La dernière partie, constitue comme un axe de perspective de ces travaux, car les copolymères à blocs ainsi produits ont pour vocation de créer de nouveaux matériaux biodégradables. C'est pourquoi, après la synthèse du copolymère PVAc-*b*-PLA, nous l'avons dégradé grâce à un complexe de zinc, comme on peut le voir sur la GPC présentée en *figure 13*. Le signal du macro-amorceur PVAc se décale vers les temps de rétention plus faibles, ce qui traduit l'extension vers le copolymère PVAc-*b*-PLA qui est ensuite dégradé, et le signal se décale à nouveau, mais vers les temps de rétention plus élevés, ce qui traduit une perte de masse sur le polymère.

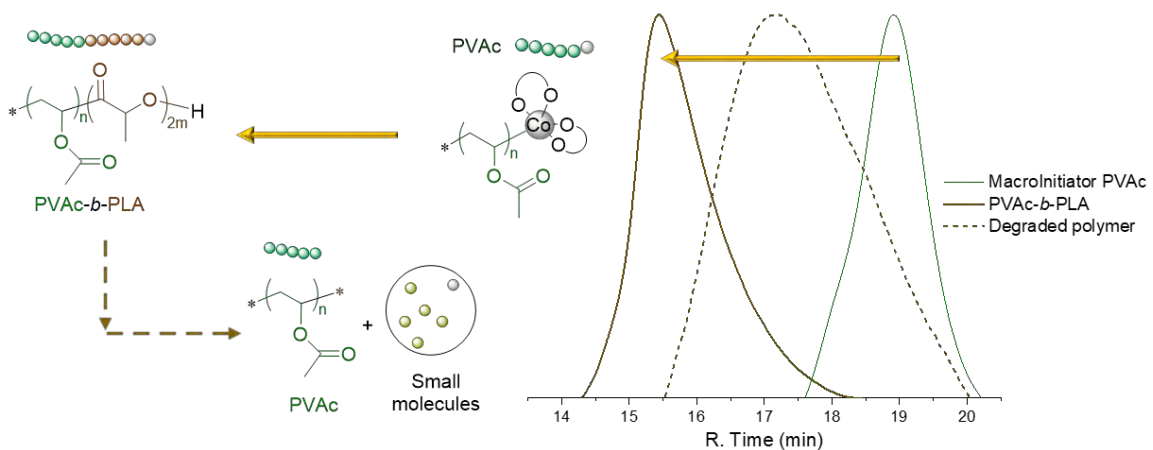


Figure 13 : Stratégie de dégradation appliqué au PVAc-*b*-PLA.

Références

1. Kazuo, S., Takesi, S., Ziegler-Natta catalysts for olefin polymerizations. *Pmg. Polym, Sci.* **1997**, *23*, 1503-1546.
2. Matyjaszewski, K., Advanced Materials by Atom Transfer Radical Polymerization. *Adv Mater* **2018**, *30* (23), e1706441.
3. Ribelli, T. G.; Fantin, M.; Daran, J. C.; Augustine, K. F.; Poli, R.; Matyjaszewski, K., Synthesis and Characterization of the Most Active Copper ATRP Catalyst Based on Tris[(4-dimethylaminopyridyl)methyl]amine. *J Am Chem Soc* **2018**, *140* (4), 1525-1534.
4. Matyjaszewski, K., Introduction to living polymerization. Living and/or controlled polymerization. *Journal of physical organic chemistry* **1995**, *8*, 197-207.
5. Wang, J.-S.; Matyjaszewski, K., Controlled/"living" radical polymerization. atom transfer radical polymerization in the presence of transition-metal complexes. *Journal of the American Chemical Society* **2002**, *117* (20), 5614-5615.
6. Charles H. J. Johnson, G. M., David H. Solomon, Thomas H. Spuvling and Davren J. veaving, The Application of Supercomputers in Modelling Chemical Reaction Kinetics: Kinetic Simulation of 'Quasi-Living' Radical Polymerization. *Aust. J. Chem.*, **1990**, *43*, 1215-30.
7. Moad, G.; Rizzardo, E., Alkoxyamine-Initiated Living Radical Polymerization: Factors Affecting Alkoxyamine Homolysis Rates. *Macromolecules* **2002**, *28* (26), 8722-8728.
8. Roshan T. A. Mayadunne, J. J., Graeme Moad and Ezio Rizzardo, Living Free Radical Polymerization with Reversible Addition-Fragmentation Chain Transfer (RAFT Polymerization): Approaches to Star Polymers. *Macromolecules* **2003**, *36*, 1505-1513.
9. Atsushi Goto, K. S., Yoshinobu Tsujii, Takeshi Fukuda,* , Graeme Moad, Ezio Rizzardo, and San H. Thang, Mechanism and Kinetics of RAFT-Based Living Radical Polymerizations of Styrene and Methyl Methacrylate. *Macromolecules* **2001**, *34*, 402-408.
10. Roshan T. A. Mayadunne, E. R., * John Chiefari, Yen Kwong Chong, Graeme Moad, and San H. Thang, Living Radical Polymerization with Reversible Addition-Fragmentation Chain Transfer (RAFT Polymerization) Using Dithiocarbamates as Chain Transfer Agents. *Macromolecules* **1999**, *32*, 6977-6980.
11. David G. Hawthorne, G. M., * Ezio Rizzardo,* and San H. Thang*, Living Radical Polymerization with Reversible Addition-Fragmentation Chain Transfer (RAFT): Direct ESR Observation of Intermediate Radicals. *Macromolecules* **1999**, *32*, 5457-5459.
12. Nothling, M. D.; Fu, Q.; Reyhani, A.; Allison-Logan, S.; Jung, K.; Zhu, J.; Kamigaito, M.; Boyer, C.; Qiao, G. G., Progress and Perspectives Beyond Traditional RAFT Polymerization. *Adv Sci (Weinh)* **2020**, *7* (20), 2001656.
13. Debuigne, A.; Poli, R.; Jérôme, C.; Jérôme, R.; Detrembleur, C., Overview of cobalt-mediated radical polymerization: Roots, state of the art and future prospects. *Progress in Polymer Science* **2009**, *34* (3), 211-239.
14. Zhu, Y.; Romain, C.; Williams, C. K., Sustainable polymers from renewable resources. *Nature* **2016**, *540* (7633), 354-362.
15. Degradable Aliphatic Polyesters. *Advances in Polymer Science* **2002**, *157*.
16. Auras, R.; Harte, B.; Selke, S., An overview of polylactides as packaging materials. *Macromol Biosci* **2004**, *4* (9), 835-64.
17. Gupta, A. P.; Kumar, V., New emerging trends in synthetic biodegradable polymers – Polylactide: A critique. *European Polymer Journal* **2007**, *43* (10), 4053-4074.

18. Philippe Degée, P. D., Robert Jerome, Sven Jacobsen and HansGerhard Fritz, New catalysis for fast bulk ring-opening polymerization of lactide monomers. *Macromol. Symp.* **1999**, *144*, 289-302
19. Löfgren, A.; Albertsson, A.-C.; Dubois, P.; Jérôme, R., Recent Advances in Ring-Opening Polymerization of Lactones and Related Compounds. *Journal of Macromolecular Science, Part C: Polymer Reviews* **1995**, *35* (3), 379-418.
20. Odile Dechy-Cabaret, B. M.-V., and Didier Bourissou, Controlled Ring-Opening Polymerization of Lactide and Glycolide. *Chem. Rev.* **2004**, *104*, 6147-6176.
21. Zhao, Y.; Yu, M.; Zhang, S.; Wu, Z.; Liu, Y.; Peng, C. H.; Fu, X., A well-defined, versatile photoinitiator (salen)Co-CO₂CH₃ for visible light-initiated living/controlled radical polymerization. *Chem Sci* **2015**, *6* (5), 2979-2988.
22. Zhao, Y.; Zhang, S.; Wu, Z.; Liu, X.; Zhao, X.; Peng, C.-H.; Fu, X., Visible-Light-Induced Living Radical Polymerization (LRP) Mediated by (salen)Co(II)/TPO at Ambient Temperature. *Macromolecules* **2015**, *48* (15), 5132-5139.
23. Fliedel, C.; Poli, R., Homolytically weak metal-carbon bonds make robust controlled radical polymerizations systems for “less-activated monomers”. *Journal of Organometallic Chemistry* **2019**, *880*, 241-252.
24. Demarteau, J.; Kermagoret, A.; German, I.; Cordella, D.; Robeyns, K.; De Winter, J.; Gerbaux, P.; Jerome, C.; Debuigne, A.; Detrembleur, C., Halomethyl-cobalt(bis-acetylacetonate) for the controlled synthesis of functional polymers. *Chem Commun (Camb)* **2015**, *51* (76), 14334-7.
25. Debuigne, A.; Champouret, Y.; Jerome, R.; Poli, R.; Detrembleur, C., Mechanistic insights into the cobalt-mediated radical polymerization (CMRP) of vinyl acetate with cobalt(III) adducts as initiators. *Chemistry* **2008**, *14* (13), 4046-59.
26. Lars P. C. Nielsen, C. P. S., Donna G. Blackmond,* and Eric N. Jacobsen*, Mechanistic Investigation Leads to a Synthetic Improvement in the Hydrolytic Kinetic Resolution of Terminal Epoxides. *J. AM. CHEM. SOC.* **2004**, *126*, 1360-1362.
27. Redjel, Y. K.; Thevenin, L.; Daran, J.-C.; Benslimane, M.; Poli, R.; Fliedel, C., Acetylacetonato cobalt(III) and iron(III) complexes of picolylamine- and aminopropylamine-bis(phenolate) ligands: Synthesis, characterization and crystal structures. *Polyhedron* **2019**, *158*, 83-90.
28. Rayna Bryaskova, C. D., Antoine Debuigne, and Robert Jerome, Cobalt-Mediated Radical Polymerization (CMRP) of Vinyl Acetate Initiated by Redox Systems: Toward the Scale-Up of CMRP. *Macromolecules* **2006**, *39*, 8263-8268.

Résumé de thèse vulgarisé

Les matériaux polymères prennent une grande place et remplacent bons nombres de matériaux traditionnels. L'objectif de cette thèse, est d'apporter un caractère biodégradable à ces polymères. Pour les fabriquer, on utilise des complexes de coordinations (catalyseurs) et dans notre cas on veut utiliser le cobalt, qui est peu couteux et moins toxique que ceux utilisés aujourd'hui dans l'industrie. D'autre part, les monomères (brique de base constituant les polymères) ont différentes réactivités de par leur structure chimique. Les monomères vinyliques, qui forment la plupart des polymères non-dégradables et pétro-sourcés, tandis que les monomères esters cycliques, forment des polymères biodégradables. Ces travaux visent à développer un catalyseur universel pour deux classes distinctes de monomères. L'idée sous-jacente est de créer des copolymères en couplant des monomères non-biodégradables et biodégradables, par un mécanisme de commutation de polymérisation entre ces 2 techniques.

Short abstract

Polymer materials take a large place and substitute large quantities of traditional materials such as wood, steel or glass. The objective of this thesis was to bring a biodegradability property to these polymers. Usually, the polymers production is carried out by coordination complexes or catalysts and, in our case, we wanted to use Cobalt, which is less expensive and less toxic than other metals nowadays used in the industry. On the other hand, the monomers (basic brick constituting the polymers) have different reactivities due to their chemical structure. For example, vinyl monomers form most of the non-degradable polymers whereas cyclic ester monomers form biodegradable polymers. We developed a universal catalyst for two distinct classes of monomers, with the idea to create copolymers coupling non-biodegradable and biodegradable monomers, switching polymerization mechanism between these two techniques.